Jürgen Weis

Electrical Transport Through Quantum Dot Systems

April 14, 2002

To my parents.

Preface

Quantum dots or *zero-dimensional electron systems* are objects where electrons are confined in a small spatial enclosure, allowing the single electron only certain eigenvalues for its energy. Quantum dots weakly linked to leads by tunnel barriers can be considered as *model systems* to study fundamental aspects of electrical transport through single atoms or molecules.

In general, such quantum dot systems consists of the quantum dot with tunnel barriers to the so-called source and drain electrodes and with electrostatically coupling to gate electrodes. A sketch of the basic arrangement is shown in Fig. 0.1. Quantum dot systems can be designed to purpose since they are usually fabricated by conventional semiconductor growth and processing technology. Drawback is that exploring their electrical properties requires low temperature. The relative magnitude of quantization energy due to the spatial confining and electron-electron interaction is preset by design. They offer at one end confined electron systems with a dense single-particle energy spectrum like in metal, on the other end electron systems with properties reminding on those in atoms. The latter case has founded the name *artifical atoms* for quantum dots. Moreover, quantum dot systems offer the ability of *in-situ control over the properties* by changing parameters like electrostatic potential, confined electron number, shape of confining potential, magnetic field, tunnel couplings and temperature. That is why such systems are of *fundamental and conceptual interest* for theoretical and experimental work.

Coulomb blockade and *single-electron charging* are observed in electrical transport as a consequence of the repelling electrostatic electron-electron interaction in quantum dots. Quantum dot systems behave as *single-electron transistors*. Transport spectroscopy delivers a tool for *investigating the few- to many-electron states formed in the quantum dot* revealing correlation effects between the electrons which are more pronounced than in real atoms due to the stronger influence of electron-electron interaction. Also the coupling to the leads give rise to peculiar quantum mechanical effects: Quantum fluctuations due to *correlated electron tunneling* between quantum dot and leads cause under circumstances the formation of a *Kondo-like state*, i.e., quantum dot systems offer a new experimental approach to an almost 40 years old field. The formation of molecule-like states by tunnel coupling of two quantum dots has been studied in electrical transport. Electrostatically coupled

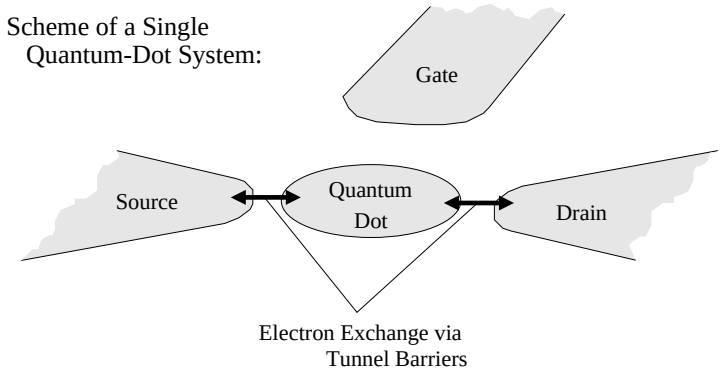

Fig. 0.1. Scheme of a single quantum-dot system consisting of the quantum dot which is weakly coupled by tunnel barriers to a source and a drain electrode. One or more gate electrodes in the surrounding of the quantum dot couple capacitively to the quantum dot, i.e., they can be used to tune the electrostatic potential of the quasi-isolated quantum dot. The quantum dot can be thought as a model system describing in one limit a metal island, in the other limit an impurity site in a dielectric, a molecule or a single atom.

quantum dots with separate leads show due to their interaction correlated tunneling in both quantum dot systems in parameter regimes where single-electron transport is prohibit. Exploring all these transport properties allows for *checking the validity of theoretical concepts*, and for *identifying strengths and* – of same importance – *weaknesses* of such quantum dot devices for *certain practical applications.*

The present work is not intended to give a complete overview over the field of electrical transport through quantum dot systems. As rich the physics of quantum dot systems is, as manifold are the interests in these systems. After more than one decade of active research by many theoretical and experimental groups, a complete and well-balanced review is not possible covering all aspects in this field and thereby satisfying all expectations. In addition, strong links exists to closely related research fields, – i.e., Coulomb blockade effects in metal and superconducting devices, and their possible application in metrology, or the optical properties of quantum dots and their possible application in optoelectronics. The preparation of respective quantum dot structures is a challenge and a broad field on its own. Actually only the collection of a number of review articles and books might fulfill this purpose, since each has its preference and quality: A good introduction into the field of Coulomb blockade and single-electron charging is given by the book 'Single Charge Tunneling' from 1991, edited by H. Grabert and M.H. Devoret [1]. An overview over the development in the field of single-electronics with a collection of references is found in the article 'Single-Electron Devices and Their Applications' by K.K. Likharev [2] from 1999. References

are found there on using the single-electron-charging effect in metrology, for instance as a single-electron pump for a frequency-controlled current standard or as a primary thermometer. Experiments on revealing the electronic properties of confined electron systems are reviewed by the articles of U. Meirav and E.B. Foxman [3] from 1995 and L.P. Kouvenhoven, Ch.M. Marcus, P.L. McEuen, S. Tarucha, R.M. Westerwelt, N.S. Wingreen [4] from 1997. The more recent experiments on atom-like quantum dot systems are summarized in the article of L.P. Kouwenhoven, D.G. Austing and S. Tarucha [5] from 2001. A collection of original papers in the field is found in the book 'Quantum Dots - A survey of the properties of artifical atoms' by T. Chakraborty [6] from 1999. An earlier work by N.F. Johnson [7] from 1996 reviews theoretical models for the description of confined electron systems in quantum dots. Correlation effect and their consequences on the properties in electrical transport are presented in the work of D. Pfannkuche [8] and D. Weinmann [9]. Dynamical aspects beyond master equation approaches, i.e., quantum fluctuations due to correlated tunneling including also phase coherence between tunneling events are covered by papers of G. Schön [10] and H. Schoeller [11]. An overview about electron transport in mesoscopic systems is found in the book 'Mesoscopic Electron Transport' [12] edited by L.L. Sohn, L.P. Kouwenhoven and G. Schön. An introduction to 'The Physics of Low-Dimensional Semiconductors' is represented by the book of J. Davies [13].

Goal of the present work is to give a coherent description of electrical transport through quantum dot systems starting from rather simple electrostatic considerations valid for metal systems. Step-by-step the description is improved by better electrostatic models, by thermodynamical and quantum mechanical considerations. By trying to be strict in certain deductions, this presentation should deliver links between experiments and theory which uses model Hamiltonians catching more or less the experimental situation. It should give a guideline for performing experiments and for interpreting experimental data, hinting at the same time to possible pitfalls in doing so. Moreover, by presenting the assumptions also the restrictions in the validity for certain models should become clear – identifying the room for improvements in the description and for further experiments.

This treatise is structured in the following way:

To start as simple as possible, the quantum dot is replaced in **Chapter 1** by an isolated mesoscopic metal conductor – denoted as *metal island*. This metal island is coupled by weak tunnel barriers to macroscopic drain and source electrodes of fixed electrostatic potential and is also coupled only capacitively to a gate electrode. The rearrangement of single electrons, treated as particles with electrical charge $-e$, between metal island, source and drain electrode is discussed. *Coulomb blockade* and *single-electron charging* are introduced in a simple electrostatic description based on the concept of capaci-

tances between the conductors. A powerful energy scheme is presented which allows to deduce some basic properties of a *single-electron transistor*. It will be developed further in Chapters 4 and 5.

To account for realistic arrangements of metal single-electron devices, in **Chapter 2** the usual treatment of *Capacitances* in textbooks is extended for an arbitrary arrangement of metal conductors and fixed ion charges embedded in an inhomogeneous anisotropic dielectric matrix. The behaviour of the capacitances with scaling the conductor arrangement is derived, and limits for the total capacitance of a metal electrode of arbitrary shape are given with proofs in the **Appendices B** and **C**.

Single-electron transistors are devices sensitive to the electric field. Hence, their electric behaviour depends strongly on the contact voltages of the chosen electrode and island material. To describe properly the Coulomb blockade and the single-electron charging effect, it is pointed out in **Chapter 3** that one has to distinguish carefully between the concepts of *Electrostatic Potential, Chemical Potential and Electrochemical Potential*. Measurements are presented which demonstrate that variations in the contact voltages between the electrodes of different material are detected by a single-electron transistor.

By scaling down the spatial lengths of a single-electron transistor, its working temperature increases. Metal islands of few nanometers are required to see Coulomb blockade and single-electron charging at room temperature. Besides the particle properties, the wave nature of an *electron as a quantum* becomes important. For electrons confined in such a small enclosure – denoted as a quantum dot –, only certain eigenvalues for the energy of an electron are possible. In **Chapter 4**, a *model Hamiltonian* for a quantum dot is derived from general electrostatic considerations mimicking basic electrostatic properties of realistic quantum dot structures. The electrons confined in the quantum dot have to be treated as an *interacting N-electron system* where the confining potential but also the electron-electron interaction depend on the electrostatic surrounding. The screened electron-electron interaction is related to the electrostatic Green's function of the arrangement. This description justifies to denote quantum dots as 'artifical atoms' with tunable parameters. On this base, the concept of capacitances for quantum dots is discussed, too.

For a still more general treatment, the results of Chapter 4 enforce to discuss the quantum dot in terms of an interacting few- or many-electron system. Therefore in **Chapter 5**, Coulomb blockade and single-electron charging effect are revisited in terms of this more general language. By thermodynamic considerations the transport regions in terms of single-electron transport are derived. By energy considerations the rearranging of single electrons between leads and quantum dot is described, i.e., as the transition between a N- and a $(N+1)$-electron system in the quantum dot. This allows to establish the method of *transport spectroscopy of ground and excited states* of the *inter-*

acting few- to many-electron system in the quantum dot. A master equation appproach is presented describing the increase, but also decrease of current with increasing drain-source voltage due to the long decay time of excited states of the confined electron system. The complications in interpreting single current-voltage characteristics is emphasized.

In **Chapter 6** experiments are discussed which demonstrate that the concept of single-electron transport for quantum dot systems breaks down under certain conditions even in the case of weak tunnel coupling to the leads. The basic physics behind this is already catched by a simple model introduced by P.W. Anderson in 1961 and applied to quantum dot systems in 1988. The tunnel coupling of the electronic states with the reservoir leads to a many-body state between leads and quantum dot described within the framework of *Kondo physics*.

Whereas the preceding treatment is more or less solely concerned with pure physical aspects of single-electron transistors, **Chapter 7** is devoted to possible practical applications, namely to the question: Are single-electron transistors suitable as ultimate transistor for very large scale integration (VLSI) of *digital circuits*? We know that single-electron transistors are dealing with the smallest charge amount, i.e., the current is carried by single electrons passing one-by-one the device and that this current flow can be controlled by a single electron charge. To work at room temperature, the device has to be extremely compact. Based on the requirements for digital circuits, the constraints on a electrostatic switch are derived showing severe limitations in using single-electron transistors for VLSI.

Finally open questions and new developments are summarized in **Chapter 8**.

This treatise is the outgrowth of the author's experimental engagement on the fundamental physical aspects associated with single-electron transistors and of the necessity for their profound theoretical understanding. Most of the experimental results presented in this treatise have been obtained in the last decade by mainly PhD works in the group of Prof. K. v. Klitzing at the Max-Planck-Institut für Festkörperforschung, Stuttgart (Germany), financially supported by the Bundesministerium für Forschung und Technologie (BMBF) and the Max-Planck Society. The presentation in Chapter 7 was mainly developed during my stay in 1995 in the group of Dr. A. Ourmazd and Dr. R.H. Yan in the Silicon Research Lab at Bell Laboratories at Holmdel in New Jersey, USA.

I would like to take the opportunity thanking Prof. K. v. Klitzing for offering me this topic ten years ago for my PhD work, for all the discussions questioning interpretations, for his believe in me setting up research projects and guiding PhD students in their work in his group. I am further indebted to my PhD supervisor Dr. R. Haug, to Dr. D. Pfannkuche, R. Blick, Dr. P. Maksym and Prof. S. Ulloa for all the 'punching' discussions leading

finally to the model description presented in Chapter 4 and 5. I gratefully acknowledge the opportunity given by Dr. A. Ourmazd and Dr. R.H. Yan to me looking into the challenges in making highly integrated circuits fulfilling customers' needs. I wish to thank Dr. H. Schoeller and Dr. J. König for the helpful discussions on correlated electron transport through quantum-dot systems. My coworkers, the PhD students J. Hüls, M. Keller, J. Schmid, Y.Y. Wei and U. Wilhelm and the Diploma student A. Welker contributed a lot to this work by their enthusiasm, although it was sometimes painful if it was not working the way it should. I am very grateful to them. I like to knowledge the support by heterostuctures from Dr. K. Ploog and Dr. K. Eberl grown by M. Hauser, and from Dr. W. Wegscheider grown by M. Bichler. I am very grateful for all the technical support in making the devices by T. Reindl, M. Riek, F. Schartner, and U. Waizmann.

Contents

1. Electrostatic Model of Coulomb Blockade, Single-Electron Charging, and Single-Electron Transistor

One fundamental property of an electron is its quantized electrical charge $-e$. In mesoscopic systems at sufficient low temperature, this discrete elementary charge gives rise to peculiar *electrostatic effects* which do not occur in macroscopic systems. Based on a simple electrostatic description, the concepts of *Coulomb Blockade* and *Single-Electron Charging* are introduced within this Chapter. An energy level scheme is presented and stressed which allows to deduce the basic properties of a metal *Single-Electron Transistor*. A deeper understanding of the phenomena will be developed thereafter in the following Chapters.

1.1 Single-Electron Charging Energy

In Fig. 1.1a, a small – electrically uncharged – metal island [1] is sketched between an arrangement of metal electrodes which are electrically connected. Transfering a single electron from one of the electrodes onto the metal island charges this island negative by $q = -e$ (see Fig. 1.1b). Image charges q_i ($i = \{1, 2\}$) are induced on the surrounding electrodes which sum up to the positive charge $+e$. Obviously the metal island forms a capacitor with the total island capacitance C_Σ in conjunction with the other electrodes. The energy $e^2/2C_\Sigma$ was required to charge the island by a single electron, and is now stored as electrostatic energy in this capacitor configuration. Instead of transfering a single electron to the electrically uncharged island, a single electron can be taken from the island. The island is now positively charged with $q = +e$ (see Fig. 1.1c). However, again the energy $e^2/2C_\Sigma$ was required for doing so. Therefore for both cases – either adding a single electron to the metal island or taking off a single electron from the metal island – the single-electron transfer between the island and the other electrodes costs the electrostatic *charging energy*

$$E_\mathrm{C} = \frac{e^2}{2\,C_\Sigma}\,. \tag{1.1}$$

[1] The term 'island' is of common use (for instance, [14, 1]) to describe a conductor completely surrounded by an insulator.

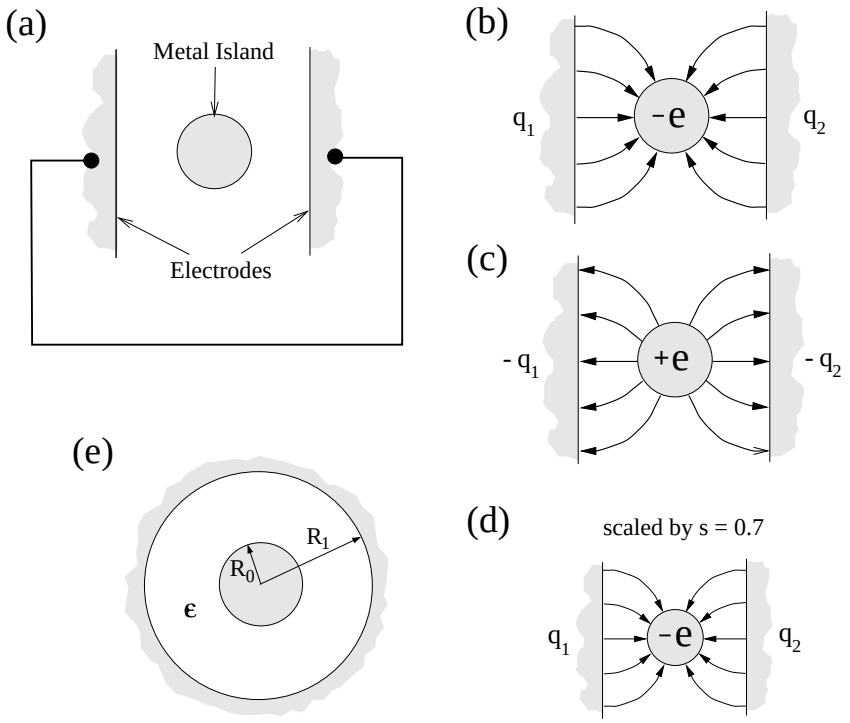

Fig. 1.1. (a) Arrangement of a metal island embedded in a dielectric medium and surrounded by other metal electrodes which are electrically connected. (b) By transfering a single electron from the electrodes to the island, the island is charged negative to $-e$. (c) By transfering a single electron from the island to the electrodes, the island is charged positive to $+e$. (d) Scaling the electrode arrangement by a factor $s < 1$ reduced the capacitances between the island and the other electrodes by the same factor. (e) A simple arrangement to estimate absolute values for the charging energy: A spheric metal island of radius R_0 located in the center of a metal hollow sphere of radius R_1.

This energy is required for the separation of a single electron from its positive counter charge spread over the other conductors.

Shrinking the absolute spatial lengths of a given island/electrodes arrangement by the scaling factor s (see Fig. 1.1d) decreases all the capacitances in the arrangement by the same scaling factor s. Since the charging energy E_{C} is inverse proportional to the total island capacitance C_{Σ}, the energy costs for transfering a single electron between island and the other electrodes increases with decreasing the spatial length scale [2]

$$E_{\mathrm{C}} \propto \frac{1}{s} \,. \tag{1.2}$$

[2] The exact scaling rules and the proof are given in Chapter 2.

For a total capacitance C_Σ of less than $10^{-15}\,\mathrm{F} = 1\,\mathrm{fF}$, the charging energy $E_\mathrm{C} = e^2/2C_\Sigma$ exceeds the thermal energy $k_\mathrm{B}T \approx 77\,\mu\mathrm{eV}$ at the temperature $T = 1\,\mathrm{K}$. Single-electron movements between island and electrodes activated by thermal fluctuations are suppressed below this temperature. This effect is named *Coulomb blockade*. Reducing the total capacitance further by scaling increases the charging energy E_C further. For a total island capacitance of $C_\Sigma < 3 \cdot 10^{-18}\,\mathrm{F} = 3\,\mathrm{aF}$, E_C exceeds the thermal energy $k_\mathrm{B}T \approx 26\,\mathrm{meV}$ at room temperature ($T = 300\,\mathrm{K}$).

Are such small capacitance values feasible? For an estimate, we consider a metal sphere of radius R_0 embedded in a dielectric medium of the relative dielectric constant ϵ in the center of a metal hollow sphere of the inner radius R_1 (see Fig. 1.1e). For this arrangement with $R_1 \gg R_0$, the sphere capacitance is given by $C_\Sigma = 4\pi\epsilon_0\epsilon R_0$. For $R_0 \approx 1\,\mu\mathrm{m}$ and $\epsilon = 10$, the spheric island has the capacitance of about $10^{-15}\,\mathrm{F}$. For $R_0 < 2.8$ nm, the single-electron charging energy is beyond the thermal energy at room temperature. We have to conclude that the single-electron charging energy is of importance to describe single-electron movements in systems of mesoscopic size.

Granular metal films consists of many metal grains electrically connected by tunnel barriers. At low temperature and small applied voltages, the electrical resistivity increases with lowering the temperature. C.J. Gorter [15] realized in 1951 that this is due to the quantization of charge. Electrons hopping from grain to grain are recharging the individual grains. It costs electrostatic energy so that at low temperature due to the lack of thermal activation the hopping is suppressed. Systematic resistivity measurements on thin metal films by C.A. Neugebauer and M.B. Webb [14] in 1962 confirmed the picture. The Coulomb blockade effect on few grains have been investigated by I. Giaever and H.R. Zeller [16], J. Lambe and R.C. Jaklevic [17], and R.E. Cavicchi and R.H. Silsbee [18]. A transport theory through granular media taking the electrostatic charging of grains by single electrons into account was developed by I.O. Kulik and R.I. Shekhter [19] in 1975.

1.2 Coulomb-Blockade Effect in Electrical Transport through a Source/Island/Drain-Arrangement

A simple arrangement to discuss the consequence of the single-electron charging energy E_C for electrical transport in small systems is shown in Fig. 1.2c. A small metal island is embedded between two lead electrodes arbitrarily denoted as source S and drain D. Thin insulator layers separate the metal island from the two electrodes. These layers should be thin enough that – due to quantum mechanics – tunneling of electrons through the insulator layers is possible, thick enough that it is plausible to describe single electrons in the system as being localized either on the metal island or the lead electrodes. *Since the metal island is almost isolated, the total charge on the metal electrode is considered as being quantized in the elementary charge e.*

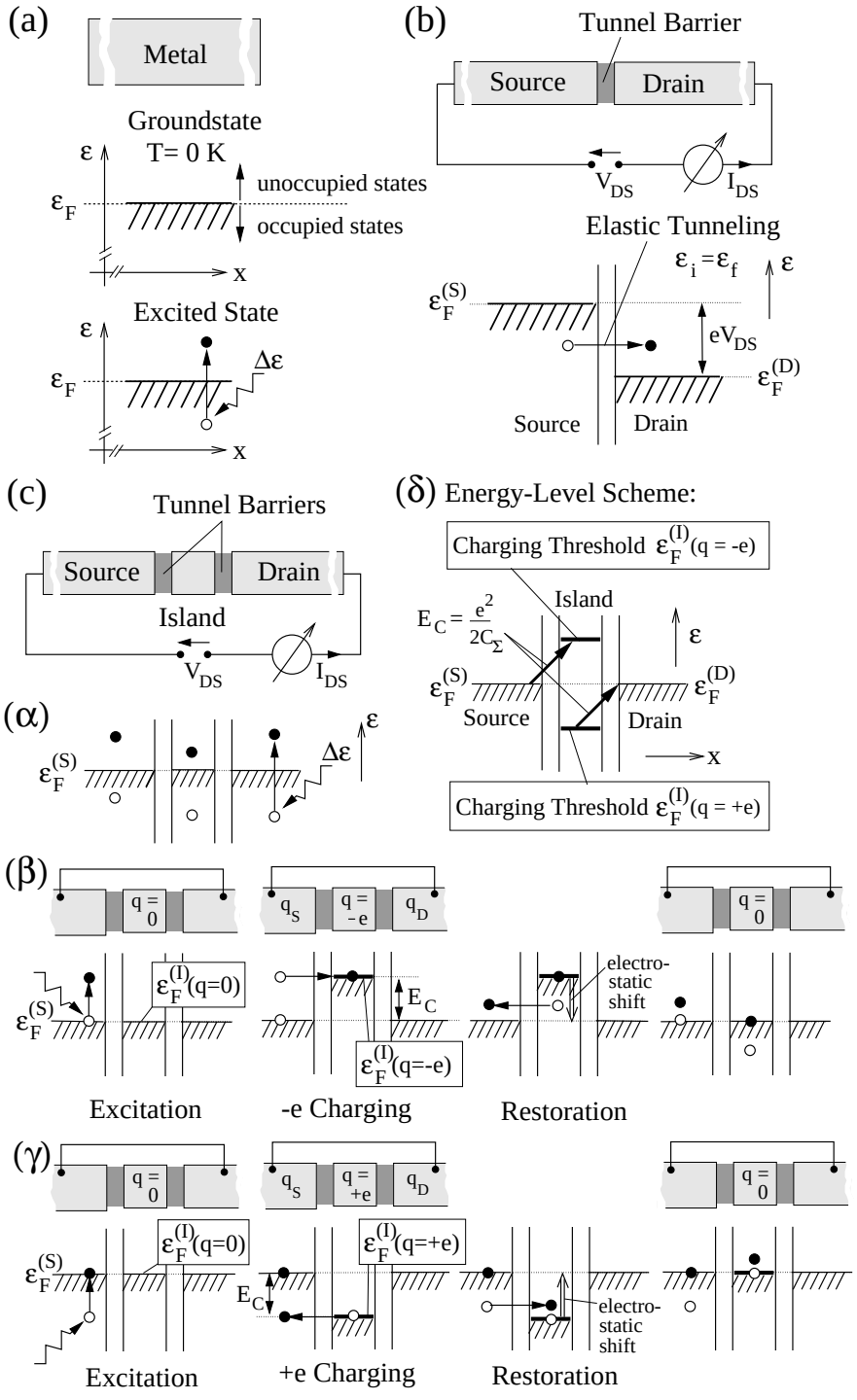
(a)
Metal
Groundstate
T= 0 K
unoccupied states
occupied states
Excited State
(b)
Tunnel Barrier
Source
Drain
Elastic Tunneling
(c)
Tunnel Barriers
Island
(δ) Energy-Level Scheme:
Charging Threshold
Charging Threshold
(α)
(β)
Excitation
-e Charging
Restoration
electro-
static
shift
(γ)
Excitation
+e Charging
Restoration

Fig. 1.2. (Left page) (a) Energy level scheme for a metal based on the Sommerfeld model: In the groundstate at $T = 0\,\mathrm{K}$, the Fermi level ε_F separates the occupied single-electron states from the unoccupied ones. By an external excitation, an 'electron-hole excitation' is created. (b) Two metals – denoted as source and drain – are connected by a voltage source V_DS and a tunnel barrier. With applied voltage $V_\mathrm{DS} > 0$, the Fermi levels of source and drain are shifted relatively. Electrons tunnel under energy conservation from source to unoccupied states on the drain site (elastic tunneling). It means in the energy scheme a horizontal move of an electron from source to drain keeping its energetical height. (c) Mesoscopic metal island connected by tunnel barriers to lead electrodes, denoted as source and drain. At $V_\mathrm{DS} = 0$, the whole arrangement is charge unpolarized. (α) Energy level scheme suggested by cutting one metal (see (a)) into three metal pieces forming source, island and drain. (β) Transfering a single electron to the island requires at least the electrostatic energy E_C which has to delivered from external. Restoration from this charge state back to $q = 0$ might happen by any electron from the island with energy $\varepsilon \geq \varepsilon_\mathrm{F}^{(\mathrm{S})}$ above the common Fermi level $\varepsilon_\mathrm{F}^{(\mathrm{S})}$ of the leads. (γ) Charging of the electrical uncharged island by a single electron leaving can occur only with an external excitation E_C. For decaying from this charge polarized state to the charge unpolarized state, any electron from the lead with energy $\varepsilon > \varepsilon_\mathrm{F}^{(\mathrm{S})} - E_\mathrm{C}$ can tunnel onto the island. (δ) On the island site, the threshold levels are indicated for charging the electrical uncharged island either to $q = -e$ or $q = +e$ by a single electron. The arrows indicate the respective energy barriers E_C between initial and final state prohibiting elastic tunneling at $V_\mathrm{DS} = 0$. Note that the energy-level scheme gives relatively to source and drain the energetic position of the Fermi level $\varepsilon_\mathrm{F}^{(\mathrm{I})}$ in the *charged* metal island. It is elevated for $q = -e$ by the electrostatic charging energy E_C and depressed for $q = +e$ by the same amount. In the following the hatching of the occupied electron states will mostly be omitted.

A drain-source voltage V_DS can be applied to this two-terminal arrangement. We will describe electron transport between source and drain electrode by single-electron hopping via the metal island assuming both tunneling processes being totally independent. This requires a recharging of the metal island by the elementary charge e. These processes can be illustrated by means of an energy-level scheme (see Fig. 1.2$c(\delta)$) where the single-electron energy ε is plotted against the spatial position x (For convenience, we omit this abscissa in the following schemes).

1.2.1 Charge Polarization Described with the Sommerfeld Model: Energy-Level Scheme

What is the idea behind this energy-level scheme? To be simple, conduction band electrons in the three metals – source, drain and island – are described by the *Sommerfeld model* (free electron model): The Fermi level ε_F separates at $T = 0\,\mathrm{K}$ the occupied single-electron states below ε_F from the empty states above (see Fig. 1.2a). All electron charges are compensated by the positive background charges of the ions. Electronic excitations from this groundstate of the metal are possible by energy transfer $\Delta\varepsilon$ from outside: An electron

with charge $-e$ is excited from an initial state i with energy $\varepsilon_\mathrm{i} \leq \varepsilon_\mathrm{F}$ to an unoccupied state f above the Fermi level with energy $\varepsilon_\mathrm{f} = \varepsilon_\mathrm{i} + \Delta\varepsilon \geq \varepsilon_\mathrm{F}$ leaving *a hole (unoccupied state) with charge* $+e$ in the 'Fermi sea' at energy ε_i. Such an *electron-hole excitation* is macroscopically electrically neutral and vanishes usually by relaxation processes (losing its surplus energy in one or more steps by phonon emission, for instance). In case of exciting the electron from the Fermi level ($\varepsilon_\mathrm{i} = \varepsilon_\mathrm{F}$), such an excitation is simpler denoted as *electron excitation*, in case of exciting an electron below the Fermi level to the Fermi level ($\varepsilon_\mathrm{f} = \varepsilon_\mathrm{F}$), such an excitation is called *hole excitation*.

The energy level scheme for a metal based on the Sommerfeld model reflects the energies of single-electron states being occupied or unoccupied. It also allows to describe electron transport between two macroscopic metals connected on one hand by a voltage source, on the other hand by a tunnel barrier (see Fig. 1.2b). Tunneling of electrons is usually described under energy conservation between initial and final state ('elastic tunneling'). Due to Pauli's exclusion principle, tunneling can occur only into an unoccupied state. Applying the voltage V_DS between the two metals causes an electric field over the tunnel barrier. As shown in Fig. 1.2b, the Fermi level $\varepsilon_\mathrm{F}^{(\mathrm{D})}$ of drain is shifted relatively to the Fermi level $\varepsilon_\mathrm{F}^{(\mathrm{S})}$ of source by eV_DS, – the electrostatic energy of an electron at source is for $V_\mathrm{DS} > 0$ higher than the one at drain. Electrons on the source site with $\varepsilon_\mathrm{i} \geq \varepsilon_\mathrm{F}^{(\mathrm{D})} = \varepsilon_\mathrm{F}^{(\mathrm{S})} - eV_\mathrm{DS}$ find unoccupied states at same energy $\varepsilon_\mathrm{f} = \varepsilon_\mathrm{i}$ at drain site, i.e., a tunneling current can flow. The surplus in kinetic energy $0 < \varepsilon_\mathrm{f} - \varepsilon_\mathrm{F}^{(\mathrm{D})} \leq eV_\mathrm{DS}$ of the injected electron is dissipated by relaxation on the drain site, – finally the injected electron ends up at the Fermi level $\varepsilon_\mathrm{F}^{(\mathrm{D})}$. Important to note, the energy level scheme of Fig. 1.2b takes into account *the response of the whole system* on the tunneling of one electron from source to drain: With the electron, the charge $-e$ is transfered via the tunnel barrier which has to be instantaneously compensated by a charge transfer between source and drain via the voltage source to keep the voltage V_DS between both metals fixed. The energy balance between initial and final state of the whole system – including the work performed by the voltage source – is mapped into the single-electron energies ε_i and ε_f which include kinetic and potential energy.

Let us come back to the device in Fig. 1.2c, where on one hand source and drain electrodes are connected by the voltage source V_DS, on the other hand by a mesoscopic metal island via tunnel barriers. In a first approach, we can think of cutting one piece of metal into three pieces forming source, drain and island. As each piece of metal is electrically uncharged, we obtain the single-electron level scheme depicted in Fig. 1.2$c(\alpha)$ with same Fermi level for all pieces. Electron-hole excitations within each of these metals are indicated. Summing up all single-electron energies of occupied states identified in this energy level scheme would give the total electron energy of the system. The scheme is suitable to describe excitation within each piece of metal, but has to be modified to describe electron exchange between those metals. Why? A

charge polarization within the whole device occurs if we transfer an electron from source or drain to the island: [3] Charge is separated into the island charge $q = -e$ and into the image charges q_S and q_D at the source and drain electrodes ($q_S + q_D = -q$). For creating such a charge polarization for $V_{DS} = 0$, it requires the charging energy E_C given by (1.1), which has to be delivered from external as an excitation to the system. In terms of rearranging an electron in the device, we can express this slightly different by mapping the total energy balance into the single-electron energy ε at the respective position x: Work has to be performed to transfer an electron from the leads onto the electrically uncharged island – the electron possesses due to its charge $-e$ an electrostatic energy on the island which is by E_C higher than on the leads' site. The energy scheme of Fig. 1.2$c(\beta)$ takes this into account: The Fermi levels of source and drain are kept fixed relative to each other by $V_{DS} = 0$. An electron from the Fermi level of the leads has first to be excited by E_C before being able to tunnel onto the island finding an unoccupied state at the Fermi level of the island metal.

> *Starting from a charge unpolarized state of the device (island charge $q = 0$), the threshold level $\varepsilon_F^{(S)} + E_C$ is the lowest energy level available for an electron in the leads for tunneling elastically onto the island and charging the neutral island to $q = -e$.*

The charged island metal itself is then in the groundstate with this additional electron since all single-electron states are filled to the Fermi level and empty above. Exciting an electron in the leads to energies higher than $\varepsilon_F^{(S)} + E_C$ allows the electron to tunnel into states on the island further above the Fermi level $\varepsilon_F^{(I)}(q = -e)$ of the island – the island metal ends up in an excited state. Therefore, the threshold level $\varepsilon_F^{(S)} + E_C$ represents the border between reaching occupied or unoccupied states on the metal island by a single electron.

The electrostatic charging energy E_C, now stored in the system, is not attributed to a specific electron. Therefore, as shown in Fig. 1.2c(β), *any* electron – but only one – with energy ε_i fulfilling $\varepsilon_F^{(S)} + E_C \geq \varepsilon_i \geq \varepsilon_F^{(S)}$ can leave the $q = -e$ charged island to source or drain under elastic tunneling leading to $q = 0$. During electron tunneling, the electrostatic field disappears and consequently the conduction band in the island shifts down by the electrostatic energy E_C. A hole is left back in the Fermi sea of the now electrically uncharged island metal, which then is filled by relaxation in the island metal. The rest of the surplus energy carried by the tunneled electron is dissipated in the leads. The whole system has finally restored the groundstate of the charge unpolarized state.

[3] To avoid charge transfer by intrinsic contact voltages, we assume that only one kind of metal is involved. Thus, at $V_{DS} = 0$ no macroscopic charge polarization exists in the device between the metals. The effect of using different metals will be discussed in Chapter 3.

The energy scheme of Fig. 1.2c(β) suggests that all electrons on the island are shifted with the Fermi level in their energies by E_C. This is wrongly interpreted if one intends to sum up all these single-electron energies to obtain the total electron energy of the system. Total energy of the charge polarized state $q = -e$ is that of the unpolarized system plus E_C. Correctly, this energy level scheme on the site of the island gives the possible energy levels for a single electron in the leads charging the initially electrically uncharged island to $q = -e$ by elastic tunneling. Starting with the $q = -e$ charged island, the same energy scheme also indicates the energy levels in the leads into which one electron from the island can elastically tunnel and thereby discharging the island to $q = 0$.

What about a single electron leaving the electrical uncharged island ($q = 0$)? Such a process causes also a charge polarization in the device: The island is charged to $q = +e$ inducing the corresponding image charges q_S and q_D at source and drain. Again the energy E_C is required allowing for such a charge polarization. A possible way is indicated in Fig. 1.2c(γ): A single electron in the leads has to be excited by at least E_C to create a hole at $\varepsilon_F^{(S)} - E_C$ which then can be occupied by elastic tunneling by an electron from the Fermi level of the island leaving back a hole at the Fermi level $\varepsilon_F^{(I)}(q = +e)$ of the island with charge $+e$. Electrons below this Fermi level of the island require a deeper hole in the leads and therefore a larger excitation for being allowed to leave the island by elastic tunneling.

> *Starting from a charge unpolarized state of the device (island charge $q = 0$), $\varepsilon_F^{(S)} - E_C$ is the closest energy level below the common Fermi level $\varepsilon_F^{(S)}$ of the leads which has to be emptied in the leads for allowing a single electron leaving the uncharged island by elastic tunneling and therefore charging it to $q = +e$.*

Alternatively, an electron from the Fermi level of the island can be excited by E_C allowing to find an unoccupied state in the leads. A decay back from $q = +e$ into the charge unpolarized state can occur by any electron – but only one – from the leads with energy ε_i in the window $\varepsilon_F^{(S)} \geq \varepsilon_i \geq \varepsilon_F^{(S)} - E_C$. Therefore, without excitation from external, $\varepsilon_F^{(S)} - E_C$ represents the maximum energy available for a single electron leaving the electrically uncharged island. Since the respective single-electron states in the leads are occupied, the island cannot be charged to $q = +e$ without excitation.

In conclusion, for charging or discharging a mesoscopic island by elastic tunneling of a single electron, the electrostatic energy change between initial and final state of the device has to be taken into account for the energy considerations. The electrostatics of the device determines the thresholds for these charging processes. The threshold energy levels – given by the electrostatics and representing the Fermi levels of the charged metal island – are drawn in the energy scheme of Fig. 1.2c(γ). For $V_{DS} = 0$ and uncharged island ($q = 0$), without external excitation the electrostatic energy barriers E_C

exist – indicated by two arrows – for a single electron entering and for a single electron leaving the island. Note that the spacing between upper and lower level shown for the island site is $2\,E_{\mathrm{C}}$. However, direct transitions between these two levels are not possible since such a transition requires recharging of the island by charge transfer from the leads in two separate processes as already explained.

1.2.2 Current-Voltage Characteristic

We are now prepared to approach the $I_{\mathrm{DS}}(V_{\mathrm{DS}})$ characteristic of the two-terminal device. We found that close to $V_{\mathrm{DS}} = 0$ the excitation energy E_{C} must be available to cause single electrons entering or leaving the island by tunneling. Since thermal energy is responsible for such excitations, we expect: Current flow from source to drain mediated by single-electron hopping is suppressed if the single-electron charging energy E_{C} of the metal island exceeds the thermal energy $k_{\mathrm{B}}T$. This is denoted as *Coulomb blockade* of electrical transport in such a two-terminal source/island/drain arrangement.

Applying the drain-source voltage $V_{\mathrm{DS}} > 0$, the electrostatic potential of the island is shifted by $C_{\mathrm{D}}/C_{\Sigma} \cdot V_{\mathrm{DS}}$ in reference to the source potential (see capacitance circuit given in Fig. 1.3b), and the electrostatic energy of a charge q on the island changes by $q{\cdot}C_{\mathrm{D}}/C_{\Sigma}{\cdot}V_{\mathrm{DS}}$. This reduces the electrostatic energy difference $\Delta E_{\mathrm{S}\to\mathrm{I}}$ which an electron sees when moving from the source electrode S to the island I,

$$\Delta E_{\mathrm{S}\to\mathrm{I}} = E_{\mathrm{C}} - e \cdot C_{\mathrm{D}}/C_{\Sigma} \cdot V_{\mathrm{DS}} \; . \tag{1.3}$$

This lowering is indicated in the energy level scheme of Fig. 1.3c(β). Also the energy barrier $\Delta E_{\mathrm{I}\to\mathrm{D}}$ valid for an electron moving from the electrically uncharged island to drain is lowered since applying V_{DS} reduces the electrostatic energy for single electrons at the drain more than at the island. From the energy scheme, given in Fig. 1.3c(β), we derive

$$\begin{aligned} \Delta E_{\mathrm{I}\to\mathrm{D}} &= \left(2\,E_{\mathrm{C}} - \Delta E_{\mathrm{S}\to\mathrm{I}}\right) - e\,V_{\mathrm{DS}} \\ &= E_{\mathrm{C}} - e \cdot C_{\mathrm{S}}/C_{\Sigma} \cdot V_{\mathrm{DS}} \; . \end{aligned} \tag{1.4}$$

The last line is obtained from (1.3) by taking into account $C_{\Sigma} = C_{\mathrm{S}} + C_{\mathrm{D}}$.

For $V_{\mathrm{DS}} < 0$, similar considerations can be done: The difference $\Delta E_{\mathrm{I}\to\mathrm{S}}$ for an electron moving from the electrically uncharged island to source reduces by

$$\Delta E_{\mathrm{I}\to\mathrm{S}} = E_{\mathrm{C}} - e \cdot C_{\mathrm{D}}/C_{\Sigma} \cdot |V_{\mathrm{DS}}| \; . \tag{1.5}$$

Also the charging energy $\Delta E_{\mathrm{D}\to\mathrm{I}}$ for an electron being transfered from drain to the electrically uncharged island decreases which leads to the relation

$$\Delta E_{\mathrm{D}\to\mathrm{I}} = \left(2\,E_{\mathrm{C}} - \Delta E_{\mathrm{I}\to\mathrm{S}}\right) - e\,|V_{\mathrm{DS}}| \tag{1.6}$$

$$= E_{\mathrm{C}} - e \cdot C_{\mathrm{S}}/C_{\Sigma} \cdot |V_{\mathrm{DS}}| \; , \tag{1.7}$$

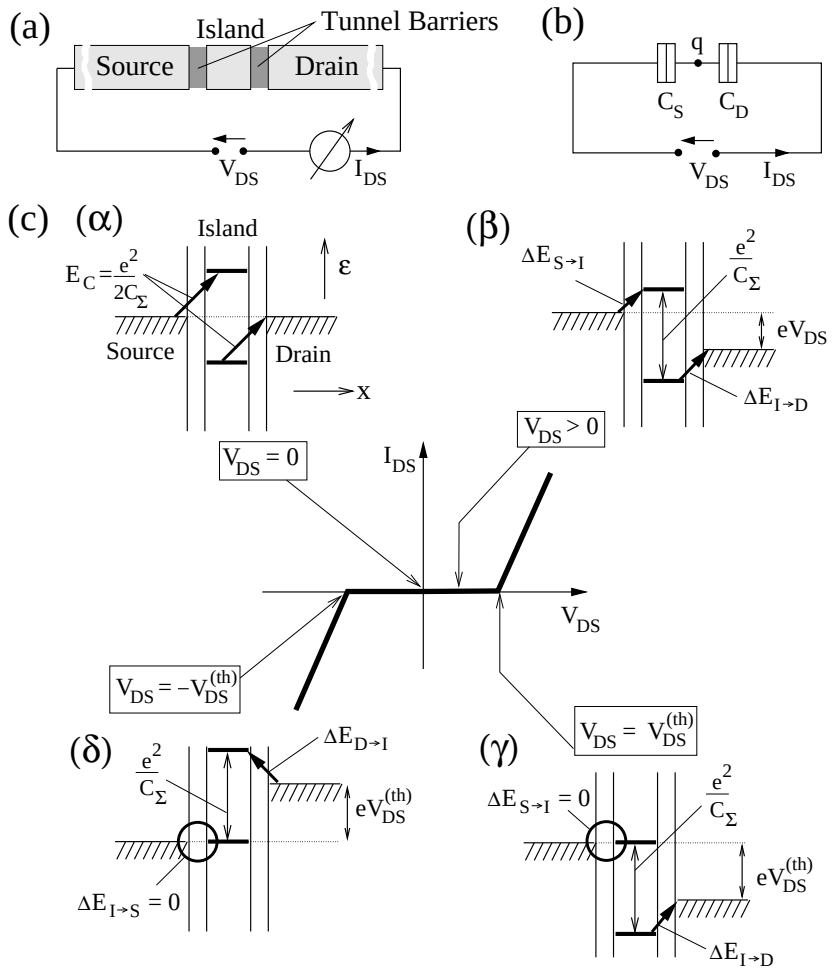

Fig. 1.3. (a) Scheme of the two-terminal device: A metal island is connected by tunnel barriers to two metal electrodes denoted as source S and drain D. (b) Capacitance circuit modelling the electrostatics of the arrangement shown in (a). The total capacitance is given by $C_\Sigma = C_\mathrm{S} + C_\mathrm{D}$. The box-like symbol denotes a capacitor where electron tunneling is possible [20, 1]. (c) Due to the presence of a single-electron charging energy, the shown nonlinear $I_\mathrm{DS}(V_\mathrm{DS})$ characteristic is expected. It can be deduced from the four depicted energy level schemes (ε is the single-electron energy and x the position) valid for different distinct V_DS values: At $V_\mathrm{DS} = 0$, the energy barrier $E_\mathrm{C} = e^2/2C_\Sigma$ exists for an electron entering and for an electron leaving the uncharged island. The current I_DS is suppressed around drain-source voltage $V_\mathrm{DS} = 0$ ('Coulomb blockade effect'). With growing $|V_\mathrm{DS}|$, the barriers $\Delta E_{\mathrm{S}\to\mathrm{I}}$, $\Delta E_{\mathrm{I}\to\mathrm{D}}$, $\Delta E_{\mathrm{I}\to\mathrm{S}}$ and $\Delta E_{\mathrm{D}\to\mathrm{I}}$ for single electrons to recharge the island are lowered. At certain positive and negative threshold values $\pm V_\mathrm{DS}^{(\mathrm{th})}$, one of the barriers has vanished first. For the energy schemes $C_\mathrm{S} < C_\mathrm{D}$ is assumed leading to $\Delta E_{\mathrm{S}\to\mathrm{I}} = 0$ at positive and $\Delta E_{\mathrm{I}\to\mathrm{S}} = 0$ at negative V_DS threshold.

By changing D with S in (1.7), the expression (1.5) is recovered, demonstrating the arbitrary choice of the electrodes as source or drain for the two-terminal arrangement.

The charging energy given by (1.3) vanishes ($\Delta E_{\mathrm{S}\to\mathrm{I}} = 0$) for $V_{\mathrm{DS}} = e/(2\,C_{\mathrm{D}})$, the energy barrier given by (1.4) disappears ($\Delta E_{\mathrm{I}\to\mathrm{D}} = 0$) for $V_{\mathrm{DS}} = e/(2\,C_{\mathrm{S}})$. Therefore, depending on the relative size of the capacitance values C_{S} and C_{D}, either the difference defined by (1.3) or by (1.4) vanishes first with increasing $V_{\mathrm{DS}} > 0$. The same is true for $|V_{\mathrm{DS}}|$ in case of negative drain-source bias ($V_{\mathrm{DS}} < 0$) as can be seen from (1.5) and (1.6). Therefore, – excluding thermal excitations – *single-electron transport between source and drain electrode* can only occur for

$$|V_{\mathrm{DS}}| \geq V_{\mathrm{DS}}^{(\mathrm{th})} \equiv \min\left(\frac{e}{2\,C_{\mathrm{S}}}\,;\,\frac{e}{2\,C_{\mathrm{D}}}\right) \tag{1.8}$$

in the two-terminal device of Fig. 1.3a. As roughly sketched in Fig. 1.3c, a symmetric $I_{\mathrm{DS}}(V_{\mathrm{DS}})$ characteristic is expected with threshold voltages $\pm V_{\mathrm{DS}}^{(\mathrm{th})}$ given by (1.8). Current carried by single electrons passing the island arises for $|V_{\mathrm{DS}}| > V_{\mathrm{DS}}^{(\mathrm{th})}$. [4]

Let us discuss in more detail the charging of the island at the threshold voltages $\pm V_{\mathrm{DS}}^{(\mathrm{th})}$ and the onset of the drain-source current I_{DS}: In case of $C_{\mathrm{S}} < C_{\mathrm{D}}$, at the corresponding positive threshold $V_{\mathrm{DS}} = V_{\mathrm{DS}}^{(\mathrm{th})} = e/(2\,C_{\mathrm{D}})$, the barrier $\Delta E_{\mathrm{S}\to\mathrm{I}}$ vanishes before $\Delta E_{\mathrm{I}\to\mathrm{D}}$ does (see Fig. 1.3c(γ)). An electron from the Fermi level of source can tunnel freely forth and back between source and island. Hence, the charge q on the metal island fluctuates between 0 and $-e$. Current I_{DS} in the circuit flows via the voltage source from drain to source ($I_{\mathrm{DS}} > 0$) due to such single electrons entering the uncharged island from source by tunneling, and in a sequential step by an electron leaving the island by tunneling to drain. The last step, discharging is possible in several ways, similar to what was described for Fig. 1.2c(β). The surplus energy $eV_{\mathrm{DS}}^{(\mathrm{th})} = e^2/(2\,C_{\mathrm{D}})$ is dissipated thereafter in relaxation processes. Such a transport process is denoted as *electron-like* because the process is enabled with an electron entering the island. At negative threshold $V_{\mathrm{DS}} = -V_{\mathrm{DS}}^{(\mathrm{th})} = -e/(2\,C_{\mathrm{D}})$, the charge q on the island fluctuates between 0 and $+e$ since $\Delta E_{\mathrm{I}\to\mathrm{D}}$ is zero (see Fig. 1.3c(δ)). A net current flows from drain to source due to single electrons which leave the island to source by tunneling creating a hole on the island which is then filled by an electron tunneling from the drain electrode. The last step can be done in several ways, similar to what was indicated in Fig. 1.2c(γ). Overall the surplus energy $eV_{\mathrm{DS}} = e^2/(2\,C_{\mathrm{D}})$ is dissipated. Such a transport process is denoted as *hole-like* because transport is enabled by creating a hole on the island. In the opposite case of $C_{\mathrm{S}} > C_{\mathrm{D}}$, the charge q fluctuates between 0 and $+e$ at posi-

[4] The increase will be described later in Chapter 5 in terms of a master equation approach.

tive threshold $V_{\mathrm{DS}} = V_{\mathrm{DS}}^{(\mathrm{th})} = e/(2\,C_{\mathrm{S}})$, enabled by a 'hole-like' process, and between 0 and $-e$ at negative threshold $V_{\mathrm{DS}} = -V_{\mathrm{DS}}^{(\mathrm{th})} = -e/(2\,C_{\mathrm{S}})$, enabled by an 'electron-like' process. The surplus energy $eV_{\mathrm{DS}} = e^2/(2\,C_{\mathrm{S}})$ is dissipated with each elementary charge transfer between source and drain. In case of $C_{\mathrm{S}} = C_{\mathrm{D}}$, both electrostatic energy barriers – on the source and the drain site – disappear at the same time at threshold (see Fig. 1.4). Due to these electrostatic energy considerations, the charge q of the island can fluctuate between $-e$, 0 and $+e$. 'Electron-like' and 'hole-like' transport processes are working in parallel. Thus, recharging of the island by two electrons at the same time from charge state $+e$ to $-e$ or vice versa becomes energetically possible.

As already pointed out with (1.8), the larger value of C_{D} and C_{S} determines the threshold values $\pm V_{\mathrm{DS}}^{(\mathrm{th})}$ for single-electron transport in the two-terminal arrangement of Fig. 1.3a. For a given C_Σ, different threshold values are obtained by varying the ratio $C_{\mathrm{D}}/C_{\mathrm{S}}$. For the symmetric case ($C_{\mathrm{S}} = C_{\mathrm{D}} = C_\Sigma/2$), single-electron transport between source and drain is

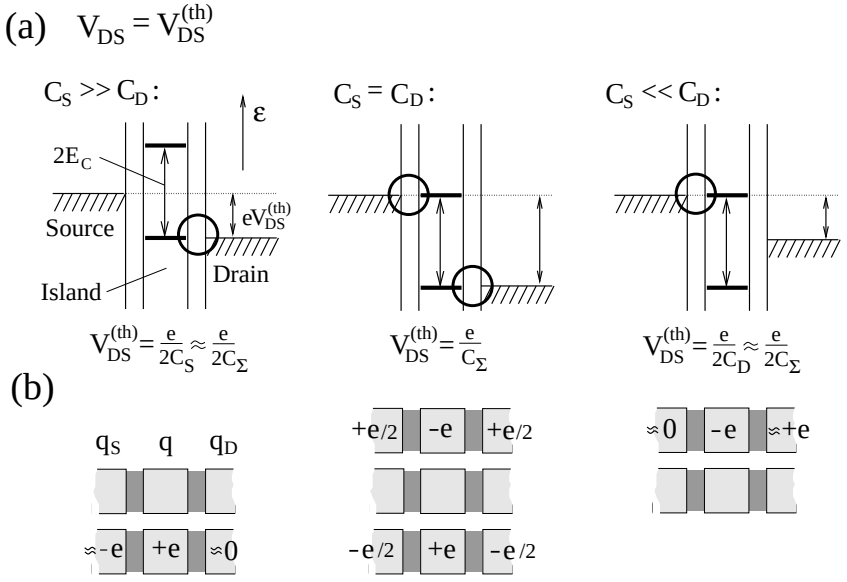

Fig. 1.4. (a) Energy scheme at positive threshold $V_{\mathrm{DS}} = V_{\mathrm{DS}}^{(\mathrm{th})}$ for a given total capacitance $C_\Sigma = C_{\mathrm{S}} + C_{\mathrm{D}}$ of the metal island but different ratios $C_{\mathrm{S}}/C_{\mathrm{D}}$. The cases $C_{\mathrm{S}} \gg C_{\mathrm{D}}$, $C_{\mathrm{S}} = C_{\mathrm{D}}$ and $C_{\mathrm{S}} \ll C_{\mathrm{D}}$ are chosen. (b) The respective charge configurations between which the system might fluctuate allowing single-electron transport between source and drain electrode. The additional image charges, present on the source and drain electrode for the island with charge $q = 0$ or $\pm e$, are indicated. For the source electrode, it is $q_{\mathrm{S}} = -C_{\mathrm{S}}/C_\Sigma \cdot q$, for the drain electrode, $q_{\mathrm{D}} = -C_{\mathrm{D}}/C_\Sigma \cdot q$. For $C_{\mathrm{S}} \gg C_{\mathrm{D}}$ hole-like, for $C_{\mathrm{S}} \ll C_{\mathrm{D}}$ electron-like transport processes are possible at positive threshold.

possible for

$$|V_{\mathrm{DS}}| \geq V_{\mathrm{DS}}^{(\mathrm{th})} = \frac{e}{C_\Sigma} ,$$

as derived from (1.8). This value multiplied by e reflects the energy gap $2E_{\mathrm{C}}$ for single-electron transport present for this two-terminal device. It is the maximum threshold which can be observed by varying the ratio $C_{\mathrm{S}}/C_{\mathrm{D}}$, since the relation $C_\Sigma \leq 2\max(C_{\mathrm{S}}; C_{\mathrm{D}})$ is generally valid for the two-terminal arrangement. For the extreme asymmetric cases of $C_{\mathrm{S}} \ll C_{\mathrm{D}}$ and $C_{\mathrm{S}} \gg C_{\mathrm{D}}$ presented in Fig. 1.4, the total capacitance is well described by $C_\Sigma \approx C_{\mathrm{D}}$ or $C_\Sigma \approx C_{\mathrm{S}}$, respectively. In that case, the threshold value $V_{\mathrm{DS}}^{(\mathrm{th})}$ is at minimum, and electron transport occurs already for

$$|V_{\mathrm{DS}}| \geq V_{\mathrm{DS}}^{(\mathrm{th})} \approx \frac{e}{2\,C_\Sigma} . \tag{1.9}$$

This is obvious from Fig. 1.4a: For $C_{\mathrm{S}} \gg C_{\mathrm{D}}$, due to the strong electrostatic coupling towards the source electrode, the energy gap for recharging the metal island remains fixed in position relative to the electronic levels of the source electrode. The minimum (1.9) in drain-source voltage is required to overcome the Coulomb blockade in transport by opening single-electron transfer with the drain electrode. For $C_{\mathrm{S}} \ll C_{\mathrm{D}}$, the energy gap is pinned in its relative position to the electronic levels of the drain electrode. Again, the minimum (1.9) in drain-source voltage is required to overcome the Coulomb blockade in transport, – now by opening single-electron transfer with the source electrode. Zero threshold is not reached by any ratio of C_{S} and C_{D}. However, by choosing the total capacitance C_Σ large ($C_\Sigma \to \infty$), zero threshold is approached ($V_{\mathrm{DS}}^{(\mathrm{th})} \to 0$, $E_{\mathrm{C}} \to 0$).

Since the Coulomb blockade effect was introduced as an electrostatic effect, i.e., the attractive and repulsive interaction between charges creates the behaviour, the effect is not only restricted to metal islands, but can also be seen with *superconducting islands*, *quantum dots*, *atom* or *molecule clusters*, *single atoms* or *molecules* (see reviews cited in the Preface). The arrangement of a two-terminal device is often found with a scanning tunneling microscope probing a conductive substrate where adsorbates are present: The adsorbates form the island, whereas the microscope tip and the conductive substrate act as the source and the drain electrodes. In such an arrangement, in 1989 the Coulomb blockade effect was demonstrated for $T = 4\,\mathrm{K}$ [21], in 1992 for room temperature [22].

1.3 Single-Electron Box: Charging or Discharging by $-e$ Quanta a Metal Island Connected to a Source Electrode by Using a Gate Electrode

In a different two-terminal device sketched in Fig. 1.5a, the island electrode is weakly coupled by a tunnel barrier to the source electrode and only capacitively coupled to the second electrode – the *gate electrode* G. If the voltage $V_{\rm GS}$ between the gate and the source electrode is near $V_{\rm GS} = 0$, the Coulomb blockade prevents charging of the island, i.e., $q = 0$. However due to the capacitance divider given in Fig. 1.5b which models the electrostatics of the two-terminal arrangement of Fig. 1.5a, the electrostatic potential of the island is shifted by changing the gate-source voltage $V_{\rm GS}$ – similar to what was discussed in the previous Section for changing $V_{\rm DS}$. The electrostatic energy of an electron on the island is changed by [5]

$$\Delta E_{\rm G} = -e \cdot C_{\rm G}/C_{\Sigma} \cdot V_{\rm GS} \; . \tag{1.10}$$

The total capacitance is given again by the sum of all partial capacitances towards the island: $C_{\Sigma} = C_{\rm S} + C_{\rm G}$. According to (1.10), for increasing $V_{\rm GS}$, the energy barrier for an electron transfered from source to the island is reduced,

$$\Delta E_{\rm S\to I} = E_{\rm C} + \Delta E_{\rm G} = E_{\rm C} - e \cdot C_{\rm G}/C_{\Sigma} \cdot V_{\rm GS} \; , \tag{1.11}$$

whereas the barrier for an electron leaving the island to source is increased,

$$\Delta E_{\rm I\to S} = E_{\rm C} - \Delta E_{\rm G} = E_{\rm C} + e \cdot C_{\rm G}/C_{\Sigma} \cdot V_{\rm GS} \; . \tag{1.12}$$

The level distance remains independent of $V_{\rm GS}$

$$\Delta E_{\rm I\to S} + \Delta E_{\rm S\to I} = 2\, E_{\rm C} = e^2/C_{\Sigma} \, . \tag{1.13}$$

For $V_{\rm GS} < 0$, the relations (1.10) to (1.13) are valid too.

If $\Delta E_{\rm S\to I} = 0$ which occurs at the gate-source voltage $V_{\rm GS}^{\rm (th)} = e/(2\, C_{\rm G})$ (see (1.11)), an electron does not feel any electrostatic energy difference between being localized on the island or the source electrode. Single electrons moves back and forth, – the charge q on the island fluctuates between 0 and $-e$. The same happens for $V_{\rm GS} = -V_{\rm GS}^{\rm (th)} = -e/(2\, C_{\rm G})$ since there $\Delta E_{\rm I\to S} = 0$ (see 1.12)): The island charge q fluctuates between 0 and $+e$. With increasing the gate-source voltage $V_{\rm GS}$ from $V_{\rm GS} = V_{\rm GS}^{\rm (th)}$ further, $\Delta E_{\rm S\to I}$ becomes negative (see (1.11)), – the electrostatic energy for an electron on the island shifts below its electrostatic energy at source. The additional electron is trapped on the island, – the charge on the island is changed to $-e$. What gate-source voltage change is required to further charge the island?

[5] The index G in $\Delta E_{\rm G}$ should remind on the gate as the cause of this contribution.

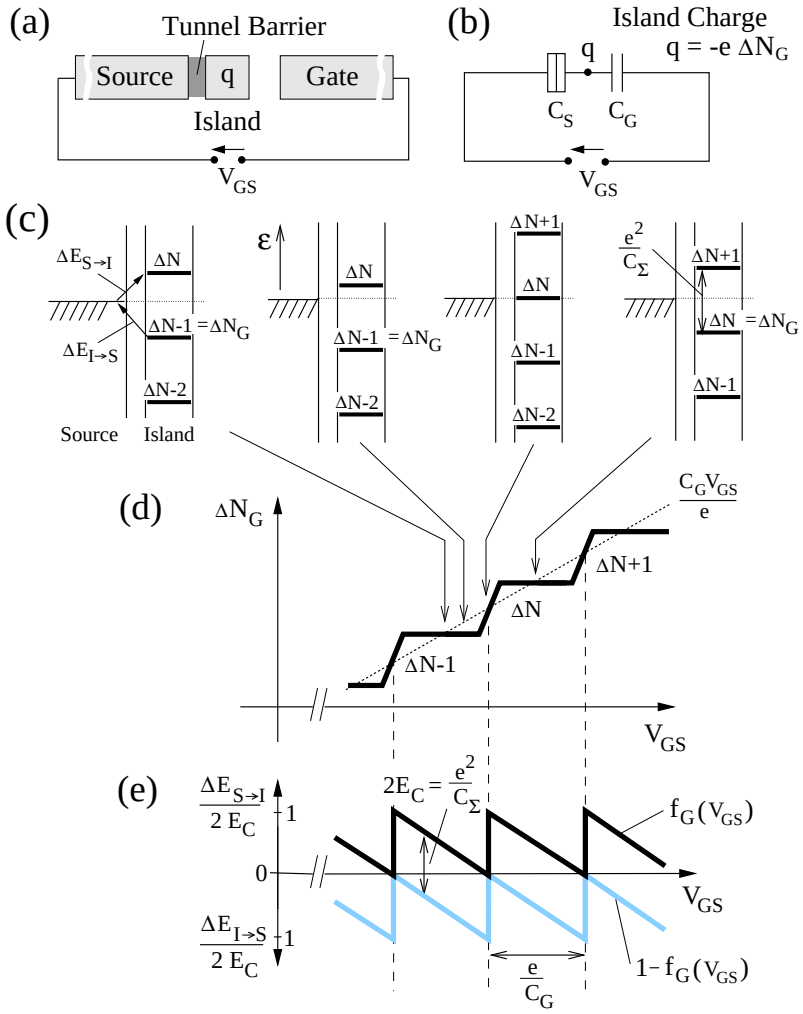

Fig. 1.5. (a) Single-electron box: A two-terminal device where a metal island is weakly connected by a tunnel barrier to the source electrode. The gate electrode couples only electrostatically by the capacitance C_G to the metal island. The island potential is shifted by the gate-source voltage V_{GS} as well as by a trapped island charge q which is changed by $\pm e$ at certain V_{GS} values where tunneling is energetically allowed. (b) Capacitance circuit of the arrangement shown in (a): C_S and C_G denote the capacitances of the island to source and gate, respectively. (c) Energy scheme representing the charging energies for certain distinct gate-source voltage values V_{GS}. The number of trapped electrons – starting counting from the electrical uncharged island – is ΔN_G. For negative V_{GS}, the value of ΔN_G becomes negative and $|\Delta N_G|$ represents the number of trapped holes. (d) The number of electrons on the metal island is increased one-by-one with increasing gate-source voltage V_{GS}. (e) The charging energy $\Delta E_{S\to I}$ for a single electron entering the metal island and the discharging energy $\Delta E_{I\to S}$ for a single electron leaving the metal island is periodically modulated with increasing gate-source voltage V_{GS}.

Charging the island at $V_{\rm GS} = 0$ with ΔN electrons at the same time requires the charging energy $E_{\rm elst}(\Delta N) = (-\Delta N e)^2/2C_\Sigma$. Applying the gate-source voltage $V_{\rm GS}$ shifts the potential energy of all ΔN electrons lowering the charging energy:

$$E_{\rm elst}(\Delta N, V_{\rm GS}) = \frac{(-\Delta N e)^2}{2\,C_\Sigma} - \Delta N e \cdot \frac{C_{\rm G}}{C_\Sigma} \cdot V_{\rm GS}\ . \tag{1.14}$$

For $\Delta N = 1$ and $V_{\rm GS} = 0$, we obtain $E_{\rm elst} = e^2/2C_\Sigma = E_{\rm C}$, consistent with our previous result (1.1).

Having already charged the island with $\Delta N - 1$ electrons, the next electron 'ΔN' moving from source to the charged island feels at fixed applied $V_{\rm GS}$ the electrostatic energy difference

$$\begin{aligned}\Delta E_{\rm S\to I}(\Delta N, V_{\rm GS}) &= E_{\rm elst}(\Delta N, V_{\rm GS}) - E_{\rm elst}(\Delta N - 1, V_{\rm GS}) \\ &= \left(\Delta N - \tfrac{1}{2}\right) \cdot \frac{e^2}{C_\Sigma} - e \cdot \frac{C_{\rm G}}{C_\Sigma} \cdot V_{\rm GS} \\ &= 2\,E_{\rm C} \cdot \left(\Delta N - \tfrac{1}{2} - \frac{C_{\rm G}\,V_{\rm GS}}{e}\right)\ .\end{aligned} \tag{1.15}$$

Depending on $V_{\rm GS}$ and ΔN, this energy difference is positive, zero or negative, i.e., the electrostatic energy for the electron ΔN lies above, at or below its potential energy at source. The energy values given by (1.15) for different ΔN at a certain $V_{\rm GS}$ are plotted as levels for the island in the energy scheme of Fig. 1.5c. A ladder of energy levels is obtained where the level distance is $2E_{\rm C} = e^2/C_\Sigma$ and the ladder shifts linearly with $V_{\rm GS}$. This energy scheme extends the one introduced in Fig. 1.2c(δ) which is valid for $\Delta N = 1$ and $\Delta N = 0$ with $V_{\rm GS} = 0$. The new energy level scheme will be used extensively in the following. It was already used by I. Giaever and H.R. Zeller [16] in 1968. Let us look closer to the meaning of the introduced ladder of energy levels:

- An electron at source at the energy level denoted by ΔN can fluctuate between source and island by elastic tunneling if the island has already trapped $\Delta N - 1$ electrons. Thus, the ΔN level represents the *charging and discharging threshold level* for the ΔNth electron.
- For $\Delta N = 1$ we have the threshold level for the first electron leading to fluctuations between $q = 0$ and $q = -e$ on the island.
- For $\Delta N = 0$ we have $\Delta N - 1 = -1$. This means that the electron moving back and forth between source and island causes charge fluctuation between $q = 0$ and $+e$. The initial state for charging the island by the electron is the presents of a hole charge ('missing electron').
- In general for $\Delta N < 0$, an electron fluctuating between source and drain leads to charge fluctuations between $\Delta N \cdot (-e) = |\Delta N| \cdot e > 0$ and $(\Delta N - 1) \cdot (-e) = (|\Delta N| + 1) \cdot e > 0$. The level ΔN indicates $|\Delta N| + 1$ hole charges trapped on the island as the initial state for adding an electron.

In conclusion, the energy level denoted by ΔN indicates the threshold level for charging and discharging the island by the ΔNth electron relatively to the Fermi levels of source if $\Delta N - 1$ electrons are already trapped on the island. Relation (1.15) is also valid for $\Delta N \leq 0$ indicating the presence of $|\Delta N| + 1$ trapped hole charges for the initial charging state.

With changing the gate-source voltage from zero to a certain value V_{GS}, electrons will move onto the island as long as the expression (1.15) is negative: The first electron will move onto the island if $\Delta E_{\mathrm{S}\to\mathrm{I}}(1, V_{\mathrm{GS}}) < 0$, the second too if $\Delta E_{\mathrm{S}\to\mathrm{I}}(2, V_{\mathrm{GS}}) < 0$. This will continue to the ΔNth electron as long as $\Delta E_{\mathrm{S}\to\mathrm{I}}(\Delta N, V_{\mathrm{GS}}) < 0$. This electron transfer will stop when the next electron $\Delta N + 1$ feels (1.15) being positive, i.e., $\Delta E_{\mathrm{S}\to\mathrm{I}}(\Delta N + 1, V_{\mathrm{GS}}) > 0$. Finally under stationary conditions, $\Delta N = \Delta N_{\mathrm{G}}$ electrons are trapped on the island, if the relations

$$\Delta E_{\mathrm{S}\to\mathrm{I}}(\Delta N_{\mathrm{G}} + 1, V_{\mathrm{GS}}) > 0 \qquad \text{and} \qquad \Delta E_{\mathrm{S}\to\mathrm{I}}(\Delta N_{\mathrm{G}}, V_{\mathrm{GS}}) < 0 \tag{1.16}$$

are fulfilled at the same time. This happened for [6]

$$\Delta N_{\mathrm{G}} = \Delta N_{\mathrm{G}}(V_{\mathrm{GS}}) = \mathrm{int}\left(\frac{C_{\mathrm{G}} V_{\mathrm{GS}}}{e} + \tfrac{1}{2}\right) = \mathrm{int}\left(\frac{E_{\mathrm{C}} - \Delta E_{\mathrm{G}}}{2\,E_{\mathrm{C}}}\right) . \tag{1.17}$$

The electrostatic energy $E_{\mathrm{elst}}(\Delta N, V_{\mathrm{GS}})$ given by (1.14) is minimized for given V_{GS} by the transfer of $\Delta N = \Delta N_{\mathrm{G}}(V_{\mathrm{GS}})$ electrons to the island. Therefore, due to the applied gate-source voltage V_{GS} the trapped charge on the metal island becomes

$$q(V_{\mathrm{GS}}) = -\Delta N_{\mathrm{G}} \cdot e \, . \tag{1.18}$$

This quantized charge is close to the charge amount q' which would be present on the capacitor with capacitance C_{G} if the tunnel barrier in Fig. 1.5b is replaced by a short: $q' = -C_{\mathrm{G}}\, V_{\mathrm{GS}}$. This case corresponds to the straight dotted line $q'/(-e) = C_{\mathrm{G}}\, V_{\mathrm{GS}}/e$ in the diagram of Fig. 1.5d where the number of electrons of the island is sketched versus V_{GS}. However, since the island is quasi-isolated, the quantized trapped charge q can adjust only in multiple of the elementary charge e. This allows the system to come close to $q = q'$, but only at the distinct gate-source voltage values $\Delta N_{\mathrm{G}}\, e/C_{\mathrm{G}}$ the island charge is exactly $q = q'$.

The additional number of electrons on the metal island fluctuates between ΔN_{G} and $\Delta N_{\mathrm{G}} - 1$ electrons at the gate-source voltage values

$$V_{\mathrm{GS}}^{(\mathrm{th})}(\Delta N_{\mathrm{G}}) = \left(\Delta N_{\mathrm{G}} - \tfrac{1}{2}\right) \cdot \frac{e}{C_{\mathrm{G}}} \, . \tag{1.19}$$

$V_{\mathrm{GS}}^{(\mathrm{th})}(\Delta N_{\mathrm{G}})$ gives the threshold value for trapping the next electron ΔN_{G} on the island. Therefore, with slowly increasing V_{GS}, the island is charged

[6] The function $\mathrm{int}(x)$ delivers the closest integer number which is smaller than x, i.e., $x \geq \mathrm{int}(x)$, valid for $x \geq 0$ and $x < 0$.

one-by-one with additional single electrons, i.e., the control over V_{GS} allows *single-electron charging* of the island (see Fig. 1.5d) with a periocity of

$$\Delta V_{\mathrm{GS}} = \frac{e}{C_{\mathrm{G}}} \,. \tag{1.20}$$

Single-electron charging of a box was clearly demonstrated experimentally by P. Lafarge and coworkers [23] in 1991. The device of Fig. 1.5a with such properties is therefore often denoted as *single-electron box*. We should emphasize here, that there might be millions or billions of conduction band electrons on the metal island and we have control over single electrons being added to this huge amount or taken off. [7]

Taking off a single electron from the metal island with ΔN_{G} trapped electrons requires – to surpass the electrostatic barrier – the discharging energy $\Delta E_{\mathrm{I}\to\mathrm{S}}(\Delta N_{\mathrm{G}}, V_{\mathrm{GS}})$. From (1.14), (1.15) and (1.17) we obtain

$$\begin{aligned}
\Delta E_{\mathrm{I}\to\mathrm{S}}(\Delta N_{\mathrm{G}}, V_{\mathrm{GS}}) &= E_{\mathrm{elst}}(\Delta N_{\mathrm{G}} - 1, V_{\mathrm{GS}}) - E_{\mathrm{elst}}(\Delta N_{\mathrm{G}}, V_{\mathrm{GS}}) \\
&= -\Delta E_{\mathrm{S}\to\mathrm{I}}(\Delta N_{\mathrm{G}}, V_{\mathrm{GS}}) = 2\,E_{\mathrm{C}} \cdot \left(\frac{C_{\mathrm{G}}\, V_{\mathrm{GS}}}{e} + \tfrac{1}{2} - \Delta N_{\mathrm{G}} \right) \\
&= 2\,E_{\mathrm{C}} \cdot \left\{ \left(\frac{C_{\mathrm{G}}\, V_{\mathrm{GS}}}{e} + \tfrac{1}{2} \right) - \mathrm{int} \left(\frac{C_{\mathrm{G}}\, V_{\mathrm{GS}}}{e} + \tfrac{1}{2} \right) \right\}
\end{aligned} \tag{1.21}$$

Introducing the 'remaining fraction' f_{G}, [8]

$$f_{\mathrm{G}} = f_{\mathrm{G}}(V_{\mathrm{GS}}) \equiv \mathrm{mod} \left(\frac{C_{\mathrm{G}} V_{\mathrm{GS}}}{e} + \tfrac{1}{2} \right) \,, \tag{1.22}$$

with the property $0 \le f_{\mathrm{G}} < 1$, the barrier for discharging is written as

$$\Delta E_{\mathrm{I}\to\mathrm{S}}(\Delta N_{\mathrm{G}}, V_{\mathrm{GS}}) = 2\,E_{\mathrm{C}} \cdot f_{\mathrm{G}} \,. \tag{1.23}$$

On the other hand, assuming ΔN_{G} electrons trapped on the metal island, an electron moving from the source to the island requires according to the obtained result (1.21) the charging energy

$$\begin{aligned}
\Delta E_{\mathrm{S}\to\mathrm{I}}(\Delta N_{\mathrm{G}} + 1, V_{\mathrm{GS}}) &= -\Delta E_{\mathrm{I}\to\mathrm{S}}(\Delta N_{\mathrm{G}} + 1, V_{\mathrm{GS}}) \\
&= 2\,E_{\mathrm{C}} \cdot \left(1 - f_{\mathrm{G}}\right) \,.
\end{aligned} \tag{1.24}$$

We note from (1.23) and (1.24) that the sum of both barriers $\Delta E_{\mathrm{S}\to\mathrm{I}}(\Delta N_{\mathrm{G}} + 1, V_{\mathrm{GS}}) + \Delta E_{\mathrm{I}\to\mathrm{S}}(\Delta N_{\mathrm{G}}, V_{\mathrm{GS}})$ is always $2E_{\mathrm{C}}$, independent of the values of ΔN_{G} and of V_{GS}.

[7] For a superconducting metal island, the odd or even parity of the electron number on the island – although billions – can be distinguished by charging or discharging the island due to the binding of electrons to Cooper pairs [24].

[8] The function $\mathrm{mod}(x)$ delivers $x - \mathrm{int}(x)$, valid for positive and negative x.

The development of the energy barriers with increasing gate-source voltage V_{GS} – allowing an adjustment of the island charge to ΔN_G – are sketched in Fig. 1.5e: They follow a left and a right going sawtooth contour line, respectively. For $f_G = 0$, the island charge can fluctuate. For $f_G = \frac{1}{2}$, mid gap condition is achieved, i.e., the barriers for single electrons recharging the island are *at maximum at the same time*: $\Delta E_{S\to I}(\Delta N_G + 1, V_{GS}) = E_C = e^2/2C_\Sigma$ and $\Delta E_{I\to S}(\Delta N_G, V_{GS}) = E_C = e^2/2C_\Sigma$. Therefore, at least the condition $e^2/2C_\Sigma > k_B T$ has to be fulfilled to observe at temperature T the charging of the metal island with electrons one-by-one.

1.4 Single-Electron Transistor (SET)

In this Section, the single-electron transistor (SET) is introduced. The basic properties of a metal SET are explained using the electrostatic description developed in the preceding Sections. The description of the physical properties of such a SET will be improved step-by-step in the following Chapters by extended electrostatics, by including thermodynamical aspects, and finally by quantum mechanical aspects.

1.4.1 Basic Concept and Special Realization of a SET. Coulomb-Blockade Oscillations

In the two-terminal device sketched in Fig. 1.3a, the metal island was weakly coupled to the source and to the drain electrode by tunnel barriers. Due to the single-electron charging energy $e^2/2C_\Sigma$, Coulomb blockade of electron transport is present around drain-source voltage $V_{DS} = 0$. The Coulomb blockade *close to zero drain-source voltage* can be overcome in the three-terminal arrangement, sketched in Fig. 1.6a, by applying a voltage V_{GS} between gate and source electrode. As it was just described for the single-electron box sketched in Fig. 1.5a, for $V_{DS} = 0$ the metal island is charged one-by-one with single electrons by increasing the applied gate-source voltage V_{GS} (see Fig. 1.6c). At certain V_{GS} values, the charge on the island fluctuates by e. With applying a small voltage V_{DS} at such V_{GS} values, a current flows between drain and source, carried by electrons passing the island one-by-one on their way from source to drain: *Single-electron transport* occurs. With slightly changing the gate-source voltage, single-electron hopping is suppressed. Therefore, for small V_{DS}, the single-electron current is periodically turned on and off with increasing the gate-source voltage V_{GS}. This current modulation, sketched in Fig. 1.6c, is denoted as *Coulomb-blockade oscillations* (CBO). Showing such a characteristic, the three-terminal arrangement sketched in Fig. 1.6a is named *single-electron transistor* (SET). The device concept was suggested in 1986 by D.V. Averin and K.K. Likharev [20] and clearly described in 1987 by K.K. Likharev [25]. A first realization was presented in the same year 1987 by T.A. Fulton and G.D. Dolan [26].

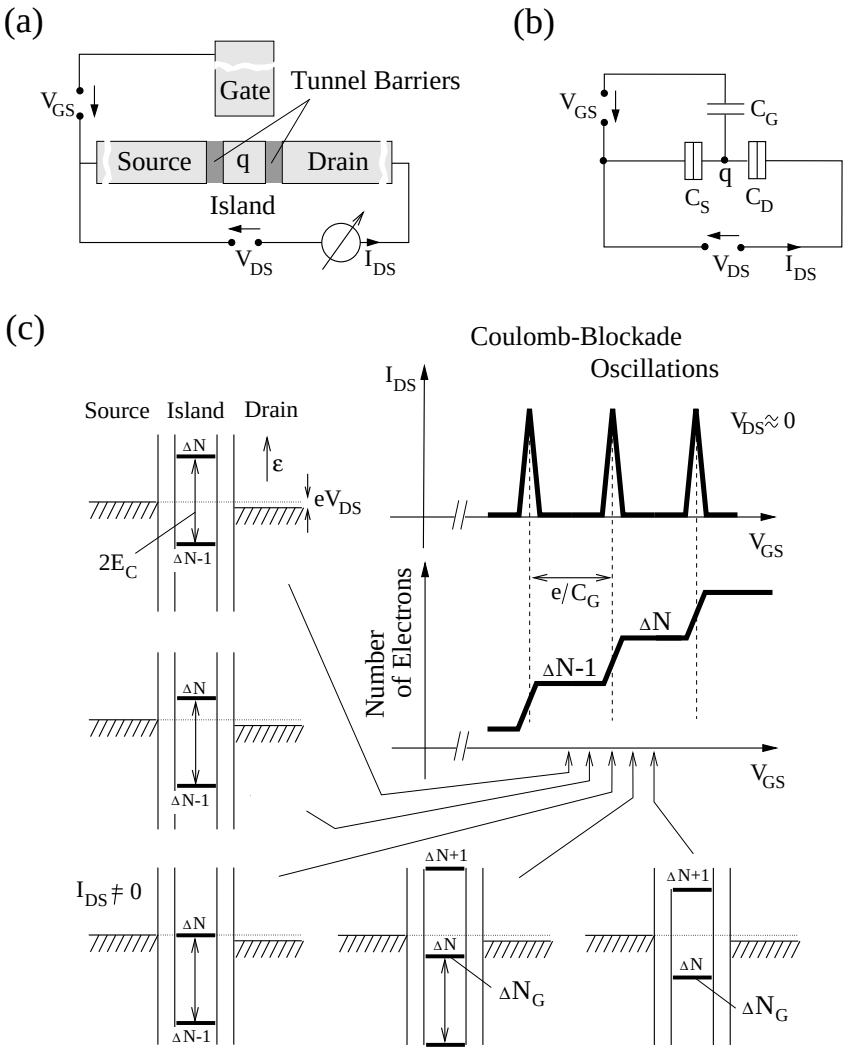

Fig. 1.6. (a) Single-electron transistor: A three-terminal device where a metal island is connected by tunnel barriers to the source and to the drain electrode. The gate electrode couples only electrostatically by the capacitance C_{G} to the metal island. (b) Capacitance circuit of the arrangement shown in (a): C_{S}, C_{D} and C_{G} denote the capacitances of the island to source, drain and gate, respectively. The total island capacitance C_{Σ} is $C_{\Sigma} = C_{\mathrm{S}} + C_{\mathrm{D}} + C_{\mathrm{G}}$, and the island charge $q = -e \cdot \Delta N_{\mathrm{G}}$. (c) Energy scheme representing the electrostatic energy differences for various gate-source voltage values V_{GS} which are seen by single electrons being either added to this island or taken off. The number of electrons on the metal island is increased one-by-one with increasing gate-source voltage V_{GS}, and the current I_{DS} of the metal single-electron transistor for small V_{DS} is periodically modulated with increasing gate-source voltage V_{GS} ('Coulomb blockade oscillations').

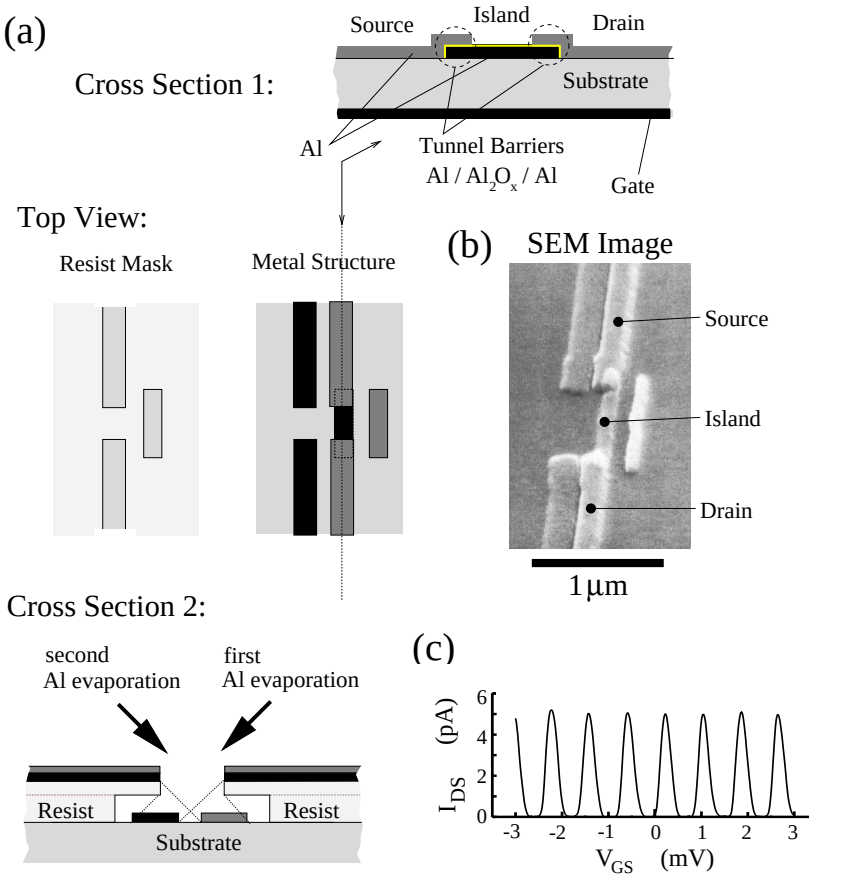

Fig. 1.7. (a) Metal single-electron transistor used in our experiments. It is made by an Al-evaporation technique: Cross Section 1 shows the whole device including the gate electrode. The fabrication of the source/island/drain system is done by a two-angle evaporation technique: With electron-beam lithography, a two-layer organic resist is patterned leading to openings to the substrate with large undercut (see 'Cross Section 2'). In vacuum, aluminum layers are evaporated twice under different angles through the openings onto the substrate. By an in-situ oxidation *between* first and second evaporation, a thin aluminum oxide of few nanometer is formed on the first aluminum layer. The resist is lifted off and a metal structure remains on the substrate. Due to the two different evaporation angles, the metal patterns of the first and second evaporation process are slightly shifted against each other leading to an overlap in certain regions. In the overlap regions, the thin aluminum oxide acts as tunnel barriers between both aluminum layers, whereas the uncovered aluminum is unavoidable oxidized further in air. (b) Scanning electron microscope (SEM) image of the single-electron transistor (from Y.Y. Wei [27]). The lengths along the vertical axis are reduced by a factor of $1/\sqrt{2}$. (c) Coulomb-blockade oscillations measured at $T = 0.1$ K by using the gate electrode buried in the substrate ($V_{\rm DS} = 80$ μV) (from Y.Y. Wei [27]). To suppress the superconductivity of aluminum, a magnetic field of 1 Tesla was applied.

In Fig. 1.7, a special kind of a metal single-electron transistor is shown which was realized in our laboratory. This SET consists of a small aluminum island (0.1 μm in width and 1 μm in length) which is coupled by aluminum oxide tunnel barriers to the aluminum source and drain electrodes. The scanning electron microscope (SEM) image is shown in Fig. 1.7b. The SET was fabricated by using the shadow-mask and two-angle evaporation technique described by Dolan and Dunsmuir [28] and other groups [29, 30]. Due to the small size of the electron island and the small area of the tunnel junctions (0.1 μm by 0.1 μm), the total capacitance of the island is small leading to a single-electron charging energy $E_{\mathrm{C}} \approx 0.1$ meV. Applying a voltage V_{GS} to the gate electrode burried at 85 nm below the surface in a GaAs/AlGaAs substrate, Coulomb blockade oscillations are observed at temperature $T \approx 0.1$ K (see Fig. 1.7c).

1.4.2 Transport Regions in the V_{GS} vs. V_{DS} Plane

The three-terminal arrangement of a single-electron transistor allows to overcome the Coulomb blockade in electrical transport by either tuning the voltage V_{GS} applied to a near-by gate electrode or by increasing the drain-source voltage V_{DS}. To obtain the Coulomb blockade regions in the parameter space of the gate-source voltage V_{GS} and the drain-source voltage V_{DS}, the lowering of the energy barriers by V_{GS} and V_{DS} have to be considered in combination. This will be done in the following. The result is plotted in Fig. 1.8 which shows the determined Coulomb blockade regions in the V_{GS} vs. V_{DS} plane and some energy schemes for certain combinations of ΔN, V_{GS} and V_{DS}.

As derived in the last Section for a single-electron box, also the characteristic of a metal single-electron transistor has to be periodic in the applied gate-source voltage V_{GS}. Therefore it is sufficient to focus the discussion near $V_{\mathrm{DS}} = 0$ on the region where, for instance, ΔN additional electrons are trapped on the metal island due to the applied gate-source voltage V_{GS}. In case of positive V_{DS}, the electrostatic charging energy $\Delta E_{\mathrm{S}\to\mathrm{I}}(\Delta N + 1, V_{\mathrm{GS}})$, found in (1.24) for an electron transfer from source to the island under the influence of V_{GS} alone, is reduced by taking V_{DS} into account,

$$\begin{aligned}\Delta E_{\mathrm{S}\to\mathrm{I}}(\Delta N + 1, V_{\mathrm{GS}}, V_{\mathrm{DS}}) &= \Delta E_{\mathrm{S}\to\mathrm{I}}(\Delta N + 1, V_{\mathrm{GS}}) - e \cdot C_{\mathrm{D}}/C_{\Sigma} \cdot V_{\mathrm{DS}} \\ &= \left(\Delta N + \tfrac{1}{2}\right) \cdot e^2/C_{\Sigma} - e \cdot C_{\mathrm{G}}/C_{\Sigma} \cdot V_{\mathrm{GS}} - e \cdot C_{\mathrm{D}}/C_{\Sigma} \cdot V_{\mathrm{DS}} \qquad (1.25)\end{aligned}$$

where $C_{\Sigma} = C_{\mathrm{S}} + C_{\mathrm{D}} + C_{\mathrm{G}}$. Whenever the electrostatic charging energy (1.25) becomes zero, single-electron tunneling forth and back between source and island is opened. Vanishing of (1.25) occurs along the straight line $C_{\mathrm{D}}\, V_{\mathrm{DS}} + C_{\mathrm{G}}\, V_{\mathrm{GS}} = (\Delta N + \frac{1}{2})\, e$ which intersects the V_{GS} axis ($V_{\mathrm{DS}} = 0$) at $V_{\mathrm{GS}} = (\Delta N + \frac{1}{2})\, e/C_{\mathrm{G}}$ and has the negative slope

$$\left.\frac{\mathrm{d}V_{\mathrm{GS}}}{\mathrm{d}V_{\mathrm{DS}}}\right|_{\Delta E_{\mathrm{S}\to\mathrm{I}}=0} = -\frac{C_{\mathrm{D}}}{C_{\mathrm{G}}}\,. \qquad (1.26)$$

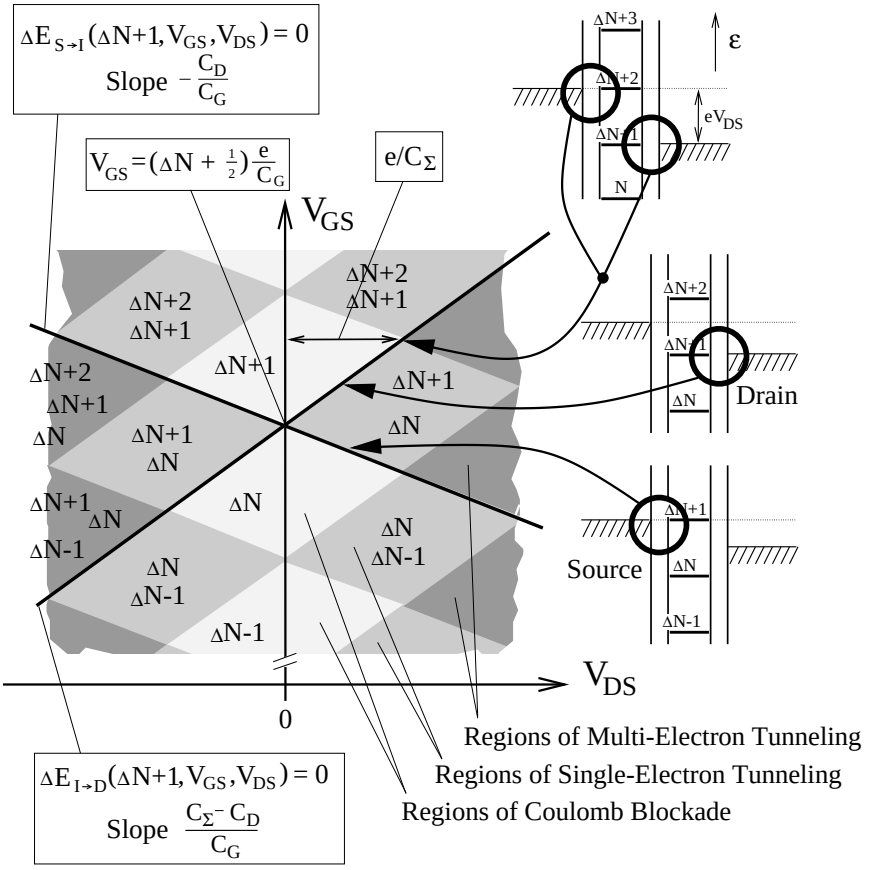

Fig. 1.8. Evaluated transport regions of a single-electron transistor as a function of the gate-source voltage V_{GS} and the drain-source voltage V_{DS}. Light grey shaded are the regions of Coulomb blockade where the electron number is fixed in the plot to $\Delta N - 1$, ΔN, or $\Delta N + 1$, respectively. Fluctuations by one electron charge $-e$ is possible in the adjacent regions. With further increasing V_{DS}, more and more charge configurations become energetically possible. Starting in a Coulomb blockade region, with increasing $V_{\mathrm{DS}} > 0$ and crossing the straight borderlines with negative slope, one electron more can enter from source to the island, and with positive slope one electron more can leave from the island to drain. Examples are illustrated in the energy schemes.

This borderline is depicted in the V_{GS} vs. V_{DS} plane of Fig. 1.8. Starting at $V_{\mathrm{DS}} > 0$ in the $(V_{\mathrm{GS}}, V_{\mathrm{DS}})$ region where ΔN electrons are trapped, and increasing V_{DS} or V_{GS} to cross this borderline makes the electrostatic charging barrier (1.25) negative. Consequently, the threshold for charging the island by the $(\Delta N + 1)$th electron is crossed, i.e., the charge state with $\Delta N + 1$ electrons on the island becomes available. Crossing in opposite direction over the borderline means that this charge state is excluded.

Let us now consider the electrostatic discharging energy which is required to transfer an electron from the island with $\Delta N + 1$ trapped electrons to the drain at prescribed voltages V_{GS} and V_{DS}. The contribution due to V_{GS} can be taken from (1.23), replacing the index S now by D and ΔN_{G} by $\Delta N + 1$. To move an electron from the island to drain under the influence of V_{DS}, the required electrostatic energy is $-e \cdot (1 - C_{\mathrm{D}}/C_{\Sigma}) \cdot V_{\mathrm{DS}}$ since the difference of the electrostatic potential between drain and the island can be taken from the capacitance circuit of Fig. 1.6b as $(1 - C_{\mathrm{D}}/C_{\Sigma}) \cdot V_{\mathrm{DS}}$. Thus we obtain for the electrostatic discharging energy from the island to drain

$$\begin{aligned} \Delta E_{\mathrm{I}\to\mathrm{D}}(\Delta N + 1, V_{\mathrm{GS}}, V_{\mathrm{DS}}) &= \Delta E_{\mathrm{I}\to\mathrm{D}}(\Delta N + 1, V_{\mathrm{GS}}) - e \cdot \left(1 - C_{\mathrm{D}}/C_{\Sigma}\right) \cdot V_{\mathrm{DS}} \\ &= \left(\Delta N + \tfrac{1}{2}\right) \cdot e^2/C_{\Sigma} + e \cdot C_{\mathrm{G}}/C_{\Sigma} \cdot V_{\mathrm{GS}} - e \cdot \left(1 - C_{\mathrm{D}}/C_{\Sigma}\right) \cdot V_{\mathrm{DS}} \,. \end{aligned} \tag{1.27}$$

This energy barrier vanishes along the straight line $C_{\mathrm{G}}\, V_{\mathrm{GS}} - (C_{\Sigma} - C_{\mathrm{D}})\, V_{\mathrm{DS}} = (\Delta N + \frac{1}{2}) \cdot e$. This borderline intersects the V_{GS} axis ($V_{\mathrm{DS}} = 0$) at gate voltage value $V_{\mathrm{GS}} = (\Delta N + \frac{1}{2}) \cdot e/C_{\mathrm{G}}$ and has a positive slope

$$\left.\frac{\mathrm{d}V_{\mathrm{GS}}}{\mathrm{d}V_{\mathrm{DS}}}\right|_{\Delta E_{\mathrm{I}\to\mathrm{D}}=0} = \frac{C_{\Sigma} - C_{\mathrm{D}}}{C_{\mathrm{G}}} \,. \tag{1.28}$$

This borderline is also shown in Fig. 1.8. Starting in the Coulomb blockade region with $\Delta N + 1$ trapped electrons, and crossing this borderline at $V_{\mathrm{DS}} > 0$ by decreasing V_{GS} or increasing V_{DS} makes (1.27) negative and allows therefore for discharging the island by transfering the $(\Delta N + 1)$th electron from the island to drain. The charge state with ΔN electrons becomes available.

As similar discussion can be done for negative V_{DS}. The same slopes are obtained. Changing the gate-source voltage, the recharging of the island occurs according to (1.20) with the periodicity $\Delta V_{\mathrm{GS}} = e/C_{\mathrm{G}}$ which means that the two borderlines have to be extended to two sets of parallel lines with distance ΔV_{GS}. These two sets of parallel lines cut the V_{GS} vs. V_{DS} plane into equal parallelograms (sometimes denoted as 'diamond-like' [5]) in which certain charge configuration are energetically allowed. In regions along the V_{GS} axis around $V_{\mathrm{DS}} = 0$ the number $\Delta N_{\mathrm{G}} = \Delta N_{\mathrm{G}}(V_{\mathrm{GS}})$ of trapped electrons is fixed to $\Delta N - 1$, ΔN, or $\Delta N + 1$ in the plot of Fig. 1.8. These are the *regions of Coulomb blockade*. In the adjacent regions, fluctuation by one electron is possible. These are the *regions of single-electron tunneling*. In the next regions with rising $|V_{\mathrm{DS}}|$ the charge on the island can fluctuate between three charge states: Energetically two electrons can enter and leave the island at the same time. For even higher drain-source voltages, more and more charge configurations become energetically possible between which the arrangement might fluctuate. Thus, we have to distinguish between regions of Coulomb blockade and the remaining *different transport regions*, defined by the energetically possible charge configurations on the island.

Let us look closer to these thresholds between regions of Coulomb blockade and electron transport in the V_{GS} vs. V_{DS} plane: For fixed V_{GS}, the threshold

values in $V_{\rm DS}$ do not lie symmetrically to $V_{\rm DS} = 0$, except for a special SET where the absolute values of the two slopes are equal which is fulfilled by $C_{\rm D} = C_{\Sigma}/2$. Such a situation is obtained, for instance, for $C_{\rm D} = C_{\rm S} \gg C_{\rm G}$. Beyond a certain $V_{\rm DS}$ value, the Coulomb blockade effect is overcome for *any* $V_{\rm GS}$ value. This maximum $V_{\rm DS}^{\rm (th)}$ in the threshold of $V_{\rm DS}$ is reached when both energy barriers – for an electron entering and for an electron leaving the island – disappear at the same time, i.e., $\Delta E_{\rm S\to I}(\Delta N + 1, V_{\rm GS}, V_{\rm DS}) = 0$ and $\Delta E_{\rm I\to D}(\Delta N, V_{\rm GS}, V_{\rm DS}) = 0$. As derived from the energy scheme Fig. 1.8 for such situation, the drain-source voltage reflects under that condition the energy-level distance $2\,E_{\rm C}$ of single-electron transport through the single-electron transistor

$$V_{\rm DS}^{\rm (th)} = \frac{e}{C_{\Sigma}} = \frac{2\,E_{\rm C}}{e}\,, \tag{1.29}$$

independent of the ratio between $C_{\rm S}$ and $C_{\rm D}$.

1.4.3 Current-Voltage Characteristics $I_{\rm DS}(V_{\rm DS}, V_{\rm GS})$

In Fig. 1.9, the measured $I_{\rm DS}(V_{\rm DS}, V_{\rm GS})$ characteristics of a metal single-electron transistor – similar to Fig. 1.7 – are shown. Clearly the Coulomb blockade regions are visible. Beyond the respective threshold in $V_{\rm DS}$, the current $I_{\rm DS}$ increases. Adjacent to the Coulomb blockade regions, the current is carried by single electrons passing one-by-one the island: In average, each time interval $\tau = e/I_{\rm DS} \leq e/40$ pA$= 4$ ns an electron passes the island between source and drain. With increasing $V_{\rm DS}$, the current modulation versus the applied gate voltage $V_{\rm GS}$ becomes smoother. Single-electron transistors have been proposed [25] as the ultimate transistors for very-large scale integration (VLSI) (see later Chapter 7), but also as highly-sensitive electrometers – described in the next Section.

It is worth to emphasize that the identification of the two different transport regions of a single-electron transistor – Coulomb blockade and single-electron transport regime – as a function of the drain-source voltage $V_{\rm DS}$ and a gate-source voltage $V_{\rm GS}$ was achieved in Section 1.4.2 only by electrostatic energy considerations. Also predicted was a multi-electron transport at higher $|V_{\rm DS}|$ values where regions of more than two charge states could exist. However, certain SETs show also single-electron transport at these high $|V_{\rm DS}|$ values. This phenomenon can be explained [32] by taking also *dynamical aspects* into account: If high electron tunnel rates exist between source and island, low ones between drain and island, or vice versa, a change of the charge state on the island via single-electron tunneling through the blocking barrier is almost immediately restored by a single-electron tunneling event through the more transparent barrier. For SETs with such *strongly asymmetric tunnel barriers* [9] we can state:

[9] Note that the kind of SET presented in Fig. 1.7 has symmetric tunnel barriers due to the design and fabrication process.

- The current I_{DS} is completely limited by tunneling through the blocking barrier.
- The tunneling between the island and the lead with the more transparent barrier determines the prefered charge state of the island.

To discuss this behaviour in case of strongly asymmetric tunnel barriers in more detail, a blocking or 'thick' drain tunnel barrier is assumed in Fig. 1.10 and a 'thick' source tunnel barrier in Fig. 1.11. The charge state regions in the V_{GS} vs. V_{DS} plane are plotted. Energy schemes are given for a fixed V_{GS} but various distinct V_{DS} values. The energy 'window' at the blocking barrier for an electron entering or leaving the island, respectively, is marked by grey shading:

- For charging the island via the blocking barrier, the width of the 'window' is determined by the difference from the Fermi level of the weakly coupled lead to the threshold energy level for charging the island which just lies above the Fermi level of the stronger coupled lead.
- For discharging the island via the blocking barrier, the energy 'window' is given by the difference between the threshold energy level for charging the

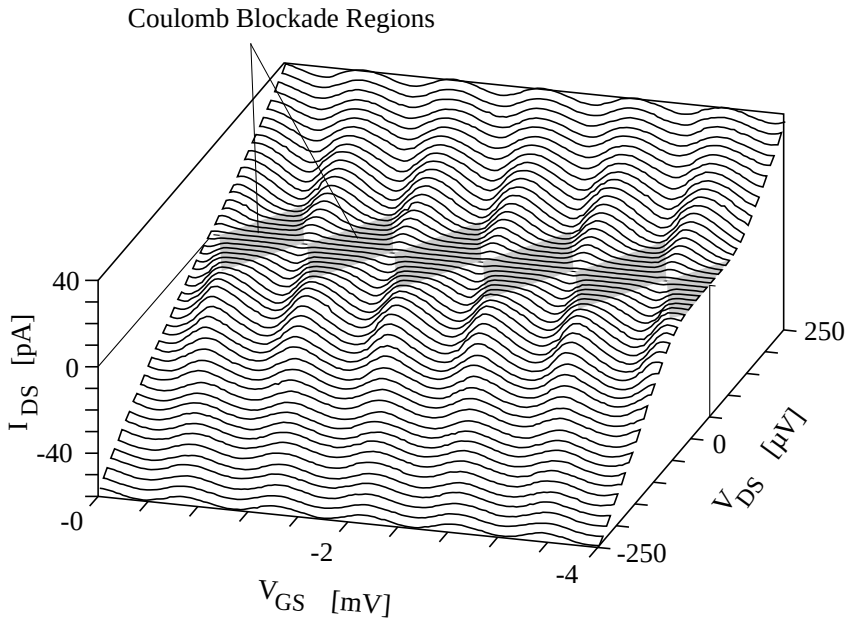

Fig. 1.9. Current I_{DS} through a single-electron transistor measured at $T = 0.1$ K for different discrete drain-source voltages V_{DS} as a function of gate-source voltage V_{GS} applied to an electrode burried in the substrate (from J. Hüls [31] measured in our lab). The SET structure corresponds to the one presented in Fig. 1.7. The Coulomb-blockade regions ($I_{\mathrm{DS}} = 0$) are roughly marked by shading.

island which just lies below the Fermi level of the stronger coupled lead and the Fermi level of the weakly coupled lead.

Note, the width of the respective 'window' is less than $e|V_{\rm DS}|$, and only equal when a threshold level for charging the island aligns with the Fermi level of the stronger coupled lead. With increasing $|V_{\rm DS}|$, the 'window' width increases, i.e., more electronic states become available above (below) the Fermi level of the island for charging (discharging) the island over the blocking barrier. The overall rate for a single-electron charging (discharging) event via the blocking barrier is enhanced, the current $|I_{\rm DS}|$ increased. Reaching a new charge state by electron exchange via the more transparent tunnel barrier, which is then the initial charge state for a tunneling event through the blocking barrier, the 'window' width changes by $2\,E_{\rm C} = e^2/C_\Sigma$ if $|V_{\rm DS}| \geq e/C_\Sigma$, and by $e|V_{\rm DS}|$ if still $|V_{\rm DS}| < e/C_\Sigma$: A step-like increase in the $I_{\rm DS}(V_{\rm DS})$ characteristic is observed at $V_{\rm DS}$ values crossing a thick marked borderline in Fig. 1.10 and Fig. 1.11. Assuming that the density of states versus ε in the metal is constant around the Fermi level and the tunneling rate does not depend on the single-electron energy ε in the range of several $\pm e|V_{\rm DS}|$ around the Fermi level $\varepsilon_{\rm F}$, the rate of a charging (discharging) event is proportional to the width of the energy window. The proportionality constant $R_{\rm T}$ is denoted as *tunnel resistance.* [10] Under these assumptions, a step of $\Delta I_{\rm DS} = e/(R_{\rm T}^{\rm max}\,C_\Sigma)$ is observed with $R_{\rm T}^{\rm max} = \max\{R_{\rm T}^{\rm (S)}, R_{\rm T}^{\rm (D)}\}$ whenever a thick marked borderline drawn in Fig. 1.10 and Fig. 1.11 is crossed. Between the steps, the current $|I_{\rm DS}|$ increases slightly linearly as the window is linearly increased with $|V_{\rm DS}|$. The whole characteristic is limited by $I_{\rm DS} = V_{\rm DS}/R_{\rm T}^{\rm max}$ since the energy window is usually less than $e|V_{\rm DS}|$. It is equal at $V_{\rm DS}$ values where a new charge state occurs by charging from the lead with the more transparent barrier. Substracting at these $V_{\rm DS}$ values, the respective change $\Delta I_{\rm DS}$ from $I_{\rm DS} = V_{\rm DS}/R_{\rm T}^{\rm max}$ and connecting the obtained $I_{\rm DS}$ values, the whole $I_{\rm DS}(V_{\rm DS})$ characteristic is obtained. Such a step-like $I_{\rm DS}(V_{\rm DS})$ characteristic, – observed for strongly asymmetric tunnel barriers is denoted as the *Coulomb staircase* characteristic. As seen from the charge state diagram, the step distance along the $V_{\rm DS}$ axis is given for a blocking source barrier ($R_{\rm T}^{\rm (S)} \gg R_{\rm T}^{\rm (D)}$) by

$$\Delta V_{\rm DS} = \frac{2\,E_{\rm C}}{e\cdot(1-C_{\rm D}/C_\Sigma)} = \frac{e}{C_\Sigma - C_{\rm D}}\;, \tag{1.30}$$

and for a blocking drain barrier ($R_{\rm T}^{\rm (D)} \gg R_{\rm T}^{\rm (S)}$) by

$$\Delta V_{\rm DS} = \frac{2\,E_{\rm C}}{e\cdot(C_{\rm D}/C_\Sigma)} = \frac{e}{C_{\rm D}}\;. \tag{1.31}$$

Relation (1.31) describes charging of the island from source with increasing $V_{\rm DS}$ by using the drain electrode like a gate electrode. Relation (1.30)

[10] The tunnel resistance is different to an ohmic resistance since in the latter case dissipation occurs within the resistor. In case of a tunnel barrier, dissipation occurs after the tunneling event in the electrodes.

SET with Strongly Asymmetric Tunnel Barriers:

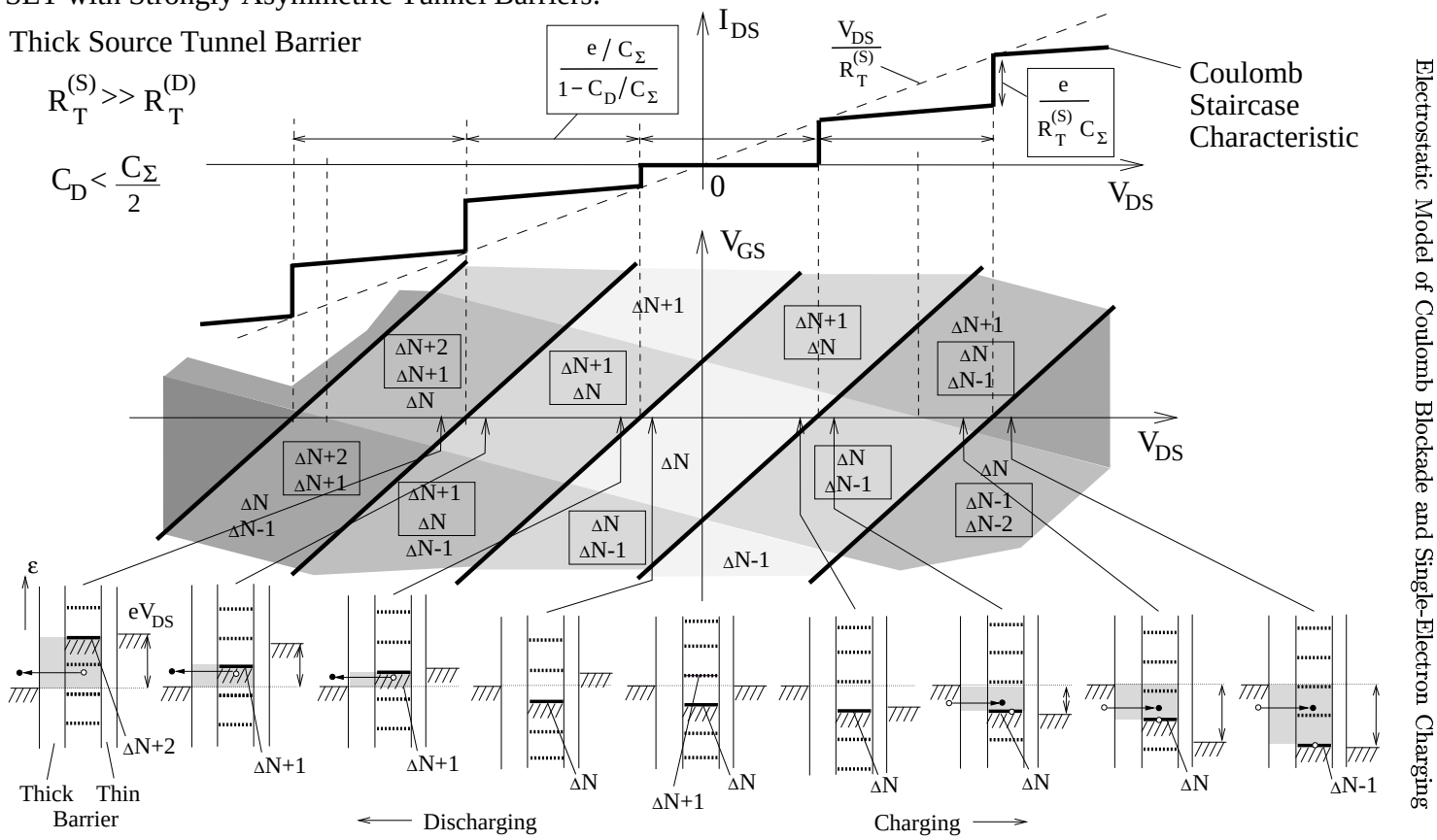

Fig. 1.10. (Left page) Coulomb staircase characteristic $I_{\rm DS}(V_{\rm DS})$ at fixed $V_{\rm GS}$ of a metal SET with strongly asymmetric tunnel barriers ($R_{\rm T}^{\rm (S)} \gg R_{\rm T}^{\rm (D)}$): From the capacitance values C_Σ, $C_{\rm D}$, and $C_{\rm G}$, the charge state diagram in the $V_{\rm GS}$ vs. $V_{\rm DS}$ plane can be constructed. Here we assume $C_{\rm D} < C_\Sigma/2$. Due to the strong asymmetry of the tunnel barriers, the charge state fluctuates even at large $|V_{\rm DS}|$ values basically between two charge states which are marked by frames in the diagram. Whenever crossing a borderline of positive slope (thick solid lines), a new charge state becomes available due to charging ($V_{\rm DS} < 0$) or discharging ($V_{\rm DS} > 0$) from drain site which is the new initial charge state for a tunnel event on the blocking source barrier. The rate for charging ($V_{\rm DS} > 0$) or discharging ($V_{\rm DS} < 0$) is suddenly enhanced due to further opening the energy window (grey shaded in the respective energy schemes) by e^2/C_Σ leading to a step-like increase in $I_{\rm DS}$ at that $V_{\rm DS}$ values by $\Delta I_{\rm DS} = e/(R_{\rm T}^{\rm (S)}\, C_\Sigma)$. The overall $I_{\rm DS}(V_{\rm DS})$ characteristics is limited by the straight line $I_{\rm DS} = V_{\rm DS}/R_{\rm T}^{\rm (S)}$ representing the case of a short instead of a thin drain barrier. Since the energy window is fully opened to $e|V_{\rm DS}|$ at $V_{\rm DS}$ values where the new charge state is reached from drain site, substracting $\Delta I_{\rm DS}$ from $I_{\rm DS} = V_{\rm DS}/R_{\rm T}^{\rm (S)}$ at the respective $V_{\rm DS}$ values also allows to construct the whole $I_{\rm DS}(V_{\rm DS})$ characteristic for the respective $V_{\rm GS}$ value. It is denoted as *Coulomb staircase* characteristic. The step width is given by $\Delta V_{\rm DS} = 2\,E_{\rm C}/(e \cdot (1 - C_{\rm D}/C_\Sigma)) = e/(C_\Sigma - C_{\rm D})$.

describes charging of the island with increasing $V_{\rm DS}$ by using the drain electrode as the electron reservoir for the island and as a gate electrode.

In conclusion, with knowing the parameters C_Σ, $C_{\rm G}$, $C_{\rm D}$ and $R_{\rm T}^{\rm max} = \max\{R_{\rm T}^{\rm (S)}, R_{\rm T}^{\rm (D)}\}$, the full $I_{\rm DS}(V_{\rm DS})$ characteristic for any value of $V_{\rm GS}$ can be sketched for strong asymmetric tunnel barriers by simple geometric considerations as done in Fig. 1.10 and Fig. 1.11. Other cases for ratios between $R_{\rm T}^{\rm (S)}$ and $R_{\rm T}^{\rm (D)}$ and finite temperature can be included by a master equation approach (see Chapter 5), – denoted as the *orthodox theory* of Coulomb blockade and single-electron tunneling [2]. The $I_{\rm DS}(V_{\rm DS})$ characteristic of the two-terminal device of Fig. 1.3 is obtained for strongly asymmetric tunnel barriers from Fig. 1.10 or Fig. 1.11, respectively, by considering a trace of $V_{\rm DS}$ crossing the $V_{\rm GS}$ axis in the middle of a Coulomb blockade region where the $I_{\rm DS}(V_{\rm DS})$ characteristic is symmetric. Setting $C_\Sigma = C_{\rm S} + C_{\rm D}$ in (1.30) and (1.31), the step width in the Coulomb staircase characteristic for a blocking source electrode is obtained to $\Delta V_{\rm DS} = e/C_{\rm S}$, for a blocking drain electrode to $\Delta V_{\rm DS} = e/C_{\rm D}$. Such a Coulomb staircase characteristic has been observed, for instance in a scanning-tunneling microscope arrangement [33].

1.5 Single-Electron Devices as Sensitive Electrometers

By applying a voltage $V_{\rm GS}$ to a gate electrode, we obtained according to (1.10) a shift $\Delta E_{\rm G}$ of the electrostatic energy of an electron on the metal island. Similarily, adding a charge Q close to the island (see Fig. 1.12a) shifts the electrostatic energy for single electrons on the island by $\Delta E_{\rm Q}$. The value of

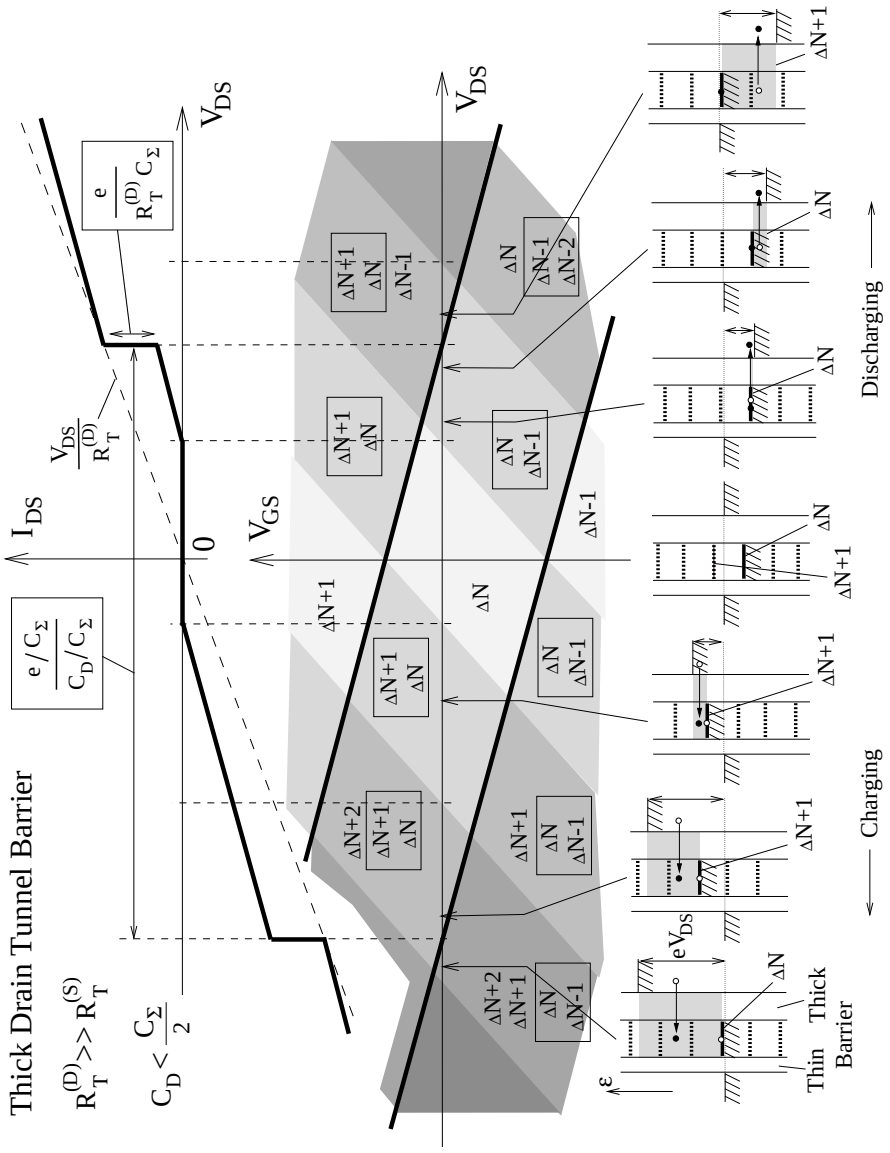

Fig. 1.11. Similar scheme and same parameters as Fig. 1.10 except that $R_{\mathrm{T}}^{(\mathrm{D})} \gg R_{\mathrm{T}}^{(\mathrm{S})}$: The current is limited by the tunneling through the drain barrier. Whenever a new charge state is reached from source site (solid borderlines in the V_{GS} vs. V_{DS} plane), a step-like increase in $|I_{\mathrm{DS}}|$ is obtained, $\Delta I_{\mathrm{DS}} = e/(R_{\mathrm{T}}^{(\mathrm{D})}\, C_{\Sigma})$. The current I_{DS} of the whole characteristic is limited by the linear relation $I_{\mathrm{DS}} = V_{\mathrm{DS}}/R_{\mathrm{T}}^{(\mathrm{D})}$. The step width in the Coulomb staircase characteristic is given by $\Delta V_{\mathrm{DS}} = 2\,E_{\mathrm{C}}/(e \cdot C_{\mathrm{D}}/C_{\Sigma}) = e/C_{\mathrm{D}}$, since the prefered charge state of the island is determined by electron exchange with the source site, – the drain electrode acts like a gate electrodes inducing a change.

ΔE_{Q} depends on the charge Q and its position within the arrangement.[11] In case of a positive charge Q, electrons on the island are attracted, i.e., $\Delta E_{\mathrm{Q}} < 0$. In the case of a negative charge added close to the island, the electrons are repelled, i.e., $\Delta E_{\mathrm{Q}} > 0$. The whole ladder of energy levels $\Delta E_{\mathrm{S}\to\mathrm{I}}(\Delta N+1, V_{\mathrm{GS}})$ described by (1.15) is shifted by ΔE_{Q} (see Fig. 1.12b), and therefore also a shift $\Delta V'_{\mathrm{GS}}$ occurs in the Coulomb blockade characteristic of the single-electron transistor (see Fig. 1.12c). How are ΔE_{Q} and $\Delta V'_{\mathrm{GS}}$ related? Assuming that the peak at V'_{GS} for $Q = 0$ is produced by fluctuation in the number of electrons on the island between ΔN and $\Delta N + 1$, the peak position is then described by $0 = \Delta E_{\mathrm{S}\to\mathrm{I}}(\Delta N + 1, V'_{\mathrm{GS}}, V_{\mathrm{DS}} = 0) = 2\,E_{\mathrm{C}} \cdot (\Delta N + \frac{1}{2} - C_{\mathrm{G}} V'_{\mathrm{GS}}/e)$ (see (1.15)). Adding the charge Q, the peak is shifted to $V'_{\mathrm{GS}} + \Delta V'_{\mathrm{GS}}$, described by $0 = \Delta E_{\mathrm{S}\to\mathrm{I}}(\Delta N + 1, V'_{\mathrm{GS}} + \Delta V'_{\mathrm{GS}}, V_{\mathrm{DS}} = 0) + \Delta E_{\mathrm{Q}} = \Delta E_{\mathrm{S}\to\mathrm{I}}(\Delta N + 1, V'_{\mathrm{GS}}, V_{\mathrm{DS}} = 0) - e \cdot C_{\mathrm{G}}/C_{\Sigma} \cdot \Delta V'_{\mathrm{GS}} + \Delta E_{\mathrm{Q}}$. Combining both expressions yields the relation we have been looking for,

$$\Delta E_{\mathrm{Q}} = e \cdot \frac{C_{\mathrm{G}}}{C_{\Sigma}} \cdot \Delta V'_{\mathrm{GS}} \; . \tag{1.32}$$

Obviously from the energy schemes of Fig. 1.12b, if $|\Delta E_{\mathrm{Q}}|$ exceeds $E_{\mathrm{C}} = e^2/2C_{\Sigma}$, the metal island is recharged by single electrons until the number $\Delta N = \Delta N_{\mathrm{Q}}$ of trapped electrons fulfills

$$\begin{aligned} &\Delta E_{\mathrm{S}\to\mathrm{I}}(\Delta N_{\mathrm{Q}}, V_{\mathrm{DS}} = 0, V_{\mathrm{GS}} = 0) + \Delta E_{\mathrm{Q}} \quad \leq 0 \quad \text{and} \\ &\Delta E_{\mathrm{S}\to\mathrm{I}}(\Delta N_{\mathrm{Q}} + 1, V_{\mathrm{DS}} = 0, V_{\mathrm{GS}} = 0) + \Delta E_{\mathrm{Q}} > 0 \; . \end{aligned} \tag{1.33}$$

The additional number ΔN_{Q} of electrons, accumulated on the island due to the presence of the charge Q in the neighbourhood of the island, is therefore given by

$$\Delta N_{\mathrm{Q}} = \mathrm{int}\left(\frac{E_{\mathrm{C}} - \Delta E_{\mathrm{Q}}}{2\,E_{\mathrm{C}}}\right) \; . \tag{1.34}$$

A similar expression (1.17) was obtained in case $Q = 0$ for applying a gate-source voltage, where the index G was used to remember the gate as the cause. The remaining fraction

$$f_{\mathrm{Q}} = f_{\mathrm{Q}}(\Delta E_{\mathrm{Q}}) = \mathrm{mod}\left(\frac{E_{\mathrm{C}} - \Delta E_{\mathrm{Q}}}{2\,E_{\mathrm{C}}}\right) \tag{1.35}$$

determines the energy barriers at $V_{\mathrm{GS}} = V_{\mathrm{DS}} = 0$ for recharging the island by single electrons,

$$\Delta E_{\mathrm{S}\to\mathrm{I}}(\Delta N_{\mathrm{Q}} + 1, V_{\mathrm{DS}} = 0, V_{\mathrm{GS}} = 0, Q) = 2E_{\mathrm{C}} \cdot (1 - f_{\mathrm{Q}}) \; , \tag{1.36}$$

$$\Delta E_{\mathrm{I}\to\mathrm{S}}(\Delta N_{\mathrm{Q}}, V_{\mathrm{DS}} = 0, V_{\mathrm{GS}} = 0, Q) \quad = 2E_{\mathrm{C}} \cdot f_{\mathrm{Q}} \; . \tag{1.37}$$

[11] An explicit expression for ΔE_{Q} is derived later in Chapter 2.

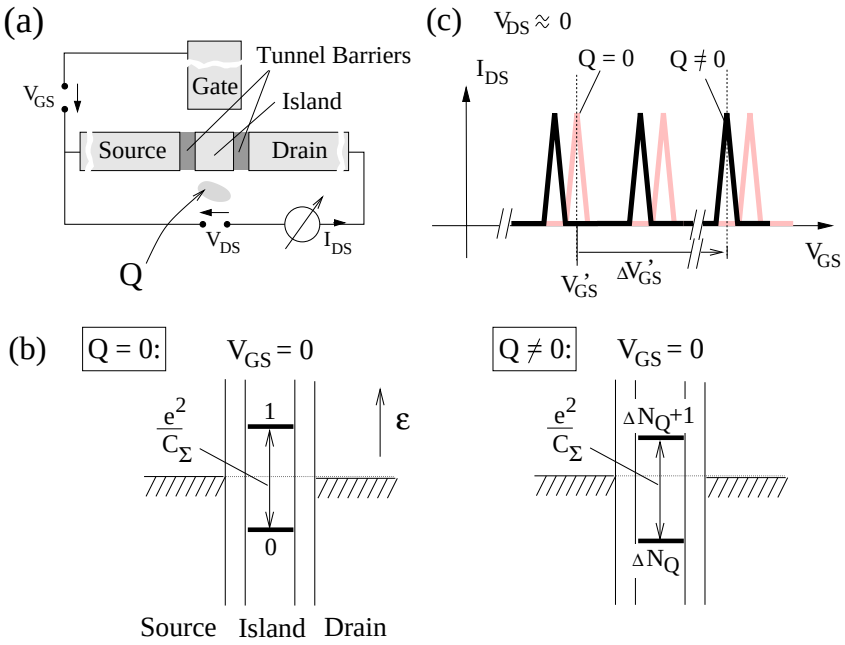

Fig. 1.12. (a) Single-electron transistor (SET) with added charge Q close to the metal island. (b) Energy scheme of the single-electron transistor without applied voltages ($V_{\rm DS} = V_{\rm GS} = 0$) with and without the charge Q. (c) Adding a charge close to the island of the SET (see (a)) shifts the Coulomb blockade oscillations along the gate voltage axis by $\Delta V'_{\rm GS}$.

When the gate-source voltage $V_{\rm GS} \neq 0$ is applied, one has to replace $\Delta E_{\rm Q}$ by $\Delta E_{\rm G} + \Delta E_{\rm Q}$ in (1.33). This yields instead of (1.34) to (1.37) the relations

$$\Delta N_{\rm G,Q} = \text{int}\left(\frac{E_{\rm C} - \Delta E_{\rm G} - \Delta E_{\rm Q}}{2\,E_{\rm C}}\right) , \tag{1.38}$$

$$f_{\rm G,Q} = f_{\rm G,Q}(\Delta E_{\rm G} + \Delta E_{\rm Q}) = \text{mod}\left(\frac{E_{\rm C} - \Delta E_{\rm G} - \Delta E_{\rm Q}}{2\,E_{\rm C}}\right) , \tag{1.39}$$

$$\Delta E_{\rm S\to I}(\Delta N_{\rm G,Q} + 1, V_{\rm DS} = 0, V_{\rm GS}, Q) = 2\,E_{\rm C} \cdot \left(1 - f_{\rm G,Q}\right) , \tag{1.40}$$

$$\Delta E_{\rm I\to D}(\Delta N_{\rm G,Q}, V_{\rm DS} = 0, V_{\rm GS}, Q) = 2\,E_{\rm C} \cdot f_{\rm G,Q} . \tag{1.41}$$

Thus, the sum of both, charging barrier $\Delta E_{\rm S\to I}(\Delta N_{\rm G,Q} + 1, V_{\rm DS} = 0, V_{\rm GS}, Q)$ and discharging barrier $\Delta E_{\rm I\to D}(\Delta N_{\rm G,Q}, V_{\rm DS} = 0, V_{\rm GS}, Q)$, is always $2\,E_{\rm C} = e^2/C_\Sigma$ independent of the magnitude of Q and $V_{\rm GS}$.

How sensitive is the single-electron transistor to charges? If the charge $Q = \pm e$ would be added directly to the metal island, then the Coulomb-blockade oscillations are shifted by one period along the gate voltage axis ($\Delta E_{\rm Q} = \mp e^2/C_\Sigma$). In this sense, the single-electron transistor is a highly

sensitive electrometer which is even able to detect a fraction of the elementary charge e by the change in its characteristic if the charge is added closely to the island. Single-electron transistors have been demonstrated as electrometers with a charge sensitivity down to $8 \cdot 10^{-6} \cdot e/\sqrt{\text{Hz}}$ at 10 Hz [34]. To improve the bandwidth, R.J. Schoelkopf and collaborators incorporated the single-electron transistor into a radio-frequency resonance circuit – denoted as RF-SET, achieving a value of $1.2 \cdot 10^{-5} e/\sqrt{\text{Hz}}$ at 1.1 MHz [35] (see also [36, 37]). This high charge sensitivity offers on one hand a *ultrasensitive electrometer*, on the other hand it is a disadvantage for applications [25] where a stable and reproducible SET characteristic is required for a large number of SET devices. Telegraph noise due to charge fluctuations in the SET surroundings [38, 39, 40] makes them almost useless for this purpose.

An additional charge Q close to the island is not only detected with a single-electron transistor arrangement, but also with the two-terminal arrangement, sketched in Fig. 1.13a. Like just discussed for the single-electron transistor, with positioning Q, single electrons will recharge the island until ΔN_{Q} (see (1.34)) is reached. The energy barriers for further recharging the island without applied V_{DS} bias are given by (1.36) and (1.37). With increasing V_{DS}, both the charging energy for an electron added from source to the island

$$\Delta E_{\text{S}\to\text{I}} = 2E_{\text{C}} \cdot (1 - f_{\text{Q}}) - e \cdot C_{\text{D}}/C_{\Sigma} \cdot V_{\text{DS}} \ , \tag{1.42}$$

and the discharging energy for an electron leaving the island to drain

$$\begin{aligned} \Delta E_{\text{I}\to\text{D}} &= \left(2E_{\text{C}} \cdot f_{\text{Q}} + e \cdot C_{\text{D}}/C_{\Sigma} \cdot V_{\text{DS}}\right) - e \cdot V_{\text{DS}} \\ &= 2E_{\text{C}} \cdot f_{\text{Q}} - e \cdot C_{\text{S}}/C_{\Sigma} \cdot V_{\text{DS}} \end{aligned} \tag{1.43}$$

are reduced. The last line is obtain with $C_{\Sigma} = C_{\text{S}} + C_{\text{D}}$. Threshold is reached first either with $\Delta E_{\text{S}\to\text{I}} = 0$ or with $\Delta E_{\text{I}\to\text{D}} = 0$. Therefore, single-electron transport is expected for

$$V_{\text{DS}} \geq V_{\text{DS}}^{(\text{th})} = \min\left(\frac{e}{C_{\text{D}}} \cdot (1 - f_{\text{Q}}) \ ; \ \frac{e}{C_{\text{S}}} \cdot f_{\text{Q}}\right) . \tag{1.44}$$

For $V_{\text{DS}} < 0$, similar considerations lead to

$$|V_{\text{DS}}| \geq V_{\text{DS}}^{(\text{th})} = \min\left(\frac{e}{C_{\text{D}}} \cdot f_{\text{Q}} \ ; \ \frac{e}{C_{\text{S}}} \cdot (1 - f_{\text{Q}})\right) . \tag{1.45}$$

As a consequence, for $C_{\text{S}} \neq C_{\text{D}}$ and $f_{\text{Q}} \neq \frac{1}{2}$, the threshold voltages lie asymmetric relative to $V_{\text{DS}} = 0$. In the symmetric case ($C_{\text{D}} = C_{\text{S}} = C_{\Sigma}/2$), we obtain for $0 < f_{\text{Q}} < 1$

$$|V_{\text{DS}}| \geq V_{\text{DS}}^{(\text{th})} = \min\left(\frac{2\,e}{C_{\Sigma}} \cdot \left(1 - f_{\text{Q}}\right) \ ; \ \frac{2\,e}{C_{\Sigma}} \cdot f_{\text{Q}}\right) \ , \tag{1.46}$$

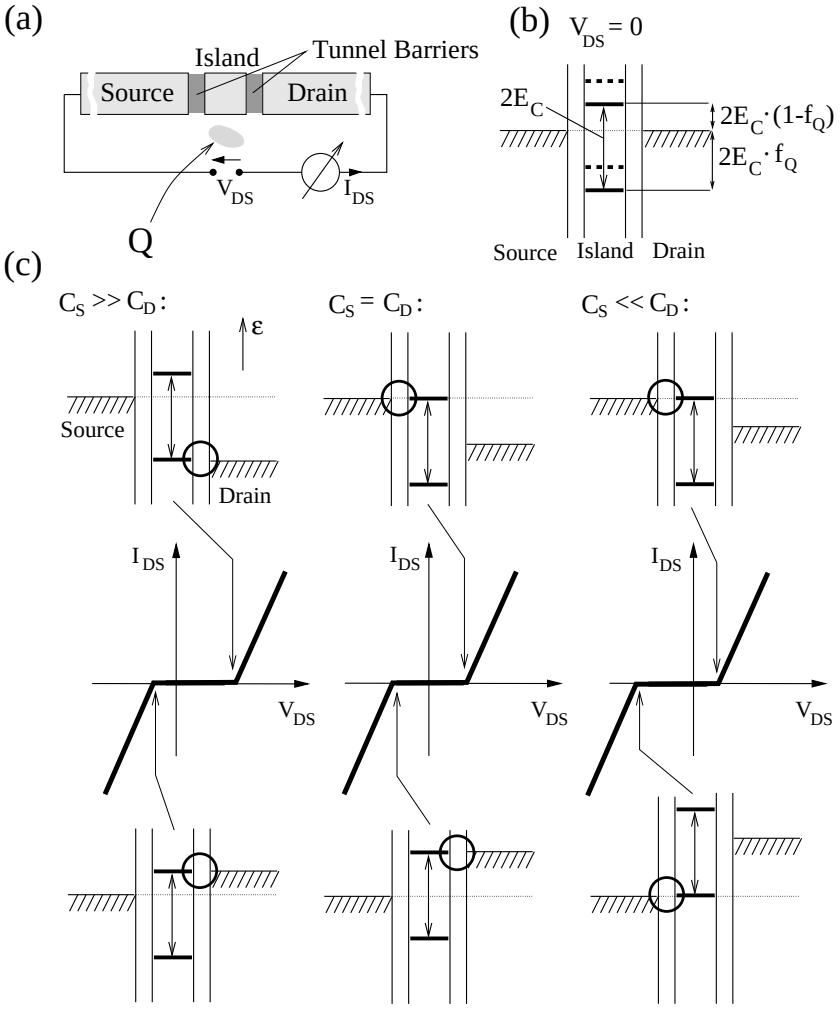

Fig. 1.13. (a) Scheme of a two-terminal arrangement: A charge Q is added close to the metal island. (b) Energy scheme of the arrangement in presence of Q at $V_{\mathrm{DS}} = 0$. (c) For different ratios $C_{\mathrm{S}}/C_{\mathrm{D}}$, $I_{\mathrm{DS}}(V_{\mathrm{DS}})$ characteristic and related energy schemes at positive and negative threshold are shown.

i.e., the thresholds lie symmetric to $V_{\mathrm{DS}} = 0$. The Coulomb blockade disappears already at the origin $V_{\mathrm{DS}} = 0$ when a charge is added so that $f_{\mathrm{Q}} = 0$. For instance, this is fulfilled for $\Delta E_{\mathrm{Q}} = \mp e^2/2C_{\Sigma}$. In case of $\Delta E_{\mathrm{Q}} = j \cdot 2E_{\mathrm{C}}$ with $j \in \{..., -2, -1, 0, 1, 2, ...\}$, we obtain $f_{\mathrm{Q}} = \frac{1}{2}$, i.e., the charging and discharging barrier are here equal leading to $V_{\mathrm{DS}}^{(\mathrm{th})} = \min\left(e/(2\,C_{\mathrm{S}}); e/(2\,C_{\mathrm{D}})\right)$, which is equal to the previous result (1.8).

1.6 Single-Electron Transistor as a Current Rectifier with Gate-Controlled Current Polarity

As derived in Section 1.4 for a single-electron transistor, the capacitance ratios $-C_D/C_G$ and $(C_\Sigma - C_D)/C_G$ are responsible for the slopes of the boundaries between Coulomb blockade and single-electron transport regions as a function of drain-source voltage V_{DS} and a gate-source voltage V_{GS}. Therefore threshold values at fixed gate voltage lie usually asymmetrically with respect to $V_{DS} = 0$. Thus, single-electron transistors display a nonlinear drain-source current-voltage characteristic $I_{DS}(V_{DS}, V_{GS})$ which is tunable by an applied gate-source voltage V_{GS}. Two-terminal single-electron devices with different source and drain capacitance values show also a nonlinear current-voltage characteristic $I_{DS}(V_{DS}, Q)$ if charge is present close to the island (see Fig. 1.13). Due to the nonlinearity of such devices around $V_{DS} = 0$, frequency mixing of *ac* voltage signals is possible around $V_{DS} = 0$. Especially a rectification process can occur: An applied *ac* bias voltage signal results in a time-averaged net *dc* current.

To discuss this effect, in Fig. 1.14a the transport regimes of a single-electron transistor are shown again as a function of the drain-source voltage V_{DS} and a gate-source voltage V_{GS}. In addition, $I_{DS}(V_{DS})$-characteristics and energy schemes are sketched for different V_{GS} values, marked by (α), (β), (γ) and (δ) in Fig. 1.14. By applying an *ac* voltage of a certain amplitude (less than e/C_Σ) to the drain contact, current flows whenever this voltage modulation $V_{DS}(t)$ exceeds either the positive or the negative threshold on the V_{DS} axis. [12] Since the thresholds are changing with the applied gate-source voltage, either a positive (α), zero (β), or a negative (γ) net *dc* current is detected. The single-electron transistor behaves as a *current rectifier* with gate-controlled current polarity. As seen from the respective energy schemes, the relative position of the energy level for charging an electron to the island for $V_{DS} = 0$, which is tuned by V_{GS}, determines whether the modulation of the potential of the drain reservoir leads to a net *dc* current either from source to drain or from drain to source.

In the example given in Fig. 1.14, the capacitive coupling of the drain electrode to the island was assumed to be $C_D/C_\Sigma < \frac{1}{2}$, i.e., $C_D/C_G < (C_\Sigma - C_D)/C_G$. This can be modified by changing the design of the single-electron transistor. Depending on the ratio C_D/C_Σ, three different behaviours are expected (see Fig. 1.15): In the case of $C_D/C_\Sigma > \frac{1}{2}$, for a fixed *ac* bias modulation with $|V_{DS}(t)| \ll e/C_\Sigma$, the sequence in the *dc* current polarity is zero/positive/negative/zero with increasing the gate-source voltage from one Coulomb blockade region to the next, whereas in the case $C_D/C_\Sigma < \frac{1}{2}$ the

[12] Only the current is plotted derived from the nonlinear *dc* characteristics. Therefore not included is the displacement current due to the capacitive coupling between drain, source and gate electrode [41]. Those are important at high frequencies.

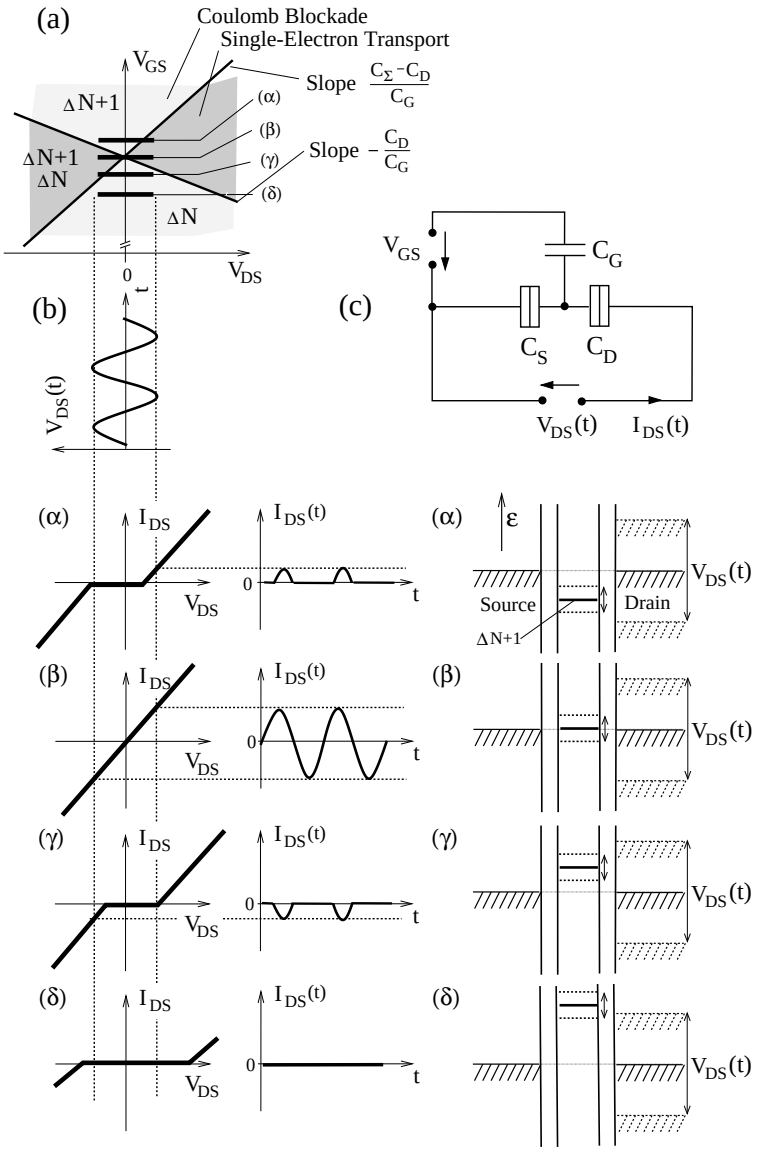

Fig. 1.14. Single-electron transistor as a rectifier: (a) Transport regions of a single-electron transistor as a function of the drain-source voltage $V_{\rm DS}$ and a gate-source voltage $V_{\rm GS}$. For the gate-source voltage values marked by (α), (β), (γ) and (δ), sketches of $I_{\rm DS}(V_{\rm DS})$-characteristic and the energy scheme are given in (b). Applying an *ac* voltage modulation $V_{\rm DS}(t)$ (see (b)) results in a time-dependent current $I_{\rm DS}(t)$ which leads in time-average to a positive, zero or negative *dc* current component depending on how the threshold voltages are lying in respect to $V_{\rm DS} = 0$. (c) Electrial circuit indicating that the source electrode is the common node for the applied *ac* drain-source voltage $V_{\rm DS}(t)$ (see (b)) and the gate-source voltage $V_{\rm GS}$. For *this* configuration the slopes between Coulomb blockade and single-electron tunneling are given as denoted in (a).

sequence is zero/negative/positive/zero. Only in the case where $C_D/C_\Sigma = \frac{1}{2}$, the net current is basically zero over the whole gate-source voltage range. The differences in the behaviour are due to the fact that the energy level on the island is modulated in its position with the modulation of the drain potential, – and this is stronger or weaker depending on C_D/C_Σ. Therefore, the relative position of the energy level *and* the capacitive coupling between the island and the drain electrode, where the voltage modulation is applied, determines the polarity of the net *dc* current. The effect was demonstrated for a quantum dot system by J. Weis and coworkers [42, 43] in 1993.[13] In

[13] The effect can be used to detect radio frequency signals usually affecting low-temperature measurements in ^{3}He/^{4}He dilution refrigerators if no appropiate RF filtering is done.

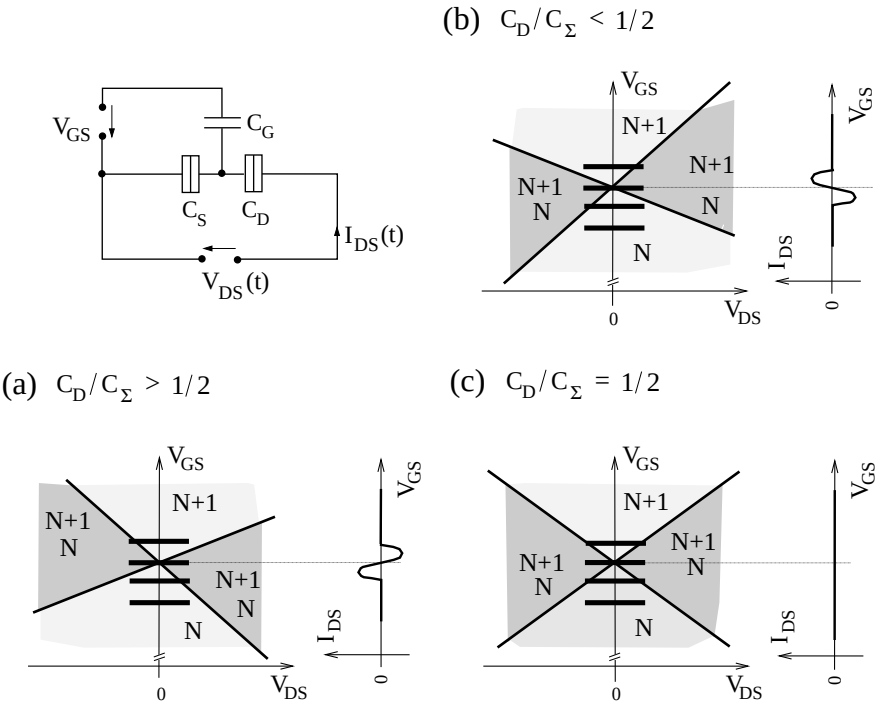

Fig. 1.15. Single-electron transistor as a rectifier with gate-controlled current polarity: Transport regions of a single-electron transistor as a function of the drain-source voltage V_{DS} and a gate-source voltage V_{GS} for different ratios C_D/C_Σ. (a) For $C_D/C_\Sigma > \frac{1}{2}$, a sequence of zero/positive/negative/zero time-averaged *dc* current is observed as a function of gate-source voltage if an *ac* voltage is applied to the drain contact. (b) For $C_D/C_\Sigma < \frac{1}{2}$, the sequence has switched to zero/negative/positive/zero *dc* current. (c) For $C_D/C_\Sigma = \frac{1}{2}$, no rectification is observed for small modulation amplitudes.

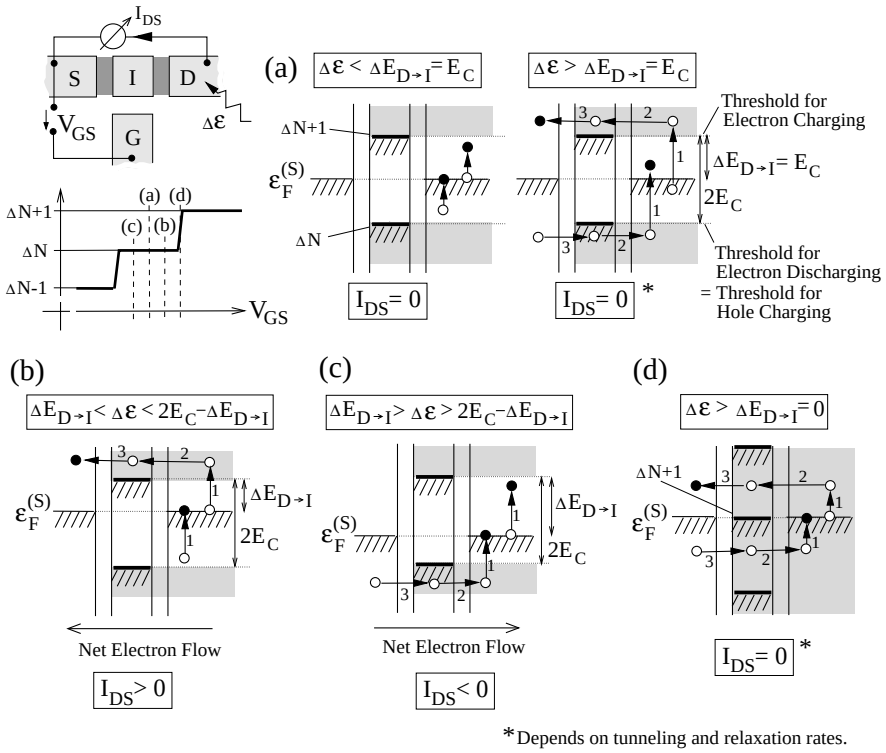

Fig. 1.16. Net current flow $I_{\mathrm{DS}} \neq 0$ for $V_{\mathrm{DS}} = 0$ caused by electron-hole excitations in the drain electrode due to a continuous external energy transfer $\Delta\varepsilon$. Distinct operation points in V_{GS} are indicated. (a) If the energy-level ladder is symmetric ($\Delta E_{\mathrm{D}\to\mathrm{I}} = E_{\mathrm{C}}$) to the common Fermi energy $\varepsilon_{\mathrm{F}}^{(\mathrm{S})}$, the current I_{DS} is zero if $\Delta\varepsilon < E_{\mathrm{C}}$, since the island cannot be charged or discharged by a single electron. For $\Delta\varepsilon > E_{\mathrm{C}}$, charging and discharging is possible, but electron and hole current compensate if the respective tunneling and relaxation rates are equal. (b) If the energy-level ladder is shifted down ($\Delta E_{\mathrm{D}\to\mathrm{I}} < E_{\mathrm{C}}$), a net electron flow is observed, i.e., $I_{\mathrm{DS}} > 0$, if the excitation is high enough to overcome the threshold for charging, $\Delta\varepsilon > \Delta E_{\mathrm{D}\to\mathrm{I}}$, but low enough for not allowing to overcome the threshold for discharging, $\Delta\varepsilon < 2\,E_{\mathrm{C}} - \Delta E_{\mathrm{D}\to\mathrm{I}}$. (c) A net current $I_{\mathrm{DS}} < 0$ is obtained if the energy-level ladder is shifted leading to $\Delta E_{\mathrm{D}\to\mathrm{I}} > \Delta\varepsilon > 2\,E_{\mathrm{C}} - \Delta E_{\mathrm{D}\to\mathrm{I}}$. (d) In case of vanishing charging barrier $\Delta E_{\mathrm{D}\to\mathrm{I}} = 0$, charging and discharging is possible, but respective hole and electron processes compensate if tunneling and relaxation rates are equal.

detail a better description of the rectification process is obtained within a master equation approach, for instance, described in [41].

A similar rectification process is observed if a higher temperature exists for the drain electrode than for the source electrode, or a continuous flow of photons is absorbed only at the drain electrode. Both lead to stationary occupation probabilities of the electronic levels at the drain electrode which

differs from that at the source electrode: Electrons are excited to higher energy and, at the same time, unoccupied states are created below the Fermi level. Depending on the position of the energy level for charging or discharging an electron to the island, a net current flows either from drain to source or from source to drain (see Fig. 1.16). For an open drain contact, a *dc* V_{DS} voltage is built up due to the rectification process. For a temperature gradient between the source and the drain, this thermally induced voltage has been observed, denoted as 'thermal power'. In several theoretical and experimental works this subject has been explored [44, 45, 46]. For monochromatic photon radiation, a model was developed in Ref. [47].

Due to its nonlinear $I_{\mathrm{DS}}(V_{\mathrm{DS}})$ characteristics, the single-electron transistor can be considered as a realization of a ratchet. [14]

1.7 Remarks on the Electrostatic Model

By simple electrostatic energy considerations for rearranging single electrons between metal electrodes, the effects named *Coulomb blockade*, *Single-Electron Charging*, and *Single-Electron-Transport* were introduced. The basic properties of a *Single-Electron-Transistor* were described. Due to the discussion, Coulomb blockade and single-electron charging should be observable in transport through quasi-isolated metal islands if, firstly, the charging energy $E_{\mathrm{C}} = e^2/2C_{\Sigma}$ of the island exceeds the thermal energy $k_{\mathrm{B}}T$, and, secondly, the applied drain-source voltage V_{DS} is small, $|eV_{\mathrm{DS}}| < 2E_{\mathrm{C}}$.

All the discussed electrical processes of the previous Sections were based on an electro*static* picture. This implies for electrical transport that with the movement of an electron from one electrode to another the respective image charges on the electrodes have to be created instantaneously and that the defined potential differences have to restore immediately. This was indicated for a two-terminal arrangement in the Fig. 1.4. However, the Coulomb blockade effect has also been characterized [20] as a time-dependent dynamical effect – denoted as '*environmental Coulomb blockade*' [2]: A tunnel junction itself is modelled by the tunnel resistance R_{J} and the small capacitance C_{J} in parallel (see Fig.1.17). The electrodynamical environment is modelled by an impedance $Z(\omega)$ in series [49, 50]. Such an arrangement with an high $|Z(\omega)|$ should show a nonlinear current-voltage characteristic. The effect is that the high impedance in series prohibits instantaneous restoration of the applied potential difference over the junction, and, therefore, an electron moving from one side of the junction to the other charges the junction capacitor on a short time scale. Current flow through the junction is suppressed at small drain-source voltage due to the required single-electron charging energy. Theoretically predicted [20], it is experimentally difficult to demonstrate the effect

[14] A ratchet consisting of a chain of asymmetric energy barriers which are deformed by a modulated bias voltage is discussed in [48].

of Coulomb blockade on this arrangement [51]. It is a challenge to create a high impedance in series to the tunnel junction since already an ohmic wire possesses due to its spatial extension a stray capacitance which reduces its impedance. A constant-voltage-driven instead of a constant-current-driven single tunnel junction does not show the Coulomb blockade effect. The easiest way to create a high impedance is to use a second tunnel junction close to the first junction [52, 51]. A small quasi-isolated region in between is obtained – an electron island. In the course of this book we restrict ourselves to Coulomb blockade effect on island in the electrostatic description. A number of theoretical papers on metal and superconducting SET include the environmental impedances [53, 54, 55]. [15]

The island has been denoted as being *quasi-isolated*: Electron exchange with source and drain should be possible to allow electrical transport between source and drain via the island. On the other hand, the charge of the island should be quantized allowing a recharging only by single electrons.

[15] Note, in those cases some of the dissipation might occur in the electrodynamical environment and not only by the relaxation of single electrons.

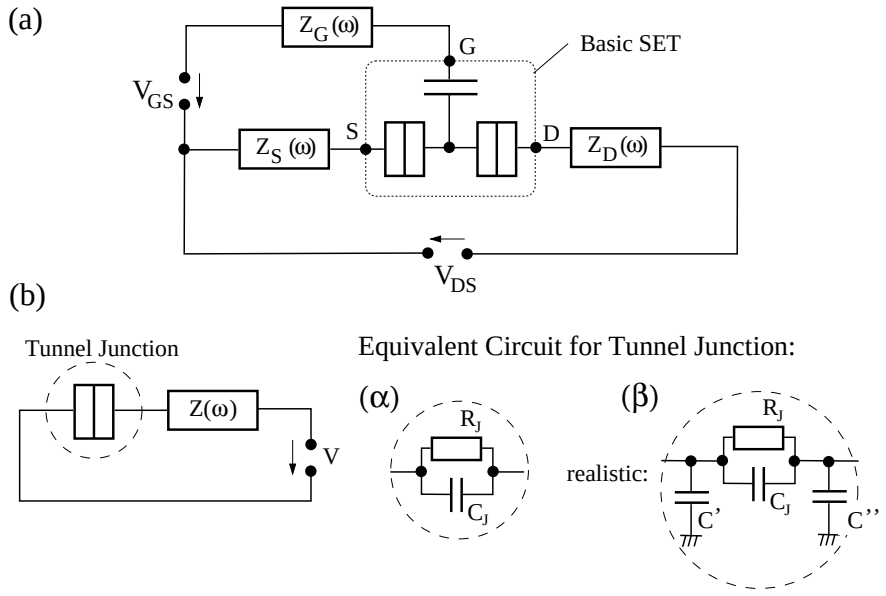

Fig. 1.17. (a) Impedances $Z_S(\omega)$, $Z_D(\omega)$, $Z_G(\omega)$ – modeling the *electromagnetic environment* – might hinder the instantaneous restoration of the electrostatic potentials on the source, drain and gate electrodes while an electron is tunneling. (b) A tunnel junction in a serial arrangement with a high impedance $Z(\omega)$. (α) The equivalent circuit of the tunnel junction consists of a tunnel resistance R_J and a parallel capacitance C_J. (β) Usually the stray capacitance C', $C''$of the leads to the tunnel junction dominate the serial impedance $Z(\omega)$ leading to a low $Z(\omega)$.

Well-defined energies have been attributed to single electrons being either located on the island or the surrounding electrodes of fixed potential. Energy differences for recharging the island by single electrons prohibit transport between source and drain. If the time τ of a single electron occupying the island is short, due to Heisenberg uncertainty relation, such an energy difference ΔE might be no hurdle for single-electron transport between source and drain. The energy difference ΔE is overcome if the life time τ_{H} of the electron on the high energy state is $\tau_{\mathrm{H}} < \hbar/\Delta E$, where $\hbar = h/(2\pi)$ and h denotes Planck's constant. Hence, the Coulomb blockade effect can only occur if $\tau_{\mathrm{H}} \gg \hbar/E_{\mathrm{C}} = \hbar/e^2 \cdot 2C_{\Sigma}$. The island is usually considered as 'quasi-isolated' [1, 3] if the tunnel resistances R_{T} between the island and leads exceeds well the value $h/e^2 \approx 26\ \mathrm{k\Omega}$ – the inverse of the conductance quantum e^2/h [56, 57].

2. Revision of the Electrostatics of Metallic Single-Electron Devices

Metallic single-electron devices are mostly composed of different shaped metal films deposited on a dielectric substrate which is often a crystal or an amorphic insulator. Some of these metal films are connected by thin dielectric layers acting as tunnel barriers. Furthermore fixed charges may exist as ions due to doping or contamination. The electrostatic model, presented in the preceding Chapter, uses the *partial capacitances* C_{S}, C_{G}, C_{D} and the total capacitance C_{Σ} between metal island and the metal electrodes as known parameters. Design and optimization of such devices require however a quantitative treatment of the electrostatics of such complicated devices. It is also needed to establish later in Chapter 4 the Hamiltonian of systems containing a quantum dot.

In the present Chapter, the usual treatment of capacitances in textbooks, which assume a homogeneous, isotropic, charge-free dielectric between the metal conductors, is generalized [42] to possibly inhomogeneous, anisotropic dielectrics containing localized charges. Integral expressions for the *capacitance coefficients* and their connection to partial capacitances are given. The behaviour of the capacitance coefficients with scaling of an arbirary conductor arrangement is derived, and limits for the total capacitance of a metal island of arbitrary shape are given. This general treatment leads also to a general expression for the total electrostatic energy of ΔN electrons on a metal island in a respective electrostatic surrounding and that prepares the step to a model Hamiltonian for quantum dots presented in Chapter 4.

2.1 Capacitance Coefficients and Partial Capacitances Between Metal Conductors

An arrangement of $M+1$ metal conductors embedded in an inhomogeneous, anisotropic dielectric medium is shown in Fig. 2.1. The conductors are labelled by an index i or j from 0 to M. For the following it is convenient to denote always metal conductors having definite electrostatic potential V_i as 'metal electrodes' and those having definite electrical charge Q_i as 'metal islands'. In Section 2.3, we will restrict the number of islands to one and label it by index

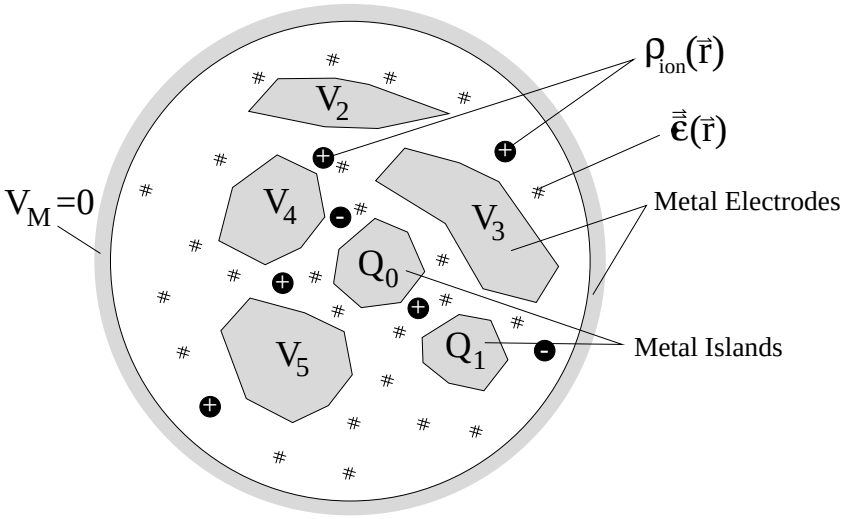

Fig. 2.1. An arbitrary arrangement of $M+1$ metal conductors and a fixed charge distribution $\rho_{\rm ion}(\boldsymbol{r})$ embedded in a dielectric matrix described by $\boldsymbol{\epsilon}(\boldsymbol{r})$. Either the charge Q_i or the electrostatic potential V_i in reference to one conductor (for example, $i = M$ with $V_M = 0$) is fixed for each conductor $i = 0$ to M. The surface $S = \{S_i\}$ of all conductors enclose the volume V filled by the dielectric matrix. For convenience, a conductor i with definite electrostatic potential V_i is denoted as 'metal electrode', a conductor j with definite charge Q_j as 'metal island'.

$i = 0$, the electrodes are then numbered from 1 to M. [1] All metal conductors should carry only surface charges as is generally assumed in the electrostatics of charged metals. In addition, a fixed charge distribution $\rho_{\rm ion}(\boldsymbol{r})$ due to ions or trapped electrons is present. Due to Maxwell's relations in the stationary case, the electric field $\boldsymbol{E}(\boldsymbol{r})$ at any position $\boldsymbol{r}$ in the space V *between* the conductors has to follow

$$\mathrm{rot}\boldsymbol{E}(\boldsymbol{r}) \equiv \boldsymbol{\nabla}_{\boldsymbol{r}} \times \boldsymbol{E}(\boldsymbol{r}) = 0\,, \tag{2.1}$$

and the dielectric field $\boldsymbol{D}(\boldsymbol{r})$ fulfills the relation

$$\mathrm{div}\boldsymbol{D}(\boldsymbol{r}) \equiv \boldsymbol{\nabla}_{\boldsymbol{r}}\,\boldsymbol{D}(\boldsymbol{r}) = \rho_{\rm ion}(\boldsymbol{r})\,. \tag{2.2}$$

As a good description for small electric field strength, the dielectric and the electric field should be linearly related by a dielectric tensor $\boldsymbol{\epsilon}(\boldsymbol{r})$ of the second rang,

$$\boldsymbol{D}(\boldsymbol{r}) = \epsilon_0 \boldsymbol{\epsilon}(\boldsymbol{r}) \cdot \boldsymbol{E}(\boldsymbol{r})\,, \tag{2.3}$$

where ϵ_0 denotes the dielectric constant of vacuum. From relation (2.1), the existence of an electrostatic potential $\Phi(\boldsymbol{r})$ follows,

[1] The metal island labelled by the index 0 will later be replaced by the quantum dot. The electrodes will then still be numbered from 1 to M.

$$\boldsymbol{E}(\boldsymbol{r}) = -\mathrm{grad}\,\Phi(\boldsymbol{r}) = -\boldsymbol{\nabla}_{\boldsymbol{r}}\,\Phi(\boldsymbol{r})\ . \tag{2.4}$$

Substituting $\boldsymbol{E}(\boldsymbol{r})$ by (2.4) in (2.2), with taking into account (2.3), an equation is obtained which the electrostatic potential $\Phi(\boldsymbol{r})$ has to fulfill at position $\boldsymbol{r}$ under the boundary conditions of given values V_i on the surfaces S_i of the conductors $i = 0$ to M,

$$\begin{aligned} -\boldsymbol{\nabla}_{\boldsymbol{r}}\left\{\epsilon_0\boldsymbol{\epsilon}(\boldsymbol{r})\cdot\boldsymbol{\nabla}_{\boldsymbol{r}}\,\Phi(\boldsymbol{r})\right\} &= \rho_{\mathrm{ion}}(\boldsymbol{r})\ ,\ \text{if}\ \boldsymbol{r}\in V\ , \\ \Phi(\boldsymbol{r}) &= V_i\qquad ,\ \text{if}\ \boldsymbol{r}\in S_i\ . \end{aligned} \tag{2.5}$$

For a homogeneous isotropic dielectric medium filling the space V between the conductors (i.e., $\boldsymbol{\epsilon}(\boldsymbol{r}) = \epsilon = \text{const}$ for $\boldsymbol{r}\in V$), the simpler Poisson equation $\Delta_{\boldsymbol{r}}\Phi(\boldsymbol{r}) = -\rho_{\mathrm{ion}}(\boldsymbol{r})/\epsilon_0\epsilon$ is recovered, and further for $\rho_{\mathrm{ion}}(\boldsymbol{r}) = 0$ the Laplace equation $\Delta_{\boldsymbol{r}}\Phi(\boldsymbol{r}) = 0$.

Due to the linearity of (2.5), which is a result of the material relation (2.3), the total electrostatic potential can be considered as being composed by the superposition of several electrostatic potential contributions. A convenient choice is

$$\Phi(\boldsymbol{r}) = \sum_{i=0}^{M}\alpha_i(\boldsymbol{r})\cdot V_i + \Phi_{\mathrm{ion}}(\boldsymbol{r})\ , \tag{2.6}$$

where – according to (2.5) – the $\alpha_i(\boldsymbol{r})$ with $i = 0$ to M have to fulfill

$$\begin{aligned} \boldsymbol{\nabla}_{\boldsymbol{r}}\left\{\epsilon_0\boldsymbol{\epsilon}(\boldsymbol{r})\cdot\boldsymbol{\nabla}_{\boldsymbol{r}}\,\alpha_i(\boldsymbol{r})\right\} &= 0\ ,\ \text{if}\ \boldsymbol{r}\in V\ , \\ \alpha_i(\boldsymbol{r}) &= \begin{cases} 1\ ,\ \text{if}\ \boldsymbol{r}\in S_i\ , \\ 0\ ,\ \text{if}\ \boldsymbol{r}\in S_j\ \text{with}\ i\neq j\ , \end{cases} \end{aligned} \tag{2.7}$$

and $\Phi_{\mathrm{ion}}(\boldsymbol{r})$ the relations

$$\begin{aligned} -\boldsymbol{\nabla}_{\boldsymbol{r}}\left\{\epsilon_0\boldsymbol{\epsilon}(\boldsymbol{r})\cdot\boldsymbol{\nabla}_{\boldsymbol{r}}\,\Phi_{\mathrm{ion}}(\boldsymbol{r})\right\} &= \rho_{\mathrm{ion}}(\boldsymbol{r})\ ,\ \text{if}\ \boldsymbol{r}\in V\ , \\ \Phi_{\mathrm{ion}}(\boldsymbol{r}) &= 0\qquad ,\ \text{if}\ \boldsymbol{r}\in S_j\ (j = 0\ \text{to}\ M)\ . \end{aligned} \tag{2.8}$$

Therefore, $\alpha_i(\boldsymbol{r})\cdot V_i$ describes the electrostatic potential profile in the space V between the conductors, if the electrostatic potential on the surface S_i of electrode i is set to V_i, and the electrostatic potential is zero on all other surfaces S_j $(i\neq j)$. The functions $\alpha_i(\boldsymbol{r})$ are completely independent of the electrostatic potentials $\{V_j\}$ on the electrodes. We name $\alpha_i(\boldsymbol{r})$ the *(electrostatic) potential profile of electrode* i. If all electrodes are at the same electrostatic potential (all $V_i = V_0$), there is due to potential theory no change of the electrostatic potential between the electrodes (except those which is caused by $\rho_{\mathrm{ion}}(\boldsymbol{r})$), i.e., $\Phi(\boldsymbol{r}) = V_0$. Hence according to (2.6) one obtains $\sum_{i=0}^{M}\alpha_i(\boldsymbol{r})\cdot V_0 = V_0$ for this case which gives the useful relation

$$\sum_{i=0}^{M}\alpha_i(\boldsymbol{r}) = 1 \tag{2.9}$$

generally valid for any position $\boldsymbol{r}$ between the electrodes.

The total charge Q_i on a metal conductor i is calculated from the Gauß' integral theorem

$$Q_i = -\oint_{S_i} \boldsymbol{D}(\boldsymbol{r})\,\mathrm{d}\boldsymbol{S}_i = \oint_{S_i} \left\{\epsilon_0 \boldsymbol{\epsilon}(\boldsymbol{r}) \cdot \boldsymbol{\nabla}_{\boldsymbol{r}}\, \Phi(\boldsymbol{r})\right\} \mathrm{d}\boldsymbol{S}_i \;, \tag{2.10}$$

where $\mathrm{d}\boldsymbol{S}_i$ denotes the vector of the surface element at position $\boldsymbol{r}$ on conductor i with the orientation normal inward to the surface of the conductor. With replacing $\Phi(\boldsymbol{r})$ by (2.6), Q_i is expressed by

$$Q_i = -\sum_{j=0}^{M} C_{ij}\, V_j + Q_{i,\mathrm{ion}} \;, \tag{2.11}$$

with

$$C_{ij} \equiv -\oint_{S_i} \left\{\epsilon_0 \boldsymbol{\epsilon}(\boldsymbol{r}) \cdot \boldsymbol{\nabla}_{\boldsymbol{r}}\, \alpha_j(\boldsymbol{r})\right\} \mathrm{d}\boldsymbol{S}_i \;, \tag{2.12}$$

and

$$Q_{i,\mathrm{ion}} \equiv \oint_{S_i} \left\{\epsilon_0 \boldsymbol{\epsilon}(\boldsymbol{r}) \cdot \boldsymbol{\nabla}_{\boldsymbol{r}}\, \Phi_{\mathrm{ion}}(\boldsymbol{r})\right\} \mathrm{d}\boldsymbol{S}_i \;. \tag{2.13}$$

For $i \neq j$, C_{ij} are positive values from their definition (2.12) and are denoted as *Capacitance Coefficients.* [2] The relation (2.11) represents $(M+1)$ coupled linear equations ($i = 0$ to M), which connects the charges and electrostatic potentials of all $(M+1)$ conductors. By setting the charge or the electrostatic potential for each of the conductors, the other quantity – electrostatic potential or charge, respectively – can be calculated from (2.11), if the coefficients C_{ij} are known. Due to (2.12) and (2.7), these capacitance coefficients C_{ij} depend only on the dielectric matrix, described by the tensor $\boldsymbol{\epsilon}(\boldsymbol{r})$, the shapes and the geometric arrangement of the conductors, as long as the finite screening length of the surface charge – which is usually in the range of less than a nanometer for a metal [58] – can be neglected.

Due to charge conservation for the whole arrangement of Fig. 2.1, the sum over all charges Q_i is constant with any variations of the electrostatic potentials V_j, i.e.,

$$\begin{aligned} 0 \;&= \sum_{i=0}^{M} \partial Q_i = \sum_i \sum_j C_{ij} \cdot \partial V_j \\ &= \sum_j \sum_i C_{ij} \cdot \partial V_j = \sum_j \left\{ \sum_{i \neq j} C_{ij} + C_{jj} \right\} \cdot \partial V_j \;. \end{aligned} \tag{2.14}$$

Since this condition is valid for any changes ∂V_j, the relation

[2] The explicit minus sign in the definition (2.12) compensates for the orientation of the surface element vector $\mathrm{d}\boldsymbol{S}_i$ which is normal *inward* to the conductor's surface.

$$C_{i\Sigma} \equiv -C_{ii} = \sum_{\substack{j=0 \\ j\neq i}}^{M} C_{ij} \tag{2.15}$$

is generally valid. The sum $C_{i\Sigma}$ of the capacitance coefficients C_{ij} is denoted as the *total capacitance* of conductor i. The total capacitance determines the total charge change ∂Q_i on conductor i, if its potential is changed by ∂V_i, while the electrostatic potential of the other conductors are kept fixed:

$$C_{i\Sigma} = \left.\frac{\partial Q_i}{\partial V_i}\right|_{\partial V_{j\neq i}=0} . \tag{2.16}$$

To obtain the total capacitance of a conductor, it is not necessary to know all $\alpha_i(\boldsymbol{r})$. Due to (2.9) or – equivalent – due to (2.15), the total capacitance $C_{i\Sigma}$ of conductor i is directly obtained from $\alpha_i(\boldsymbol{r})$,

$$C_{i\Sigma} = \oint_{S_i} \left\{\epsilon_0 \boldsymbol{\epsilon}(\boldsymbol{r}) \cdot \boldsymbol{\nabla}_{\boldsymbol{r}}\, \alpha_i(\boldsymbol{r})\right\} \mathrm{d}\boldsymbol{S}_i \, . \tag{2.17}$$

Since the $\alpha_i(\boldsymbol{r})$ are independent of $\{V_i\}$, the total capacitance $C_{i\Sigma}$ is determined from the electrostatic potential profile which is obtained for setting electrode i to potential $V_i = 1\,\mathrm{V}$ and keeping all other electrodes grounded ($V_{j\neq i} = 0$).

In addition, the capacitance coefficient fulfill the symmetry relation

$$C_{ij} = -\left.\frac{\partial Q_i}{\partial V_j}\right|_{\partial V_{i\neq j}=0} = C_{ji} = -\left.\frac{\partial Q_j}{\partial V_i}\right|_{\partial V_{j\neq i}=0} , \tag{2.18}$$

which is easy to show from the definitions of C_{ij} and C_{ji}:

$$\begin{aligned} C_{ij} &\overset{(2.12)}{=} -\oint_{S_i} \left\{\epsilon_0 \boldsymbol{\epsilon}(r) \cdot \nabla_{\boldsymbol{r}}\, \alpha_j(\boldsymbol{r})\right\} \mathrm{d}\boldsymbol{S}_i \\ &\overset{(2.7)}{=} -\oint_{S} \left\{\epsilon_0 \boldsymbol{\epsilon}(r) \cdot \nabla_{\boldsymbol{r}}\, \alpha_j(\boldsymbol{r})\right\} \cdot \alpha_i(\boldsymbol{r})\, \mathrm{d}\boldsymbol{S} \, , \\ &\qquad \text{since } \alpha_i(\boldsymbol{r}) = \begin{cases} 1, \text{ if } \boldsymbol{r} \in S_i \, , \\ 0, \text{ if } \boldsymbol{r} \in S_i \text{ with } i \neq j \, . \end{cases} \end{aligned}$$

Here S describes the sum of all conductors' surfaces and, therefore, encloses the whole space V between the conductors. With Gauß' integral theorem, the integral over the surface S can be replaced by an integral of the enclosed volume V,

$$C_{ij} = -\int_V \nabla_{\boldsymbol{r}} \Big[\left\{\epsilon_0 \boldsymbol{\epsilon}(\boldsymbol{r}) \cdot \nabla_{\boldsymbol{r}}\, \alpha_j(\boldsymbol{r})\right\} \cdot \alpha_i(\boldsymbol{r})\Big] \, \mathrm{d}^3\boldsymbol{r} \, .$$

With using $\nabla_{\boldsymbol{r}} \left\{\epsilon_0 \boldsymbol{\epsilon}(\boldsymbol{r}) \cdot \nabla_{\boldsymbol{r}}\, \alpha_j(\boldsymbol{r})\right\} = 0$, valid in the space V due to (2.7), finally, one obtains

$$C_{ij} = -\int_V \left\{\epsilon_0 \boldsymbol{\epsilon}(\boldsymbol{r}) \cdot \nabla_{\boldsymbol{r}}\, \alpha_j(\boldsymbol{r})\right\} \cdot \nabla_{\boldsymbol{r}}\, \alpha_i(\boldsymbol{r})\, \mathrm{d}^3\boldsymbol{r}\ . \tag{2.19}$$

Since the static dielectric tensor $\boldsymbol{\epsilon}(\boldsymbol{r})$ is symmetric in its components, $\nabla_{\boldsymbol{r}}\, \alpha_i(\boldsymbol{r})$ and $\nabla_{\boldsymbol{r}}\, \alpha_j(\boldsymbol{r})$ can be exchanged in the product of (2.19) so that

$$C_{ij} = -\int_V \left\{\epsilon_0 \boldsymbol{\epsilon}(\boldsymbol{r}) \cdot \nabla_{\boldsymbol{r}}\, \alpha_i(\boldsymbol{r})\right\} \cdot \nabla_{\boldsymbol{r}}\, \alpha_j(\boldsymbol{r})\, \mathrm{d}^3\boldsymbol{r}\ .$$

By comparing this result with (2.19), the symmetry $C_{ij} = C_{ji}$ is shown.

The symmetry $C_{ij} = C_{ji}$ reflects the reciprocity of the system: A electrostatic potential change $\partial V_i = \partial V$ on electrode i induces a charge change $\partial Q_j = \partial Q$ on electrode j, while the potentials V_j $(j \neq i)$ are kept constant. In reverse, the same potential change $\partial V_j = \partial V$ on electrode j, while all V_k $(k \neq j)$ are kept fixed, enforces the same charge change $\partial Q_i = \partial Q$ on electrode i: Important is only the electrostatic potential difference between the electrodes, and not its absolute potential for the charge induced on the electrodes. Therefore, the relation (2.11) can be transfered with (2.15) to the differential form

$$\partial Q_i = \sum_{\substack{j=0 \\ j\neq i}}^{M} C_{ij} \cdot \partial\left\{V_i - V_j\right\}\ . \tag{2.20}$$

The capacitance coefficients C_{ij} have been introduced by (2.11) as the linear coefficients between the electrostatic potentials V_i and the charges Q_i of all the conductors. In experiment, usually the concept of partial capacitances is used where those relate the charge *change* ΔQ_i to the *change in the electrostatic potential difference* ('voltage') $\Delta(V_i - V_j)$ between two electrodes. Relation (2.20) demonstrates that the partial capacitances between conductor i and j are numerically the same as the capacitance coefficient C_{ij} in our treatment. That is because charge conservation (2.14) leads to (2.15), which is used to obtain (2.20) from (2.11). For convenience, we can chose one electrode as the reference electrode with electrostatic potential equal to zero (in Fig. 2.1, electrode M with $V_M = 0$).

To determine the single-electron charging energy $E_\mathrm{C} = e^2/2C_\Sigma$ introduced in Chapter 1 for the special conductor arrangement under consideration, one has to evaluate the total capacitance $C_\Sigma \equiv C_{0\Sigma}$ of the metal island favorably by means of (2.17). This relation provides us also with the information that, due to certain shape modification of the metal island or the surrounding electrodes, the total capacitance increases or decreases, respectively. This is quantitatively proven in Appendix B. Knowing this result, geometrically simpler capacitors can be constructed which are mathematically tractable and allow to estimate upper and lower limits for the total capacitance of the original island. This problem is treated in Appendix C. Pushing the electrodes to

infinite distance from the island defines the *self-capacitance* $C_{0\Sigma}^{(\infty)}$ of the island (see Appendix C) which just depends on the shape of the metal island and the surrounding dielectric medium. The self-capacitance gives a lower limit to the total capacitance of the island in the original arrangement. Furthermore, it delivers the highest single-electron charging energy E_{C} achievable for a certain island shape and size,

$$E_{\mathrm{C}} = \frac{e^2}{2\,C_{0\Sigma}} \leq \frac{e^2}{2\,C_{0\Sigma}^{(\infty)}} \; . \tag{2.21}$$

Expressing the capacitance coefficients C_{ij} for an arbitrary arrangement by relation (2.12) allows to identify certain dependencies, for instance, as shown in the next Section, the scaling behaviour of the capacitance coefficients of a conductor arrangement with an inhomogeneous, anisotropic dielectric filling including ions.

2.2 Shrinking of a Metal Conductor Arrangement by Scaling

It was already pointed out that the single-electron charging energy becomes larger the smaller the total capacitance of the metal island is. Reducing the linear spatial dimensions of a conductor arrangement by a scaling factor $s < 1$ (see Fig. 2.2a to Fig. 2.2b), means to replace in (2.6), (2.7) and (2.8) the unprimed original quantities by the primed quantities of the scaled system,

$$\boldsymbol{r}' = s \cdot \boldsymbol{r} \; , \qquad \boldsymbol{\epsilon}'(\boldsymbol{r}') = \boldsymbol{\epsilon}(\boldsymbol{r}) \; , \qquad \rho'_{\mathrm{ion}}(\boldsymbol{r}') = \rho_{\mathrm{ion}}(\boldsymbol{r}) \; . \tag{2.22}$$

Since the same equations have to be solved – with scaled spatial coordinates $\boldsymbol{r}'$ – the functional dependence of the physical quantities in the scaled arrangement can be expressed by those of the unscaled arrangement, under the assumption of the same electrostatic potentials V_j or charge Q_j, respectively, on the conductors for both scaled and unscaled arrangement:

$$\begin{aligned} \Phi'(\boldsymbol{r}') &= \Phi'(s \cdot \boldsymbol{r}) &&= \Phi(\boldsymbol{r}) \; , \\ \Phi'_{\mathrm{ion}}(\boldsymbol{r}') &= \Phi'_{\mathrm{ion}}(s \cdot \boldsymbol{r}) &&= \Phi_{\mathrm{ion}}(\boldsymbol{r}) \; , \\ \alpha'_i(\boldsymbol{r}') &= \alpha'_i(s \cdot \boldsymbol{r}) &&= \alpha_i(\boldsymbol{r}) \; . \end{aligned}$$

The capacitance coefficients C'_{ij} are defined due to (2.12) by an integral over the surface S'_j of conductor j. With the scaling, the area of a surface element on a conductor has decreased by

$$\mathrm{d}\boldsymbol{S}'_j = \mathrm{d}^2\boldsymbol{r}' = s^2 \cdot \mathrm{d}^2\boldsymbol{r} = s^2 \cdot \mathrm{d}\boldsymbol{S}_j \; . \tag{2.23}$$

The definition for C'_{ij} includes the term $\boldsymbol{\nabla}_{\boldsymbol{r}'}\,\alpha'_j(\boldsymbol{r}')$ in the integrand which contributes to the electric field in the arrangement, $\boldsymbol{E}'(\boldsymbol{r}') = -\sum_j \boldsymbol{\nabla}_{\boldsymbol{r}'}\,\alpha'_j(\boldsymbol{r}') \cdot V_j$. From

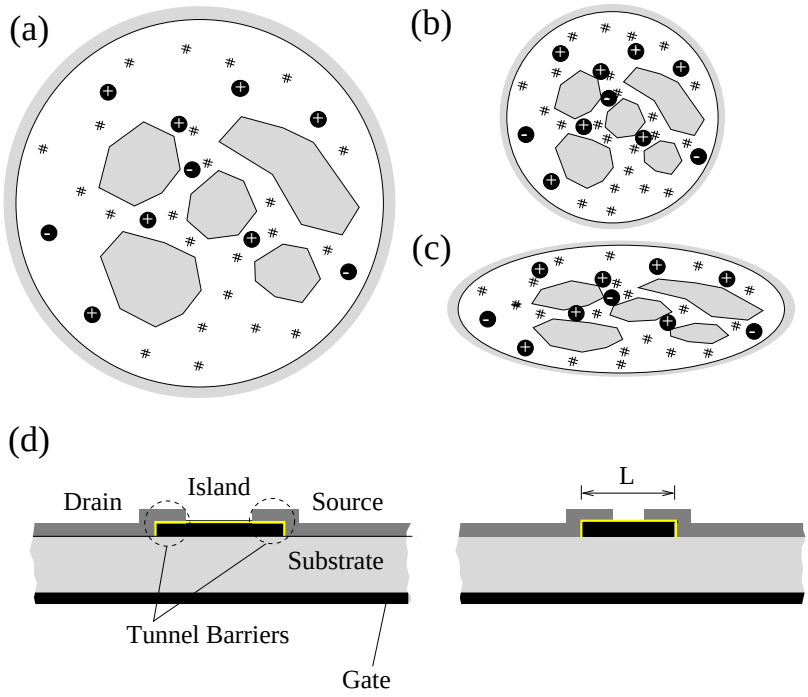

Fig. 2.2. (a),(b) Scaling a conductor arrangement by a factor $s < 1$ decreases the capacitances between the conductors by the factor s. (c) An example which does not follow such a simple linear scaling relation (2.22). (d) Reducing only the island's length L of a single-electron transistor by a factor s while keeping all other spacial lengths unaffected *does not* reduce the total capacitance of the island by s.

$$\boldsymbol{\nabla}_{\boldsymbol{r}'}\,\alpha'_j(\boldsymbol{r}') = \boldsymbol{\nabla}_{s\cdot\boldsymbol{r}}\,\alpha'_j(s\cdot\boldsymbol{r}) = \boldsymbol{\nabla}_{s\cdot\boldsymbol{r}}\,\alpha_j(\boldsymbol{r}) = s^{-1}\cdot\boldsymbol{\nabla}_{\boldsymbol{r}}\,\alpha_j(\boldsymbol{r})\;, \qquad (2.24)$$

it is obvious, that the local electric field strength $|\boldsymbol{E}(\boldsymbol{r})|$ has increased by s^{-1} with decreasing the spatial dimensions in the conductor arrangement by s:

$$\begin{aligned}\boldsymbol{E}'(\boldsymbol{r}') &= -\sum_{j=0}^{M}\boldsymbol{\nabla}_{\boldsymbol{r}'}\,\alpha'_j(\boldsymbol{r}')\cdot V_j \\ &= -\sum_{j=0}^{M} s^{-1}\cdot\boldsymbol{\nabla}_{\boldsymbol{r}}\,\alpha_j(\boldsymbol{r})\cdot V_j = s^{-1}\cdot\boldsymbol{E}(\boldsymbol{r})\;. \qquad (2.25)\end{aligned}$$

It just reflects the fact that the same electrostatic potential difference between conductors is present on a smaller length scale.

Therefore, with (2.23) and (2.24), the capacitance coefficients scale linear with s,

$$C'_{ij} = -\oint_{S'_i}\left\{\epsilon_0\boldsymbol{\epsilon}'(\boldsymbol{r}')\cdot\boldsymbol{\nabla}_{\boldsymbol{r}'}\,\alpha'_j(\boldsymbol{r}')\right\}\mathrm{d}\boldsymbol{S}'_i$$

$$= -\oint_{S_i} \left\{\epsilon_0 \boldsymbol{\epsilon}(\boldsymbol{r}) \cdot s^{-1} \cdot \boldsymbol{\nabla}_{\boldsymbol{r}}\, \alpha_j(\boldsymbol{r})\right\} s^2 \cdot \mathrm{d}\boldsymbol{S}_i = s \cdot C_{ij} \ . \qquad (2.26)$$

This proves the statement of Section 1.1: The total capacitance scales linearly with reducing the spatial lengths,

$$C'_{i\Sigma} = s \cdot C_{i\Sigma} \ . \qquad (2.27)$$

To emphasize, this relation is valid if the scaling of the conductor arrangement follows (2.22). Examples not obeying this relation are shown in Fig. 2.2c and Fig. 2.2d. It is important to realize that we assume that the dielectric matrix does not become 'denser' with scaling: A homogeneous matrix remains homogeneous with the same dielectric constant value. Different, the ion concentration becomes higher by shrinking the arrangement. These scaling rules (2.22) will become important again in Chapter 7 when comparing a single-electron transistor with a conventional field-effect transistor for application in highly integrated digital circuits.

2.3 Total Electrostatic Energy of a Charged Metal Island Surrounded by an Inhomogeneous, Anisotropic Dielectric Containing Ion Charges and Metal Electrodes of Fixed Electrostatic Potential

Our aim is to derive a general expression for the total electrostatic energy of electrons on a metal island of devices described in Chapter 1. This is needed to establish later in Chapter 4 the Hamiltonian of systems containing a quantum dot. Therefore we specify the electrostatic properties obtained in Section 2.1 for the general arrangement (M pieces of equal metal having definite charge or electrostatic potential) to our system consisting of only 'one metal island' and 'M metal electrodes'. The charge Q_0 of the metal island ($i = 0$) can be changed only in multiples of the elementary charge e.

2.3.1 Assuming ΔN Electron Charges on the Island

This quantized charge $Q_0 = \Delta N \cdot (-e)$ can be chosen arbitrarily by transfering (adding or substracting) ΔN electrons from the reference electrode M ('ground') defining the electrostatic potential zero (see Fig. 2.3). This choice of the island charge is independent of the electrostatic potential V_i of the metal electrodes ($i = 1$ to M) which are fixed by external voltage sources applied between each metal electrode and the reference electrode M. The total charge Q_i of each metal electrode i is according to (2.11) linearly related to the electrostatic potential V_i of all metal pieces $i = 0$ to M and to the ion contribution $Q_{i,\mathrm{ion}}$. These surface charges Q_i can change continuously and are built up by slightly shifting the 'free' electrons in the metal against the

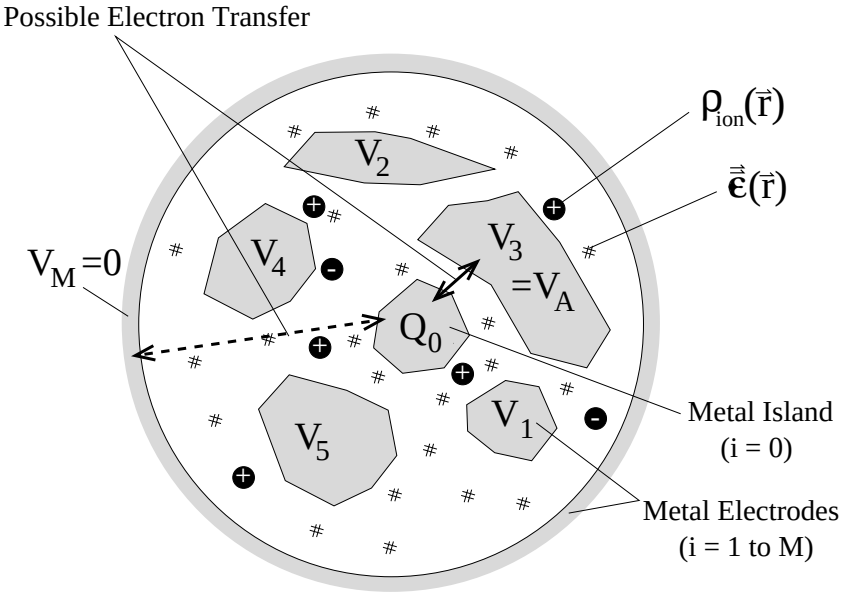

Fig. 2.3. An arbitrary arrangement consisting of one metal island ($i = 0$), M metal electrodes ($i = 1$ to M), and fixed charge distribution $\rho_{\rm ion}(\boldsymbol{r})$ embedded in a dielectric matrix described by $\boldsymbol{\epsilon}(\boldsymbol{r})$. The electrostatic potential V_i is fixed for all electrodes by external voltage sources applied between each electrode and the reference electrode M ('ground') at potential $V_M = 0$. The island is considered as (quasi-)isolated and carries the quantized charge Q_0. When we allow electron exchange between the metal island and the electrode M at potential $V_M = 0$ or with an electrode A at potential $V_{\rm A}$, the system minimizes its energy by adjusting the electron number on the island.

fixed positive charged ions of the crystal lattice associated with the corresponding charge transfer from one electrode to the other through the voltage sources.

The electrostatic potential V_0 of the metal island, derived from (2.11), consists of the contribution Q_0/C_Σ due to its charge Q_0 and the contribution from all other charges in the system,

$$V_0(Q_0;\{V_{j\neq 0}\};Q_{0,\rm ion}) = \frac{Q_0}{C_{0\Sigma}} + \sum_{j=1}^{M} \frac{C_{0,j}}{C_{0\Sigma}} \cdot V_j - \frac{Q_{0,\rm ion}}{C_{0\Sigma}} \,. \qquad (2.28)$$

If we replace (as is formally allowed) the quantized charge Q_0 of the metal island by a continuous charge q, the total electrostatic energy $E^0_{\rm elst}(\Delta N;\{V_{j\neq 0}\})$ of ΔN electrons stored on the island can now be calculated from expression (2.28) by integrating the differential contributions $V_0(q;\{V_{j\neq 0}\};Q_{0,\rm ion}) \cdot {\rm d}q$ from $q = 0$ to $q = Q_0 = -\Delta N\, e$,

$$E^0_{\mathrm{elst}}(\Delta N;\{V_{j\neq 0}\};Q_{0,\mathrm{ion}}) = \int_0^{-\Delta N e} V_0(q;\{V_{j\neq 0}\};Q_{0,\mathrm{ion}})\,\mathrm{d}q$$

$$= -\Delta N e\cdot\sum_{j=1}^{M}\frac{C_{0,j}}{C_{0\Sigma}}V_j + \frac{(\Delta N e)^2}{2\,C_{0\Sigma}} + E_{\mathrm{Q}}(\Delta N;Q_{0,\mathrm{ion}})\,. \qquad (2.29)$$

The first term describes the potential energy of ΔN electrons at the electrostatic potential which is found due to the capacitance divider at the electrically neutral island ($Q_0 = 0$) without the presence of ion charges ($Q_{0,\mathrm{ion}} = 0$). The second term takes into account the work which has to be done to separate the charge $Q_0 = -\Delta N\,e$ from its counter charge spread on the electrodes $j = 1$ to M. This energy term is independent of the electrostatic potential of the electrodes. It is the energy stored in the capacitor formed by the island with all electrodes and charged by $-\Delta N\,e$. One should emphasize here again, that ΔN denotes only the change in the total number of electrons on the metal island in reference to the electrically uncharged island. ΔN can be either positive or negative describing an increase or decrease of the electron number. The third term in (2.29) takes into account any fixed charges in the arrangement,

$$E_{\mathrm{Q}}(\Delta N;Q_{0,\mathrm{ion}}) = \frac{\Delta N e\cdot Q_{0,\mathrm{ion}}}{C_{0\Sigma}}\,, \qquad (2.30)$$

where $Q_{0,\mathrm{ion}}$ is given by (2.8) and (2.13). The quantity ΔE_{Q}, introduced in Section 1.5 to describe the shift of the electrostatic energy of a *single* electron by the presence of charges in the surrounding of the island, is related to $E_{\mathrm{Q}}(\Delta N;Q_{0,\mathrm{ion}})$ by $\Delta E_{\mathrm{Q}} = E_{\mathrm{Q}}(\Delta N;Q_{0,\mathrm{ion}})/\Delta N$, leading to

$$\Delta E_{\mathrm{Q}} = \frac{e\,Q_{0,\mathrm{ion}}}{C_{0\Sigma}}\,. \qquad (2.31)$$

The ion charges felt by the electrons on the island are partially screened by the electrodes. This is correctly included in (2.13) via the boundary conditions defined by (2.8).

Inserting (2.31) into (2.29) yields for the total electrostatic energy the expression

$$E^0_{\mathrm{elst}}(\Delta N;\{V_{j\neq 0}\};Q_{0,\mathrm{ion}}) =$$

$$= \frac{1}{2\,C_{0\Sigma}}\cdot\left\{\Big(-e\,\Delta N\Big)^2 - 2\,e\,\Delta N\cdot\left[\sum_{j=1}^{M}C_{0,j}\,V_j - Q_{0,\mathrm{ion}}\right]\right\} \qquad (2.32)$$

Introduction as an abbreviation the 'offset charge' Q_0^*,

$$Q_0^* = -\sum_{j=1}^{M}C_{0,j}\,V_j + Q_{0,\mathrm{ion}} \qquad (2.33)$$

and using $Q_0 = -e\,\Delta N$ allows to rewrite (2.32) in a simpler form

$$E^0_{\rm elst}(\Delta N; \{V_{j\neq 0}\}; Q_{0,\rm ion}) = \frac{\left(Q_0 - Q_0^*\right)^2}{2\,C_{0\Sigma}} - \frac{\left(Q_0^*\right)^2}{2\,C_{0\Sigma}}\,. \tag{2.34}$$

Since the electrostatic potentials $\{V_{j\neq 0}\}$ and the ion charge distribution are kept constant when electrons are moved between electrode of electrostatic potential zero and the island, the constant term $-(Q_0^*)^2/(2\,C_{0\Sigma})$ depending only on $\{V_{j\neq 0}\}$ and/or $Q_{0,\rm ion}$ can be omitted in determining the energetical favourable value for the charge amount on the island. [3] Therefore, instead of giving the relation (2.29) or (2.32), an expression like

$$E^0_{\rm elst}(\Delta N; \{V_{j\neq 0}\}; Q_{0,\rm ion}) = \frac{\left(Q_0 - Q_0^*\right)^2}{2\,C_{0\Sigma}} \tag{2.35}$$

is found. Formally this expression reminds on the electrostatic energy $Q^2/2C_\Sigma$ stored in a capacitor with capacitance C_Σ when it is charged with $Q = Q_0 - Q_0^*$. But one should be careful in interpreting the quantity Q as the charge being present on the island. Due to the Gauß integral over the dielectric field (2.10), this is given by Q_0. For an isolated conductor, Q_0 cannot change continuously and is restricted to multiple of the elementary charge, $Q_0 = -\Delta N\,e$, whereas Q_0^* shifts continously with the electrostatic potentials V_i of the electrodes capacitively coupling to the island (see (2.33)).

2.3.2 Adjusting ΔN by Electron Exchange either with Ground Electrode M or an Arbitrary Electrode A

For given ΔN, the electrostatic energy term (2.35) describes a parabola as the function of any $V_{j\neq 0}$. For fixed $\{V_{j\neq 0}\}$, the electrostatic energy depends also quadratic on ΔN. Allowing electron exchange with the electrode M with $V_M = 0$, the electrostatic energy $E^0_{\rm elst}(\Delta N; \{V_{j\neq 0}\}; Q_{0,\rm ion})$ – expressed by (2.29) or (2.35) – minimizes by adjusting the electron number ΔN on the island. Minimum is reached for $\Delta N = \Delta N_0$ with

$$-\frac{e}{2} \leq \left(-\Delta N_0\,e + \sum_{j=1}^{M} C_{0,j}\,V_j - Q_{0,\rm ion}\right) \leq \frac{e}{2}\,.$$

Therefore, allowing electrons to rearrange between the island and the electrode of electrostatic potential zero, the energetical minimum is reached when

[3] Actually due to the electrostatic potential differences and ion charges between the electrodes, additional electrostatic energy is stored in the arrangement not included in (2.29) which does not depend on the electron number on the island. Therefore that part is not affected by rearranging electrons between island and the electrode M, and therefore need not to be considered.

the 'charge' $Q = Q_0 - Q_0^*$ is at or within half of the elementary charge e close to zero.

Allowing only electron exchange with the electrode A of electrostatic potential V_A, it has to be taken into account the potential energy of the electrons on the electrode A from where they are taken. By substrating this potential energy $-\Delta N\, e \cdot V_\mathrm{A}$ from (2.29) leads to the modified electrostatic energy

$$E_\mathrm{elst}^{(\mathrm{A})}(\Delta N; \{V_{j\neq 0}\}; Q_{0,\mathrm{ion}}) = E_\mathrm{elst}^{0}(\Delta N; \{V_{j\neq 0}\}; Q_{0,\mathrm{ion}}) + e\,\Delta N \cdot V_\mathrm{A} \qquad (2.36)$$

which is minimized by the rearranging of electrons while $\{V_{i\neq 0}\}$ and $Q_{0,\mathrm{ion}}$ are kept fixed. [4] Minimum is reached for $\Delta N = \Delta N_0^{(\mathrm{A})}$ with

$$-\frac{e}{2} \leq \left(-\Delta N_0^{(\mathrm{A})} e + \sum_{\substack{j=1 \\ j\neq \mathrm{A}}}^{M} C_{0,j}\, V_j - \Big(C_{0\Sigma} - C_{0,\mathrm{A}}\Big) \cdot V_\mathrm{A} - Q_{0,\mathrm{ion}} \right) \leq \frac{e}{2}\,,$$

which yields explicitely for the number of trapped electrons

$$\Delta N_0^{(\mathrm{A})} = \mathrm{int}\left(\sum_{\substack{j=1 \\ j\neq \mathrm{A}}}^{M} \frac{C_{0,j}\, V_j}{e} - \frac{\big(C_{0\Sigma} - C_{0,\mathrm{A}}\big) \cdot V_\mathrm{A}}{e} - \frac{Q_{0,\mathrm{ion}}}{e} + \tfrac{1}{2} \right). \qquad (2.37)$$

For $\Delta N = \Delta N_0^{(\mathrm{A})}$, the *electrostatic potential V_0 of the island*, expressed by (2.28), adjusts close to the electrostatic potential V_A of electrode A,

$$V_\mathrm{A} - \frac{e}{2\,C_{0\Sigma}} \;\leq\; V_0(Q_0 = -e\,\Delta N_0^{(\mathrm{A})}; \{V_{j\neq i}\}; Q_{0,\mathrm{ion}}) \;\leq\; V_\mathrm{A} + \frac{e}{2\,C_{0\Sigma}}\,.$$

The smaller the total capacitance $C_{0\Sigma}$ of the island, the larger the possible deviation of the island's potential V_0 from the electrostatic potential V_A of the respective electrode with which electron exchange is possible.

With $\Delta N_0^{(\mathrm{A})}$ electrons trapped on the island defined by (2.37), the energy barriers $\Delta E_{\mathrm{A}\to\mathrm{I}}$ and $\Delta E_{\mathrm{I}\to\mathrm{A}}$ for recharging the island by a single electron are derived as

$$\begin{aligned}
&\Delta E_{\mathrm{A}\to\mathrm{I}}(\Delta N_0^{(\mathrm{A})} + 1; \{V_{i\neq 0}\}; Q_{0,\mathrm{ion}}) \\
&\quad = E_\mathrm{elst}^{(\mathrm{A})}(\Delta N_0^{(\mathrm{A})} + 1; \{V_{i\neq 0}\}; Q_{0,\mathrm{ion}}) - E_\mathrm{elst}^{(\mathrm{A})}(\Delta N_0^{(\mathrm{A})}; \{V_{i\neq 0}\}; Q_{0,\mathrm{ion}}) \\
&\quad = 2\,E_\mathrm{C} \cdot \Big(1 - f^{(\mathrm{A})}\Big)\,, \qquad (2.38)
\end{aligned}$$

$$\begin{aligned}
&\Delta E_{\mathrm{I}\to\mathrm{A}}(\Delta N_0^{(\mathrm{A})}; \{V_{i\neq 0}\}; Q_{0,\mathrm{ion}}) = -\Delta E_{\mathrm{A}\to\mathrm{I}}(\Delta N_0^{(\mathrm{A})}; \{V_{i\neq 0}\}; Q_{0,\mathrm{ion}}) \\
&\quad = E_\mathrm{elst}^{(\mathrm{A})}(\Delta N_0^{(\mathrm{A})} - 1; \{V_{i\neq 0}\}; Q_{0,\mathrm{ion}}) - E_\mathrm{elst}^{(\mathrm{A})}(\Delta N_0^{(\mathrm{A})}; \{V_{i\neq 0}\}; Q_{0,\mathrm{ion}}) \\
&\quad = 2\,E_\mathrm{C} \cdot f^{(\mathrm{A})}\,, \qquad (2.39)
\end{aligned}$$

[4] Relation (2.36) has to be replaced if different metals for the conductors are involved. In such a case the following relations are modified.

with

$$f^{(\mathrm{A})} = f^{(\mathrm{A})}_{\{V_{i\neq 0}\},Q_{0,\mathrm{ion}}}$$
$$\equiv \mathrm{mod}\left(\sum_{\substack{j=1 \\ j\neq \mathrm{A}}}^{M} \frac{C_{0,j}\, V_j}{e} - \frac{\left(C_{0\Sigma} - C_{0,\mathrm{A}}\right)\cdot V_{\mathrm{A}}}{e} - \frac{Q_{0,\mathrm{ion}}}{e} + \tfrac{1}{2} \right) . \quad (2.40)$$

The result (2.40) generalizes f_{G} (1.22), f_{Q} (1.35) and $f_{\mathrm{G,Q}}$ (1.39), introduced in Chapter 1.

To emphasize again, the results of this Section were derived under the assumption that the metal conductors are made from the same material. Metal conductors of different material show intrinsic contact voltages (see next Chapter 3) and thus modifications are expected.

2.4 Application to an Arbitrary Arrangement of a Single-Electron Transistor with Several Gate Electrodes, All Made of Same Metal

To find the link to the discussion of Chapter 1 and furthermore to prepare also the description of experiments with quantum dots as island in the following Chapters, an arbitrary arrangement of a metal single-electron transistor is sketched in Fig. 2.4a containing now as an extension two gate electrodes G1 and G2. Both are used to tune the electrostatic potential V_0 of the island. The charge state of the island adjusts by electron exchange via tunnel barriers with the source and the drain electrode. Further electrodes might be present also capacitively coupling to the island with capacitance C_{r}, but those are kept at fixed electrostatic potential for convenience. It is of importance to denote the common reference point for the applied voltages since the characteristics of the single-electron transistor are affected by its choice as can be seen from the results derived in the following. For practical purpose, the electrostatic potentials $V_i = V_{i,\mathrm{M}}$ of all electrodes are refered to the source electrode by voltage sources $V_{i,\mathrm{S}}$, i.e., $V_i = V_{\mathrm{M,S}} + V_{i,\mathrm{S}}$ as depicted in Fig. 2.4b. The capacitance coefficients can be replaced by the partial capacitances of the island, and vice versa, i.e., for example $C_{0,\mathrm{S}} = C_{\mathrm{S}}$, $C_{0,\mathrm{D}} = C_{\mathrm{D}}$, $C_{0,\mathrm{G1}} = C_{\mathrm{G1}}$, $C_{0,\mathrm{G2}} = C_{\mathrm{G2}}$. Note that the total capacitance $C_\Sigma = C_{0\Sigma}$ contains the partial capacitances of the island to all electrodes, i.e., in general $C_\Sigma \geq C_{\mathrm{S}} + C_{\mathrm{D}} + C_{\mathrm{G1}} + C_{\mathrm{G2}}$.

For equal potentials for source and drain electrode, i.e., $V_{\mathrm{DS}} = V_{\mathrm{D}} - V_{\mathrm{S}} = 0$, the number of trapped electrons $\Delta N_0 = \Delta N_0^{(\mathrm{S})} = \Delta N_0^{(\mathrm{D})}$ is determined for a certain set of parameters from (2.37) by replacing the index A by S (or D),

$$\Delta N_0^{(\mathrm{S})}(V_{\mathrm{DS}} = 0; V_{\mathrm{G1,S}}; V_{\mathrm{G2,S}}) = \mathrm{int}\left(\frac{C_{\mathrm{G1}}\, V_{\mathrm{G1,S}}}{e} + \frac{C_{\mathrm{G2}}\, V_{\mathrm{G2,S}}}{e} - \frac{Q_0^*}{e} + \tfrac{1}{2} \right) .$$

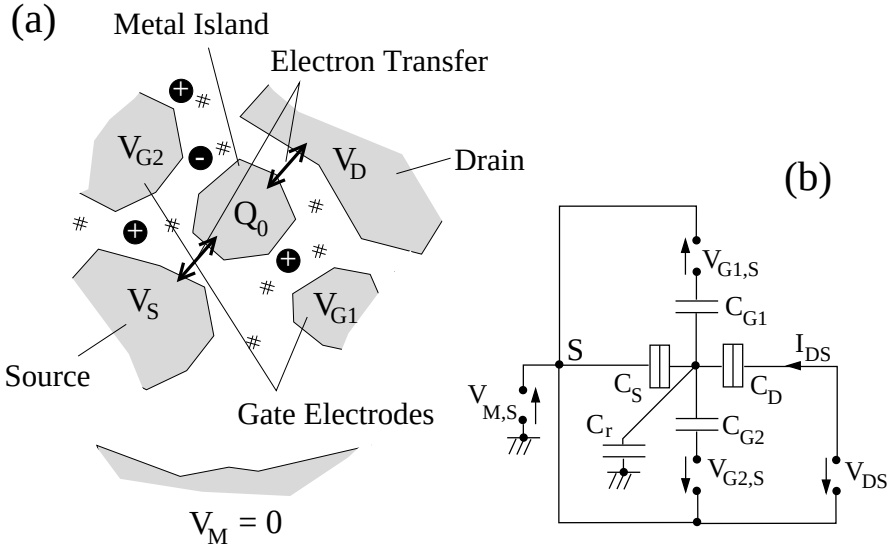

Fig. 2.4. (a) Arbitrary arrangement of a single-electron transistor: Metal island between source, drain and gate electrodes embedded in a dielectric with fixed ion charges. The two gate electrodes G1 and G2 are used to tune the electrostatic potential of the metal island. (b) Equivalent capacitance circuit denoting the partial capacitances and voltages applied in reference to the source electrode.

The offset charge Q_0^* of (2.33) is given by

$$\begin{aligned} Q_0^* &= Q_0^*(V_{\mathrm{DS}} = 0; V_{\mathrm{G1,S}} = 0; V_{\mathrm{G2,S}} = 0) \\ &= -\sum_{\substack{j=1 \\ j \neq \{\mathrm{G1,G2,D}\}}}^{M} C_{0,j}\, V_{j,\mathrm{S}} + Q_{0,\mathrm{ion}} \,. \end{aligned} \tag{2.41}$$

In Fig. 2.5a, the electron number $\Delta N_0^{(\mathrm{S})}$ on the island and the respective borderlines between two adjacent charge states of the island are indicated in the plane of the two gate voltages $V_{\mathrm{G1,S}}$ and $V_{\mathrm{G2,S}}$. Note that only at the borderlines a single-electron transfer is possible and Coulomb blockade exists in the regions in between. The *absolute* values where these borderlines intersect the gate voltage axes are affected by the electrostatic potentials of *all* electrodes and the ion charges, as seen from (2.41). In contrast, insensitive to these are the periodic distance between adjacent borderlines and their common slope. Along the $V_{\mathrm{G1,S}}$ axis the distance is given by $\Delta V_{\mathrm{G1,S}} = e/C_{\mathrm{G1}}$, along the $V_{\mathrm{G2,S}}$ axis given by $\Delta V_{\mathrm{G2,S}} = e/C_{\mathrm{G2}}$. The slope of the borderlines is described by

$$\frac{\partial V_{\mathrm{G1,S}}}{\partial V_{\mathrm{G2,S}}} = -\frac{C_{\mathrm{G2}}}{C_{\mathrm{G1}}} \,. \tag{2.42}$$

The relation (2.42) expresses that along these borderlines a change in the electrostatic potential of the island by $C_{\mathrm{G1}}/C_{\Sigma} \cdot \partial V_{\mathrm{G1,S}}$ due to the potential change $\partial V_{\mathrm{G1,S}}$ on gate electrode G1 is compensated by a change $\partial V_{\mathrm{G2,S}} = -C_{\mathrm{G1}}/C_{\mathrm{G2}} \cdot \partial V_{\mathrm{G1,S}}$ on gate electrode G2. Furthermore, *any path in parallel to or at the borderlines keeps equal energetic barriers for recharging the metal island.* Energy level schemes for distinct situations are also depicted in Fig. 2.5a, valid along the respective line with slope given by (2.42). In general, also a change in the ion charge contribution $Q_{0,\mathrm{ion}}$ can be compensated by changes in the electrostatic potential of one or more gate electrodes.

On the borderlines single-electron transport between source and drain is observable if a small drain-source voltage V_{DS} is applied. Any straight path in the $V_{\mathrm{G1,S}}$ vs. $V_{\mathrm{G2,S}}$ plane *crossing* the borderlines allows to observe periodic Coulomb blockade oscillations. Such straight paths are, for instance, parameterized by

$$V_{\mathrm{G2,S}} = \beta_1 \cdot V_{\mathrm{G1,S}} + \beta_0 \ , \tag{2.43}$$

and realized by varying $V_{\mathrm{G1,S}}$ and taking always $V_{\mathrm{G2,S}}$ proportional to $V_{\mathrm{G1,S}}$. By changing the proportionality constant β_1 and the offset β_0, any straight path can easily be chosen. Each path leads to an effective change in the electrostatic potential of the island. This change can be thought of being caused by a voltage change V^*_{GS} applied to a fictitious gate electrode G*. According to (2.41) we have the identification

$$\begin{aligned} C^*_{\mathrm{G}}\, V^*_{\mathrm{GS}} &\equiv C_{\mathrm{G1}}\, V_{\mathrm{G1,S}} + C_{\mathrm{G2}}\, V_{\mathrm{G2,S}} \\ &= \Big(C_{\mathrm{G1}} + \beta_1\, C_{\mathrm{G2}}\Big) \cdot \left\{ V_{\mathrm{G1,S}} + \frac{\beta_0}{\beta_1 + C_{\mathrm{G1}}/C_{\mathrm{G2}}} \right\} \end{aligned} \tag{2.44}$$

where in the last line (2.43) has been inserted.

The periodicity of the Coulomb blockade oscillations along such a straight path is given by

---

Fig. 2.5. (Right Page) (a) Borderlines between two charge states of the island sketched in Fig. 2.4 at $V_{\mathrm{DS}} = 0$ in the plane of two gate voltages $V_{\mathrm{G1,S}}$ and $V_{\mathrm{G2,S}}$. At these borderlines charge flucuations by a single-electron charge are obserable (for instance as single-electron transport at small V_{DS}). Along paths in parallel to these borderline with slope $-C_{\mathrm{G1}}/C_{\mathrm{G2}}$, equal energetical situation is present for recharging the metal island. (b) Charge states in the plane of the drain-source voltage V_{DS} and a gate voltage path V^*_{GS} crossing the borderlines in (a) (see Fig. 1.8). Insert: Energy level scheme denoting the energy barriers $\Delta E_{\mathrm{S}\to\mathrm{I}}$, $\Delta E_{\mathrm{I}\to\mathrm{S}}$, $\Delta E_{\mathrm{D}\to\mathrm{I}}$ and $\Delta E_{\mathrm{I}\to\mathrm{D}}$ for charging and discharging the island either with source or drain. The relative height of those can be identified for each point in the V^*_{GS} vs. V_{DS} as indicated for one point. (c) For $V_{\mathrm{DS}} > 0$, the regions of stable charge configuration (Coulomb blockade regions) in the $V_{\mathrm{G1,S}}$ vs. $V_{\mathrm{G2,S}}$ plane decrease, the regions of charge flucuations (single-electron tunneling regions) increase. The dotted line in (b) and (c) indicates the common path through the parameter space $(V_{\mathrm{G1,S}}, V_{\mathrm{G2,S}}, V_{\mathrm{DS}})$.

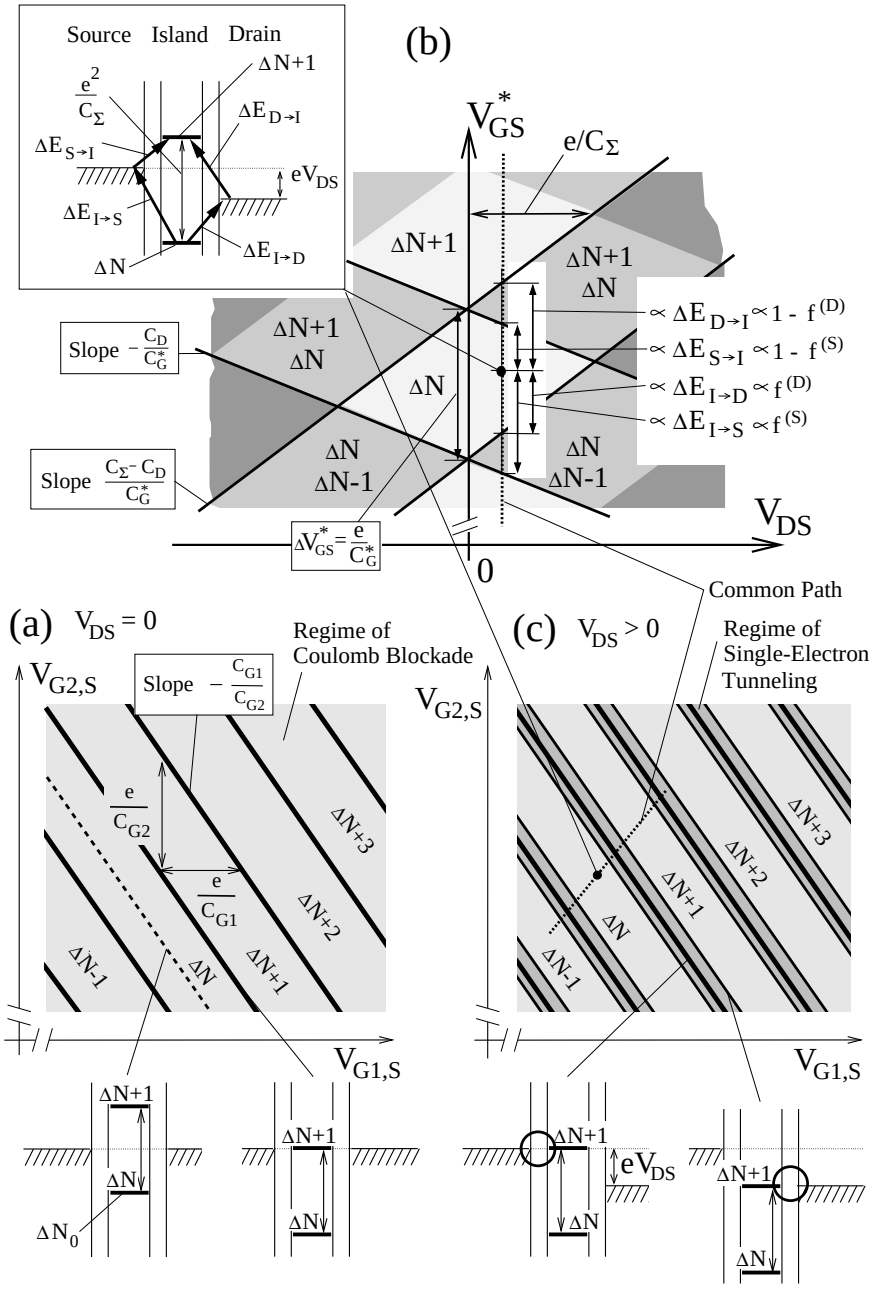
Source Island Drain
(b)
(a) $V_{DS} = 0$
(c) $V_{DS} > 0$
V^*_{GS}
e/C_Σ
V_{DS}
$V_{G2,S}$
$V_{G1,S}$
Slope $-\frac{C_D}{C^*_G}$
Slope $\frac{C_\Sigma - C_D}{C^*_G}$
Slope $-\frac{C_{G1}}{C_{G2}}$
$\Delta V^*_{GS} = \frac{e}{C^*_G}$
Common Path
Regime of Coulomb Blockade
Regime of Single-Electron Tunneling
$\propto \Delta E_{D\to I} \propto 1 - f^{(D)}$
$\propto \Delta E_{S\to I} \propto 1 - f^{(S)}$
$\propto \Delta E_{I\to D} \propto f^{(D)}$
$\propto \Delta E_{I\to S} \propto f^{(S)}$
$\frac{e^2}{C_\Sigma}$
$\Delta E_{D\to I}$
$\Delta E_{S\to I}$
eV_{DS}
$\Delta E_{I\to S}$
$\Delta E_{I\to D}$
ΔN_0

$$\Delta V_{\mathrm{GS}}^{*} = \frac{e}{C_{\mathrm{G}}^{*}} = \frac{e}{C_{\mathrm{G1}} + \beta_1 \, C_{\mathrm{G2}}} \, , \tag{2.45}$$

and hence variable by the chosen proportionality constant β_1:

- For $\beta_1 = -C_{\mathrm{G1}}/C_{\mathrm{G2}}$ the path is parallel to the borderlines and $\Delta V_{\mathrm{GS}}^{*} = \infty$,
- for $\beta_1 = 0$ the periodicity is $\Delta V_{\mathrm{GS}}^{*} = e/C_{\mathrm{G1}}$, i.e., identical to those of tuning only gate G1, and
- for $|\beta_1| \to \infty$, $\Delta V_{\mathrm{GS}}^{*}$ becomes e/C_{G2}, i.e., identical to those of tuning only gate G2. [5]

Building up a drain-source V_{DS} while V_{S} and all other electrostatic potentials of the electrodes except of drain remain fixed, the $I_{\mathrm{DS}}(V_{\mathrm{DS}})$ characteristics of the single-electron transistor can be measured at each point in the $V_{\mathrm{G1,S}}$ vs. $V_{\mathrm{G2,S}}$ plane. Taking such $I_{\mathrm{DS}}(V_{\mathrm{DS}})$ characteristics along a straight path crossing the borderlines, the 'diamond-like' Coulomb blockade regions are obtained in the V_{GS}^{*} vs. V_{DS} plane (see Fig. 2.5b), similar to what is described in Chapter 1 by Fig. 1.8. Starting in the Coulomb blockade region, one of the barriers for recharging the island, i.e.,

$$\Delta E_{\mathrm{S}\to\mathrm{I}} = 2E_{\mathrm{C}} \cdot \left(1 - f^{(\mathrm{S})}\right) \quad , \quad \Delta E_{\mathrm{I}\to\mathrm{S}} = 2E_{\mathrm{C}} \cdot f^{(\mathrm{S})} \, ,$$
$$\Delta E_{\mathrm{D}\to\mathrm{I}} = 2E_{\mathrm{C}} \cdot \left(1 - f^{(\mathrm{D})}\right) \quad , \quad \Delta E_{\mathrm{I}\to\mathrm{D}} = 2E_{\mathrm{C}} \cdot f^{(\mathrm{D})} \, ,$$

with $f^{(\mathrm{S})}$ and $f^{(\mathrm{D})}$ derived from (2.40) to

$$f^{(\mathrm{S})} = \mathrm{mod}\left(\frac{C_{\mathrm{D}} \, V_{\mathrm{DS}}}{e} + \frac{C_{\mathrm{G1}} \, V_{\mathrm{G1,S}}}{e} + \frac{C_{\mathrm{G2}} \, V_{\mathrm{G2,S}}}{e} - \frac{Q_0^{*}}{e} + \tfrac{1}{2}\right) ,$$
$$f^{(\mathrm{D})} = \mathrm{mod}\left(\frac{(C_{\Sigma} - C_{\mathrm{D}}) \, V_{\mathrm{DS}}}{e} + \frac{C_{\mathrm{G1}} \, V_{\mathrm{G1,S}}}{e} + \frac{C_{\mathrm{G2}} \, V_{\mathrm{G2,S}}}{e} - \frac{Q_0^{*}}{e} + \tfrac{1}{2}\right) ,$$

is reduced first with increasing $|V_{\mathrm{DS}}|$. The respective borderlines in the V_{GS}^{*} vs. V_{DS} plane are obtained by evaluating $f^{(\mathrm{S})} = 0$, $1 - f^{(\mathrm{S})} = 0$, $f^{(\mathrm{D})} = 0$ and $1 - f^{(\mathrm{D})} = 0$. The slopes of these borderlines, as given in Fig. 2.5b, are described by

$$\frac{\partial V_{\mathrm{GS}}^{*}}{\partial V_{\mathrm{DS}}} = \frac{C_{\Sigma} - C_{\mathrm{D}}}{C_{\mathrm{G}}^{*}} \, , \quad \text{and} \quad \frac{\partial V_{\mathrm{GS}}^{*}}{\partial V_{\mathrm{DS}}} = -\frac{C_{\mathrm{D}}}{C_{\mathrm{G}}^{*}} \, . \tag{2.46}$$

Note, we have refered all applied voltages to the source electrode. Another choice would affect the slope of the borderlines.

Choosing a certain point in the V_{GS}^{*} vs. V_{DS} plane, certain energy barriers for recharging the island are present. Due to the linear relation between electrode voltages and shift of the electrostatic potential of the island, the

[5] This can be seen starting from the reversed relation $V_{\mathrm{G1,S}} = 1/\beta_1 \cdot V_{\mathrm{G2,S}} - \beta_0/\beta_1$ of (2.43).

relative heights of these barriers can directly be extracted from the charge state scheme of Fig. 2.5b.

For fixed $V_{\mathrm{DS}} > 0$, in Fig. 2.5c the borderlines for vanished charging and discharging barriers, respectively are plotted in the $V_{\mathrm{G1,S}}$ vs. $V_{\mathrm{G2,S}}$ plane. In the dark shaded regions, the charge state of the island fluctuates by one electron, i.e., these are the regions of single-electron tunneling. The regions of stable charge configuration – the Coulomb blockade regions (light shaded) – are reduced in comparison to the case of $V_{\mathrm{DS}} = 0$ in Fig. 2.5a. With increasing V_{DS} further, the regions of Coulomb blockade disappear completely as is evident from Fig. 2.5b. This threshold is reached for $|V_{\mathrm{DS}}| = e/C_{\Sigma}$. Choosing a path in the $V_{\mathrm{G1,S}}$ vs. $V_{\mathrm{G2,S}}$ plane in parallel to the borderlines, *no* 'diamond-like structure' is observed since $\Delta V^{*}_{\mathrm{GS}}$ is infinite. The positive and negative thresholds in V_{DS} are independent of the gate voltage value V^{*}_{GS} along such a path. They depend on the distance in the $V_{\mathrm{G1,S}}$ vs. $V_{\mathrm{G2,S}}$ plane to the adjacent borderline depicted in Fig. 2.5a.

2.5 Summary

In this Chapter, starting from Maxwell's relations, the concepts of *Capacitance Coefficients*, *Total Capacitance* and *Self Capacitance* were introduced for an arrangement of metal conductors embedded in an anisotropic and/or inhomogeneous dielectric matrix. It was shown generally that by scaling the conductor arrangement linearly in all its spatial dimensions, the capacitances change linearly by the same scaling parameter. The self-capacitance can be used to give a lower limit for the total capacitance of a metal island. Expressions for the total electrostatic energy of a charged metal island were derived, generalizing the expressions derived in Chapter 1. Some useful properties of a SET using two gate electrodes for tuning the electrostatic potential of the island were also explained.

For the discussions up to now, it was assumed that the metal conductors consist of the same material. The use of different materials enforces to distinguish carefully between the concept of *Electrostatic Potential*, *Chemical Potential*, and *Electrochemical Potential*. This will be done in the next Chapter.

3. Single-Electron Transistor as a Sensor of Contact Voltage Variations

The sensitivity of a metal single-electron transistor to the electrostatic environment can be used to measure chemical potential variations of conducting materials affected by an external parameter, – for instance, the magnetic field. It enforces to distinguish carefully between the concepts of *Electrostatic Potential*, *Chemical Potential*, and *Electrochemical Potential* to describe electrical transport in such devices which are sensitive to the electric field. The conditions for Coulomb blockade and single-electron charging, as obtained in Chapter 1, have to be modified *if* electrodes of different materials or electronic properties are involved.

3.1 Reminding on the Concepts of Electrostatic, Chemical and Electrochemical Potential

Let us consider two macroscopic *electrically uncharged* metal conductors i and j of different material. Usually they have different *chemical potentials* $\mu_i^{\rm ch}$ and $\mu_j^{\rm ch}$, i.e., there exists a difference in their Fermi levels towards the same reference. [1] Or in other words, different energies W_i, W_j are required in thermodynamic equilibrium for taking off an electron from the electrically uncharged metals and bringing that electron into the vacuum far away at rest, i.e., to the vacuum energy level $\varepsilon(x = \infty)$. The jump W_i or W_j between metal and vacuum level is called *work function of the metal*. If electron exchange is allowed between both metals – for instance by a metal wire (see Fig. 3.1b) –, electrons will move from the metal of higher chemical potential to the metal of lower chemical potential to get both in thermodynamical equilibrium. Due to this electron exchange, both metals are electrically charged: the one with the higher chemical potential to positive, the one of lower chemical potential to negative. The charges are present as surface charges on the metal conductors causing an electric field between both metals. Because of the macroscopic

[1] The chemical potential usually denotes the difference in the inner energy for a given temperature T between the $(N + 1)$- and the N-electron system, where the electron systems are compensated in their electrical charge by background ions. For mesoscopic metals, single-electron charging effects occur contributing by $E_{\rm C}$ to the energy. For macroscopic metals, this electrostatic energy part is negligible, and therefore ignored.

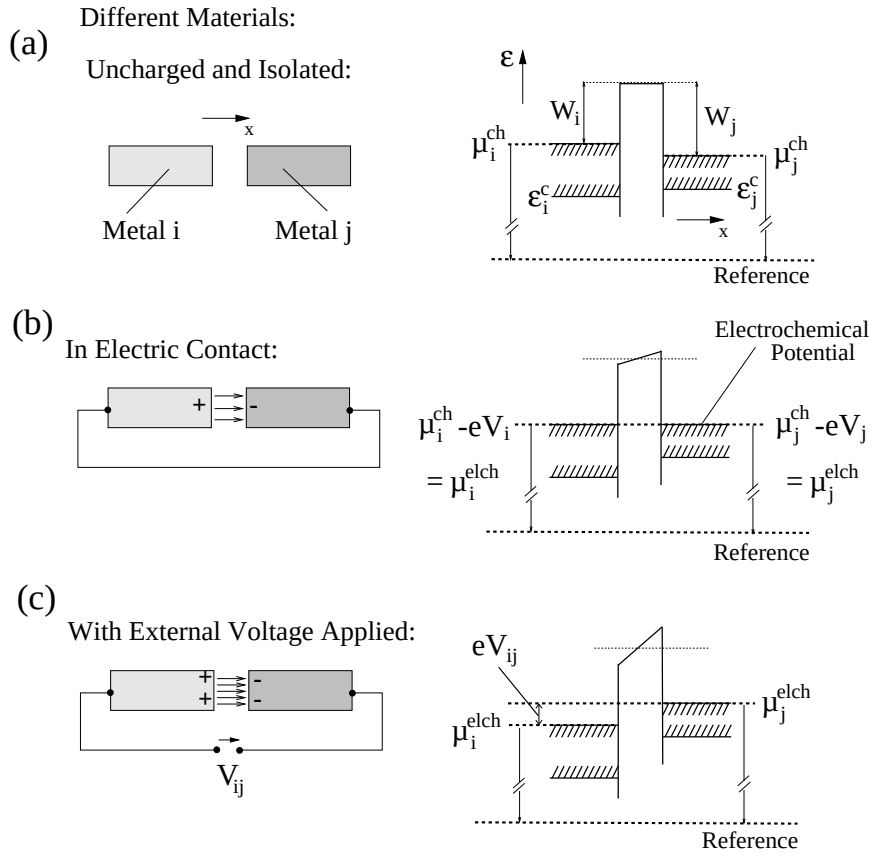

Fig. 3.1. Arrangement of two metal conductors of different materials: (a) Energy scheme of the conduction bands of two electrically uncharged metal conductors of different chemical potentials $\mu_i^{\rm ch}$ and $\mu_j^{\rm ch}$ (work functions), i.e., their Fermi levels lie differently with respect to a reference. Often the vacuum level is taken as the reference by setting $\varepsilon(x=\infty)=0$. The conduction band minima are denoted by $\varepsilon_i^{\rm c}$ and $\varepsilon_j^{\rm c}$. (b) By connecting both electrodes, electron exchange equilibrates the Fermi levels – a contact voltage (electrostatic potential difference) is built up between both metals. The electrochemical potential, considered as being locally composed of the electrostatic potential and the chemical potential, is the same everywhere in the combined system. (c) The electrochemical potentials of the electrodes are shifted against each other by an externally applied voltage V_{ij}. The jumps W_i, W_j in all three cases remain the same.

size, the electron density in the bulk of the metals is almost not affected by this electron exchange. The integral over the electric field along a path connecting the bulks of both metals defines the *electrostatic potential difference* $V_i - V_j$ between both metals. The Fermi level of the metal i shifts by the change in the electrostatic potential V_i. Thermodynamical equilibrium between both metals is obtained if $\mu_i^{\rm ch} - e \cdot V_i = \mu_j^{\rm ch} - e \cdot V_j$, i.e., the chemical

potential difference is just compensated by the electrostatic energy difference due to electrically charging (see Fig. 3.1b). An intrinsic *contact voltage* V_{ij}^{C} (Volta voltage) is built up between both metals given by the difference of the chemical potentials and hence also of the work functions of the metals,

$$e \cdot V_{ij}^{\mathrm{C}} = \mu_i^{\mathrm{ch}} - \mu_j^{\mathrm{ch}} \,. \tag{3.1}$$

The sum $\mu_i^{\mathrm{elch}} \equiv \mu_i^{\mathrm{ch}} - e \cdot V_i$ is denoted as the *electrochemical potential* of the metal i. It defines the Fermi level of the *electrically charged* metal with respect to the reference. In thermodynamical equilibrium, the electrochemical potential is the same everywhere in the combined system. This is also correct for an inhomogeneous material,

$$\mu^{\mathrm{elch}}(\boldsymbol{r}) = \mu^{\mathrm{ch}}(\boldsymbol{r}) - e\,V(\boldsymbol{r}) \,. \tag{3.2}$$

Locally the electrochemical potential can be considered as being composed of the local electrostatic energy of an electron feeling the local electrostatic potential $V(\boldsymbol{r})$ and the local chemical potential $\mu^{\mathrm{ch}}(\boldsymbol{r})$ which depends on the local material parameters. At $T = 0$, the electrochemical potential separates the energies of occupied and unoccupied electronic states in the metal.

By putting a voltage source between both metals (see Fig. 3.1c), the electrochemical potential of the metal i is shifted against the electrochemical potential of metal j. An additional electrical connection between both metal conductors (for instance by a tunnel junction or by inserting a metal island with two tunnel junctions) would cause a permanent electron flow from the metal of higher electrochemical potential to the metal of lower electrochemical potential. [2] In this sense the metal conductors are out of thermodynamical equilibrium due to the externally applied bias voltage. If the electrical connection does not exists or is very weak, each metal can be described by a Fermi-Dirac function with the electrochemical potential of the respective metal, and the applied voltage V_{ij} determines the difference in the electrochemical potential of both conductors:

$$\mu_i^{\mathrm{elch}} - \mu_j^{\mathrm{elch}} = e \cdot V_{ij} \,. \tag{3.3}$$

Therefore, the total electrostatic potential difference $V_i - V_j$, defined by the integral over the electric field along a path connecting both metals, is given by the *sum* of the intrinsic contact voltage V_{ij}^{C} and the externally applied voltage V_{ij}:

$$V_i - V_j = V_{ij} + V_{ij}^{\mathrm{C}} \,. \tag{3.4}$$

The consequence of such intrinsic contact voltages for the characteristics of a single-electron transistor is discussed in the following Section.

[2] Usual voltmeters are measuring the electrochemical potential difference and *not* necessarily the electrostatic potential difference between two terminals.

3.2 Single-Electron Transistor Made of Different Metals

As presented in Chapter 1, a single-electron transistor is sensitive to changes in the electrostatic environment of the metal island: Adding a charge or varying the electrostatic potential of a nearby gate electrode affects the transport characteristics of the single-electron transistor. Or in other words, the electrons on the island feel the additional electric field created by such changes.

As pointed out in the previous Section, the electrostatic potential between electrodes of different electronic properties is not only defined by the externally applied voltage, but also by the intrinsic contact voltage due to the work function difference between the electrodes. To see the consequence for single-electron devices, let us consider the following arrangement: In Fig. 3.2a, a sketch of a single-electron transistor is given which consists of same metal for the electrodes and for the island. As a function of the gate voltage $V_{\rm GS}$, Coulomb blockade oscillations are observable as described in Chapter 1. By replacing the gate electrode by an electrode of *different* metal (see Fig. 3.2b), an additional contact voltage $V_{\rm GS}^{\rm C}$ occurs – defining already at applied gate voltage $V_{\rm GS} = 0$ an electrostatic potential difference between gate electrode and leads. Due to this replacement, the electrostatic potential of the island is shifted (holding $V_{\rm GS} = 0$) and $\Delta N_{\rm C}$ additional electrons are trapped on the island,

$$\Delta N_{\rm C} = {\rm int}\left(\frac{C_{\rm G} V_{\rm GS}^{\rm C}}{e} + \tfrac{1}{2}\right) , \tag{3.5}$$

in analogy to (1.17). With varying the gate voltage $V_{\rm GS}$, the Coulomb-blockade oscillations appear shifted along the gate voltage axis by $\Delta V_{\rm GS} = -V_{\rm GS}^{\rm C}$ (see Fig. 3.2b).

What happens if one of the lead electrodes, for instance the drain electrode (Fig. 3.2c), is replaced by an electrode of different metal? Again, an intrinsic contact voltage $V_{\rm DS}^{\rm C}$ occurs between drain electrode and other electrodes. The electrochemical potential difference between source and drain electrode is *not* affected by the intrinsic contact voltage. As described in the previous Section, a difference in the electrochemical potential, i.e., a non-equilibrium situation between both lead electrodes occurs if $V_{\rm DS}$ is applied defined by an external voltage source, driving the current $I_{\rm DS}$. [3] However due to the intrinsic contact voltage $V_{\rm DS}^{\rm C}$, the electrostatic potential of the island is shifted, and therefore, for $V_{\rm GS} = 0$, $\Delta N_{\rm C}$ additional electrons are trapped on the island,

$$\Delta N_{\rm C} = {\rm int}\left(\frac{C_{\rm D} V_{\rm DS}^{\rm C}}{e} + \tfrac{1}{2}\right) . \tag{3.6}$$

The Coulomb blockade oscillations appear again shifted along the gate voltage axis – now by $\Delta V_{\rm GS} = -C_{\rm D}/C_{\rm G} \cdot V_{\rm DS}^{\rm C}$.

[3] Usual experiments are performed with the sample at low temperatures but the measurement setup at room temperture. If wires of different metal are used, thermal voltage do create differences in the electrochemical potential. The thermal voltages should be avoided or be compensated.

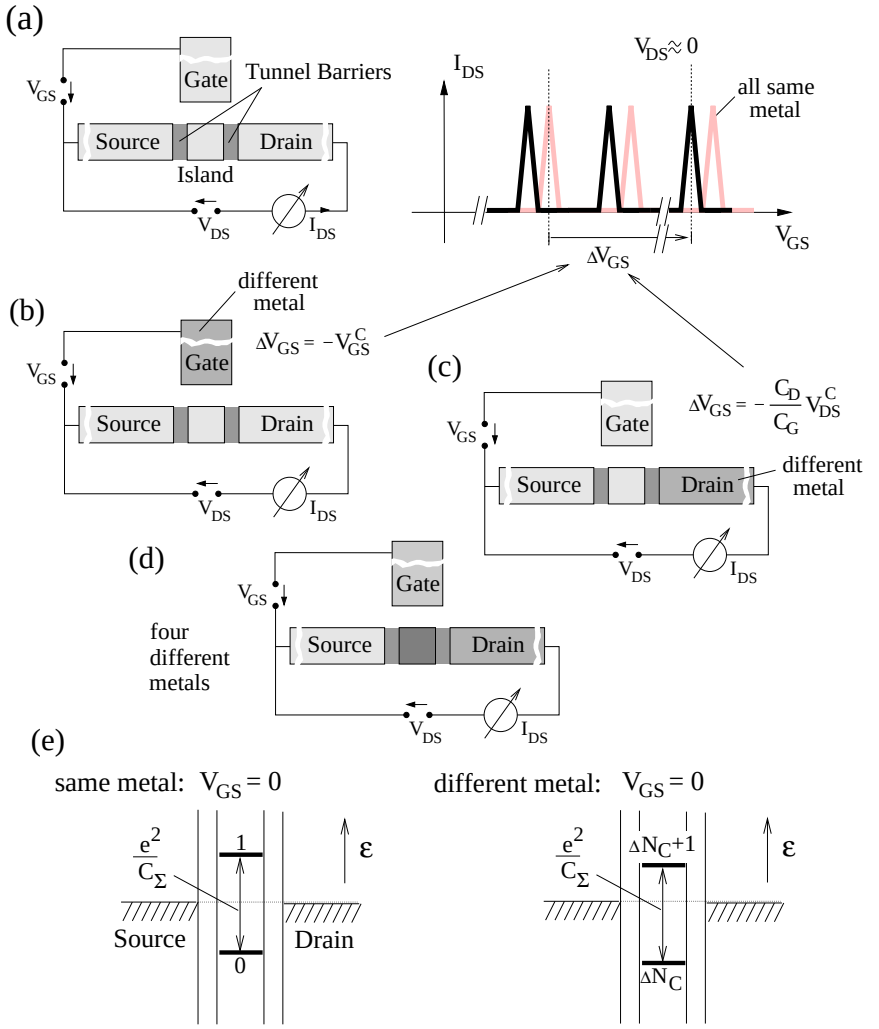

Fig. 3.2. Effect of intrinsic contact voltages on the transport properties of a single-electron transistor: (a) Sketch of a single-electron transistor made of the same metal for all electrodes. As a function of the gate voltage V_{GS}, Coulomb blockade oscillations are observable (grey-coloured line). (b) Replacing the gate electrode of a single-electron transistor by a electrode of different metal shifts the Coulomb blockade oscillations (black coloured line) (c) Replacing the source or the drain electrode by an electrode of different metal also shifts the Coulomb blockade oscillations. (d) Replacing all electrodes around the island by electrodes of different metals causes a similar shift as for (b) and (c) (see text). (e) The energy schemes of an single-electron transistor made of only one kind of metal and made of different metals are shown for $V_{GS} = 0$. Due to the intrinic contact voltages, ΔN_C additional electrons are trapped if different metals are used. The electrochemical potential difference between source and drain remains uneffected since it is given by V_{DS} defined by an external voltage source.

For the case that all electrodes around the metal island are replaced by electrodes all made of different metals (see Fig. 3.2d), ΔN_{C} is given by

$$\begin{aligned} \Delta N_{\mathrm{C}} &= \mathrm{int}\left(\frac{C_{\mathrm{D}}V_{\mathrm{DI}}^{\mathrm{C}} + C_{\mathrm{S}}V_{\mathrm{SI}}^{\mathrm{C}} + C_{\mathrm{G}}V_{\mathrm{GI}}^{\mathrm{C}}}{e} + \tfrac{1}{2}\right) \\ &= \mathrm{int}\left(\frac{C_{\Sigma}V_{\mathrm{GI}}^{\mathrm{C}}}{e} + \tfrac{1}{2}\right) , \end{aligned} \tag{3.7}$$

where the last line is obtained for the case $C_{\Sigma} = C_{\mathrm{D}} + C_{\mathrm{S}} + C_{\mathrm{G}}$ and $V_{\mathrm{GI}}^{\mathrm{C}} = V_{\mathrm{SI}}^{\mathrm{C}} = V_{\mathrm{DI}}^{\mathrm{C}}$. Here $V_{i,\mathrm{I}}^{\mathrm{C}}$ denotes the contact voltage between the type of metal used for the island and the metal of electrode i ($i \in \{\mathrm{S}, \mathrm{D}, \mathrm{G}\}$). The Coulomb blockade oscillations are shifted by

$$\Delta V_{\mathrm{GS}} = -\frac{C_{\mathrm{D}}V_{\mathrm{DI}}^{\mathrm{C}} + C_{\mathrm{S}}V_{\mathrm{SI}}^{\mathrm{C}} + C_{\mathrm{G}}V_{\mathrm{GI}}^{\mathrm{C}}}{C_{\mathrm{G}}} \tag{3.8}$$

along the V_{GS} axis.

The systems just described are realized in the following experiment: A metal single-electron transistor is fabricated on top of a microscopic tip which is then scanned over a substrate containing enclosures of other conductive materials at the surface (see Fig. 3.3). As a function of the position, the local contact voltage contribute to the local electrostatic potential difference between the SET and the substrate. Monitoring the changes in the SET characteristics, the SET can be used as a local probe for the electrostatic potential variations along the substrate surface. Such an application has already been demonstrated by M. Yoo and coworkers [59] [4]: With reducing the distance between SET and substrate, the capacitance between substrate and SET island increases roughly to $1/d$ with the distance d. Therefore the Coulomb blockade oscillations, observable as a function of the externally applied SET-substrate voltage (see Fig. 3.3b), decrease in their periodicity, squeezing to a fix point on the SET-substrate voltage axis where the electrostatic potential between SET island and substrate becomes zero. In case of no additional charges trapped between SET and surface, at that point, the externally applied SET-substrate voltage just compensates for the intrinsic contact voltage between SET and substrate. Such an SET probe on a scanning tip can be considered as an alternative to a scanning force microscope running in the Kelvin probe mode where the local electrostatic force between tip and substrate is minimized by tuning the tip-substrate voltage [59].

Extracting the real contact voltage in the thermodynamical sense from such measurements is usually complicated due to the presence of charges being trapped between the tip and the substrate. Under circumstances it might be easier to measure the variations of the intrinsic contact voltage as a

[4] The setup was used to probe electrostatic potential fluctuations in GaAs/AlGaAs heterostructures and later to investigate two-dimensional electron systems in high magnetic fields [60].

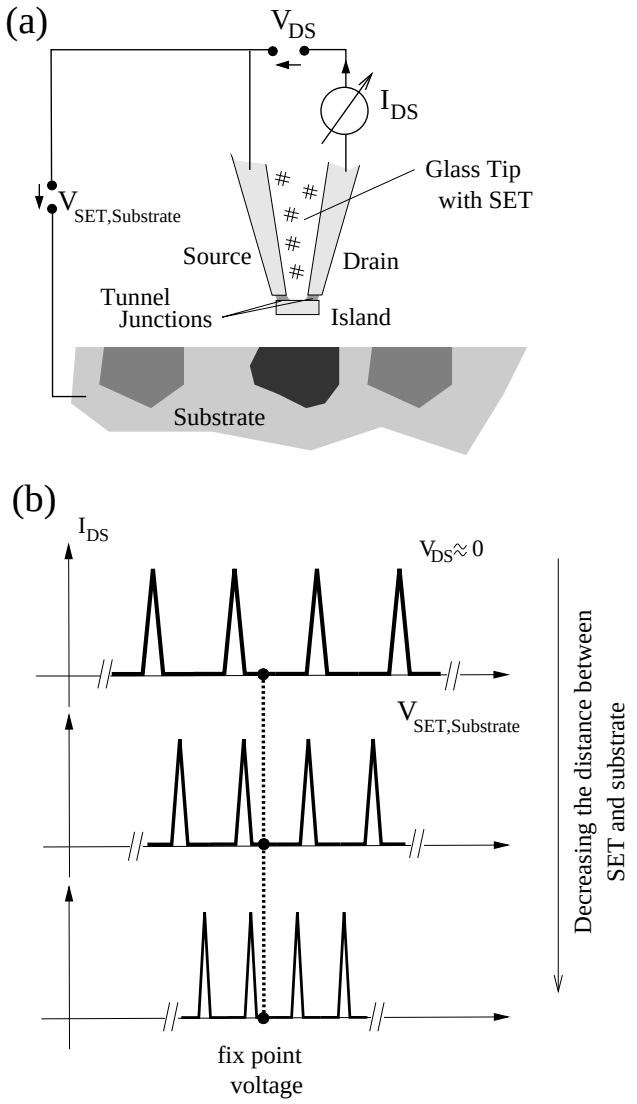

Fig. 3.3. (a) A single-electron transistor on a glass tip probing a conductive substrate with metal enclosures at the surface. (b) Measuring the current I_{DS} through the SET as a function of the SET-substrate voltage reveal Coulomb blockade oscillations (CBO). With decreasing the distance between SET and substrate, the periodicity of the CBO reduces, the CBO squeeze to a fix point voltage on the SET-substrate voltage axis basically given by the local intrinsic contact voltage (adopted from M. Yoo et al. [59]).

function of other parameters like temperature, pressure or applied magnetic field. An example for such a measurement will be presented in the following Section. Compressibility measurements of two-dimensional hole system, i.e., variations of the chemical potential with the carrier concentration, were performed by S. Ilani et al. [61] using a similar setup as presented in the following.

3.3 Metal Single-Electron Transistor as a Probe of Chemical Potential Variations of a Two-Dimensional Electron System in High Magnetic Fields

Measuring the Hall effect on a two-dimensional electron system in high magnetic field at temperatures typically below 4 K leads to the observation of the *Integer Quantum Hall Effect* (IQHE), and in high quality samples and at lower temperature in addition to the observation of the *Fraction Quantum Hall Effect* (FQHE) (see for review [62]). The IQHE was discovered in 1980 by K. von Klitzing [63], the FQHE in 1982 by D.C. Tsui, H.L. Störmer, and A.C. Gossard [64]. Since the year 1990, the IQHE is used as the international resistance standard. The quantized Hall resistance values are in agreement with $h/(i\,e^2)$ (i is an integer number) within an uncertainty of $2.4 \cdot 10^{-8}$ [65, 66] and no difference between samples (including different materials) is observed to an uncertainty of $3.5 \cdot 10^{-10}$ [67, 68]. Although such a fundamental effect is observed and used in metrology, still a basic controversy exists where microscopically the externally biased current is flowing through the two-dimensional electron system (2DES) to build up the well-defined Hall voltage. Local probes – like the single-electron transistor as a local electrometer – are an ideal tool to obtain information about the local electrostatic potential variations in the 2DES under quantum Hall conditions. Measurements using a stationary SET are presented in [69, 70, 71, 27, 31]. A SET as a scanning probe was used by A. Yacoby and coworkers [60]. In the following, we discuss results obtained in our group [72], showing that indeed the SET is sensitive to variations of intrinsic contact voltages.

Fig. 3.4a shows a sketch of a metal single-eletron transistor which is deposited on top of a GaAs/$Al_{0.33}Ga_{0.67}As$ heterostructure. Such a typical heterostructure contains a two-dimensional electron system (2DES) at the AlGaAs-GaAs heterojunction [73] 85 nm below the surface: Due to the lower conduction band minimum of GaAs, the electrons from the donors in the AlGaAs layer have moved to the GaAs. They are attracted by the remaining positive charged donors and are therefore trapped at the interface between the GaAs and the AlGaAs layer. The strong triangular-shaped confining potential freeze in their motion in z direction [74]: Electrons can only move freely only along the interface in x and y direction. At low enough electron concentration and temperature, a two-dimensional electron system is formed.

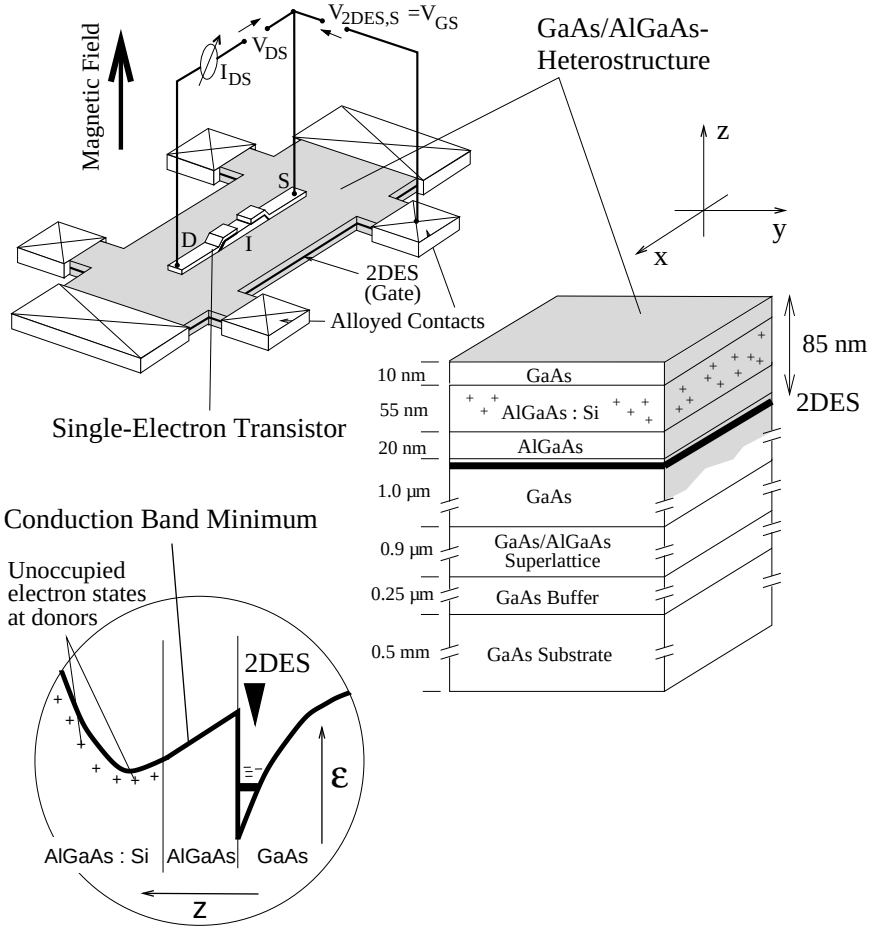

Fig. 3.4. Sketch of a metal single-electron transistor deposited on top of a GaAs/AlGaAs heterostructure containing in a depth of about 85 nm a two-dimensional electron system (2DES with electron concentration $n_s = 2.9 \cdot 10^{15}$ m^{-2}, electron mobility $\mu_e = 40$ m^2/Vs at $T = 4$ K). The fabrication of the SET and the Coulomb blockade oscillations have already been presented in Fig. 1.7.

Due to the spacial separation between ionized donors and electrons – denoted as modulation doping [75], scattering of electrons at the donor potentials is reduced. Two-dimensional electron systems, defined in such modulation-doped heterostructure, have electron concentrations typically in the range of $5 \cdot 10^{14}$ to $5 \cdot 10^{15}$ electrons per m^2 and electron mobilities [5] of about 10^2 m^2/Vs, leading to a ballistical mean free path of several tens of μm.

The SET structure was already presented in Chapter 1. Due to the small size of the electron island and the small area of the tunnel junctions (0.1 μm

[5] Up to about $3 \cdot 10^3$ m^2/Vs has been recently reported by L. Pfeiffer (Bell Labs).

by 0.1 μm), the total capacitance of the island is small leading to a single-electron charging energy $E_C \approx 0.1$ meV. Alloyed ohmic contacts to the 2DES allow to use the 2DES as a gate electrode for the SET island. With changing $V_{2DES,S}$, Coulomb blockade oscillations are observed at temperature $T \approx 0.1$ K.

Applying a magnetic field B perpendicularly to the plane of the 2DES, the Coulomb blockade oscillations – measured as a function of the externally applied voltage $V_{2DES,S}$ – shift with magnetic field (see Fig. 3.5a). As will become clear from the following, this shift of the CBO reflects the variations of the chemical potential of the 2DES at constant electron concentration with changing the magnetic field.

The electrostatic potential difference between the SET and the 2DES is proportional to the intrinsic contact voltage between aluminum electrodes and the 2DES in the heterostructure. With applying the homogeneous magnetic field B, the chemical potentials of both materials are affected, causing a change of the contact voltage given by the relation [6]

$$e \cdot \frac{\mathrm{d}V^{\mathrm{C}}_{2DES,SET}}{\mathrm{d}B} = \frac{\mathrm{d}\mu^{\mathrm{ch}}_{2DES}}{\mathrm{d}B} - \frac{\mathrm{d}\mu^{\mathrm{ch}}_{SET}}{\mathrm{d}B} \; . \tag{3.9}$$

Since the effect of the magnetic field on the aluminum electrodes in the non-superconducting state is negligible, the magnetic field effect on the 2DES dominates the contact voltage changes between the aluminum electrodes of the SET and the 2DES gate. Therefore the shift of the CBO, measured in $V_{2DES,S}$, should reflect the chemical potential changes of the 2DES with magnetic field.

With B applied perpendicularly to the 2DES plane, the energy spectrum of the 2DES splits into a series of Landau levels (see Fig. 3.5b). The energy difference between Landau levels increased linearly with B and at the same time the density of states within each Landau level increases with B. Electronic states become available at lower energy. Therefore the electrons in the 2DES are redistributed from Landau levels of higher energy to Landau levels of lower energy, i.e., with increasing B, a Landau level is depopulated at each integer value of the Landau level filling factor ν, defined as $\nu = hn_s/Be$, where n_s denotes the sheet electron concentration in the 2DES. Thus μ^{ch}_{2DES} changes in the zigzag-like manner as observed in the measurements shown in Fig. 3.5a. As long as the Fermi level is within a Landau level, μ^{ch}_{2DES} increases continuously with B. This corresponds to shifts towards more negative $V_{2DES,S}$ values in Fig. 3.5a. Around integer filling factors, sharp changes in the chemical potential indicate just the complete depopulation of a Landau level. There the Fermi level is situated between two Landau levels: The bulk of the

[6] A depletion in the 2DES electron density due to the contact voltage between SET and 2DES has been compensated by applying a constant bias voltage between SET and 2DES. There might remain a modulation of the electron density in the 2DES by mechanical strain produced at the edges of the SET at the heterostructure surface.

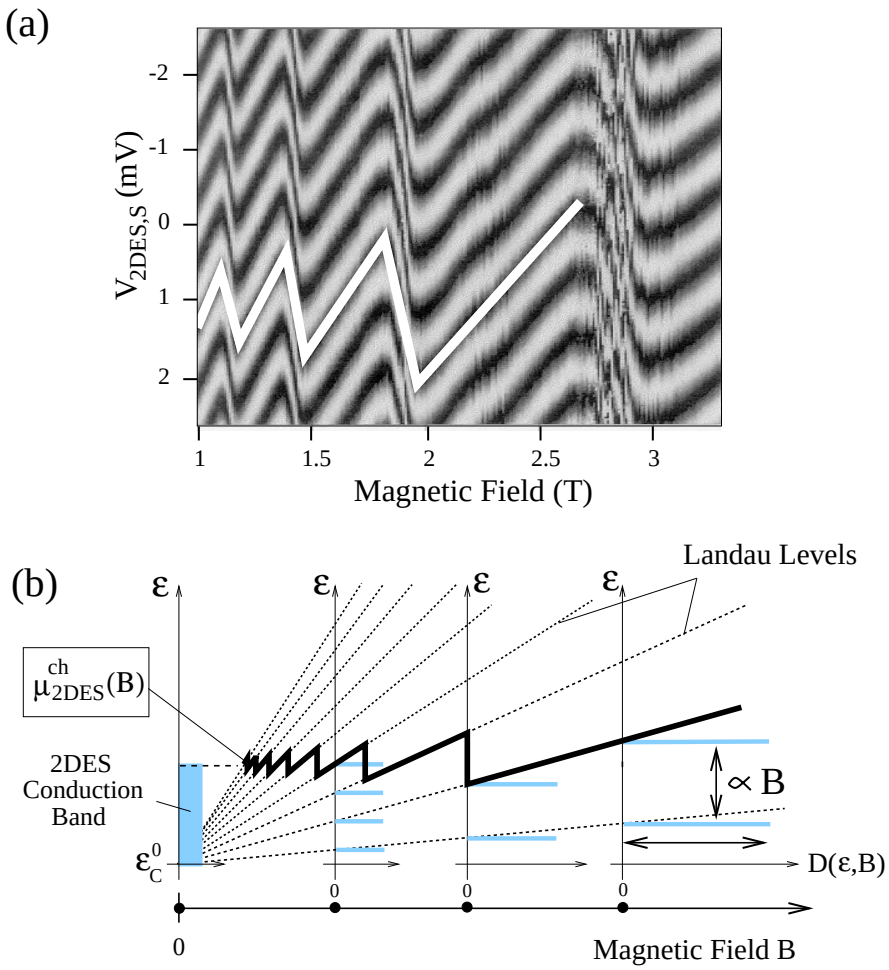

Fig. 3.5. Variation of the chemical potential of the 2DES with magnetic field at constant electron concentration: (a) Measured current through the SET shown in greyscale ('light' low current, 'dark' high current) as a function of gate voltage $V_{GS} = V_{2DES,S}$ and of magnetic field. The current modulation versus V_{GS} at constant magnetic field B reflects the Coulomb blockade oscillations. The zigzag-like shifts of the Coulomb blockade oscillations – marked by the white line – reflect the variations of the chemical potential of the 2DES with magnetic field. (b) Sketch of the chemical potential variations (solid zig-zag line) of an idealized two-dimensional electron system (spin-splitting of the Landau levels neglected) as a function of applied magnetic field B. The density of states $D(\varepsilon, B)$ of the 2DES is depicted in four diagrams for the marked distinct B fields.

2DES behaves at low temperature as an insulator decoupling the local 2DES below the SET island from the contact where $V_{2DES,S}$ is applied. Therefore, around integer filling factors the 2DES cannot work as a gate electrode for

the SET as it is observed in Fig. 3.5a around magnetic field value $B = 2.8$ T. This effect is less pronounced at this temperature at large integer filling factors, i.e., at small magnetic field values, where the conductivity of the bulk 2DES is still large enough to establish thermodynamical equilibrium within the whole 2DES at time scales accessible in the experiment. The slopes of the shifts in the chemical potential give information about the effective mass of the electrons, the electron-electron interaction, the spin splitting and the Landau level broadening.

Due to the small island size, the SET is able to detect the chemical potential change of the *local* 2DES region below the SET island. To demonstrate this ability, we measured the change of the chemical potential variations versus magnetic field for different values of the *local electron concentration*. To change the local electron concentration, a sidegate electrode is deposited on the heterostructure, 5 μm away from the SET (see Fig. 3.6a). Applying a bias voltage between the sidegate electrode and the 2DES, the local electron concentration near the SET is tuned. Calculated electron concentration profiles are shown in Fig. 3.6b for the geometry sketched in the inset. In Fig. 3.6d, the chemical potential variations with magnetic fields are shown, measured at different sidegate voltages $V_{\mathrm{Side,S}} = 0$ V to -9 V. These curves reflect the shift of the CBOs, directly obtained by using the feedback circuit sketched in Fig. 3.6c. This feedback loop keeps the current I_{DS} through the SET constant which means that according to Fig. 3.6 the feedback signal gives directly the zigzag shift of the CBO as a function of B. It can also directly be used to compensate for the contact voltage present between SET and 2DES at $B = 0$ by applying an additional voltage to the 2DES. Actually this configuration assures that the electrostatic potential difference between the SET and the 2DES is kept constant when changing B. Therefore, the presence of the SET does not cause an additional depletion effect on the 2DES when changing B. As seen in Fig. 3.6d, the measured curves scale in the B axis for all $V_{\mathrm{Side,S}}$ values. Therefore, the shift ΔB reflects the change of the local electron concentration n_{s}. With decreasing the electron concentration by

Fig. 3.6. (Right page) Variation of chemical potential versus magnetic field for different local electron concentrations of the 2DES: (a) In addition to the setup of Fig. 3.4a, a sidegate electrode is added. (b) Calculated electron concentration profile $n_{\mathrm{s}}(y)$ for the geometry given in the inset for different sidegate electrode voltages $V_{\mathrm{side,2DES}}$ (taken from relations given in Ref. [76]; 'frozen surface model' with the parameters $d = 90$ nm, $V_{\mathrm{del}} = -0.29$ V). (c) Feedback circuit keeping the current I_{DS} through the SET constant by tuning the voltage $V_{\mathrm{2DES,S}}$. In this case, the B dependence of $V_{\mathrm{2DES,S}}$ reflects directly the zigzag shift of the CBO shown in Fig. 3.5a. The voltage V_{bias} is used to compensate for the contact voltage at $B = 0$ T. (d) Zigzag-like shifts of Coulomb blockade oscillations with magnetic field (measured with the feedback circuit of (c)) for distinct sidegate voltages $V_{\mathrm{Side,S}} = 0$ V to -9 V (adopted from Y.Y. Wei et al. [72]). Shift ΔB is caused by the depletion of the electron concentration.

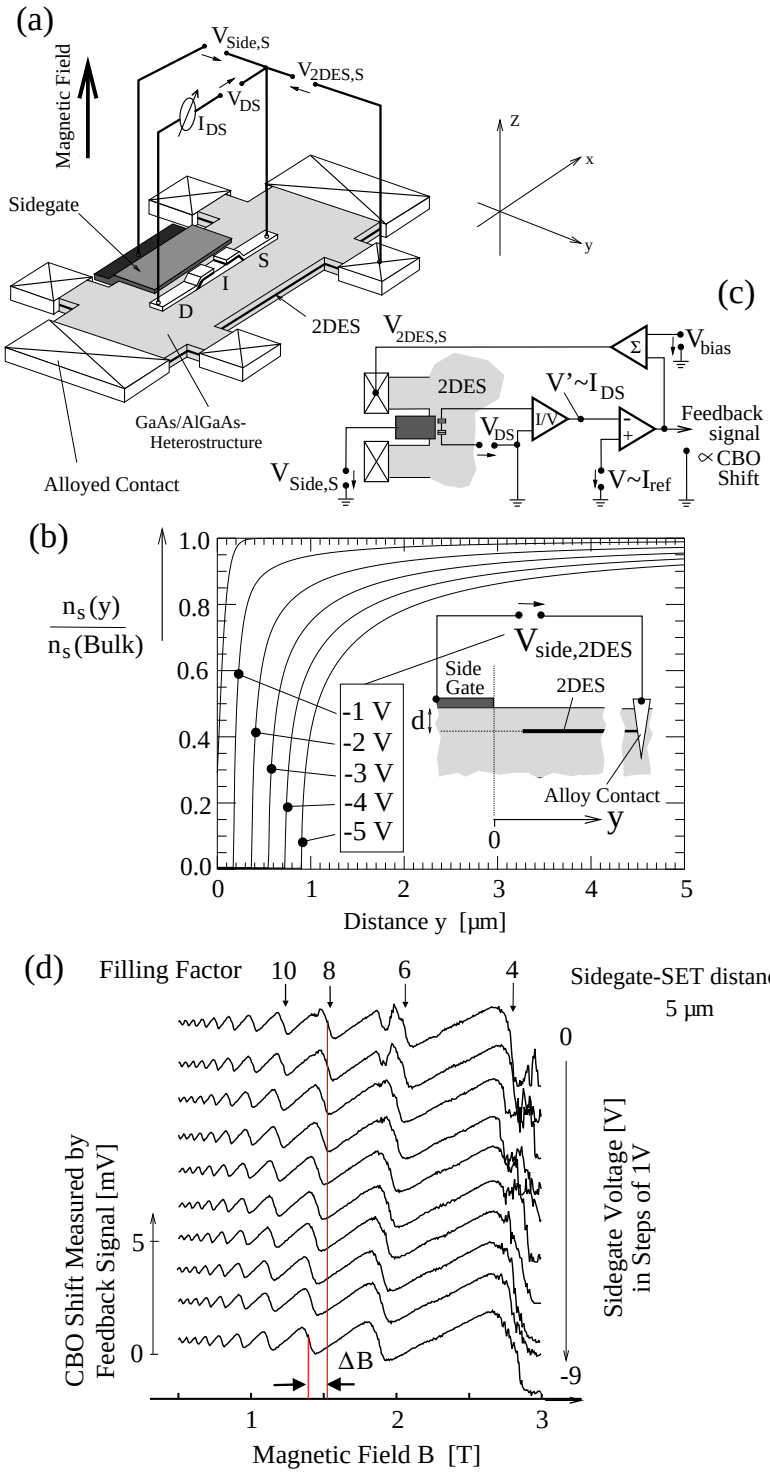
(a)
Magnetic Field
$V_{Side,S}$
$V_{2DES,S}$
V_{DS}
I_{DS}
Sidegate
S
I
D
2DES
GaAs/AlGaAs-
Heterostructure
Alloyed Contact
z
x
y
(c)
$V_{2DES,S}$
2DES
V_{bias}
$V'\sim I_{DS}$
I/V
V_{DS}
Feedback
signal
$\propto$ CBO
Shift
$V_{Side,S}$
$V\sim I_{ref}$
(b)
$\frac{n_s(y)}{n_s(Bulk)}$
1.0
0.8
0.6
0.4
0.2
0.0
-1 V
-2 V
-3 V
-4 V
-5 V
$V_{side,2DES}$
Side
Gate
2DES
d
Alloy Contact
0
y
0
1
2
3
4
5
Distance y [µm]
(d)
Filling Factor
10
8
6
4
Sidegate-SET distance
5 µm
0
-9
Sidegate Voltage [V]
in Steps of 1V
CBO Shift Measured by
Feedback Signal [mV]
5
0
ΔB
1
2
3
Magnetic Field B [T]

Δn_s, the depopulation of a Landau level at filling factor ν occurs at B value decreased by $\Delta B = h\Delta n_s/e\nu$. With this relation we calculate that the local electron concentration is depleted by about 8% with decreasing $V_{\mathrm{Side,S}}$ from 0 V to −9 V, which is in the range of what is expected from Fig. 3.6b for a gate distance of 5 μm.

Using a similar arrangement, the electrostatic potential profile in the depletion region of a two-dimensional electron system in high magnetic field has been probed. The so-called compressible and incompressible strips have been resolved [69, 70, 71, 27, 31]. They are important for understanding the Hall potential profile in a 2DES under quantum Hall effect conditions [77].

3.4 Summary

Changing the *electrostatic* potential of one electrode of a single-electron device shifts the electrostatic potential of the island. This is caused by either changing the externally applied voltages *or* by affecting the intrinsic contact voltages between the electrodes. Like additional charges in the surrounding, intrinsic contact voltages cause additional electrons to be trapped on the SET island. But these intrinsic contact voltages do not affect the electrochemical potential differences between the electrodes. Only the electrochemical potential differences are responsible for directed currents in the system. They are defined by externally applied voltages.

In the further course of this treatise, conditions for Coulomb blockade and single-electron charging are therefore expressed by the electrochemical potentials of the source and drain electrodes instead of their electrostatic potentials.

4. Quantum Dot as an Interacting N-Electron System: an Artifical Atom with Tunable Properties

In Chapter 1, the Coulomb blockade effect and single-electron charging have been introduced based on the existence of the elementary charge $-e$ of electrons combined with simple electrostatic energy considerations. Sofar the islands of the single-electron devices have been described as bulk metal. By choosing the island size smaller and smaller, we must take into account that electrons are quantum mechanical particles: They show a wave-particle duality. For electrons confined on a sufficiently small island, only certain kinetic energies are possible. In that case, the mesoscopic island is denoted as a *quantum dot*. In the simplest approach for a description, electrons of the island are moving in a phenomenological confining potential chosen as a 'box confinement' or as a 'parabolic confinement'. But what are the contributions to the confining potential of real quantum dots? What can be identified as 'capacitance coefficients' and the 'total capacitance' of a quantum dot, used in the previous Chapters to decribe single-electron charging effects? To clarify these questions is goal of the discussion in this Chapter. It requires more fundamental quantum mechanical considerations of the electron system in the quantum dot. To this purpose, the Hamiltonian for a quantum dot confining N electrons of the conduction band is derived for an arbitary electrostatic surrounding – inhomogeneous anisotropic dielectric medium containing a fixed charge distribution and electrodes of fixed electrostatic potential [42, 78]. The charges of the N movable electrons in the quantum dot are macroscopically compensated by the fixed ion charges and image charges on the electrodes. The fixed valence band electrons contribute to the dielectric matrix. It generalizes the description of the electron island including in one limit the metal island where the quantum confining effect is negligible, and mimicking in the other limit atoms and molecules dominated by quantization effects. [1] As a result, the confining potential, but also the electron-electron interaction in the quantum dot depend on the electrostatic surrounding: Quantum dots can

[1] Conformation changes of molecules with adding an electron are of course not modelled in such a system. However the general language developed here can also be adopted including such effects. Recent experiments [79] on single-electron transistors embedding a C_{60} molecule as the island indicate excitations due to the motion of the molecule in its binding potential to the surface. Also such effects might have to be included for decribing single-electron transport through real molecules or clusters.

be considered as *artifical atoms* [80, 81, 6, 5] with – in principle – tunable properties.

4.1 Quantum Dot: Electron Island on which the Energy of Single Electrons is Quantized

It was pointed out in Chapter 1 that for smaller metal islands the single-electron charging energy becomes larger. Metal islands of few nanometers are required to see Coulomb blockade and single-electron charging at room temperature. Enclosing an electron into a small box, only certain values for its kinetic energy become possible due to the quantum nature of electrons: An electron in a small enclosure shows a discrete energy spectrum similar to what is known from atoms where electrons are closely bound to a positive charged nucleus. [2]

The deBroglie wavelength λ is attributed to a free propagating electron due to its kinetic momentum $p = \hbar k = \hbar \cdot 2\pi/\lambda$. Since the kinetic momentum is directly related to the kinetic energy of the electron, $\varepsilon(k) = (\hbar\, k)^2/2m_e^*$, where m_e^* denotes the effective electron mass in the material, we obtain

$$\lambda = \frac{2\pi\hbar}{\sqrt{2\, m_e^*\, \varepsilon}} = \frac{h}{\sqrt{2\, m_e^*\, \varepsilon}}\,. \tag{4.1}$$

The electron density in the conduction band of metals is high which leads in the Sommerfeld model [82] of free electrons due to the Pauli exclusion principle to a high Fermi energy, i.e., a high kinetic energy of the electrons at the Fermi level. Therefore, the wavelength of an electron at the Fermi level in metals is usually only few tenths of a nanometer. Semiconductor materials have lower concentrations of free electrons and therefore lower Fermi energies. A smaller effective mass m_e^* results in a larger deBroglie wavelength for the same kinetic energy ε. Conduction band electrons in Gallium Arsenide (GaAs) are treated well in an effective mass approximation with $m_e^* = 0.067 \cdot m_e$, where m_e denotes the free electron mass. Thus, for a Fermi energy of $\varepsilon_\mathrm{F} = 10$ meV, the Fermi wavelength is $\lambda_\mathrm{F} = 46$ nm in GaAs.

By reducing the size of the bulk material, pronounced quantization effects can be expected when the size of the bulk becomes comparable with the wavelength λ_F of an electron at the Fermi level of the bulk material (see Fig. 4.1). If this confinement occurs in all directions, we speak from a *quantum dot* [3] or *zero-dimensional electron system.*

The simplest evaluation of a quantum dot can be done in Cartesian coordinates using an electron box with the side lengths L_{x_i} with $x_i \in \{x, y, z\}$ and a confining potential with infinite high walls:

[2] The confining potential in atoms is given by an attractive Coulomb potential $V(\boldsymbol{r}) = -Z\, e^2/|\boldsymbol{r}|$ where Ze denotes the charge of the nucleus sitting at $\boldsymbol{r} = 0$.

[3] The term 'quantum dot' has been used in literature for a variety of systems, not all of them fulfilling above definition.

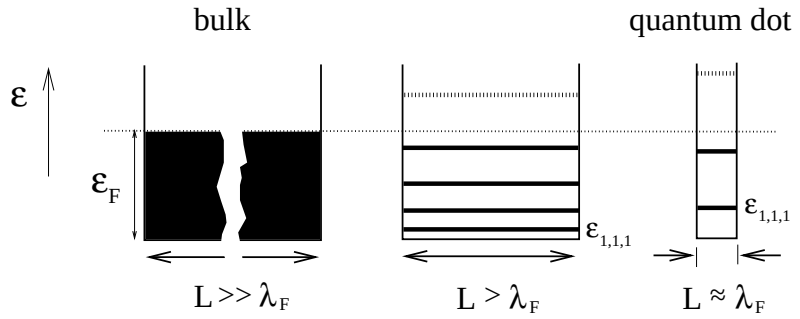

Fig. 4.1. The possible kinetic energies of electrons in a cubic box. The ratio of the side length L of the cube to the Fermi wavelength λ_F determines the spacing between the energy levels.

• **Box confinement**

$$V(\boldsymbol{r}) = V_1(x) \cdot V_2(y) \cdot V_3(z) \tag{4.2}$$

$$\text{with} \qquad V_i(x_i) = \begin{cases} 0 & \text{if } 0 \le x_i \le L_{x_i} \ , \\ \infty & \text{else} \ . \end{cases}$$

Solving the respective single-particle Schrödinger equation, it is easy to show that only certain discrete kinetic energies for the electrons are allowed in such a quantum dot,

$$\varepsilon_{i_x,i_y,i_z} = \frac{\pi^2\hbar^2}{2\,m_e^*}\left(\frac{i_x^2}{L_x^2} + \frac{i_y^2}{L_y^2} + \frac{i_z^2}{L_z^2}\right) \tag{4.3}$$

with L_x, L_y and L_z denoting the length of the box in the respective directions. The numbers i_x, i_y and i_z are integer values starting from one and labeling the electronic states in the box. The lowest possible energy is given by $i_x = i_y = i_z = 1$,

$$\varepsilon_{1,1,1} = \frac{\pi^2\hbar^2}{2\,m_e^*}\left(\frac{1}{L_x^2} + \frac{1}{L_y^2} + \frac{1}{L_z^2}\right) \ . \tag{4.4}$$

This represents the energy of the groundstate of a single electron in the box. For a box with same side lengths $L_x = L_y = L_z = L$, i.e., for a cube, the groundstate energy becomes

$$\varepsilon_{1,1,1} = \frac{3\pi^2\hbar^2}{2\,m_e^*\,L^2} \ . \tag{4.5}$$

For convenience, the energy levels of a cubic 3D box are depicted in Fig. 4.1, showing the spacing of the discrete energies as a function of side length L.

Depending on the aspect ratio of the quantum dot's extensions in three orthogonal spatial directions, we distinguish between 3D, 2D and 1D quantum dots [7]:

$$\begin{aligned} &\text{3D}: \; L_x \approx L_y \approx L_z \;, \\ &\text{2D}: \; L_x \approx L_y \gg L_z \;, \\ &\text{1D}: \; L_x \gg L_y, L_z \;, \end{aligned}$$

where the largest length is in the order of the Fermi wavelength λ_{F}.

The shape and strength of the confining potential determines the energy spectrum of an electron in the confinement. A simpler energy spectrum is obtained for an electron in a three-dimensional *parabolic* potential:

• **Parabolic confinement**

$$V(\boldsymbol{r}) = \tfrac{1}{2} m_e^* \omega_0^2 \cdot |\boldsymbol{r}|^2 = \tfrac{1}{2} m_e^* \omega_0^2 \cdot (x^2 + y^2 + z^2) \,. \tag{4.6}$$

It reveals the energy spectrum of a harmonic oscillator, – an equidistant ladder of energy levels with $\hbar\omega_0$ as the level distance,

$$\varepsilon_{i_x, i_y, i_z} = \hbar\omega_0 \cdot \left(i_x + i_y + i_z + \tfrac{3}{2}\right) \;, \tag{4.7}$$

where $i_{x_i} = 0, 1, 2, \cdots$. The quantization energy $\hbar\omega_0$ depends on the effective mass m_e^* attributed to the electron and the curvature of the confining potential at its potential minimum. It is convenient to introduce an effective diameter D for the quantum dot with a parabolic confinement in order to give an impression of its spatial extension. To this purpose, D is taken as the distance between opposite turnaround points for a classical particle having the energy $\hbar\omega_0/2$, i.e., D is determined from $V(|\boldsymbol{r}| = D/2) = \hbar\omega_0/2$. [4] This definition D leads to the following relation between $\hbar\omega_0$ and D,

$$\hbar\omega_0 = \frac{4\hbar^2}{m_e^* D^2} \;. \tag{4.8}$$

Like already found for the confining potential of a box where the distance between the energy levels scales with $1/L^2$ of the box's side length L, the distance between the single-particle energies in a parabolic confining potential increases with $1/D^2$ of the effective diameter D. On the other hand, we found that with decreasing the linear spatial dimension D, the self-capacitance of a metal island decreases causing that the single-electron charging energy increases linearly with the inverse of the island's diameter.

> Therefore, with decreasing the island size, the influence of the quantization effect increases and exceeds the single-electron charging energy scale at a certain island size.

For estimating the transition, in Fig. 4.2, the scaling of the single-electron charging energy E_{C} of a metal sphere with diameter D, which is $E_{\mathrm{C}} = e^2/2C_\Sigma = e^2/4\pi\epsilon_0\epsilon D$, is compared with the scaling of the quantization energy $\hbar\omega_0 = 4\hbar^2/m_e^* D^2$ in a 3D parabolic confinement with the effective diameter

[4] The length $l^* \equiv \sqrt{\hbar/(m_e^*\,\omega_0)} = D/2$ is sometimes denoted as 'oscillator length'.

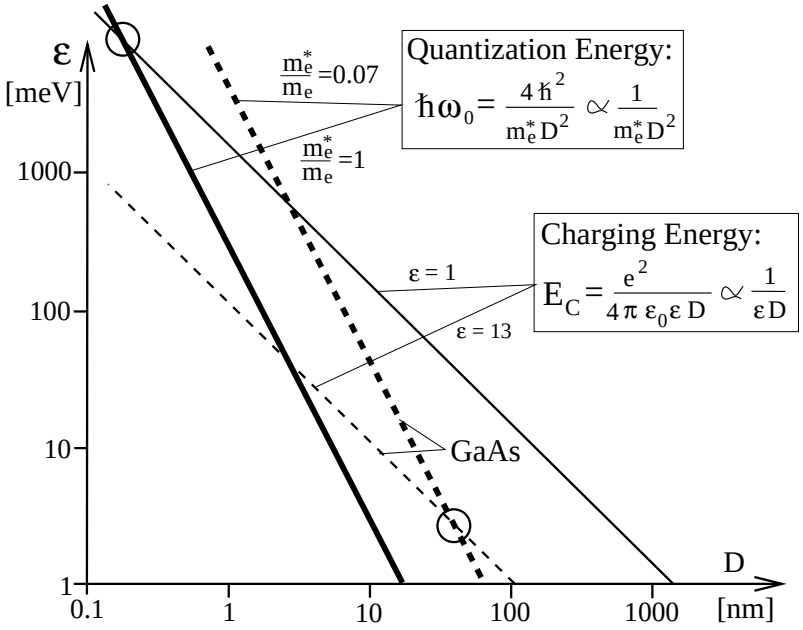

Fig. 4.2. Comparison of the quantization energy $\hbar\omega_0$ in a 3D parabolic confinement with effective diameter D and the single-electron charging energy E_C of a metal sphere of diameter D for different ϵ and m_e^* as a function of D in a log-log plot. At small D below the crossing point, the quantization energy becomes dominant.

D. They become equal ($E_C = \hbar\omega_0$) for the diameter $D = 16\pi\epsilon_0\epsilon\hbar^2/e^2m_e^* \approx 0.2\,\mathrm{nm}\cdot\epsilon\cdot m_e/m_e^*$. This diameter below which the quantization energy starts to dominate depends on the effective mass m_e^* and the dielectric constant ϵ. For $\epsilon = 1$, $m_e^* = m_e$, the transition occurs at 0.2 nm, i.e., on atomic scale. Conventional processing technology allows to structure materials on the hundred nanometer scale. For such large systems, a small effective mass is required to have both energy scales in the same range. Due to the small effective mass in GaAs ($m_e^* = 0.067\cdot m_e$) and the dielectric constant $\epsilon = 13$, quantum dot systems realized in GaAs/AlGaAs heterostructures offer the transition at about 40 nm. [5] Therefore such quantum dots with a diameter from several hundreds to few tens of nanometers give access to investigate the interplay between single-electron charging energy and single-particle quantization energy on an energy scale of 0.01 meV to few meV. To suppress ther-

[5] Usually such an estimate is expressed by the 'oscillator length' $l^* = \sqrt{\hbar/(m_e^*\,\omega_0)}$ and by the effective Bohr radius $a_B^* = (\hbar^2\,4\pi\epsilon_0\epsilon)/(m_e^*\,e^2)$: The quantization energy scales like $\hbar^2/(m_e^*\cdot(l^*)^2)$, whereas the Coulomb energy between two electrons in distance $D = 2\,l^*$ is given by $e^2/(4\pi\epsilon_0\epsilon\,D)$. Both become equal at $l^* = 2\,a_B^*$, i.e., for GaAs at $l^* \approx 20\,\mathrm{nm}$. This is equal to the estimate presented in the text. Note, this should be taken as a rough estimate.

mal fluctuations, low temperatures (typically below 0.1 Kelvin) are required which are accessible in commercially available ^{3}He-^{4}He-dilution refrigerators.

4.2 Various Realizations of Quantum Dot Systems for Electrical Transport Measurements

Quantum dot systems for electrical transport measurements have been realized in different ways, for instance,

- by shaping bulky materials like Silicon by etching and enhanced local oxidation [83, 84],
- by embedding small particles in a thin Si_xN_y membrane which is contacted in a small area from both sides by metal electrodes [85],
- by self-formation during epitaxial growth of lattice-mismatched III-V semiconductor materials [86],
- by molecular beam epitaxy of III-V materials on a prepatterned substrate [87, 88],
- by depositing semiconductor clusters from colloids between metal electrodes [89],
- by arranging single carbon nanotube [90, 91], C_{60}-buckyballs [79], molecules or atom clusters between metal electrodes or mechanical breakjunctions, or
- by structuring GaAs/AlGaAs heterostructures.

Structuring GaAs/AlGaAs heterostructures is a very usual approach to form well-defined 2D quantum dots with *in-situ* tunable parameters and is therefore used in all the experiments presented in this work. Base is a $GaAs/Al_{1-x}Ga_xAs$-heterostructure which contains a two-dimensional electron system (2DES). The 2DES is located either at a GaAs/AlGaAs heterojunction or in a AlGaAs/GaAs/AlGaAs quantum well below the surface (see Fig. 4.3). Such GaAs/AlGaAs heterostructures offer several advantages:

- GaAs, AlAs and $Al_{1-x}Ga_xAs$ alloys can be grown with almost no lattice mismatch monolayer by monolayer with molecular beam epitaxy (MBE), forming a crystal.
- The energetic position of the conduction band minimum is tunable by varying the stochiometry between Ga and Al. Potential steps or wells are easily obtained by abruptly changing the stochiometry.
- Due to the high growth quality and the modulation-doped technique, two-dimensional electron systems (2DES) are created as conduction band in such heterostructure offering a mean free path for electrons without being scattered for even up to 100 μm at temperatures below 4 K.
- The 2DES layer is typically 10 nm thick and lies 35 to 250 nm below the surface. The concentration is usually in the range of $5 \cdot 10^{14}$ to $5 \cdot 10^{15}$

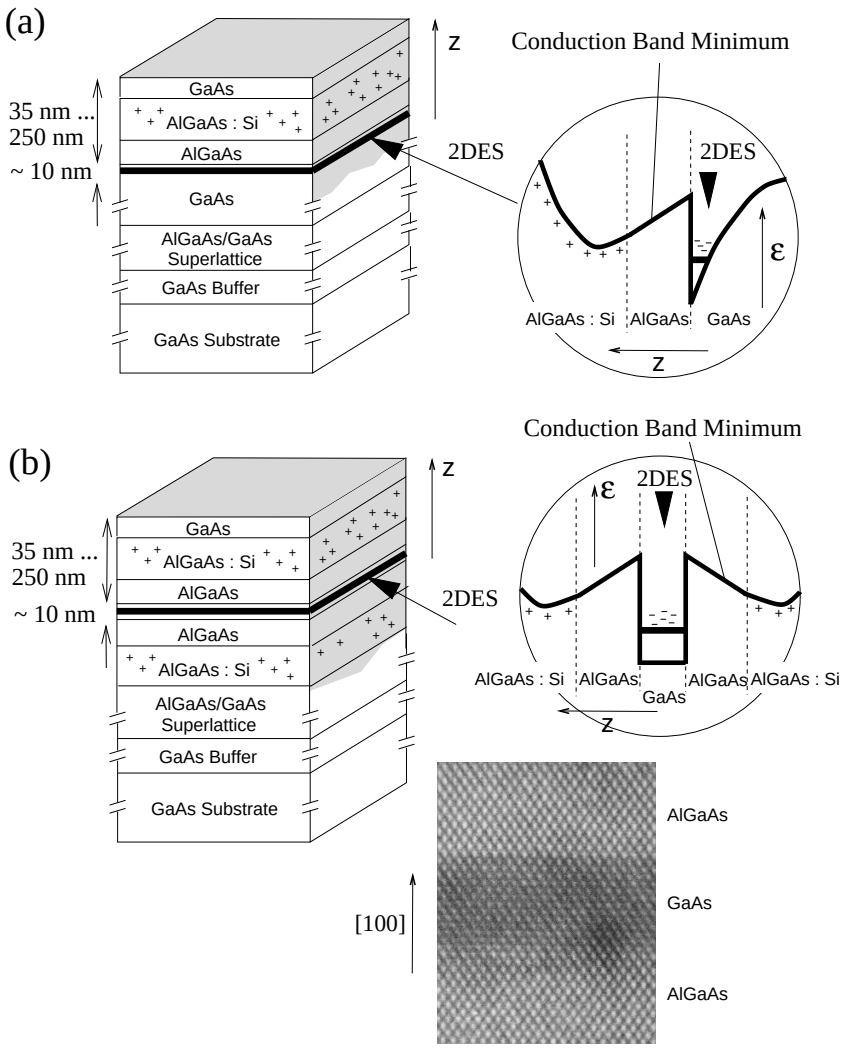

Fig. 4.3. Examples of GaAs-AlGaAs heterostructures containing two-dimensional electron systems: (a) at a heterojunction, (b) in a quantum well. On the right bottom a highly resolved transmission electron micropscope image is shown of such a heterostructure layer sequence. The lattice period in [100] direction is about 0.57 nm.

electrons per m^2, i.e., in a square of 100 nm by 100 nm there are about 5 to 50 electrons.

- The electron concentration in the 2DES can easily be varied locally by applying voltages to metal electrodes on the surface.

- The conduction band electrons are described well within an effective mass approximation. The effective mass is low and thus favours a large Fermi wavelength and therefore quantum confining effects.

To realize a quantum dot system in such heterostructures, the following approaches are common for dividing the 2DES laterally in different functional regions (see Fig. 4.4):

- By using electron-beam lithography, structured metal electrodes – denoted as *split-gate electrodes* [95]– are deposited on top of this heterostructure. Such kind of structures were the first for studying Coulomb-blockade effects in quantum dot systems (see historic review by M. Kastner [96]). An example is given in Fig. 4.4a. In this case, the split-gate electrodes consists of six electrodes, – three on each side: two outer electrodes and one inner electrode. With applying negative voltages to these gate electrodes, the electrons are electrostatically depleted below each gate: The 2DES is divided into a small region between the gate fingers – the quantum dot – and two large areas of 2DES acting as source and drain electrode to the quantum dot. The heights and widths of the *tunnel barriers are tunable* by the voltage applied to the outer gate electrodes. The inner gate electrodes should screen the cross acting of the outer electrodes and act as gate electrodes for the quantum dot.
- In an another approach, the 2DES is divided by etching grooves into the heterostructure which are defined by electron-beam lithography. An example is shown in Fig. 4.4b. The diverse regions act as source, drain, gate electrodes and the quantum dot. Since all these components are realized in the same plane, such an arrangement is denoted as *in-plane gate structure* [97]. At the constriction between two etched grooves, tunnel barriers are formed due to electrostatic depletion around the grooves which is always present due to negative surface charges trapped on the free surface of GaAs and AlGaAs. The electrostatic depletion length is typically 0.1 to 0.2 μm for such 2DES reducing the actually size of the electron system in the quantum dot respectively. In this realization the barriers are also tunable by the gate electrodes. The present design avoids problems of earlier layouts [98], where the gate electrodes got partially depleted with negative gate voltages.
- Instead of etching, a focused Ga-ion beam (FIB) has been used to distort locally the 2DES leading to insulating lines which divide the 2DES in different regions acting as source, drain or gate electrodes, and as the quantum dot [99]. The technique has also been combined with the split-gate technique [100]. Risk is that single ions implanted by the FIB are trapped in the region of the quantum dot causing disturbed confining potentials.
- Isolating lines in the 2DES are also obtained by a focused laser beam inducing p-dopant diffusion from a surface layer into the heterostructure. A single-electron transistor has been defined by this technique [101].

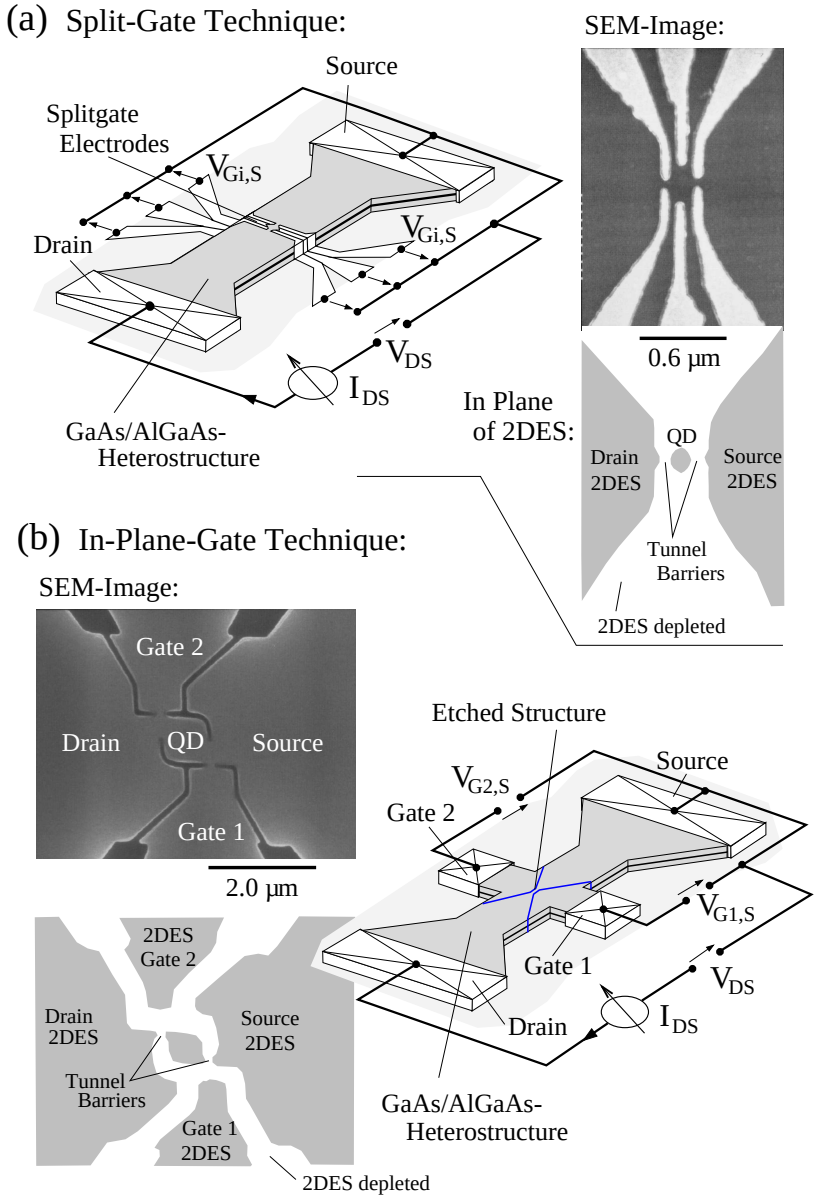

Fig. 4.4. Examples of lateral 2D quantum dot systems: (a) 2D quantum dot defined by partial electrostatic depletion of a 2DES with split-gate electrodes. Here the 2DES is located at a GaAs-AlGaAs heterojunction or GaAs quantum well (from J. Schmid [92] after J. Weis [42]) (b) Lateral quantum dot system by dividing a 2DES by etching grooves. The typical depletion length at an etched groove is between 0.1 to 0.2 μm, reducing the size of the quantum dot respectively. (from M. Keller [93] after U. Wilhelm [94])

- Recently scanning probes microscopes have been used to modify locally the heterostructure by scratching or oxidizing the surface. The 2DES becomes depleted below the modified surface, allowing to divide the 2DES into single-electron transistor arrangements [102, 103]. The technique also allows to combine in-plane with split-gate technique.

With these techniques, quantum dots have been realized with a typical diameter between 0.1 to 1 μm. The leads are laterally arranged to the quantum dot, i.e., electrical transport takes place in parallel to the plane of the heterostructure layers. That is why such realizations are denoted as *lateral quantum dot systems*. Electron transport has to occur via the edge region of the quantum dot. An advantage is the in-situ tunability of the tunnel barriers, a disadvantage is that these tunnel barriers are long in their spatial extensions and shallow in energetical height. [6] The latter also restricts the magnitude of drain-source voltage which can be applied. Recently, Ciorga and coworkers [104] have demonstrated single-electron transport on a split-gate quantum dot system, where the total electron number in the quantum dot could be tuned starting with an empty dot.

Realizations of *vertical quantum dot systems* where electron transport occurs perpendicularly to the plane of the heterostructure layers and therefore via the whole area of the 2D quantum dot are sketched in Fig. 4.5:

- The structure of Fig. 4.5a was presented in 1988 by M. Reed and coworkers [105] and further developed by M. Tewordt and coworkers, B. Su and coworkers, Th. Schmid and coworkers (see references in [106]). Firstly a heterostructure is grown with a quantum well embedded between two highly doped layers which are separated by thin layers acting as tunnel barriers. In the second step a pillar is etched out of the heterostructure.
- S. Tarucha, D.G. Austing and T. Honda [107] have extended the structure in a third step by a metal electrode surrounding the quantum dot (see Fig. 4.5b). This was an important step for exploring the energy spectrum of atom-like quantum dots.
- Fig. 4.5c shows a quantum-dot box used by R. Ashoori and coworkers [108] for capacitance spectroscopy: The quantum dot is formed by means of a top gate electrode producing an electrostatic depletion except in a small area due to a larger distance of the gate metal to the quantum well. Tunneling is only possible between quantum dot and substrate.

Such vertical quantum dot systems offer energetically high tunnel barriers. They are defined by the conduction band offset of the grown layers which has the drawback of not being in-situ tunable. However, since it is easy to start with an empty quantum dot by choosing the right thickness of the layer

[6] Due to these properties, the tunnel barrier regions are very sensitive to local potential fluctuations leading to local potential valleys acting as unintentional quantum dots in series to the lithographically defined quantum dot [94, 93].

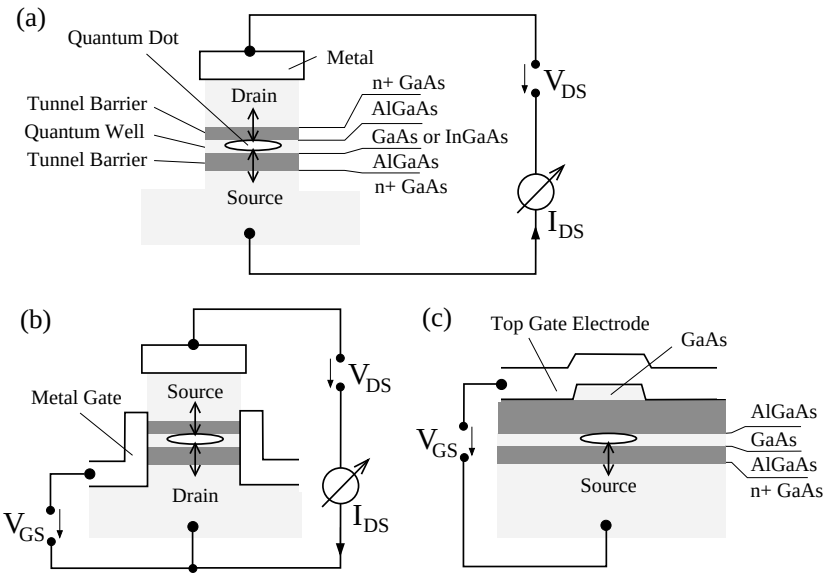

Fig. 4.5. Example of a vertical 2D quantum dot systems (not on scale): (a) The quantum dot system defined by etching a pillar out of a heterostructure with a 2DES embedded between two conducting layers. The quantum dot is coupled by tunnel barriers to source and drain. (b) Full single-electron transistor: A metal gate electrode around the quantum dot allows to change at fixed drain-source voltage the number of electrons confined in the quantum dot. (c) Quantum-dot single-electron box: Thick barrier between quantum dot and top gate electrode prohibits tunneling. The gate electrode allows for loading the quantum dot by tunneling from the substrate site. Such a structure has been used for capacitance spectroscopy.

containing the quantum dot, beautiful experiments could be done [108, 5] which demonstrate quantum dots with properties reminding on real atoms.

Quantum dots of various shape have been presented, – for instance, circular [107], elliptical [109], ring-like [86, 110], and irregular [111]. One should have always in mind that intrinsic potential fluctuations due to donor distributions might break any symmetry intended by the lithography [93, 94]. The larger the device, the larger the risk of having these disturbed confining potentials. This is not unusual: Devices originally intended as quantum wires break up into several valleys acting as a series of strongly or weakly coupled quantum dots [112]. Quantum dots are found below the finger of a split-gate structure [113] or in the depletion region of a split-gate defined quantum point contact [114]. The characteristic might even change with each warming-up and cooling-down cycle. Therefore, quantum dot system require extensive characterization measurements by tuning several parameters:

Although prepared in the same way, quantum dots are individuals distinct more or less in their properties due to variations in the confining potential.

Common of all mentioned quantum dot structures is that various materials are combined, and metal electrodes and charges are present to form the quantum dot. The diverse regions of semiconductor heterostructures behave under experimental conditions, i.e., low temperature, either metal- or insulator-like. Donors and acceptors are fixed in their charge state. Therefore the diverse regions can be treated either as a metal electrode or as a dielectric with a fixed charge distribution. [7] To determine the confining potential for the electrons in the quantum dot, these ingredients have to be taken into account. Finding an adequate description is goal of the following Sections of this Chapter.

4.3 Popular Model of a Quantum Dot: The Constant Interaction Model (CIM)

A simple model was proposed and elaborated in 1991 by different authors [32, 115, 116]. To take into account the quantization of the kinetic energy on the electron island, the single-electron energies ε_i due to the kinetic energy of the electrons in are added to the electrostatic energy term (2.29) derived for the metal island arrangement. The energies ε_i are measured with respect to the bottom of the confining potential with is the conduction band minimum $\varepsilon_0^{\mathrm{C}}$, where $\varepsilon_0^{\mathrm{C}}$ is given relative to a common reference for the case of an electrically neutral bulk material. This yields the total energy

$$E_{\mathrm{tot}}(N;\{V_i\}) = \sum_{i=1}^{N} \left(\varepsilon_i + \varepsilon_0^{\mathrm{C}}\right) \; - \Delta N e \cdot \sum_{j=1}^{M} \frac{C_{0,j}}{C_{0\Sigma}} \cdot V_j + \frac{(\Delta N e)^2}{2C_{0\Sigma}} \qquad (4.9)$$

where $\Delta N = N - N_0$. Here, N_0 denotes the total number of (conduction band) electrons for the electrical uncharged quantum dot, i.e., N_0 electrons of the total number N are compensated in their negative charge by positive background charges, and ΔN is therefore the number of additional electrons. [8]

[7] The term 'semiconductor quantum dot' found in literature has to be understood as 'quantum dot being realized from a (at room temperature) semiconducting material'.

[8] E_{tot} has also been written with ΔN being replaced by N, the total electron number. There was some argueing [117] whether $(Ne)^2/2C_{0\Sigma}$ or $N(N-1)e^2/2C_{0\Sigma}$ is the correct ansatz. As one can see from the discussion in Section 4.8.2, for a pure Coulomb interaction between the electrons in the quantum dot, the ansatz $N(N-1)e^2/2C_{0\Sigma}$ is more feasible. In case of nearby electrodes, the interaction with the induced image charges have to be taken into account which are seen even by the first electron, i.e., a dependence $(Ne)^2/2C_{0\Sigma}$ might become plausible, although not exact.

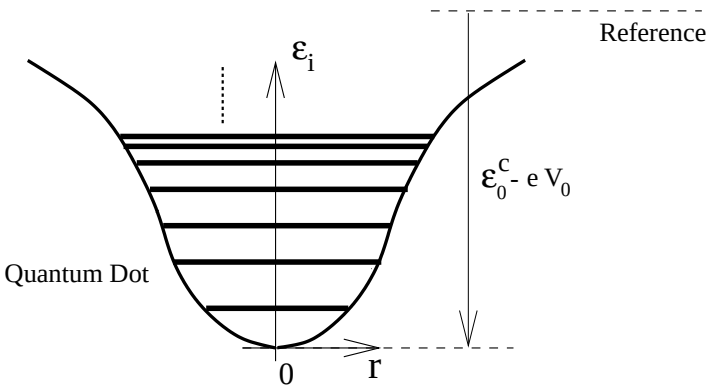

Fig. 4.6. Energy scheme for the *Constant Interaction Model*: Single-electron energies ε_i are measured relatively to the bottom of the confining potential which is the bottom $\varepsilon_0^{\mathrm{C}}$ of the conduction band. The position of the bottom of the confining potential is shifted by $-eV_0$ with the electrostatic potential V_0 of the island, which depends on the electron number N and the electrostatic potentials of the surrounding electrodes.

The energy spectrum describes the possible energy levels for the electrons in an effective confining potential. One should note:

> The single-electron energies $\varepsilon_i + \varepsilon_0^{\mathrm{C}}$ are assumed to be affected neither by the electron number nor by the electrostatic potential changes on the electrodes.

For charging the quantum dot with the $(N+1)$th electron from a reference electrode with the electrochemical potential zero, not only the electrostatic charging energy is required but also the energy for getting into the first unoccupied single-particle state with energy ε_{N+1}. Therefore the energy difference $\Delta E_{\mathrm{tot}}(N+1;\{V_i\})$, which an electron feels between being located on the quantum dot and being located on the reference electrode with the electrochemical potential equal zero, is given by

$$\begin{aligned}\Delta E_{\mathrm{tot}}(N+1;\{V_i\}) &= E_{\mathrm{tot}}(N+1;\{V_i\}) - E_{\mathrm{tot}}(N;\{V_i\}) \\ &= \varepsilon_{N+1} + \varepsilon_0^{\mathrm{C}} - e\sum_{j=1}^{M} \frac{C_{0,j}}{C_{0\Sigma}} \cdot V_j + \left(N - N_0 + \tfrac{1}{2}\right) \frac{e^2}{C_{0\Sigma}} \,. \end{aligned} \tag{4.10}$$

The charging energy is modified by $\varepsilon_{N+1} + \varepsilon_0^{\mathrm{C}}$ in comparison to (1.15). Changing N, the energy difference (4.10) defines energy levels for charging the quantum dot, similar to what was used in Chapter 1. With other words: The Constant Interaction Model with the ansatz (4.9) implies that

- a single-electron spectrum exists which is not affected by the number of electrons in the quantum dot. Moreover,

- the interaction between charges are only described by capacitances which are independent of the electron number on the quantum dot. This founds the name 'Constant Interaction Model (CIM)'.

Both are *ad hoc* assumptions usually not valid. [9] A more accurate description is developed in the following. A comparison between the Constant Interaction Model and the general description in terms of an interacting N-electron system is done in Section 4.8 and in Chapter 5. There the spectroscopy of energy levels of a quantum dot is described, visible in electrical transport experiments with increasing drain-source voltage.

4.4 Electrostatics of Realistic Quantum Dots: N Electrons Embedded in an Inhomogeneous Anisotropic Dielectric Medium with Charged Ions and Surrounded by Metal Electrodes

As presented in Section 4.2, a quantum dot is usually defined in semiconductor materials by etching, by electrostatic depletion due to voltages applied to gate electrodes, by local doping and/or by changing the stochiometry of the compound semiconductor material. To find a more proper description of a quantum dot confining N conduction-band electrons, we have first to consider the physical elements, i.e., the electrostatic arrangement, modelling the *essentials of a real quantum dot.* Thereafter we are able to derive in this Section expressions for the electrostatic potential and the classical potential energy of the electron system, needed to establish in Section 4.6 the Hamiltonian of a realistic quantum dot. This description was introduced in 1994 [42] and published in 1996 [78].

In Fig. 4.7, the physical elements of a real quantum dot are sketched in which N conduction-band electrons are confined. The negative electron charges of these N electrons are partly or fully compensated by an explicitely given charge density $\rho_{\rm ion}(\boldsymbol{r})$, – a homogeneous positive background charge is not assumed as usually done. The environment is composed of M metal electrodes ($i = 1$ to M) with fixed electrostatic potential V_i and a dielectric matrix, filling the volume V between the electrodes, in which the electrons are embedded. The dielectric matrix contains the contribution of the valence band electrons being shifted against the positive nuclei lattice and is described by the dielectric tensor $\boldsymbol{\epsilon}(\boldsymbol{r})$ which allows for the dielectric matrix being anisotropic and/or inhomogeneous. Charged impurities, dopants or trapped surface charges, usually present in real systems, are modelled

[9] The Constant Interaction Model has been applied to rather large quantum dots of irregular shape to extract level spacings for a comparison with Random Matrix Theory. The status is discussed in [118]. A detailed analysis [5] on experimental data obtained on atom-like quantum dots shows some trues but also limitations in the use of the CIM in such a case.

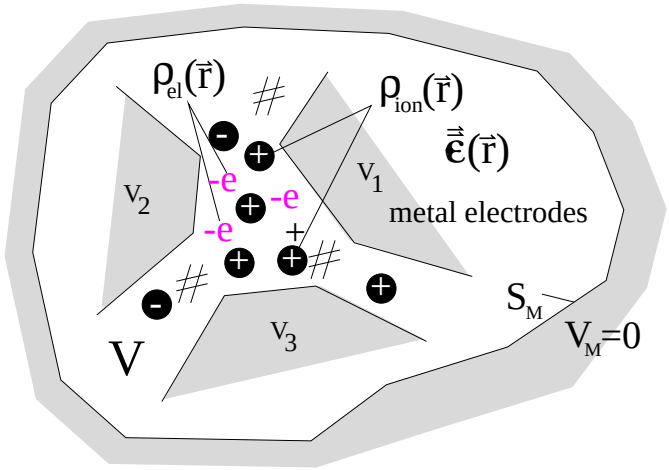

Fig. 4.7. Sketch of the physical elements of the electrostatic environment present for N conduction-band electrons confined in a real quantum dot. The electrons and a fixed charge distribution $\rho_{\rm ion}(\boldsymbol{r})$ are embedded in a dielectric matrix which fills up the space V. The properties of the dielectric matrix are decribed by $\boldsymbol{\epsilon}(\boldsymbol{r})$. M metal electrodes ($i = 1$ to M) of fixed electrostatic potential $\{V_i\}$ enclose the whole space V by their surfaces $\{S_i\}$.

by the charge distribution $\rho_{\rm ion}(\boldsymbol{r})$. The quantities $\boldsymbol{\epsilon}(\boldsymbol{r})$ and $\rho_{\rm ion}(\boldsymbol{r})$, and the shape and position of the metal electrodes are considered as being given for a certain arrangement. They are unaffected by the redistribution of the N movable electrons.

These electrons are treated as point charges at the positions $\boldsymbol{r}_s \in V$, $s = 1$ to N, i.e., the electron charge density $\rho_{\rm el}(\boldsymbol{r})$ is written as

$$\rho_{\rm el}(\boldsymbol{r}) = -e \sum_{s=1}^{N} \delta^3(\boldsymbol{r} - \boldsymbol{r}_s) \; . \tag{4.11}$$

Each electron s at location $\boldsymbol{r}_s$ is interacting with the charges present on the electrodes, with the fixed charge distribution $\rho_{\rm ion}(\boldsymbol{r})$ and with all other $(N-1)$ electrons.

The total electrostatic potential $\Phi_N(\boldsymbol{r})$ at location $\boldsymbol{r}$ between the electrodes ($\boldsymbol{r} \in V$), in the presence of the N electrons, is determined by the Poisson equation under the boundary condition of defined values $\{V_i\}$ on the surfaces $\{S_i\}$ of the M electrodes:

$$\begin{aligned} -\boldsymbol{\nabla}_{\boldsymbol{r}} \left\{ \epsilon_0 \boldsymbol{\epsilon}(\boldsymbol{r}) \cdot \boldsymbol{\nabla}_{\boldsymbol{r}} \, \Phi_N(\boldsymbol{r}) \right\} &= \rho_{\rm ion}(\boldsymbol{r}) + \rho_{\rm el}(\boldsymbol{r}) \; , \text{ if } \boldsymbol{r} \in V \; , \\ \Phi_N(\boldsymbol{r}) &= V_i \qquad\qquad\quad \; , \text{ if } \boldsymbol{r} \in S_i \; . \end{aligned} \tag{4.12}$$

Because of the linearity of (4.12), the total electrostatic potential $\Phi_N(\boldsymbol{r})$ can be written as a sum of three contributions: $\Phi_{\rm E}(\boldsymbol{r})$ of the electrodes, $\Phi_{\rm ion}(\boldsymbol{r})$ of the fixed charge distribution and $\Phi_{\rm el}(\boldsymbol{r})$ of the N electrons,

$$\Phi_N(\boldsymbol{r}) = \Phi_{\mathrm{E}}(\boldsymbol{r}) + \Phi_{\mathrm{ion}}(\boldsymbol{r}) + \Phi_{\mathrm{el}}(\boldsymbol{r}) \; . \tag{4.13}$$

Each of these potential contributions has to fulfill either the Poisson equation or the Laplace equation with specific boundary conditions. For the following discussion it is convenient to satisfy the boundary conditions of (4.12) on the electrodes entirely via $\Phi_{\mathrm{E}}(\boldsymbol{r})$, i.e., demanding $\Phi_{\mathrm{E}}(\boldsymbol{r}) = V_i$ if $\boldsymbol{r} \in S_i$ ($i = 1$ to M). Therefore, due to (4.13), the other potential contributions $\Phi_{\mathrm{el}}(\boldsymbol{r})$ and $\Phi_{\mathrm{ion}}(\boldsymbol{r})$ have to vanish on each electrode, i.e., $\Phi_{\mathrm{el}}(\boldsymbol{r}) = 0$ and $\Phi_{\mathrm{ion}}(\boldsymbol{r}) = 0$ if $\boldsymbol{r} \in \{S_i\}$. Then $\Phi_{\mathrm{el}}(\boldsymbol{r})$ is the electrostatic potential caused by the electrons and $\Phi_{\mathrm{ion}}(\boldsymbol{r})$ the electrostatic potential caused by the ions in the presence of *grounded* electrodes, whereas $\Phi_{\mathrm{E}}(\boldsymbol{r})$ is the electrostatic potential of the system when the electrodes are set to their respective potential values V_i, but the electrons and ions are absent. Therefore, the electrostatic potential contribution $\Phi_{\mathrm{el}}(\boldsymbol{r})$ of the N electrons obeys the Poisson equation

$$\begin{aligned} -\boldsymbol{\nabla}_{\boldsymbol{r}} \left\{ \epsilon_0 \boldsymbol{\epsilon}(\boldsymbol{r}) \cdot \boldsymbol{\nabla}_{\boldsymbol{r}} \Phi_{\mathrm{el}}(\boldsymbol{r}) \right\} &= \rho_{\mathrm{el}}(\boldsymbol{r}) \; , \text{ if } \boldsymbol{r} \in V \; , \\ \Phi_{\mathrm{el}}(\boldsymbol{r}) &= 0 \qquad , \text{ if } \boldsymbol{r} \in \{S_i\} \; . \end{aligned} \tag{4.14}$$

The electrostatic potential contribution $\Phi_{\mathrm{ion}}(\boldsymbol{r})$ due to the fixed charge distribution has to fulfill the Poisson equation

$$\begin{aligned} -\boldsymbol{\nabla}_{\boldsymbol{r}} \left\{ \epsilon_0 \boldsymbol{\epsilon}(\boldsymbol{r}) \cdot \boldsymbol{\nabla}_{\boldsymbol{r}} \Phi_{\mathrm{ion}}(\boldsymbol{r}) \right\} &= \rho_{\mathrm{ion}}(\boldsymbol{r}) \; , \text{ if } \boldsymbol{r} \in V \; , \\ \Phi_{\mathrm{ion}}(\boldsymbol{r}) &= 0 \qquad , \text{ if } \boldsymbol{r} \in \{S_i\} \; . \end{aligned} \tag{4.15}$$

The solutions for (4.14) and (4.15) can be expressed by

$$\Phi_{\mathrm{ion}}(\boldsymbol{r}) = \int_V \rho_{\mathrm{ion}}(\boldsymbol{r}') \cdot G(\boldsymbol{r}, \boldsymbol{r}') \, \mathrm{d}^3 \boldsymbol{r}' \; , \tag{4.16}$$

$$\Phi_{\mathrm{el}}(\boldsymbol{r}) \;\; = \int_V \rho_{\mathrm{el}}(\boldsymbol{r}') \cdot G(\boldsymbol{r}, \boldsymbol{r}') \, \mathrm{d}^3 \boldsymbol{r}' = -e \sum_{s=1}^{N} G(\boldsymbol{r}, \boldsymbol{r}_s) \; , \tag{4.17}$$

where the Green's function $G(\boldsymbol{r}, \boldsymbol{r}')$ is the solution of

$$\begin{aligned} -\boldsymbol{\nabla}_{\boldsymbol{r}} \left\{ \epsilon_0 \boldsymbol{\epsilon}(\boldsymbol{r}) \cdot \boldsymbol{\nabla}_{\boldsymbol{r}} G(\boldsymbol{r}, \boldsymbol{r}') \right\} &= \delta^3(\boldsymbol{r} - \boldsymbol{r}') \; , \text{ if } \boldsymbol{r} \in V \; , \\ G(\boldsymbol{r}, \boldsymbol{r}') &= 0 \qquad , \text{ if } \boldsymbol{r} \in \{S_i\} \; . \end{aligned} \tag{4.18}$$

For the last result in (4.17), expression (4.11) has been inserted. The relations (4.16) and (4.17) show: By multiplying the Green's function $G(\boldsymbol{r}, \boldsymbol{r}')$ with the charge q, the electrostatic potential is obtained at location $\boldsymbol{r}$, caused by the charge q located at position $\boldsymbol{r}' \in V$, in the case of all electrodes being grounded, i.e., $V_i = 0$ for $i = 1$ to M. The associated dielectric field is due to (2.3) and (2.4) described by

$$\boldsymbol{D}(\boldsymbol{r}) = -\epsilon_0 \boldsymbol{\epsilon}(\boldsymbol{r}) \cdot \boldsymbol{\nabla}_{\boldsymbol{r}} G(\boldsymbol{r}, \boldsymbol{r}') \cdot q \; . \tag{4.19}$$

The electrostatic potential contribution $\Phi_{\mathrm{E}}(\boldsymbol{r})$ due to the electrodes at certain potential values V_i ($i = 1$ to M) obeys the Laplace equation

$$\begin{aligned} \boldsymbol{\nabla}_{\boldsymbol{r}} \left\{ \epsilon_0 \boldsymbol{\epsilon}(\boldsymbol{r}) \cdot \boldsymbol{\nabla}_{\boldsymbol{r}} \, \Phi_{\mathrm{E}}(\boldsymbol{r}) \right\} &= 0 \quad , \text{if } \boldsymbol{r} \in V \ , \\ \Phi_{\mathrm{E}}(\boldsymbol{r}) &= V_i \ , \text{if } \boldsymbol{r} \in S_i \ . \end{aligned} \tag{4.20}$$

The solution $\Phi_{\mathrm{E}}(\boldsymbol{r})$ of (4.20) can be written as a superposition of contributions from each electrode

$$\Phi_{\mathrm{E}}(\boldsymbol{r}) = \sum_{i=1}^{M} \alpha_i(\boldsymbol{r}) \cdot V_i \tag{4.21}$$

where the dimensionless $\alpha_i(\boldsymbol{r})$ are determined by

$$\begin{aligned} \boldsymbol{\nabla}_{\boldsymbol{r}} \left\{ \epsilon_0 \boldsymbol{\epsilon}(\boldsymbol{r}) \cdot \boldsymbol{\nabla}_{\boldsymbol{r}} \, \alpha_i(\boldsymbol{r}) \right\} &= 0 \ , \quad \text{if } \boldsymbol{r} \in V \ , \\ \alpha_i(\boldsymbol{r}) \ &= \begin{cases} 1 & , \text{if } \boldsymbol{r} \in S_i \ , \\ 0 & , \text{if } \boldsymbol{r} \in S_j \text{ with } i \neq j \ . \end{cases} \end{aligned} \tag{4.22}$$

Physically, $\alpha_i(\boldsymbol{r}) \cdot V_i$ describes the electrostatic potential of the system without electrons and ions, with the potential of the electrode i fixed to V_i and all other electrodes grounded. These functions $\alpha_i(\boldsymbol{r})$ were named electrostatic potential profile of electrode i in Chapter 2 and used to express the capacitance coefficients C_{ij} between electrode i and electrode j.

The functions $\alpha_i(\boldsymbol{r})$ and $G(\boldsymbol{r}, \boldsymbol{r}')$ are determined by the shapes and geometric arrangement of the electrodes and the dielectric medium in between. They are independent of the electrostatic potential $\{V_i\}$ of the electrodes. But they are not independent themselves. Indeed, $\alpha_i(\boldsymbol{r})$ can be expressed by $G(\boldsymbol{r}, \boldsymbol{r}')$:

Using the integral definition of the delta function, relation (4.18) and the product rule of differential calculus, we obtain

$$\begin{aligned} \alpha_i(\boldsymbol{r}) &= \int_V \delta^3(\boldsymbol{r}' - \boldsymbol{r}) \cdot \alpha_i(\boldsymbol{r}') \, \mathrm{d}^3\boldsymbol{r}' \\ &= \int_V -\boldsymbol{\nabla}_{\boldsymbol{r}'} \left\{ \epsilon_0 \boldsymbol{\epsilon}(\boldsymbol{r}') \boldsymbol{\nabla}_{\boldsymbol{r}'} \, G(\boldsymbol{r}', \boldsymbol{r}) \right\} \cdot \alpha_i(\boldsymbol{r}') \, \mathrm{d}^3\boldsymbol{r}' \\ &= \int_V -\boldsymbol{\nabla}_{\boldsymbol{r}'} \left\{ \epsilon_0 \boldsymbol{\epsilon}(\boldsymbol{r}') \boldsymbol{\nabla}_{\boldsymbol{r}'} \, G(\boldsymbol{r}', \boldsymbol{r}) \cdot \alpha_i(\boldsymbol{r}') \right\} \mathrm{d}^3\boldsymbol{r}' \\ &\qquad + \int_V \left\{ \epsilon_0 \boldsymbol{\epsilon}(\boldsymbol{r}') \boldsymbol{\nabla}_{\boldsymbol{r}'} \, G(\boldsymbol{r}', \boldsymbol{r}) \right\} \cdot \boldsymbol{\nabla}_{\boldsymbol{r}'} \, \alpha_i(\boldsymbol{r}') \, \mathrm{d}^3\boldsymbol{r}' \ . \end{aligned}$$

Applying Gauß's law to the first integral, and considering the symmetry of the dielectric tensor in its components for the second integral, one finds

$$\begin{aligned} \alpha_i(\boldsymbol{r}) &= -\oint_S \left\{ \epsilon_0 \boldsymbol{\epsilon}(\boldsymbol{r}') \boldsymbol{\nabla}_{\boldsymbol{r}'} \, G(\boldsymbol{r}', \boldsymbol{r}) \right\} \cdot \alpha_i(\boldsymbol{r}') \, \mathrm{d}\boldsymbol{S}' \\ &\qquad + \int_V \left\{ \epsilon_0 \boldsymbol{\epsilon}(\boldsymbol{r}') \boldsymbol{\nabla}_{\boldsymbol{r}'} \, \alpha_i(\boldsymbol{r}') \right\} \cdot \boldsymbol{\nabla}_{\boldsymbol{r}'} \, G(\boldsymbol{r}', \boldsymbol{r}) \, \mathrm{d}^3\boldsymbol{r}' \ . \end{aligned}$$

The surface integral over S covers all electrode surfaces ($S = \{S_i\}$) and, therefore, encloses the whole space V between the electrodes. The surface element vector $\mathrm{d}\boldsymbol{S}$ directs normal inward into the electrode, i.e., normal outward to the surface of V. Since $\alpha_i(\boldsymbol{r}') = 0$ for $\boldsymbol{r}' \in S_j$ $(j \neq i)$, the surface integral has to be taken only over the surface S_i of electrode i, on which $\alpha_i(\boldsymbol{r}') = 1$. The volume integral vanishes due to Gauß's law, (4.18) and (4.22).

Therefore, the relation looked for is

$$\alpha_i(\boldsymbol{r}) = -\oint_{S_i} \left\{\epsilon_0 \boldsymbol{\epsilon}(\boldsymbol{r}') \boldsymbol{\nabla}_{\boldsymbol{r}'} G(\boldsymbol{r}', \boldsymbol{r})\right\} \mathrm{d}\boldsymbol{S}_i' \,. \tag{4.23}$$

What is expressed by this relation? The integrand times charge q represents according to (4.19) the dielectric field $\boldsymbol{D}(\boldsymbol{r}')$ at location $\boldsymbol{r}'$ caused by the point charge q at position $\boldsymbol{r}$. Thus

$$-q \cdot \alpha_i(\boldsymbol{r}) = q \cdot \oint_{S_i} \left\{\epsilon_0 \boldsymbol{\epsilon}(\boldsymbol{r}') \boldsymbol{\nabla}_{\boldsymbol{r}'} G(\boldsymbol{r}', \boldsymbol{r})\right\} \mathrm{d}\boldsymbol{S}_i' = -\oint_{S_i} \boldsymbol{D}(\boldsymbol{r}') \, \mathrm{d}\boldsymbol{S}_i' = \delta Q_i \tag{4.24}$$

determines due to Gauß the image charge δQ_i on the surface S_i of electrode i induced by this point charge q located at $\boldsymbol{r}$. Since $\sum_{i=1}^{M} \alpha_i(\boldsymbol{r}) = 1$ (see (2.9)), the total charge, induced on all electrodes by a charge q at position $\boldsymbol{r}$, sum up to the counter charge $-q = \sum_{i=1}^{M} \delta Q_i$ (see Fig.4.8a).

In Chapter 2, it was pointed out that $\alpha_i(\boldsymbol{r}) \cdot V_i$ represents the electrostatic potential at location $\boldsymbol{r}$, if the electrode i is set to V_i, the other M electrodes are grounded and $\rho_{\mathrm{ion}}(\boldsymbol{r}) = 0$ (see Fig. 4.8b). Combining both physical interpretations of $\alpha_i(\boldsymbol{r})$ reveals an equivalency for interpreting $q \cdot \alpha_i(\boldsymbol{r}) \cdot V_i$: The charge q possesses the electrostatic energy $q \cdot \alpha_i(\boldsymbol{r})\, V_i$ which is equal to the work which was done to transfer the image charge $-q \cdot \alpha_i(\boldsymbol{r})$ onto the electrode i with potential V_i. We will refer to this equivalency – denoted as the *electrostatic reciprocity between charge/image charges and potential/electrode potentials* – in several contexts (see discussion to (4.39) and Chapter 7).

Assuming that the Green's function of the electrostatic arrangement is known, the total electrostatic potential $\Phi_N(\boldsymbol{r})$ of N electrons can be expressed by combining (4.13), (4.16), (4.17), (4.21), and (4.23), as

$$\begin{aligned} \Phi_N(\boldsymbol{r}) &= \Phi_{\mathrm{el}} + \Phi_{\mathrm{ion}} + \Phi_{\mathrm{E}} \\ &= -\sum_{s=1}^{N} e\, G(\boldsymbol{r}, \boldsymbol{r}_s) + \int_V \rho_{\mathrm{ion}}(\boldsymbol{r}')\, G(\boldsymbol{r}', \boldsymbol{r})\, \mathrm{d}^3\boldsymbol{r}' + \sum_{i=1}^{M} \alpha_i(\boldsymbol{r})\, V_i \,. \end{aligned} \tag{4.25}$$

This expression takes into account the electrostatic potential of the electrodes $\{V_i\}$, the fixed charge distribution $\rho_{\mathrm{ion}}(\boldsymbol{r})$, the N electrons, and the image charges on the electrodes induced by $\rho_{\mathrm{ion}}(\boldsymbol{r})$ and the N electrons. Due to (2.4),

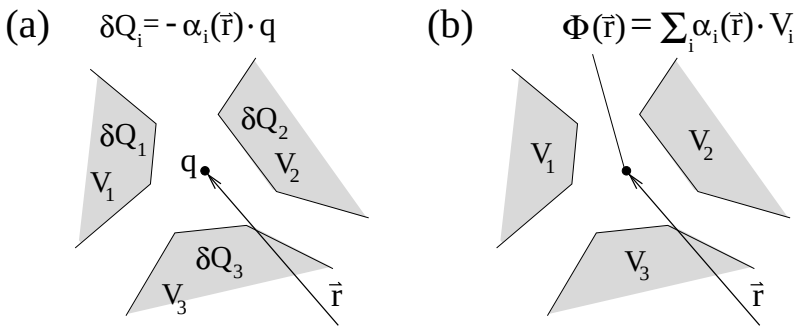

Fig. 4.8. The twofold meaning of the dimensionless function $\alpha_i(\boldsymbol{r})$: (a) Putting a charge q to position $\boldsymbol{r}$ induces the additional image charge $\delta Q_i = -\alpha_i(\boldsymbol{r}) \cdot q$ on electrode i if the electrodes' potentials V_j ($j = 1$ to M) are fixed. Therefore $\alpha_i(\boldsymbol{r})$ gives the fraction of image charge induced on electrode i. (b) The electrostatic potential $\Phi(\boldsymbol{r})$ at position $\boldsymbol{r}$ is proportional to the electrostatic potential V_i of electrode i. The proportionality factor is given by $\alpha_i(\boldsymbol{r})$.

the electric field $\boldsymbol{E}(\boldsymbol{r})$ present in the arrangement at position $\boldsymbol{r}$ is obtained by

$$\boldsymbol{E}(\boldsymbol{r}) = -\boldsymbol{\nabla}_{\boldsymbol{r}} \Phi_N(\boldsymbol{r}) \,. \tag{4.26}$$

Let us consider for the moment such a system containing not N but $s-1$ electrons. Taking one electron from a reference electrode with electrostatic potential zero and putting it to position $\boldsymbol{r}_s$ while keeping the electrostatic potentials $\{V_i\}$ of the electrodes fixed, work has to be performed: [10] The electron feels along its way the electric field $-\boldsymbol{\nabla}_{\boldsymbol{r}} \Phi_{s-1}(\boldsymbol{r})$, caused by the $(s-1)$ electrons already present, by the ion charge distribution $\rho_{\mathrm{ion}}(\boldsymbol{r})$ and by the gate electrode potentials $\{V_i\}$. They finally contribute by $-e\,\Phi_{s-1}(\boldsymbol{r}_s)$ to the potential energy of the electron s at position $\boldsymbol{r}_s$. However, the electron induces its own image charges on the electrodes also contributing to its potential energy. Like it was done for obtaining the electrostatic energy of the charge Q_0 on a metal island (see (2.29)), the potential energy $\Delta E^{(s)}_{\mathrm{pot}}(\boldsymbol{r})$ of the electron s at position $\boldsymbol{r}$ is obtained by integrating the differential electrostatic energy contributions $\{\Phi_{s-1}(\boldsymbol{r}) + q\,G(\boldsymbol{r},\boldsymbol{r})\} \cdot \mathrm{d}q$ from $q = 0$ to $q = -e$, leading to

$$\Delta E^{(s)}_{\mathrm{pot}}(\boldsymbol{r}) = \int_0^{-e} \Big\{ \Phi_{s-1}(\boldsymbol{r}) + q \cdot G(\boldsymbol{r},\boldsymbol{r}) \Big\}\, \mathrm{d}q = -e\,\Phi_{s-1}(\boldsymbol{r}) + \tfrac{1}{2} e^2\, G(\boldsymbol{r},\boldsymbol{r}) \,. \tag{4.27}$$

[10] The system fulfills charge conservation, i.e., the total charge of the system is uneffected, since respective image charges are induced on the electrodes.

One should note, the force $\boldsymbol{F}(\boldsymbol{r})$ felt by the electron s at position $\boldsymbol{r}$ is obtained from the gradient of $\Delta E^{(s)}_{\rm pot}(\boldsymbol{r})$ in position,

$$\boldsymbol{F}(\boldsymbol{r}) = -\boldsymbol{\nabla}_{\boldsymbol{r}}\left[\Delta E^{(s)}_{\rm pot}(\boldsymbol{r})\right] = e\,\boldsymbol{\nabla}_{\boldsymbol{r}}\Phi_{s-1}(\boldsymbol{r}) - \tfrac{1}{2}e^2\boldsymbol{\nabla}_{\boldsymbol{r}}G(\boldsymbol{r},\boldsymbol{r})\;, \qquad (4.28)$$

which is different to $-e\cdot\boldsymbol{E}(\boldsymbol{r})$, where $\boldsymbol{E}(\boldsymbol{r})$ is the electric field in the arrangement at position $\boldsymbol{r}$ given by (4.26),

$$-e\,\boldsymbol{E}(\boldsymbol{r}) = e\,\boldsymbol{\nabla}_{\boldsymbol{r}}\Phi_s(\boldsymbol{r}) = e\,\boldsymbol{\nabla}_{\boldsymbol{r}}\Phi_{s-1}(\boldsymbol{r}) - e^2\boldsymbol{\nabla}_{\boldsymbol{r}}G(\boldsymbol{r},\boldsymbol{r})\;. \qquad (4.29)$$

Comparing the second term of (4.28) with that of (4.29), it deviates by the prefactor $\frac{1}{2}$ since this force contribution is induced by the electron charge itself. [11]

The potential energy $E_{\rm pot}(N)$ for a total of N electrons in the arrangement is found by adding one electron after the other from the reference electrode to its positions into the system while keeping the electrostatic potential of all electrodes constant:

$$E_{\rm pot}(N) = \sum_{s=1}^{N}\Delta E^{(s)}_{\rm pot}(\boldsymbol{r}_s) = \sum_{s=1}^{N}\Big[-e\,\Phi_{s-1}(\boldsymbol{r}_s) + \tfrac{1}{2}e^2\,G(\boldsymbol{r}_s,\boldsymbol{r}_s)\Big]\;. \qquad (4.30)$$

Inserting $\Phi_{s-1}(\boldsymbol{r}_s)$ from expression (4.25) yields for the potential energy of N electrons confined in the quantum dot

$$\begin{aligned} E_{\rm pot}(N) = \sum_{s=1}^{N}\Bigg[\sum_{s'=1}^{s-1} e^2\,G(\boldsymbol{r}_s,\boldsymbol{r}_{s'}) + \tfrac{1}{2}e^2\,G(\boldsymbol{r}_s,\boldsymbol{r}_s) \\ -e\int_V \rho_{\rm ion}(\boldsymbol{r}')\,G(\boldsymbol{r}',\boldsymbol{r}_s)\,{\rm d}^3\boldsymbol{r}' - e\sum_{i=1}^{M}\alpha_i(\boldsymbol{r}_s)\,V_i\Bigg] \\ = \tfrac{1}{2}\sum_{s=1}^{N}\sum_{\substack{s'=1\\ s\neq s'}}^{N} e^2\,G(\boldsymbol{r}_s,\boldsymbol{r}_{s'}) + \tfrac{1}{2}\sum_{s=1}^{N} e^2\,G(\boldsymbol{r}_s,\boldsymbol{r}_s) \\ -e\sum_{s=1}^{N}\int_V \rho_{\rm ion}(\boldsymbol{r}')\,G(\boldsymbol{r}',\boldsymbol{r}_s)\,{\rm d}^3\boldsymbol{r}' - e\sum_{s=1}^{N}\sum_{i=1}^{M}\alpha_i(\boldsymbol{r}_s)\,V_i\;. \end{aligned} \qquad (4.31)$$

The first term of (4.31) represents the *electrostatic electron-electron energy*, the second *the electrostatic self-energy of the electrons* for the given electrode arrangement and the dielectric matrix. Both are determined by the Green's function. The third term takes into account the *ion charge* distribution, the fourth term the *electrode potentials*. Also their contributions are expressed by the Green's function.

[11] The factor $\frac{1}{2}$ in the second term of (4.28) is also found in the force between two charged conductors in a capacitor arrangement, – due to the same reason.

4.5 Electrostatic Green's Function for Special Arrangements

The electrostatic Green's function was defined by (4.18). For a homogeneous, isotropic dielectric medium without any electrodes, the Green's function is

$$G^{(\infty)}(\boldsymbol{r}, \boldsymbol{r}_s) = \frac{1}{4\pi\epsilon_0\epsilon\,|\boldsymbol{r} - \boldsymbol{r}_s|}\,. \tag{4.32}$$

Multiplying with the electron charge $-e$ yields the well-known Coulomb potential at $\boldsymbol{r}$ caused by an electron at position $\boldsymbol{r}_s$. If we put a second electron a position $\boldsymbol{r} = \boldsymbol{r}_{s'}$, the Green's function (4.32) describes a pure Coulomb interaction between both electrons (compare first term in (4.31)). In presence of electrodes or an inhomogeneous dielectric matrix, $G(\boldsymbol{r}_s, \boldsymbol{r}_{s'})$ deviates from (4.32) taking into account the induced image charges. The electron-electron interaction is therefore reduced by the presence of the metal electrodes in comparison to the pure Coulomb interaction. This is understood by a simple example (see Fig. 4.9c): Two electrons are confined in the (x, y)-plane between two parallel metal plate electrodes at distances d_1 and d_2 (see Fig. 4.9c(right)). These are, for instance, electrons of a 2D quantum dot between parallel electrodes. The Green's function for the more general case of this arrangement (see Fig. 4.9c(left)), has been derived 1996 by Hallam, Weis and Maksym [78]. Expressed by the point to point separation, projected into the (x, y)-plane, $\boldsymbol{\rho} = \boldsymbol{r}_{s\parallel} - \boldsymbol{r}_{s'\parallel}$ where $\boldsymbol{r}_{s\parallel}$, $\boldsymbol{r}_{s'\parallel}$ denote the in-plane component of $\boldsymbol{r}_s$ or $\boldsymbol{r}_{s'}$, respectively, and the z and z' coordinates of these points, the solution for Fig. 4.9c(left) reads in a two-dimensional Fourier representation as

$$G(\boldsymbol{r}_s, \boldsymbol{r}_{s'}) = G(\boldsymbol{\rho}; z, z') = \left(\frac{1}{2\pi}\right)^2 \int g_{\boldsymbol{k}}(z, z') \exp(i\boldsymbol{k}\,\boldsymbol{\rho})\,\mathrm{d}^2\boldsymbol{k} \tag{4.33}$$

with the Fourier transform $g_{\boldsymbol{k}}(z, z')$ for given z, z'

$$g_{\boldsymbol{k}}(z, z') = \begin{cases} \dfrac{\sinh\big(k\cdot\{d_1 + d_2 - z'\}\big)\,\sinh\big(k\,z\big)}{\epsilon_0\epsilon\,k\sinh\big(k\cdot\{d_1 + d_2\}\big)} & \text{, if } 0 \le z < z' \\[2ex] \dfrac{\sinh\big(k\,z'\big)\,\sinh\big(k\cdot\{d_1 + d_2 - z\}\big)}{\epsilon_0\epsilon\,k\sinh\big(k\cdot\{d_1 + d_2\}\big)} & \text{, if } z' < z \le d_1 + d_2\,. \end{cases} \tag{4.34}$$

Special cases of (4.34):

- The electron-electron interaction in a plane parallel to the electrodes ($z = z' = d_1$, see Fig. 4.9c(right)) is therefore determined by

$$G(\rho; d_1, d_1) = \frac{1}{4\pi\epsilon_0\epsilon}\frac{1}{2\pi}\int \frac{f(k)}{k}\exp\Big(i\boldsymbol{k}\,\boldsymbol{\rho}\Big)\,\mathrm{d}^2\boldsymbol{k} \tag{4.35}$$

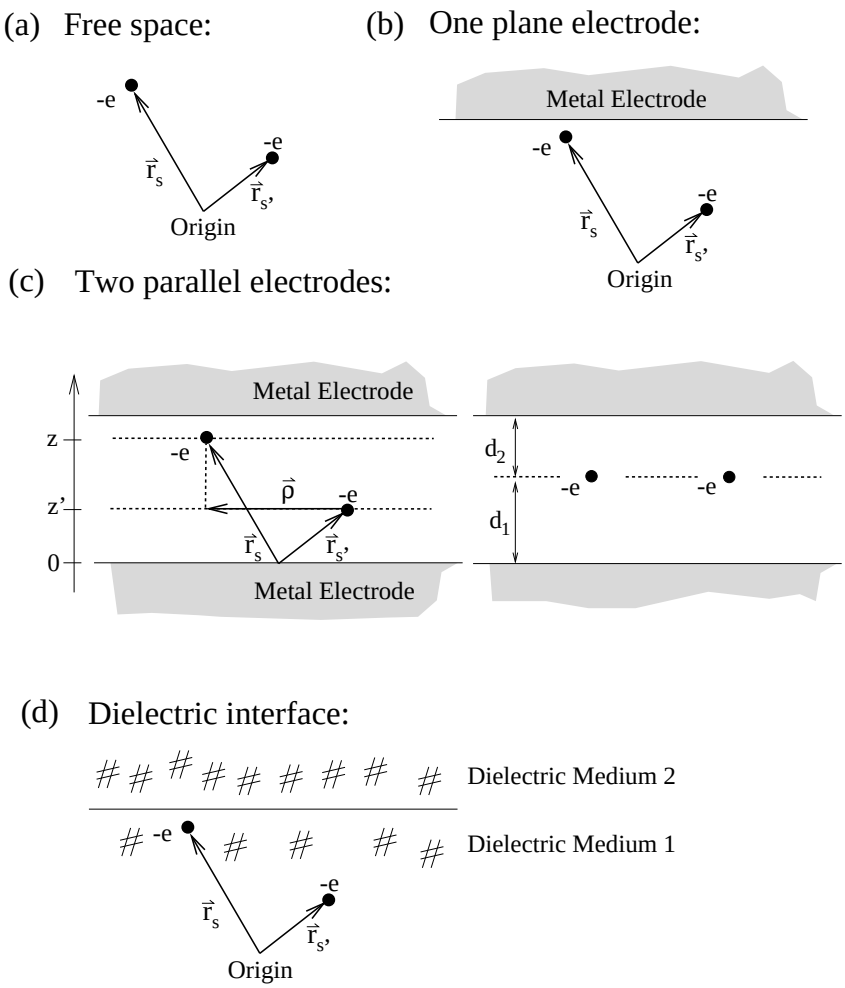

Fig. 4.9. Electrostatic electron-electron interaction: (a) In free space, the interaction between two electrons located at $\boldsymbol{r}_s$ and $\boldsymbol{r}_{s'}$ is decribed by the Green's function of infinite space, i.e., a pure Coulomb interaction. (b) The presence of a metal electrode screens the electron-electron interaction. (c) Left: For two parallel electrodes, the Green's function is known (see (4.34)). It contains as limits the cases (a) and (b). (c) Right: Electrons restricted to a plane between the electrodes simplifies the description (see (4.35)). (d) The electron-electron interaction is also affected by the polarization at interfaces between media of different dielectric constants.

with

$$f(k) = \frac{2\sinh\big(k\,d_1\big)\,\sinh\big(k\,d_2\big)}{\sinh\big(k\cdot\{d_1+d_2\}\big)}\ . \tag{4.36}$$

- For large electron-plate separations ($d_1 \to \infty$ and $d_2 \to \infty$), $f(k)$ becomes unity and (4.35) reduces to the pure Coulomb interaction potential.

- For only one plate electrode close-by, i.e., $d_2 \gg d_1$, $f(k)$ reduces to $f(k) \approx 1 - \exp(-2kd_1)$, leading to the electrostatic electron-electron interaction [78]

$$G(\boldsymbol{r}_s, \boldsymbol{r}_{s'}) = \frac{1}{4\pi\epsilon_0\epsilon}\frac{1}{|\boldsymbol{\rho}|}\left\{1 - \left(1 + \frac{4\,{d_1}^2}{|\boldsymbol{\rho}|^2}\right)^{-1/2}\right\} . \tag{4.37}$$

  For small electron-electron distances $|\boldsymbol{\rho}| \ll d_1$, the interaction follows $1/|\boldsymbol{\rho}|$, whereas for $|\boldsymbol{\rho}| \gg d_1$, the screening by the plate electrode leads to an interaction following $1/|\boldsymbol{\rho}|^3$: Two electrons at a distance d in front of a plane metal electrode feel at large distances $|\boldsymbol{r}_s - \boldsymbol{r}_{s'}| \gg d$ between them only the dipole formed by an electron and its image charge on the metal electrode.

The discussed examples shows clearly that the electrode arrangements determines the electron-electron interaction. This is also true for the self-energy, governed by $G(\boldsymbol{r}_s, \boldsymbol{r}_s)$ which gives divergent energy contributions. However, the self-energy term in (4.31) cannot just be excluded from the sum since it contains the contributions of the electron with its image charges induced on the electrodes. For a continuous charge distribution, techniques are known to overcome the self-energy divergency. Since later, quantum mechanical expectation values are calculated and the electrons are represented by a continuous wavefunction in space, the self-energy divergency need not be cancelled for the following. A discussion how to exclude this self-interaction term at this stage is done by Hallam, Weis and Maksym [78].

4.6 Hamiltonian of N Electrons Confined in a Realistic Quantum Dot

We consider a realistic quantum dot, as discussed in Section 4.4 and schematically depicted in Fig. 4.7, containing N (conduction band) electrons. The Hamiltonian for these electrons is obtained by adding the kinetic energy $\sum_{s=1}^{N}\{{\boldsymbol{p}_s}^2/(2m_e^*) + \varepsilon_0^{\mathrm{C}}(\boldsymbol{r}_s)\}$ to the potential energy $E_{\mathrm{pot}}(N)$ of (4.31). By replacing the moment vector $\boldsymbol{p}_s$ and the position vector $\boldsymbol{r}_s$ of the electrons by their respective operators $\hat{\mathbf{p}}_s$ and $\hat{\mathbf{r}}_s$, the Hamilton operator $\hat{\mathbf{H}}$ for the N electron system with fixed electrostatic potential at all electrodes can be written in coordinate representation ($\hat{\mathbf{r}}_s = \boldsymbol{r}_s$) as

$$\hat{\mathbf{H}}(N;\{V_i\}) = \sum_{s=1}^{N}\left[\frac{\hat{\mathbf{p}}_s^2}{2m_e^*} - e\,\Phi_{\mathrm{ext}}(\boldsymbol{r}_s)\right] + \frac{1}{2}\sum_{s=1}^{N}\sum_{\substack{s'=1\\ s'\neq s}}^{N} e^2\,G(\boldsymbol{r}_s, \boldsymbol{r}_{s'}) \tag{4.38}$$

with the *external* or bare confining potential

$$\Phi_{\mathrm{ext}}(\boldsymbol{r}) = \Phi_{\mathrm{ion}}(\boldsymbol{r}) - \tfrac{1}{2}e\,G(\boldsymbol{r}, \boldsymbol{r}) + \Phi_{\mathrm{E}}(\boldsymbol{r}) - \varepsilon_0^{\mathrm{C}}(\boldsymbol{r})/e$$

$$= \int_V \rho_{\mathrm{ion}}(\boldsymbol{r}')\, G(\boldsymbol{r}', \boldsymbol{r})\, \mathrm{d}^3\boldsymbol{r}' - \tfrac{1}{2} e\, G(\boldsymbol{r}, \boldsymbol{r}) + \sum_{i=1}^{M} \alpha_i(\boldsymbol{r})\, V_i - \varepsilon_0^{\mathrm{C}}(\boldsymbol{r})/e \ . \tag{4.39}$$

Energetical differences in the conduction-band minima between the different materials have been taken into account by the position-dependence of $\varepsilon_0^{\mathrm{C}}(\boldsymbol{r})$. For considering a local variation of the effective mass due to the local variation of the material, the kinetic energy operator has to be modified (see [74]). Such a general treatment including band structure effects is beyond the scope of what should be discussed here. Let us now have a closer look to the different terms of the Hamiltonian derived.

4.6.1 Electron-Electron Interaction

The electron-electron interaction in the quantum dot is described in the Hamilton operator (4.38) by the term

$$\hat{\mathbf{H}}_{\mathrm{el,el}} = \frac{1}{2} \sum_{s=1}^{N} \sum_{\substack{s'=1 \\ s \neq s'}}^{N} e^2\, G(\boldsymbol{r}_s, \boldsymbol{r}_{s'})$$

and is therefore directly given by the electrostatic Green's function for the given electrode arrangement and dielectric matrix. Hence, the electron-electron interaction is reduced by the presence of the metal electrodes in comparison to the pure Coulomb interaction $\propto 1/|\boldsymbol{r}_s - \boldsymbol{r}_{s'}|$ between two point charges as was explained in Section 4.5. That is, the electrode arrangement determines the electron-electron interaction. This modification is especially important in cases where the diameter of the quantum dot is comparable to distances to metal-like electrodes [78]. In vertical quantum dot systems presented in Fig. 4.5, the source and drain leads are only separated by tunnel barriers of few tens of nanometers whereas the quantum dot diameter is in the range of hundred nanometers. Therefore in such structure, the close-by leads might screen [12] the electron-electron interaction in the embedded quantum dot. [13]

Also an inhomogeneous dielectric matrix or a dielectric mismatch causes modifications of a pure Coulomb interaction. For instance, such dielectric mismatch is found at the surface of an etched structure, at the interfaces of heterostructures [74], at semiconductor/insulator interfaces or at the surface of colloidally prepared semiconductor clusters with organic surface passivation [119]. These modifications are also taken into account by the Green's

[12] Metal electrodes or the dielectric *screen* the electron-electron interaction. Fixed ion charges do not screen but *compensate* for electrical charges.

[13] Usually calculations refering to the experiments using these structures assume a pure Coulomb interaction adopting the dielectric constant ϵ and the confining energy to the experimental results.

function (4.18) describing the complete electrostatic arrangement. Recently in 2001, Orlandi and coworkers [120] calculated spherical quantum dots with a radial dielectric mismatch. The respective Green's function is found there. For a quantum dot embedded in a matrix of lower dielectric constant, the electron-electron interaction is enhanced, and also the many-electron states in the quantum dot are modified compared to the case without dielectric mismatch.

4.6.2 External Confining Potential

The *external confining potential* $\Phi_{\mathrm{ext}}(\boldsymbol{r})$ for the electrons which depends on the arrangement but not on the electron number N is given by (4.39). The contributions are interpreted in the following, and sketched in Fig. 4.10:

1. The first term $\Phi_{\mathrm{ion}}(\boldsymbol{r})$ describes the electrostatic potential contribution caused by the fixed charge distribution $\rho_{\mathrm{ion}}(\boldsymbol{r})$ if the electrostatic potentials of the electrodes are set to zero. Image charges of this ion charge distribution induced on the electrodes and seen by the electrons are taken into account by the Green's function $G(\boldsymbol{r}, \boldsymbol{r}')$ (Fig. 4.10a).
2. The second term $-\frac{1}{2}e \cdot G(\boldsymbol{r}, \boldsymbol{r})$ contains the interaction of the electron at position $\boldsymbol{r}$ with *its own image charges* on all the M electrodes. This term was already mentioned at the end of Section 4.5. The following examples may illustrate its importance: An electron in front of a metal electrode (Fig. 4.10b) is attracted by its image charges, i.e., its electrostatic potential varies with its position $\boldsymbol{r}$ relative to the metal electrode. It is the origin, for instance, of the Schottky effect of lowered barriers in field emission devices. It contributes to the external confining potential since it does not depend on the position of the other electrons, only on the position of the electron itself in the arrangement. Also interfaces, giving a local change in the dielectric properties, create a contribution to the confining potential via $G(\boldsymbol{r}, \boldsymbol{r})$ [74]. An example is given in Fig. 4.10b. Goldoni, Rossi and Molinari [121] proposed using the dielectric confinement for enhancing exciton binding energies in nanostructures. A dielectric mismatch can be either attractive or repulsive for the electrons.
3. The third term $\Phi_{\mathrm{E}}(\boldsymbol{r})$ in (4.39) depends linearly on the electrostatic potentials $\{V_i\}$ of the electrodes: The electrostatic potential change of an electron at position $\boldsymbol{r}$ due to a change in the electrostatic potential V_i of electrode i is proportional to the fraction of image charge $e\,\alpha_i(\boldsymbol{r})$ (see (4.22)) induced by the electron on the electrode i,

$$\Phi_{\mathrm{ext}}(\boldsymbol{r}) \propto e\,\alpha_i(\boldsymbol{r}) \cdot V_i \ . \tag{4.40}$$

This reflects the electrostatic reciprocity (see discussion to (4.22)). Voltages applied to gate electrodes can be used intentionally to change the bare confining potential of the quantum dot [111, 109].

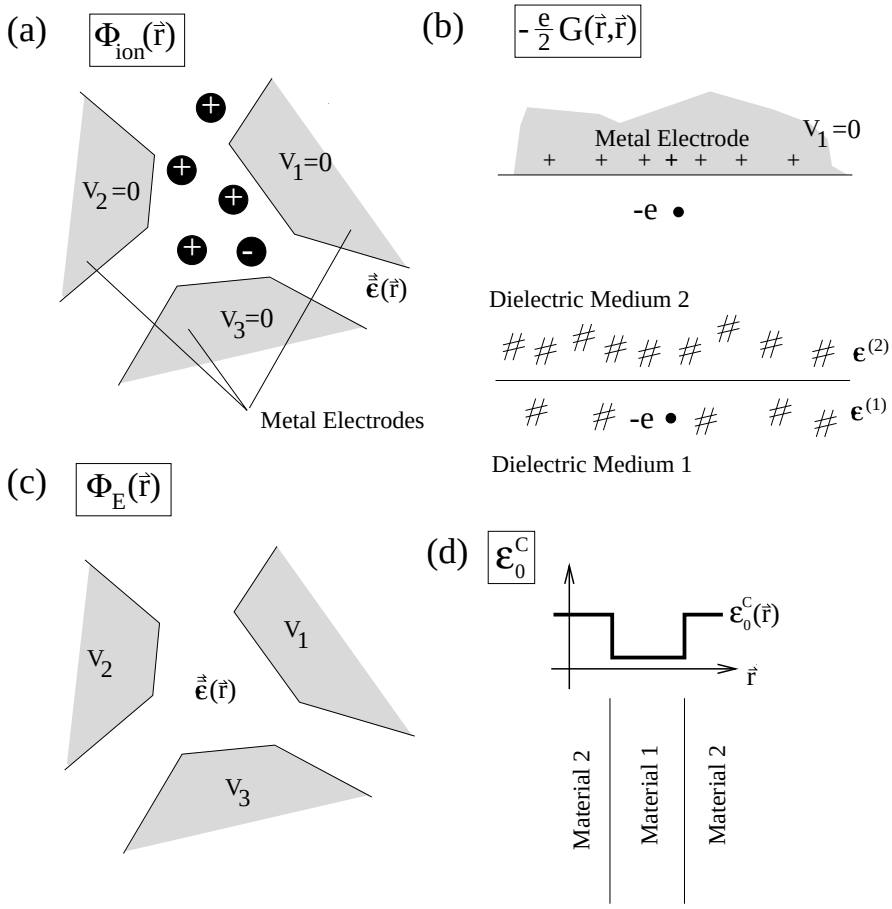

Fig. 4.10. Contributions to the external confining potential of the quantum dot: (a) A fixed charge distribution with its image charges. (b) The image charge of a single electron induced on a metal electrode. Also the field induced polarisation of an interface between dielectric media of different electric constants attracts the electron to the interface if $\epsilon^{(1)} < \epsilon^{(2)}$ or repels the electron from the interface if $\epsilon^{(1)} > \epsilon^{(2)}$. (c) The electrostatic potential differences between the electrodes define an electrostatic potential landscape. (d) The variation of the conduction-band minimum due to material varying with position.

4. The last term $\varepsilon_0^{\mathrm{C}}(\boldsymbol{r})$ describes a position dependent conduction-band minimum due to different materials at positions of the quantum dot. It includes, for instance, the conduction-band offset at heterojunctions or the steep confinement present at etched surfaces due to the transition to vacuum (see Fig. 4.10d). Surface charges usually present on such surfaces and repelling the electrons from such surfaces are modelled by the first term in (4.39) via $\rho_{\mathrm{ion}}(\boldsymbol{r})$.

To emphasize, the external confining potential $\Phi_{\text{ext}}(\boldsymbol{r})$ is *not* equal to the electrostatic potential profile with no electrons present in the quantum dot. The latter neglects the second term $-\frac{1}{2}e\cdot G(\boldsymbol{r},\boldsymbol{r}')$ describing the contribution due to the own image charges. One should also be aware of that the external confining potential is different to the effective confining potential seen by the single electrons in a Hartree- or Hartree-Fock-like ansatz.

4.7 Energy Spectrum, Groundstate, Excited States, and Addition Spectrum of an N-Electron System Confined in a Quantum Dot

Due to the wide variety of arrangements for a quantum dot, the exact solution of the Schrödinger equation for N electrons in a quantum dot cannot in general be given. In this Section, firstly a notation is introduced labeling the N-electron states starting from the groundstate of the N-electron system. Then some approximations for treating N interacting electrons in a quantum dot are briefly mentioned. Thereafter, the total energy spectra of a parabolic 2D quantum dot with one, two and three electrons are presented to emphasize the importance of talking in terms of few or many-electron states instead of single-electron states when discussing in general the electronic properties of quantum dots. Finally the concepts *Addition Spectrum* and *Excitation Spectrum* are distinguished.

4.7.1 Exact Solution of the N-Electron Schrödinger Equation

The energy spectrum of the quantum dot, filled with N electrons, is obtained by solving the N-electron Schrödinger equation

$$\hat{\mathbf{H}}(N;\{V_i\})\ \big|N,l;\{V_i\}\big\rangle = E(N,l;\{V_i\})\cdot\big|N,l;\{V_i\}\big\rangle\,. \tag{4.41}$$

$E(N,l;\{V_i\})$ denotes the total energy of the state $|N,l;\{V_i\}\rangle$ of the N electrons in the quantum dot. The number l stands for a multiplet of quantum numbers which have be chosen properly for characterizing the states of the N-electron system. Good quantum numbers are found for quantum dots possessing certain symmetries, leading to integrals of motion (like angular momentum), but also other quantities like the total spin or the spin projection characterize the N-electron system as quantum numbers. Irregular shaped quantum dots usually do not offer integrals of motions. Nevertheless for each set of parameters N and $\{V_i\}$, it should be possible to denote the N-electron states definitely. To avoid explicit quantum numbers in the following, the states are labeled by $l=0,1,2,\cdots$, starting from $l=0$ for the groundstate of the N-electron system in the quantum dot. The excited states are numbered unambiguously with increasing energy, i.e., $E(N,l;\{V_i\}) \le E(N,l+1;\{V_i\})$,

allowing also for degeneracy due to the spatial symmetry of the quantum dot or due to the spin, for instance.

None has solved the N-electron system for arbitrary confining potential and electron-electron interaction. The physics of quantum dots is rich

- due to the variety of the external confining potenial, – for instance, with or without geometrical symmetry,
- due to the variations in screening the electron-electron interaction, and
- due to different relative magnitude of quantization energy by confining and electron-electron interaction energy.

The Schrödinger equation (4.41) covers in one limit metals, in the other limit single atoms. The interesting physics in the interplay between confinement and electron-electron interaction leading to correlations between the electrons is found between both limits.

4.7.2 Approximations for Treating N Electrons in a Quantum Dot

Models for quantum dots have been investigated and applied to certain experiments. A more complete presentation of the large amount of theoretical work which has been done is found in the collection of diverse reviews [7, 6, 8]. Here we emphasize only certain aspects.

- Usually a box-like [122] or parabolic confining potential [123, 124] is assumed for describing the shape of the external confining potential. The latter gives a first approximation to a local minimum in a potential landscape of the true external confining potential.
- With few electrons in such a system (less then 10), the Hamiltonian of the interaction electrons can be exactly solved numerically with reasonable effort. As the base for the few-electron wavefunction, the superposition of Slater determinants with single-electron states fitting to the external confining potential are used and the Hamiltonian in the matrix presentation of this base is numerically diagonalized (see, for instance, [122]).
- For high electron numbers approximations have to be done – usually based on Hartree or Hartree-Fock-like states. An effective confining potential is obtained for the single electrons. Single-electron states are obtained with eigenenergies ε_i. These might be more adequate to be used in the Constant Interaction Model than those electronic states and single-electron energies found for the external confining potential.
- For high electron numbers, the Thomas-Fermi approximation has been used combined with Poisson equation [125].
- Usually for the description of a quantum dot, a $1/|\boldsymbol{r}-\boldsymbol{r}'|$ interaction is assumed (see, for instance, [122, 123, 124, 126]). As pointed out, this is equal to the Green's function of the infinite space filled by a homogeneous dielectric medium.

- If the Poisson equation and Schrödinger equation are solved self-consistently [127] for a given electrostatic surrounding, image charges are taken into account by the boundary conditions for the total electrostatic potential. These calculations are usually based on a Hartree-like or a Hartree-Fock-like ansatz. Correlation effects between the electrons (besides exchange interaction) are excluded by such an ansatz since those are not described by a single product ansatz of single-particle states (for instance, by a single Slater determinant). Functional density methods are used for improving here [128].
- Spherical symmetry in the bare confining potential and in the Coulomb interaction leads to a shell-like structure in the energy spectrum minimizing the energy for adding an electron to the quantum dot for certain 'magic' numbers. It reminds on the variation of the ionisation energy in the periodic system of real atoms. Hund's rule is found, well known for real atoms. A generalized Hund's rule can be derived for such quantum dots in magnetic fields [129].
- Correlations in the spatial position of the electrons are found for low density quantum dots, since the electrons prefer due to the electrostatic Coulomb interaction certain configurations between point charges.
- The modifications of the few-electron states in a 2D quantum dot by screening the electron-electron interaction by parallel plate electrodes was investigated by Hallam and coworkers [78].
- For an electron-electron interaction term following $1/|\boldsymbol{r}-\boldsymbol{r}'|^2$ instead of a pure Coulomb interaction, even analytical solutions have been found for parabolic confining potentials [7]. Such an ansatz mimicks screening of wide range Coulomb interaction.
- For large quantum dots of irregular shape, the Constant-Interaction Model has been applied to extract single-particle energy level spacings and compare it statistically with Random Matrix Theory (for review: [118]).
- A systematic comparison between CIM model and experimental data was presented by L. Kouwenhoven, D.G. Austing and S. Tarucha [5] for vertical quantum dot systems, denoted as atom-like quantum dots where the quantization energy due to confining just dominates over the electron-electron interaction. Some trues but also limitations of the CIM are presented. Modifications due to electron exchange interaction and correlations have to be taken into account for a proper desciption of the experimental data.

Applying a *magnetic field* B modifies the electronic states of the quantum dot. That is why the magnetic field is an important tuning parameter to learn more about the realized quantum dot and the confined interacting few- or many-electron system. The effect is stronger for quantum dots than for real atoms since the magnetic confinement – expressed by the cyclotron energy $\hbar\omega_{\mathrm{c}} = e\,B/m_e^*$ – increases with 1.7 meV per Tesla for the effective mass in GaAs, i.e., exceeds at few Tesla the typical quantization energy $\hbar\omega_0$ given by a parabolic electrostatic confining. The Zeeman energy $E_{\mathrm{Z}} = g\mu_{\mathrm{B}}B$ is small

(0.33 meV/T) since the Landé g-factor for GaAs is only $g = -0.44$. The following remarks to quantum dots in magnetic fields:

- The single-particle states of a 2D quantum dot with a parabolic external confining potential are described in a perpendicular magnetic field by so-called Fock-Darwin states [130, 131].
- With the first experiments in 1991 on 2D quantum dots in high magnetic fields the Thomas-Fermi approximation has been applied [125] leading to so-called compressible and incompressible regions [132] in the quantum dot. It was the first demonstration that the CIM model is not the adequate description for such a quantum dot system.
- Most of the calculation on few-electron quantum dots focus on changes in the energy spectrum with applying magnetic field. Since an in-situ tunable parameter, it allows to reveal correlation effects –like, for instance, a singlet-triplet transition induced by magnetic field [133].

4.7.3 N Electrons in 2D Quantum Dot With Parabolic Confining Potential and Pure Coulomb Electron-Electron Interaction: The Total Energy Spectrum

To demonstrate the complexity of an interacting N electron system already in a simple example, the total energy spectra are shown in Fig. 4.11 for one, two and three electrons in a 2D quantum dot with a parabolic confining potential:

- A single electron in the quantum dot has a groundstate energy $E(N = 1, l = 0) = \hbar\omega_0$ and an excitation spectrum revealing an equidistant ladder of energy levels.
- For two electrons in the system, the total energy $E(N = 2, l = 0)$ for the groundstate includes the kinetic energy of both electrons and the electron-electron interaction. Important to realize, the excitation spectrum of this two-electron system does not reflect simply the excitation of the electrons in higher single-particle states with constant electron-electron interaction. It is more complex.
- With three electrons, the excitation spectrum becomes already dense at low excitation energies, i.e., below the confining quantization energy $\hbar\omega_0$.

To keep the discussion for electrical transport through quantum dots general, such an energy spectrum asks to talk of *few-* or *many-electron states* on the quantum dot instead of single-electron states.

4.7.4 Addition Spectrum and Excitation Spectrum of a Quantum Dot

To describe the rearrangement of electrons between quantum dot and electrodes, it is convenient to introduce the minimum energy which is required

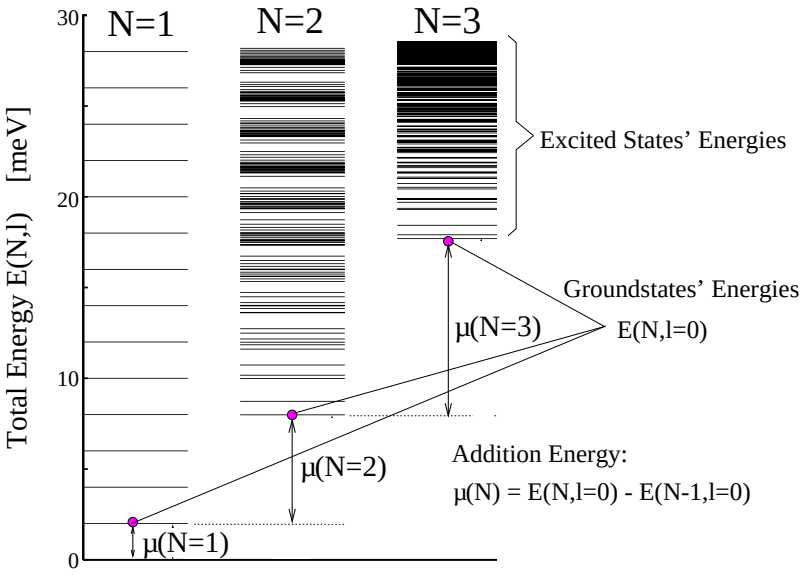

Fig. 4.11. Total energy spectrum of one, two and three electrons in a two-dimensional parabolic confining potential assuming $\hbar\omega_0 = 2$ meV and a pure Coulomb electron-electron interaction. The parameters are $m_e^* = 0.067\, m_e$ and $\epsilon = 12.4$ leading to an effective diameter (4.8) for the quantum dot of $D = 45$ nm. The electron-electron interaction between two electrons dominates the quantization energy $\hbar\omega_0$. The system with one electron has been denoted as QD *Hydrogen*, with two electrons as QD *Helium*, and with three electrons as QD *Lithium* (adopted from D. Pfannkuche and S. Ulloa [134]).

to add the next electron from a reference electrode to the quantum dot when already N electrons are present there in their groundstate. This *addition energy* $\mu(N+1;\{V_i\})$ is defined by the difference between the groundstate energy $E(N+1, l=0;\{V_i\})$ of $(N+1)$ electrons in the quantum dot and the groundstate energy $E(N, l=0;\{V_i\})$ of N electrons in the quantum dot,

$$\mu(N+1;\{V_i\}) \equiv E(N+1, l=0;\{V_i\}) - E(N, l=0;\{V_i\})\,. \qquad (4.42)$$

It is sometimes denoted as the *(electro-)chemical potential of the quantum dot.* Starting with N electrons in the quantum dot and adding the next electron, this energy is the analogous of the *affinity* of real atoms. The other process – starting with N electrons in the groundstate and taking off one electron to the reference electrode with electrochemical potential $\mu_S^{\rm elch}$ – reflects an *ionisation* process of the quantum dot and requires the minimum energy $\mu_S^{\rm elch} + E(N-1, l=0;\{V_i\}) - E(N, l=0;\{V_i\}) = \mu_S^{\rm elch} - \mu(N;\{V_i\})$.

The energies $\mu(N;\{V_i\})$ with $N = \{0,1,2,\cdots\}$ are defining an energy ladder, which will be used in the next Chapter 5 to describe the thresholds for single-electron transport through a quantum dot and generalize the energy ladder introduced in Chapter 1. Variations in the level distance of this energy ladder [14]

$$\Delta E_{\rm add} = \mu(n+1;\{V_i\}) - \mu(n;\{V_i\}) \quad \text{with } n = \cdots N-1, N, N+1\cdots \tag{4.43}$$

are referred as *addition spectrum* of the quantum dot and should not be mixed up with the *excitation spectrum* of the quantum dot of a fixed electron number,

$$\Delta E_{\rm exc} = E(n, l\neq 0;\{V_i\}) - E(n,0;\{V_i\}) \quad \text{with } n = \cdots N-1, N, N+1\cdots . \tag{4.44}$$

These quantities are indicated in the energy spectrum depicted in Fig.4.11.

4.7.5 Collective Excitations and Single-Particle Excitations

It is worthwhile to emphasize that different kind of excitations might exist in quantum dots:

- Exciting an electron from a single-particle state to a single-particle state of higher energy and thereby creating a hole at lower energy is denoted *single-particle excitation* (see Fig. 4.12). These are the only excitations described in the Constant-Interaction Model.
- Electron systems in quantum dots with a parabolic confining potential characterized by $\hbar\omega_0$ and bare Coulomb interaction obey the Kohn's theorem [135] which allows to separate between the center-of-mass motion of the whole electron system and the relative motion of the electrons. Far infrared spectroscopy on 2D quantum dots [136] reveals this center-of-mass motion as a collective excitation of the electron system. It is quantized in $\hbar\omega_0$ independently of the number N of confined electrons. Applying a magnetic field, so-called *magneto-plasmons* are found as collective excitations [136]. Those can still be found if a slightly anharmonic potential contribution is introduced [137].
- As indicated in Fig. 4.12b also vibrational or rotational collective excitations might be observable. Those have been predicted for electron systems in quantum dots dominated by Coulomb interaction. For large electron numbers, a hydrodynamical model might be applicable [138, 139].

[14] In literature the term 'addition energy' is also used to denote the quantity $\mu(n+1;\{V_i\})-\mu(n;\{V_i\})$ instead of our association with $\mu(n+1;\{V_i\})$. Both definitions are in use.

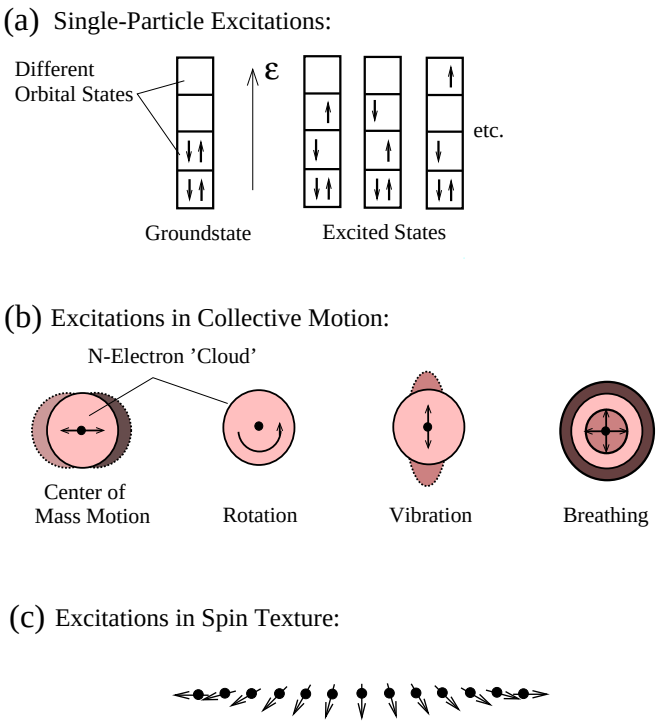

Fig. 4.12. Examples for various kinds of excitations which might exist for the few- or many-electron system confined in a quantum dot: (a) Single-particle exitations: Single electrons are lifted to single-particle states of higher energy. (b) Excitations in the collective motion of the electrons, i.e., for instance, center-of-mass motion, rotation, vibration, or breathing. For a large number of electrons, these excitations are plasma-like excitations. (c) Spin texture in which excitations, i.e., spin-waves or skyrmions, can occur.

- High magnetic fields applied to a two-dimensional electron system freeze the motion of the electrons so that the electron-electron interaction in the system leads to correlated states which have been related to states present in the *Fractional Quantum Hall Effect* or in a Wigner solid. Collective excitations within a spin-texture – so-called *skyrmions* – have been predicted (for instance, [140]). Similar excitations can be expect under circumstances also for 2D quantum dots, denoted as quantum Hall droplets. For such systems low-lying charge density excitations have been predicted (for instance, [141]).

Within the Constant Interaction Model, there is an obvious identity of addition spectrum and excitation spectrum: Single-electron states are consecutively filled with adding single electrons, and are also used for single-particle

excitations. For collective excitations in real many-electron systems, such a correlation is not obvious. D. Stewart and coworkers [142] reported from their experiments some correlations in comparing the addition and the excitation spectrum of a rather large quantum dot.

4.8 Is the Concept of Capacitance Coefficients for a Quantum Dot Reasonable?

To describe the effect of Coulomb blockade and single-electron charging, the concepts of capacitance coefficients were introduced in Chapter 2. The definition (2.12) of capacitance coefficients C_{ij} are based on the assumption of the *existence of surface charges* at the electrodes where the dielectric field ends. This treatment involves that the bulk density n_0 of free electrons in the electrodes is sufficiently high in order that the external dielectric field can end on the surface charge within atomic distances near the surface of electrodes. Due to the Thomas-Fermi theory of screening by a Sommerfeld electron gas [82] with fixed ion background, the screening length is

$$\ell = \sqrt{\frac{2\,\epsilon_0\epsilon}{3\,n_0\,e^2}\,\varepsilon_\mathrm{F}} = \left(\frac{\pi}{3}\right)^{\frac{1}{6}} \frac{1}{2} \sqrt{\epsilon\,\frac{m_e}{m_e^*}\,a_\mathrm{B}\,n_0^{-1/3}} \tag{4.45}$$

where $\varepsilon_\mathrm{F} = (3\pi^2 n_0)^{2/3}\hbar^2/2m_e^*$, the bulk electron concentration n_0 and the Bohr radius $a_\mathrm{B} = 4\pi\epsilon_0\hbar^2/m_e e^2 = 5.3 \cdot 10^{-11}$ m. Since for metals the mean distance $n_0^{-1/3}$ between conduction-band electrons is in the range of 0.2 nm to 0.5 nm, the Thomas-Fermi screening length ℓ becomes smaller than the distance between atoms in the crystal lattice which justifies the concept of surface charges for usual metal electrodes.

In contrary, the system of conduction-band electrons in a quantum dot has a more or less pronounced discrete energy spectrum due to the mesoscopic size, and the electron concentration n_0 is usually less than in a metal system. The screening length ℓ obtained from (4.45) for much smaller electron concentrations is comparable or even larger than the diameter of the quantum dot. Therefore, does it make physically sense to define capacitance coefficients $C_{0,j}$ and $C_{0\Sigma}$ between the quantum dot (index '0') and the M electrodes $j = 1 \cdots M$ surrounding this quantum dot? To address this issue, we compare the electrostatic energy (2.29), derived for a metal island which is surrounded by M metal electrodes and charged by ΔN electrons under the assumption $Q_{0,\mathrm{ion}} = 0$,

$$E_\mathrm{elst}(\Delta N) = -\Delta N e \cdot \sum_{j=1}^{M} \frac{C_{0,j}}{C_{0\Sigma}} V_j + \frac{(\Delta N e)^2}{2C_{0\Sigma}}\,, \tag{4.46}$$

with the total energy of N electrons in the state $|N, l; \{V_i\}\rangle$ (normalized to N) in the quantum dot,

$$E(N,l;\{V_i\}) = \langle N,l;\{V_i\}|\ \hat{\mathbf{H}}(N;\{V_i\})\ |N,l;\{V_i\}\rangle$$

$$= \left\langle N,l;\{V_i\}\right|\ \sum_{s=1}^{N}\left[\frac{\hat{\mathbf{p}}_s^2}{2m_e^*} - e\,\Phi_{\rm ext}(\boldsymbol{r}_s)\right]\ \left|N,l;\{V_i\}\right\rangle$$

$$+\left\langle N,l;\{V_i\}\right|\ \frac{e^2}{2}\sum_{s=1}^{N}\sum_{\substack{s'=1\\ s'\neq s}}^{N} G(\boldsymbol{r}_s,\boldsymbol{r}_{s'})\ \left|N,l;\{V_i\}\right\rangle . \quad (4.47)$$

To find expressions for the capacitance coefficients for a quantum dot by comparing (4.46) and (4.47), we will follow different approaches which are characterized by the following questions:

- In Section 4.8.1: How does the total energy of the quantum dot change with varying the electrostatic potential of a gate electrode? For a metal system, this depends on the ratios of capacitance coefficients.
- In Section 4.8.2 and Section 4.8.4: How does the electron-electron interaction varies with the electron number? For a metal island, it is described by a constant – the total capacitance.
- In Section 4.8.3: How large is the gate voltage change needed to add an additional electron to the quantum dot? For a metal island, it is given by e divided by the capacitance coefficient to the respective electrode.

These comparisons will reveal that the concept of capacitance coefficients might be reasonable only under certain circumstances. However, they may be fulfilled by special geometric arrangements of quantum dot and metal electrodes.

4.8.1 Ratios of Capacitance Coefficients

For the quantum dot, N electrons in the normalized state $|N,l;\{V_j\}\rangle$ induce the *image charge* δQ_i on the electrode i which is obtained as the quantum mechanical expectation value

$$\delta Q_i = \left\langle N,l;\{V_j\}\right|\ e\sum_{s=1}^{N}\alpha_i(\boldsymbol{r}_s)\ \left|N,l;\{V_j\}\right\rangle , \quad (4.48)$$

where (4.24) has been used.

For the metal system, the ratio between the capacitance coefficient $C_{0,i}$ and the total capacitance $C_{0\Sigma}$ determines the charge fraction δQ_i which is induced on electrode i by the charge $Q_0 = -\Delta N e$ on the metal island,

$$\delta Q_i = C_{0,i}/C_{0\Sigma}\cdot\Delta N\, e\,. \quad (4.49)$$

A comparison of the results (4.49) and (4.48) suggests to define a 'capacitance ratio' for N electrons in the state $|N,l;\{V_j\}\rangle$ by

$$N \cdot \left[\frac{C_{0,i}}{C_{0\Sigma}}\right]_{|N,l;\{V_j\}\rangle} \equiv \left\langle N,l;\{V_j\}\right| \sum_{s=1}^{N} \alpha_i(\boldsymbol{r}_s) \left|N,l;\{V_j\}\right\rangle . \qquad (4.50)$$

This quantity governs also the change of system energy with electrostatic potential variations: For N electrons in state $|N,l;\{V_j\}\rangle$ the *change of the total energy by a change of* V_i follows from (4.47) and (4.50). In first approximation, i.e., neglecting a change in the wavefunction with V_i, i.e., $\partial|N,l;\{V_j\}\rangle/\partial V_i = 0$, we obtain

$$\left.\frac{\partial E(N,l;\{V_j\})}{\partial V_i}\right|_{V_{k\neq i}} = -Ne \cdot \left[\frac{C_{0,i}}{C_{0\Sigma}}\right]_{|N,l;\{V_j\}\rangle} . \qquad (4.51)$$

In case of a metal island, varying V_i by ∂V_i, the total electrostatic energy for the electrons on the island is changed by $-\Delta N\, e \cdot C_{0,i}/C_{0\Sigma} \cdot \partial V_i$, i.e., from (4.46) we obtain

$$\frac{\partial E_{\mathrm{elst}}(N;\{V_j\})}{\partial V_i} = -e\Delta N \, \frac{C_{0,i}}{C_{0\Sigma}} . \qquad (4.52)$$

The definition (4.50) indicates that the ratios of capacitance coefficients for a quantum dot depend explicitly on the N-electron state $|N,l;\{V_j\}\rangle$, which is denoted by the corresponding index. This is contrary to the classical concept of capacitance coefficients which should be independent of any electron number and electrostatic potentials $\{V_j\}$. Thus, (4.50) delivers formally only an abbreviation.

> The circumstances have to be checked under which such defined ratios of capacitance coefficients become *almost* independent of $|N,l;\{V_j\}\rangle$. Only then it can be considered as a classical $C_{0,i}/C_{0\Sigma}$ ratio.

- **Arbitrary Electrode Arrangement:**
  Obviously from (4.50), a state dependence is expected if strong variations occur with N and l in the normalized position probability density $\langle N,l;\{V_j\}|N,l;\{V_j\}\rangle/N$, which is presumable important for small quantum dots with a small electron number N, or for quantum dots with more than one valley in the confining potential. This statement is valid for an arbitrary geometry as indicated in Fig. 4.13. Choosing carefully the gate electrode for tuning the electrostatic potential of the quantum dot might allow to dissolve in such arrangements *internal structure* of the confined N-electron system, since the total energy of states with different spatial distribution change differently with the electrostatic potential variations of the electrodes. [15]

[15] Large quantum dots might possess more than one valley in the external confining potential. In such a case, the charge distributions of the diverse N-electron states differ significantly inducing different image charge fractions on the respective electrodes. With changing an electrode voltage, even groundstate transitions might be induced, changing to a N-electron state with more favourable charge

- **Special Electrode Arrangements:**
  In special arrangements and situation, this is different: In Fig. 4.13b, a spherical or cylindical electrode arrangement is depicted. Any spherical (cylindrical) charge distribution present in the center induces the same image charge fraction on the respective electrode. [16] In Fig. 4.13c, two parallel plate electrodes are shown. Any strict 2D charge distribution between these electrodes induces the same image charge fraction on the respective electrode. Such an arrangement is in favour for investigating the energy spectrum of a N-electron system in a *fixed confining potential shape*: All energies $E(n,l)$ are shifted by the same amount by changing the electrostatic potential of the respective electrode if the distance remains unaffected. It allows to do spectroscopy of confined N-electron systems. With the formalism developed above, this can be proven: The $\alpha_i(\boldsymbol{r})$, defined by (4.22), is easily found for this arrangement in the strict 2D case to be

$$\alpha_1(\boldsymbol{r}) = \alpha_1(z) = \frac{d_1 + d_2 - z}{d_1 + d_2}\,, \qquad \alpha_2(\boldsymbol{r}) = \alpha_2(z) = \frac{z}{d_1 + d_2}\,. \tag{4.53}$$

  The image charge $-q\,\alpha_i(\boldsymbol{r}_s)$ on electrode i induced by a charge q at $\boldsymbol{r}_s$ between the plate electrodes depends only on the z coordinate of the charge q. A single electron in the plane of the 2D quantum dot at $z = d_1$ induces therefore the image charge fractions $\alpha_1(d_1) = d_2/(d_1 + d_2)$ on electrode i and $\alpha_2(d_1) = d_1/(d_1 + d_2)$ on electrode 2. For a strict 2D N-electron system, the charge fractions become independent of the state $|N, l; \{V_j\}\rangle$,

$$N^{-1} \cdot \Big\langle N, l; \{V_j\} \Big| \sum_{s=1}^{N} \alpha_1(\boldsymbol{r}_s) \Big| N, l; \{V_j\} \Big\rangle = \alpha_1(d_2) = \frac{d_2}{d_1 + d_2}\,, \tag{4.54}$$

$$N^{-1} \cdot \Big\langle N, l; \{V_j\} \Big| \sum_{s=1}^{N} \alpha_2(\boldsymbol{r}_s) \Big| N, l; \{V_j\} \Big\rangle = \alpha_2(d_1) = \frac{d_1}{d_1 + d_2}\,. \tag{4.55}$$

  Due to the electrostatic reciprocity, the ratios $\alpha_1(d_1)$ and $\alpha_2(d_1)$ describe also the fraction by which the electrostatic potential of each electron is shifted in the plane $z = d_1$ by tuning the electrostatic potential V_1 and V_2, respectively. This behaviour has been denoted as the 'lever arm' mechanism [108]. In view of (4.50), we can state that the strict 2D quantum dot between two plane electrodes can exactly be treated by the classical ratios

distribution for $\{V_i\}$. Note, the states differ in their charge distribution with respect to the electrodes, and only this causes the different 'capacitance ratios'. Experimental data on carbon nanotubes have been overinterpreted [90] in this context as being indicative for electron-electron correlations. Experiments on vertical quantum dots used the effect to resolve the redistribution of charge in the quantum dot with increasing magnetic field [143].

[16] Note, the confinement potential for the electrons might be dominated by other contributions, i.e., with changing the electrode potentials, the spherical symmetry remains unaffected.

(a) Arbitrary Electrode Arrangement:

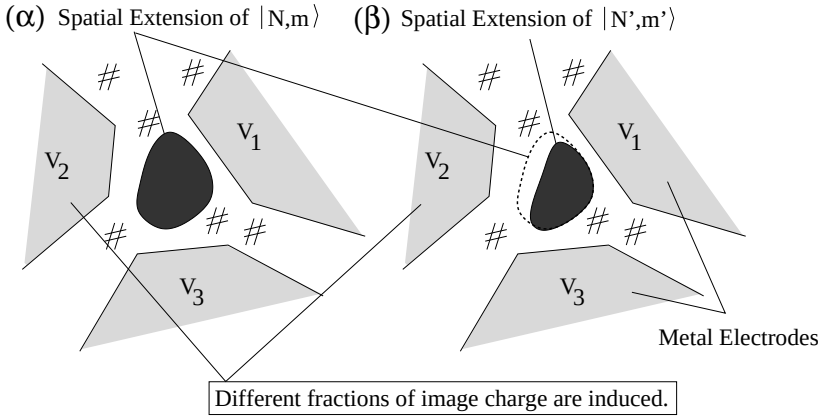

(b) Spherical or Cylindrical Electrode Arrangement:

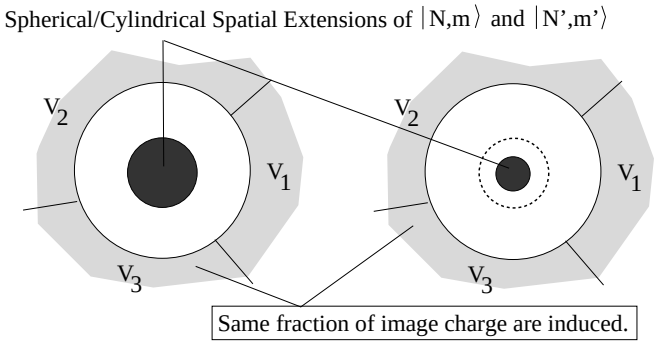

(c) Parallel Plane Electrode Arrangement:

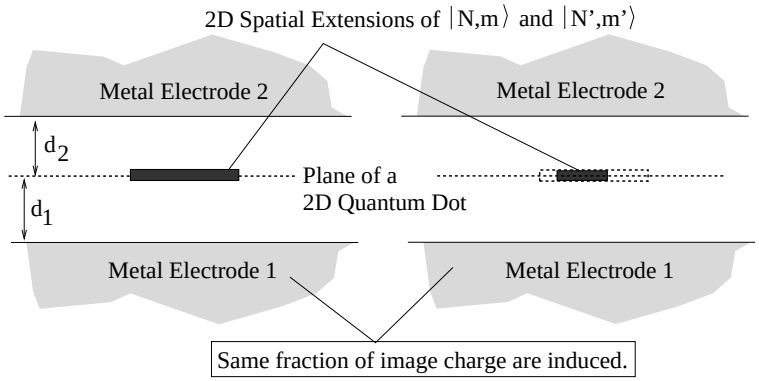

Fig. 4.13. (Left page) (a) Arbitary electrode arrangement: (α) A N-electron system in state $|N, m; \{V_j\}\rangle$ in the quantum dot induces a certain fraction of image charge on the electrode i. (β) A many-electron state $|N', m'; \{V_j\}\rangle$ with different spatial extension – due to different electron number or different quantum number – induces in general a different fraction of image charge on the electrode i, since this fraction depends on the spatial extension of the many-electron state relatively to the electrodes. Therefore, with varying the electrostatic potential V_i of electrode i, the potential energy per electron is changed differently by comparing (α) and (β). Only in keeping certain symmetries, these fractions are independent of the many-electron-state: (b) In a spherical or cylindrical electrode arrangement, any spherical/cylindrical many-electron state induces the same fraction of image charge on the respective electrode. (c) Confining electrons in the plane of a strict 2D quantum dot, the shift of the electrostatic potential with varying the electrostatic potential of one of the plane electrodes is described by a 'lever arm' ratio (or 'leverage' factor), i.e, independently of the two-dimensional many-electron state. In this case, the fractions of image charges are independent of $|N, m; \{V_j\}\rangle$, which is in favour of doing spectroscopy of an interaction N-electron system in a confining potential of fixed shape.

---

of capacitance coefficient to describe the energy shift due to changes in V_i. It is also the optimal arrangement for doing transport spectroscopy (see Chapter 5). Vertical 2D quantum dot systems can come close to such conditions. To be applicable, the extension of the wavefunction in z direction has to be much smaller than the distance d_1 and d_2 to the electrodes.

4.8.2 Total Capacitance (Version I)

The electron-electron interaction in (4.38) gives an energy contribution which is proportional to the square of the total charge in the quantum dot. A similar term is found for the metal case – the charging energy for the capacitor formed by the metal island and the other electrodes. Therefore it is tempting to relate the quantum mechanical expectation value of the electron-electron interaction in the quantum dot with this electrostatic energy. Hence we choose the abbreviation

$$\left[\frac{(N\,(N-1)\,e)^2}{2C_{0\Sigma}}\right]_{|N,l;\{V_i\}\rangle} \equiv \left\langle N, l; \{V_i\}\right| \frac{e^2}{2} \sum_{s=1}^{N} \sum_{\substack{s'=1 \\ s' \neq s}}^{N} G(\boldsymbol{r}_s, \boldsymbol{r}_{s'}) \left|N, l; \{V_i\}\right\rangle . \tag{4.56}$$

This definition includes only the (screened) interaction between electrons. The interaction of each electron with its image – in the previous Section described as a contribution to the external confining potential – might also be considered as a contribution to the capacitance, especially in case of $N = 1$. Then one might consider

$$\left[\frac{(N\,e)^2}{2C_{0\Sigma}}\right]_{|N,l;\{V_i\}\rangle} \equiv \left\langle N,l;\{V_i\}\right| \frac{e^2}{2}\sum_{s=1}^{N}\sum_{s'=1}^{N} G(\boldsymbol{r}_s,\boldsymbol{r}_{s'}) \left|N,l;\{V_i\}\right\rangle . \quad (4.57)$$

Again such an attempt of identification depends on the state $|N,l;\{V_i\}\rangle$, in which the electron system of the quantum dot is found. Describing $|N,l;\{V_i\}\rangle$ by a Hartree-like ansatz, the expression (4.57) delivers the classical Coulomb interaction of the charge distribution in the quantum dot taking the induced image charges into account. The closer the electrodes, the better the screening: The total capacitance value calculated from (4.57) becomes large. The lowest value is obtained by replacing the real Green's function of the arrangement by the Green's function $G^{(\infty)}(\boldsymbol{r}_s,\boldsymbol{r}_{s'})$ of infinite space with an adequate dielectric constant $\epsilon = \min[\boldsymbol{\epsilon}(\boldsymbol{r});\boldsymbol{r}\in V]$,

$$\left[\frac{\big(N(N-1)e\big)^2}{2C_{0\Sigma}}\right]_{|N,l;\{V_i\}\rangle} \leq \left[\frac{\big(N(N-1)e\big)^2}{2C^{(\infty)}_{0\Sigma}}\right]_{|N,l;\{V_i\}\rangle}$$

$$\equiv \left\langle N,l;\{V_i\}\right| \frac{e^2}{2}\sum_{s=1}^{N}\sum_{\substack{s'=1\\ s'\neq s}}^{N} \frac{1}{4\pi\epsilon_0\epsilon\,|\boldsymbol{r}_s-\boldsymbol{r}_{s'}|} \left|N,l;\{V_i\}\right\rangle , \quad (4.58)$$

while keeping the same state $|N,l;\{V_i\}\rangle$. This could be interpreted as the *self-capacitance* of the quantum dot.

For a Hartree-like ansatz for $|N,l;\{V_i\}\rangle$, relation (4.57) gives the classical Coulomb interaction of the charge distribution $-e\,\langle N,l;\{V_i\}|N,l;\{V_i\}\rangle$. For a Hartree-Fock-like ansatz for $|N,l;\{V_i\}\rangle$, exchange terms due to the indistinguishability of electrons are included in (4.57). In an exact treatment, even contributions due to electron-electron correlation might be contained. Only if (4.57) becomes independent of the many-body state $|N,l;\{V_i\}\rangle$, a mapping on the Constant Interaction Model becomes reasonable.

4.8.3 Capacitance Coefficients

Capacitance coefficients C_{ij} have been introduced in Chapter 2 for arrangements of metal conductors to relate the charge Q_i which is induced on conductor i by an electrostatic potential change V_j of electrode j,

$$C_{ij} = -\frac{\partial Q_i}{\partial V_j} . \quad (4.59)$$

For quasi-isolated metal conductors, the charge on the conductor is quantized in units of e. A finite electrode potential change of $\Delta V_j = e/C_{ij}$ is required for recharging the island by e.

Adopted to quantum dots, the change required for charging another electron onto the quantum dot is given by the electrostatic potential difference

$\Delta V_j = V_j' - V_j$, where V_j and V_j' are implicitly given by the resonance conditions in V_j for charging the Nth and the $(N+1)$th electron onto the quantum dot,

$$\begin{aligned} \mu(N+1; V_j', \{V_{k\neq j}\}) &= \mu_{\rm S}^{\rm elch} \,, \\ \mu(N; V_j, \{V_{k\neq j}\}) &= \mu_{\rm S}^{\rm elch} \,. \end{aligned} \tag{4.60}$$

If $\mu(n; V_j', \{V_{k\neq j}\})$ shifts linearly by changing V_j with the factor α_j (see discussion in Section 4.8.1), then we obtain from (4.60)

$$\mu(N+1; V_j, \{V_k\}) - \alpha_j\, e \cdot (V_j' - V_j) = \mu(N; V_j, \{V_k\}) \,, \tag{4.61}$$

leading to the attempt of identification

$$\begin{aligned} \Big[C_{0,j}\Big]_{|N,l=0;\{V_i\}\rangle}^{|N+1,l=0;\{V_i\}\rangle} &\equiv \frac{e}{V_j' - V_j} \\ &= \alpha_j \cdot \frac{e^2}{\mu(N+1; V_j, \{V_k\}) - \mu(N; V_j, \{V_k\})} \,. \end{aligned} \tag{4.62}$$

This reminds on the thermodynamical definition of a capacitance in mesoscopic electron systems. As can already be seen from the Constant Interaction Model, leading to

$$\Big[C_{0,j}\Big]_{|N,l=0;\{V_i\}\rangle}^{|N+1,l=0;\{V_i\}\rangle} = \alpha_j \cdot \frac{e^2}{\varepsilon_{N+1} - \varepsilon_N + e^2/C_{0\Sigma}} \,, \tag{4.63}$$

the electrostatic potential change $\Delta V_j = V_j' - V_j$ depends on the quantization effect and on the electron number N, and therefore varies. High degeneracy or constant level spacing without degeneracy lead to a constant spacing. In general, such a 'capacitance coefficient' depends on the groundstates of the N- and the $(N+1)$-electron system.

4.8.4 Total Capacitance (Version II)

The difference in the energy ladder $\mu(N+1; \{V_j\})$ for a metal island is given by e^2/C_Σ. Therefore, it has been suggested [128] to define the total capacitance of a quantum dot by the distance in the energy ladder for charging a quantum dot – denoted as the *addition spectrum*:

$$\Big[C_{0\Sigma}\Big]_{|N,l=0;\{V_i\}\rangle}^{|N+1,l=0;\{V_i\}\rangle} \equiv \frac{e^2}{\mu(N+1) - \mu(N)} \,. \tag{4.64}$$

Such an approach delivers a similar result as the one discussed in the previous Section since $\sum_i \alpha_i = 1$ as long as indeed capacitance coeffients as discussed in Section 4.8.1 can be defined. The definition (4.64) is different to the first definition of a total capacitance given by (4.57). Here the *total energy* is

included into the definition whereas in (4.57) only *the interaction term* is considered. However also here, this is not a quantity which is in general independent of the N- and $(N+1)$-electron groundstate.

If the quantization effect due to the confining environment are negligible in comparison to the electron-electron interaction, the quantum dot resembles a metallic island. For such a system, the effects Coulomb blockade and single-electron charging are reasonably well described by the concept of capacitances.

4.9 Summary

The energy spectrum for N electrons confined in a realistic electrostatic surrounding is described by the Hamiltonian (4.38). An expression for the external confining potential, which characterizes the realistic quantum dot, is given by (4.39). In case of a small change of the electrostatic potentials of one of the electrodes, the quantities (4.51) reflect the change in the total energy of the N-electron system in the state $|N, l; \{V_i\}\rangle$. In general, this shift depends on the state $|N, l; \{V_i\}\rangle$. The electron-electron interaction present between the electrons is characterized by the electrostatic Green's function $G(\boldsymbol{r}, \boldsymbol{r}')$. Therefore, it usually deviates from a pure Coulomb interaction between two point charges due to screening by electrodes or inhomogenities in the dielectric matrix. The electron-electron interaction (4.57) is responsible for the Coulomb blockade effect.

Although the electrostatic Green's function is known as an analytical expression only for certain specific arrangements, it is a useful concept to define notations and – more important – to identify what contributes to the external (bare) confining potential and the electron-electron interaction. It helps to choose the right approximations for the proper theoretical description of a real quantum dot. Moreover, it allows to estimate how strong the bare confining potential shape is affected by the change of the respective electrode potential change in experiments.

Band structure effects – like spatial variations of the effective mass, nonparabolicity of the conduction band dispersion, band mixing and spin-orbital coupling due to the lack in the inversion symmetry of the underlying crystal structure – have not been included here since we have focused on getting the link in the description between the capacitive description of a metal island and the quantum mechanical description of a quantum dot. Due to the gradient in the confining potential, the Hamiltonian might even have to be extended by a spin-orbital coupling term. This so-called Rashba effect might play a role for 2D quantum dots [144, 145] at heterojunctions where electrons feel the steep asymmetric effective confining potential perpendicular to its plane leading to such spin-orbital coupling.

The popular Constant Interaction Model is in general not suitable. Therefore, to account for the complexity of the electron system confined in the

quantum dot system, we will describe in the following the single-electron transport through quantum dot systems in terms of few- and many-electron states, i.e., in terms of the difference in the total energy between a N- and a $(N+1)$-electron system.

5. Transport Spectroscopy on a Quantum Dot

In the previous Chapter 4, the electron system confined in a quantum dot has been described as an interacting N-electron system. As a consequent continuation, single-electron transport through such a quantum dot is discussed in this Chapter by using the general description in terms of N-electron states in the quantum dot. The spectroscopy of ground- and excited states of the few- to many-electron system in the quantum dot is discussed by energy conservation arguments for rearranging an electron between quantum dot and leads, and by Pauli's exclusion principle. The access to excited states leads usually to an increase but sometimes also to a decrease of current with increasing magnitude of the drain-source voltage. The dynamics leading to this behaviour is discussed within a master equation approach. The complexity of the dynamics with opening channels to excited states on emitter *and* on collector side makes it difficult to deduce from a single $I_{\mathrm{DS}}(V_{\mathrm{DS}})$ curve information about the energy spectrum of the quantum dot without further assumptions. In case of correlations in the electron system of the quantum dot, (quasi)-selection rules exists weighing transitions between N- and $(N+1)$-electron states for adding or taking off an electron.

5.1 Measured Coulomb-Blockade Oscillations of a Quantum Dot System

In Fig. 5.1a, the experimental setup of a quantum dot is shown which will be used in this Chapter to demonstrate some of the electrical transport properties of quantum dots. The quantum dot system is defined by partial electrostatic depletion of a two-dimensional electron system (2DES) [1] in a $GaAs/Al_{0.33}Ga_{0.67}As$ heterostructure (see also Fig. 4.3a) at the GaAs/AlGaAs heterojunction interface 86 nm below the surface: Metallic split-gates were deposited on top of a mesa remained after partially etching the surface of the heterostructure. The diameter of the area between the tips of the gates is about 350 nm. In addition to these topgates, a metallic backgate electrode on the reverse side of the undoped substrate (0.5 mm thick) was used *to change*

[1] Electron density $n_{\mathrm{s}} = 3.4 \cdot 10^{15}$ m^{-2}, electron mobility $\mu_{\mathrm{e}} = 60$ m^2/Vs at the temperature of $T = 4.2$ K.

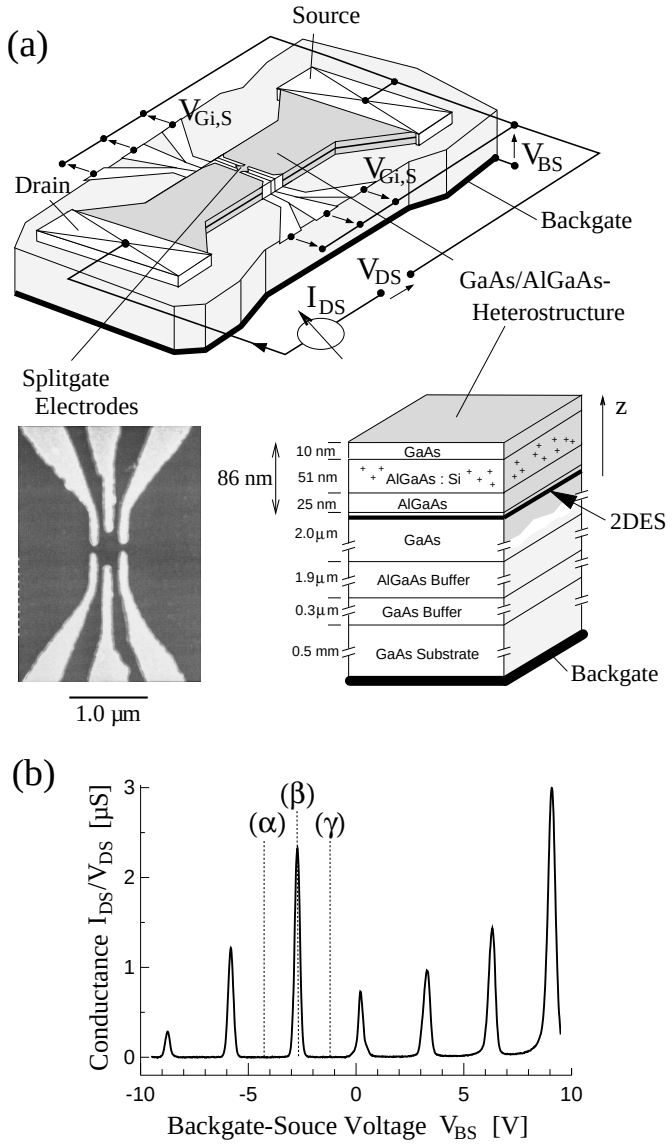

Fig. 5.1. (a) Setup of a quantum dot system realized by partial electrostatic depletion of a two-dimensional electron system (2DES) contained in a GaAs/AlGaAs hetereostructure. Splitgate-electrodes (see SEM image) with suitable gate-source voltages $V_{\mathrm{G}i,\mathrm{S}}$ are used to form the quantum dot between source and drain. Here in addition a backgate electrode is used to tune the electrostatic potential of the quantum dot. (b) Coulomb blockade oscillations: Conductance modulation measured as a function of the backgate-source voltage V_{BS} ($V_{\mathrm{DS}} = 5\ \mu$V, $T = 0.1$ K). The marks (α), (β) and (γ) denote distinct V_{BS} values and are used in conjunction with Fig. 5.3. (data from [42])

the electrostatic potential of the quantum dot. Note that the application of a backgate ensures that the *shape* of the external confining potential remains almost unaffected. Therefore, to emphasize this property, the hitherto used gate-source voltage $V_{\rm GS}$ is now specified to be the backgate-source voltage $V_{\rm BS}$. The sample was mounted in a ^{3}He/^{4}He dilution refrigerator with a base temperature of 22 mK.

In Fig. 5.1b, a typical curve of conductance $I_{\rm DS}/V_{\rm DS}$ versus the backgate-source voltage $V_{\rm BS}$ for small drain-source voltage $V_{\rm DS}$ is shown. A series of conductance peaks is observed which is interpreted in the following as *Coulomb Blockade Oscillations* (CBO). In contrary to the characteristics shown for a metal single-electron transistor (see Fig. 1.7c), the peak heights are *strongly modulated.* Applying in addition a magnetic field B (see Fig. 5.2),

- these peaks of CBO are shifting,
- their distance in the gate voltage is changed, and
- the heights are modulated.

This indicates that the *character of the electronic states of the quantum dot* – changed by the magnetic field – *affects the electrical transport.* This property was demonstrated first by P. McEuen and coworkers in 1991 [146]. In the last decade it has been used by many groups to explore the electronic properties of confined N-electron systems (see for review [3, 4, 6, 5]).

By using the general description in terms of N-electron states on the quantum dot, in the following the regimes of Coulomb blockade and single-electron transport are reconsidered for the quantum dot system and the base for interpreting transport data is given.

5.2 Coulomb Blockade in a Quantum Dot System: Thermodynamical Considerations

Let us start looking at a quantum dot weakly coupled by electron tunneling to an electron reservoir with the electrochemical potential $\mu_{\rm S}^{\rm elch}$ of the source. It generalizes the arrangement of a single-electron box discussed in Chapter 1. The electron states of the quantum dot, denoted by $|N, l; \{V_i\}\rangle$ with the total energy $E(N, l; \{V_i\})$, are considered as being those of the isolated quantum dot.[2] Allowing electron exchange between the quantum dot and the weakly coupled electron reservoir, the quantum dot can come to an equilibrium with the reservoir for fixed electrostatic potentials $\{V_i\}$ on the surrounding electrodes.

[2] Although at first view a reasonable approach, this assumption is not generally valid as will be discussed in Chapter 6 where under certain conditions a new state is formed between the electron system confined in the quantum dot and the reservoir even in case of weak tunnel coupling with approaching zero temperature – a Kondo state.

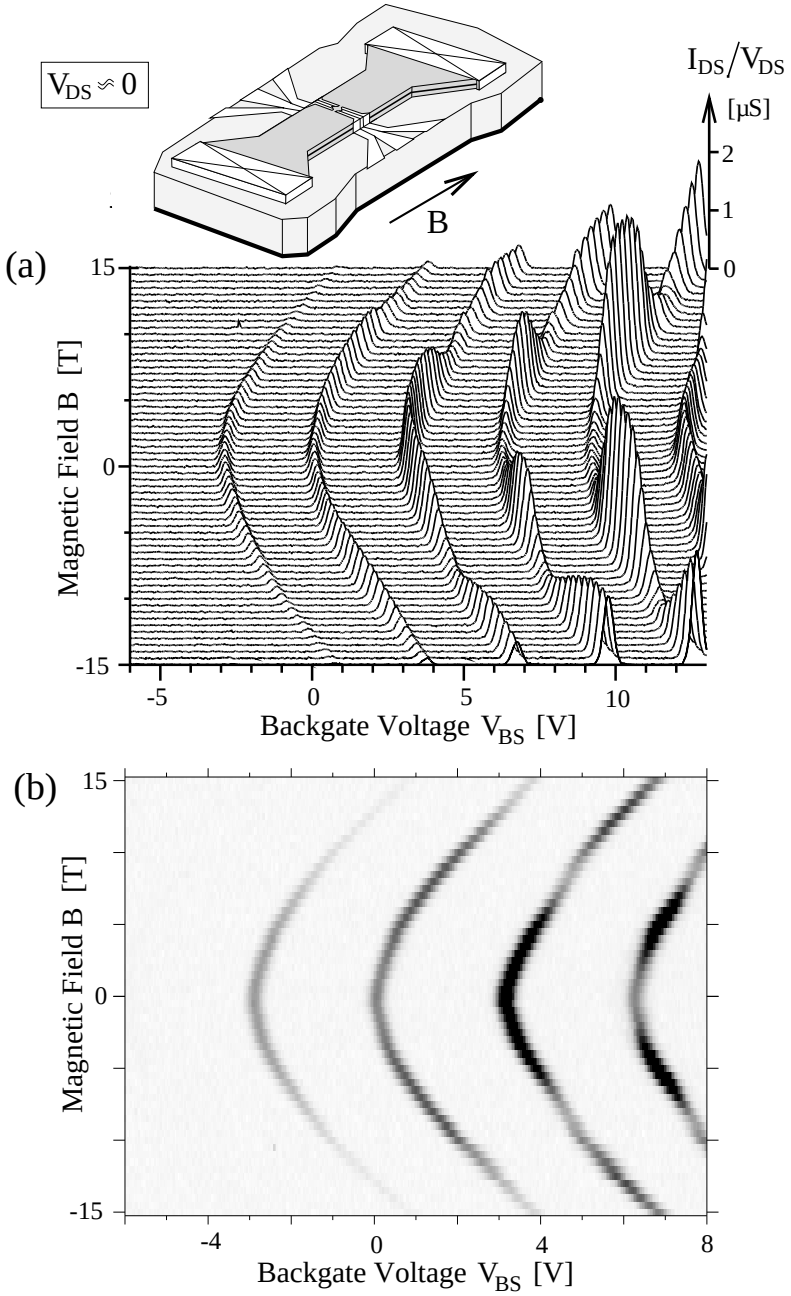

Fig. 5.2. (a) Conductance $I_{\rm DS}/V_{\rm DS}$ through quantum dot system at $V_{\rm DS} \approx 0$ as a function of magnetic field B applied parallel to the plane of the 2DES. (b) Same data as (a) presented in a greyscale plot. (adopted from [144])

The question arises: Which number N of electrons will be found at sufficient low temperature in the quantum dot in thermodynamic equilibrium? The probability $P(N,l;\{V_i\})$ of finding the electron system in the quantum dot in the state $|N,l;\{V_i\}\rangle$ is given by the Gibbs' distribution function [115],

$$P(N,l;\{V_i\}) = Z^{-1}\cdot\exp\left(-\frac{E(N,l;\{V_i\})-N\,\mu_{\rm S}^{\rm elch}}{k_{\rm B}T}\right)\,, \tag{5.1}$$

where Z is the partition function

$$Z=\sum_{\text{all }|n,k;\{V_i\}\rangle}\exp\left(-\frac{E(n,k;\{V_i\})-n\,\mu_{\rm S}^{\rm elch}}{k_{\rm B}T}\right)\,,$$

summing over all n-electron states $|n,k;\{V_i\}\rangle$ of all electron numbers $n=1,2,3\cdots$ at given $\{V_i\}$.

The probability $P(N;\{V_i\})$ for having N electrons in the quantum dot is the probability of finding the quantum dot in any state of the N-electron system,

$$\begin{aligned}P(N;\{V_i\}) &= \sum_{\text{all }l}P(N,l;\{V_i\})\\ &= Z^{-1}\cdot\exp\left(-\frac{E(N,0;\{V_i\})-N\,\mu_{\rm S}^{\rm elch}}{k_{\rm B}T}\right)\\ &\quad\cdot\left\{1+\sum_{l=1}^{\infty}\exp\left(-\frac{E(N,l;\{V_i\})-E(N,0;\{V_i\})}{k_{\rm B}T}\right)\right\}\,.\end{aligned} \tag{5.2}$$

Thermal fluctuations of the number of electrons in the quantum dot are suppressed and the number fixed to N if $P(N-1;\{V_i\})\ll P(N;\{V_i\})$ and $P(N+1;\{V_i\})\ll P(N;\{V_i\})$. Due to the first exponential factor in (5.2) at low temperature, one obtains with the quantities already introduced in (4.42)

$$\begin{aligned}\mu(n;\{V_i\}) &\equiv E(n,0;\{V_i\})-E(n-1,0;\{V_i\})\\ &\qquad\text{with } n\in\{\cdots N-1,N,N+1,\cdots\}\end{aligned} \tag{5.3}$$

the conditions

$$\begin{aligned}\mu(N+1;\{V_i\})-\mu_{\rm S}^{\rm elch} &\gg k_{\rm B}T\,, \qquad \text{and}\\ \mu_{\rm S}^{\rm elch}-\mu(N;\{V_i\}) &\gg k_{\rm B}T\,.\end{aligned} \tag{5.4}$$

The $\mu(n;\{V_i\})$ according to (5.3) are the differences in the groundstate energies of the n- and the $(n-1)$-electron system at fixed electrostatic potentials $\{V_i\}$.[3] The relation (5.3) defines a ladder of energy levels which is plotted

[3] Here, $\mu(n;\{V_i\})$ denotes the difference between groundstate energies. We will avoid the term *chemical* or *electrochemical potential of the quantum dot* used in other publications for $\mu(n;\{V_i\})$. In the combined system quantum dot/reservoir, at thermal equilibrium, there exists only one electrochemical potential, although none of these levels $\mu(n;\{V_i\})$ might be aligned with $\mu_{\rm S}^{\rm elch}$.

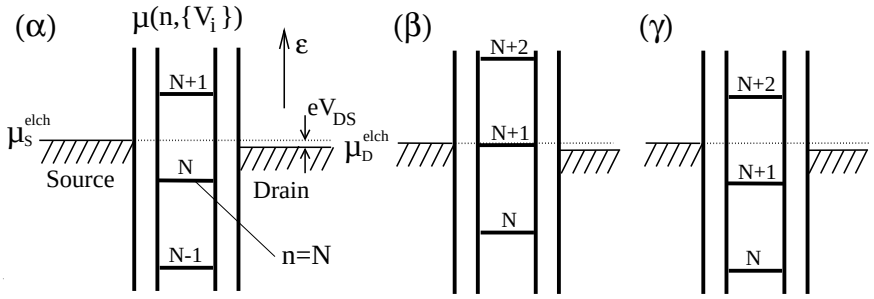

Fig. 5.3. Quantum dot system: Energy scheme for the different $V_{\rm BS}$ marked by (α), (β) and (γ) in Fig. 5.1b. For the source and the drain electrode, the respective electrochemical potential $\mu_{\rm S}^{\rm elch}$ and $\mu_{\rm D}^{\rm elch}$ are indicated. For the quantum dot, the energy ladder $\mu(n;\{V_i\})$ defined by (5.3) is plotted shifting relatively to $\mu_{\rm S}^{\rm elch}$ with varying any electrostatic potential V_i. In general, distances between energy levels in the ladder are not equal.

in Fig. 5.3 relative to the electrochemical potential $\mu_{\rm S}^{\rm elch}$ of the source electrode. A similar energy scheme was already presented in Chapter 1 for metal single-electron charging devices.

The energy barriers for changing the number of electrons in the quantum dot is maximal if $\mu_{\rm S}^{\rm elch}$ lies in the middle between $\mu(N+1;\{V_i\})$ and $\mu(N;\{V_i\})$ as depicted in Fig. 5.3α. At certain values of $\{V_i\}$ where $\mu(N+1;\{V_i\}) = \mu_{\rm S}^{\rm elch}$, the number of electrons in the quantum dot fluctuates between N and $(N+1)$ even at lowest temperature (see Fig. 5.3β).

For electrical transport investigations, the quantum dot has to be coupled to a second reservoir with the electrochemical potential $\mu_{\rm D}^{\rm elch}$. Depending on the sign of the applied drain-source voltage $V_{\rm DS}$, which defines the difference $\mu_{\rm S}^{\rm elch} - \mu_{\rm D}^{\rm elch} = eV_{\rm DS}$, the electrons flow from the source to the drain reservoir, or vice versa. To cover both cases within one discussion, in the following the reservoir with the higher electrochemical potential will be denoted as *emitter* E, the reservoir with the lower electrochemical potential as *collector* C. The respective electrochemical potentials are

$$\mu_{\rm E}^{\rm elch} \equiv \max\{\mu_{\rm S}^{\rm elch}, \mu_{\rm D}^{\rm elch}\} \qquad \text{and} \qquad \mu_{\rm C}^{\rm elch} \equiv \min\{\mu_{\rm S}^{\rm elch}, \mu_{\rm D}^{\rm elch}\}\ .$$

Due to Pauli's exclusion principle, at low temperature, the electrochemical potentials $\mu_{\rm E}^{\rm elch}$ and $\mu_{\rm C}^{\rm elch}$ separate the occupied from the unoccupied states in the emitter and collector reservoir, respectively. Since $\mu_{\rm E}^{\rm elch} \geq \mu_{\rm C}^{\rm elch}$, electrons with higher energy are available in the emitter, whereas unoccupied states of lowest energy are available in the collector.

Finding the quantum dot in the groundstate $|N,0;\{V_i\}\rangle$ of the N-electron system, single-electron transport through the quantum dot is blocked if the

minimal energy

$$\Delta E_{\mathrm{E}\to\mathrm{QD}} = \mu(N+1;\{V_i\}) - \mu_{\mathrm{E}}^{\mathrm{elch}} ,$$

for the $(N+1)$th electron being added from emitter to the quantum dot, and the minimal energy

$$\Delta E_{\mathrm{QD}\to\mathrm{C}} = \mu_{\mathrm{C}}^{\mathrm{elch}} - \mu(N;\{V_i\}) ,$$

for the Nth electron being taken off the quantum dot to the collector, greatly exceeds the thermal energy $k_{\mathrm{B}}T$. Similar energy differences for recharging the electron island were given for the metal single-electron transistor in Chapter 1. Thus, an electron transport process from emitter to collector, changing the number of electrons in the quantum dot in the meantime, is suppressed, if the relation

$$\mu(N+1;\{V_i\}) > \mu_{\mathrm{E}}^{\mathrm{elch}} \geq \mu_{\mathrm{C}}^{\mathrm{elch}} > \mu(N;\{V_i\}) \tag{5.5}$$

holds. The condition (5.5) is sketched in Fig. 5.3(α). The quantum dot system is in the *Coulomb blockade regime*.[4] Changing the electrostatic potential of a gate electrode (for our sample the backgate electrode), the energy barrier is overcome and electron transport through the quantum dot occurs if $\mu(N+1;\{V_i\})$ lies between $\mu_{\mathrm{E}}^{\mathrm{elch}}$ and $\mu_{\mathrm{C}}^{\mathrm{elch}}$. Electron transport happens due to *single* electrons passing the quantum dot one after the other if

$$\mu(N+2;\{V_i\}) > \mu_{\mathrm{E}}^{\mathrm{elch}} \geq \mu(N+1;\{V_i\}) \geq \mu_{\mathrm{C}}^{\mathrm{elch}} > \mu(N;\{V_i\}) .$$

This situation is sketched in Fig. 5.3β. It is the regime of *single-electron tunneling* where the electron number on the quantum dot fluctuates between N and $N+1$. Increasing the gate-source voltage further, the number of electrons becomes fixed to $N+1$, because

$$\mu(N+2;\{V_i\}) > \mu_{\mathrm{E}}^{\mathrm{elch}} \geq \mu_{\mathrm{C}}^{\mathrm{elch}} > \mu(N+1;\{V_i\})$$

suppresses the fluctuations by one or more electron charges (see Fig. 5.3(γ)).

Therefore, when increasing the gate-source voltage at vanishingly small bias between $\mu_{\mathrm{E}}^{\mathrm{elch}}$ and $\mu_{\mathrm{C}}^{\mathrm{elch}}$, a series of conductance peaks are observable similar to a metal single-electron transistor – the *Coulomb blockade oscillations* (see Fig. 5.1b). A conductance peak is observed at $V'_{j,\mathrm{S}}$ if

$$\mu_{\mathrm{E}}^{\mathrm{elch}} \gtrapprox \mu(N;V'_{j,\mathrm{S}})\Big|_{\{V_{i\neq j}\}} \gtrapprox \mu_{\mathrm{C}}^{\mathrm{elch}} . \tag{5.6}$$

The resonance condition for the *next* conductance peak along the gate voltage axis $V_{j,\mathrm{S}}$ is achieved at $V'_{j,\mathrm{S}} + \Delta V_{j,\mathrm{S}}$ if

[4] Suppression of conductance might not exist for correlated multi-electron tunneling processes which change the electron number in the quantum dot only virtually [147]. This will be discussed in Chapter 6.

$$\mu_{\mathrm{E}}^{\mathrm{elch}} \gtrapprox \mu(N+1; V'_{j,\mathrm{S}} + \Delta V_{j,\mathrm{S}})\Big|_{\{V_{i\neq j}\}} \gtrapprox \mu_{\mathrm{C}}^{\mathrm{elch}} \,. \tag{5.7}$$

One should note that with changing a gate electrode potential, in general, the confining potential for the electron system in the quantum dot is affected. Let us look closer to this problem: For small changes of the electrostatic potential V_j, the total energy $E(N,l;\{V_i\})$ of N electrons in the state $|N,l;\{V_i\}\rangle$ is shifted linearly with V_j, which can be described by

$$\frac{\partial E(N,l;V_j)}{\partial V_j}\bigg|_{\{V_{i\neq j}\}} = -\alpha_j\big(|N,l;\{V_i\}\rangle\big)\cdot Ne \,,$$

where $\alpha_j(|N,l;\{V_i\}\rangle)$ denotes the fraction of image charge induced in the electrode j by the confined N-electron system in the state $|N,l;\{V_i\}\rangle$ (see Section 4.8):

$$\alpha_j\big(|N,l;\{V_i\}\rangle\big) \equiv N^{-1}\cdot\Big\langle N,l;\{V_i\}\Big|\sum_{s=1}^{N}\alpha_j(\boldsymbol{r}_s)\Big|N,l;\{V_i\}\Big\rangle \,.$$

As pointed out in Chapter 4, under certain conditions the fraction might become independent of the n-electron state, so that we can assume that

$$\alpha_j\big(|N,l;\{V_i\}\rangle\big) = \alpha_j\big(|N+1,l';\{V_i\}\rangle\big) \equiv \alpha_j \tag{5.8}$$

is valid over a wider range for the gate-source voltage $V_{j,\mathrm{S}}$ and the electron number. The energy ladder $\mu(n;\{V_i\})$ with $n \in \{\cdots N-1, N, N+1, \cdots\}$, depicted in Fig. 5.3, is just shifted linearly with the change of the gate-source voltage $V_{j,\mathrm{S}}$. We obtain

$$\mu(n; V_{j,\mathrm{S}} + \Delta V_{j,\mathrm{S}}) = \mu(n; V_{j,\mathrm{S}}) - \alpha_j \cdot e\Delta V_{j,\mathrm{S}} \,. \tag{5.9}$$

Substracting (5.6) from (5.7) and taking into account (5.9), the distance $\Delta V_{j,\mathrm{S}}$ between adjacent conductance peaks is derived to

$$\alpha_j \cdot e\Delta V_{j,\mathrm{S}} = \mu(N+1;\{V_i\}) - \mu(N;\{V_i\}) \,. \tag{5.10}$$

To emphasize, for obtaining (5.10), the geometric arrangement between gate electrode j, where the electrostatic potential is changed, and quantum dot has to be chosen in favour of the validity of (5.8). On one hand, the factor α_j gives the fraction of image charge present on electrode j induced by the charge in the quantum dot. On the other hand, as given by relation (5.10), it converts changes $\Delta V_{j,\mathrm{S}}$ to the real energy shift of the quantum dot. For a metallic single-electron transistor or within the Constant Interaction Model, α_j is given by the capacitance ratio $C_{0,j}/C_{0\Sigma}$. For a metal system the distance $\Delta V_{j,\mathrm{S}}$ is periodic, $\Delta V_{j,\mathrm{S}} = e/C_{0,j}$ (see Chapter 1). For a quantum dot system, – in general – deviations from this periodicity are expected as can be seen, for instance, from the calculated energy spectrum shown in Fig. 4.11. Clearly

observable are these in the magnetic field dependent measurements presented in Fig. 5.1c where the distance between two adjacent conductance peaks varies with magnetic field. Within the framework of the Constant Interaction Model, the distance between two conductance peaks is described by

$$\frac{C_{0,j}}{C_{0\Sigma}} \cdot e\Delta V_{j,\mathrm{S}} = \varepsilon_{N+1} - \varepsilon_N + \frac{e^2}{C_{0\Sigma}},$$

i.e., not periodic if the energies ε_n of the single-particle eigenstates are not degenerate, i.e., $\varepsilon_{n+1} \neq \varepsilon_n$ for $n = \{\cdots N-1, N, N+1 \cdots\}$.

5.3 Charge-Stability Regions of a Quantum Dot in the (V_{BS},V_{DS}) Plane

In Chapter 1 we have discussed the occurrence of charge-stability regions in the (V_{GS},V_{DS}) plane – the Coulomb blockade regions where only one definite number N of electrons exists on the island. Adjacent to these are the single-electron transport regions where two definite numbers N and $N+1$ of electron charges are allowed on the metal island, and finally regions with even more possible charge states. We investigate in this Section the corresponding regions in the (V_{BS},V_{DS}) plane for a quantum dot.

5.3.1 Basic Experiment

In Fig. 5.4, the $I_{DS}(V_{DS})$ characteristics, measured on the quantum dot system depicted in Fig. 5.1a, are shown for distinct backgate-source voltage values V_{BS}. Clearly the Coulomb-blockade regions are visible. In addition, 'step-like' increases in the current are observed. Some $I_{DS}(V_{DS})$ characteristics show even a decrease in I_{DS} with increasing $|V_{DS}|$. To better resolve the changes in I_{DS}, the differential conductance $\mathrm{d}I_{DS}/\mathrm{d}V_{DS}$ is prefered for presentation because changes in the $I_{DS}(V_{DS})$ are enhanced – a step-like increase becomes a peak in $\mathrm{d}I_{DS}/\mathrm{d}V_{DS}$ at the respective value of V_{DS}.

In Fig. 5.5 the differential conductance $\mathrm{d}I_{DS}/\mathrm{d}V_{DS}$ is shown in greyscale as a function of the backgate voltage V_{BS} for the different bias voltages V_{DS}. [5] At vanishingly small V_{DS}, the Coulomb blockade oscillations are observed as described in the previous Section. Note, the differential conductance $\mathrm{d}I_{DS}/\mathrm{d}V_{DS}$ at $V_{DS} = 0$ is equal to the conductance I_{DS}/V_{DS} for small $|V_{DS}|$. By increasing the absolute value of V_{DS}, the range in backgate voltage V_{BS} where transport

[5] The differential conductance through the quantum dot was measured by using an ac lock-in technique at a frequency of 13 Hz and an effective ac drain-source voltage of 5 μV. In addition to the ac source-drain voltage (5 μV), a dc voltage V_{DS} in the range of mV could be applied.

through the quantum dot occurs is broadened linearly with $|V_{\mathrm{DS}}|$. These regions of transport enclose almost rhombically shaped [6] regions between them, where transport through the quantum dot is blocked – the Coulomb blockade regimes.

5.3.2 Comparison with Expectations from Energy Considerations

In Fig. 5.6, a scheme is given for the different transport regimes in the (V_{BS},V_{DS}) plane, derived from energy considerations:

- In the *Coulomb blockade regime*, the number of electrons on the quantum dot is fixed, for instance to N, since

$$\mu(N+1;\{V_i\}) > \mu_{\mathrm{E}}^{\mathrm{elch}} > \mu_{\mathrm{C}}^{\mathrm{elch}} > \mu(N;\{V_i\}) \; . \tag{5.11}$$

  With increasing $|V_{\mathrm{DS}}|$, the energy ladder $\mu(n;\{V_i\})$ is shifted due to the capacitive coupling to the drain electrode. At certain positive and negative V_{DS} threshold values, the Coulomb blockade is overcome and the number of electrons on the quantum dot can energetically fluctuate, for instance between N and $N+1$, if

$$\mu_{\mathrm{E}}^{\mathrm{elch}} \geq \mu(N+1;\{V_i\}) \geq \mu_{\mathrm{C}}^{\mathrm{elch}} \; . \tag{5.12}$$

  In Fig. 5.6, such a region is marked by hatching.
- The larger the bias $|V_{\mathrm{DS}}|$, the more charge states for the quantum dot become possible. The *regimes of single-electron tunneling*, where energetically the electron number is only allowed to fluctuate between N and $N+1$, are defined by the condition

$$\mu(N+2;\{V_i\}) > \mu_{\mathrm{E}}^{\mathrm{elch}} \geq \mu(N+1;\{V_i\}) \geq \mu_{\mathrm{C}}^{\mathrm{elch}} > \mu(N;\{V_i\}) \; . \tag{5.13}$$

  The possible (V_{BS},V_{DS}) values fulfilling (5.13) are restricted to the rhombically shaped regions adjacent to the Coulomb blockade regimes (see Fig. 5.6).
- Due to (5.12), the boundaries $V_{\mathrm{BS}}^{(\mathrm{S})}(V_{\mathrm{DS}})$ and $V_{\mathrm{BS}}^{(\mathrm{D})}(V_{\mathrm{DS}})$ in the (V_{BS},V_{DS}) plane, between which the electron numbers N and $N+1$ on the quantum dot are energetically possible, are defined by the conditions

$$\mu_{\mathrm{S}}^{\mathrm{elch}} = \mu(N+1;V_{\mathrm{BS}}^{(\mathrm{S})},V_{\mathrm{DS}}) \quad \text{and} \quad \mu_{\mathrm{D}}^{\mathrm{elch}} = \mu(N+1;V_{\mathrm{BS}}^{(\mathrm{D})},V_{\mathrm{DS}}) \; , \quad \text{where} \quad \mu_{\mathrm{S}}^{\mathrm{elch}} - \mu_{\mathrm{D}}^{\mathrm{elch}} = eV_{\mathrm{DS}} \; . \tag{5.14}$$

  These borderlines are plotted in Fig. 5.6. As visible in the experimental data of Fig. 5.5, these borderlines $V_{\mathrm{BS}}^{(\mathrm{S})}$ and $V_{\mathrm{BS}}^{(\mathrm{D})}$ depend linearly on V_{DS}. It tells that indeed in this experiment the energy ladder $\mu(n;\{V_i\})$ is shifted

[6] More correct: 'parallelogram-like shaped'. Of common use is the term 'diamond-like shaped' [5].

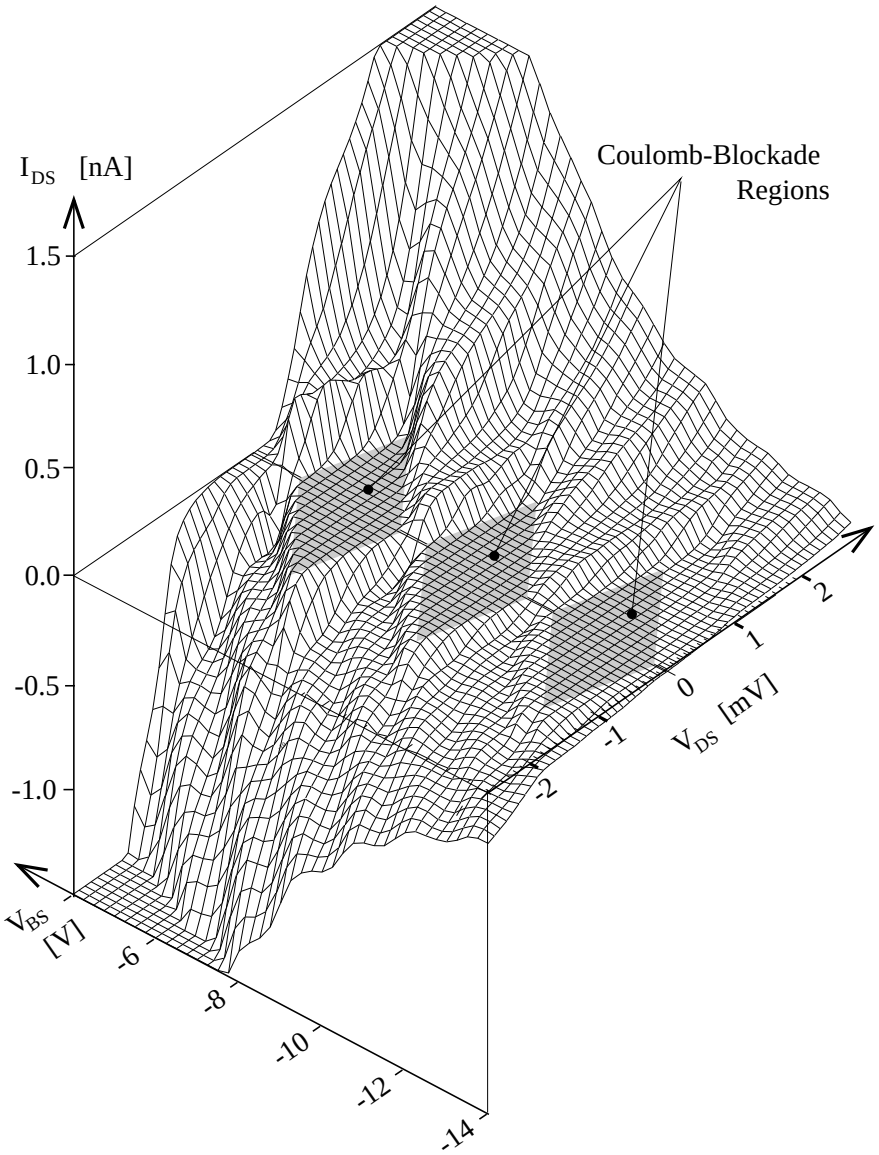

Fig. 5.4. Current-voltage characteristics $I_{DS}(V_{DS})$ for distinct backgate-source voltages V_{BS}, measured for the quantum dot system presented in Fig. 5.1a. Grey-shaded are three Coulomb-blockade regions. Note by tracing single $I_{DS}(V_{DS})$ curves that the current $|I_{DS}|$ increases but sometimes also decreases with increasing $|V_{DS}|$. (Data from J. Weis, 1993, unpublished)

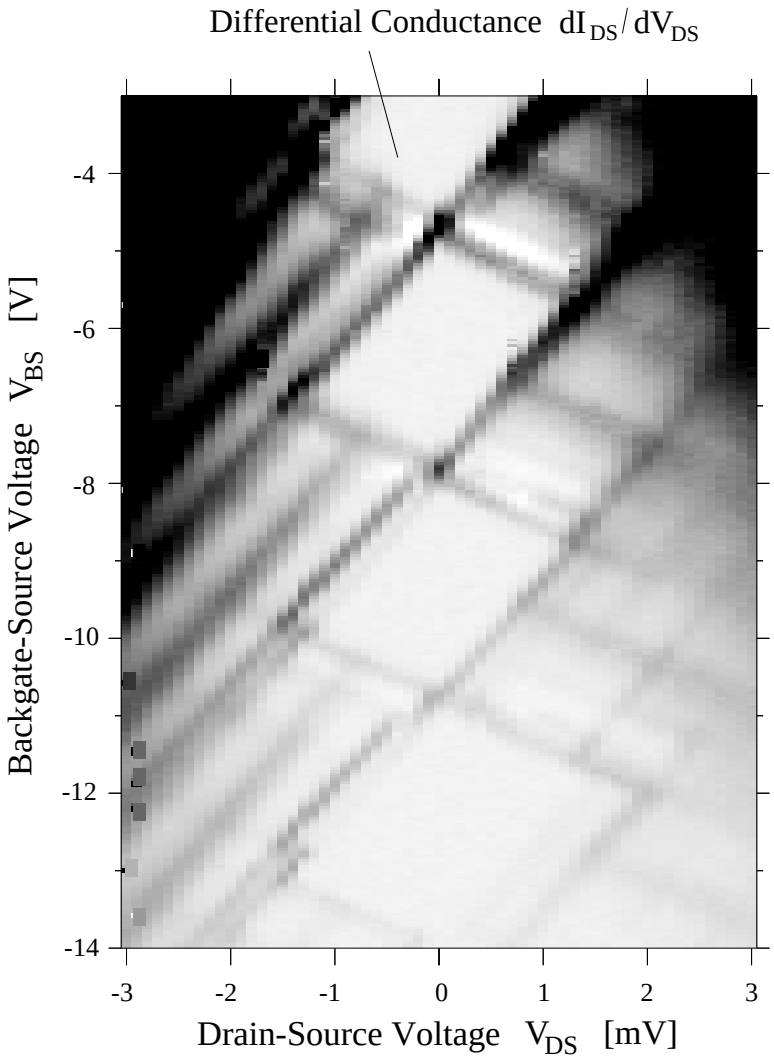

Fig. 5.5. Differential conductance $\mathrm{d}I_{\mathrm{DS}}/\mathrm{d}V_{\mathrm{DS}}$ through the quantum dot system shown in Fig. 5.1a, measured as a function of drain-source voltage V_{DS} (between -3 mV and 3 mV in 0.1 mV steps) and backgate voltage V_{BS}. In the linear greyscale plot, white regions correspond to $\mathrm{d}I_{\mathrm{DS}}/\mathrm{d}V_{\mathrm{DS}}$ below -0.1 μS and black ones to $\mathrm{d}I_{\mathrm{DS}}/\mathrm{d}V_{\mathrm{DS}}$ above 2 μS. Positive peaks in the differential conductance indicate a step-like increase in the $I_{\mathrm{DS}}(V_{\mathrm{DS}})$ characteristics at the respective gate voltage value V_{BS}, negative peaks a step-like decrease in the current. Interpreting the height of peaks in the differential conductance $\mathrm{d}I_{\mathrm{DS}}/\mathrm{d}V_{\mathrm{DS}}$, one has to be careful: The height depends on how the current step shifts in the $(V_{\mathrm{BS}},V_{\mathrm{DS}})$ plane. In the extreme case, that the step in the current I_{DS} shifts almost parallel to the V_{DS} axis, $\mathrm{d}I_{\mathrm{DS}}/\mathrm{d}V_{\mathrm{DS}}$ is almost zero, i.e., the smaller the slope $|\mathrm{d}V_{\mathrm{BS}}/\mathrm{d}V_{\mathrm{DS}}|$, the smaller the height in $\mathrm{d}I_{\mathrm{DS}}/\mathrm{d}V_{\mathrm{DS}}$. (adopted from J. Weis et al. [148, 149])

linearly with changing the electrostatic potential V_{B} of the backgate electrode by V_{BS} and the electrostatic potential V_{D} of the drain electrode by V_{DS}:

$$\frac{\partial\mu(n;\{V_i\})}{\partial V_{\mathrm{DS}}} = -e\,\alpha_{\mathrm{D}} \quad \text{and} \quad \frac{\partial\mu(n;\{V_i\})}{\partial V_{\mathrm{BS}}} = -e\,\alpha_{\mathrm{B}}\ . \tag{5.15}$$

Here α_{B} denotes the fraction of image charge induced on the backgate electrode by the electron charges in the quantum dot and α_{D} the fraction induces on the drain electrode. The two slopes $\mathrm{d}V_{\mathrm{BS}}/\mathrm{d}V_{\mathrm{DS}}$, characterizing the borderlines $V_{\mathrm{BS}}^{(\mathrm{S})}$ and $V_{\mathrm{BS}}^{(\mathrm{D})}$, are obtained by differentiating (5.14) with respect to V_{DS} and to V_{BS} and taking into account (5.15):

$$\frac{\mathrm{d}V_{\mathrm{BS}}^{(\mathrm{S})}}{\mathrm{d}V_{\mathrm{DS}}} = -\frac{\alpha_{\mathrm{D}}}{\alpha_{\mathrm{B}}} \quad \text{and} \quad \frac{\mathrm{d}V_{\mathrm{BS}}^{(\mathrm{D})}}{\mathrm{d}V_{\mathrm{DS}}} = \frac{1-\alpha_{\mathrm{D}}}{\alpha_{\mathrm{B}}}\ . \tag{5.16}$$

In case of the Constant Interaction Model or a metal single-electron transistor, the slopes are given by $-C_{0\mathrm{D}}/C_{0\mathrm{B}}$ and $(C_{0\Sigma}-C_{0\mathrm{D}})/C_{0\mathrm{B}}$, respectively (see also Fig. 1.8).

- At certain $(V_{\mathrm{BS}}, V_{\mathrm{DS}})$ values, the relations

$$\mu_{\mathrm{E}}^{\mathrm{elch}} = \mu(N+1;V_{\mathrm{BS}},V_{\mathrm{DS}}) \quad \text{and} \quad \mu_{\mathrm{C}}^{\mathrm{elch}} = \mu(N;V_{\mathrm{BS}},V_{\mathrm{DS}}) \tag{5.17}$$

are fulfilled at the same time. The respective energy scheme is shown in Fig. 5.6. It allows to obtain the difference $\mu(N+1;\{V_i\})-\mu(N;\{V_i\})$, the distance in the energy ladder, directly from the respective drain-source voltage $V_{\mathrm{DS}}^{\mathrm{max}}$:

$$\mu(N+1;\{V_i\}) - \mu(N;\{V_i\}) = e\cdot V_{\mathrm{DS}}^{(\mathrm{max})}\ . \tag{5.18}$$

In the quantum dot under investigation the distance is about 1.3 meV with variations in the order of 10% for different N. In Chapter 1 for a metal single-electron transistor, $\mu(N+1;\{V_i\}) - \mu(N;\{V_i\}) = e^2/C_{0\Sigma}$ was used. For a quantum dot within the Constant Interaction Model, we obtain $\mu(N+1;\{V_i\})-\mu(N;\{V_i\}) = \varepsilon_{N+1}-\varepsilon_N+e^2/C_{0\Sigma}$. In general, the variations in $\mu(N+1;\{V_i\}) - \mu(N;\{V_i\})$ have been denoted as *addition spectrum* of the quantum dot (see Section 4.7.4).

- The *fraction of image charges α_i on the electrodes* (i = {B,D,S} can also be determined from the experimental data:
  Comparing (5.18) with (5.10), one obtains the proportionality factor

$$\alpha_{\mathrm{B}} = V_{\mathrm{DS}}^{(\mathrm{max})}/\Delta V_{\mathrm{BS}}\ . \tag{5.19}$$

Thus, the scaling factor between a change of V_{BS} and the shift of the energy ladder relatively to the Fermi level of the source electrode is obtained by comparing the distance ΔV_{BS} in gate voltage between two adjacent

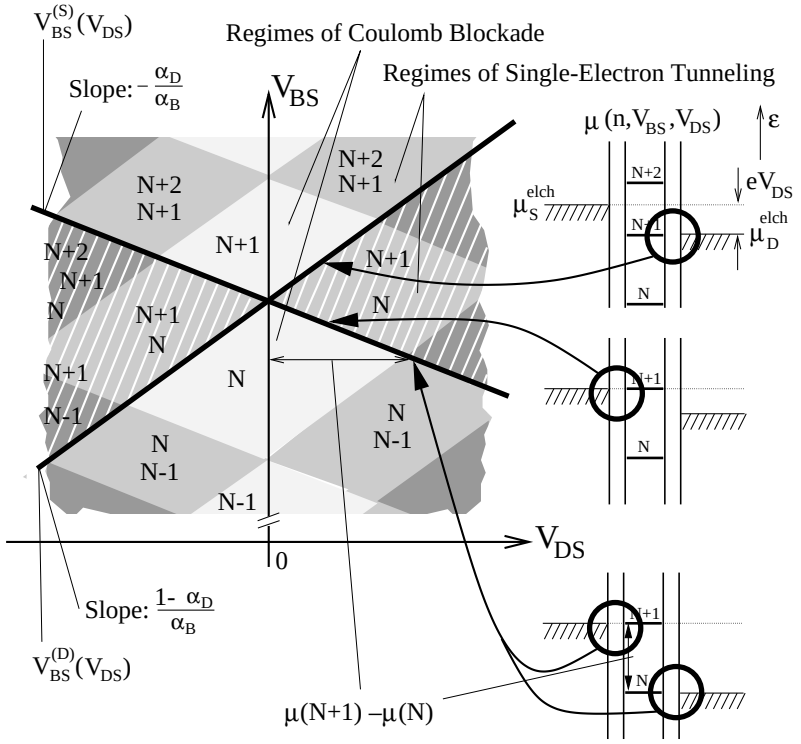

Fig. 5.6. Transport regions of the quantum dot system. The scheme is similar to the one presented for a metal single-electron transistor in Fig. 1.8, except that in general the size of the Coulomb blockade regions varies with the electron number. The hatched region marks where the electron number N and $N+1$ might be found. Single-electron transport, restricted to transitions only between $n+1$ and n electrons on the quantum dot, is found by energetical considerations in the rhombically shaped regions adjacent to the Coulomb blockade region of n and $n+1$ electrons. Such regions are denoted here as regimes of single-electron tunneling.

conductance peaks at $V_{\mathrm{DS}} = 0$ and the maximum threshold value $V_{\mathrm{DS}}^{(\max)}$ of the respective Coulomb blockade region: $\alpha_{\mathrm{B}} = V_{\mathrm{DS}}^{(\max)}/\Delta V_{\mathrm{BS}} = (4.5 \pm 0.2) \times 10^{-4}$. To emphasize again, besides the scaling factor, α_{B} gives the fraction of image charge on the backgate electrode induced by the electrons in the quantum dot (see electrostatic reciprocity, Fig. 4.8).

From the slopes in Fig. 5.5 and the relation (5.16), the fraction α_{D} of image charge induced on the drain lead is obtain to $\alpha_{\mathrm{D}} = 0.30 \pm 0.02$.

By redoing the measurements of Fig. 5.5 by choosing the drain instead of the source contact as the reference for all applied voltages to the system,

the relations derived above remain valid by exchanging the index S with D. Then α_S is obtained instead of α_D (here $\alpha_S = 0.21 \pm 0.02$).
The sum $\alpha_S + \alpha_D + \alpha_B = (0.51 \pm 0.04)$ is less than unity, since further image charges are induced on the split-gate electrodes on top of the heterostructure defining the quantum dot. This is proven by determine their α_i.

5.4 Quantitative Transport Spectroscopy of Ground and Excited States of the Quantum Dot

In the previous Section, the regimes of Coulomb blockade and single-electron tunneling have been identified within the parameter space (V_{BS},V_{DS}) by energy considerations and are schematically given in Fig. 5.6. In experimental data of Fig. 5.5, *within* the regimes of single-electron tunneling, additional peaks in the differential conductance dI_{DS}/dV_{DS} occur, forming a grid-like structure in the (V_{BS},V_{DS}) plane. They indicate that additional transport channels through the quantum dot become available in the region of single-electron tunneling, leading each time to a step-like increase of the current I_{DS} with increasing $|V_{DS}|$. Such additional transport channels have been reported and interpreted in 1992 by several groups [150, 113, 151, 148]. Impressive results are obtained later from vertical quantum dots [5]. Since in such a single-electron tunneling regime the number of electrons can energetically fluctuate only between n and $n+1$ with $n \in \{\cdots N-1, N, N+1 \cdots\}$, these additional single-electron tunneling channel have been attributed to excited states of the quantum dot being used by electrons tunneling into and out of the quantum dot. Following [148, 149, 152], here we will discuss this in terms of n-electron states without restricting the description to a specific model for the quantum dot.

As visible in the experimental data of Fig. 5.5, the peaks in the differential conductance dI_{DS}/dV_{DS} shift either parallel to the borderline $V_{BS}^{(S)}$ or the borderline $V_{BS}^{(D)}$ of the region of single-electron tunneling. This indicates that new channels are either opened in resonance with the Fermi level μ_S^{elch} of source or the Fermi level μ_D^{elch} of drain. For $V_{DS} > 0$, the source electrode acts as the emitter, for $V_{DS} < 0$ as the collector, for the drain electrode it is vice versa. With applied bias V_{DS}, electrons from the emitter are entering the quantum dot, and electrons are leaving the quantum dot to the collector side. It is therefore natural to distinguish between additional channels being opened on the emitter side and additional channels being opened on the collector side.

5.4.1 Single-Electron Tunneling Regime of N and $(N+1)$ Electrons: Additional Channels on the Emitter Side due to Excited States of the $(N+1)$-Electron System

In Fig. 5.7, a single-electron tunneling regime is schematically shown, in which the number of electrons can fluctuate between N and $N+1$. One additional transport channel of those observed in Fig. 5.5 is depicted with its borderline (dotted line) parallel to the borderline to the Coulomb blockade regime with N electrons, i.e., it opens in resonance to the Fermi level of the *emitter*. [7] To explain the origin, let us consider what happens at finite bias $V_{\rm DS}$ with varying the gate voltage $V_{\rm BS}$ along the path indicated by the dashed line in Fig. 5.7a. Due to the fixed $V_{\rm DS}$, the electrochemical potential difference between drain and source is fixed. With changing $V_{\rm BS}$, the electrostatic potential of the quantum dot is shifted. For some $V_{\rm BS}$ values (marked in Fig. 5.7a by (α), (β), (γ), (δ) and (ε)) the respective energy schemes are given in Fig. 5.7b. Let us discuss in the following the electronic properties of the quantum dot for four of these ($V_{\rm BS}$,$V_{\rm DS}$) values:

- **Operation point α:** In the Coulomb blockade regime at $V_{\rm BS}^{\alpha}$, the number of electrons in the quantum dot is fixed to N, since

$$\mu(N+1;V_{\rm BS}^{\alpha},V_{\rm DS}) > \mu_{\rm E}^{\rm elch} > \mu_{\rm C}^{\rm elch} > \mu(N;V_{\rm BS}^{\alpha},V_{\rm DS}) \ ,$$

  shown in Fig. 5.7b(α). On one hand, the electrons from the Fermi level of the emitter do not enter the quantum dot since for them the energy barrier $\mu(N+1;V_{\rm BS}^{\alpha},V_{\rm DS})-\mu_{\rm E}^{\rm elch}$ exists. On the other hand, no electron can leave the quantum dot since by starting from the groundstate of the N-electron system, an electron would gain at maximum the energy $\mu(N;V_{\rm BS}^{\alpha},V_{\rm DS}) = E(N,0;V_{\rm BS}^{\alpha},V_{\rm DS})-E(N-1,0;V_{\rm BS}^{\alpha},V_{\rm DS})$ which is less than $\mu_{\rm C}^{\rm elch}$, i.e., the energy to reach an unoccupied state in the collector.
- **Operation point β and δ:** By increasing the backgate voltage $V_{\rm BS}$, the energy ladder $\mu(n;V_{\rm BS},V_{\rm DS})$ is shifted down relatively to $\mu_{\rm E}^{\rm elch}$ and $\mu_{\rm C}^{\rm elch}$.

[7] Parallel to $V_{\rm BS}^{\rm (S)}$ for $V_{\rm DS}>0$, and parallel to $V_{\rm BS}^{\rm (D)}$ for $V_{\rm DS}<0$.

Fig. 5.7. (Right page) (a) Sketch of the transport regions between the Coulomb blockade regions of N and $(N+1)$ electrons around zero $V_{\rm DS}$ in the ($V_{\rm BS}$,$V_{\rm DS}$) plane. An additional single-electron transport channel (the position is indicated by the dotted line) opens within a single-electron tunneling region, parallel to the borderline to the Coulomb blockade regime of N electrons. (b) Energy schemes to ($V_{\rm BS}$,$V_{\rm DS}$) values indicated in (a) with (α) to (ε). In case of (γ), an additional channel is opened for electrons entering the quantum dot by inducing a transition to an excited state $|N+1,k\rangle$ of the $(N+1)$-electron system. This is done (see (c)) either by starting from the groundstate $|N,0\rangle$ of the N-electron system or by starting from an excited state $|N,l\rangle$ of the N-electron system. The latter has to be reached by the preceeding process, for instance, by a tunneling process of the $(N+1)$th electron to collector, leaving behind the excited state $|N,l\rangle$.

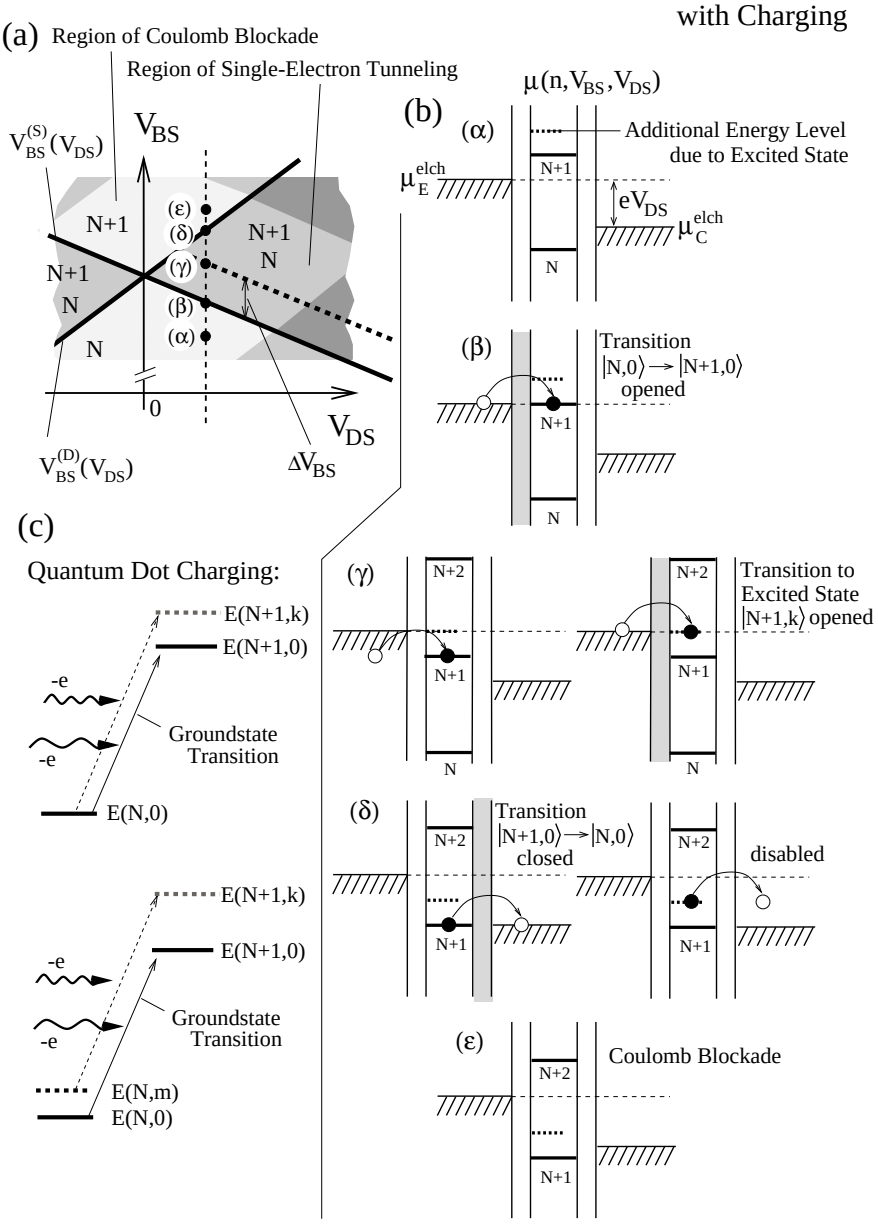
Additional Channel on Emitter Side by Reaching Excited State |N+1,k⟩ with Charging
(a)
Region of Coulomb Blockade
Region of Single-Electron Tunneling
V_{BS}
$V_{BS}^{(S)}(V_{DS})$
$V_{BS}^{(D)}(V_{DS})$
V_{DS}
ΔV_{BS}
(ε)
(δ)
(γ)
(β)
(α)
N+1
N
0
(b)
$\mu(n,V_{BS},V_{DS})$
(α)
Additional Energy Level due to Excited State
μ_E^{elch}
eV_{DS}
μ_C^{elch}
(β)
Transition
|N,0⟩ → |N+1,0⟩
opened
(c)
Quantum Dot Charging:
E(N+1,k)
E(N+1,0)
E(N,0)
E(N,m)
-e
Groundstate Transition
(γ)
N+2
Transition to Excited State |N+1,k⟩ opened
(δ)
Transition
|N+1,0⟩ → |N,0⟩
closed
disabled
(ε)
Coulomb Blockade

At $V_{\rm BS}^{\beta}$, where

$$\mu_{\rm E}^{\rm elch} \overset{(>)}{=} \mu(N+1; V_{\rm BS}^{\beta}, V_{\rm DS}) \ ,$$

an electron from the Fermi level of the emitter has enough energy to allow with entering a transition from the groundstate of the N to the groundstate of the $(N+1)$-electron system in the quantum dot (see Fig. 5.7b(β)). This is the transition with lowest possible energy when starting from the groundstate of the N electron system. Single-electron tunneling remains possible within the gate voltage interval $V_{\rm BS}^{\beta} \leq V_{\rm BS} \leq V_{\rm BS}^{\delta}$ since there

$$\mu_{\rm E}^{\rm elch} \geq \mu(N+1; V_{\rm BS}, V_{\rm DS}) \geq \mu_{\rm C}^{\rm elch} \ . \tag{5.20}$$

The right side of relation (5.20) ensures that starting from the groundstate of the $(N+1)$-electron system in the quantum dot, the $(N+1)$th electron leaving the quantum dot finds with its energy $\mu(N+1; V_{\rm BS}, V_{\rm DS})$ an unoccupied state in the collector. This becomes blocked at $V_{\rm BS}^{\delta}$ (see Fig. 5.7b(δ)) with entering the Coulomb blockade regime of $N+1$ electrons.

- **Operation point γ:** At $V_{\rm BS}^{\gamma}$ within the gate voltage interval defined by (5.20), a step-like increase in the current occurs, indicated by a peak in the differential conductance at that position: Electrons from the Fermi level of the emitter seems to have an additional channel for entering the quantum dot. What defines such a level as indicated in Fig. 5.7b(γ)? Starting from the groundstate $|N, 0; V_{\rm BS}^{\gamma}, V_{\rm DS}\rangle$ of the N-electron system in the quantum dot, with an additional electron entering the quantum dot from the emitter, the quantum dot ends in an excited state $|N+1, k; V_{\rm BS}^{\gamma}, V_{\rm DS}\rangle$ of the $(N+1)$-electron system (see Fig. 5.7c). Such a process is opened at $V_{\rm BS}^{\gamma}$ if

$$\mu_{\rm E}^{\rm elch} \overset{(>)}{=} E(N+1, k; V_{\rm BS}^{\gamma}, V_{\rm DS}) - E(N, 0; V_{\rm BS}^{\gamma}, V_{\rm DS}) \, . \tag{5.21}$$

By opening this channel, electrons for the emitter can *either* use the way via the groundstate *or* via the excited state of the $(N+1)$-electron system as depicted in Fig. 5.7b(γ). These channels are taken from electrons of different energy, but *they cannot be used at the same time* due to the electron-electron interaction in the quantum dot allowing fluctuations only between N and $(N+1)$ electrons in this parameter regime. Therefore, the additional channel increases only the probability that an electron enters the quantum dot from the emitter side, and leads by this to an increase in the current $I_{\rm DS}$.

Actually it is not obligatory that the quantum dot is in the groundstate of the N-electron system before the $(N+1)$th electron enters the quantum dot. As we will see in the next Section, also excited states of the N-electron system become accessible in this single-electron tunneling regime. Therefore, starting from the excited state $|N, l; V_{\rm BS}^{\gamma}, V_{\rm DS}\rangle$, in general, an additional channel to the emitter is opened, leading to an excited state of the $|N+1, k; V_{\rm BS}^{\gamma}, V_{\rm DS}\rangle$ (see Fig. 5.7c), if

$$\mu_{\rm E}^{\rm elch} \overset{(>)}{=} E(N+1,k;V_{\rm BS}^{\gamma},V_{\rm DS}) - E(N,l;V_{\rm BS}^{\gamma},V_{\rm DS}) \tag{5.22}$$

$$> \mu(N+1,k;V_{\rm BS}^{\gamma},V_{\rm DS}) \geq \mu_{\rm C}^{\rm elch} \; . \tag{5.23}$$

This additional single-electron channel described by (5.21) or by (5.22) is only possible if anyhow the quantum dot can fluctuate between $N+1$ and N electrons, i.e., (5.23) is fulfilled. Otherwise, although the energy difference $E(N+1,k;\{V_i\}) - E(N,l;\{V_i\})$ might fall between $\mu_{\rm E}^{\rm elch}$ and $\mu_{\rm C}^{\rm elch}$, this channel via the excited state cannot be used. An example is given with Fig. 5.7b(ε).

At $V_{\rm BS}^{\beta}$ and $V_{\rm BS}^{\gamma}$, the respective resonance conditions

$$\mu_{\rm E}^{\rm elch} \overset{(>)}{=} E(N+1,0;V_{\rm BS}^{\beta},V_{\rm DS}) - E(N,0;V_{\rm BS}^{\beta},V_{\rm DS}) \; ,$$

$$\mu_{\rm E}^{\rm elch} \overset{(>)}{=} E(N+1,k;V_{\rm BS}^{\gamma},V_{\rm DS}) - E(N,l;V_{\rm BS}^{\gamma},V_{\rm DS})$$

are obtained. Based on the assumption (5.8), the difference $\Delta V_{\rm BS} = V_{\rm BS}^{\gamma} - V_{\rm BS}^{\beta}$ in the gate voltage $V_{\rm BS}$ between (β) and (γ) in Fig. 5.7a is then given by

$$\begin{aligned} \alpha_{\rm B} \cdot e\,\Delta V_{\rm BS} = \; & E(N+1,k;\{V_i\}) - E(N,l;\{V_i\}) \\ & - \Big[E(N+1,0;\{V_i\}) - E(N,0;\{V_i\})\Big] \; . \end{aligned} \tag{5.24}$$

The processes leading to excited states of the N-electron system are described in the following Section.

5.4.2 Single-Electron Tunneling Regime between N and $(N+1)$ Electrons: Additional Channels on the Collector Side due to Excited States of the N-Electron System

Once again, a single-electron tunneling regime is schematically shown in Fig. 5.8, in which the number of electrons can fluctuate between N and $N+1$. But now an additional transport channel is opened with its borderline (dotted line) parallel to the borderline to the Coulomb blockade regime with $N+1$ electrons, i.e., it is opened in resonance to the Fermi level of the *collector*. [8] Again, to explain the origin, let us consider what happens at a bias $V_{\rm DS}$ with varying the gate voltage $V_{\rm BS}$ along the path indicated by the dashed line in Fig. 5.8a. The respective energy schemes for different gate voltages – marked in Fig. 5.7a by (α), (β), (γ), (δ) and (ε), are given in Fig. 5.8b. Here we take the opposite direction in $V_{\rm BS}$ – starting from the Coulomb blockade regime of $N+1$ electrons.

- **Operation point α:** At $V_{\rm BS}^{\alpha}$, the quantum dot is in the Coulomb blockade regime of $N+1$ electrons, i.e., (see Fig. 5.8b(α))

$$\mu(N+2;V_{\rm BS}^{\alpha},V_{\rm DS}) > \mu_{\rm E}^{\rm elch} > \mu_{\rm C}^{\rm elch} > \mu(N+1;V_{\rm BS}^{\alpha},V_{\rm DS}) \; .$$

[8] Parallel to $V_{\rm BS}^{\rm (D)}$ for $V_{\rm DS} > 0$, and parallel to $V_{\rm BS}^{\rm (S)}$ for $V_{\rm DS} < 0$.

Additional Channel on Collector Side by Reaching Excited State $|N,m'\rangle$ with Discharging

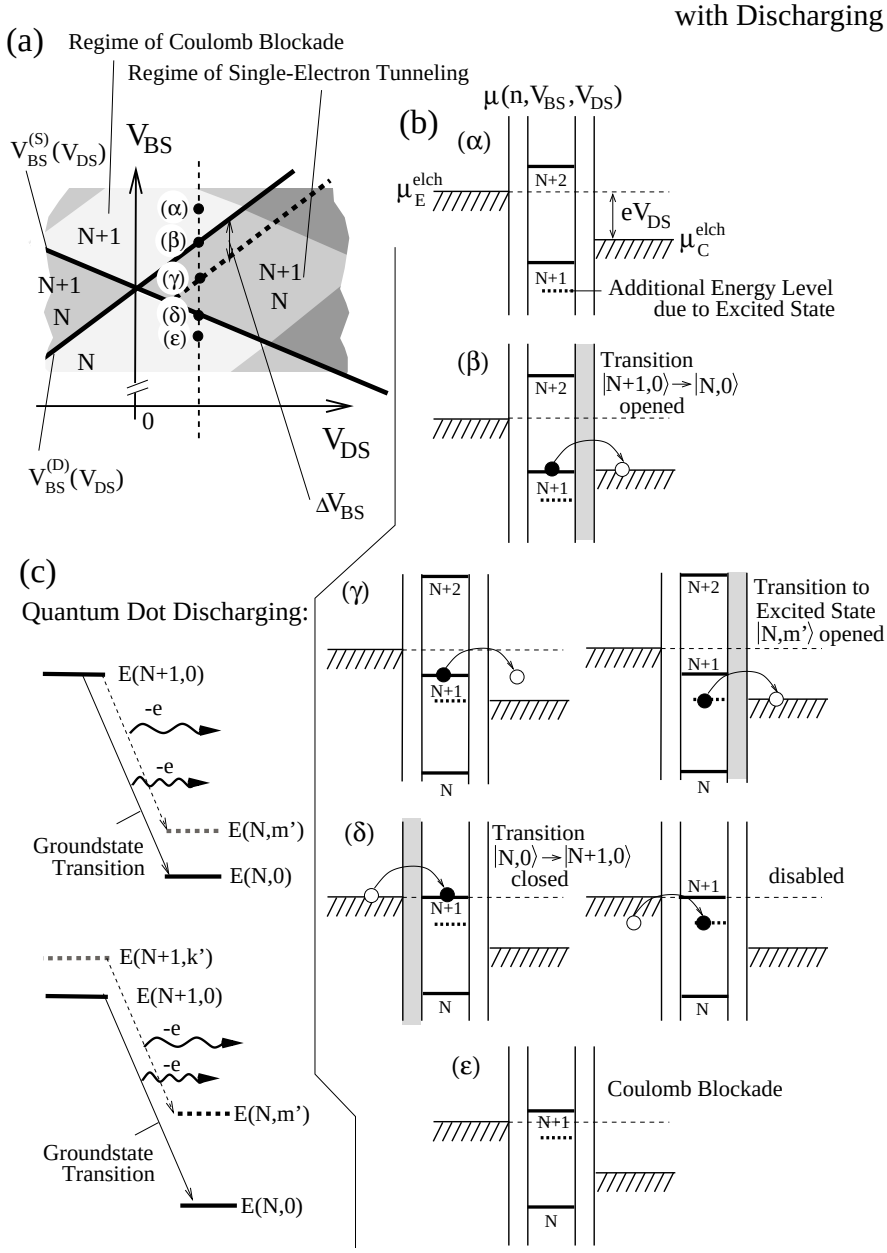

Fig. 5.8. (Left page) (a) Similar to Fig. 5.7a, except that an additional single-electron transport channel (the position is indicated by the dotted line) opens within a single-electron tunneling region, parallel to the borderline to the Coulomb blockade regime of $N+1$ electrons instead of N electrons. (b) Energy schemes to the $V_{\rm BS}$ values indicated in (a) with (α) to (ε). In case of (γ), an additional channel is opened for electrons leaving the quantum dot by ending in an excited state $|N,l'\rangle$ of the N-electron system. This is done (see (c)) either by starting from the groundstate $|N+1,0\rangle$ of the $(N+1)$-electron system or by starting from an excited state $|N+1,k'\rangle$ of the $(N+1)$-electron system. The latter has to be reached by the preceeding process, for instance, by a tunneling process adding the $N+1$ electron from emitter (see Fig. 5.7).

- **Operation point β:** With decreasing the gate voltage $V_{\rm BS}$, single-electron transport becomes possible at $V_{\rm BS}^{\beta}$ since there

$$\mu(N+1;V_{\rm BS}^{\beta},V_{\rm DS}) \overset{(\geq)}{=} \mu_{\rm C}^{\rm elch}$$

(see Fig. 5.8b(β)). Starting from the groundstate of the $(N+1)$-electron system in the quantum dot, maximum energy is obtained for an electron leaving the quantum if the quantum dot ends in the groundstate of the N-electron system. At $V_{\rm BS}^{\beta}$ the energy $\mu(N+1;V_{\rm BS}^{\beta},V_{\rm DS})$ of the electron is just enough to reach an unoccupied state at the Fermi level of the collector. For $V_{\rm BS}^{\beta} \geq V_{\rm BS} \geq V_{\rm BS}^{\delta}$, single-electron transport remains possible since

$$\mu_{\rm E}^{\rm elch} \geq \mu(N+1;V_{\rm BS},V_{\rm DS}) \geq \mu_{\rm C}^{\rm elch} \,. \tag{5.25}$$

- **Operation point γ:** At $V_{\rm BS}^{\gamma}$ within the gate voltage interval defined by (5.25), an additional channel is opened in resonance to the collector: There is another channel for electrons *leaving* the quantum dot. Starting from the groundstate $|N+1,0;V_{\rm BS}^{\gamma},V_{\rm DS}\rangle$ of the $(N+1)$-electron system in the quantum dot, an electron can escape from the quantum dot to the collector so that the quantum dot is left behind in an excited state $|N,l';V_{\rm BS}^{\gamma},V_{\rm DS}\rangle$ of the N-electron system (see Fig. 5.8c). This becomes possible at $V_{\rm BS}^{\gamma}$ if

$$E(N+1,0;V_{\rm BS}^{\gamma},V_{\rm DS}) - E(N,l';V_{\rm BS}^{\gamma},V_{\rm DS}) \overset{(\geq)}{=} \mu_{\rm C}^{\rm elch} \,, \tag{5.26}$$

i.e, the electron gains enough energy to find an unoccupied state at the Fermi level of the collector.
By opening this channel, a single electron from the quantum dot can leave to the collector by *either* transfering the quantum dot into an excited state *or* into the groundstate of the N-electron system. As in the case of an additional channel from the emitter side, these channels at the collector side are taken from electrons of different energy, but again *they cannot be used at the same time.* The additional channel increases only the probability that an electron is leaving the quantum dot to the collector side.

Due to the possibility of obtaining an excited state $|N+1,k';V_{\rm BS}^{\gamma},V_{\rm DS}\rangle$ of the $(N+1)$-electron system by tunneling from emitter into the quantum dot, the relation (5.26) has to be generalized to

$$\mu_{\rm C}^{\rm elch} \overset{(<)}{=} E(N+1,k';V_{\rm BS}^{\gamma},V_{\rm DS}) - E(N,l';V_{\rm BS}^{\gamma},V_{\rm DS}) \tag{5.27}$$

$$< \mu(N+1,k;V_{\rm BS}^{\gamma},V_{\rm DS}) \leq \mu_{\rm E}^{\rm elch} \,. \tag{5.28}$$

This transition between the N and the $(N+1)$-electron system is indicated in Fig. 5.8c.

The additional single-electron channel described by (5.26) or by (5.27) is only possible if anyhow the quantum dot can fluctuate between $N+1$ and N electrons, i.e., (5.28) is fulfilled. Otherwise, although the energy difference $E(N+1,k';\{V_i\}) - E(N,l';\{V_i\})$ might fall between $\mu_{\rm E}^{\rm elch}$ and $\mu_{\rm C}^{\rm elch}$, this channel via the excited state cannot be used (see Fig. 5.8b(ε)).

At $V_{\rm BS}^{\beta}$ and $V_{\rm BS}^{\gamma}$, the respective resonance conditions

$$E(N+1,0;V_{\rm BS}^{\beta},V_{\rm DS}) - E(N,0;V_{\rm BS}^{\beta},V_{\rm DS}) \overset{(>)}{=} \mu_{\rm C}^{\rm elch} \,,$$

$$E(N+1,k';V_{\rm BS}^{\gamma},V_{\rm DS}) - E(N,l';V_{\rm BS}^{\gamma},V_{\rm DS}) \overset{(>)}{=} \mu_{\rm C}^{\rm elch}$$

are obtained. Based on the assumption (5.8), the difference $\Delta V_{\rm BS} = V_{\rm BS}^{\beta} - V_{\rm BS}^{\gamma}$ in the gate voltage $V_{\rm BS}$ between (γ) and (β) in Fig. 5.8a is then given by

$$\begin{aligned} \alpha_{\rm B} \cdot e\,\Delta V_{\rm BS} = \; & E(N+1,k';\{V_i\}) - E(N,l';\{V_i\}) \\ & - \Big[E(N+1,0;\{V_i\}) - E(N,0;\{V_i\})\Big] \,. \end{aligned} \tag{5.29}$$

This result is very similar to the result (5.24) for opening an additional channel for electrons entering the quantum dot from emitter side.

5.4.3 Is Separate Quantitative Spectrocopy of the N- and of the $(N+1)$-Electron System Possible?

Eqn. (5.22) describes the situation when an excited state of the $(N+1)$-electron system is reached, whereas Eqn. (5.27) describes the condition for an excited state of the N-electron system becoming accessible. In the general case where the initial state before tunneling is an excited state, these resonance conditions include the total energy of excited states of *both* systems which makes the spectroscopy rather complex.

But if the initial state of the quantum dot before the $(N+1)$th electron enters the quantum dot from the emitter is always the groundstate $|N,0\rangle$ of the N-electron system (see Fig. 5.9a), then (5.22) reduces to

$$\mu_{\rm E}^{\rm elch} \overset{(>)}{=} E(N+1,k;V_{\rm BS}^{\gamma},V_{\rm DS}) - E(N,0;V_{\rm BS}^{\gamma},V_{\rm DS}) \tag{5.30}$$

$$> \mu(N+1,k;V_{\rm BS}^{\gamma},V_{\rm DS}) \geq \mu_{\rm C}^{\rm elch} \,.$$

As a consequence, the distance ΔV_{BS} in the backgate-source voltage from the borderline to the Coulomb-blockade regime of N electrons to opening the additional channel on the emitter side is given by

$$\alpha_{\mathrm{B}} \cdot e\,\Delta V_{\mathrm{BS}} = E(N+1,k;\{V_i\}) - E(N+1,0;\{V_i\})\ . \tag{5.31}$$

Similar for the channels to the collector: If the initial state of the quantum dot before the Nth electron leaves the quantum dot to the collector is always the groundstate $|N+1,0\rangle$ of the $(N+1)$-electron system (see Fig. 5.9a), then (5.27) reduces to

$$\begin{aligned}\mu_{\mathrm{C}}^{\mathrm{elch}} \overset{(\leq)}{=} E(N+1,0;V_{\mathrm{BS}}^{\gamma},V_{\mathrm{DS}}) - E(N,l';V_{\mathrm{BS}}^{\gamma},V_{\mathrm{DS}}) \\ < \mu(N+1,k;V_{\mathrm{BS}}^{\gamma},V_{\mathrm{DS}}) \leq \mu_{\mathrm{E}}^{\mathrm{elch}}\ .\end{aligned} \tag{5.32}$$

The distance ΔV_{BS} in the backgate-source voltage from the borderline to the Coulomb blockade regime of $(N+1)$ electrons to opening the additional channel on the collector side is given by

$$\alpha_{\mathrm{B}} \cdot e\,\Delta V_{\mathrm{BS}} = E(N,k;\{V_i\}) - E(N,0;\{V_i\})\ . \tag{5.33}$$

Under such conditions, indeed, quantitative spectroscopy of the $(N+1)$- and the N-electron system can be done separately, just distinguished by the shift of their borderline in the (V_{BS},V_{DS}) plane (see Fig. 5.9b):

> Within the single-electron tunneling regime of N and $N+1$ electrons, a quantitative spectroscopy of the $(N+1)$-electron system is done with respect to the borderline to the Coulomb blockade regime of N electrons,[9] whereas a quantitative spectroscopy of the N-electron system is done with respect to the borderline to the Coulomb blockade regime of $N+1$ electrons.[10] This is possible if a fast and complete relaxation to the groundstate of the confined electron system in the quantum dot occurs before the next tunneling process through one of the barriers starts.

However, negative differential conductance in Fig. 5.5 indicates that (at least for some excited states) relaxation does not occur within the mean time $\tau = e/|I_{\mathrm{DS}}|$ between successive electrons passing through the quantum dot [148]. We will come back to this effect in Section 5.8. The question arises: Are there other features indicating that the initial states for the tunneling process are in the respective groundstates? This topic will be addressed in the following Sections.

[9] Parallel to $V_{\mathrm{BS}}^{(\mathrm{S})}$ for $V_{\mathrm{DS}} > 0$, and parallel to $V_{\mathrm{BS}}^{(\mathrm{D})}$ for $V_{\mathrm{DS}} < 0$.
[10] Parallel to $V_{\mathrm{BS}}^{(\mathrm{D})}$ for $V_{\mathrm{DS}} > 0$, and parallel to $V_{\mathrm{BS}}^{(\mathrm{S})}$ for $V_{\mathrm{DS}} < 0$.

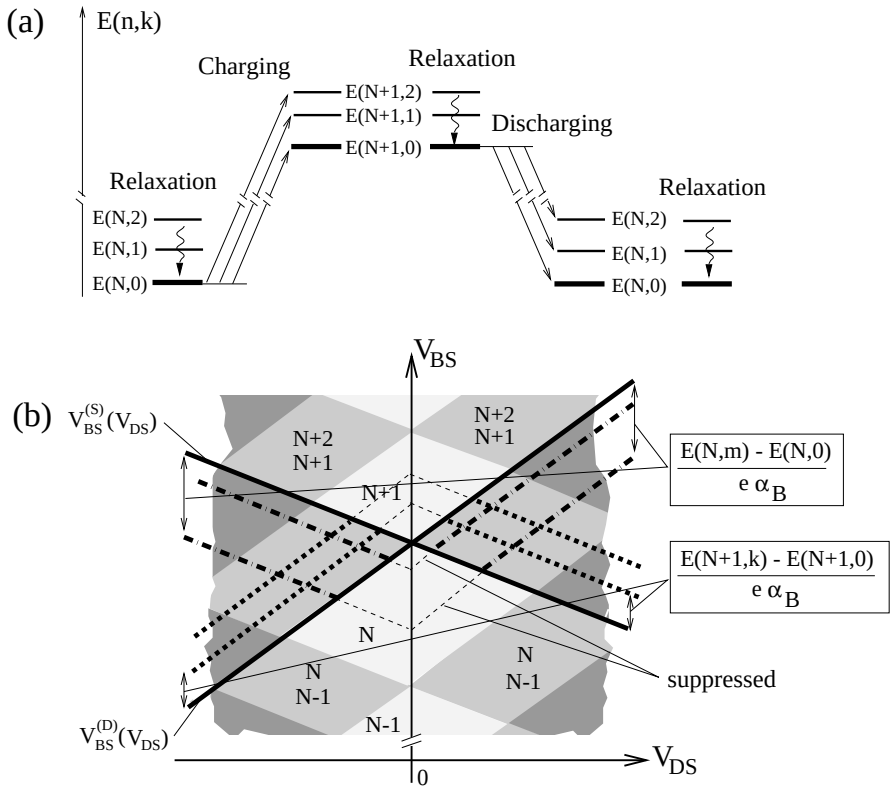

Fig. 5.9. Separate spectroscopy of the N- and the $(N+1)$-electron system can be done if the initial state of the quantum dot before a tunneling process starts is always the groundstate of the respective n-electron system. (a) If an excited state has been reached, a relaxation process to the respective groundstate has to occur before the next tunneling event takes place. (b) Sketch of the single-electron tunneling regimes of N and $(N+1)$ electrons on the quantum dot: The dotted lines mark the borderline for opening an additional channel on the emitter side and are therefore due to excited states of the $(N+1)$-electron system. The dashed-dotted lines mark the borderline for opening an additional channel on the collector side and are therefore due to excited states of the N-electron system. These channels are suppressed in the Coulomb blockade regime since there the number of electrons on the quantum dot is fixed.

5.5 Construction of Possible Transport Threshold Lines in the (V_{BS},V_{DS}) Plane from the Known Energy Spectra of the Quantum Dot

Is it possible to construct the positions for opening additional single-electron transport channels in the (V_{BS},V_{DS}) plane if we know the energy spectra for

the N- and the $(N+1)$-electron system in the quantum dot? A scheme for doing so is derived here [42]:

Let us assume the total energy spectra for the N- and the $(N+1)$-electron system as shown in Fig. 5.10a. For simplicity, degeneracy in the spectrum is absent, i.e., with increasing quantum number index the energy of the n-electron states increases. The differences between the energy spectrum of the $(N+1)$-electron system and those of the N-electron system for fixed potential $\{V_i\}$ are denoted in the following as *transition energies*. They are plotted in Fig. 5.10b with respect to the electrochemical potentials of emitter and collector represented by the horizontal lines. By changing a gate electrode potential V_j by $\mathrm{d}V_j$, all transition energies are shifted relatively to $\mu_{\mathrm{E}}^{\mathrm{elch}}$ and $\mu_{\mathrm{C}}^{\mathrm{elch}}$ by $-e\alpha_j\,\mathrm{d}V_j$.

The scheme of Fig. 5.10b is constructed in the following way: First the transition energies $E(N+1,k) - E(N,0)$ from the groundstate of the N-electron system to the ground- and excited states of the $(N+1)$-electron system ($k \in \{0,1,2,\cdots\}$) are plotted along the vertical energy axis. The exact vertical position of this ladder with respect to $\mu_{\mathrm{E}}^{\mathrm{elch}}$ and $\mu_{\mathrm{C}}^{\mathrm{elch}}$ depends on the operation point in the (V_{BS},V_{DS}) plane. The respective levels are marked by $(0,k)$. At horizontal distances, given by the transition energies $E(N+1,0) - E(N,l)$ with $l \in \{0,1,2,\cdots\}$, the ladder of transition energies $E(N+1,k) - E(N,l)$ with $k \in \{0,1,2,\cdots\}$ are plotted, marked by (l,k). We obtain a grid-like pattern with nodes each indicating an energy level with respect to $\mu_{\mathrm{E}}^{\mathrm{elch}}$ and $\mu_{\mathrm{C}}^{\mathrm{elch}}$ for a transition between the N- and the $(N+1)$-electron system. By the vertical solid line crossing a node (l,k) all transitions are connected involving the same state $|N,l\rangle$ of the N-electron system. By the dashed oblique line, the transitions involving the same state $|N+1,k\rangle$ of the $(N+1)$-electron system are connected. The arrows on the connecting lines indicate possible directions for relaxation in the system for fixed electron number. Any path following the arrows will end at the transition between the groundstates, denoted by $(0,0)$.

How to interpret this scheme to derive the possible transitions for the given drain-source voltage V_{DS} and gate-source voltage V_{BS}. To succeed, consider the following statements:

1. A direct transition from $|N,l\rangle$ to $|N+1,k\rangle$ is only allowed if

$$\mu_{\mathrm{E}}^{\mathrm{elch}} \geq E(N+1,k;\{V_i\}) - E(N,l;\{V_i\})\,.$$

   The node (l,k) has to lie below $\mu_{\mathrm{E}}^{\mathrm{elch}}$. Prerequisite for such a transition is that the state $|N,l\rangle$ is the initial state, i.e., $|N,l\rangle$ has been prepared by a preceeding process. This might happen due to a direct transition from a $(N+1)$-electron state or by relaxation from a N-electron state of higher energy. A transition from $|N+1,k'\rangle$ to $|N,l\rangle$ is only energetically allowed if

$$E(N+1,k';\{V_i\}) - E(N,l;\{V_i\}) \geq \mu_{\mathrm{C}}^{\mathrm{elch}}\,.$$

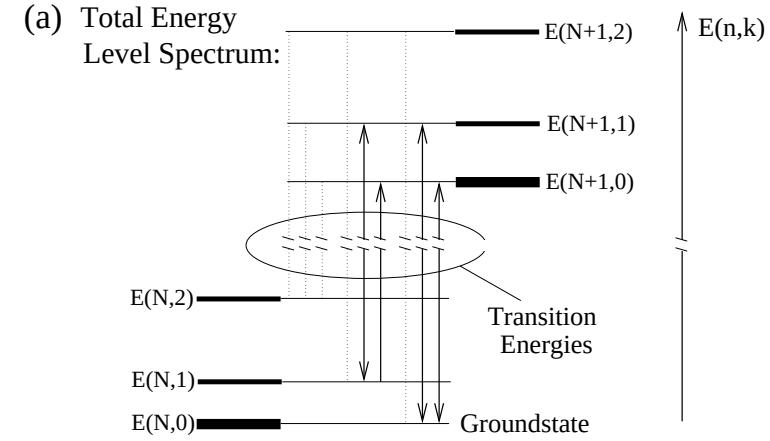

(b) Transition Energies at Distinct (V_{BS}, V_{DS}) Values

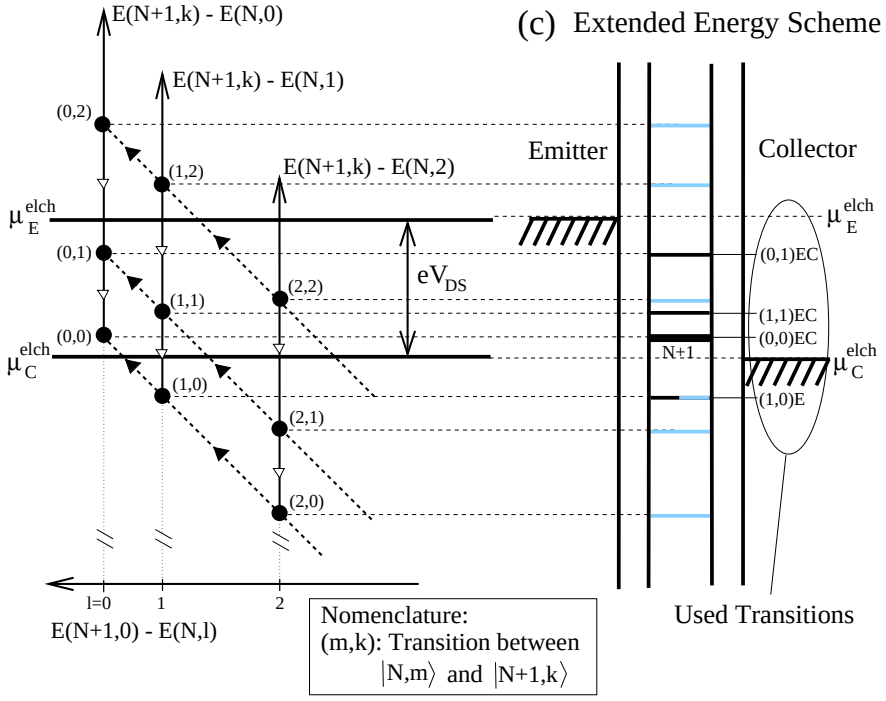

(c) Extended Energy Scheme

Fig. 5.10. (Left page) Interrelation between the total energy spectrum and extended energy-level scheme: (a) Fictitious total energy spectra of the N- and the $(N+1)$-electron system. The distance between the N- and the $(N+1)$-electron spectrum increases linearly with changing an electrode potential V_i. Transitions are indicated, possible for the situation depicted in (b). (b) Scheme where the transition energies $E(N+1,k)-E(N,l)$ derived from (a) are plotted for a certain drain-source voltage and gate voltage combination relatively to the electrochemical potentials of emitter and collector. Construction and interpretation: see text. (c) Extended energy scheme for the quantum dot to decribe single-electron transport: All transition energies $E(N+1,k)-E(N,l)$ are plotted. The thick solid line represents the transition between the groundstates, i.e., $\mu(N+1)$. Black are marked possible transitions, grey those which cannot be used under these conditions. The transition (1,0) is usable only from the emitter side, i.e., (1,0)E (black to emitter side, grey to collector side).

The node (l,k') has to lie above $\mu_{\mathrm{C}}^{\mathrm{elch}}$ and prerequisite is that the initial state $|N+1,k'\rangle$ has been prepared by the preceeding process.

2. If the transition $|N,l\rangle \rightarrow |N+1,k\rangle$ becomes possible, all transitions $|N,l\rangle \rightarrow |N+1,k'\rangle$ with $0 \leq k' \leq k$ become energetically allowed. It means in Fig. 5.10b: If the transition $|N,l\rangle \rightarrow |N+1,k\rangle$ occurs, transitions to all states of the $(N+1)$-electron system become energetically possible which are reached along the *solid* line through (l,k) for which the transition energy lies *below* $\mu_{\mathrm{E}}^{\mathrm{elch}}$.
3. Similar, if the transition $|N+1,k\rangle \rightarrow |N,l\rangle$ occurs, all transitions $|N+1,k\rangle \rightarrow |N,l'\rangle$ with $0 \leq l' \leq l$ are energetically allowed. It means in Fig. 5.10b: If the transition $|N+1,k\rangle \rightarrow |N,l\rangle$ is possible, transitions to all states of the N-electron system become possible which are reached along the *dashed* line through (l,k) for which the transition energy lies *above* $\mu_{\mathrm{C}}^{\mathrm{elch}}$.
4. If the state $|N+1,k\rangle$ is reached, by relaxation also the states $|N+1,k'\rangle$ with $k' < k$ might occur. Similar, if the state $|N,l\rangle$ is obtained, by relaxation also the states $|N,l'\rangle$ with $l' < l$ might be present.

In Fig. 5.10b, the transition energy between the groundstate of the N- and the $(N+1)$-electron system lies between $\mu_{\mathrm{E}}^{\mathrm{elch}}$ and $\mu_{\mathrm{C}}^{\mathrm{elch}}$, i.e., single-electron tunneling is possible and the electron system in the quantum dot is found in both groundstates $|N,0\rangle$ and $|N+1,0\rangle$ from time to time. Which other transitions are possible? Starting from $(0,0)$ along the connecting lines further transitions have to be searched. Along the solid vertical line, transitions are only possible if the respective transition energy lies below $\mu_{\mathrm{E}}^{\mathrm{elch}}$. It is a channel for an electron entering the quantum dot. Along the dashed oblique line, a transition is only possible if its transition energy lies above $\mu_{\mathrm{C}}^{\mathrm{elch}}$. It is a channel for an electron leaving the quantum dot. If a possible transition is found, from this node further transitions can be searched along its connecting lines to neighboring nodes.

We can summarize: If the transition (l,k) is possible, all transitions are energetically possible which are

- reached along the solid vertical line with transition energy below $\mu_{\mathrm{E}}^{\mathrm{elch}}$, or
- reached along the dashed oblique line with transition energy above $\mu_{\mathrm{C}}^{\mathrm{elch}}$.

Let us apply this result to the situation depicted in Fig. 5.10b: Starting from $(0,0)$, along the solid line, transitions from the groundstate $|N,0\rangle$ to excited state $|N+1,k\rangle$ of the $(N+1)$-electron system are found marked by $(0,k)$. Only the transition $(0,1)$ is possible since its transition energy lies below $\mu_{\mathrm{E}}^{\mathrm{elch}}$. Therefore, the state $|N+1,1\rangle$ is reached. Again, starting from $(0,0)$, along the dashed line the transition $(1,0)$ is reached which cannot be used since it lies below $\mu_{\mathrm{C}}^{\mathrm{elch}}$. Therefore the transition $|N+1,0\rangle \to |N,1\rangle$ is not energetically allowed. From $(0,1)$ only $(0,0)$ (solid line, below $\mu_{\mathrm{E}}^{\mathrm{elch}}$) and $(1,1)$ (dashed line, above $\mu_{\mathrm{C}}^{\mathrm{elch}}$) lead to possible transitions. From $(1,1)$, also $(1,0)$ is reached along the solid line. Since it lies below $\mu_{\mathrm{E}}^{\mathrm{elch}}$, the transition $|N,1\rangle \to |N+1,0\rangle$ is energetically allowed. In summary, for the situation in Fig. 5.10b the following transitions are energetically accessible:

$$
\begin{aligned}
&(0,0)\mathrm{EC} : |N,0\rangle \leftrightarrow |N+1,0\rangle \ , \\
&(0,1)\mathrm{EC} : |N,0\rangle \leftrightarrow |N+1,1\rangle \ , \\
&(1,1)\mathrm{EC} : |N,1\rangle \leftrightarrow |N+1,1\rangle \ , \\
&(1,0)\mathrm{E} \quad : |N,1\rangle \to |N+1,0\rangle \ .
\end{aligned}
$$

The transition $|N,1\rangle \to |N+1,0\rangle$ but not the transition $|N+1,0\rangle \to |N,1\rangle$ is possible, whereas all other transitions are bidirectional. All these transitions are marked in total energy spectra shown Fig. 5.10a. Is the key transition $|N,0\rangle \to |N+1,1\rangle$ not allowed due to other selection rules besides energy conservation, then all transitions described above are not usable since these are linked to $(0,1)$E. If this key transition occurs, then all transitions described above are energetically allowed.

In conclusion, the dynamics of single-electron transport is rather complex, since by opening a transition to a new excited state of the N or the $(N+1)$-electron system, generally a whole series of other transitions between both electron systems become energetically allowed. The scheme presented in Fig. 5.10b allows to explore systematically these energetically possible transitions as described above.

How does it looks like in the $(V_{\mathrm{BS}},V_{\mathrm{DS}})$ plane? In Fig. 5.11, the borderlines derived from the fictitious energy spectrum and described by the relations

$$
E(N+1,k;V_{\mathrm{BS}},V_{\mathrm{DS}}) - E(N,l;V_{\mathrm{BS}},V_{\mathrm{DS}}) \overset{(\leq)}{=} \mu_{\mathrm{E}}^{\mathrm{elch}} \ , \tag{5.34}
$$

$$
E(N+1,k;V_{\mathrm{BS}},V_{\mathrm{DS}}) - E(N,l;V_{\mathrm{BS}},V_{\mathrm{DS}}) \overset{(\geq)}{=} \mu_{\mathrm{C}}^{\mathrm{elch}} \tag{5.35}
$$

are plotted in the $(V_{\mathrm{BS}},V_{\mathrm{DS}})$ plane. By (l,k)E, the borderline decribed by (5.34) is marked, by (l,k)C that described by (5.35). The borderline for

single-electron tunneling towards the Coulomb blockade regimes are equivalent to $(0,0)$E and $(0,0)$C. Borderlines involving excited state can only be used within the single-electron tunneling regime, and there only if the initial state has been reached by another process. The lines (l,k)E and (l,k)C are drawn as a thick line for $(V_{\mathrm{DS}}, V_{\mathrm{BS}})$ where these transitions become possible for higher $|V_{\mathrm{DS}}|$. There a peak in the differential conductance is expected. For example, the borderline $(1,1)$E is drawn as a thick line after crossing a line $(1,0)$C because the initial state $|N,1\rangle$ for $(1,1)$E became available at the crossing with $(1,0)$C.

The pattern of transport spectroscopy of Fig. 5.11 is obtained by considering direct transitions between the N and the $(N+1)$-electron system. Under this assumption, it seems to be possible to conclude on the initial state for each transition visible in the transport spectrum. Unfortunately, if certain transitions are not allowed, the story is not so easy as the following example shows: Let us assume the transition (l,k)E, i.e., $|N,l\rangle \rightarrow |N+1,k\rangle$, is not possible although energetically allowed. But $|N+1,k\rangle$ might be obtained from relaxation from a state $|N+1,k'\rangle$ of higher energy, which was reached by the transition (l',k')E. Therefore transitions involving the state $|N+1,k\rangle$ are not enabled by (l,k)E but by (l',k')E: Borderlines of (l'',k)C end on (l',k')E instead of (l,k)E. Therefore, from the transport spectrum, in general, we cannot conclude unambituously on the initial state!

Additional channels which are opened from groundstates as the initial state are ending at the borderlines $(0,0)$E and $(0,0)$C. Can be concluded in the opposite direction that all those borderlines ending at the borderlines of single-electron tunneling are due to transitions involving a groundstate? Unfortunately not: Let us look at the following example. We assume that the transition energy for $(1,1)$ is the same as for $(0,0)$. Then $(1,1)$E falls in Fig. 5.11 *onto* the borderline $(0,0)$E and is activated with $(0,1)$C for increasing $|V_{\mathrm{DS}}|$. Therefore (2,1)C which is linked to $(1,1)$E ends also on the borderline $(0,0)$E.

Obvious from Fig. 5.11, transitions (k,l) with

$$E(N+1,k) - E(N,l) > \mu(N+1)\ , \tag{5.36}$$

i.e., with an energy level above the groundstate transition are candidates for opening additional channels on the emitter side, whereas, transitions (k',l') with

$$E(N+1,k') - E(N,l') < \mu(N+1)\ , \tag{5.37}$$

i.e., with an energy level below the transition energy between groundstates might open additional channels on the collector side. In the first case, a new channel is created for an electron entering the quantum dot, whereas in the second case a new channel is created for electrons leaving the quantum dot. In analogy to Section 1.2, the first one can be denoted as an 'electron-like' channel whereas the second one as a 'hole-like' channel.

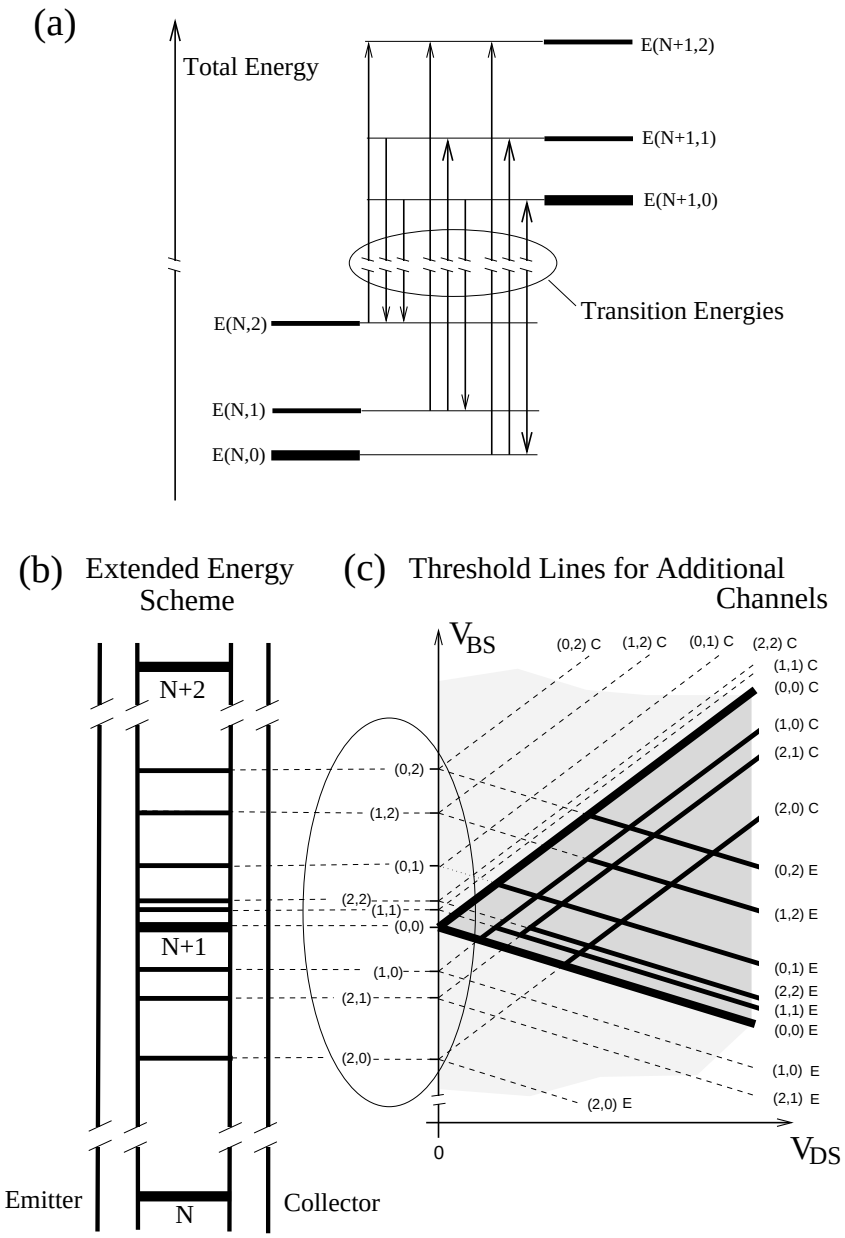
(a)
Total Energy
E(N+1,2)
E(N+1,1)
E(N+1,0)
Transition Energies
E(N,2)
E(N,1)
E(N,0)
(b) Extended Energy Scheme
N+2
N+1
N
Emitter
Collector
(0,2)
(1,2)
(0,1)
(2,2)
(1,1)
(0,0)
(1,0)
(2,1)
(2,0)
(c) Threshold Lines for Additional Channels
V_{BS}
V_{DS}
0
(0,2) C
(1,2) C
(0,1) C
(2,2) C
(1,1) C
(0,0) C
(1,0) C
(2,1) C
(2,0) C
(0,2) E
(1,2) E
(0,1) E
(2,2) E
(1,1) E
(0,0) E
(1,0) E
(2,1) E
(2,0) E

Fig. 5.11. (Left page) Interrelation between total energy levels and borderlines in the (V_{BS}, V_{DS}) plane: In (a) a fictitious energy spectrum is given which leads to the energy ladder defined by the transition energies $E(N+1,k) - E(N,l)$ and plotted in (b). It includes $\mu(N+1) = E(N+1,0) - E(N,0)$, i.e., the transition between the groundstates. With changing the gate voltage V_{GS}, the energy ladder is shifted, i.e., these levels come in resonance for certain V_{GS} values as marked in (c). These transitions might open an additional channel on the emitter or the collector side defining the borderline shifting up or down with $|V_{DS}|$. If these borderlines fall into the single-electron tunneling regime, they might be usable. Prerequisite is that the initial state has been reached: Groundstates are reached at the borderlines of single-electron tunneling, excited states usually after crossing another borderline which leads to the required initial state.

In conclusion, from experimental transport spectrum it is not straight forward to extract unambiguously the energy spectra for the N- and the $(N+1)$-electron system. Further information about the system has to be collected and incorporated into the interpretation of such an experimental transport spectrum.

5.6 Transport Spectrum: From Metal-Like to Atom-Like Quantum Dot

Single-electron transport is caused by the repulsive electron-electron interaction on the island, described in metal systems by the electrostatic single-electron charging energy E_C. As described in Chapter 4, with descreasing the size of an island, the kinetic energy of the electrons gets quantized. The single-particle level spacing $\Delta\varepsilon_{qu}$ [11] increases and even exceeds E_C.

The energy scheme to describe single-electron transport through the quantum dot includes all possible transitions between the N- and the $(N+1)$-electron system. Depending on the relative size of the single-electron charging energy E_C and the quantization energy $\Delta\varepsilon_{qu}$, one can distinguish the following cases:

- For a metal island, the single-electron charging energy is the dominant energy scale: $E_C \gg \Delta\varepsilon_{qu}$. The single-particle excitation spectrum is continuously dense, i.e., the transition energies between the N- and the $(N+1)$-electron system are also dense. As sketched in Fig. 5.12a, very regular and uniform regions of Coulomb blockade should be observed as a function of a gate voltage V_{GS} and drain-source voltage V_{DS}. Due to the dense excitation spectra of a metal island, continuously additional single-electron transport channels are opened with increasing $|V_{DS}|$ (see $I_{DS}(V_{DS})$ characteristics in Fig. 1.9, Fig. 1.10 and Fig.1.11).

[11] For a harmonic confining potential, we have $\Delta\varepsilon_{qu} = \hbar\omega_0$.

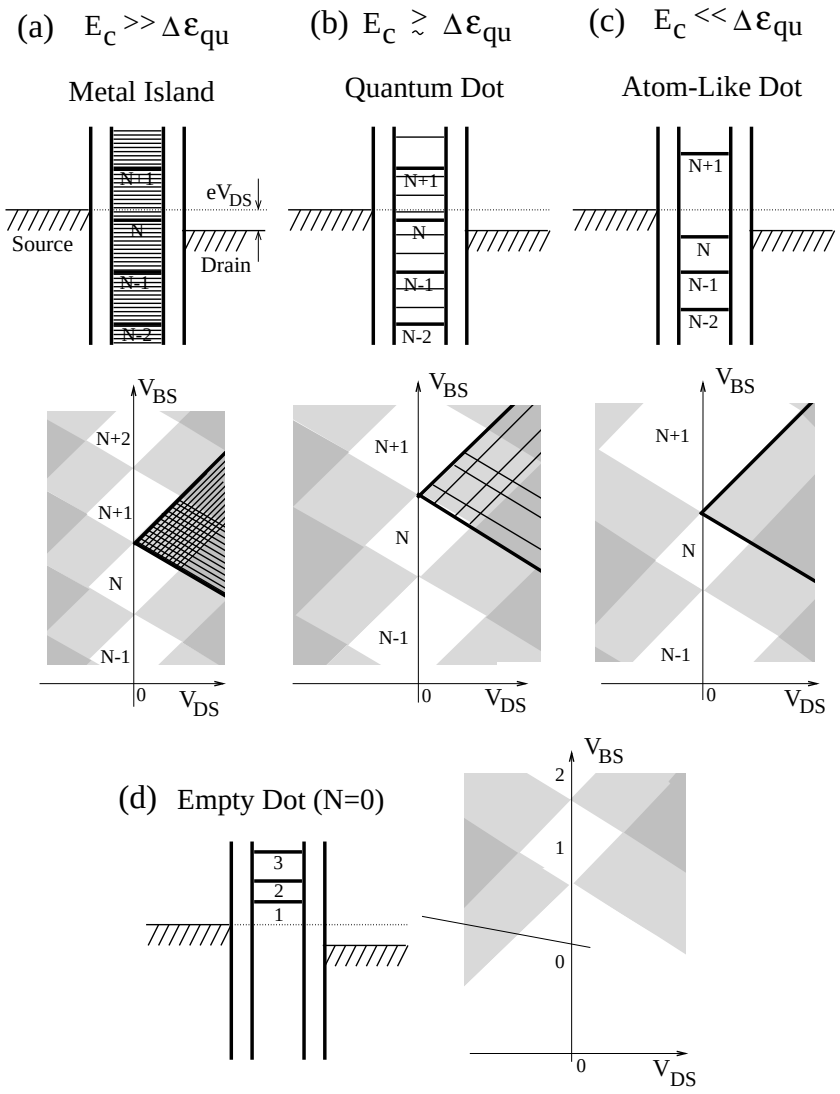

Fig. 5.12. With decreasing the typical size of a quantum dot, the quantum-mechanical energy-level spacing $\Delta\varepsilon_{\rm qu}$ increases and might even exceed the single-electron charging energy $E_{\rm C}$ due to the electron-electron interaction in the quantum dot. With increasing the ratio $\Delta\varepsilon_{\rm qu}/E_{\rm C}$, the Coulomb blockade regions in the $(V_{\rm BS}, V_{\rm DS})$ plane vary more and more in size with the electron number, and a less number of additional channels occur in the single-electron tunneling regime.

- For a typical quantum dot obtained by structuring bulk material, the quantization energy $\Delta\varepsilon_{\rm qu}$ is comparable to the single-electron charging energy: $E_{\rm C} \approx \Delta\varepsilon_{\rm qu}$. The excitation spectrum is discrete close to the respective

groundstate. The shapes of the Coulomb blockade regions vary in size with the electron number and additional channels in the single-electron tunneling regime should be resolved (see Fig. 5.12b).

- In case of really small islands, the quantization due to the confinement dominates – like in atoms: $\Delta\varepsilon_{\mathrm{qu}} \gg E_{\mathrm{C}}$. Almost no additional channels are expected to be opened within the single-electron tunneling regime since the single-electron excitation energies usually exceeds the classical single-electron charging energy (see Fig. 5.12c). Reminiscences of the electron-electron interaction in the n-electron system might still deliver low-energy excitations.

In the case that the quantum dot becomes completely empty of conduction-band electrons, the Coulomb blockade region $N = 0$ is not closed as indicated in Fig. 5.12d. Such transport spectra were observed by Kouwenhoven, Austing, Tarucha and coworkers [5]. Such a Coulomb-blockade region gets in principle closed by taking off the first electron from the valence band ($N = 0$): The distance in the addition energies $\mu(N = 1) - \mu(N = 0)$ becomes about the relatively large semiconductor's bandgap energy.

5.7 Transport Spectroscopy by Applying a Magnetic Field

We have already presented in Fig. 5.2 conductance measurements versus V_{BS} at $V_{\mathrm{DS}} \approx 0$ for varying an applied magnetic field B. We found that the distance in the Coulomb blockade oscillations varies with magnetic field: Each CBO peak shifts slightly differently, i.e., shows a characteristic 'magnetic field dispersion'. Furthermore, the peak heights in the CBOs are modulated. The effects are independent of positive or negative magnetic field orientation. From these observations we conclude: Applying a magnetic field to the quantum dot system changes the energy spectrum of the electron system confined in the quantum dot. This leads to changes in the transition energies between the N- and the $(N + 1)$-electron system in the quantum dot for fixed electrostatic potentials $\{V_i\}$ on the surrounding electrodes. The change in the transition energies $E(N + 1, k; \{V_i\}, B) - E(N, l; \{V_i\}, B)$, induced by the magnetic field B, can be compensated by a change in an applied gate voltage, for instance, V_{BS}. Therefore, the values of the applied gate voltage V_{BS}, which fulfill the resonance conditions

$$E(N + 1, k; V_{\mathrm{BS}}, V_{\mathrm{DS}}, B) - E(N, l; V_{\mathrm{BS}}, V_{\mathrm{DS}}, B) \overset{(\leq)}{=} \mu_{\mathrm{E}}^{\mathrm{elch}} , \quad (5.38)$$

$$E(N + 1, k; V_{\mathrm{BS}}, V_{\mathrm{DS}}, B) - E(N, l; V_{\mathrm{BS}}, V_{\mathrm{DS}}, B) \overset{(\geq)}{=} \mu_{\mathrm{C}}^{\mathrm{elch}} , \quad (5.39)$$

for opening transport channels, are shifted along the V_{BS} axis. McEuen *et al.* [146] demonstrated this kind of transport spectroscopy in a magnetic field

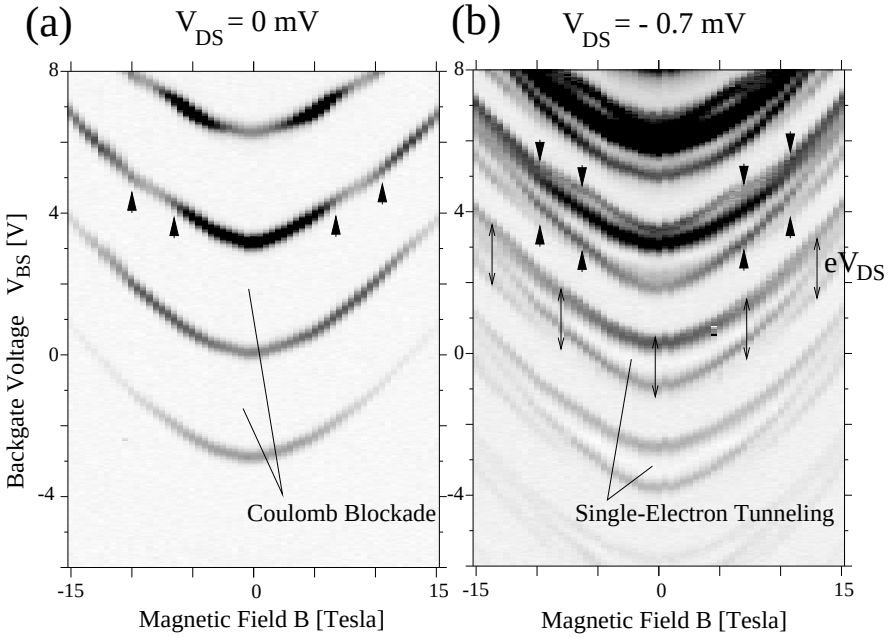

Fig. 5.13. Differential conductance $\mathrm{d}I_{\mathrm{DS}}/\mathrm{d}V_{\mathrm{DS}}$ in greyscale through the quantum dot system of Fig. 5.1 with magnetic field parallel to the plane of the 2DES, measured as a function of V_{BS} for the magnetic field range $-15\,\mathrm{T}$ to $+15\,\mathrm{T}$ in $0.5\,\mathrm{T}$ steps: (a) for drain-source voltage $V_{\mathrm{DS}} = 0$, (b) for $V_{\mathrm{DS}} = -0.7$ (white regions corresponds to $\mathrm{d}I_{\mathrm{DS}}/\mathrm{d}V_{\mathrm{DS}} \leq 0\,\mu\mathrm{S}$, black ones to $\mathrm{d}I_{\mathrm{DS}}/\mathrm{d}V_{\mathrm{DS}} \geq 2\,\mu\mathrm{S}$). Arrows indicate where a degeneracy in the groundstate either of the n- or the $(n+1)$-electron system occurs. (adopted from J. Weis et al. [149])

in 1991. The magnetic field B was orientated perpendicular to the plane of their 2D quantum dot realized in an AlGaAs/GaAs-heterostructure by split-gates. Due to the weak confinement in the plane *perpendicular* to the magnetic field orientation, defined by the split-gate electrodes, the spectrum is dominated by orbital effects. The method has been used by several groups to explore the electronic structure of quantum dots in high magnetic field (for review see for instance [81, 3, 4, 6, 5]). In Fig. 5.13, some of our own data are shown from the quantum dot presented in Fig. 5.1 where the magnetic field is applied *parallel* to the plane of the two-dimensional electron system. Due to the strong confinement for the 2DES in the growth direction of the heterostructure, orbital effects are diminished and the observed magnetic field dispersions are less complex, allowing to discuss the principles of transport spectroscopy with applying a magnetic field.

In Fig. 5.13a the differential conductance $\mathrm{d}I_{\mathrm{DS}}/\mathrm{d}V_{\mathrm{DS}}$ measured at $V_{\mathrm{DS}} = 0\,\mathrm{mV}$ is plotted in greyscale as a function of the backgate voltage V_{BS} and of

the magnetic field B between $-15\,\mathrm{T}$ and $15\,\mathrm{T}$ in $0.5\,\mathrm{T}$ steps. [12] In Fig. 5.13b similar measurements are shown for $V_{\mathrm{DS}} = -0.7\,\mathrm{mV}$. In Fig. 5.13b the backgate-voltage regions, where single-electron-tunneling occurs, are broadened since the difference between the electrochemical potentials of emitter and collector has been increased. Additional transport channels due to excited states of the quantum dot become accessible and the magnetic field dispersions of V_{BS} for opening these channels by the resonance conditions (5.38) and (5.39) are visible. The magnetic field behaviour is symmetric in changing the sign of the magnetic field B.

> The upper and lower boundaries $V_{\mathrm{BS}}^{(\mathrm{D})}(B)$ and $V_{\mathrm{BS}}^{(\mathrm{S})}(B)$ of each single-electron tunneling regime show the same magnetic field dispersion as predicted by conditions $\mu(n; V_{\mathrm{BS}}^{(\mathrm{D})}, V_{\mathrm{DS}}, B) = \mu_{\mathrm{D}}^{\mathrm{elch}}$, respectively $\mu(n; V_{\mathrm{BS}}^{(\mathrm{S})}, V_{\mathrm{DS}}, B) = \mu_{\mathrm{S}}^{\mathrm{elch}}$, where the difference $\mu_{\mathrm{S}}^{\mathrm{elch}} - \mu_{\mathrm{D}}^{\mathrm{elch}} = e|V_{\mathrm{DS}}|$ is *independent* of the magnetic field and defined by the externally applied drain-source voltage V_{DS} [149].

This is the same magnetic field dispersion which is observed at vanishingly small bias voltage $|V_{\mathrm{DS}}|$ in Fig. 5.13a. The kinks observable in Fig. 5.13a can be identified with crossings of different magnetic field dispersions in Fig. 5.13b (marked by arrows). Therefore, kinks in the magnetic field dispersion of the boundaries $V_{\mathrm{BS}}^{(\mathrm{D})}$ and $V_{\mathrm{BS}}^{((\mathrm{S})}$ of a single-electron tunneling regime indicate a change in the character of the groundstate of the N- or $(N+1)$-electron system (change in the quantum numbers): The groundstate of the quantum dot is degenerate either for the N- or the $(N+1)$-electron system, at these magnetic field values, i.e., $E(n, 0; B) = E(n, l; B)$.

Different magnetic field dispersions are visible in Fig. 5.13b. In principle, one should be able to derive further information about the magnetic field dependence of the transition energies $E(N+1, k; \{V_i\}, B) - E(N, l; \{V_i\}, B)$ between states of the N and the $(N+1)$-electron system of the quantum dot from such measurements. However, in interpreting the shift of V_{BS} values with B, that fulfills the condition (5.38) or (5.39), one has to be careful:

- On the one hand the magnetic field changes the states of the quantum dot.
- On the other hand the magnetic field also affects the states of the 2DES electrodes, acting as leads, and of the metal electrodes used as gates: The electronic states of the electrodes are energetically shifted and the density of states is changed by the magnetic field.

The latter effect causes a change in the electrostatic environment of the quantum dot: As discussed in Chapter 3, the differences of the *electrostatic* potentials of the electrodes are *not* given by the external electrical circuit, only the differences of the *electrochemical* potentials of the electrodes are given by the *external applied* voltages (V_{BS}, V_{DS}, etc.). Intrinsic contact voltages between

[12] Note, at $V_{\mathrm{DS}} = 0$ the differential conductance $\mathrm{d}I_{\mathrm{DS}}/\mathrm{d}V_{\mathrm{DS}}$ is equal to the conductance $I_{\mathrm{DS}}/V_{\mathrm{DS}}$ for $V_{\mathrm{DS}} \approx 0$.

the electrodes lead to a shift of the electrostatic potential of the quantum dot by $\alpha_i \cdot \Delta V_i^{\mathrm{C}}(B)$. Thus, the differential shift $(\partial V_{\mathrm{BS}}/\partial B) \cdot \mathrm{d}B$ of the applied gate voltage V_{BS}, required to remain at the resonance position for opening a transport channel, can be obtained from (5.38), (5.39) and the shift of the electrostatic potential of the electrodes with magnetic field [42, 144, 153]):

$$e \cdot \alpha_{\mathrm{B}} \frac{\partial V_{\mathrm{BS}}}{\partial B} = \frac{\partial}{\partial B} \left[E(N+1,k;V_{\mathrm{BS}},V_{\mathrm{DS}},B) - E(N,l V_{\mathrm{BS}},V_{\mathrm{DS}},B) \right] \Big|_{\{V_i\}} - e \cdot \sum_i \alpha_i \cdot \frac{\partial V_i^{\mathrm{C}}}{\partial B} \; . \tag{5.40}$$

The essential result of (5.40) is:

> The measured magnetic field dispersion of the applied gate voltage $V_{\mathrm{BS}}(B)$, fulfilling the resonance condition for opening a new transport channel, is due to the change in $E(N+1,k;V_{\mathrm{BS}},V_{\mathrm{DS}},B) - E(N,l;V_{\mathrm{BS}},V_{\mathrm{DS}},B)$ at fixed electrostatic potentials $\{V_i\}$, and due to the changes in the electrostatic potential of the surrounding electrodes by variations in the contact voltages induced by the magnetic field.

Therefore, if $\partial V_i^{\mathrm{C}}(B)/\partial B$ is unknown, the interpretation of the measured magnetic field dispersion $V_{\mathrm{BS}}(B)$ is difficult. [13] However, since the last term in (5.40) can be replaced by using $e \cdot \partial V_i^{\mathrm{C}}/\partial B = \partial \mu_i^{\mathrm{ch}}/\partial B$, it gives a contribution to all magnetic field dispersions. Consequently, reliable information about the magnetic field dispersion of $E(N+1,k;V_{\mathrm{BS}},V_{\mathrm{DS}},B) - E(N,l;V_{\mathrm{BS}},V_{\mathrm{DS}},B)$ at fixed electrostatic potentials $\{V_i\}$ can be obtained by a direct comparison of two magnetic field dispersions.

5.8 Dynamics of Single-Electron Transport Through Quantum Dots

If excited states of the electron system in the quantum dot become accessible, usually the current through the quantum dot is increased. But this is not true in all cases as visible in the experimental data of Fig. 5.5 where negative differential conductance occurs: The electrical transport seems to be suppressed by accessing certain excited states. Why is this possible? In the regime of single-electron tunneling, the number of electrons in the quantum dot fluctuates by one during electron transport. At finite drain-source voltage, electrons of different energy in the emitter are competing in entering the quantum dot, and electrons of different energy in the quantum dot

[13] This is a consequence of $\mu_i^{\mathrm{elch}} = -e\,V_i + \mu_i^{\mathrm{ch}} = \mathrm{const}$ (see relation (3.2)), i.e., the change of the electrostatic potential V_i is given by the change of the chemical potential μ_i^{ch} of the electrode i.

are competing for leaving the quantum dot to collector. The electrons are *competing* [148], since within the regime of single-electron tunneling only *one* electron can tunnel at a time: Due to the repulsive electron-electron interaction, tunneling of electrons using different channels is not independent of each other. *Long life times in certain excited states might lead to blocking of single-electron tunneling through the other channels.* The dynamics of single-electron transport through quantum dots will be discussed in the following based on a master equation approach.

5.8.1 Master-Equation Ansatz for Describing the Dynamics of Single-Electron Transport

A first approach to the dynamics of single-electron tunneling in a quantum dot system is a master equations ansatz [32, 115, 9, 134]: After preparing the quantum dot in the state $|n,l;\{V_i\}\rangle$, the quantum dot system develops in changing its state because

- single electrons are entering,
- single electrons are leaving,
- the electron system in the quantum dot relaxes to a state of lower energy of the same electron number, or
- the electron system is excited to a state of higher energy of same electron number.

These transitions can be described by rates giving the time scale for the respective changes. Such rates can be derived from Fermi's golden rule [9].

A transition from the state $|n,l;\{V_i\}\rangle$ to $|n+1,k;\{V_i\}\rangle$ is either induced by an electron entering from the source or from the drain side. Both tunneling processes occur under energy conservation between initial and final state of the system, i.e., $E(n+1,k;\{V_i\}) - E(n,l;\{V_i\}) - \varepsilon = 0$, where ε denotes the energy of the electron entering. The *tunneling rate* $\Gamma^{(r)}_{(n,l)\to(n+1,k)}$ for the transition from the respective reservoir $r \in \{\mathrm{S},\mathrm{D}\}$ is described by [14]

$$\Gamma^{(r)}_{(n,l)\to(n+1,k)} = \frac{2\pi}{\hbar}\sum_s \Big|T_r(|n,l\rangle,|n+1,k\rangle;\varepsilon_s)\Big|^2 \cdot \delta\big(E(n+1,k) - E(n,l) - \varepsilon_s\big)\cdot f_{\mathrm{FD}}\big(\varepsilon_s,\mu_r^{\mathrm{elch}},T\big)\ . \quad (5.41)$$

The factor $|T_r(|n,l\rangle,|n+1,k\rangle;\varepsilon)|^2$ represents the tunneling matrix element for the transition $|n,l;\{V_i\}\rangle$ to $|n+1,k;\{V_i\}\rangle$ with an electron of energy ε entering the quantum dot from the reservoir r. The Fermi-Dirac distribution function $f_{\mathrm{FD}}(\varepsilon,\mu_r^{\mathrm{elch}},T) = 1/\{\exp((\varepsilon-\mu_r)/k_{\mathrm{B}}T)+1\}$ gives the occupation

[14] The sum over s, numbering the single-particle states of reservoir $r \in \{S,D\}$, can be replaced by an integral with introducing the density of states $D_r(\varepsilon)$ in the reservoir r at the energy ε: $\sum_s \to \int_\varepsilon D_r(\varepsilon)\,\mathrm{d}\varepsilon$

probability of finding an electron at energy ε in the reservoir r at temperature T for a Fermi level μ_r^{elch}.

The *tunneling rate* for a transition from the state $|n+1,k;\{V_i\}\rangle$ to the state $|n,l;\{V_i\}\rangle$, induced by an electron leaving the quantum dot to reservoir r, is given by

$$\Gamma^{(r)}_{(n,l)\leftarrow(n+1,k)} = \frac{2\pi}{\hbar}\sum_s \Big|T_r(|n,l\rangle,|n+1,k\rangle;\varepsilon_s)\Big|^2 \cdot \delta\big(E(n+1,k)-E(n,l)-\varepsilon_s\big)\cdot\Big(1-f_{\mathrm{FD}}\big(\varepsilon_s,\mu_r^{\mathrm{elch}},T\big)\Big)\ . \quad (5.42)$$

The rate is proportional to the probabilty of finding an unoccupied state in the reservoirs r at the respective energy ε which is given by $(1-f_{\mathrm{FD}}(\varepsilon,\mu_r^{\mathrm{elch}},T))$.

By relaxation the electron system in the quantum dot reaches a state of same electron number at lower energy. These *relaxation rates* are denoted by

$$\Gamma^{(\mathrm{rel})}_{(n,l')\leftarrow(n,l)} \qquad \text{with} \quad 0\le l'<l\in\{0,1,2,\cdots\}\ ,$$
$$\text{i.e.,} \quad E(n,l';\{V_i\})\le E(n,l;\{V_i\})\ . \quad (5.43)$$

Excitations from energetically low lying states to states of higher energy can also be incorporated with respective *excitation rates*,

$$\Gamma^{(\mathrm{exc})}_{(n,l')\to(n,l)} \qquad \text{with} \quad 0\le l<l'\in\{0,1,2,\cdots\}\ ,$$
$$\text{i.e.,} \quad E(n,l';\{V_i\})> E(n,l;\{V_i\})\ . \quad (5.44)$$

Preparing the quantum dot in a certain state, the time evolution of the probability $P(n,l;\{V_i\},\mu_{\mathrm{S}}^{\mathrm{elch}},\mu_{\mathrm{D}}^{\mathrm{elch}})$ of finding the electron system in the quantum dot in the state $|n,l;\{V_i\}\rangle$ is given by the *master equation* [15]

$$\begin{aligned}\frac{\mathrm{d}P(n,l)}{\mathrm{d}t} = &\sum_m\Big(\Gamma^{(\mathrm{S})}_{(n-1,m)\to(n,l)}+\Gamma^{(\mathrm{D})}_{(n-1,m)\to(n,l)}\Big)\cdot P(n-1,m)\\ &-\sum_m\Big(\Gamma^{(\mathrm{S})}_{(n-1,m)\leftarrow(n,l)}+\Gamma^{(\mathrm{D})}_{(n-1,m)\leftarrow(n,l)}\Big)\cdot P(n,l)\\ &+\sum_k\Big(\Gamma^{(\mathrm{S})}_{(n,l)\leftarrow(n+1,k)}+\Gamma^{(\mathrm{D})}_{(n,l)\leftarrow(n+1,k)}\Big)\cdot P(n+1,k)\\ &-\sum_k\Big(\Gamma^{(\mathrm{S})}_{(n,l)\to(n+1,k)}+\Gamma^{(\mathrm{D})}_{(n,l)\to(n+1,k)}\Big)\cdot P(n,l)\\ &+\sum_{l'>l}\Gamma^{(\mathrm{rel})}_{(n,l)\leftarrow(n,l')}\cdot P(n,l')-\sum_{l'<l}\Gamma^{(\mathrm{rel})}_{(n,l')\leftarrow(n,l)}\cdot P(n,l)\\ &+\sum_{l'<l}\Gamma^{(\mathrm{exc})}_{(n,l')\to(n,l)}\cdot P(n,l')-\sum_{l'>l}\Gamma^{(\mathrm{exc})}_{(n,l)\to(n,l')}\cdot P(n,l)\ . \quad (5.45)\end{aligned}$$

[15] For brevity, $P(n,l)\equiv P(n,l;\{V_i\},\mu_{\mathrm{S}}^{\mathrm{elch}},\mu_{\mathrm{D}}^{\mathrm{elch}})$.

Such a master equation exists for each state $|n,l;\{V_i\}\rangle$ with $n \in \{\cdots N-1, N, N+1\cdots\}$ and $l \in \{0,1,2,\cdots\}$. Since the quantum dot has to be found in one of these states, the probabilities of all states should sum up to unity,

$$\sum_n \sum_l P(n,l) = 1 \,. \tag{5.46}$$

The rates and the energies depend on the electrochemical potentials of source and drain and the electrostatic potentials of all surrounding electrodes including source, drain and gate electrodes. Therefore, the rate have to be determined for each set of parameters $\mu_{\mathrm{S}}^{\mathrm{elch}}$, $\mu_{\mathrm{D}}^{\mathrm{elch}}$ and $\{V_i\}$.

Under stationary conditions, the probabilities do not change, i.e.,

$$\frac{\mathrm{d}P(n,l)}{\mathrm{d}t} = 0, \quad \text{for all} \quad n \in \{\cdots N-1, N, N+1\cdots\} \quad \text{and} \quad l \in \{0,1,2,\cdots\} \,. \tag{5.47}$$

With drain-source voltage $V_{\mathrm{DS}} = 0$, the probability of finding the quantum dot in a certain state is given by the Gibbs' distribution function (5.1), solving (5.45) for the case of thermodynamical equilibrium at temperature T.

For $V_{\mathrm{DS}} \neq 0$, a situation of non-equilibrium is enforced. If possible, electrons will hop between quantum dot and reservoir leading to a net stationary current from the reservoir of higher electrochemical potential to the reservoir of lower electrochemical potential. Whether transitions are allowed and on which time scale, this is described by the respective rates. Starting from a state $|n+1,k;\{V_i\}\rangle$, the $(n+1)$th electron can tunnel either to source or drain given by the respective tunneling rate. The stationary current I_{DS}, defined positive if a net flow of positive charges occurs from drain to source with $V_{\mathrm{DS}} > 0$, can be determined from the net single-electron hopping towards drain, i.e., for the transitions $|n+1,k;\{V_i\}\rangle$ to $|n,l;\{V_i\}\rangle$, electron hopping to drain is counted positive, electron hopping to source negative:

$$I_{\mathrm{DS}} = e \sum_n \sum_k \sum_l \left(\Gamma^{(\mathrm{D})}_{(n,l)\leftarrow(n+1,k)} - \Gamma^{(\mathrm{S})}_{(n,l)\leftarrow(n+1,k)} \right) \cdot P(n+1,k) \,. \tag{5.48}$$

A similar relation for the same I_{DS} is obtained by considering the probability $P(n,l;\{V_i\})$ of finding the quantum dot in any of the states $|n,l;\{V_i\}\rangle$, and counting per time interval the transitions $|n,l;\{V_i\}\rangle$ to any $|n+1,k;\{V_i\}\rangle$ induced by electrons entering from source positive, by electrons entering from drain negative:

$$I_{\mathrm{DS}} = e \sum_n \sum_k \sum_l \left(\Gamma^{(\mathrm{S})}_{(n,l)\rightarrow(n+1,k)} - \Gamma^{(\mathrm{D})}_{(n,l)\rightarrow(n+1,k)} \right) \cdot P(n,l) \,. \tag{5.49}$$

Restriction to Low Temperatures. At low temperature, the edge between occupied and unoccupied single-particle states in the reservoirs is sharp. Therefore, we can assume

$$f_{\mathrm{FD}}(\varepsilon,\mu_r^{\mathrm{elch}}) = 0 \qquad \text{for } \varepsilon > \mu_r^{\mathrm{elch}} \qquad \text{and}$$
$$f_{\mathrm{FD}}(\varepsilon,\mu_r^{\mathrm{elch}}) = 1 \qquad \text{for } \varepsilon < \mu_r^{\mathrm{elch}} \; . \tag{5.50}$$

With applied drain-source voltage V_{DS}, either the drain or the source reservoir becomes the emitter, the other the collector. Due to (5.50), certain tunneling rates, defined by (5.41) and (5.42), vanish:

$$\Gamma^{(\mathrm{C})}_{(n,l)\to(n+1,k)} = 0 \quad \text{for } \varepsilon > \mu_{\mathrm{C}}^{\mathrm{elch}} \; , \text{ since } \quad f_{\mathrm{FD}}(\varepsilon,\mu_{\mathrm{C}}^{\mathrm{elch}}) = 0 \; ,$$
$$\Gamma^{(\mathrm{E})}_{(n,l)\leftarrow(n+1,k)} = 0 \quad \text{for } \mu_{\mathrm{E}}^{\mathrm{elch}} > \varepsilon \; , \text{ since } \quad 1 - f_{\mathrm{FD}}(\varepsilon,\mu_{\mathrm{E}}^{\mathrm{elch}}) = 0 \; .$$

As a consequence, electrons can enter the quantum dot only from emitter side, and leave to collector side. It is the factor $(1 - f_{\mathrm{FD}}(\varepsilon,\mu_r^{\mathrm{elch}}))$ prohibiting that an electron enters the reservoir with an energy ε below the electrochemical potential μ_r^{elch} of the reservoir r: Single particle states at the respective energy are already occupied and Pauli's exclusion principle does not allow double occupation of states. Therefore this factor is denoted in this context as *Pauli blocking factor*.

The master equations (5.45) simplify under these low temperature conditions, and the stationary current is obtained from (5.48) and (5.49) to

$$\begin{aligned} I_{\mathrm{CE}} &= e \sum_n \sum_k \sum_l \Gamma^{(\mathrm{C})}_{(n,l)\leftarrow(n+1,k)} \cdot P(n+1,k) \\ &= e \sum_n \sum_k \sum_l \Gamma^{(\mathrm{E})}_{(n,l)\to(n+1,k)} \cdot P(n,l) \; . \end{aligned} \tag{5.51}$$

Transitions might contribute if their respective tunneling rates differ from zero. Due to

$$\Gamma^{(\mathrm{C})}_{(n,l)\leftarrow(n+1,k)} \;\propto\; \delta\big(E(n+1,k) - E(n,l) - \varepsilon\big) \cdot \Big(1 - f_{\mathrm{FD}}\big(\varepsilon,\mu_{\mathrm{C}}^{\mathrm{elch}}\big)\Big) \; ,$$
$$\Gamma^{(\mathrm{E})}_{(n,l')\to(n+1,k')} \;\propto\; \delta\big(E(n+1,k') - E(n,l') - \varepsilon\big) \cdot f_{\mathrm{FD}}\big(\varepsilon,\mu_{\mathrm{E}}^{\mathrm{elch}}\big) \; ,$$

the respective transitions might be active in the (V_{BS},V_{DS}) plane beyond certain threshold lines $V_{\mathrm{DS}}(V_{\mathrm{BS}})$ defined by

$$E(n+1,k;\{V_i\}) - E(n,l;\{V_i\}) \gtreqless \mu_{\mathrm{C}}^{\mathrm{elch}} \; ,$$
$$E(n+1,k';\{V_i\}) - E(n,l';\{V_i\}) \lesseqgtr \mu_{\mathrm{E}}^{\mathrm{elch}} \; .$$

These resonance conditions have been used before to derive a transport spectrum from fictitious energy spectra $E(n+1,k)$ and $E(n,l)$ shown in Fig. 5.11.

Restriction to Single-Electron Tunneling Regime. In the regime of single-electron tunneling, the number of electrons in the quantum dot fluctuates between N and $N+1$, i.e., the quantum dot is only found in states of these two electron numbers. Therefore the constraint (5.46) reduces to

$$\sum_l P(N,l) + \sum_k P(N+1,k) = 1 \; . \tag{5.52}$$

and the stationary current I_{CE} is expressed by

$$\begin{aligned} I_{\mathrm{CE}} &= e \sum_k \sum_l \Gamma^{(\mathrm{C})}_{(N,l)\leftarrow(N+1,k)} \cdot P(N+1,k) \\ &= e \sum_k \sum_l \Gamma^{(\mathrm{E})}_{(N,l)\rightarrow(N+1,k)} \cdot P(N,l) \; . \end{aligned} \tag{5.53}$$

Let us first assume that electron transfer from emitter to collector can only occur by transitions between the groundstates of the N- and the $(N+1)$-electron system as it is the only possibility at small drain-source voltage. Then the master equations (5.45) reduce under stationary conditions further to

$$\begin{aligned} 0 &= \mathrm{d}P(N+1,0)/\mathrm{d}t = -\mathrm{d}P(N,0)/\mathrm{d}t \\ &= \Gamma^{(\mathrm{E})}_{(N,0)\rightarrow(N+1,0)} \cdot P(N,0) - \Gamma^{(\mathrm{C})}_{(N,0)\leftarrow(N+1,0)} \cdot P(N+1,0) \; , \end{aligned} \tag{5.54}$$

with the constraint $P(N,0) = 1 - P(N+1,0)$. The stationary current $I^{(0,0)}_{\mathrm{CE}}$ – where the superscript $(0,0)$ denotes the transition between groundstates – is obtained from (5.53) and (5.54) to

$$\begin{aligned} I^{(0,0)}_{\mathrm{CE}} &= e \cdot \Gamma^{(\mathrm{C})}_{(N,0)\leftarrow(N+1,0)} \cdot P(N+1,0) \\ &= e \cdot \left[\left[\Gamma^{(\mathrm{C})}_{(N,0)\leftarrow(N+1,0)} \right]^{-1} + \left[\Gamma^{(\mathrm{E})}_{(N,0)\rightarrow(N+1,0)} \right]^{-1} \right]^{-1} \; . \end{aligned} \tag{5.55}$$

The inverse tunneling rates through emitter and collector are adding to the inverse of an effective rate for single-electron transport from emitter to collector. The inverse of the tunneling rate to collector can be interpreted as the *life time* τ_{N+1} of the charge state of $N+1$ electrons in the quantum dot,

$$\tau_{N+1} = \left[\Gamma^{(\mathrm{C})}_{(N,0)\leftarrow(N+1,0)} \right]^{-1} \; , \quad \text{whereas} \quad \tau_N = \left[\Gamma^{(\mathrm{E})}_{(N,0)\rightarrow(N+1,0)} \right]^{-1}$$

denotes the life time of the charge state with N electrons in the quantum dot under these conditions. By comparing with (5.55), the current is expressed by

$$I^{(0,0)}_{\mathrm{CE}} = \frac{e}{\tau_{N+1} + \tau_N} \; .$$

Under the low temperature condition (5.50) we will discuss in the following within a single-electron tunneling regime (see constraint (5.52)) the increase and decrease of current through the quantum dot by reaching an excited state of long life time.

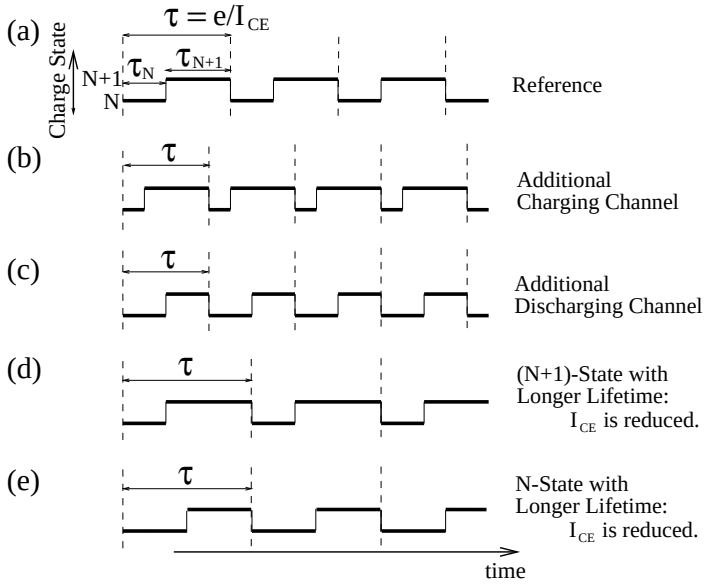

Fig. 5.14. Affecting the lifetime of charge state of the quantum dot changes the current $I_{\rm DS}$ through quantum dot: (a) Every mean time $\tau = e/I_{\rm CE} = e/|I_{\rm DS}|$ a single electron is passing the quantum dot. (b) By reducing the life time τ_N of the N-electron charge state by an additional channel for entering the quantum dot, the period τ is decreased and the current is increased. (c) By reducing the life time τ_{N+1} of the $(N+1)$-electron charge state by an additional channel for a single electron leaving the quantum dot, the period τ is also decreased and the current is increased. (d),(e) Due to excited states of long life time which are reached from time to time, the life time of the respective electron system is increased reducing the current $|I_{\rm DS}|$.

5.8.2 Long Decay Time of an Excited State Can Block Single-Electron Transport

During single-electron tunneling, every mean time $\tau = e/I_{\rm CE} = e/|I_{\rm DS}|$ a single electron is passing the quantum dot. In average, during such a single-electron tunneling process, the quantum dot is found for the time $\tau_{N+1} = \sum_k P(N+1,k)\cdot\tau$ in a state of the $(N+1)$-electron system and for the time $\tau_N = \sum_l P(N,l)\cdot\tau$ in a state of the N-electron system (see Fig. 5.14a). $\tau = \tau_{N+1} + \tau_N$ is valid (see (5.52)). By opening a channel to an additional excited state, these life times are affected. How, this depends on the efficiency of relaxation processes occuring in the quantum dot.

Instantanous Relaxation. With instantanous and complete relaxation, i.e.,

$$\begin{aligned} \Gamma^{(\rm rel)}_{(N,0)\leftarrow(N,l)} &\gg \Gamma^{\rm E}_{(N,l)\rightarrow(N+1,k)}, \\ \Gamma^{(\rm rel)}_{(N+1,0)\leftarrow(N+1,k)} &\gg \Gamma^{\rm C}_{(N,l)\leftarrow(N+1,k)}\ , \end{aligned} \tag{5.56}$$

the initial state for the following tunneling process is always the groundstate of the respective electron system. Let us assume that L excited states of the N-electron system and K of the $(N+1)$-electron system are accessible. The master equations become under stationary conditions

for the groundstate of the N-electron system:

$$\begin{aligned} 0 &= \mathrm{d}P(N,0)/\mathrm{d}t \\ &= \Gamma^{(\mathrm{C})}_{(N,0)\leftarrow(N+1,0)} \cdot P(N+1,0) - \Gamma^{(\mathrm{E})}_{(N,0)\rightarrow(N+1,0)} \cdot P(N,0) \\ &\quad + \sum_{l>0} \Gamma^{(\mathrm{rel})}_{(N,0)\leftarrow(N,l)} \cdot P(N,l) \ , \end{aligned}$$

for the L excited states of the N-electron system $(1 \le l \le L)$:

$$\begin{aligned} 0 &= \mathrm{d}P(N,l)/\mathrm{d}t \\ &= \Gamma^{(\mathrm{C})}_{(N,l)\leftarrow(N+1,0)} \cdot P(N+1,0) - \Gamma^{(\mathrm{rel})}_{(N,0)\leftarrow(N,l)} \cdot P(N,l) \ , \end{aligned}$$

for the groundstate of the $(N+1)$-electron system:

$$\begin{aligned} 0 &= \mathrm{d}P(N+1,0)/\mathrm{d}t \\ &= \Gamma^{(\mathrm{E})}_{(N,0)\rightarrow(N+1,0)} \cdot P(N,0) - \Gamma^{(\mathrm{C})}_{(N,0)\leftarrow(N+1,0)} \cdot P(N+1,0) \\ &\quad + \sum_{k>0} \Gamma^{(\mathrm{rel})}_{(N+1,0)\leftarrow(N+1,k)} \cdot P(N+1,k) \ , \end{aligned}$$

for the K excited states of the $(N+1)$-electron system $(1 \le k \le K)$:

$$\begin{aligned} 0 &= \mathrm{d}P(N+1,k)/\mathrm{d}t \\ &= \Gamma^{(\mathrm{E})}_{(N,0)\rightarrow(N+1,k)} \cdot P(N,0) - \Gamma^{(\mathrm{rel})}_{(N+1,0)\leftarrow(N+1,k)} \cdot P(N+1,k) \ , \end{aligned}$$

with the constraint

$$\sum_{k=0}^{K} P(N+1,k) + \sum_{l=0}^{L} P(N,l) = 1 \ .$$

Solving for $P(N,l)$, from (5.53) the stationary current is deduced to

$$\begin{aligned} I_{\mathrm{CE}}(K,L) &= \frac{e}{\tau_{N+1} + \tau_N} \ , \ \text{where} \\ \tau_{N+1} &= \left[\sum_{l=0}^{L} \Gamma^{(\mathrm{C})}_{(N,l)\leftarrow(N+1,0)} \right]^{-1} , \quad \tau_N = \left[\sum_{k=0}^{K} \Gamma^{(\mathrm{E})}_{(N,0)\rightarrow(N+1,k)} \right]^{-1} . \end{aligned} \tag{5.57}$$

The terms τ_N and τ_{N+1} can again be interpreted as the life times of the respective charge state in the quantum dot. With each additional channel, the current is increased by

$$I_{\mathrm{CE}}(K+1,L)-I_{\mathrm{CE}}(K,L)=\frac{e\cdot\Gamma^{(\mathrm{E})}_{K+1}\cdot\sum_{l=0}^{L}[]\cdot\sum_{l=0}^{L}[]}{\left(\sum_{k=0}^{K}[]+\sum_{l=0}^{L}[]\right)^{2}+\Gamma^{(\mathrm{E})}_{K+1}\cdot\left(\sum_{k=0}^{K}[]+\sum_{l=0}^{L}[]\right)}\,,$$

$$I_{\mathrm{CE}}(K,L+1)-I_{\mathrm{CE}}(K,L)=\frac{e\cdot\Gamma^{(\mathrm{C})}_{L+1}\cdot\sum_{k=0}^{K}[]\cdot\sum_{k=0}^{K}[]}{\left(\sum_{l=0}^{L}[]+\sum_{k=0}^{K}[]\right)^{2}+\Gamma^{(\mathrm{C})}_{L+1}\cdot\left(\sum_{l=0}^{L}[]+\sum_{k=0}^{K}[]\right)}\,,$$

with

$$\sum_{k=0}^{K}[]\equiv\sum_{k=0}^{K}\Gamma^{(\mathrm{E})}_{(N,0)\to(N+1,k)}\,,\qquad\sum_{l=0}^{L}[]\equiv\sum_{l=0}^{L}\Gamma^{(\mathrm{C})}_{(N,l)\leftarrow(N+1,0)}\,,$$

$$\Gamma^{(\mathrm{E})}_{K+1}\equiv\Gamma^{(\mathrm{E})}_{(N,0)\to(N+1,K+1)}\,,\qquad\Gamma^{(\mathrm{C})}_{L+1}\equiv\Gamma^{(\mathrm{C})}_{(N,L+1)\leftarrow(N+1,0)}\,.$$

The increase becomes simple for very asymmetric tunnel barriers: [16]

$$\text{For}\quad\Gamma^{(\mathrm{E})}_{(N,0)\to(N+1,k)}\ll\Gamma^{(\mathrm{C})}_{(N,l)\leftarrow(N+1,0)}\,,\ \text{and}\ K\approx L\,,\ \text{then}$$
$$I_{\mathrm{CE}}(K+1,L)-I_{\mathrm{CE}}(K,L)=e\cdot\Gamma^{(\mathrm{E})}_{(N,0)\to(N+1,K+1)}\,,$$

$$\text{for}\quad\Gamma^{(\mathrm{E})}_{(N,0)\to(N+1,k)}\gg\Gamma^{(\mathrm{C})}_{(N,l)\leftarrow(N+1,0)}\,,\ \text{and}\ K\approx L\,,\ \text{then}$$
$$I_{\mathrm{CE}}(K,L+1)-I_{\mathrm{CE}}(K,L)=e\cdot\Gamma^{(\mathrm{C})}_{(N,L+1)\leftarrow(N+1,0)}\,.$$

How to interpret the result (5.57)? By opening an additional channel on the emitter side, the rate for an electron entering the quantum dot is increased. Therefore the life time τ_N, in which the quantum dot remains in a N-electron state, is reduced. Due to the instantaneous relaxation, nothing has changed for electrons leaving the quantum dot since for this the initial state is still the groundstate of the $(N+1)$-electron system: the life time τ_{N+1} in the $(N+1)$-electron charge state remains unaffected. With τ_N the sum $\tau=\tau_{N+1}+\tau_N$ is reduced, and therefore the current $I_{\mathrm{CE}}=e/\tau$ increased (see Fig. 5.14b).

Similar with opening an additional channel on the collector side: The rate for an electron leaving the quantum dot is increased reducing the life time τ_{N+1} of the quantum dot being in a $(N+1)$-electron charge state. Due to the instantanous relaxation from the excited state of the N-electron system, the initial state for adding an electron from emitter is always the groundstate of

[16] Note, this result describes also the linear increase $|\mathrm{d}I_{\mathrm{DS}}|=|\mathrm{d}V_{\mathrm{DS}}|/R_{\mathrm{T}}^{\max}$ between steps in the Coulomb staircase characteristics derived in Fig. 1.10 and Fig. 1.11 for strong asymmetric tunnel barriers of a metal single-electron transistor.

the N-electron system, i.e., the life time τ_N in the N electron charge state remains unaffected. But with τ_{N+1} the sum $\tau = \tau_{N+1} + \tau_N$ is reduced, and therefore the current $I_{\mathrm{CE}} = e/\tau$ increased (see Fig. 5.14c).

We can conclude: With instantanous relaxation, the current is increased with each additional channel becoming available because the rate for entering (leaving) the quantum dot is increased towards the one reservoir whereas the rate of leaving (entering) to the other reservoir remains unaffected: The life time of one charge state is shorten whereas the life time of the other remains unchanged. The situation allows to do spectroscopy of the N- and $(N+1)$-electron system independently as given in Fig. 5.9.

Since in the data of Fig. 5.5 negative differential conductance occurs, we have to conclude that this is not completely true for the quantum dot system here.

Without Relaxation. Without fast and complete relaxation, i.e.,

$$\begin{aligned} \Gamma^{\mathrm{rel}}_{(N,0)\leftarrow(N,l)} &\ll \Gamma^{(\mathrm{E})}_{(N,l)\rightarrow(N+1,k)}, \\ \Gamma^{\mathrm{rel}}_{(N+1,0)\leftarrow(N+1,k)} &\ll \Gamma^{(\mathrm{C})}_{(N,l)\leftarrow(N+1,k)} , \end{aligned} \tag{5.58}$$

the change in the dynamics with opening a channel to an additional excited state is complex. But by a simple example, we can show that besides the usual increase also a decrease in the current might occur with increasing $|V_{\mathrm{DS}}|$: Let us assume that L excited states of the N-electron system and K of the $(N+1)$-electron system are accessible. For simplicity, only the tunneling process sequences

$$\begin{aligned} |N,0\rangle \rightarrow \quad |N+1,k\rangle \quad &\rightarrow |N,0\rangle \qquad \text{for} \quad k \geq 0 , \\ |N+1,0\rangle \rightarrow \quad |N,l\rangle \quad &\rightarrow |N+1,0\rangle \qquad \text{for} \quad l \geq 0 , \end{aligned}$$

are allowed, i.e.,

$$\Gamma^{(\mathrm{E})}_{(N,l)\rightarrow(N+1,k)} = 0 \ , \ \text{if } l > 0 \ , \qquad \Gamma^{(\mathrm{C})}_{(N,l)\leftarrow(N+1,k)} = 0 \ , \ \text{if } k > 0 \ .$$

The master equations become under stationary conditions

for the groundstate of the $(N+1)$-electron system $(1 \leq k \leq K)$:

$$\begin{aligned} 0 &= \mathrm{d}P(N+1,0)/\mathrm{d}t \\ &= \Gamma^{(\mathrm{E})}_{(N,0)\rightarrow(N+1,0)} \cdot P(N,0) - \sum_{l=0}^{L} \Gamma^{(\mathrm{C})}_{(N,l)\leftarrow(N+1,0)} \cdot P(N+1,0) \ , \end{aligned}$$

for the K excited states of the $(N+1)$-electron system:

$$\begin{aligned} 0 &= \mathrm{d}P(N+1,k)/\mathrm{d}t \\ &= \Gamma^{(\mathrm{E})}_{(N,0)\rightarrow(N+1,k)} \cdot P(N,0) - \Gamma^{(\mathrm{C})}_{(N,0)\leftarrow(N+1,k)} \cdot P(N+1,k) \ , \end{aligned}$$

for the groundstate of the N-electron system:

$$\begin{aligned} 0 &= \mathrm{d}P(N,0)/\mathrm{d}t \\ &= \Gamma^{(\mathrm{C})}_{(N,0)\leftarrow(N+1,0)} \cdot P(N+1,0) - \sum_{k=0}^{K} \Gamma^{(\mathrm{E})}_{(N,0)\rightarrow(N+1,k)} \cdot P(N,0) \ , \end{aligned}$$

for the L excited states of the N-electron system ($1 \leq l \leq L$):

$$\begin{aligned} 0 &= \mathrm{d}P(N,l)/\mathrm{d}t \\ &= \Gamma^{(\mathrm{C})}_{(N,l)\leftarrow(N+1,0)} \cdot P(N+1,0) - \Gamma^{(\mathrm{E})}_{(N,l)\rightarrow(N+1,0)} \cdot P(N,l) \ , \end{aligned}$$

with the constraint

$$1 = \sum_{k=0}^{K} P(N+1,k) + \sum_{l=0}^{L} P(N,l) \ .$$

Solving the master equations by expressing $P(N,0)$, the stationary current is given by

$$\begin{aligned} I_{\mathrm{CE}}(K,L) &= e \cdot \sum_{k=0}^{K} \Gamma^{(\mathrm{E})}_{(N,0)\rightarrow(N+1,k)} \cdot P(N,0) \\ &= \frac{e \cdot \displaystyle\sum_{k=0}^{K} \Gamma^{(\mathrm{E})}_{(N,0)\rightarrow(N+1,k)}}{1 + \displaystyle\sum_{k=1}^{K} \frac{\Gamma^{(\mathrm{E})}_{(N,0)\rightarrow(N+1,k)}}{\Gamma^{(\mathrm{C})}_{(N,0)\leftarrow(N+1,k)}} + \left[1 + \sum_{l=1}^{L} \frac{\Gamma^{(\mathrm{C})}_{(N,l)\leftarrow(N+1,0)}}{\Gamma^{(\mathrm{E})}_{(N,l)\rightarrow(N+1,0)}}\right] \cdot \frac{\Gamma^{(\mathrm{E})}_{(N,0)\rightarrow(N+1,0)}}{\displaystyle\sum_{l=0}^{L} \Gamma^{(\mathrm{C})}_{(N,l)\leftarrow(N+1,0)}}} \ . \end{aligned}$$

Solving the master equations by expressing $P(N+1,0)$, the stationary current is written as

$$\begin{aligned} I_{\mathrm{CE}}(K,L) &= e \cdot \sum_{l=0}^{L} \Gamma^{(\mathrm{C})}_{(N,l)\leftarrow(N+1,0)} \cdot P(N+1,0) \\ &= \frac{e \cdot \displaystyle\sum_{l=0}^{L} \Gamma^{(\mathrm{C})}_{(N,l)\rightarrow(N+1,0)}}{1 + \displaystyle\sum_{l=1}^{L} \frac{\Gamma^{(\mathrm{C})}_{(N,l)\leftarrow(N+1,0)}}{\Gamma^{(\mathrm{E})}_{(N,l)\rightarrow(N+1,0)}} + \left[1 + \sum_{k=1}^{K} \frac{\Gamma^{(\mathrm{E})}_{(N,0)\rightarrow(N+1,k)}}{\Gamma^{(\mathrm{E})}_{(N,0)\leftarrow(N+1,k)}}\right] \cdot \frac{\Gamma^{(\mathrm{C})}_{(N,0)\leftarrow(N+1,0)}}{\displaystyle\sum_{k=0}^{K} \Gamma^{(\mathrm{E})}_{(N,0)\rightarrow(N+1,k)}}} \ . \end{aligned}$$

By adding the excited state $|N+1, K+1\rangle$, the current $I_{\mathrm{CE}}(K+1,L)$ is *reduced* if

$$\Gamma^{(\mathrm{C})}_{(N,0)\leftarrow(N+1,K+1)} < \frac{I_{\mathrm{CE}}(K,L)}{e}$$

is fulfilled. In the opposite case, the current is increased. Therefore, if the life time $[\Gamma^{(\mathrm{C})}_{(N,0)\rightarrow(N+1,K+1)}]^{-1}$ of state $|N+1,K+1;\{V_i\}\rangle$ exceeds the mean time τ for electrons passing the quantum dot in case of K channels, then the single-electron transport is depressed (see Fig. 5.14d), leading to negative differential conductance with opening the transition to the excited state $|N+1,K+1;\{V_i\}\rangle$. The same might happen by reaching the excited state $|N,L+1;\{V_i\}\rangle$. The current $I_{\mathrm{CE}}(K,L+1)$ is less (see Fig. 5.14e), if

$$\Gamma^{(\mathrm{E})}_{(N,L+1)\rightarrow(N+1,0)} < \frac{I_{\mathrm{CE}}(K,L)}{e}\,.$$

Let us generalize: We assume that an additional channel (l,k)E opens on the emitter side (see Fig. 5.15). Without relaxation, an electron has to leave starting with the initial state $|N+1,k\rangle$. If the rate for doing so is low, then the quantum dot remains in the $(N+1)$-electron state $|N+1,k\rangle$ and the life time τ_{N+1} becomes long and may even exceed τ valid without this additional channel. In such a case, the single-electron transport through the quantum dot is blocked leading to negative differential conductance with opening (l,k)E. But to obtain this effect, it is not necessary that the quantum dot remains in the state $|N+1,k\rangle$ itself: By relaxation the $(N+1)$-electron system might end in an energetically lower state $|N+1,k'\rangle$ (see Fig. 5.15b)

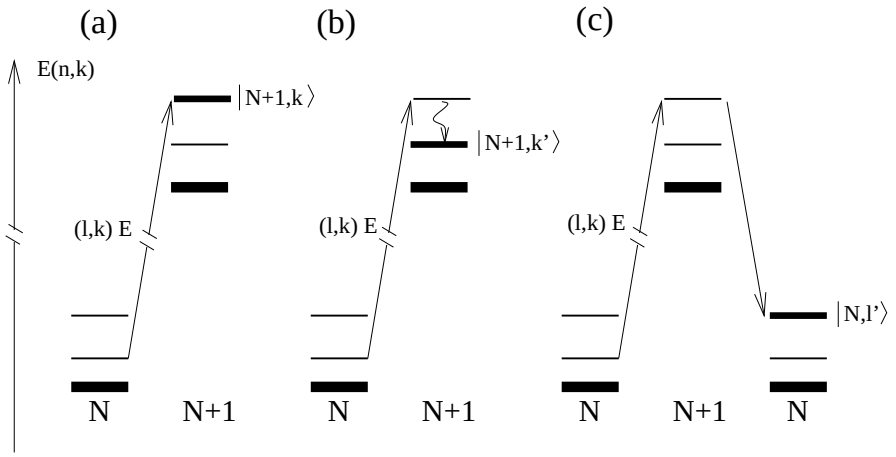

Fig. 5.15. Opening the transition (l,k)E, the single-electron transport might be blocked because (a) the quantum dot remains for a long time in $|N+1,k\rangle$, (b) the quantum dot relaxed from $|N+1,k\rangle$ to a state $|N+1,k'\rangle$ of long life time, or (c) the quantum dot is transferred to the excited state $|N,l'\rangle$ of the N electron system and sticking there. All these three processes will lead to negative differential conductance at the borderline of (l,k)E.

from where an electron escape to collector is depressed. It is also possible that an excited state $|N, l'\rangle$ of the N-electron system is reached (see Fig. 5.15c) and from there the transition to an $(N+1)$-electron system is blocked. Since the state $|N, l'\rangle$ has been reached by the state $|N+1, k\rangle$, the blocking occurs with opening the transition (l, k)E. Similar conclusions can be drawn for opening additional channels on the collector side.

5.9 Tunneling-Matrix Elements Weigh the Transition Rates

Within the Constant Interaction Model, single-electron tunneling is described by transitions of single electrons from a single-particle state in the emitter to an unoccupied single-particle state in the quantum dot and then to an unoccupied single-particle state in the collector. If the *spatial* overlap between single-particle states in the quantum dot and those in the leads is different for the different states of the quantum dot, then the tunneling matrix element varies. It might lead to negative differential conductance if the spatial overlap of an excited single-particle state is low (A.T. Johnson and coworkers [150] in 1992).

Degeneracy in the energy spectrum of the N-electron systems – by spin degeneracy or orbital degeneracy due to a rotational symmetry – allows for more possible transitions at same energy. Several channels are opened in parallel, leading to an enhanced step-like change of the current.

D. Weinmann *et al.* [154] pointed out that the spin orientation is usually conserved for a tunneling process. Therefore not all transitions between states of the N and the $(N+1)$-electron system are possible. By adding an electron to the quantum dot or taking off an electron from the quantum dot, the electron number changes by one, the total spin of the electron system in the quantum dot by $\pm\frac{1}{2}$ and the spin projection by $\pm\frac{1}{2}$:

$$S(N,l) \pm \tfrac{1}{2} \stackrel{!}{=} S(N+1,k)\ , \text{ and } S_z(N,l) \pm \tfrac{1}{2} \stackrel{!}{=} S_z(N+1,k)\ . \quad (5.59)$$

Transitions between N- and $(N+1)$-electron states not fulfilling these *spin selection rules* are forbidden. The respective tunneling matrix element becomes zero and therefore the respective tunneling rate.

Rotational symmetry in the confining potential of the quantum dot ensures that the angular momentum is a good quantum number to describe the n-electron states. In vertical quantum dots, electrons are tunneling along such a symmetry axis: Like the spin, the projection of the angular momentum onto this axis should be a quantum number being conserved, leading also to selection rules for transitions between N- and $(N+1)$-electron states.

Correlated electron systems are not described by a single Slater determinant of single-particle states – an assumption of the Constant Interaction Model. Theoretical works of J.M. Kinaret *et al.* [155], J.J. Palacios *et al.* [156],

D. Pfannkuche and S. Ulloa [157] K. Jauregui *et al.* [158] describe the tunneling matrix elements being weighed by a correlation factor. This is given by the projection of the N electron state $|N,l\rangle$ plus a single-particle state $|s\rangle$ – being part of the base to describe the n-electron states – onto the $(N+1)$-electron state $|N+1,k\rangle$:

$$\left|T_r(|N,l\rangle,|N+1,k\rangle;\varepsilon_s)\right|^2 \quad \propto \quad \left|\langle N+1,k|\,|s\rangle|N,l\rangle\right|^2 . \qquad (5.60)$$

If the n-electron states are described by a Slater determinant, the correlation factor is unity if the N and the $(N+1)$-electron system differ by the single particle state $|s\rangle$ and is zero for single-particle states $s' \neq s$. In case of a correlated state, the factor is less than unity since it is only partially occupied to describe the correlated state. This correlation factor leads – besides the spin-selection rule – to quasi-selection rules for transitions between the N- and the $(N+1)$-electron system.

Transport spectra of correlated electron systems based on above (quasi-) selection rules have been presented in several theoretical works [9, 134].

5.10 Complications in Interpreting Single $I_{\mathrm{DS}}(V_{\mathrm{DS}})$ Characteristics

Measuring the current I_{DS} versus the applied drain-source voltage V_{DS} for a fixed gate voltage value, steps in the $I_{\mathrm{DS}}(V_{\mathrm{DS}})$ characteristics of the quantum dot are usually observable. Such staircase-like characteristics were already described for metal islands with two asymmetric tunnel junctions to drain and source. A single $I_{\mathrm{DS}}(V_{\mathrm{DS}})$ curve of a quantum dot system lacks the information on which side – source or drain – an additional channel is opened leading to the step-like increase in the characteristic. Such information is obtained by following the direction of how the step positions are shifted along the V_{DS} axis with changing a gate voltage V_{BS}. Full information is obtained by doing transport spectroscopy in the (V_{BS},V_{DS}) plane as presented in Fig. 5.5.

In Fig. 5.16 for a fictitious transport spectrum, single $I_{\mathrm{DS}}(V_{\mathrm{DS}})$ characteristics are shown for two different V_{BS} values. Obviously it is not clear for a single $I_{\mathrm{DS}}(V_{\mathrm{DS}})$ curve, how to relate the step length ΔV_{DS} to an energy difference in the quantum dot spectrum: If the energies between two transitions, for instance $(l,k)=(0,0)$ and $(l',k')=(1,1)$, differ by ΔE,

$$\Delta E \equiv E(N+1,k') - E(N,l') - \Big[E(N+1,k) - E(N,l)\Big] ,$$

the step length ΔV_{DS} between the two channels opening on source side (in Fig. 5.16c for $V_{\mathrm{DS}} > 0$) is given by

$$\Delta V_{\mathrm{DS}} = \frac{\Delta E}{e \cdot \alpha_{\mathrm{D}}} ,$$

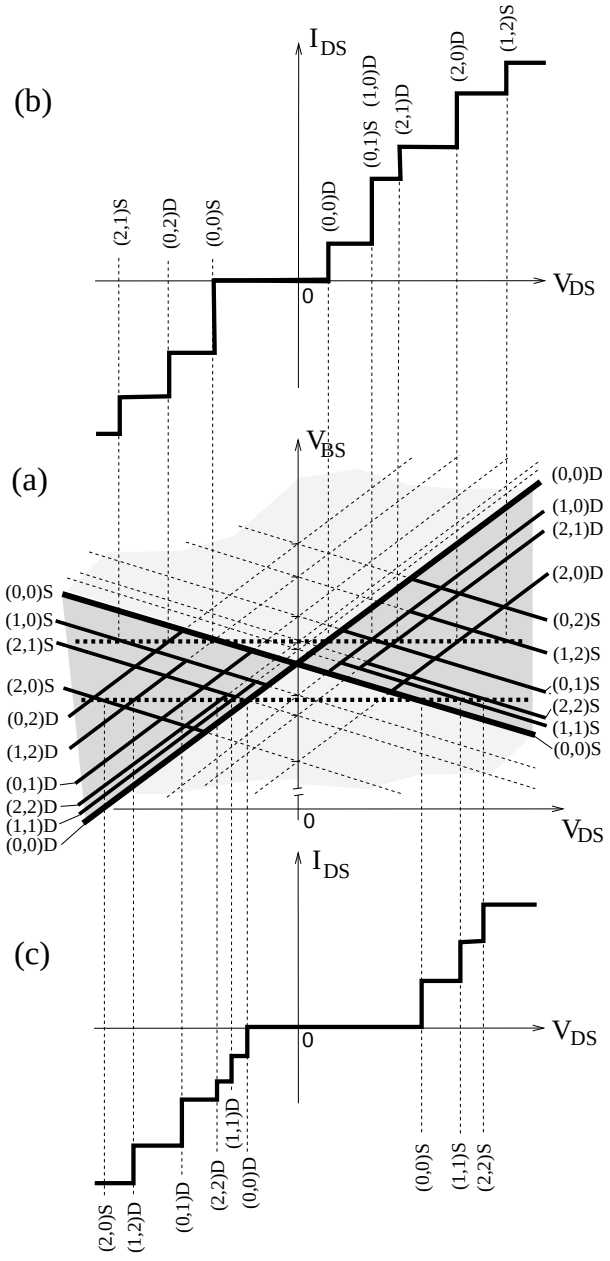

Fig. 5.16. Staircase-like charcteristic $I_{\rm DS}(V_{\rm DS})$ of a quantum dot: (a) Fictitious transport spectrum: At each borderline in the ($V_{\rm BS}$,$V_{\rm DS}$) plane, a step-like increase in the $I_{\rm DS}(V_{\rm DS})$ characteristic is observed. (b),(c) Guess for a single $I_{\rm DS}(V_{\rm DS})$ trace taken along the dotted lines in (a). The step length between opening two channels cannot be interpreted simple if channels are opened alternately on source and drain side with increasing drain-source voltage. A careful analysis requires the full transport spectrum obtained in the ($V_{\rm BS}$,$V_{\rm DS}$) plane.

which can be derived by substracting the two resonance conditions

$$E(N+1,k;V_{\mathrm{BS}},V_{\mathrm{DS}}) - E(N,l;V_{\mathrm{BS}},V_{\mathrm{DS}}) = \mu_{\mathrm{S}}^{\mathrm{elch}} ,$$
$$E(N+1,k';V_{\mathrm{BS}},V_{\mathrm{DS}}+\Delta V_{\mathrm{DS}}) - E(N,l';V_{\mathrm{BS}},V_{\mathrm{DS}}+\Delta V_{\mathrm{DS}}) = \mu_{\mathrm{S}}^{\mathrm{elch}} .$$

If both channels are opened on drain side (in Fig. 5.16c for $V_{\mathrm{DS}} < 0$), the step length changes to

$$\Delta V_{\mathrm{DS}} = \frac{\Delta E}{e \cdot (1-\alpha_{\mathrm{D}})} , \tag{5.61}$$

which can be derived by substracting the two resonance conditions

$$E(N+1,k;V_{\mathrm{BS}},V_{\mathrm{DS}}) - E(N,l;V_{\mathrm{BS}},V_{\mathrm{DS}}) = \mu_{\mathrm{D}}^{\mathrm{elch}} ,$$
$$E(N+1,k';V_{\mathrm{BS}},V_{\mathrm{DS}}+\Delta V_{\mathrm{DS}}) - E(N,l';V_{\mathrm{BS}},V_{\mathrm{DS}}+\Delta V_{\mathrm{DS}}) = \mu_{\mathrm{D}}^{\mathrm{elch}} + e\Delta V_{\mathrm{DS}} .$$

The energy ΔE scales differently for both cases along the V_{DS} axis! Such a result was already presented in Fig. 1.10 and Fig. 1.11 for metal single-electron transistors. If the opening of channels occurs alternately – for instance in Fig. 5.16b for $V_{\mathrm{DS}} < 0$ in the order $(0,0)$S, $(0,2)$D, $(2,1)$S –, the step length between $(0,0)$S and $(0,2)$D, and $(0,2)$D and $(2,1)$S depends even on the gate voltage value where the $I_{\mathrm{DS}}(V_{\mathrm{DS}})$ trace is taken.

Therefore further information or assumptions are required for the interpretation of the step lengths in $I_{\mathrm{DS}}(V_{\mathrm{DS}})$ curves of quantum dot systems. If the tunnel barriers are very asymmetric, i.e., the tunneling matrix elements to one lead are much smaller than to the other one, then the current through the quantum dot is limited by the tunneling to the weakly tunnel-coupled lead. Any additional channel on this side would enhance single-electron transport through the quantum dot system whereas an additional channel to the other lead increases the current not significantly – except if by this channel additional transitions on the weak tunnel barrier side become possible. Examples are shown in Fig. 5.17, derived from the fictitious transport spectrum in Fig. 5.16a: For instance in Fig. 5.17a for $V_{\mathrm{DS}} > 0$, the transition $(1,1)$S opening on source side is visible since it provides the initial state $|N,1\rangle$ for opening $(2,1)$D which helps to reduce the weak link to drain.

Asymmetric barriers and the assumption of a complete relaxation process between the tunnel events allow to relate the step length to energy differences of the quantum dot by a single proportionality factor – either α_{D} or $1-\alpha_{\mathrm{D}}$. Under such conditions, spectroscopy on quantum dots in a two-terminal arrangements have been done. Starting with an empty quantum dot, the quantitative spectroscopy of the single-particle states ($N = 1$) in such a quantum dot could be performed (see [106] with references in there).

5.11 Summary and Conclusions

Starting from thermodynamical considerations, the regions are derived within this Chapter, where certain electron numbers become possible for the quan-

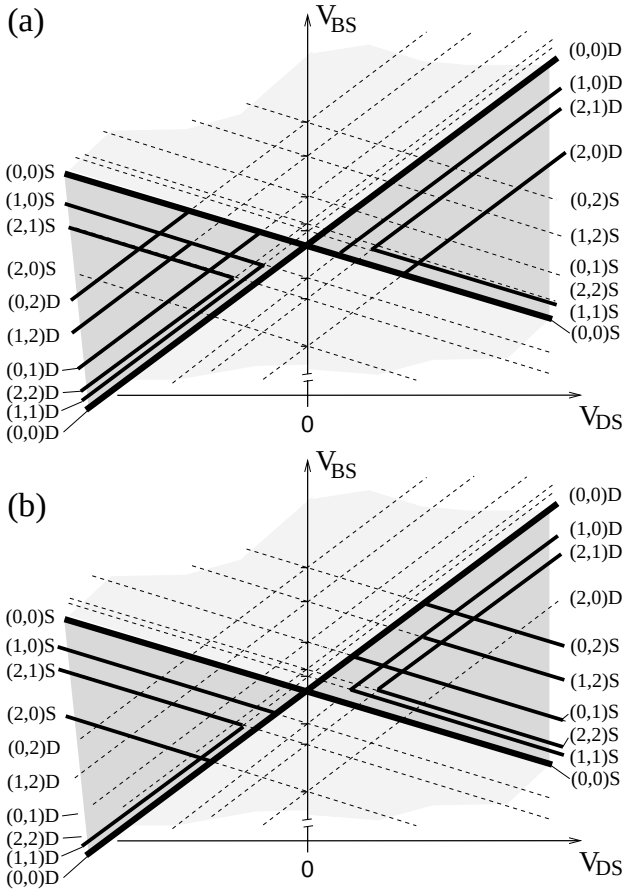

Fig. 5.17. Same as in Fig. 5.16, except that strongly asymmetric tunnel coupling is assumed: In (a) weak tunnel coupling to source, in (b) to drain.

tum dot as a function of drain-source voltage V_{DS} and a (back-)gate voltage V_{BS}. The regime of Coulomb blockade and single-electron tunneling are identified. During single-electron transport at vanishingly small V_{DS}, the quantum dot changes between the groundstates of two different electron systems, e.g., between a N- and a $(N+1)$-electron system. Increasing the bias voltage V_{DS}, excited states for both electron systems become accessible, providing new transport channels through the quantum dot. These additional channels can be classified as being opened in resonance to the Fermi level of the emitter or of the collector. In the first case, an excited state of the $(N+1)$-electron system is reached, whereas in the second case an excited state of the N-electron system is reached.

For fictitious energy spectra for the N- and the $(N+1)$-electron system, the borderlines for opening these additional channels in the (V_{BS},V_{DS}) plane

are derived from energy considerations. It demonstrates the complexity in interpreting experimental data without further assumptions about the dynamics. Separate spectroscopy of the N- and the $(N+1)$-electron system is possible if the respective groundstates are the initial states for the tunneling processes. That requires an instantaneous and complete relaxation process before each tunneling event.

Applying a magnetic field affects the electronic spectrum of the quantum dot. Transport spectroscopy at finite drain-source voltage allows to follow the dispersions of transition energies between the groundstates but also excited states of the N- and $(N+1)$-electron system. The character of the respective groundstate – described by its set of quantum numbers – might change with magnetic field. However, when performing transport spectroscopy in a magnetic field, one might have to take into account changes in the contact voltages of the leads and gate electrodes: As already pointed out in Chapter 3, the electrochemical potential differences and not the electrostatic potential differences are fixed by the electrical circuit: The electron system in the quantum dot is sensitive to the electric field and therefore to the electrostatic potential variations.

Within a master equation approach it has been discussed that with opening a channel of an excited state, the current is not necessarily increased but might also decrease. This is also observed as negative differential conductance in the experimental data, indicating that (1) different tunnel matrix elements exist wheighing the tunneling rates for the different channels, (2) instantaneous relaxation is absent and (3) excited states of long life time exist exceeding the mean time of single electron transport through the quantum dot when not reaching this excited state.

A simple $I_{\mathrm{DS}}(V_{\mathrm{DS}})$ characteristic of a quantum dot system does not allow to relate unambiguously step-like changes in I_{DS} to certain transitions in the quantum dot. The complexity is partially resolved by measuring the current or differential conductance in the full $(V_{\mathrm{BS}},V_{\mathrm{DS}})$ plane. It allows to extract whether an excited state of the N- or the $(N+1)$-electron system becomes accessible. Further the transition energy differences are extracted correctly by distinguishing between channels being opened in resonance to source or drain. The two voltages V_{BS} and V_{DS} allow to tune to any position of $\mu(n)$ relatively to $\mu_{\mathrm{S}}^{\mathrm{elch}}$ or $\mu_{\mathrm{D}}^{\mathrm{elch}}$, and to define the difference $\mu_{\mathrm{S}}^{\mathrm{elch}}$ to $\mu_{\mathrm{D}}^{\mathrm{elch}}$ independently. Therefore, for certain combinations of $(V_{\mathrm{BS}},V_{\mathrm{DS}})$, the situation is exceptional: The difference $\mu(n+1)-\mu(n)$ is obtained from the maximum V_{DS} value found for the Coulomb blockade region with n electrons. No proportionality factor besides e is required for converting the voltage scale to the energy scale of the quantum dot.

The leads to the quantum dot have been treated as electron reservoirs without specific assumption about the density of states in these. Actually, transport experiments on quantum dots can be used to resolve these density-

of-state of the leads superposed to the transport spectra just described (for instance, [159]).

Describing the dynamics by a master equation approach ('Orthodox Theory' [2]) allows to include thermal effects. The current steps smear out by thermal activations. But the approach treats each single-electron tunneling process crossing a tunnel barrier as a single and independent event in the sense that there is no quantum mechanical phase correlation between two or more tunneling events. It is denoted as *sequential tunneling*. It seems to be plausible if, for instance, the quantum dot indeed relaxes to its ground-state between tunneling events since by transfering energy to a bath, the quantum mechanical phase correlation is destroyed. But the experimental data indicate that relaxation is not present – at least – in some cases. Dual path arrangements allow to test the phase coherence of electrical transport through quantum dot systems. Such kind of experiments were pioneered by A. Yacoby and coworkers [160].

6. Kondo Effect in a Single Quantum-Dot System

Electrical transport through a quantum-dot system has been discussed in the previous Sections in terms of Coulomb blockade and single-electron tunneling. We remember: These effects are caused by the electron-electron interaction of the electrons confined on the SET island, only partially screened by the surrounding electrodes. For small drain-source voltage the electron transport between drain and source is usually blocked and only for certain values of the electrostatic potentials of the surrounding electrodes a single electron can enter the island and leave before the next electron can follow. The quantum dot has been denoted as being weakly coupled to drain and source so that the tunneling events through the tunnel barriers are considered as being independent: Energy conservation arguments for rearranging single electrons combined with a master equation approach captures basic features of the dynamics of electron transport through the quantum-dot system. This *sequential tunneling* description is denoted as *orthodox theory* [2, 10].

However, this sequential tunneling description is incomplete since it does not take into consideration that energy requirements can be raised for short time events according to Heisenberg uncertainty relation for energy and time: By correlating tunneling events of two or more electrons entering and leaving the island *at almost the same time*, the number of electrons on the island fluctuates only on short time scale. A charging or discharging of the quantum dot by an elementary charge occurs only as an intermediate state of short life time or – as better denoted – *virtually by quantum fluctuations*. Such correlated tunneling events involving two or more electrons cause electron transport between source and drain even in the regimes where single-electron tunneling – i.e., a recharging of the island by a single electron – is energetically suppressed [147]. As excepted, these correlated tunneling processes are usually strongly diminished with decreasing the tunnel coupling between quantum dot and leads. However, this is not true under all circumstances:

- Under certain conditions the quantum-dot system becomes conductive again over the whole Coulomb-blockade regime *with lowering the temperature*.
- The conductance reaches the order of $2\,e^2/h$ which is equal to the conductance of a spin-degenerate one-dimensional channel [56, 57].

Here, the description of Coulomb blockade and single-electron tunneling by master equations breaks down even in the case of weak tunnel coupling. The effect can be discussed by using a most simple model – the *Anderson impurity model* [161] which has also been used to describe the *Kondo effect* [162]. Experimental indications to the Kondo effect in a single quantum-dot systems is topic of this Chapter.

6.1 Zero-Bias Anomaly in the Differential Conductance in the Coulomb-Blockade Regime at $V_{DS} = 0$

In Fig. 6.1a the experimental setup of a split-gate quantum-dot system is shown. The structure is very similar to the one already described and used in the Chapters 4 and 5. Different is that the size of the quantum dot area has been reduced. This has been achieved by the smaller geometric size of the split-gate electrodes – now 180 nm as the open diameter between the gate fingers –, and by getting the two-dimensional electron system closer to the heterostructure surface – the depth of the AlGaAs/GaAs heterojunction is now 50 nm. [1]

In Fig. 6.1b the measured $I_{DS}(V_{DS}, V_{BS})$ characteristics are plotted. They are taken at a temperature of about 30 mK. Clearly three Coulomb blockade regions are visible and adjacent to these the single-electron tunneling regimes where step-like changes in the current I_{DS} with increasing $|V_{DS}|$ are noticeable indicating transport channels through excited states. These are better to see in Fig. 6.2a where the differential conductance dI_{DS}/dV_{DS} measured around a chosen Coulomb-blockade region is plotted in the (V_{BS}, V_{DS}) plane. Step-like changes in $I_{DS}(V_{DS})$ appear in $dI_{DS}/dV_{DS}(V_{DS})$ as peaks with positive, but also negative amplitude (see Section 5.8).

By tuning the outer split-gate electrodes, the tunnel coupling to source and drain is increased. As seen in Fig. 6.2 the borderlines between Coulomb blockade and single-electron transport regions smear out: Due to the reduced life time of single electrons on the quantum dot, occupation is possible within Heisenberg uncertainty relation of energy and time. The borderlines – derived by strict energy considerations – are no longer well defined. The stronger the tunnel coupling, the less visible is the Coulomb blockade region. However, striking in Fig. 6.2 is the occurrence of a peak in the differential conductance dI_{DS}/dV_{DS} at $V_{DS} = 0$ which is *not shifting* with the gate voltage V_{BS} as it is usually the case due to opening channels for single-electron tunneling. This

[1] Like for the MOSFET discussed in Chapter 7, *all* spatial dimensions have to be scaled by the same factor to reduce the size but still keeping the functionality of the quantum-dot system. Only shrinking the split-gate structure without reducing the distance to the 2DES would finally lead to a depletion of the 2DES without the possibility of forming a quantum dot between the gate electrode fingers.

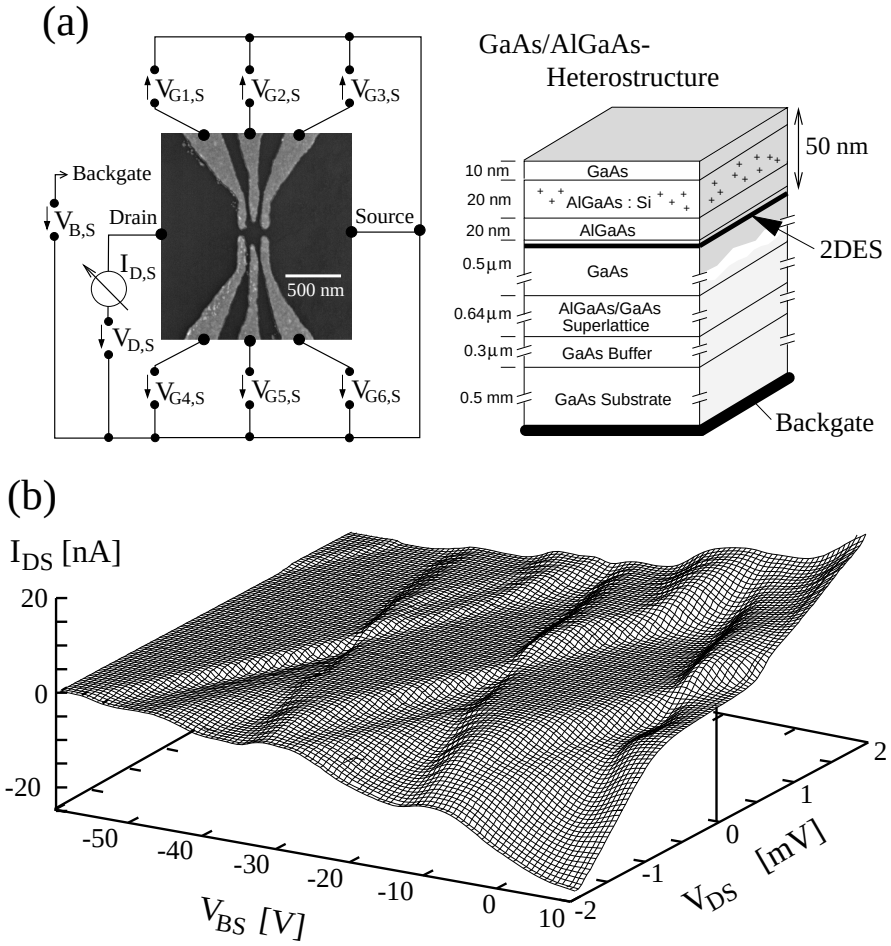

Fig. 6.1. (a) Setup of a quantum-dot system using split-gates to partially deplete a two-dimensional electron system: (Left) Scanning-electron-microscope image of the metal split-gate fingers. The voltages applied to the structures are indicated. (Right) GaAs-$Al_xGa_{1-x}As$ heterostructure containing the 2DES at the heterojunction 50 nm below the surface (2DES with electron concentration $3.2 \cdot 10^{15}$ m^{-2} and electron mobility 30 m^2/Vs at the temperature of 4.2 K). (b) Current $I_{\rm DS}$ measured as a function of the drain-source voltage $V_{\rm DS}$ and the backgate-source voltage $V_{\rm BS}$. The voltages applied to the split-gate electrodes are kept fixed. The measurement were performed at about 30 mK in our laboratory. (adopted from J. Schmid [92])

zero-bias anomaly does not fit into the picture of single-electron transport and does not occur in all Coulomb blockade regions.

As described in Chapter 4, without tunnel coupling to the leads, N electrons confined in the quantum dot own a total energy spectrum $E(N, k; \{V_i\})$ which can be labeled by the parameter k where $k = 0$ denotes the ground-

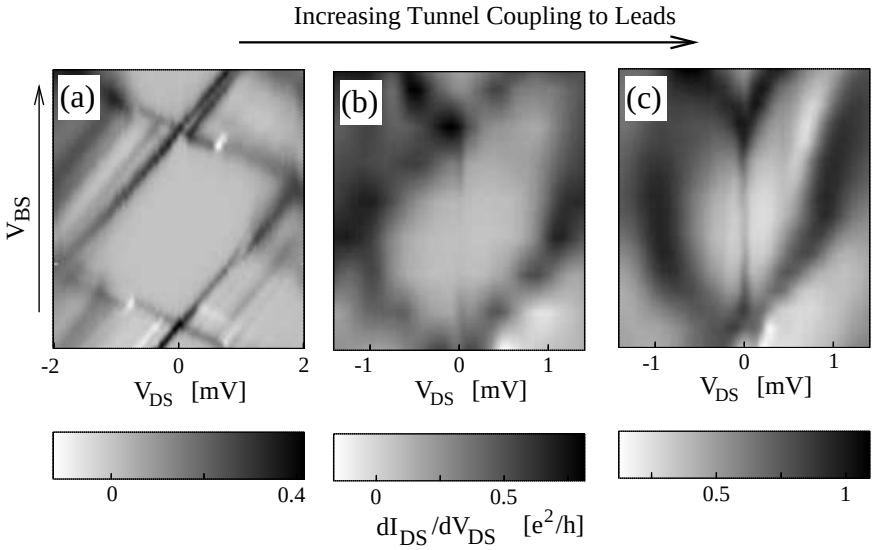

Fig. 6.2. Coulomb blockade region with a fixed number N of electrons confined in the quantum dot at about 30 mk: The differential conductance is plotted in greyscale versus $V_{\rm DS}$ and $V_{\rm BS}$. From (a) to (c) the tunnel coupling to the leads is increased by reducing the voltages applied to the outer pairs of the splitgate structure depicted in Fig. 6.1a. The backgate voltage $V_{\rm BS}$ has been adjusted to keep the same Coulomb blockade region. Striking is the occurrence of a peak in the differential conductance around $V_{\rm DS} = 0$ in (c) which does not shift with $V_{\rm BS}$. This zero-bias anomaly is identified with the Kondo effect in quantum-dot systems. (adopted from J. Schmid *et al.* [163])

state of the N-electron system. The total energy depends besides other parameters on the electrostatic potentials $\{V_i\}$ of the electrodes (split-gates, backgate, source and drain) surrounding the quantum dot. To describe electron transport through the quantum dot in the regime of weak tunnel coupling to the leads, the energies required for adding the $(N+1)$th electron into the N-electron system ('electron-like' process) and for taking off the Nth electron from the quantum dot ('hole-like' process) have to be considered. This was described in Chapter 5, leading to the energy scheme shown in Fig. 5.3, where the groundstate energy differences $\mu(N+1;\{V_i\}) \equiv E(N+1,0;\{V_i\}) - E(N,0;\{V_i\})$ between the $(N+1)$- and the N-electron system are plotted for different N but fixed $\{V_i\}$ relatively to the Fermi levels, i.e., the electrochemical potentials $\mu_{\rm S}^{\rm elch}$ and $\mu_{\rm D}^{\rm elch}$ of the source and drain leads.

As a reminder, by changing one of the applied voltages, these energy levels $\mu(n;\{V_i\})$ with $n \in \{\cdots, N-1, N, N+1, \cdots\}$ are – in first approximation – linearly shifted relatively to the Fermi levels while the distance $\mu(n+1;\{V_i\}) - \mu(n;\{V_i\})$ between the levels remains constant. In the case of $\mu(N+1;\{V_i\}) > \{\mu_{\rm S}^{\rm elch}; \mu_{\rm D}^{\rm elch}\} > \mu(N;\{V_i\})$, energy barriers exist for an electron entering or

leaving. Therefore at low temperature single-electron transport is blocked and we are in the regime of Coulomb blockade (CB) where the number of electrons on the quantum dot is fixed to N. Whenever $\mu(N+1;\{V_i\})$ lies between the Fermi levels of source and drain leads, the number of electrons on the quantum dot is fluctuating between N and $N+1$, and single-electron tunneling through the quantum dot between source and drain can occur.

As shown in Fig. 5.6, Coulomb blockade and single-electron transport regimes are found as a function of drain-source voltage V_{DS} and gate-source voltage V_{GS}. The boundaries between Coulomb blockade and transport regimes are given by the condition that the respective $\mu(n;\{V_i\})$ is either aligned with $\mu_{\mathrm{S}}^{\mathrm{elch}}$ or $\mu_{\mathrm{D}}^{\mathrm{elch}}$, giving two different slopes for the borderlines in the $(V_{\mathrm{GS}}, V_{\mathrm{DS}})$ plane. Within the single-electron transport regimes at finite drain-source voltage $eV_{\mathrm{DS}} = \mu_{\mathrm{D}}^{\mathrm{elch}} - \mu_{\mathrm{S}}^{\mathrm{elch}}$, additional channels in the transport through the quantum dot become available which have been related to excited states of the confined n- and $(n+1)$-electron system (see Section 5.4). The borderlines for opening these additional single-electron transport channels are described by $E(n+1,k;\{V_i\}) - E(n,l;\{V_i\}) = \{\mu_{\mathrm{S}}^{\mathrm{elch}}, \mu_{\mathrm{D}}^{\mathrm{elch}}\}$, i.e., they are in the $(V_{\mathrm{GS}}, V_{\mathrm{DS}})$ plane parallel to the borderlines of the respective Coulomb blockade and single-electron transport regime (see Fig. 5.11). At these borderlines, peaks in the differential conductance $\mathrm{d}I_{\mathrm{DS}}/\mathrm{d}V_{\mathrm{DS}}$ can be expected. The peak line in Fig. 6.2c at $V_{\mathrm{DS}} = 0$ is not parallel to one of these borderlines and can therefore not be related to single-electron transport through the quantum dot.

The question arises whether the peak line in Fig. 6.2 at $V_{\mathrm{DS}} = 0$ can be explained by tunneling of two electrons at nearly the same time. Such correlated two-electron tunneling is denoted as *cotunneling*. We have to distinguish especially between two kinds of cotunneling with only virtual charge change:

- *Hole-like cotunneling*: an electron leaves the quantum dot and immediately thereafter an electron enters.
- *Electron-like cotunneling:* an electron enters the quantum dot and immediately thereafter an electron leaves.

In both cases we have to distinguish whether the whole transfer occurs *elastically* (i.e., the initial and final energies of the quantum dot is the same) or *inelastically* (i.e., they are different). Furthermore, the intermediate state of the electron system in the quantum dot can be a groundstate or an excited state. Examples of these cases are depicted in Fig. 6.3 and Fig. 6.4.

6.2 Correlated Two-Electron Tunneling: Electron Transport without the Need of Charging Energy

- **Hole-like cotunneling**:
  Let us assume that the quantum dot is in the Coulomb blockade regime,

Hole-Like Elastic Cotunneling

(a) via Groundstate:

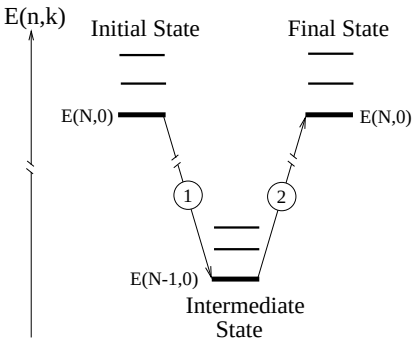

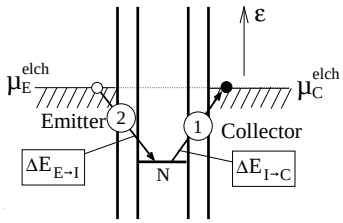

(b) via Excited State:

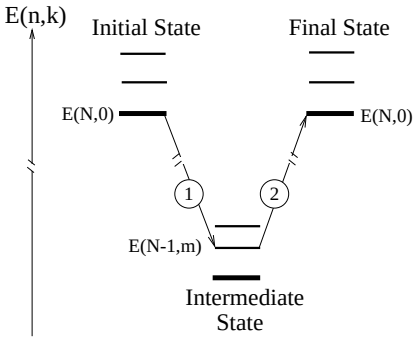

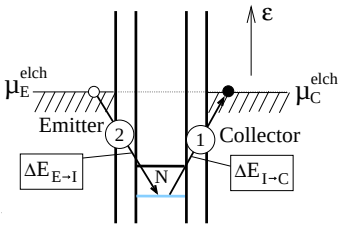

Hole-Like Inelastic Cotunneling

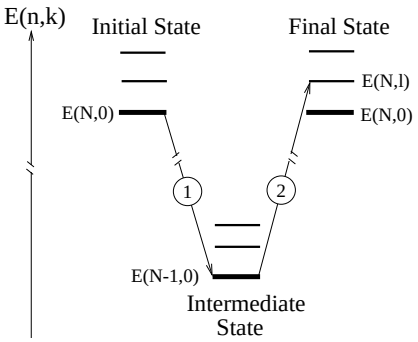

(c) at Threshold:

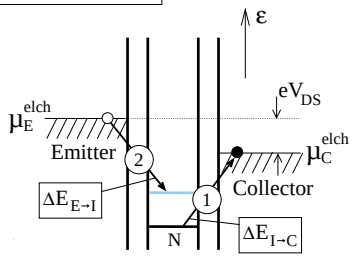

(d) beyond Threshold:

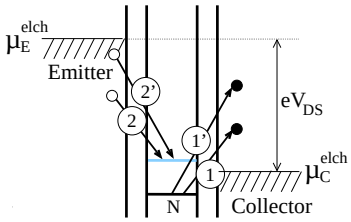

Fig. 6.3. (Left page) Hole-like cotunneling: An electron leaves the quantum dot, immediately followed by an electron entering the quantum dot. A change in the charge state of the quantum dot appears only virtually. These cotunneling processes are visualized by indicating the respective transitions in the total energy spectrum $E(n,k;\{V_i\})$ of the quantum dot, and below in the energy scheme where the transition energies $E(n,k;\{V_i\}) - E(n-1,l;\{V_i\})$ for single-electron charging are plotted relatively to the electrochemical potentials of the leads. If initial and final state of the N-electron system in the quantum dot have same energy, the cotunneling process is denoted as 'elastic' (see (a) and (b)), otherwise as 'inelastic' (see (c) and (d)). In (a) elastic cotunneling occurs via the groundstate of the $(N-1)$-electron system, in (b) via an excited state of the $(N-1)$-electron system. Note, (b) requires a higher energy cost $\Delta E_{\mathrm{I}\to\mathrm{C}}$ for creating the intermediate state than (a). (c) Inelastic cotunneling transfers the N-electron system to an excited state which requires a bias between the electrochemical potentials of the leads fulfilling $E(N,l;\{V_i\}) - E(N,0;\{V_i\}) \leq e|V_{\mathrm{DS}}|$. Beyond this threshold, more and more cotunneling processes become available as indicated by two examples in (d), for which $\Delta E_{\mathrm{I}\to\mathrm{C}} + \Delta E_{\mathrm{E}\to\mathrm{I}} = 0$, $\varepsilon_{\mathrm{C}} \geq \mu_{\mathrm{C}}^{\mathrm{elch}}$ and $\varepsilon_{\mathrm{E}} \leq \mu_{\mathrm{E}}^{\mathrm{elch}}$.

in the groundstate $|N,0;\{V_i\}\rangle$ of the N-electron system. [2] An electron leaving towards an empty collector state of energy $\varepsilon_{\mathrm{C}} \geq \mu_{\mathrm{C}}^{\mathrm{elch}}$ transfers the quantum dot into the groundstate $|N-1,0;\{V_i\}\rangle$ shown in Fig. 6.3a or – more general – into the state $|N-1,m;\{V_i\}\rangle$ of Fig. 6.3b.
Such a hole-like process requires the energy

$$\Delta E_{\mathrm{I}\to\mathrm{C}} = \Big[\varepsilon_{\mathrm{C}} + E(N-1,m;\{V_i\})\Big] - E(N,0;\{V_i\}) \geq 0\ , \qquad (6.1)$$

and can only work if the life time τ of the state $|N-1,m;\{V_i\}\rangle$ is short, estimated by Heisenberg uncertainty relation of energy and time,

$$\Delta E_{\mathrm{I}\to\mathrm{C}} \cdot \tau < \hbar\ . \qquad (6.2)$$

Under condition (6.2), the state $|N-1,m;\{V_i\}\rangle$ can be considered as a *virtual intermediate state*, almost immediately decaying by an electron entering the quantum dot from an emitter state with energy $\varepsilon_{\mathrm{E}} \leq \mu_{\mathrm{E}}^{\mathrm{elch}}$. With entering, the electron-system in the quantum dot changes its state to the previous initial state (Fig. 6.3a and b), or – more general – to the state $|N,l;\{V_i\}\rangle$ (Fig. 6.3c). By such a transition the system gains energy,

$$\Delta E_{\mathrm{E}\to\mathrm{I}} = \Big[E(N,l;\{V_i\}) - E(N-1,m;\{V_i\})\Big] - \varepsilon_{\mathrm{E}} \leq 0\ . \qquad (6.3)$$

The overall process is working without violating energy conservation if the energy gain (6.3) just compensates for the energy cost (6.1), i.e.,

$$\Delta E_{\mathrm{I}\to\mathrm{C}} + \Delta E_{\mathrm{E}\to\mathrm{I}} = 0\ . \qquad (6.4)$$

[2] Note that for the sake of brevity the constants $\{V_i\}$ are omitted in the state kets and total energies in all diagrams.

Since for ε_{E} and ε_{C} the restrictions $\varepsilon_{\mathrm{E}} \leq \mu_{\mathrm{E}}^{\mathrm{elch}}$ and $\varepsilon_{\mathrm{C}} \geq \mu_{\mathrm{C}}^{\mathrm{elch}}$ exist at low temperature, such a cotunneling process is energetically allowed under the condition

$$E(N,l;\{V_i\}) - E(N,0;\{V_i\}) = \varepsilon_{\mathrm{E}} - \varepsilon_{\mathrm{C}} \leq \mu_{\mathrm{E}}^{\mathrm{elch}} - \mu_{\mathrm{C}}^{\mathrm{elch}} = e|V_{\mathrm{DS}}| \,. \tag{6.5}$$

Relation (6.5) expresses that the energy difference $\varepsilon_{\mathrm{E}} - \varepsilon_{\mathrm{C}}$ of the electron entering and the electron leaving has to reflect the energy difference between initial and final state of the N-electron system in the quantum dot. Moreover, the possible energy difference between excited state and groundstate is limited by the applied bias $e|V_{\mathrm{DS}}|$ between the electrochemical potentials of the leads.

With the cotunneling process just described, an excited state of the quantum dot is obtained under condition (6.5) although the quantum dot is in the Coulomb blockade regime. This excited state $|N,l;\{V_i\}\rangle$ can now act as the initial state for cotunneling processes leading to other excited states. In general, if a state $|N,l;\{V_i\}\rangle$ is accessible, a state $|N,l';\{V_i\}\rangle$ is energetically reached by cotunneling if

$$\left|E(N,l';\{V_i\}) - E(N,l;\{V_i\})\right| = \left|\varepsilon_{\mathrm{E}} - \varepsilon_{\mathrm{C}}\right| \leq \mu_{\mathrm{E}}^{\mathrm{elch}} - \mu_{\mathrm{C}}^{\mathrm{elch}} = e|V_{\mathrm{DS}}| \,. \tag{6.6}$$

Since $\varepsilon_{\mathrm{E}} - \varepsilon_{\mathrm{C}}$ can be either positive or negative, the quantum dot can be excited or can loose energy by correlated electron exchange between quantum dot and leads if $|V_{\mathrm{DS}}| > 0$.

Note, the probability for a cotunneling process is higher, the lower the energy cost (6.1) is for the intermediate state. For given $\{V_i\}$, the position of the energy ladder $E(n,k;\{V_i\}) - E(n-1,l;\{V_i\})$ relatively to the electrochemical potential of the leads is fixed: Starting from the groundstate $|N,0;\{V_i\}\rangle$, an electron leaving to the Fermi level of the collector ($\varepsilon_{\mathrm{C}} = \mu_{\mathrm{C}}^{\mathrm{elch}}$) and transfering the quantum dot to the groundstate $|N-1,0;\{V_i\}\rangle$ as the intermediate state requires the least energy (compare Fig. 6.3a and b), and has therefore the highest probability for a hole-like cotunneling process if not other selection rules weigh the cotunneling transitions.

- **Electron-like cotunneling**:
  Instead of starting such a correlated two-electron process by an electron leaving the quantum dot (hole-like process), an electron can enter the quantum dot (electron-like process), leading to an intermediate state with $N+1$ electrons on the quantum dot (see Fig. 6.4): The quantum dot is transfered from $|N,0;\{V_i\}\rangle$ to $|N,l;\{V_i\}\rangle$ via the intermediate state $|N+1,k;\{V_i\}\rangle$. Entering of an electron costs the energy

$$\Delta E_{\mathrm{E}\to\mathrm{I}} = E(N+1,k;\{V_i\}) - \Big[\varepsilon_{\mathrm{E}} + E(N,0;\{V_i\})\Big] \geq 0 \,. \tag{6.7}$$

The life time τ of this state has to be short,

$$\Delta E_{\mathrm{E}\to\mathrm{I}} \cdot \tau < \hbar \; . \tag{6.8}$$

The energy cost is compensated by the energy gain with an electron leaving,

$$\Delta E_{\mathrm{I}\to\mathrm{C}} = \Big[\varepsilon_{\mathrm{C}} + E(N,l;\{V_i\})\Big] - E(N+1,k;\{V_i\}) \leq 0 \; . \tag{6.9}$$

Comparing (6.7) and (6.9), such a cotunneling process can be expected if

$$\Delta E_{\mathrm{E}\to\mathrm{I}} + \Delta E_{\mathrm{I}\to\mathrm{C}} = 0 \tag{6.10}$$

is fulfilled. With $\varepsilon_{\mathrm{E}} \leq \mu_{\mathrm{E}}^{\mathrm{elch}}$ and $\varepsilon_{\mathrm{C}} \geq \mu_{\mathrm{C}}^{\mathrm{elch}}$, it leads to the restriction

$$\begin{aligned} E(N,l;\{V_i\}) - E(N,0;\{V_i\}) &= \varepsilon_{\mathrm{E}} - \varepsilon_{\mathrm{C}} \\ &\leq \mu_{\mathrm{E}}^{\mathrm{elch}} - \mu_{\mathrm{C}}^{\mathrm{elch}} = e|V_{\mathrm{DS}}| \; , \end{aligned} \tag{6.11}$$

which is the same as found with (6.5) for the hole-like cotunneling process. If the state $|N,l;\{V_i\}\rangle$ is accessible, further states $|N,l';\{V_i\}\rangle$ are energetically allowed if (6.6) is fulfilled.

Therefore, starting with $|N,l;\{V_i\}\rangle$ and ending with $|N,l';\{V_i\}\rangle$, the electron- and hole-like cotunneling process are energetically allowed at the same time. Note, since however different intermediate states are used, in general the probability between hole-like and electron-like cotunneling process might be different, especially if the energy costs for the intermediate state are different, or the tunneling couplings differ.

We can conclude for low temperature:

- For correlated tunneling of two electrons in the Coulomb blockade regime confining N electrons in the quantum dot, the energy difference between the inital and the final state of the N-electron system in the quantum dot has to be less than the energy window opened by the drain-source voltage between the electrochemical potential of source and drain.
- Since relation (6.5) and (6.11) are independent of the electrostatic potentials $\{V_i\}$, the borderlines for opening such cotunneling processes lie in the $(V_{\mathrm{GS}}, V_{\mathrm{DS}})$ plane at $V_{\mathrm{DS}} = \pm|E(N,l;\{V_i\}) - E(N,0;\{V_i\})|/e$ parallel to the V_{GS} axis. As indicated in Fig. 6.5, they are linked to borderlines in the single-electron transport regime using the respective state $|N,l;\{V_i\}\rangle$ for single-electron transport.
- For $V_{\mathrm{DS}} = 0$, the initial and final state of the cotunneling process have the same energy. It is denoted as *elastic cotunneling*. Since the quantum dot is usually found in the groundstate, the initial and final state of a cotunneling process lie at the groundstate energy, i.e., excited states are not reached.

Electron-Like Elastic Cotunneling

(a) via Groundstate:

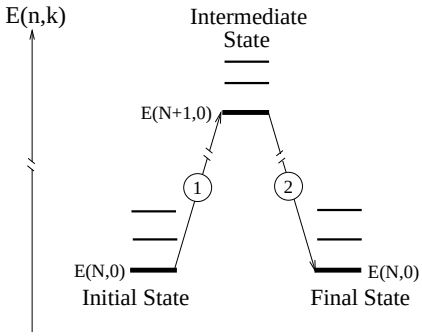

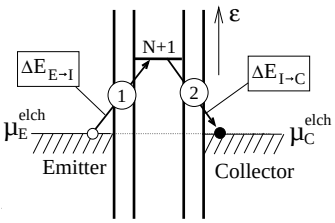

(b) via Excited State:

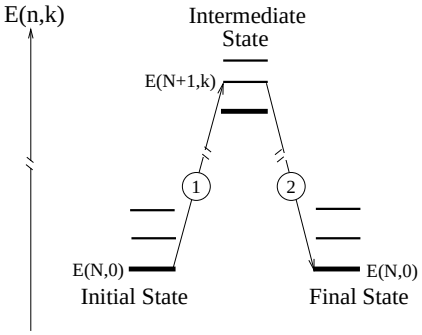

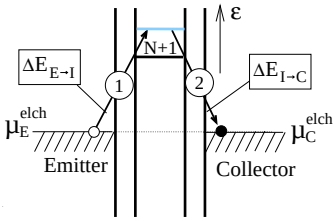

Electron-Like Inelastic Cotunneling

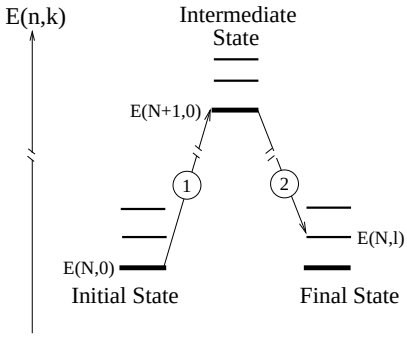

(c) at Threshold:

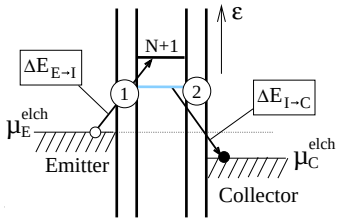

(d) beyond Threshold:

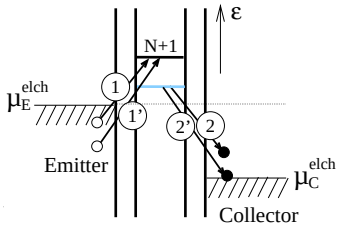

Fig. 6.4. (Left page) Electron-like cotunneling: An electron enters the quantum dot, immediately followed by an electron leaving the quantum dot. A change in the charge state of the quantum dot appears only virtually. Visualized are the processes corresponding to the hole-like cotunneling processes shown in Fig. 6.3. In (a) elastic cotunneling occurs via the groundstate of the $(N+1)$-electron system, in (b) via an excited state of the $(N+1)$-electron system. Note, (b) requires a higher energy cost $\Delta E_{\mathrm{E}\to\mathrm{I}}$ for creating the intermediate state than (a). (c) Inelastic cotunneling transfers the N-electron system to an excited state which requires a bias between the electrochemical potentials of the leads fulfilling $E(N,l;\{V_i\}) - E(N,0;\{V_i\}) \leq e|V_{\mathrm{DS}}|$. Beyond this threshold, more and more cotunneling processes become available as indicated by two examples in (d), for which $\Delta E_{\mathrm{E}\to\mathrm{I}} + \Delta E_{\mathrm{I}\to\mathrm{C}} = 0$, $\varepsilon_{\mathrm{E}} \leq \mu_{\mathrm{E}}^{\mathrm{elch}}$ and $\varepsilon_{\mathrm{C}} \geq \mu_{\mathrm{C}}^{\mathrm{elch}}$.

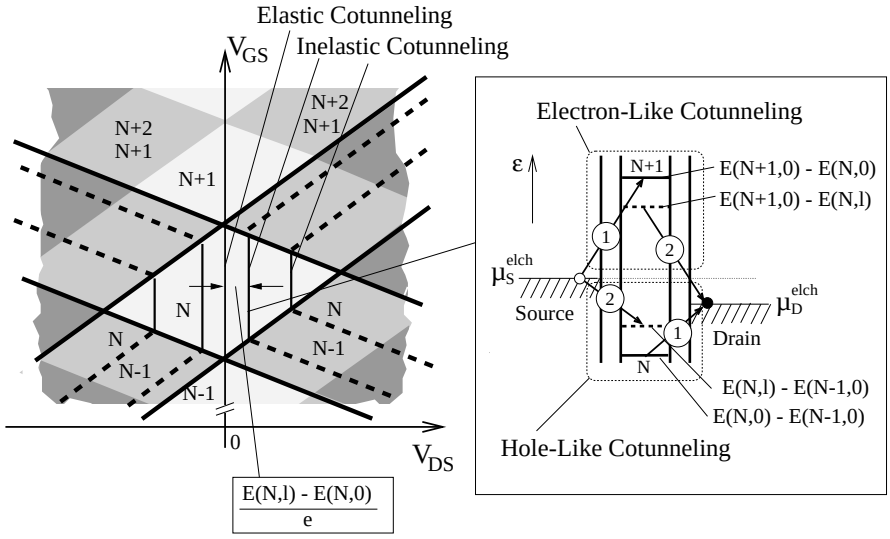

Fig. 6.5. Sketch of the transport regions of a quantum-dot system in the $(V_{\mathrm{GS}}, V_{\mathrm{DS}})$ plane. In the Coulomb blockade region confining N electrons in the quantum dot, borderlines are drawn at which inelastic cotunneling ending in an excited state of the N-electron system becomes possible. These borderlines end at respective borderlines of the single-electron transport channels using the same excited state. Right: Energy scheme demonstrating that electron- and hole-like cotunneling can both occur at the marked $(V_{\mathrm{GS}}, V_{\mathrm{DS}})$ operation point, although differently weighed by the energy costs for the intermediate state. In this case the hole-like cotunneling might dominate.

- For $|V_{\mathrm{DS}}| > 0$, the initial and final state of the N-electron system in the quantum dot can differ in energy, but they need not. Therefore, the quantum dot can be excited, and can loose again its excitation. If such an energy transfer between quantum dot and leads occurs, such a correlated two-electron tunneling process is denoted as *inelastic cotunneling*.

Since in a small quantum dot only few excited states are found in a certain energy window close to the groundstate, basically only elastical cotunneling occurs. This is different for a metal-like quantum-dot system where inelastic cotunneling is also found at small drain-source voltage.

With increasing $|V_{\mathrm{DS}}|$ beyond a borderline described by the general relation (6.6), more and more occupied states of the emitter and unoccupied states of the collector can be used for such electron-like and hole-like cotunneling processes involving the same initial and final states $|N, l; \{V_i\}\rangle$ and $|N, l'; \{V_i\}\rangle$ (see Fig. 6.3d and Fig. 6.4d). Therefore, not a peak but more a step-like change in the differential conductance $\mathrm{d}I_{\mathrm{DS}}/\mathrm{d}V_{\mathrm{DS}}$ can be expected at the vertical borderline in the $(V_{\mathrm{GS}}, V_{\mathrm{DS}})$ plane described by (6.6).

As it turns out, cotunneling can hardly explain the zero-bias anomaly observed at $V_{\mathrm{DS}} = 0$ in Fig. 6.2. Correlated tunneling processes involving more electrons have to be taken into account. In general, different cases for the quantum dot have to be distinguished leading to different behaviour:

- The energy ladder $E(n, k; \{V_i\}) - E(n-1, l; \{V_i\})$ with $n \in \{\cdots, N-1, N, N+1, \cdots\}$ and its position relatively to the electrochemical potentials of the leads determines the number of energy levels which are of importance.
- These levels can be either degenerate or non-degenerate.
- The tunnel coupling strength and the temperature are of importance, defining different behaviour of the quantum dot under same conditions given by $\{V_i\}$. The quantum mechanical phase coherence is destroyed with increasing temperature.

Even at parameter values where single-electron transport occurs, such correlated electron tunneling events modify the result compared to the orthodox theory. There, the energy costs for the intermediate state are the lowest. It leads for instance to *resonant tunneling* if $\mu(n; \{V_i\})$ is aligned with the electrochemical potentials $\mu_{\mathrm{S}}^{\mathrm{elch}}$ and $\mu_{\mathrm{D}}^{\mathrm{elch}}$: The quantum mechanical phase is preserved for electrons passing the island. For a small quantum dot with a well pronounced discrete excitation spectrum the line-shape of Coulomb blockade oscillations resembles at low temperature a Lorentzian [115].

In the following, we will restrict ourselves to small quantum dots for understanding the zero-bias anomaly observable in Fig. 6.2.

6.3 A Simple Model with Strong Impact: The Anderson Impurity Model

Before starting – a brief historic review:
Usually the resistivity of metal decreases with reducing the temperature due to the reduced electron scattering at thermal phonons and becomes constant at low temperature limited by the static disorder in the host crystal lattice

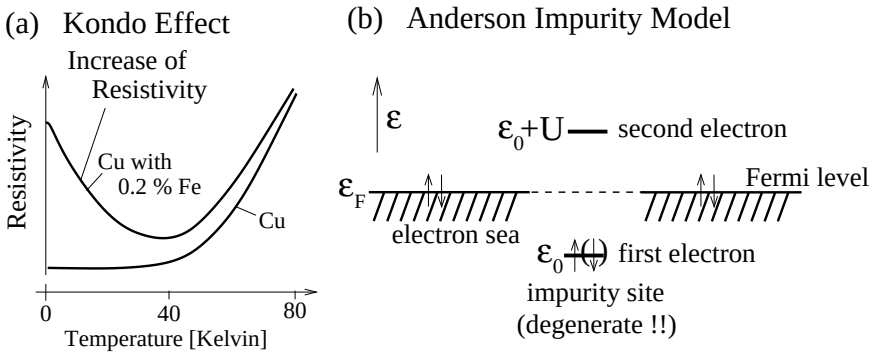

Fig. 6.6. (a) Kondo effect: Cu with diluted Fe impurities shows an increase in the resistivity at low temperature. (b) The Anderson impurity model describes an electronic level ε_0 bound to an impurity below the Fermi level ε_F of the conduction band which can be occupied either by a spin-up or spin-down electron due to tunneling between impurity site and conduction band. Occupation by two electrons at the same time is suppressed at low temperatures due to the interaction energy U.

felt by the conduction band electrons. In the 1930's it was observed [164] that in contrary to this expectation the resistivity increases again at low temperature for metals like Cu which include so-called magnetic impurities like Co or Fe in a concentration of less than 1% (see sketch in Fig. 6.6a). It took almost 30 years when in 1964 Jun Kondo demonstrated [165] that spin-scattering of conduction band electrons at these magnetic impurities explains this phenomenon. That is why this resistivity increase in metals with magnetic impurities is called *Kondo effect*. Another model introduced by P.W. Anderson in 1961 [161] – the so-called *Anderson impurity model* – can also be used to describe the essential physics. The Anderson Hamiltonian and the Kondo Hamiltonian map under certain conditions [166]. Techniques have been developed in the following years – denoted as numerical renormalization group techniques pioneered by K.G. Wilson [167]– allowing to solve these and extended models which predict the formation of non-trivial many-body states with approaching low temperature.

The basic ingrediences for the Anderson impurity model are sketched in Fig. 6.6b: A localized electronic site – caused for instance by a bound electronic state to an impurity ion – is embedded in a Fermi sea of conduction band electrons. Electrons of the conduction band can hop by quantum mechanical tunneling onto this impurity site and vice versa. Since the energy ε_0 for a single electron at the impurity site is below the Fermi level ε_F of the conduction band electrons, the energy level ε_0 at the impurity site is always

occupied by an electron. Important is the assumption that the energy level can be occupied by either an electron with the quantum number spin-up or spin-down – the energy level is *degenerate*. The occupation by two electrons at the same time is suppressed since this requires to overcome the Coulomb repulsion on this site described by the parameter U, and the energy level for the second electron lies therefore above the Fermi level, $\varepsilon_0 + U > \varepsilon_\mathrm{F}$.

Solving the Anderson impurity model, it turns out that it cannot be treated in perturbation at low temperature: Only considering the lowest-order tunneling processes, starting with elastic cotunneling between impurity and Fermi sea described in the previous Section, is not enough. At low temperature, all higher-order correlated tunneling events have to be included – a many-body state is formed, denoted as the *Kondo state*. Therefore, the internal degree of freedom in occupying the impurity site by a spin-up or spin-down electron acts as an effective scattering mechanism for conduction band electrons. The Kondo state is well developed below the so-called Kondo temperature T_K given by [168]

$$k_\mathrm{B}\, T_\mathrm{K} = \frac{\sqrt{\Gamma\, U}}{2} \cdot \exp\left[-\frac{\pi\left(\varepsilon_\mathrm{F} - \varepsilon_0\right) \cdot \left(U + \varepsilon_0 - \varepsilon_\mathrm{F}\right)}{\Gamma\, U} \right] . \qquad (6.12)$$

The Kondo temperature depends on the tunnel coupling described by $\Gamma = \hbar/\tau$, on the energetic distance $\varepsilon_\mathrm{F} - \varepsilon_0$, and on the on-site interaction energy U.

In 1988, two publications (L.I. Glazman and M.É. Raĭkh [169]; T.K. Ng and P.A. Lee [170]) pointed out that a single quantum-dot system resembles an extended Anderson impurity model. By this analogy, a link from quantum-dot systems to Kondo physics is given. About ten years later, in 1998 D. Goldhaber-Gordon and coworkers [171] could demonstrate the Kondo effect experimentally in quantum-dot systems, confirmed by Cronenwett *et al.* [172] and J. Schmid *et al.* [173]. The data of J. Schmid *et al.*, obtained in our laboratory, are used here. Earlier experiments by D. Ralph and coworkers [174] on a small charge trap embedded in a thin silicon nitride membrane between metal electrodes have also been interpreted as the Kondo effect.

The mapping of the quantum-dot system onto the (extended) Anderson impurity model could work under the following conditions (see Fig. 6.7):

1. The energy levels ε_0 and $\varepsilon_0 + U$ of the Anderson model are identified with the levels $\mu(N; \{V_i\})$ and $\mu(N+1; \{V_i\})$, respectively.
2. Although in most quantum dots N is not equal to 1, the fluctuation in the electron number are almost restricted to N and $N+1$ if the level spacings $\mu(N+2; \{V_i\}) - \mu(N+1; \{V_i\})$ and $\mu(N; \{V_i\}) - \mu(N-1; \{V_i\})$ are large compared to the thermal energy $k_\mathrm{B}T$ and the tunnel coupling $\Gamma = \hbar/\tau$.
3. Levels due to excited states of the N or $N+1$ electron system should be energetically well separated from the groundstate or not accessible due to

too small tunnel coupling to the leads and/or selection rules (see Section 5.9).

4. To observe (the later discussed) Kondo resonance in the region of N electrons confined to the dot, the *groundstate of the N-electron system on the dot has to be degenerate*, i.e., two orthogonal N-electron states should exist at the groundstate energy: $E(N,1;\{V_i\}) - E(N,0;\{V_i\}) = 0$. Usually, a spin degeneracy is assumed.

Due to the degeneracy, cotunneling through the quantum dot can occur in either state. Actually the quantum-dot system prefers both states, i.e., the systems gains energy by doing correlated electron tunneling permanently flipping the spin orientation leading to no preferred spin-polarization on the quantum dot site. The Kondo state is described as a spin-singlet state. Since for correlated tunneling, electrons have to come from occupied states in the leads and have to end in unoccupied states in the leads, the electronic states at the Fermi level are of importance. Evaluating the simple Anderson impurity model, correlated many-electron tunneling processes between dot and reservoir(s) lead to a sharp peak in the effective density of state (denoted as spectral function $A(\varepsilon)$) at the impurity site pinned to the Fermi level ε_F of the reservoir(s) (see Fig. 6.8a). This sharp peak disappears if the temperature T of the system is increased above the Kondo temperature T_K (see Fig. 6.8b). Although $\varepsilon_0 < \varepsilon_F$ and $\varepsilon_0 + U > \varepsilon_F$, due to this effective density of state at the Fermi level on the impurity site (respectively, quantum dot site), there is a peak in the differential conductance through this impurity (respectively, quantum dot) around $V_{DS} = 0$. This pinning to ε_F is independent of the position of ε_0 below ε_F. It affects only the Kondo temperature T_K, i.e., the temperature below which the Kondo resonance saturates. As described

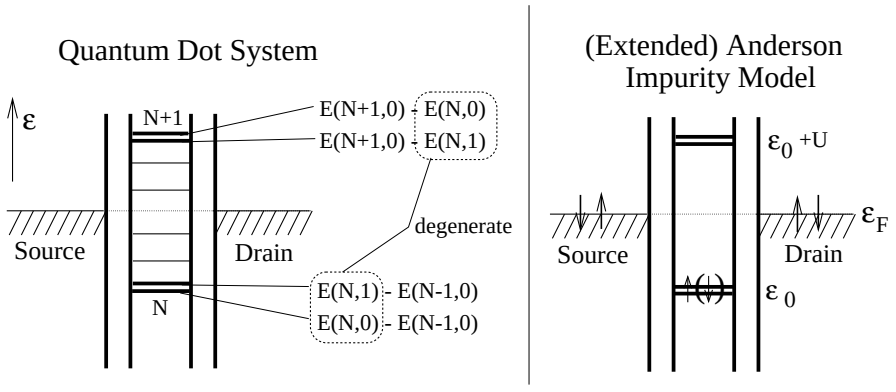

Fig. 6.7. Mapping of a quantum-dot system onto the (extended) Anderson impurity model. A degeneracy in the groundstate of the N-electron system is required. The degeneracy is indicated by the double-line. Here, the degeneracy in the Anderson impurity model is explicitely shown in the same way.

by (6.12), T_K is lowest for $\varepsilon_F - \varepsilon_0 = \varepsilon_0 + U - \varepsilon_F$, i.e., in the middle of the Coulomb blockade regime, where $\varepsilon_F - \varepsilon_0 = U/2$. At this position, (6.12) reads

$$k_B T_K^{min} = \frac{\sqrt{\Gamma U}}{2} \cdot \exp\left[-\frac{\pi U}{4\Gamma}\right] . \tag{6.13}$$

For a certain ratio between U and Γ, i.e., $\Gamma = \beta \cdot U$, the Kondo temperature increases linearly with U. For $\Gamma \approx 0.2 \cdot U$ and values $U = 1$ meV to $U = 2$ meV, which are typical for the presented quantum-dot systems, we obtain $T_K^{min} = 50$ mK to 100 mK. Below T_K^{min}, the quantum-dot system described by the Anderson impurity model becomes conductive over the whole Coulomb blockade regime reaching even the conductance $2e^2/h$, which is equal to the conductance of a spin-degenerate one-dimensional channel where no tunnel barriers are present. This behaviour is sketched in Fig. 6.8c.

From the dependence (6.12) of the Kondo temperature T_K on the tunnel coupling it is clear, that with enhancing the coupling T_K is increased. This is consistent with the experimental data presented in Fig. 6.2: At fixed temperature, a peak develops at $V_{DS} = 0$ with increasing the tunnel coupling. The

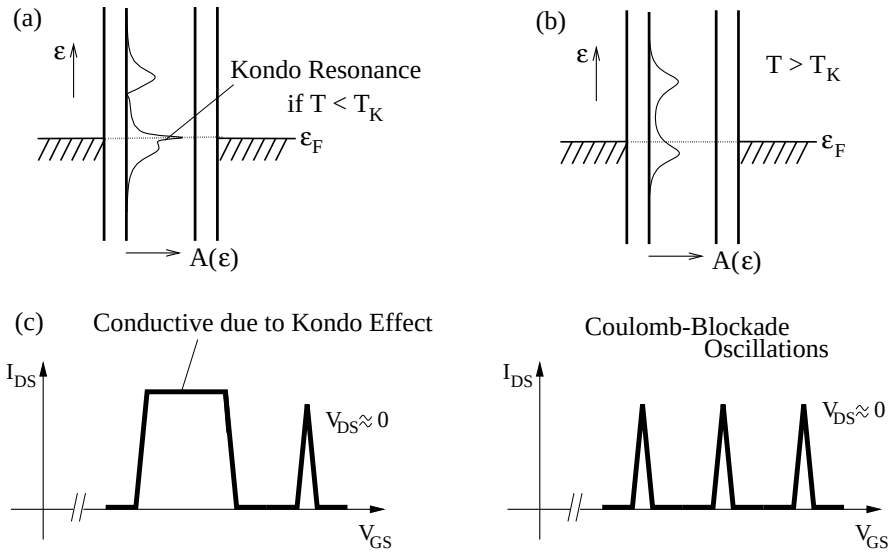

Fig. 6.8. The spectral function $A(\varepsilon)$ on the quantum dot site: It reflects in the limit of vanishing tunnel coupling the energy scheme used before. (a) below Kondo temperature, (b) above Kondo temperature (from J. Schmid, parameters are $(\varepsilon_F - \varepsilon_0)/U = 0.2$, $\Gamma/U = 0.075$, $k_B T/U = 0.01$ for (a) and 10 for (b)). For increasing the drain-source voltage, the whole spectral function changes. Two peaks are expected, pinned to both Fermi levels of the leads. [175, 176]. (c) If the prerequistes for the formation of a Kondo state are fulfilled, the quantum dot is highly conductive over the whole Coulomb blockade region. At higher temperature, the Kondo state is destroyed and the usual Coulomb blockade oscillations are recovered.

peak is first to be seen close to the single-electron-tunneling peaks, and with further increasing the tunnel coupling in the middle of the Coulomb blockade regime. Further experiments are presented in the following supporting the link to Kondo physics.

6.4 Test of Further Experimental Properties Predicted by the Anderson Impurity Model

First is tested the temperature dependence of the zero-bias anomalies, then – by applying a magnetic field – the degeneracy of the electron system confined in the quantum dot. Both results confirm what is expected from a Kondo resonance.

6.4.1 Temperature Dependence

In Fig. 6.9a, a zero-bias anomaly is presented, measured on a similar quantum-dot system but under better experimental conditions than the one presented in Fig. 6.2. The peak in the differential conductance $\mathrm{d}I_{\mathrm{DS}}/\mathrm{d}V_{\mathrm{DS}}$ at $V_{\mathrm{DS}} = 0$ is strongly expressed at $T = 25$ mK. With increasing the temperature to 800 mK (see Fig. 6.9b), this peak disappears, whereas the other features in the differential conductance in the $(V_{\mathrm{GS}}, V_{\mathrm{DS}})$ regime remain almost unaffected. In Fig. 6.9c the temperature dependence of the differential conductance along the trace marked in Fig. 6.9a is plotted: At low temperature the peak at $V_{\mathrm{DS}} = 0$ exceeds e^2/h, at $T = 800$ mK the peak is completely disappeared whereas the background is not changing with temperature. The observation of a peak in the differential conductance disappearing with increasing the temperature is in qualitative agreement with the predictions of a Kondo resonance, and fits to the estimate given with (6.13).

At each gate-source voltage value V_{GS}, the Kondo temperature is a different one. The peak height should just depend on the ratio T/T_{K}, i.e., the temperature dependence at the respective gate voltage position can be rescaled. Systematic measurements have been undertaken [177, 178, 92], demonstrating that indeed an universal behaviour exists, confirming the interpretation.

6.4.2 Lifting the Degeneracy with Magnetic Field

To investigate whether a degeneracy exists for the groundstate of the electron system confined in the quantum dot, a magnetic field is applied in the plane of the two-dimensional electron system (see Fig.6.10a). The differential conductance $\mathrm{d}I_{\mathrm{DS}}/\mathrm{d}V_{\mathrm{DS}}$ is measured in the $(V_{\mathrm{GS}}, V_{\mathrm{DS}})$ plane for various magnetic field values B. In Fig.6.10b, the data are show for $B = 0$ T, $B = 2$ T, and $B = 4$ T. A splitting of the Kondo resonance is observed, with a suppression of the differential conductance at $V_{\mathrm{DS}} = 0$.

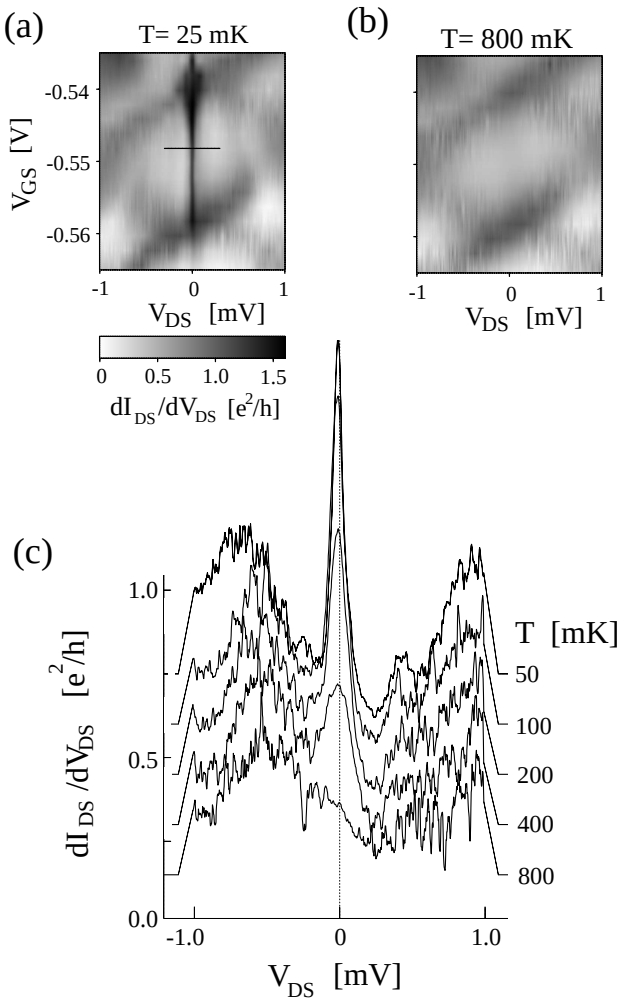

Fig. 6.9. Temperature dependence of the zero-bias anomaly: (a) Differential conductance $\mathrm{d}I_{\mathrm{DS}}/\mathrm{d}V_{\mathrm{DS}}$ in greyscale in the $(V_{\mathrm{GS}}, V_{\mathrm{DS}})$ plane, measured at $T = 25$ mK. A well pronounced zero-bias anomaly is observed in the Coulomb blockade regime. (b) At $T = 800$ mK, the zero-bias anomaly is not visible. (c) Differential conductance traces $\mathrm{d}I_{\mathrm{DS}}/\mathrm{d}V_{\mathrm{DS}}$ vs. V_{DS} in the middle of the Coulomb blockade region along the line indicated in (a) for different temperature values given on the right side. The axis on the left is valid for the trace taken at highest temperature. The other traces are offset. (adopted from measurements of J. Schmid [92] in our laboratory)

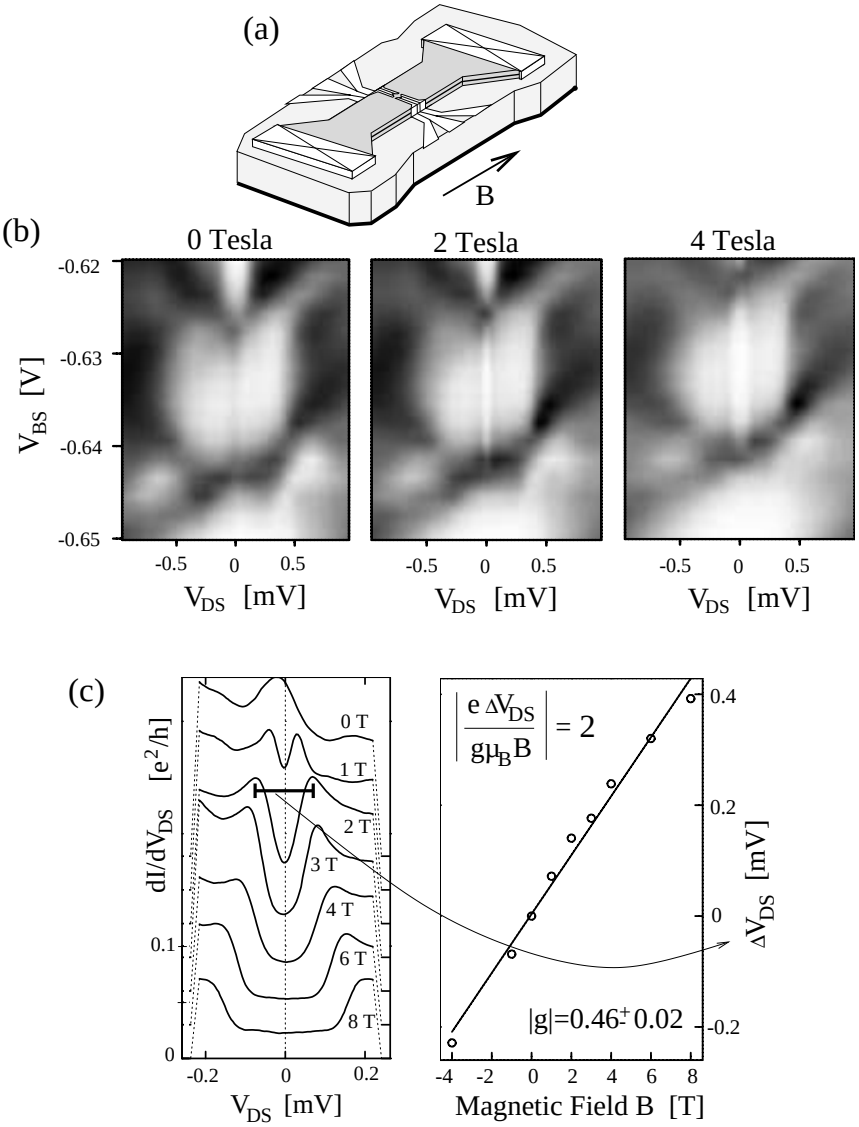

Fig. 6.10. (a) A magnetic field B is applied in the plane of the quantum dot system. (b) Differential conductance $\mathrm{d}I_{\mathrm{DS}}/\mathrm{d}V_{\mathrm{DS}}$ in the $(V_{\mathrm{GS}}, V_{\mathrm{DS}})$ plane in greyscale for three different magnetic field values. The data are taken under same condition as those of Fig. 6.2. (c) Traces $\mathrm{d}I_{\mathrm{DS}}/\mathrm{d}V_{\mathrm{DS}}$ vs. V_{DS} taken in the middle of the Coulomb blockade regime for different B. Obviously, the zero-bias anomaly splits with magnetic field. The splitting $\Delta V_{\mathrm{DS}}(B)$ fits to twice the Zeeman splitting.

This is expected: With applying the magnetic field B the spin-degeneracy is lifted by the Zeeman energy $E_Z = g\mu_B B$ where g denotes the Landé factor and μ_B the Bohr magneton. Since at $V_{DS} = 0$ only elastic processes are possible, spin-flip processes by correlated tunneling are suppressed. The internal degree of freedom can no longer be used. The Kondo state cannot develop. This becomes different at finite bias voltage V_{DS} fitting to the Zeeman energy, $e|V_{DS}| = E_Z$. Spin-flip fluctuations become possible again by inelastic correlated tunneling, similar to what was described in Section 6.2 for the lowest-order correlated tunneling process – the cotunneling. Indeed, calculation [175, 179, 176] confirm that peaks in the differential conductance should be observable at the respective bias, although with reduced amplitude.

The splitting, i.e., the voltage difference ΔV_{DS} between the V_{DS} values at which the peak appears on either sides of $V_{DS} = 0$ should reflect twice the Zeeman energy E_Z. The respective values ΔV_{DS} are plotted versus the applied magnetic field B in Fig.6.10c. Deducing the slope $\mathrm{d}\Delta V_{DS}/\mathrm{d}B$ from the data and using

$$g = \frac{1}{\mu_B}\frac{\mathrm{d}E_Z}{\mathrm{d}B} = \frac{1}{2}\frac{e}{\mu_B}\frac{\mathrm{d}\Delta V_{DS}}{\mathrm{d}B}, \tag{6.14}$$

we extracted $|g| = 0.46 \pm 0.02$ which is close to the g-factor of bulk GaAs, indicating that a spin-degenerate groundstate is present at $B = 0$ for this Coulomb blockade regime.

6.5 Absence of Odd-Even Parity Behaviour for Kondo Resonances in Quantum Dots

In several papers [171, 172], an odd-even parity behaviour with the number of electrons in the quantum dot has been expected and reported for the occurrence of the Kondo resonance. Often this was not the case for our quantum-dot systems where we observe [180] the zero-bias anomaly in two adjacent Coulomb blockade regimes (see Fig. 6.11), i.e., for N and $N + 1$. Where does the expectation for an odd-even parity behaviour comes from? It is based on the Constant Interaction Model described in Section 4.3 where the electron-electron interaction on the dot is taken to be constant – decribed by a capacitance – and where a single-particle energy spectrum is assumed which does not depend on the electron number. By filling up single-particle levels which are spin-degenerate, at each odd number of electrons on the dot, the highest electron level is half-filled, i.e., degenerate and occupied only by one electron. This is one supposition of the Anderson model predicting a Kondo resonance. With even number of electrons the highest single-particle level is filled with two electrons – a Kondo resonance should not occur.
Is this Constant Interaction Model a realistic model?

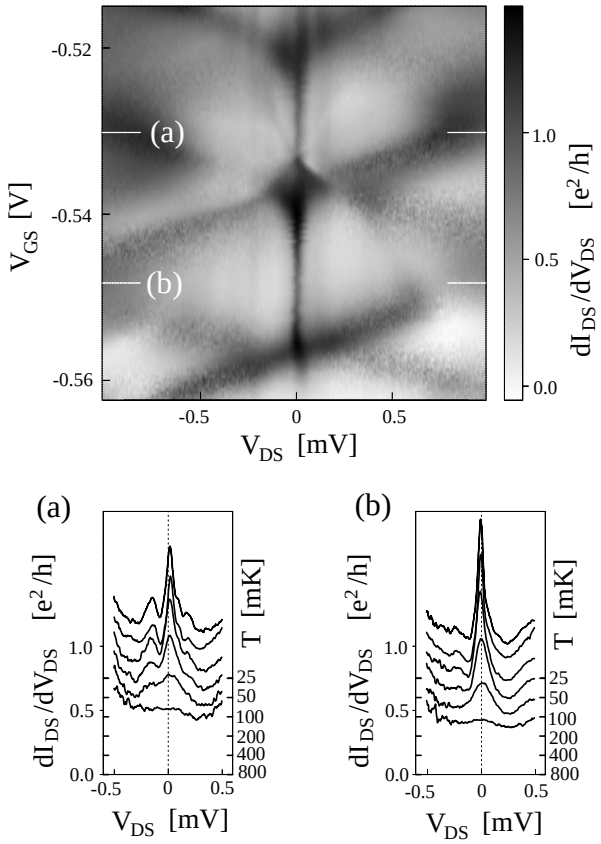

Fig. 6.11. Differential conductance $\mathrm{d}I_{\mathrm{DS}}/\mathrm{d}V_{\mathrm{DS}}$ in the $(V_{\mathrm{GS}}, V_{\mathrm{DS}})$ plane enclosing two Coulomb blockade regions. Obviously zero-bias anomalies are observed in both Coulomb blockade regions. The zero-bias anomalies disapear with increasing the temperature as shown in (a) and (b) for traces marked in the greyscale plot. (adopted from J. Schmid *et al.* [180])

1. Transport experiments on quantum dots defined in III-V semiconductor heterostructure pillars have shown that Hund's rule is working in such dots [107]: Instead of filling up the levels with spin-up and spin-down electrons consecutively, parallel spin configurations are favourable due to exchange interaction. The odd-even behaviour in N for the occurrence of Kondo resonances should be broken in such a case.
2. In quantum dots of few electrons where the electron-electron interaction is dominating over the confinement energy, correlation effects due to electron-electron interaction have to be taken into account [8]: The degeneracy of the groundstate energy of the N-electron system is not expected to change obviously in an odd-even manner with N.

Degeneracy of the level besides spin degeneracy – for instance, orbital degeneracy due to the symmetry of the confining potential – is not treated by the Anderson impurity model. Kondo effect at a transition point between a singlet and triplet state of the quantum dot has been reported by Sasaki *et al.* [181].

6.6 Conclusions

In conclusion, the picture of single-electron tunneling breaks down under certain conditions. Correlated electron tunneling becomes important with lowering the temperature. In certain Coulomb blockade regions, the conductance reaches values up to $2\,e^2/h$ as was demonstrated by van der Wiel and coworkers [178]. Evaluating a simple model – the Anderson impurity model – predicts basic features observed in experiments. Meanwhile, the Kondo effect has also been reported for quantum dot systems embedding a carbon nanotube [182].

A quantitative comparison has to be done with caution: All experimentally investigated quantum-dot systems have still excited states close to the groundstate. These have to be taken into account. Additional peaks in the differential conductance present in the experimental data of Fig. 6.11a indicate this. Correlating experimentally the energy spectrum of the quantum dot with the observation of zero-bias anomalies is still a challenge. This would allow a quantitative comparison with theoretical predictions done in the last years for $V_{\mathrm{DS}} = 0$, but also for $|V_{\mathrm{DS}}| > 0$.

Especially the more complex spin configurations due to electron correlations in the quantum dot are here of interest. However, not only the total spin of the confined electron system in the quantum dot seems to be important, but also the tunnel coupling to the leads. This could be concluded from recent experiments of our group [183, 184].

7. Fundamental Physical Contraints on Single-Electron Transistors for Highly Integrated Digital Circuits

At first glance, single-electron transistors can be considered as the ultimate transistors: The current is carried by single electrons passing the island one-by-one, switched on and off by single electron charges in the island's surrounding. Dealing with the smallest amount of charge, K.K. Likharev [25] suggested in 1987 that integrated circuits based on single-electron transistors would lead to lowest power consumption. In the same article it was also pointed out that the sensivity to single electron charges is a weakness if a large number of such transistors have to work reliable in a circuit. Fluctuations and rearrangements of background charges can hardly be controlled: They are strongly affecting the characteristics of these ultimate transistors. Later, simulations were presented by A.N. Korotkov, R.H. Chen and K.K. Likharev emphasizing this weakness [185].

The metal-oxide-semiconductor field-effect-transistor (MOSFET) is *the common* device of today's integrated digital circuits. SETs and MOSFETs belong to the class of electronic devices where an energy barrier is electrostatically controlled to turn on and off the current through the device. Belonging to the same class of switches, SETs and MOSFETs obey the same electrostatical constraints and limitations. Can the single-electron transistor be a candidate for replacement of MOSFETs as it still seems to be the belief (for instance, [186, 187, 188]), although pessimistic views are given [189, 185, 2]?

To address this question, the fundamental physics constraints on the devices for application in highly-integrated digital circuits have to be discussed. These are given by

- the integration density,
- the overall power dissipation,
- the energy dissipation per operation,
- the reliability of the circuit,
- speed consideration, and
- manufacturability.

These constraints defines the most suitable device for the respective circuit concept, and its limitations. Here we will analyse by fundamental physical considerations what single-electron transitors have to fulfill and how they behave in comparison to MOSFETs. The final result in this Chapter is that SETs are not capable in replacing MOSFETs in highly integrated digital

circuits. An analysis based on numerical simulations of SET circuits has been done by A.N. Korotkov and coworkers [185, 190] exploring the parameters space for getting these circuits into operation. Also their results demonstrate the limits in using these transistors in digital circuits. [1]

7.1 On the Evolution, Nature, and Limitations of Highly Integrated Digital Circuits

N. Negroponte [191] described in his book 'Being Digital' the advantages of digital representation of information for storage and transfer in comparison to an analogeous representation. Working with digital representation allows manipulation of the data for data compression, data packaging, encryption and error corrections. The limited bandwidth of transmission channels or the limited capacity of storage media can be better used by doing compression and packaging of data. Shortly, using digital representation of information enables 'Multimedia'. However, taking advantages of digital information representation requires computation power at information source and drain: The more 'knowledge' and 'computational power' is usable, the less information has to be transmitted and stored. Typical examples are the compression and decompression of audio and video data. Tasks like speech recognition and video animation require complex computation limited in time. This is done in integrated digital circuits where high complexity – a measure might be the number of point-to-point connections [192] – is realized cheaply in parallel by lithography.

Integrated circuits (ICs) were invented independently by J.S. Kilby [193, 194] and by R. Noyce [195] in 1959, honoured by the Nobel prize in the year 2000. [2] They described and demonstrated how transistors and other components can be integrated on a single piece of semiconductor material, connected by small metal lines to an electrically functional circuit. In 1975 G. Moore [196] presented his observation of the *exponential increase* in functionality of integrated circuits on a chip over the past years. This had been achieved by improvements in photolithography, by increasing the die (chip) size and cleverness in layout and circuit design. Such an exponential improvement – denoted as the 'learning curve' [3] – is also known for other products. But the semiconductor industry has succeeded in extending the progress described by Moore's plot by several orders of magnitude over the last decades: Every three years a new IC generation has been introduced to the market. The number of bit memory cells on a memory chip has been four times higher

[1] A.N. Korotkov and coworkers emphasize from the beginning differences between SETs and MOSFETs whereas here first the common properties are discussed before pointing out the differences.

[2] For J.S. Kilby. R. Noyce died in 1990.

[3] Decay in price per transistor (respectively, bit cell) versus cumulative number of produced transitors (respectively, bit cells).

than on a memory chip three years before, the number of logic gates has been two to three times higher than in the previous generation. The speed of microprocessors, measured in millions of instructions per second (MIPS), has improve by 40% to 50% every year. By learning how to implement, design and manufacture integrated circuits denser and more efficient – for instance also by using wafers of larger diameter –, the cost per function has reduced 30% per year and the processing cost of silicon ICs has remained almost constant at 4 US$/cm^2 to 10 US$/cm^2 over the years. In 2002 memory chips can be made offering 1 Gigabits of storage capacity, and the number of transistors in a microprocessor-like logic circuit has grown to about $2 \cdot 10^7/\text{cm}^2$. To reach such densities, the ICs nowadays are realized with up to six metal wiring layers connecting the transistors. The on-chip clock frequency has reached 2 GHz. [4] As a drawback, the power dissipation has rised to several tens of Watt.

Due to their improved performance versus price relation, integrated circuits have become more and more attractive for diverse applications and have enabled other technologies which creates new customers' 'needs'. Digital ICs are a mainstream technology which justifies huge investments in developing this technology. But huge investments forces the industry to converge in their processing technology using the same equipment pushing non-mainstream technology into niche applications.

The overall power dissipation in highly-integrated electronic circuits is a big concern due to several reasons: It limits the integration density of logic gates on chip, but also the integration of many chips into large systems. High-performance processor chips are going to dissipate about 100 W which requires an effective heat removal technique making their application expensive or even unpractical. High temperature affects the characteristics of the electrical devices and causes reliability and degradation problems. Large power dissipation increases packaging costs and limits the use of portable devices due to the limited battery capacity. High energy consumption are costs and an environmental concern. Therefore, concepts of reducing the energy dissipation in highly-integrated circuits are required which still fulfill complex computation tasks in an appropriate time. [5]

Concepts have to tackle on different, but not necessarily separated levels: software algorithm, algorithm implementation, circuit design, and – of course – hardware technology.

The key device in today's highly-integrated digital circuits is the metal-oxide-semiconductor field-effect transistor (MOSFET), demonstrated by D. Kahng and M.M. Atalla [198] in 1960, patent filed by M.M. Atalla [199] in 1960 and described in detail by S.R. Hofstein and F.P. Heimann [200] in 1963.

[4] Pentium 4 with $4 \cdot 10^7$ transistors.

[5] High-performance chips are limited to 30 to 100 W/cm^2, battery powered systems to 1 W/cm^2 and low-power chips to 1 mW/cm^2 when doing computation [197].

Early proposals of solid state field effect triodes were done by J.E. Lilienfeld [201] in 1926 and O. Heil [202] in 1935, and conductance modulation in thin semiconductor films by field effect was demonstrated by W. Shockley and G.L. Pearson [203] in 1948. A schematic cross-section of a MOSFET is shown in Fig. 7.1. Due to different type of doped areas in the semiconductor, free majority carriers (electrons in case of nMOSFET, holes in case of pMOSFET) are hindered in crossing the channel region between source and drain contact: In case of a nMOSFET, there is an energy barrier for the electrons in the conduction band entering the channel region, in case of pMOSFETs, there exists an energy barrier for electrons in the valence band leaving the channel region, and therefore creating holes in the filled valence band. Thermal activation allows charge carriers to overcome this energy barrier but the probability becomes exponentially small with lowering the temperature or with increasing the height of the energy barrier. By changing the electrostatic potential of the gate electrode, this energy barrier is changed near the surface of the semiconductor below the gate leading to an exponential dependence of the current I_{DS} between drain and source as a function of the gate-voltage change ΔV_{GS},

$$I_{\mathrm{DS}} \propto \exp\left[\pm\frac{e\Delta V_{\mathrm{GS}}}{\eta\, k_{\mathrm{B}} T}\right] \ . \tag{7.1}$$

The positive sign is valid for electrons as carriers in the channel, negative sign for holes. The factor η is limited to $0 < 1/\eta \leq 1$. This *ideality factor* $1/\eta$ will become very important in the later discussion.

Depending on the type of free charge carriers – electrons or holes – a positive change in the gate-source voltage increases or decreases the current. A nMOSFET behaves therefore complementary to a pMOSFET on a gate voltage change of same polarity (see Fig. 7.1). Changing the gate-source voltage for nMOSFET above a certain threshold value $V_{\mathrm{GS}}^{(\mathrm{thr,n})}$, the energy barrier is overcome. Further increasing the gate-source voltage leads to accumulation

---

Fig. 7.1. (Right page) (a) Schematic cross sections through Metal-Oxide-Semiconductor Field Effect Transistors of n- and p-type. A doped silicon substrate is partially highly counter-doped. These regions act as source and drain with electrons or holes as free charge carriers. A gate electrode, made of highly doped poly-silicon and isolated by an oxide from the substrate, covers the channel region between source and drain. By applying a gate voltage, the carrier concentration in the channel is controlled. (b) Conduction and valence band profile between source and drain along the channel of the nMOSFET (left) and pMOSFET (right) at 'off'-state, at threshold and at 'on'-state. In case of the nMOSFET, electrons of the conduction band are acting as free charge carriers in the channel, whereas in case of the pMOSFET holes in the valence band are used. (c) With increasing the gate-source voltage V_{GS}, the current I_{DS} is turned on for the nMOSFET, and turned off for the pMOSFET. The turn-off is done in both cases exponentially with the applied gate voltage.

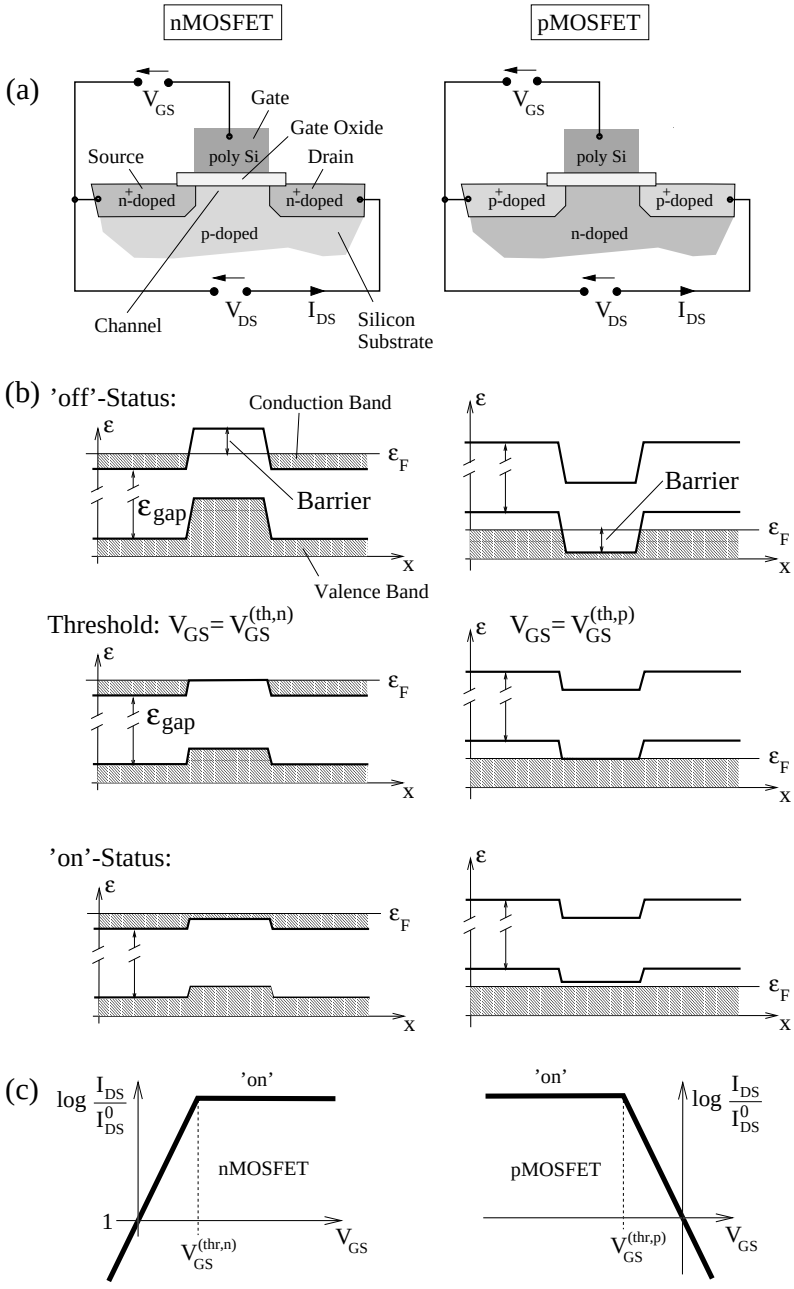
nMOSFET
pMOSFET
(a)
V_{GS}
Gate
Gate Oxide
Source
poly Si
Drain
n-doped
n-doped
p-doped
Channel
V_{DS}
I_{DS}
Silicon Substrate
p-doped
p-doped
n-doped
(b) 'off'-Status:
Conduction Band
ε
ε_F
ε_{gap}
Barrier
Valence Band
x
Threshold: $V_{GS} = V_{GS}^{(th,n)}$
$V_{GS} = V_{GS}^{(th,p)}$
'on'-Status:
(c)
$\log \frac{I_{DS}}{I_{DS}^0}$
'on'
nMOSFET
pMOSFET
1
$V_{GS}^{(thr,n)}$
$V_{GS}^{(thr,p)}$
V_{GS}

of electrons under the gate enhancing the conductivity. Similar behaviour is observed for the pMOSFET with holes, but for negative going gate voltage below $V_{\mathrm{GS}}^{(\mathrm{thr,p})}$. Therefore, beyond turn-on threshold, MOSFETs offer

$$I_{\mathrm{DS}} \propto |\Delta V_{\mathrm{GS}}| \,. \tag{7.2}$$

The industry has succeeded in keeping the 'on' current per channel width w in the range of $I_{\mathrm{DS}}^{\max}/w = 0.5$ mA/μm over the years.

Integrated digital circuits, based on complementary MOSFETs, are called CMOS circuits. The circuit concept based on complementary working transistors was introduced 1964 by W.K. Reymond [204]. Examples for basic circuits acting as logic gates are given later.

Mainly by lithography improvements, the transistors and the circuit can be shrinked down in its spatial dimensions. In 1974, R.H. Dennard and coworkers described a constant-electric-field scaling concept [205]. The industry has not followed all the years these scaling rules [206, 197], but they reflect the basic trend:

> All lateral and vertical spatial dimensions are shrinked down by a scaling factor $\kappa < 1$ (see Fig.7.2). To scale the depletion lengths like the spatial dimensions, the dopant concentration must be increased by $1/\kappa$. The applied voltages have to be reduced by a factor κ. As the result the gate and junction capacitances decrease with κ. Therefore the delay (due to the RC time constant) in switching a logic gate is reduced by κ, and the energy dissipation per switching is reduced by κ^3.

Therefore, only due to shrinking the circuit's functional density increases, the circuit becomes faster and consumes less energy which leads to improved performance. [6]

CMOS circuits cover most of today's integrated circuit market. The reason is given by the US Semiconductor Industry Association (SIA) stating in 1994 [207]:

> *CMOS transistors enable the only known circuit configuration that draws 'zero power' when not switching; it is the only known technology that is capable of achieving the required computational complexity and still satisfy the power dissipation limitations of low-cost packaging technology.*

This statement has to be challenged by any new proposal intended to replace this circuit concept in their task. The advantages of CMOS base on three transistor characteristics, mainly responsible for these esteemed properties:

- Transistors with exponential switch-off characteristic.

[6] The metal wiring has not been shrink in the same way: To keep the resistance low, the number of wiring layers has increased. Nowadays up to six Cu wiring layers are used in high performance microprocessors.

- Two types of transistors behaving complementary in gate-source voltage.
- Charge accumulation in the turned-on region increasing the conductivity.

To emphasize, the CMOS technology was not used from the beginning for integrated circuits, but has become the dominating technology in the 1990's due to an evolutionary process.

Several papers have described in the past the possible showstoppers for shrinking the transistors: Dopant distribution or oxide thickness variations might limit the manufacturability of highly-integrated circuits [208, 209, 210], since too large variations in the electrical parameters of single transistors lead to malfunction of the whole electronic circuit. It is the nature of today's digital integrated circuits, that millions of transistors on a single chip and billions of transistors on a wafer have to work for matching the designed circuit performances and for giving a reasonable manufacturing yield keeping

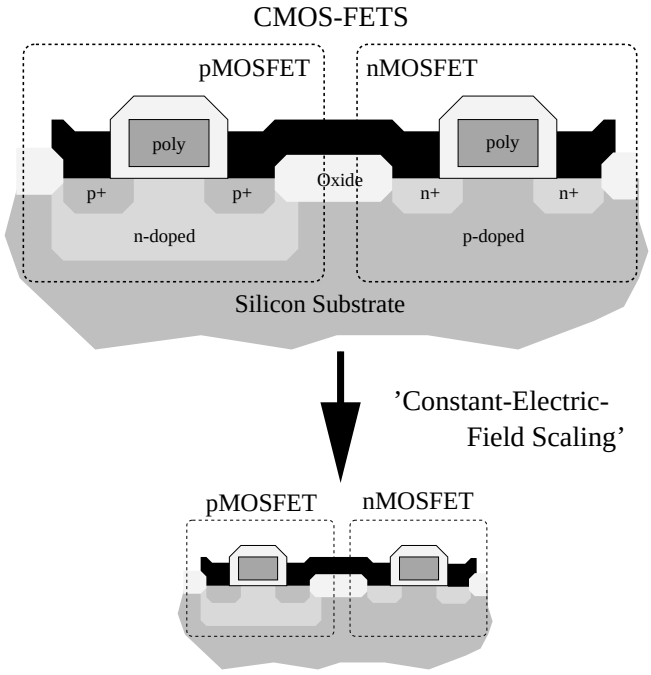

Fig. 7.2. Constant-Electrical-Field Scaling of CMOS: All spatial dimensions – horizontally and vertically – are shrinked by the scaling factor $\kappa < 1$, the dopant concentrations N_A and N_D must be increased by $1/\kappa$ to scale the depletion lengths, and the applied voltages have to be reduced by the factor κ. Such scaling increases the density by $1/\kappa^2$, the speed by $1/\kappa$ and decreases the energy dissipation by κ^3 for the same task. As the result, shrinking leads to a high gain in performance of the circuitry.

the manufacturing costs low. Replacement of non-working circuit parts by a substitutional circuit, co-integrated on the chip for this purpose, does not overcome this constraint. Unreliable logic gate would require additional overhead circuitry, and therefore costs silicon real estate and energy. Redundant integration is a practicable concept to increase the manufacturing yield where many identical circuit part exists (like in a memory array).

In 2002, for commercially available high-end ICs, the minimum feature size – typically the gate length between source and drain – has decreased to 0.13 μm. But more severe, the gate oxide thickness has decreased to about 4 nm which is less than eight times the lattice constant (0.54 nm) in [100] direction of the silicon crystal. A further decrease leads to the regime where the gate oxide becomes leaky due to quantum mechanical tunneling – a fundamental limit for the device. Silicon MOS transistors with about 50 nm gate length have been presented on electron device conferences in the 1990s with reasonable dc characteristics [211, 212, 213]. Even smaller transistors have been investigated in the last years down to 20 nm gate length [214], where the gate oxide becomes leaky and where from 30 nm to 20 nm a degradation of the 'on' to 'off' current ratio due to 'short channel effects' is significant. The perspect, challenges and limitations of CMOS in view of the year 2001 is given in a special issue of the Proceeding of the IEEE [215].

On the same conferences and in journals, realizations for single-electron transistors made from Silicon [83, 216, 217, 218] or metal [219, 220, 221, 222, 187] were presented goaling 77 K or even room-temperature operation. Circuit proposals for the use of single-electron transistors remind on circuit concepts used for conventional transistors [25, 223, 224, 225].

7.2 Basic Concept of Digital Circuits

A.W. Lo described the basic concept of digital circuits in the early 60's [226, 227]. It was repeated, emphasized and applied several times over the decades by researchers from IBM, like R. Keyes [228, 229, 230, 231, 232] and R. Landauer [233, 234, 235]. The whole digital circuit consists of elementary networks which fulfill Boolean logic functions and network elements which allow to store the bit information if required. The elementary networks has to deliver a complete set of *logic gates* like {NOT; AND} or {NOT; OR}. The output of a logic gate has to act as an input to the next logic gate. A.W. Lo characterized the **basic requirements for the elementary network** by the keywords 'Quantization', 'Fan-out and Fan-in', 'Directively and Isolation', sketched in Fig. 7.3.

- **'Quantization'** means in his words *the ability to preserve the standard physical representation of the bit representation '0' and '1'.*
- **'Fan-out'** describes the requirement that *the output of an elementary network serves as inputs to more than one elementary network.*

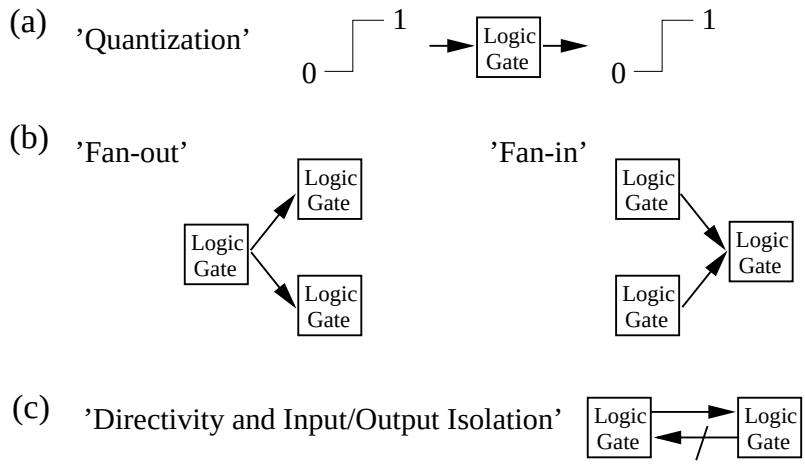

Fig. 7.3. Basic requirement due to A.W. Lo (1961) for the physical realization of logic gates: (a) 'Quantization', i.e., the ability to preserve the physical representation of logic '0' and '1'. (b) 'Fan-out' and 'Fan-in'. (c) Directivity and Input/output Isolation.

- **'Fan-in'** describes the requirement that *the output of more than one elementary network can jointly serve as the input to another network.*
- **'Directively and Isolation'** – denoted by R. Keyes as 'Input-Output separation'– means *a clear designation of cause and effect to insure that the controlling networks dictate the behaviour of the controlled networks.*

Nowaday's digital ICs rely on these concepts. They insure that the behaviour of the circuit is well predicable, and therefore easy to design and extend by additional circuits without interfering.

> The physical bit representation is done in today's digital electronic circuits by working between two electron reservoirs of different electrochemical potentials allowing locally bit signal restoration. These two electrochemical potential levels ('voltage levels') which are present on the input and output nodes connecting the logic gates. During computation, charges are moved around to change the electrochemical potentials and – linked to that – the electrostatic potentials of the nodes.

The amount of charge required to change the bit status depends on the node capacitance inherently given by the electronic devices used in the logic gates and their interconnects. Drawback of working between reservoirs of different electrochemical potentials is a permanent stand-by current which has to be minimized. The concept of complementary working switches helps here.

Note, computational concepts which rely only on guiding energy or charge quantities – representing the bit status – through a network doing computation *do not fulfill Lo's requirements*, because imperfection or distortion of

the circuit causes a degradation of the physical bit representation. Therefore errors in the computation result are unavoidable if these concepts do not incorporate a mechanism which allows bit signal restoration.

7.3 Power Dissipation in Logic Gates with Complementary Working Switches

In Fig. 7.4, two elementary logic gates – a 'NOT' and a 'AND-NOT' gate – are shown realized by using complementary working switches – denoted as n- and p-switch. [7] Between the supply terminals, the voltage V_{DD} is applied. The logic state '0' is represented by a voltage level close to the 0 V level of the negative supply terminal, the logic state '1' by a voltage level close to the voltage level V_{DD} of the positive supply terminal. With an input signal representing the logic status '0', the n-switch is 'off' whereas the p-switch is 'on'. With a logic '1' at the input, the n-switch is 'on' and the p-switch is 'off'. Therefore, with either '0' or '1' at the inputs, the elementary circuits of Fig. 7.4 connect the output node Y *either* to the positive *or* the negative supply terminal. At the same time, the node Y is almost disconnected from the respective other terminal. This is the strength of these circuit configurations:

> Circuits using complementary working switches in series ensure under static conditions that no high conductive connection exists between the positive and the negative supply terminal.

Current flow between both terminals is limited to a *leakage current* I_{off} through a switch in the 'off' state driven by almost the full voltage V_{DD} dropping over the switch. It leads to a permanent dissipation for each elementary logic gate of the order

$$P_{\mathrm{leak}} = I_{\mathrm{off}} \cdot V_{\mathrm{DD}} \ . \tag{7.3}$$

Small *standby power* P_{leak} would allow the integration of a large number of logic gates.

For switching the output node Y from '0' to '1' and back to '0', positive charge is transferred from the positive terminal onto the node and then to the negative terminal (see Fig. 7.4d). The node Y performs a *voltage swing* ΔV_{Y} which is limited by the voltage V_{DD} applied between both terminals.[8] For the whole switching cycle the charge $\Delta Q_{\mathrm{Y}} = C_{\mathrm{Y}}\, \Delta V_{\mathrm{Y}}$ is transferred between both terminals, where C_{Y} denotes the total capacitance of the node Y. Therefore the *switching energy*

[7] To a certain amount so-called pass-switches (= transistors) can be used to reduce the number of switches (= transitors) needed in more complex logic gates [236].

[8] ΔV_{Y} is less than V_{DD} if the leakage current I_{off} is large enough to cause a significant voltage drop over the switch being 'on'.

$$E_{\text{active}} = C_{\text{Y}}\,\Delta V_{\text{Y}} \cdot V_{\text{DD}} \geq C_{\text{Y}} \cdot \left(\Delta V_{\text{Y}}\right)^2 \tag{7.4}$$

is dissipated by this '0'-'1'-'0' process of an active logic gate. To emphasize,

> the energy (7.4) is not dissipated because the switches are resistive, but because charge is finally transferred between two terminals of different electrochemical potentials.

Dissipation can be reduced by using an adiabatic switching technique [237], but it slows down the switching and requires additional overhead circuitry. The industry has not taken this path up to now, however the concept is still under investigation.

In today's microprocessors typically less than a percent of the logic gates are switching in the same clock interval. Therefore, the overall power consumption of an integrated circuit can be described by

$$P_{\text{total}} = \text{NumberLogicGates} \cdot \left(P_{\text{leak}} + E_{\text{active}} \cdot \text{ClockFrequency} \cdot \text{PercentageActive}\right),$$

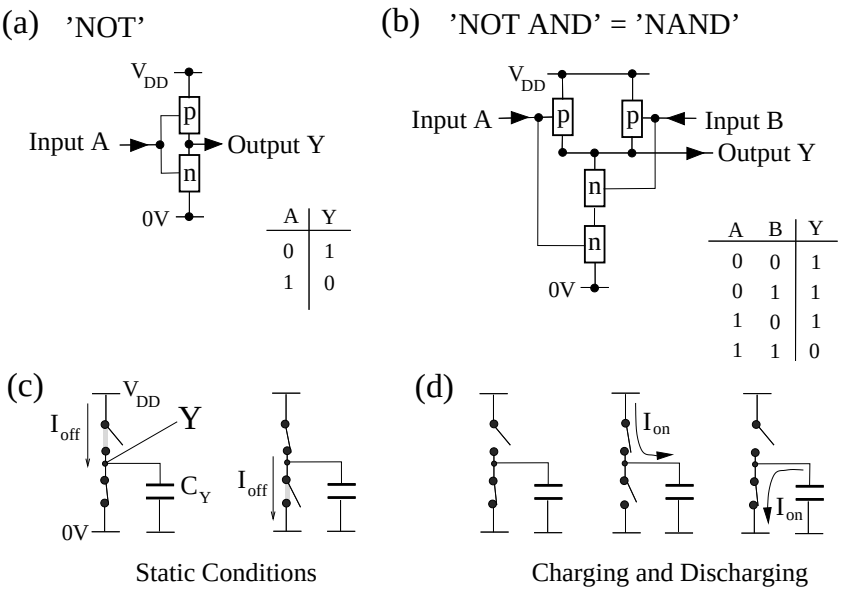

Fig. 7.4. Two elementary circuits based on complementary working switches, denoted as n- and p-switch: (a) 'NOT' gate or inverter, (b) 'AND-NOT' gate, which is usually named 'NAND' gate. (c) Under static conditions, permanent dissipation is limited to a leakage current I_{off} through a switch in 'off' state. (d) Charging the total node capacitance C_{Y} with I_{on} and then discharging C_{Y} cause dissipation due to charge transfer between both supply terminals.

Note, most of the logic gates are in a standby mode, enforcing to keep P_{leak} low.

Therefore, to integrate a large number of logic gates, the 'off' current I_{off} (respectively conductance σ_{off}) of the switch has to be small. On the other hand, a certain 'on' current I_{on} (respectively conductance σ_{on}) is required to recharge the ouput node capacitance in a short time via a switch. Therefore a high ratio of drive current I_{on} to leakage current I_{off} is required to keep leakage low but the switching delay short. Here the characteristics of the switch is of importance transducing the voltage swing ΔV_{Y} at its input, driven by the output node of the preceding logic gate, to a high ratio in the 'on' to 'off' current (respectively conductance). Using a high voltage swing ΔV_{Y} helps here, however it counteracts the requirement of low energy dissipation by switching, since $E_{\mathrm{active}} \propto (\Delta V_{\mathrm{Y}})^2$.

7.4 Availability of a Variety of Complementary Working Electrostatic Switches

The *ideal switch* controlled by an input voltage swing ΔV_{Y} changes the current step-like between $I_{\mathrm{off}} = 0$ to $I_{\mathrm{on}} = \infty$. Such a device does not exist in practice.

The second best choice of what is known is an *exponential* characteristic containing a Boltzmann factor including also the temperature influence,

$$\frac{I_{\mathrm{on}}}{I_{\mathrm{off}}} = \exp\left[\frac{e\Delta V_{\mathrm{Y}}}{\eta\, k_{\mathrm{B}} T}\right] . \tag{7.5}$$

Such switches showing the exponential generic characteristic (7.5) are obtained if a *classical energy barrier* exists between source and drain for free charge carriers and if the barrier can be removed electrostatically by the voltage swing on a close-by gate electrode, being part of the input node of the logic gate. Best performance as a switch is obtained if the ratio $I_{\mathrm{on}}/I_{\mathrm{off}}$ is as large as possible for a given voltage swing ΔV_{Y} at the input node, i.e., for an ideality factor $1/\eta = 1$ since $1/\eta$ is limited to $0 \leq 1/\eta \leq 1$.

- Field-effect transistors and especially MOSFETs can be appointed to the generic switches obeying relation (7.5). They come close to such an exponential characteristic with $\eta \to 1$.
- For a single-electron transistor, the classical energy barrier is given by the charging energy for adding an electron to the island or discharging energy for taking off an electron. The relation (7.5) holds if the island or the quantum dot is *weakly coupled to the leads*, i.e., the master equation approach of Section 5.8 is a reasonable description.

In *case of stronger coupling*, quantum mechanical aspects have to be taken into account. The exponential dependence has to be replaced by a less effective Lorentzian dependence on ΔV_{Y}, as we will derive later in Section 7.8.

Are there other electronic devices which may show similar complementary switching characteristics? For these devices we require essentially only

- an electrostatically removable barrier for adding an electron from source to the 'channel', as we denote henceforth the region between source and drain, and
- an electrostatically removable barrier for taking off an electron from the channel to drain, i.e., creating a hole in the channel.

In the following, the energy threshold for charging the channel by an electron is denoted as 'n-level', for electron discharging as 'p-level' (see Fig. 7.5). Obviously, a variety of physical arrangements exists for creating a 'np-gap', i.e., an energy gap between the n-level for electron charging and the p-level for electron discharging. Such a np-gap becomes possible

- by the bandstructure, – for instance, by using the gap between the conduction and valence band of a semiconductor,
- by the gap between the lowest unoccupied molecule orbital (LUMO) and highest occupied molecule orbital (HOMO) of a large molecule,
- by using a small island where electron-electron interaction leads to Coulomb blockade and single-electron tunneling,
- by using a small quantum dot or small molecule where the quantum mechanical confinement effect causes a well-pronounced discrete energy spectrum.

Such a structure can act as an electronic switch if a switchable gate-source voltage is applied. Whether such a switch acts as a n- or as a p-switch depends on how this np-gap is energetically positioned at small V_{GS} relatively to the electrochemical potentials of source and drain, as shown in Fig. 7.5:

> With positive going gate-source voltage, the energy barrier in the channel should diminish for a n-switch, and arise for a p-switch.

The np-gap is always shifted down with positive going gate-source voltage. Therefore, for a n-switch, at small gate-source voltage the electrochemical potentials of source and drain have to fall into the np-gap region. With positive going gate-source voltage the electron charging level (n-level) is reached falling between the electrochemical potentials of source and drain. For a p-switch, at small gate-source voltage, the energy barrier is not present because the electron discharging level (p-level) falls between the electrochemical potentials of source and drain. With positive going gate-source voltage, the p-level shifted below both electrochemical potentials, i.e., both electrochemical potentials fall into the np-gap region. Therefore, transport through a p-switch is enabled by hole-like transport processes, whereas transport through the n-switch is enabled by electron-like transport processes.

Since the position of the np-gap relatively to the electrochemical potentials of source and drain is affected electrostatically, several options are avail-

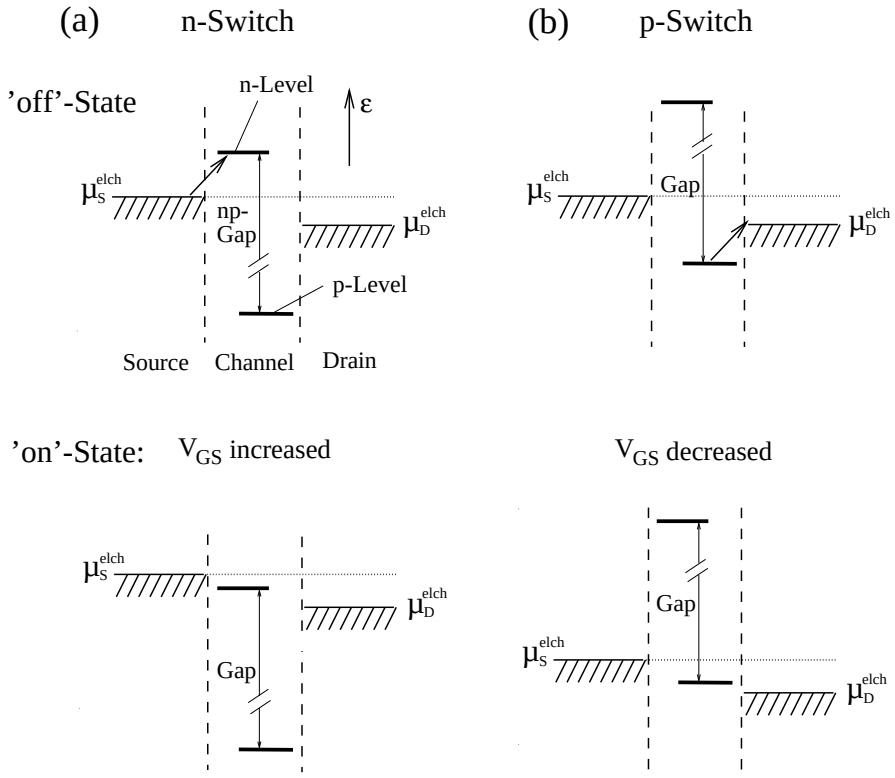

Fig. 7.5. The concept of complementary working electrostatic switches require a np-gap in the energy spectrum for adding electrons (threshold denoted as n-level) and taking off electrons (threhold denoted as p-level) from the channel region between source and drain. The position of the np-gap relatively the electrochemical potentials of source and drain at small gate-source voltage defines the type of the switch: (a) The n-level close to μ_S^{elch} defines a n-switch, (b) the p-level between μ_S^{elch} and μ_D^{elch} defines a p-switch. The n-switch is turned on with positive going gate-source voltage V_{GS} shifting down the np-gap: electrons are allowed to enter the channel region from source and leave to drain ('electron-like' transport process). The p-switch is turned on by negative going gate-source voltage shifting up the np-gap: electrons can leave to drain creating a hole which is filled again from source ('hole-like' transport process).

able to define the same device as a n- or a p-switch, i.e., intrinsically *shifting the np-gap to either direction.* It can be achieved

- by combining different materials and therefore using intrinsic contact voltages due to workfunction differences,
- by adding fixed charge close to the region between source and drain,
- by using a second gate electrode close-by which is positively or negatively biased.

In conclusion, electrostatic switches are not restricted to the concept of MOSFETs. Besides semiconductor material or organic materials, small islands weakly coupled to source and drain offer an additional way creating gaps in the energy spectrum for adding and taking off electrons in the channel region of the switch. Recent examples for logic gates based on unconventional field-effect transistors are

- a 'NOT'-gate realized by carbon nanotubes acting as n- and p-switch [238], or carbon nanotubes operating as p-switches [239], and
- a 'NOT' gate obtained from FETs with a self-assembled layer of organic molecules acting as the channel [240],
- a 'NOT' gate and a half-adder [9] realized by using single-electron transistors running a low temperature [188, 241].

Step by step, we will discuss in the following the constraints for a generic switch obeying (7.5) for fulfilling the requirements for highly integrated digital circuits.

7.5 Constraints for the Generic Electrostatic Switch Requested by Minimizing the Switching Energy

As described before in Section 7.3, the energy dissipation by changing the output state of a logic gate is proportional to the charge $\Delta Q_{\mathrm{Y}} = C_{\mathrm{Y}} \Delta V_{\mathrm{Y}}$ by which the node capacitance C_{Y} is recharged for the '0' to '1' transition and is proportional to the supply voltage V_{DD} which is at least the voltage swing ΔV_{Y}. To mimimize this energy dissipation, the node capacitance C_{Y} and/or the voltages V_{DD} and ΔV_{Y} should be reduced. Following the 'constant-electric-field-scaling' concept, the switching energy reduces by κ^3. As we will discuss in the following in more detail, there exists restrictions of doing this:

1. A fundamental limit is given by the *thermal fluctuations* occuring in the system. A low bit error probability requires a certain minimum of electrostatical energy stored on the node capacitor to distinguish reliable between the bit representations '0' and '1'.
2. The functionality of the logic gate having *bit level restoration* and *noise margins* limits the minimum in the supply voltage.
3. A stronger constraint than (2) is the *low standby power* requirement allowing still a reasonable short delay time for switching a logic gate.
4. Lowering the voltage swing too much leads to performance degradation in the *delay time* in switching a logic gate.

As we will see, especially the constraints (2), (3) and (4) affect the physics of the electrostatic switch: The minimum in the voltage swing requires the

[9] The half-adder was realized in a pass-switch logic technique, i.e. without bit-signal restoration.

optimum in the electrostatics of the switch. The switch device should allow charge accumulation above threshold to prevent degradation in the speed performance.

7.5.1 Limit due to Thermal Fluctuations on Bit Representation by Voltage Swing

Computational tasks require typically 10^{19} bit operations without an error, communication tasks require less since error correcting information is included. The number of 10^{19} bit operation is reached by a periodically sensing of 10^6 logic gates in a large system with a frequency of 10^8 Hz within one day. Nowadays high-performance microprocessors reach 1 GFlops, i.e., about 10^{11} bit operations per second.

Thermal noise is usually considered as being a negligible concern in electronic digital circuits. This is not true for circuits with small node capacitances where only few electrons might be used to represent the bit information. K.U. Stein [242] pointed out that thermal fluctuations give a fundamental minimum limit $\Delta E_{\mathrm{Y}}^{\mathrm{min}}$ on the electrostatic energy $\Delta E_{\mathrm{Y}} \equiv \frac{1}{2} C_{\mathrm{Y}} \, (\Delta V_{\mathrm{Y}})^2$ by which the node capacitor has to be recharged to distinguish reliable between the bit representation '0' and '1'. This switching energy $\Delta E_{\mathrm{Y}}^{\mathrm{min}}$ is determined by the bit error probability $\mathcal{P}^{\mathrm{err}}$ which could be tolerated in the application. K.U. Stein considered a computational bit operation as sensing the voltage level over the node capacitor *at a certain time*. In the case of dynamically working logic circuits, the switching operation freezes the electron number N – present on the node at that time – by disconnecting the node from the supply terminals. Both computational bit results '0' and '1' depend on the electron number present at a certain time on the node electrode which is affected by fluctuations due to thermal noise. An estimate for the error probability sensing the bit information at a certain time will be given in the following by using thermal equilibrium statistics. A more sophisticated analysis has to take into acccount quantum mechanical fluctuations and the coupling to the second electron reservoir which we expect to aggravate the requirement.

In complementary switch circuits, the node electrode is connected to one supply terminal and is almost disconnected from the other supply terminal. This is true for the '0' and the '1' state (see Fig. 7.6). From the physical point of view, both stationary states reflect almost the thermal equilibrium situation of an electron island – the node electrode with the total capacitance C_{Y} – connected to a large electron reservoir with a certain electrochemical potential, i.e., to one of the supply terminals. Switching between the low-level state '0' and the high-level state '1' state is done by changing the connection from one supply terminal to the other, i.e., by changing to the electron reservoir with the other electrochemical potential. This changes the thermodynamical probability distribution of the number N_0 of electrons on the node electrode. The electron number with highest probability changes between N_0^{l} for '1' and

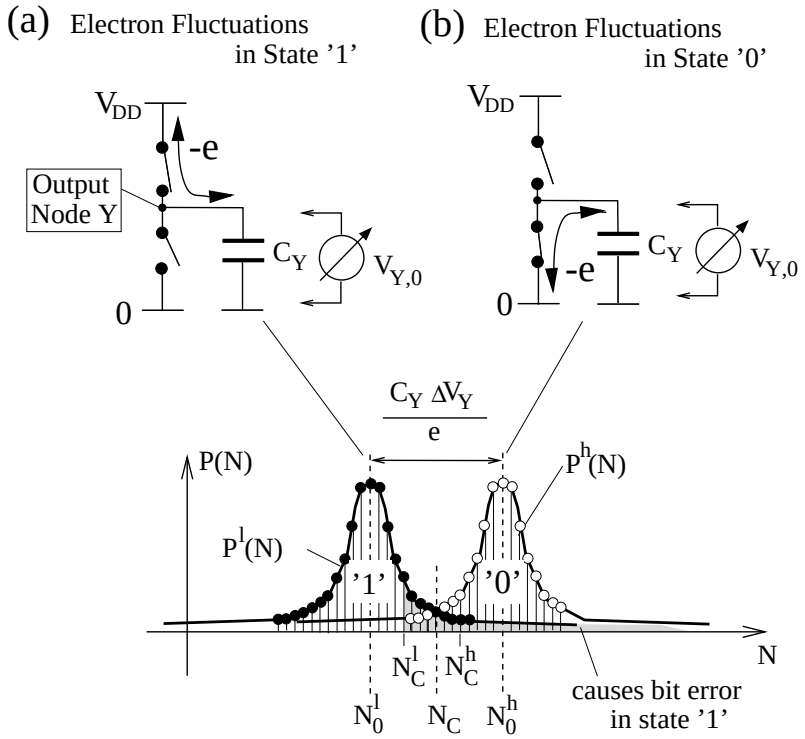

Fig. 7.6. Thermal fluctuations in the number N of electrons present on the node capacitor with capacitance C_Y causes fluctuations in the voltage $V_{Y,0}$ over the capacitor and therefore bit errors: (a) Connecting the node to the positive supply terminal, thermodynamic electron fluctuations occur (as indicated) around N_0^l, (b) connecting the node to the negative supply terminal, fluctuations occur around N_0^h, where the difference is given by $N_0^h - N_0^l = C_Y \cdot \Delta V_Y / e$. If the state '1' is intended, but the threshold N_C^l is exceeded by the fluctuating electron number N while sensing the voltage level on the node, a bit error occurs.

$N_0^h > N_0^l$ for '0'. [10] Fig. 7.6 shows the thermal fluctuations in the number N of electrons on the node around N_0^h, respectively N_0^l. These normalized probability distributions $P^l(N)$ and $P^h(N)$ cross in their tails at the critical value N_C which represents the logic threshold between the bit representation '0' and '1'. An even stronger criterion uses different critical electron numbers N_C^l and N_C^h as shown in Fig. 7.6. Such a fluctuation event causes errors in the computational process sensing the electrostatic potential which is given by the electron number N at that time: Errors occur for the logic '1' state with $N > N_C^l$ (marked in Fig. 7.6) or for the logic '0' level with $N > N_C^h$.

[10] Note that we count all free electrons including those which are compensated in their charge by ions.

In thermal equilibrium with any of the two electron reservoirs, the ratio between the probability $P(N_0 \pm n)$ of having $N_0 \pm n$ electrons on the node and the highest probability $P(N_0)$ of having N_0 electrons on the node depends exponentially on the energy $\Delta E(\pm n, N_0)$ which is required to add the n electrons from the reservoir to the N_0 electrons on the node, respectively to take off the n electrons from the node back into the reservoir:

$$\frac{P(N_0 \pm n)}{P(N_0)} = \frac{\text{const} \cdot \exp\big(-E(N_0 \pm n)/k_\mathrm{B}T\big)}{\text{const} \cdot \exp\big(-E(N_0)/k_\mathrm{B}T\big)} \equiv \exp\left(-\frac{\Delta E(\pm n, N_0)}{k_\mathrm{B}T}\right) . \tag{7.6}$$

The probability $P(N)$ is normalized by $\sum_{N=0}^{\infty} P(N) = 1$, fixing the value of const. The 'activation' energy $\Delta E(\pm n, N_0)$ in (7.6) is the electrostatic energy required to add n electrons when N_0 electrons are already present,

$$\begin{aligned} \Delta E(\pm n, N_0) &= E(N_0 \pm n) - E(N_0) \\ &= \frac{\big(-(N_0 \pm n)\, e + Q_0^*\big)^2}{2\, C_\Sigma} - \frac{\big(-N_0\, e + Q_0^*\big)^2}{2\, C_\Sigma} \\ &= \frac{\big(n^2 \pm 2\, f_{\mathrm{Q}_0^*}\, n\big) \cdot e^2}{2\, C_\Sigma} . \end{aligned} \tag{7.7}$$

Here, the quantity Q_0^* denotes the 'offset charge' already introduced in previous Chapters. It accounts for shifts in the electrostatic potential of the node due to background charges, workfunction differences and/or voltage offsets. The introduced abbreviation

$$f_{\mathrm{Q}_0^*} = N_0 - Q_0^*/e \tag{7.8}$$

is limited due to Section 2.3.2 to the range $-\frac{1}{2} \le f_{\mathrm{Q}_0^*} \le \frac{1}{2}$. This factor $f_{\mathrm{Q}_0^*}$ is negligible for large n but is important when considering changes by few electrons since this affects $\Delta E(\pm n, N_0)$ and therefore $P(N_0 \pm n)$. For $f_{\mathrm{Q}_0^*} = 0$, the number of electrons is fixed to N_0 at lowest temperature. For $f_{\mathrm{Q}_0^*} = \pm\frac{1}{2}$, the charge fluctuates because the activation energy (7.7) for $n = 1$ or $n = -1$ is zero, respectively.

We now apply the results (7.6) to (7.8) to the cases of an expected '0' or '1' on the node and add the corresponding superscripts 'h' and 'l': In case of an expected '0' the result of a computational operation is considered as being 'wrong' if the number of electrons has been equal or even below the chosen critical value $N_\mathrm{C}^\mathrm{h} = N_0^\mathrm{h} - \Delta N_\mathrm{C}^\mathrm{h}$. The probability of such an error is

$$\mathcal{P}^\mathrm{err}('0') = \sum_{n=\Delta N_\mathrm{C}^\mathrm{h}}^{N_0^\mathrm{h}} P^\mathrm{h}(N_0^\mathrm{h} - n, f_{\mathrm{Q}_0^*}^\mathrm{h}) , \tag{7.9}$$

where $f_{\mathrm{Q}_0^*}^\mathrm{h}$ is added in the argument of $P(N)$ to indicate that $f_{\mathrm{Q}_0^*} = f_{\mathrm{Q}_0^*}^\mathrm{h}$ in (7.6).

In the case of a '1' on the node, the result of a computational operation is considered as being 'wrong' if the number of electrons has been equal or even exceeded a certain value $N_{\mathrm{C}}^{\mathrm{l}} = N_0^{\mathrm{l}} + \Delta N_{\mathrm{C}}^{\mathrm{l}}$. The probability for this error is given by the sum of the probabilities of having $N > N_{\mathrm{C}}^{\mathrm{l}}$

$$\mathcal{P}^{\mathrm{err}}('1') = \sum_{n=\Delta N_{\mathrm{C}}^{\mathrm{l}}}^{\infty} P^{\mathrm{l}}(N_0^{\mathrm{l}} + n, f_{\mathrm{Q}_0^*}^{\mathrm{l}}) \; . \tag{7.10}$$

The assumption for the previous considerations was that the state '0' is correctly obtained if the number of electrons is above the critical value $N_{\mathrm{C}}^{\mathrm{h}} = N_0^{\mathrm{h}} - \Delta N_{\mathrm{C}}^{\mathrm{h}}$ and the state '1' is correctly obtained if the number of electrons is below the critical value $N_{\mathrm{C}}^{\mathrm{l}} = N_0^{\mathrm{l}} + \Delta N_{\mathrm{C}}^{\mathrm{l}}$. As the representations of the '0' and the '1' state could not have an overlap, a certain electron number N between N_0^{l} and N_0^{h} has to belong unambiguously to one binary state or to none of both if N is between $N_{\mathrm{C}}^{\mathrm{h}}$ and $N_{\mathrm{C}}^{\mathrm{l}}$. Therefore, the choices for a small change $\Delta N = N_0^{\mathrm{h}} - N_0^{\mathrm{l}}$ in the electron number between the binary states are

$$\Delta N_{\mathrm{C}}^{\mathrm{l}} = \Delta N_{\mathrm{C}}^{\mathrm{h}} = \tfrac{1}{2}\Delta N \quad \text{if } \Delta N \text{ is even, and} \tag{7.11}$$

$$\Delta N_{\mathrm{C}}^{\mathrm{l}} = \Delta N_{\mathrm{C}}^{\mathrm{h}} = \tfrac{1}{2}\big(\Delta N + 1\big) \quad \text{if } \Delta N \text{ is odd.} \tag{7.12}$$

As the numbers of electrons N_0^{l}, N_0^{h} are large, the sum in (7.9) can be extended to $n = \infty$. Using (7.6) and (7.7), Eqn. (7.9) and Eqn. (7.10) result in

$$\mathcal{P}^{\mathrm{err}} = \frac{\displaystyle\sum_{n=\Delta N_{\mathrm{C}}}^{\infty} \exp\left(-\frac{(n^2 \pm 2\, f_{\mathrm{Q}_0^*}\, n)\, e^2}{2\, C_{\mathrm{Y}}\, k_{\mathrm{B}} T}\right)}{\displaystyle\sum_{n=-\infty}^{\infty} \exp\left(-\frac{(n^2 + 2\, f_{\mathrm{Q}_0^*}\, n)\, e^2}{2\, C_{\mathrm{Y}}\, k_{\mathrm{B}} T}\right)} \; , \tag{7.13}$$

where the '+' sign is for calculating $\mathcal{P}^{\mathrm{err}}('0')$ with $f_{\mathrm{Q}_0^*} = f_{\mathrm{Q}_0^*}^{\mathrm{h}}$, and the '−' sign is for calculating $\mathcal{P}^{\mathrm{err}}('1')$ with $f_{\mathrm{Q}_0^*} = f_{\mathrm{Q}_0^*}^{\mathrm{l}}$. The error probability becomes equal for '0' and '1' if $f_{\mathrm{Q}_0^*} = f_{\mathrm{Q}_0^*}^{\mathrm{l}} = f_{\mathrm{Q}_0^*}^{\mathrm{h}} = 0$.

In Fig. 7.7, the error probability calculated by using (7.13) is plotted versus the change of the electrostatic energy ΔE_{Y} on the node capacitor C_{Y} between '1' and '0' state

$$\Delta E_{\mathrm{Y}} \equiv \frac{C_{\mathrm{Y}} \cdot (\Delta V_{\mathrm{Y}})^2}{2} = \frac{(\Delta N\, e)^2}{2\, C_{\mathrm{Y}}} \, , \tag{7.14}$$

which is normalized in Fig. 7.7 by the thermal energy $k_{\mathrm{B}}T$. The different curves belong to different change ΔN in the number of electrons on the node between the states '0' and '1'. The parameter along each curve of given ΔN is the node capacitance C_{Y}. The limiting cases of large and small ΔN are

Bit Errors Due to Thermal Fluctuations of the Electron Number

(a) No 'Offset Charge':

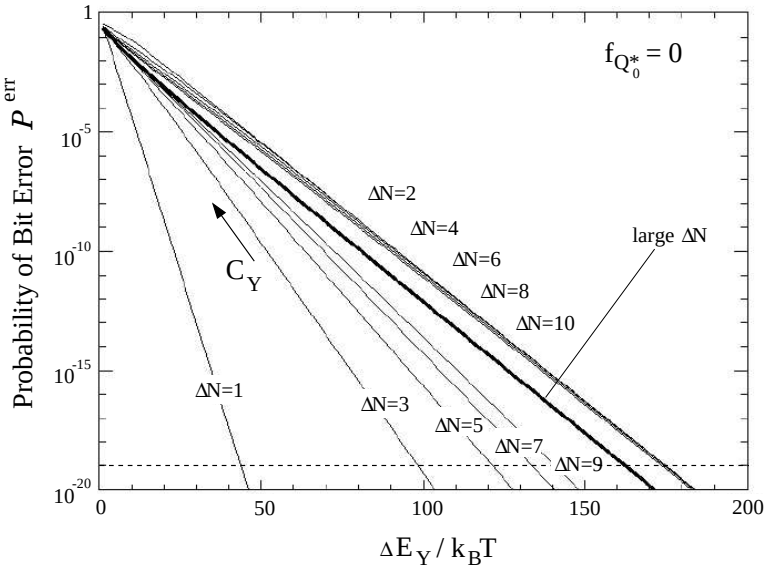

(b) Maximum 'Offset Charge':

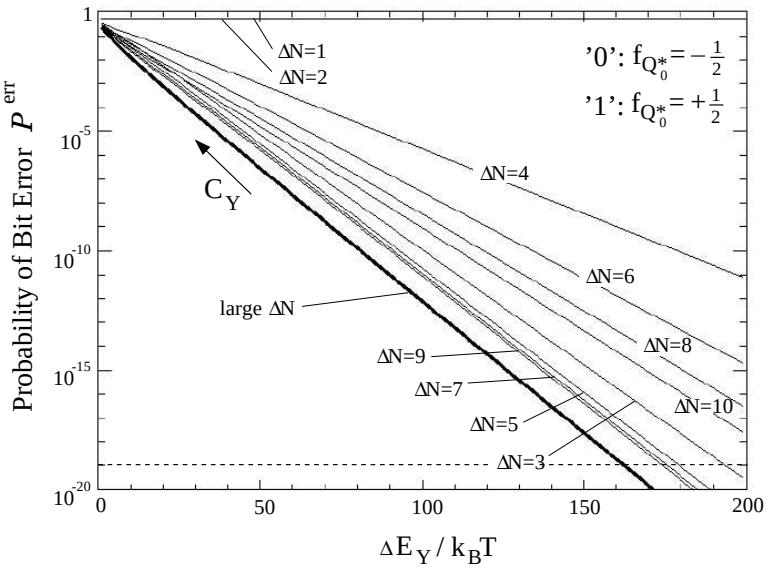

Fig. 7.7. (Left page) Thermally induced bit errors $\mathcal{P}^{\rm err}$, calculated from relation (7.13) for three prominent values of $f_{\rm Q_0^*}$, versus the electrostatic energy difference $\Delta E_{\rm Y} = \frac{1}{2} C_{\rm Y} \Delta V_{\rm Y}^2$ on the output node capacitor Y between '1' and '0' state, normalized by $k_{\rm B}T$. Curve parameter is the change $\Delta N = C_{\rm Y}\,\Delta V_{\rm Y}/e$ in mean electron number to distinguish between '0' and '1' on the node. The thick solid curve is valid for large ΔN and shows the limit $k_{\rm B}T \gg e^2/2C_{\rm Y}$. (a) $f_{\rm Q_0^*} = 0$: For odd ΔN, the error probability is below, for even ΔN above the thick solid curve. (b) To simulate background charge, worst cases for $f_{\rm Q_0^*}$ are chosen: $f_{\rm Q_0^*} = -\frac{1}{2}$ for $\mathcal{P}^{\rm err}('0')$, $f_{\rm Q_0^*} = \frac{1}{2}$ for $\mathcal{P}^{\rm err}('1')$. For $\Delta N = 1$ and $\Delta N = 2$, no $\Delta E_{\rm Y}/k_{\rm B}T$ helps to suppress bit errors.

discussed in the following:

Large ΔN:
The solid curve in Fig. 7.7 for large ΔN shows the limit $k_{\rm B}T \gg e^2/2C_{\rm Y}$ where the required energy $\Delta E_{\rm Y}$ has become almost independent of the electron number and the offset charges, i.e., of $f_{\rm Q_0^*}$. For this limit, the sum in (7.13) can be approximated by an integral and with using the error function [11], the error probability $\mathcal{P}^{\rm err} = \mathcal{P}^{\rm err}('0') = \mathcal{P}^{\rm err}('1')$ is expressed in this limit by

$$\mathcal{P}^{\rm err} = \frac{\int_{\Delta N/2}^{\infty} \exp\left(-\frac{n^2 e^2}{2\,C_{\rm Y}\,k_{\rm B}T}\right) \cdot {\rm d}n}{\int_{-\infty}^{\infty} \exp\left(-\frac{n^2 e^2}{2\,C_{\rm Y}\,k_{\rm B}T}\right) \cdot {\rm d}n} = \frac{1}{2}\left(1 - {\rm erf}\left(\sqrt{\frac{\Delta E_{\rm Y}}{4\,k_{\rm B}T}}\right)\right) \quad . \tag{7.15}$$

This represents the result which was already given in 1977 by K.U. Stein [242] who treated only this special case. The error probability $\mathcal{P}^{\rm err}$ in (7.15) depends on the ratio of stored electrostatic energy $\Delta E_{\rm Y}$ to thermal energy $k_{\rm B}T$. In the limit $\mathcal{P}^{\rm err} \ll 1$, the first term of the asymptotic representation [12] for (7.15) leads to

$$\mathcal{P}^{\rm err} = \frac{1}{\sqrt{\pi\,\Delta E_{\rm Y}/k_{\rm B}T}} \cdot \exp\left(-\frac{\Delta E_{\rm Y}}{4\,k_{\rm B}T}\right) \tag{7.16}$$

and we obtain as an estimate of the change of electrostatic energy the minimum value $\Delta E_{\rm Y} = \Delta E_{\rm Y}^{\rm min}$,

$$\Delta E_{\rm Y}^{\rm min} \approx -4\,k_{\rm B}T \cdot \ln\left(\mathcal{P}^{\rm err}\right) \quad . \tag{7.17}$$

[11] ${\rm erf}(x) \equiv 2/\sqrt{\pi} \cdot \int_0^x \exp(-t^2)\,{\rm d}t$, and $\lim_{x\to\infty} {\rm erf}(x) = 1$.

[12] See (8.254) in [243]: $1 - {\rm erf}(\sqrt{\rm x}) = \frac{1}{\pi} \cdot \exp(-{\rm x}) \cdot \left[\sqrt{\frac{\pi}{\rm x}} + \sum_{\rm k=1}^{\infty} \frac{(-1)^{\rm k} \cdot (2{\rm k}-1)!!}{2^{\rm k}\,{\rm x}^{\rm k+1/2}}\right]$

Therefore, it requires $\Delta E_{\mathrm{Y}} \geq \Delta E_{\mathrm{Y}}^{\min}$ in order to fulfill the demand that the desired error probability $\mathcal{P}^{\mathrm{err}}$ is not surpassed.

Small ΔN:
For small ΔN, there is a strong dependence for $\Delta E_{\mathrm{Y}}^{\min}$ on $f_{\mathrm{Q}_0^*}$ and on ΔN being odd or even. This becomes obvious by the following consideration: For $(\Delta N_{\mathrm{C}}\, e)^2/2C_{\mathrm{Y}} \gg k_{\mathrm{B}}T$, the first term in the sum of (7.13) dominates the error probability, [13]

$$\mathcal{P}^{\mathrm{err}} \approx \exp\left(-\frac{\left(\Delta N_{\mathrm{C}}^2 \pm 2\, f_{\mathrm{Q}_0^*}\, \Delta N_{\mathrm{C}}\right) e^2}{2C_{\mathrm{Y}}\, k_{\mathrm{B}}T}\right) . \tag{7.18}$$

Therefore the minimum $\Delta E_{\mathrm{Y}}^{\min}$ in energy $\Delta E_{\mathrm{Y}} = (\Delta N\, e)^2/2C_{\mathrm{Y}}$ fulfilling (7.18) is given by

$$\Delta E_{\mathrm{Y}}^{\min} \approx -4\,\beta\, k_{\mathrm{B}}T \cdot \ln\left(\mathcal{P}^{\mathrm{err}}\right) \tag{7.19}$$

where, due to the critical value $\Delta N_{\mathrm{C}} = \frac{1}{2}\Delta N$,

$$\frac{1}{\beta} = 1 \pm \frac{2\, f_{\mathrm{Q}_0^*}}{\Delta N} \quad \text{if } \Delta N_{\mathrm{C}} \text{ is even} , \tag{7.20}$$

and, due to the critical value $\Delta N_{\mathrm{C}} = \frac{1}{2}(\Delta N + 1)$,

$$\frac{1}{\beta} = \left(1 + \frac{1}{\Delta N}\right) \cdot \left(1 + \frac{1}{\Delta N} \cdot \left(1 \pm 2\, f_{\mathrm{Q}_0^*}\right)\right) \quad \text{if } \Delta N_{\mathrm{C}} \text{ is odd} . \tag{7.21}$$

The required energies $\Delta E_{\mathrm{Y}}^{\min}$ to achieve certain $\mathcal{P}^{\mathrm{err}}('0')$ and $\mathcal{P}^{\mathrm{err}}('1')$ are listed in Table 7.1 for some values of ΔN and $f_{\mathrm{Q}_0^*}$:

- The factor β, given by Eqn. (7.20) and Eqn. (7.21), converge with increasing ΔN to unity. Thus, (7.17) is obtained again.
- The lowest energy $\Delta E_{\mathrm{Y}}^{\min}$ for being below a certain error probability occurs – see also Fig. 7.7 – for $\Delta N = 1$ and $f_{\mathrm{Q}_0^*} = 0$ which yields to $\beta = 1/4$ in (7.19), and hence to

$$\Delta E_{\mathrm{Y}}^{\min} \approx k_{\mathrm{B}}T \cdot \ln\left(\mathcal{P}^{\mathrm{err}}\right) . \tag{7.22}$$

  Thus, this lowest energy is required in the case of representing the difference between '0' and '1' state by the absence or presence of one additional electron on the node capacitor. However this requires very small capacitance values C_{Y} due to the relation $\Delta E_{\mathrm{Y}}^{\min} = e^2/2C_{\mathrm{Y}}$.

[13] The sum of the nominator in (7.13) is dominated in this case by the contributions of $n = 0$, and $n = 1$ if $f_{\mathrm{Q}_0^*} \to -\frac{1}{2}$ or $n = -1$ if $f_{\mathrm{Q}_0^*} \to \frac{1}{2}$. This leads to a nominator value of about 1 to 2.

		$f_{Q_0^*}=0$	$f_{Q_0^*}=-\frac{1}{2}$	$f_{Q_0^*}=\frac{1}{2}$	required β if Q_0^* fluctuates
$\Delta N=1,$	'0'	$\beta=1$	∞	1/2	∞
	'1'	1	1/2	∞	∞
$\Delta N=2,$	'0'	4	∞	2	∞
	'1'	4	2	∞	∞
$\Delta N=3,$	'0'	9/4	9/2	3/2	9/2
	'1'	9/4	3/2	9/2	9/2
$\Delta N=4,$	'0'	4	8	8/3	8
	'1'	4	8/3	8	8
$\Delta N=5,$	'0'	25/9	25/6	25/12	25/6
	'1'	25/9	25/12	25/6	25/6
⋮		⋮	⋮	⋮	⋮
$\Delta N=9,$	'0'	81/25	81/20	81/30	81/20
	'1'	81/25	81/30	81/20	81/20
$\Delta N=10,$	'0'	4	5	10/3	5
	'1'	4	10/3	5	5

Table 7.1. Values of β derived from (7.20) and (7.21) which determines as factor the minimum electrostatic energy change $\Delta E_{\mathrm{Y}}^{\mathrm{min}} = -\beta \cdot 4\,k_{\mathrm{B}}T \ln \mathcal{P}^{\mathrm{err}}$ (see (7.19), required to represent the bit status '0' and '1' below a certain error probability $\mathcal{P}^{\mathrm{err}}$ due to thermal fluctuations. The factor β depends on ΔN, the bit status and $f_{Q_0^*}$. Fluctuations in the background charge cause a change in $f_{Q_0^*}$. To ensure the reliability in such a case, the worst value for β (from $f_{Q_0^*} = \{0, -\frac{1}{2}, \frac{1}{2}\}$) is listed in the right column. Note that for $\Delta N = 1$ and $\Delta N = 2$, no reliable bit representaion is possible in case of background charge fluctuations.

- Moreover, the bit representation by one electron is very sensitive to background charges which are fluctuating around. By setting $f_{Q_0^*} = \pm\frac{1}{2}$, the requirement on $\Delta E_{\mathrm{Y}}^{\mathrm{min}}$ diverges in case $\Delta N = 1$ but also for $\Delta N = 2$ (see Table 7.1). Finite values are obtained for $\Delta N \geq 3$ for any $f_{Q_0^*}$. For large ΔN, the requirement for $\Delta E_{\mathrm{Y}}^{\mathrm{min}}$ becomes independent of $f_{Q_0^*}$.
- For larger C_{Y}, more electrons ΔN have to be stored on the node capacitor maintaining the same low error probability. Advantage is that a large charge mount is less sensitive to a single electron charge fluctuating in the vicinity of the node or onto the node.

In conclusion, to suppress thermal induced bit errors, a minimum electrostatic energy $\Delta E_{\mathrm{Y}}^{\mathrm{min}}$ has to be stored on the node capacitor to distinguish reliable between the binary '0' and the binary '1' state. Fig. 7.8a shows $\Delta E_{\mathrm{Y}}^{\mathrm{min}}/k_{\mathrm{B}}T$ versus C_{Y} for a given $\mathcal{P}^{\mathrm{err}} = 10^{-19}$, obtained from Fig. 7.7. This diagram reveals that for $\mathcal{P}^{\mathrm{err}} = 10^{-19}$, an switching energy $\Delta E_{\mathrm{Y}} > 165\,k_{\mathrm{B}}T$ has to be stored. This means $\Delta E_{\mathrm{Y}} > 4.3$ eV for $T = 300$ K. [14]

[14] Note, by a computational operation which allows to *average over the thermal fluctuations over long time periods*, this energy can be reduced limited by

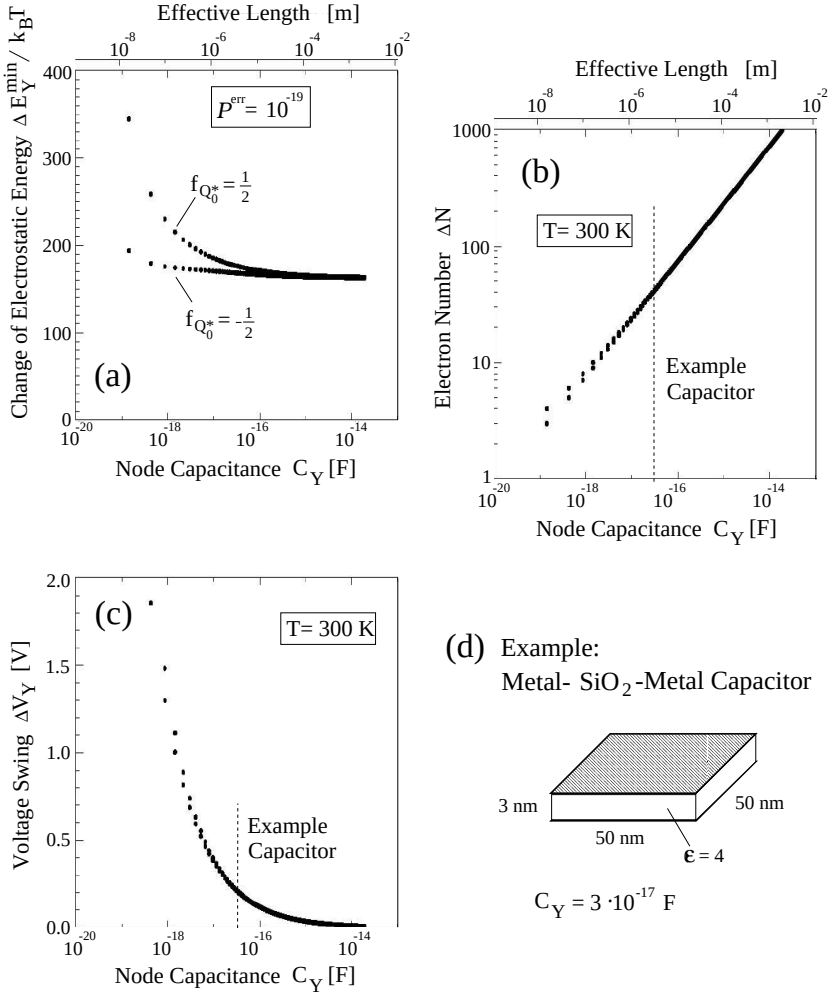

Fig. 7.8. (a) Evaluated mininum electrostatic energy $\Delta E_Y^{\min}$ versus C_Y required to avoid bit errors due to thermal fluctuations to $\mathcal{P}^{\rm err} = 10^{-19}$. For the '0' state, $f_{Q_0^*} = -\frac{1}{2}$ is assumed, for the '1' state $f_{Q_0^*} = \frac{1}{2}$. At top of the diagrams, an effective length is given, calculated by $l_{\rm eff} = C_Y/\epsilon_0$ which estimates the possible length L of a metal wire via its self-capacitance $C = 2\pi\epsilon_0\epsilon\, L/\ln(L/R_0)$ (see (C.11)): $L \leq l_{\rm eff}/\epsilon$ for a length-to-radius ratio of about 500. (b) Change ΔN in electron number on node versus C_Y required to suppress thermal errors. (c) Required voltage swing ΔV_Y versus C_Y. (d) Example of a metal-SiO_2-metal plate capacitor of 50 nm by 50 nm area with 3 nm plate distance leading to $C_Y \approx 3 \cdot 10^{-17}$ F.

In Fig. 7.8c the required minimum voltage swing $\Delta V_{\mathrm{Y}} = \sqrt{2\,\Delta E_{\mathrm{Y}}^{\mathrm{min}}/C_{\mathrm{Y}}}$ is plotted versus the node capacitance C_{Y}. Illustrating is the following example: The value of a metal-SiO_2-metal plate capacitor (see Fig. 7.8d) of 50 nm by 50 nm area, 3 nm plate distance and $\epsilon_{\mathrm{SiO_2}} = 4$ has the capacitance $C \approx 3 \cdot 10^{-17}\,\mathrm{F} = 30\,\mathrm{aF}$. Such a small capacitance requires already a voltage swing ΔV_{Y} larger than 0.2 V for $\mathcal{P}^{\mathrm{err}} = 10^{-19}$ at $T = 300\,\mathrm{K}$. About 38 electrons have to be stored under these conditions (see Fig. 7.8b). Of course, the bit representation with even less electrons is also possible choosing smaller node capacitances C_{Y} and higher voltage swings ΔV_{Y}, but the reliability of the bit representation is then sensitive to single background charges fluctuating around.

It is worth to emphasize again that it does not require the bit representation by few electrons to reach minimum in the electrostatic energy change ΔE_{Y} demanded by a low thermal-induced error probability requirement. A large number of electrons on a large capacitor leads to almost the same minimum in energy, accompanied by a small voltage swing ΔV_{Y} (see Fig. 7.8c). However for *large* node capacitance values other contraints become important not allowing to minimize the voltage swing ΔV_{Y} to the lower limit given by a low thermal-induced error probability requirement.

7.5.2 Limit due to Requirement of Bit Level Restoration

The concept of digital circuits (see Section 7.2) demands bit signal restoration. The degradation of bit signal levels leads to information loss and computational errors. As shown in Fig. 7.9 and explained in the Figure Caption, differential voltage gain $|\mathrm{d}V_{\mathrm{out}}/\mathrm{d}V_{\mathrm{in}}| < 1$ of the logic gate everywhere produces degradation. Differential voltage gain greater than unity has to be suppressed at the bit signal levels to avoid amplification of noise through the network which would cause computational errors after passing several logic gates. Noise suppression is important since 'noise' sources are inherently in digital circuits, for instance, due to capacitive cross talk, due to voltage drops on series resistances in the power lines, or due to induced voltages at the inductance of bond wires. A transfer function of the logic gate with discriminative amplification (sigmoid-like response of the output voltage on the input voltage, see Fig. 7.9d) allows to fulfill the requirements of bit signal restoration and noise suppression at same time [226, 227, 229].

The difference between the nominal bit signal input level and the input voltage where the differential voltage gain become equal to one gives the *noise margin* V_{nm} of the transfer characteristics. An input voltage can vary within this range without bit signal level degradation or noise accumulation. For the sigmoid transfer function, the differential voltage gain $\mathrm{d}V_{\mathrm{out}}/\mathrm{d}V_{\mathrm{in}}$ at

$\Delta E_{\mathrm{Y}}^{\mathrm{min}} > k_{\mathrm{B}}T \ln 2$, which gives the thermodynamic limit allowing to attribute a probability slightly higher than $\frac{1}{2}$ for one state in a two-state system (see also relation (7.22) for $\mathcal{P}^{\mathrm{err}} \approx \frac{1}{2}$).

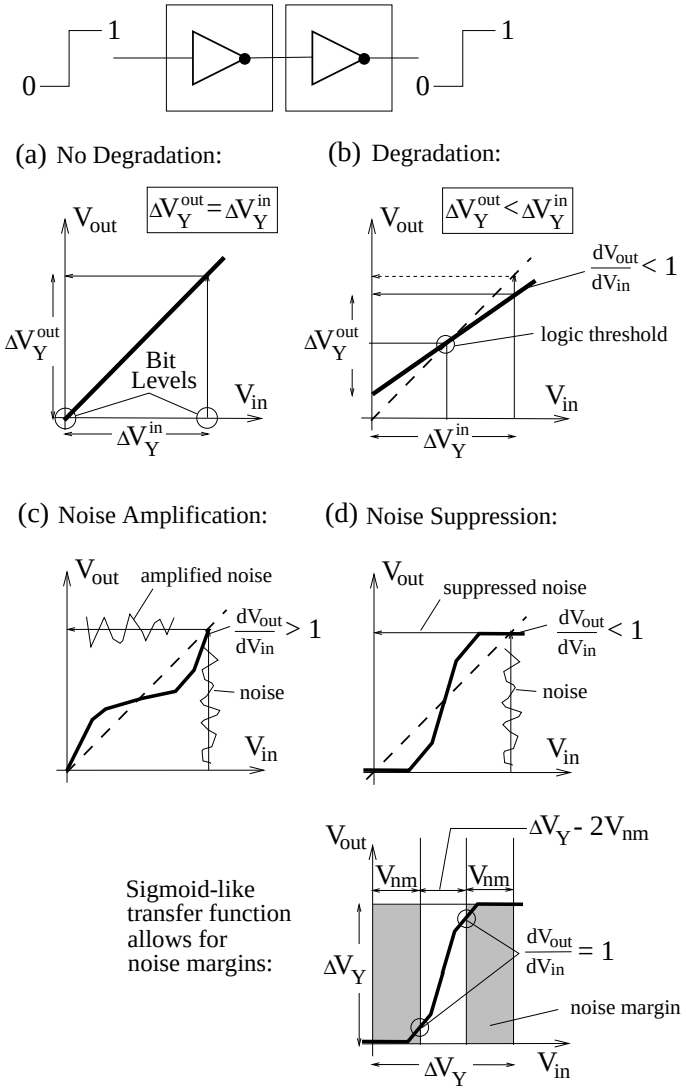

Fig. 7.9. Bit-signal degradation and restoration: Let us assume two 'NOT' gates in series. (a) The bit input signals will be transmitted at their respective level if the overall network has the slope $|dV_{out}/dV_{in}| = 1$ everywhere in its characteristics. (b) A slope $|dV_{out}/dV_{in}| < 1$ everywhere leads to a degradation of the bit signals. Several of such logic gates in series degrade the bit signals to the logic threshold level. (c) A slope $|dV_{out}/dV_{in}| > 1$ at the bit levels amplifies noise and induces therefore bit errors. (d) Discriminative amplification (sigmoid-like transfer function) prohibits bit signal degradation and suppresses noise at the bit signal levels. The noise margin V_{nm} becomes larger with steeper slope $|dV_{out}/dV_{in}|$ around logic threshold.

logic threshold is a measure for the possible noise margins. The steeper the sigmoid transfer function of the logic gate, the larger are the noise margins. By using Fig. 7.9d, the slope at logic threshold is estimated to

$$\text{gain} \equiv \left| \frac{\mathrm{d}V_{\mathrm{out}}}{\mathrm{d}V_{\mathrm{in}}} \right| \geq \frac{\Delta V_{\mathrm{Y}}}{\Delta V_{\mathrm{Y}} - 2\,V_{\mathrm{nm}}} = \frac{1}{1 - 2\,V_{\mathrm{nm}}/\Delta V_{\mathrm{Y}}} \,. \tag{7.23}$$

We call this the *voltage-gain requirement at threshold* since giving the ratio between noise margin V_{nm} and voltage swing ΔV_{Y} leads to the constraint (7.23) for the required differential gain $|\mathrm{d}V_{\mathrm{out}}/\mathrm{d}V_{\mathrm{in}}|$ at logic threshold. Taking for example a noise margin of $V_{\mathrm{nm}} = 0.3\,\Delta V_{\mathrm{Y}}$ for both bit levels, a differential gain at threshold of at least 2.5 is required, taking a noise margin of $0.45\,\Delta V_{\mathrm{Y}}$ at least a differential gain of 10.

How does the requirement (7.23) affect the device used as the switch? The voltage gain requirement at logic threshold gives a *constraint on the device geometry* due to the electrostatics by which the energy barrier of the device is controlled. To prove this statement and in order to obtain quantitative design rules, we consider the realization of a 'NOT' gate (or inverter) in Fig. 7.10: First we consider an electron in the channel between the electrodes – i.e., the input node A (the gate G of the switches), the output node Y (the drain D of the switches) and the supply terminals T (the source S of the respective switch). Putting an electron at position $\boldsymbol{r}$ induces image charges on each of these electrodes, i.e., on electrode i the charge fraction $\alpha_i(\boldsymbol{r}) < 1$. Further, the energy of the electron at $\boldsymbol{r}$ is changed by $-e\,\mathrm{d}\Phi(\boldsymbol{r})$ when changing the electrostatic potential of one of the electrodes by $\mathrm{d}V_i$. Due to the electrostatic reciprocity, this energy shift $-e\,\mathrm{d}\Phi(\boldsymbol{r})$ depends on the fraction $\alpha_i(\boldsymbol{r})$ induced by this electron on the respective electrode i. However, by changing the input voltage V_{in} on the gate electrodes (input node A) of the inverter shown in Fig. 7.10, also the output voltage V_{out}, i.e., the output-node potential of the logic gate is changed. Therefore the energy barrier height at position $\boldsymbol{r}$ in the channel between the electrodes of the n-switch is shifted for an electron with respect to the supply terminal T by

$$-e\,\mathrm{d}\Phi(\boldsymbol{r}) = -e\,\alpha_{\mathrm{A}}(\boldsymbol{r}) \cdot \mathrm{d}V_{\mathrm{in}} - e\,\alpha_{\mathrm{Y}}(\boldsymbol{r}) \cdot \mathrm{d}V_{\mathrm{out}} \,, \tag{7.24}$$

with the condition $\alpha_{\mathrm{A}}(\boldsymbol{r}) + \alpha_{\mathrm{Y}}(\boldsymbol{r}) + \alpha_{\mathrm{T}}(\boldsymbol{r}) \leq 1$. The same relation is obtained for an electron in the channel of the p-switch (see Fig. 7.10a).

We expect that $\mathrm{d}V_{\mathrm{out}} \propto -\mathrm{d}V_{\mathrm{in}}$. The more accurate dependence is obtained as follows: The output signal V_{out} depends on the 'resistance divider' formed by the n- and the p-switch in series,

$$V_{\mathrm{out}} = \frac{R_{\mathrm{n}}}{R_{\mathrm{n}} + R_{\mathrm{p}}} \cdot V_{\mathrm{DD}} \,, \tag{7.25}$$

where the 'resistances' R_{n} and R_{p} depend on the actual values of V_{in}, V_{out} and V_{DD}. At logic threshold, i.e., $V_{\mathrm{out}} = \frac{1}{2}V_{\mathrm{DD}}$, we have $R_{\mathrm{n}} = R_{\mathrm{p}} \equiv R_{\mathrm{thr}}$.

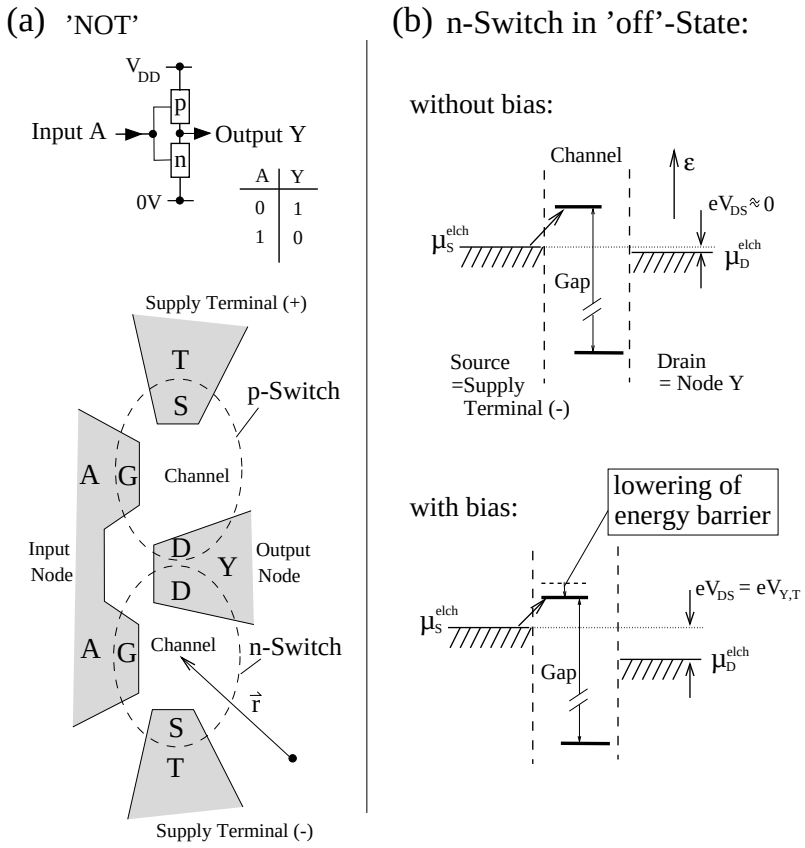

Fig. 7.10. (a) Abritary electrode arrangement modelling a 'NOT' gate or inverter formed by a n-switch and a p-switch in series. The electrostatic potential at position $\boldsymbol{r}$ in the respective channel depend on the potential of all surrounding electrodes, i.e., the input node A (gate electrode G), the output node Y (drain electrode D), the supply terminals T (source electrode S) and possible other electrodes in the surrounding which are not shown. (b) Energy scheme for the n-switch demonstrating the lowering of the energy barrier with changing the drain-source voltage, i.e., in this case the output node voltage $V_{\mathrm{Y,T}}$.

Changing slightly the input voltage around threshold, the energy barrier for electrons is lowered which decreases the resistance for the n-switch by [15]

$$\mathrm{d}R_{\mathrm{n}} = R_{\mathrm{thr}} \cdot \Big(\exp\big(- e\,\mathrm{d}\Phi / k_{\mathrm{B}}T \big) - 1 \Big) \approx R_{\mathrm{thr}} \cdot \big(- e\,\mathrm{d}\Phi / k_{\mathrm{B}}T \big) \ ,$$

[15] The dependence on the position $\boldsymbol{r}$ can be omitted since we assume that the position in the channel with maximum energy barrier does not change and determines the switch current.

whereas the energy barrier for holes rises which increases the resistance of the p-switch by [16]

$$\mathrm{d}R_\mathrm{p} = R_\mathrm{thr} \cdot \Big(\exp\left(e\,\mathrm{d}\Phi/k_\mathrm{B}T\right) - 1 \Big) \approx R_\mathrm{thr} \cdot \left(e\,\mathrm{d}\Phi/k_\mathrm{B}T\right) = -\mathrm{d}R_\mathrm{n}\,.$$

Taking the differential change of (7.25) by $\mathrm{d}V_\mathrm{in}$, the output voltage change $\mathrm{d}V_\mathrm{out}$ at the logic threshold becomes due to (7.24) implicitly

$$\mathrm{d}V_\mathrm{out} = -\frac{\mathrm{d}R_\mathrm{n}}{2\,R_\mathrm{thres}} \cdot V_\mathrm{DD} = -\frac{e\,\alpha_\mathrm{A} \cdot \mathrm{d}V_\mathrm{in} + e\,\alpha_\mathrm{Y} \cdot \mathrm{d}V_\mathrm{out}}{2\,k_\mathrm{B}T} \cdot V_\mathrm{DD}$$

leading to the voltage gain around the logic threshold

$$\mathrm{gain} = \left| \frac{\mathrm{d}V_\mathrm{out}}{\mathrm{d}V_\mathrm{in}} \right| = \frac{\alpha_\mathrm{A}}{2\,k_\mathrm{B}T/(eV_\mathrm{DD}) + \alpha_\mathrm{Y}}\,. \tag{7.26}$$

To get differential voltage gain > 1 at threshold, due to relation (7.26) it requires

- a better electrostatic coupling to the input node A (gate electrode G of the switch) than to the output node Y (drain electrode D of the switch),

$$\alpha_\mathrm{A} > \alpha_\mathrm{Y}\,, \tag{7.27}$$

- and a minimum $V_\mathrm{DD}^\mathrm{min}$ in the supply voltage V_DD,

$$V_\mathrm{DD} \geq V_\mathrm{DD}^\mathrm{min} \equiv \frac{k_\mathrm{B}T}{e} \cdot \frac{2}{\alpha_\mathrm{A}/\mathrm{gain} - \alpha_\mathrm{Y}} > 0\,. \tag{7.28}$$

- For a special arrangement fulfilling $\alpha_\mathrm{T} + \alpha_\mathrm{Y} + \alpha_\mathrm{A} = 1$ and $\alpha_\mathrm{T} = \alpha_\mathrm{Y}$, i.e., symmetric electrostatic coupling to the supply terminal T (source electrode S) and output node Y (drain electrode D), the requirement (7.28) reads

$$V_\mathrm{DD}^\mathrm{min} = \frac{k_\mathrm{B}T}{e} \cdot \frac{4}{\alpha_\mathrm{A} \cdot (1 + 2/\mathrm{gain}) - 1}\,. \tag{7.29}$$

Therefore the supply voltage V_DD should be several times $k_\mathrm{B}T/e$ to get signal level restoration as was pointed out in 1972 by R.M. Swanson and J.D. Meindl [244] in case of MOSFETs. However, result (7.26) and thus the design rules (7.27) and (7.28) are independent of how the energy barrier is defined: by workfunction engineering, by quantum mechanical confinement effect or by the Coulomb-blockade effect. It needs a fundamental minimum supply voltage for all switches based on electrostatically controlling the conductance or current. In the case of $\alpha_\mathrm{A} \to \mathrm{gain} \cdot \alpha_\mathrm{Y}$, the required supply voltage $V_\mathrm{DD}^\mathrm{min}$ grows dramatically as can be seen from (7.28). For $\alpha_\mathrm{A} < \alpha_\mathrm{Y}$, no gain is achievable at all!

[16] For convenience, we assume same geometry for the p- and n-switch, i.e., $\mathrm{d}\Phi$ is the same, described by (7.24).

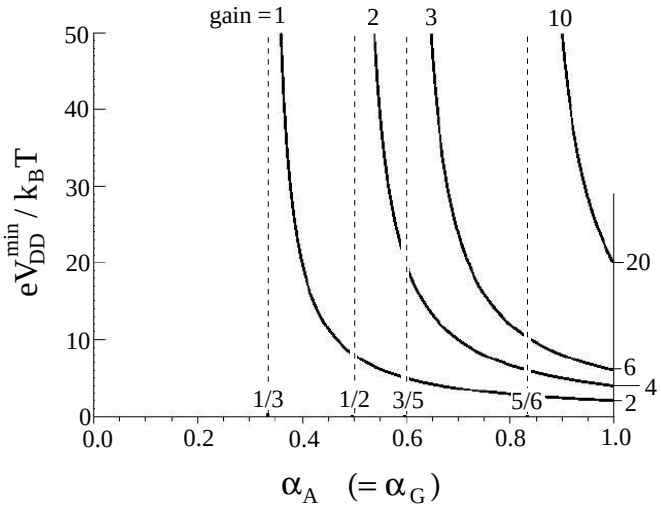

Fig. 7.11. A certain minimum V_{DD}^{min} in the supply voltage V_{DD} is required to obtain a certain differential gain at threshold of the logic 'NOT' gate. V_{DD}^{min} depends on the electrostatics of the switch – characterized by the electrostatic coupling α_A $(= \alpha_G)$ to the input node A –, and thermal fluctuations. For this plot the relation (7.29) is taken, i.e., symmetric capacitive coupling $\alpha_T = \alpha_Y$ and $\alpha_T + \alpha_Y + \alpha_A = 1$, respectively $\alpha_D = \alpha_D$ and $\alpha_S + \alpha_D + \alpha_G = 1$, is assumed. The required V_{DD}^{min} diverges for $\alpha_A = \text{gain} \cdot \alpha_Y$.

Relations (7.27) and (7.28) define severe constraints on the electrostatics of the switch. It is part of what defines a useful transistor.

Taking (7.29), the minimum V_{DD}^{min} in the supply voltage V_{DD} required for certain gain of the network acting as a 'NOT' gate is plotted in Fig. 7.11 versus α_A. Best performance, i.e., lowest V_{DD} is obtained for $\alpha_A \to 1$: Almost the whole image charge for an electron in the channel is induced on the gate electrode (input node A). The required supply voltage diverges for $\alpha_A \to \alpha_Y$, i.e., when the image charge fraction induced on the node electrode (drain electrode) becomes equal the fraction induced on the input node (gate electrode).

7.5.3 Limit due to the Requirement of Low Standby-Power

The intention exists, of course, to minimize the standby power of the logic gate in order to lower the power consumption as far as possible. Which restriction do exist? With changing abruptly the input voltage to the logic gate, the output node capacitor has to be loaded by ΔV_Y in a certain short *delay time* τ. This requires a current I_{on} through the switch in the 'on'-state

delivering the charge $C_Y \Delta V_Y$ by which the node with capacitance C_Y has to recharged within the delay time τ,

$$I_{on} > \frac{C_Y \, \Delta V_Y}{\tau} \, . \tag{7.30}$$

In the best case of our generic switch, this 'on' current I_{on} is related exponentially to the 'off' current I_{off},

$$I_{off} \approx I_{on} \cdot \exp\left(-\frac{e \, \alpha_A \, \Delta V_Y}{k_B T}\right) \, , \tag{7.31}$$

where α_A is again the charge fraction induced on the input node A (gate electrode G). However for a 'NOT' gate as shown in Fig. 7.4b, the change ΔV_Y in the input voltage with switching causes a complementary change $-\Delta V_Y$ in the output voltage: Either the n- or p-switch is in the 'off' state and therefore under drain-source voltage bias in the order of $\Delta V_Y \leq V_{DD}$. Therefore, also the modification of the energy barrier by the change in the electrostatic potential of the output node Y (drain electrode of the switch) has to be taken into account. As a consequence the relation (7.31) has to be modified due to (7.24) to

$$I_{off} \approx I_{on} \cdot \exp\left(-\frac{e \, (\alpha_A - \alpha_Y) \cdot \Delta V_Y}{k_B T}\right) \, . \tag{7.32}$$

The 'on' to 'off' current ratio is according to (7.32) affected by the electrostatics of the switch.

The standby power P_{leak} per logic gate (due to the current leakage I_{off} through the switch in the 'off'-state) is estimated due to (7.32) and (7.30) to

$$P_{leak} \geq I_{off} \cdot V_{DD} \approx \frac{C_Y \Delta V_Y \, V_{DD}}{\tau} \cdot \exp\left(-\frac{e \, (\alpha_A - \alpha_Y) \, \Delta V_Y}{k_B T}\right) \, . \tag{7.33}$$

By defining the *efficiency factor*,

$$\text{EfficiencyFactor} \equiv \frac{C_Y \, \Delta V_Y \, V_{DD}}{P_{leak} \cdot \tau} \approx \frac{I_{on}}{I_{off}} \, , \tag{7.34}$$

the performance of a single logic gate is characterized: The efficiency factor becomes worse if the dissipated energy $C_Y \Delta V_Y \, V_{DD}$ due to switching the bit status is high, and if it requires a long delay time τ for doing this switching. It becomes better if the dissipation under stationary condition due to the leakage current I_{off} between the supply terminals is highly suppressed. [17]

[17] Note, the 'off' current I_{off} is the leakage current under full drain-source bias since under stationary conditions almost the whole voltage V_{DD} drops over the switch in 'off' state. Also I_{on} is defined at full bias over the switch since at the beginning of recharging the output node the voltage drops over the switch although in 'on' state.

The efficiency factor gives a measure for the ratio between the power dissipation due to switching for doing computation ($\propto C_{\rm Y}\,\Delta V_{\rm Y}\,V_{\rm DD}/\tau$) and stand-by power dissipation due to leakage ($\propto I_{\rm off}\cdot V_{\rm DD}$). A high efficiency factor is required allowing for highly integrated circuits with millions of logic gates with a still reasonable low power consumption.

Today's MOSFETs in digital integrated circuits offer $I_{\rm on}/I_{\rm off} > 10^8$, i.e., an efficiency factor of larger than 10^8. [18]

With the efficiency factor (7.34), the constraint on the voltage swing $\Delta V_{\rm Y}$ to suppress standby power dissipation but delivering the required short delay follows from (7.33),

$$\Delta V_{\rm Y} \geq \Delta V_{\rm Y}^{\rm min} \equiv \frac{k_{\rm B}T}{e}\cdot\ln\Big(\text{EfficiencyFactor}\Big)\cdot\frac{1}{\alpha_{\rm A}-\alpha_{\rm Y}}\,. \tag{7.35}$$

Or if the arrangement of electrodes allows to take $\alpha_{\rm Y}+\alpha_{\rm T}+\alpha_{\rm A}=1$ and $\alpha_{\rm T}=\alpha_{\rm Y}$, relation (7.35) reads

$$\Delta V_{\rm Y}^{\rm min} = \frac{k_{\rm B}T}{e}\cdot\ln\Big(\text{EfficiencyFactor}\Big)\cdot\frac{2}{3\,\alpha_{\rm A}-1}\,. \tag{7.36}$$

In Fig. 7.12, the limit for $\Delta V_{\rm Y}$ given by (7.36) is shown for different efficiency factors as a function of $\alpha_{\rm A}$. If the electrostatics of the switch deviates from $\alpha_{\rm A}=1$, higher voltage swings $\Delta V_{\rm Y}$ are required. Especially for large node capacitances $C_{\rm Y}$, i.e., large fan-out and long wire lines, this relation reflects the dominant constraint on $\Delta V_{\rm Y}$ if short switching delay and low standby power are requested. The required mininum $\Delta V_{\rm Y}^{\rm min}$ in voltage swing $\Delta V_{\rm Y}$ diverges for $\alpha_{\rm A}\to\alpha_{\rm Y}$.

In conclusion, limiting the voltage swing $\Delta V_{\rm Y}$ and the efficiency factor, the relation (7.35) gives another constraint on the electrostatics of a switch operated by controlling an electrostatic energy barrier. Or vice versa:

- Bad electrostatic arrangement leads to the requirement of a large voltage swing $\Delta V_{\rm Y}$. Optimum, i.e., lowest voltage swing keeping low standby power, is achievable for $\alpha_{\rm A}\to 1$.
- For $\alpha_{\rm A}<\alpha_{\rm Y}$, the switch cannot be turned off since the lowering of the energy barrier by the change $-\Delta V_{\rm Y}$ of the drain-source voltage just compensates for the rise by the gate-source voltage $\Delta V_{\rm Y}$. Therefore, in this

[18] Other device concepts like interference devices or two-terminal resonant tunneling devices are restricted to much lower 'on' to 'off' current ratios. MOSFETs offer in 'on' state 0.5 mA to 1 mA per μm channel width and about 10 nm channel height, – a value which has been kept constant over the years and therefore describes the expectation on drive capability for transistors used in VLSI. On the other hand, a leakage current of $I_{\rm off}=1\,\mu$A would mean for the small number of 10^6 logic gates, a permanent total current of 1 A, for 10^8 a current of 100 A and for 10^{10} a current of 10^4 A, just causing dissipation without doing any computation.

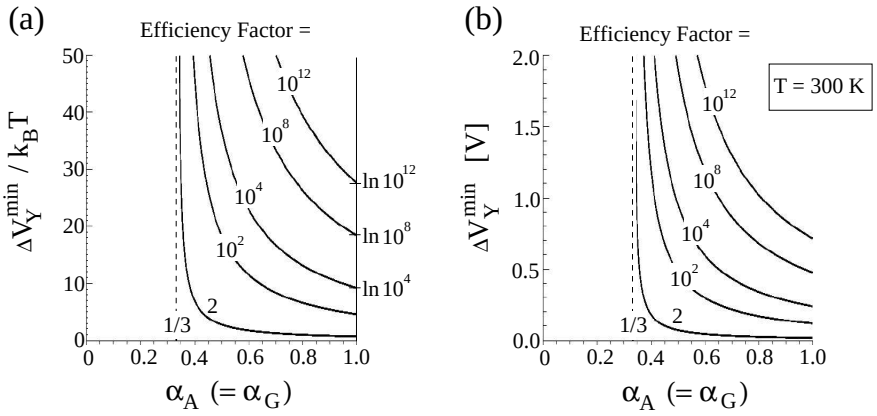

Fig. 7.12. The minimum ΔV_Y^{min} in voltage swing ΔV_Y as a function of the switch characteristic α_A to obtain a certain efficiency factor, i.e., a certain 'on' to 'off' current ratio: (a) Voltage swing ΔV_Y^{min} normalized to $k_B T$. (b) Voltage swing ΔV_Y^{min} for room temperature ($T = 300\,K$). For these plots the relation (7.36) is taken, i.e., symmetric capacitive coupling $\alpha_T = \alpha_Y$ and $\alpha_T + \alpha_Y + \alpha_A = 1$, respectively $\alpha_D = \alpha_S$ and $\alpha_S + \alpha_D + \alpha_G = 1$, is assumed. The required voltage swing ΔV_Y^{min} diverges at $\alpha_A = 1/3$ since there $\alpha_A = \alpha_Y$.

case the logic 'NOT' gate is not working and no suppression of the standby power dissipation in a logic gate due to leakage is possible.

7.6 Generalization: All Electrostatic Switches Suffer the Same Constraints and Therefore Limitations

Derived in the previous Section 7.5, the constraints on a generic switch, where an energy barrier between source S and drain D is electrostatically controlled by a gate electrode G, can be summarized by the following statements:

1. To obtain the necessities 'voltage gain' and 'noise margins' in the elementary logic circuit, a better electrostatic coupling α_G to the gate electrode G, which is part of the input node A and controls the energy barrier in the switch, than to the drain electrode, which is part of output node, is required: $\alpha_G >$ gain $\cdot\, \alpha_D$.
2. To avoid dissipation due to leakage between the supply voltage terminals via the logic gate, the bias induced lowering of the energy barrier has to be suppressed, i.e., it should be $\alpha_G \gg \alpha_D$.
3. For small voltage swing ΔV_Y on the input and output nodes, it has to be α_G close to 1, i.e., full control of the energy barrier between source and drain by the gate electrode is required.

These properties characterize a useful electrostatically controlled transistor.

These electrostatic requirements also demonstrate why for a MOSFET *all* spatial dimensions have to be shrinked by the same factor – described by the 'constant electric field scaling' rule. Let us look at the consequences of deviating from these rules::

- Keeping the insulator at same thickness while reducing the gate length would lead to a reduction of α_G, and therefore to a loss of control over the energy barrier.
- Keeping the depth of the source and drain regions close to the channel region constant while shrinking the channel length would increase α_S and α_D, diminishing α_G.

Such effects have been denoted as *short channel effects* [245]. To fulfill 'constant electric field scaling' requirements with shrinking, the insulator oxide between the gate electrode and channel must be thinned and /or increased in its dielectric constant. A superior insulator is required to get the gate electrode as close as possible to the channel region for controlling the energy barrier between source and drain, and allowing therefore for reaching short channel length. Since the usual insulator of MOSFETs, the SiO_2 becomes intolerable leaky below 1.3 nm [246], large efforts are undertaken to find a replacement – an insulator with higher dielectric constant and at least same insulating properties. The search has not been successful up to now.

Not being able to follow any longer the scaling rule for the conventional MOSFET, the electrostic design of MOSFETs have to be changed [247, 248]:

- A better electrostatic behaviour is obtained for MOSFETs fabricated in a thin silicon layer on top of an insulator (Silicon-on-Insulator (SOI) substrate) [249].
- Since the electrostatic coupling to the drain electrode (the output node in the logic gate) has to be kept small, electrodes under the channel have been proposed which are connected to the source electrode [248]. Therefore α_S is enhanced, diminishing α_D.
- The most powerful design is a 'double-gate' [250, 251, 252, 253] or 'gate-all-around' [254] arrangements where the channel is sandwiched between gate electrodes commonly controlled by the voltage swing. The electrostatic coupling α_G is significantly improved in comparison to the usual design. By this improved electrostatics, a channel length of few 10 nm for MOSFETs is possible still offering reasonable good characteristics.

What about the SET? A better electrostatic coupling of the island to a gate electrode than to the drain electrode is achievable if the spatial dimensions of the island are in the range of few hundred nanometers. For metal single-electron transistors this is expressed by $C_G > C_D$, i.e., the partial capacitance of the island to the gate has to be larger than to the drain electrode [25]. SETs with gain in the respective circuitry have been demonstrated [255, 256, 257], however only with gain ≤ 3 and working at low temperature

due to the rather small single-electron charging energy E_C caused by the large island size. Operation at room temperature requires island sizes in the range of few nanometers since the np-gap [19] has to be more than 3/2 of the applied bias $e\,\Delta V_Y$ given by the voltage swing ΔV_Y of the output node. The island has to be coupled to source and drain electrodes by tunneling barriers – unavoidable accompanied by electrostatic couplings α_S and α_D to these lead electrodes –, and at the same time capacitively coupled by α_G to a gate electrode controlling the electrostatic potential of the island. However, the electrostatic requirement for a useful transistor $\alpha_G > \alpha_D$ or even $\alpha_G \to 1$ are hardly achievable at that small island size. This was already pointed out by L.I. Lutwyche and Y. Wada [189] in 1994.

In summary, fulfilling $\alpha_G \to 1$ and keeping it even at shortest channel lengths is the problem of *any* switch operated by controlling an electrostatic energy barrier – MOSFETs made of Silicon, GaAs, plastic or other semiconductor material, single-electron transistors or transistors embedding quantum dots, single molecules or atoms.

7.7 Requirements due to Variations in Individual Device Characteristics

Manufacturing components of a circuit, individual samples show always deviations in their characteristics between each other. They are due to several causes, for example:

- geometric manufacturing tolerances,
- variations in doping and impurties,
- aging, and
- temperature variations.

Therefore, also composed devices like logic gates show a certain spread in their operating parameters and characteristics.

In practice, digital circuits with MOSFETs are not running at the minimum in voltage swing ΔV_Y or supply voltage V_{DD} as just derived from fundamental considerations. The reason is that relying on the exponential $I_{DS}(V_{GS})$ characteristics of a MOSFET would require perfect control over the threshold voltage for turning on and off the MOSFETs: Small deviations would lead to large deviations from the designed 'on' and 'off' current, which increases the leakage current and/or slows down the switching. To ensure low leakage current and full speed for all logic gates in the whole circuit, an *enlarged voltage swing* has to be used in order to reach with certainty the required 'on' and 'off' currents for all transistors in the circuit (see Fig. 7.13) [228]. MOSFETs allow to do this since *their* $I_{DS}(V_{GS})$ *characteristics are monotonic in* V_{GS}.

[19] Quantum confinement effect might help here to obtain a large np-gap since these dominate at small island size over the single-electron charging energy.

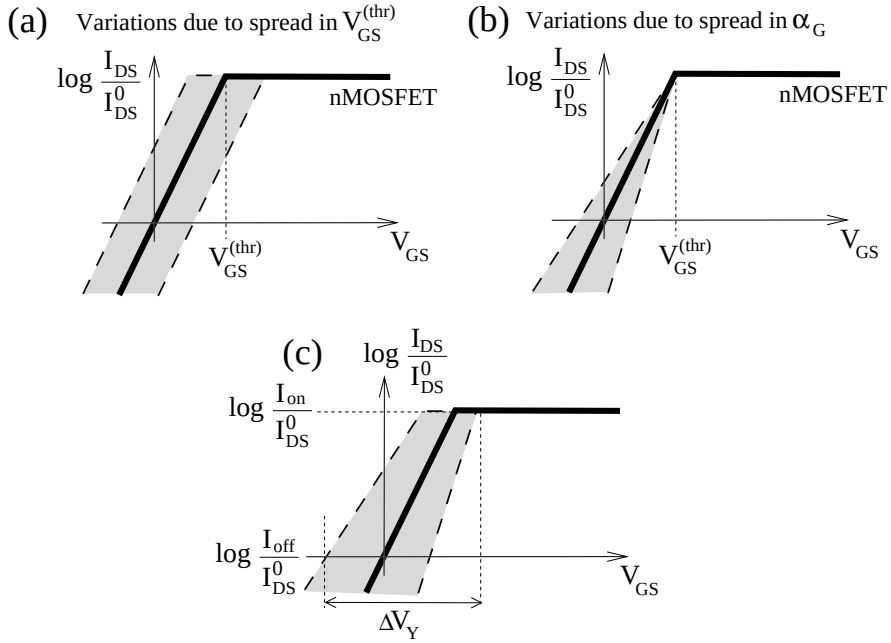

Fig. 7.13. Variations in the device characteristics of an ensemble of MOSFETs: for instance, (a) due to the spread in the threshold voltage $V_{GS}^{(th)}$, or (b) due to variations in α_A (for example, by variations in the oxide thickness) or by temperature variations. (c) The required 'on' to 'off' current ratio is ensured for the whole ensembles by a larger voltage swing ΔV_Y than required in case of identical MOSFETs.

What about a SET? As described in Chapter 1, the characteristics of a single-electron transistor shows for $V_{DS} < 2\,E_C/e$ Coulomb blockade oscillations.

> Due to the *non-monotonic characteristics of SETs*, the voltage swing has to fit exactly for turning on and off the transistor. There is no tolerance built in the $I_{DS}(V_{GS})$ characteristics of a SET, – an important disadvantage in comparison with MOSFETs. [20]

Up to now, the MOSFET characteristics is dominated by bulk properties modified by doping. Size effects – like variations in the gate insulator thickness, gate length, channel thickness – are considered as limiting factor for the fabrication of reliable working highly integrated circuits since they lead to strong variations in the MOSFET characteristics.

[20] It has been proposed of using the specific SET characteristics to implement compact logic gates. However, also this requires perfect control over the design and background charges. Such designs even propose the use of several gates coupling to the SET island.

For SETs, the important parameters – single-electron charging energy and/or quantization energy determining the np-gap of this transitor – are controlled by the geometry. More severe, the tunnel coupling between island and leads depends exponentially on the barrier height and spatial length. Therefore, geometries needs to be far better controlled in comparison with MOSFETs.

These requirements are also valid for all new kinds of transistors depending in their characteristics on geometical sizes and proposed as candidates for VLSI. For making uniform devices, molecular electronics based on self-assembly is usually proposed as the solution [258, 259], although not demonstrated.

7.8 SET: Efficiency Factor and Constraint due to Speed Performance

There is a second reason for running MOSFET transistors with higher voltage swing $\Delta V_{\rm Y}$: Although beyond threshold for turning on the MOSFET the conductance, respectively current increases only linearly with the gate voltage before reaching saturation, it speeds up the switching. Not using this additional increase in conductance, respectively current would mean a loss in speed performance.

For SETs acting as a switch, the np-gap cannot be smaller than the drain-source bias: We are restricted to the single-electron tunneling regime. The current is carried by single electrons passing the island one by one. In conventional MOSFETs, the Coulomb blockade effect is not present and therefore charge carriers are passing the channel almost independently which allows to increase the conductance by charge accumulation.

How far can we rise with a single-electron transistor the 'on' to 'off' current ratio $I_{\rm on}/I_{\rm off}$? To obtain the 'on' current $I_{\rm on} > C_{\rm Y}\Delta V_{\rm Y}/\tau$ required for the switching time τ, a single electron has to pass the island in the time

$$\tau_e < \frac{e}{I_{\rm on}} < \frac{e\,\tau}{C_{\rm Y}\,\Delta V_{\rm Y}}\,. \tag{7.37}$$

This requirement defines the strength of the tunnel coupling of the island to the leads, i.e., it determines the width and height of the tunnel barrier between island and leads. With switching off the transistor, the electrostatic energy barrier ΔE arises for charging the island, not affecting the tunnel coupling to the leads. *Heisenberg uncertainty relation* comes into play: Although the electron from source feels the energy barrier $\Delta E = \Delta E_{\rm S\to I}$, the island can be occupied by an electron if the life time for the electron on the island, which can be estimated by τ_e, is short enough: $\Delta E = \hbar/\tau_e$. To evaluate the ratio $I_{\rm on}/I_{\rm off}$, we consider first the transmisson probability $t(\Delta E)$ for an electron passing the island if the occupation would cost the energy ΔE: In the strong tunnel coupling regime the corresponding transmission probability depends

on ΔE given by a Lorentzian function. [21] Therefore the current from source to drain [115] becomes

$$I_{\mathrm{DS}} \propto \frac{1}{1+\left(\Delta E\, 2\,\tau_e/\hbar\right)^2}\,. \tag{7.38}$$

The 'on' current is obtained for $\Delta E = 0$, and should fulfill

$$I_{\mathrm{on}} > \frac{C_{\mathrm{Y}}\Delta V_{\mathrm{Y}}}{\tau}. \tag{7.39}$$

This fixes the proportionality factor in (7.38) to $> I_{\mathrm{on}}$. The 'off' current I_{off} is related to the 'on' current I_{on} due to (7.38) with rising the energy barrier ΔE by

$$\frac{I_{\mathrm{off}}}{I_{\mathrm{on}}} = \frac{1}{1+\left(\Delta E\, 2\,\tau_e/\hbar\right)^2}\,,\ \text{where}\ \Delta E = e\cdot(\alpha_{\mathrm{A}}-\alpha_{\mathrm{Y}})\cdot\Delta V_{\mathrm{Y}}\,. \tag{7.40}$$

Relation (7.40) expresses the following:

> A short life time τ_e of electrons on the island allows a leak current I_{off} between source and drain due to tunneling which depends with ΔE by a Lorentzian on I_{on}. The 'off' current I_{off} is no longer exponentially suppressed by ΔE as it occurs for a pure classical barrier.

With (7.40) and (7.39), the standby power P_{leak} can be estimated to

$$\begin{aligned} P_{\mathrm{leak}} > I_{\mathrm{off}}\cdot\Delta V_{\mathrm{Y}} &= \frac{C_{\mathrm{Y}}\left(\Delta V_{\mathrm{Y}}\right)^2}{\tau}\cdot\left[1+\left(\frac{e^2\,2\tau\cdot(\alpha_{\mathrm{A}}-\alpha_{\mathrm{Y}})}{\hbar\, C_{\mathrm{Y}}}\right)^2\right]^{-1} \\ &\approx \left(\frac{\hbar}{e^2}\right)^2\cdot\left(\frac{\Delta V_{\mathrm{Y}}}{\alpha_{\mathrm{A}}-\alpha_{\mathrm{Y}}}\right)^2\cdot\left(\frac{C_{\mathrm{Y}}}{2\,\tau}\right)^3\,. \end{aligned} \tag{7.41}$$

Obviously, an increase of ΔV_{Y} does not help here to suppress leakage which is in contrary possible in the case of an exponential dependence of the 'on' to 'off' current ratio on ΔV_{Y} leading to (7.33). Restricting P_{leak} and prescribing τ for given C_{Y} allows only a certain *maximum* $\Delta V_{\mathrm{Y}}^{\max}$ in voltage swing ΔV_{Y},

$$\Delta V_{\mathrm{Y}} < \Delta V_{\mathrm{Y}}^{\max} \equiv \frac{e^2\cdot 2\,(\alpha_{\mathrm{A}}-\alpha_{\mathrm{Y}})}{\hbar}\cdot\left(\frac{\tau}{C_{\mathrm{Y}}}\right)^{\frac{3}{2}}\cdot\left(P_{\mathrm{leak}}\right)^{\frac{1}{2}}\,, \tag{7.42}$$

[21] The same result is found for a MOSFET transistor of very short channel length or any other electronic devices with a short energy barrier: Let us consider tunneling of an electron with incident kinetic energy $\varepsilon = \frac{1}{2}m_e^* v^2$ through a rectangular barrier of height V_0 and length ℓ. For a thin and low barrier ($\sqrt{2m_e^*\Delta E/\hbar^2}\cdot\ell \ll 1$ with $\Delta E = V_0 - \varepsilon$), the transmission probability for the electron becomes $t(\Delta E) = 1/\{1+(\Delta E/\hbar^2\cdot 4\,\ell^2/v^2)\}$ as can be deduced from treatments found in textbooks on quantum theory [260]. Setting approximately $\ell/v \approx \tau_e$, the current through the barrier is described by the Lorentzian given with (7.38).

which goes down to zero for short switching time, respectively delay time τ and large node capacitances C_Y. The largest value for ΔV_Y^{max} are possible for $\alpha_A \to 1$. For $\alpha_A \leq \alpha_Y$, the logic 'NOT' gate does not work at all.

Relation (7.40) gives directly the *efficiency factor for a single-electron transistor in the strong tunnel coupling regime*,

$$\text{EfficiencyFactor} \approx \frac{I_{on}}{I_{off}} < 1 + \left(\frac{e^2\, 2\tau \cdot (\alpha_A - \alpha_Y)}{\hbar\, C_Y} \right)^2 . \qquad (7.43)$$

Thus, the efficiency factor of a SET is limited by the ratio of the required delay time τ in switching the bit status and the node capacitance C_Y. Large node capacitances allow only a large delay time τ. Otherwise the leakage current I_{off} and therefore the standy-by power P_{leak} is increased. In Fig. 7.14 the efficiency factor (7.43) is plotted versus the node capacitance C_Y for different delay times τ. To reach a short delay time τ for a certain efficiency

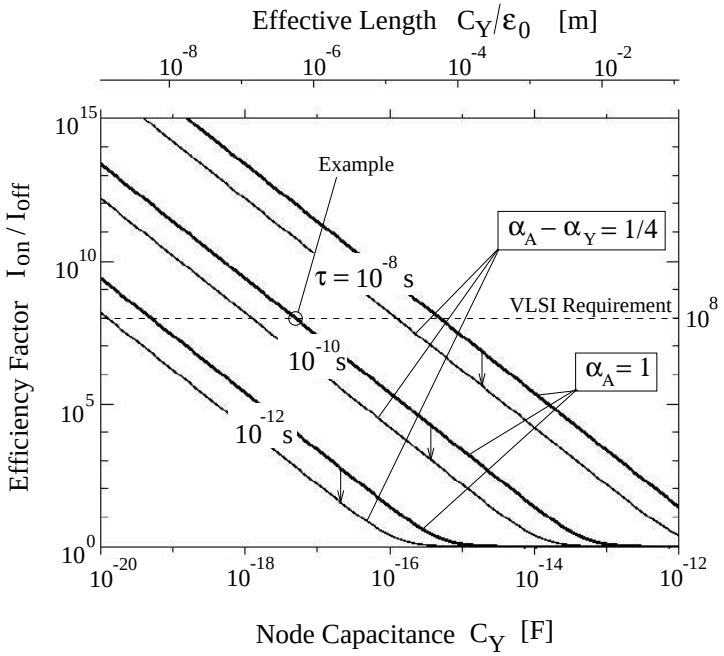

Fig. 7.14. For a transistor based on electrostatically controlling a tunnel barrier – like in a strong tunnel-coupled single-electron transistor –, the efficiency factor I_{on}/I_{off} is limited by the node capacitance C_Y and the required short delay time τ for switching the bit status. For $\alpha_A = 1$, best performance is obtained. The efficiency factor becomes worse with the factor $\alpha_A - \alpha_Y < 1$ as indicated by the respective arrow. The case $\alpha_A - \alpha_Y = 1/4$ is shown. For $\alpha_A \leq \alpha_Y$, the efficiency factor becomes unity for any C_Y value: The logic gate does not operate properly since the output swing ΔV_Y is zero.

factor, the node capacitance C_Y has to be restricted to [22]

$$C_\mathrm{Y} < \frac{e^2}{\hbar} \cdot \frac{2\,\tau \cdot (\alpha_\mathrm{A} - \alpha_\mathrm{Y})}{\sqrt{\mathrm{EfficiencyFactor}}} \,. \tag{7.44}$$

For $\tau = 0.1$ ns [23], $\alpha_\mathrm{A} = 1$ and an efficiency factor of 10^8 required for VLSI, the node capacitance has to be limited to $C_\mathrm{Y} < 4.8 \cdot 10^{-18}$ F. For such small capacitances, the single-electron charging energy $E_\mathrm{C} = e^2/2C_\mathrm{Y}$ already exceeds the thermal energy $k_\mathrm{B}T$ at room temperature: The bit is represented only by few electrons making the representation fragile. Relaxing the efficiency factor to 10^6 (which does not allow high integration), the maximum node capacitance is limited to $C_\mathrm{Y} < 4.8 \cdot 10^{-17}$ F, which corresponds to a node limited by the *effective length* $C_\mathrm{Y}/\epsilon_0 = 5$ μm. This effective length l_eff estimates the possible *maximum length L of a metal wire* via its self-capacitance $C = 2\pi\epsilon_0\epsilon\, L/\ln(L/R_0)$ (see (C.11)), where R_0 denotes the wire radius: $L \leq l_\mathrm{eff}/\epsilon$ for a L-to-R_0 ratio of about 500. Note, the effective length l_eff becomes worse if $\alpha_\mathrm{A} - \alpha_\mathrm{Y} < 1$. For $\alpha_\mathrm{A} - \alpha_\mathrm{Y} = 1/4$, i.e., $\alpha_\mathrm{D} = 1/4$, $\alpha_\mathrm{S} = 1/4$, $\alpha_\mathrm{G} = 1/2$ which means gain ≤ 2 in an inverter arrangement, this effective length is only $C_\mathrm{Y}/\epsilon_0 = 1.3$ μm, in a dielectric like SiO_2 with $\epsilon = 4$ we have $C_\mathrm{Y}/(\epsilon_0\epsilon) = 0.3$ μm. From this estimate, it would mean that for an efficiency factor of 10^6 even a wire of 0.3 μm length and radius of few atoms cannot be driven without exceeding the prescribed delay time $\tau = 0.1$ ns. [24]

7.9 Conclusion: Replacing MOSFETs in Logic Gates by SETs Yields No Advantage at All

As we know, highly integrated digital circuits suffer the problem of overall power dissipation. Controlling electrostatically an energy barrier between source and drain is the best known operation mode of a solid state device allowing minimum in the voltage swing between 'on' and 'off' state. Moreover, it allows for complementary working switches. The constraints to minimize the voltage swing ΔV_Y for representing the two bit states are discussed for the circuit of a logic 'NOT' gate in the previous Sections. They are summarized in Fig. 7.15 for three different electrostatics $\alpha_\mathrm{A} = 1$, $\alpha_\mathrm{A} - \alpha_\mathrm{Y} = 0.25$, and $\alpha_\mathrm{A} - \alpha_\mathrm{Y} = 0.1$:

[22] This result reminds on estimating the possible τ by a RC constant with $R > h/e^2$ which was given in Section 1.7 as the requirement on the tunnel barrier resistance of a metal SET.

[23] For comparison, sub-0.1 μm MOSFETs allow switching times of few 10 ps demonstrated in ring oscillator arrangements (for example, realized in 0.07μm CMOS with $I_\mathrm{on}/I_\mathrm{off} \approx 10^5$ [213]).

[24] Note, statistics has to be used to estimate the error probability that the node capacitor is not recharged at a certain time. This aggravates further the requirement on a short delay time τ for a given clock period T by which the whole circuit should run with high certainty. For typically $\tau = 0.01 \cdot T$ to $\tau = 0.1 \cdot T$, the clock frequency is limited to 0.1 to 1 GHz.

- At small node capacitance values C_{Y}, the bit representation is affected by thermal fluctuations. To suppress errors, a certain minimum $\Delta E_{\mathrm{Y}}^{\mathrm{min}} = \frac{1}{2} C_{\mathrm{Y}} \Delta V_{\mathrm{Y}}^2 = (\Delta N\, e)^2 / 2 C_{\mathrm{Y}}$ of electrostatic energy has to be stored on the node capacitor. The required minimum voltage swing ΔV_{Y} is plotted versus the node capacitance C_{Y} for the error probability $\mathcal{P}^{\mathrm{err}} = 10^{-19}$ at room temperature. The required voltage swing increases with decreasing C_{Y}.
- To allow bit signal restoration, a minimum in supply voltage is required – strongly affected by the electrostatics of the switch. Supply voltages of several $k_{\mathrm{B}}T/e \approx 26$ mV have to be applied, independently of the output node capacitance C_{Y}.
- More severe, the requirement due to leak by thermal activation of electrons over a pure classical barrier limits the reduction of ΔV_{Y} especially for large node capacitance values C_{Y}: To suppress this standby power dissipation while allowing a high speed performance requires the optimum in the electrostatics of the switch. Using the estimate (7.33), the minimum in voltage swing $\Delta V_{\mathrm{Y}}^{\mathrm{min}}$ is plotted in Fig. 7.15 for rather moderate values of $P_{\mathrm{leak}} = 0.1$ nW, $\tau = 0.1$ ns. [25] The optimum of electrostatics for the switches is $\alpha_{\mathrm{A}} = 1$, respectively $\alpha_{\mathrm{G}} = 1$.
- Single-electron transistors – or in general transistors with thin and low barriers – are limited in their efficiency factor $\approx I_{\mathrm{on}}/I_{\mathrm{off}}$ because – due to quantum mechanical tunneling – a relatively large current I_{off} is related to it in the 'off' state. A large voltage swing increases $I_{\mathrm{on}}/I_{\mathrm{off}}$ but requires an increase in I_{on} for a given τ. This actually limits the possible voltage swing for large C_{Y}, which is not the case for an exponential dependence assumed for our generic switch. In Fig. 7.15 the maximum value for the voltage swing is indicated as a function of the node capacitance C_{Y}, obtained from (7.42) for a standy power of $P_{\mathrm{leak}} = 0.1$ nW and a delay time τ of 0.1 ns. [26]

We can summarize: The minimum voltage swing $\Delta V_{\mathrm{Y}}^{\mathrm{min}}$ required due to fundamental constraints depicted in Fig. 7.15 are for sufficient high α_{A} in the range of several hundreds of milliVolts at room temperature. The np-gap in the channel region of the transistor has to be at least 3/2 of the value $e\Delta V_{\mathrm{Y}}^{\mathrm{min}}$. To get a large np-gap for a single-electron transistor, the island has to be small which is of course possible: In the ultimate limit, such an island might be represented by an impurity state in a dielectric. However, it makes it almost impossible in a simple arrangement of a single-electron-transistor to fulfill the electrostatic requirements and keeping the tunnel coupling of the island to the leads. To come around the electrostatic constraint, several islands can be arranged in series forming the channel between source and drain [189]. To obtain a higher drive current I_{on}, several of such islands can be arranged in parallel. Such an array of islands would not lead to an improve in performance when comparing with a conventional FET, – in contrary, it

[25] See footnote 24.
[26] See footnote 24.

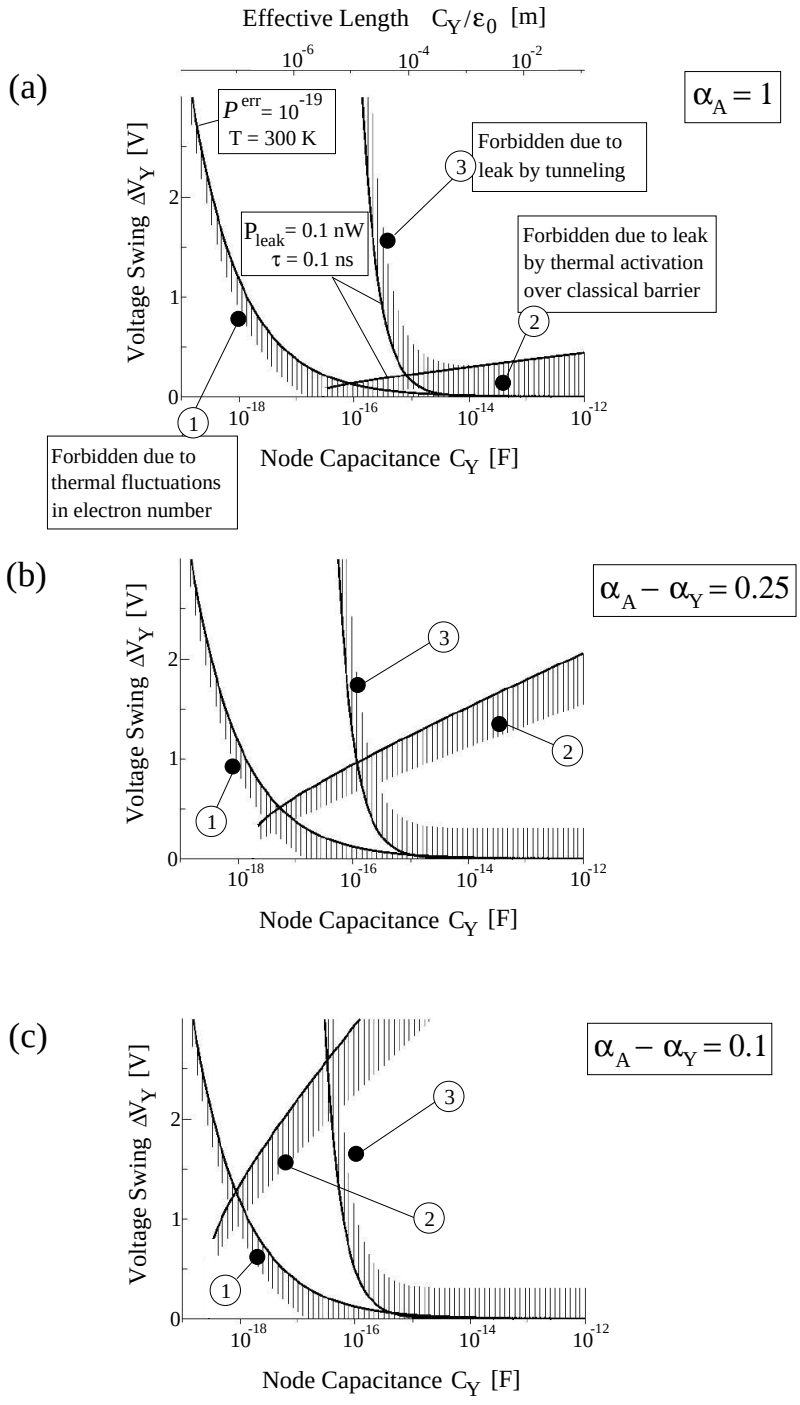
(a)
Effective Length C_Y/ε_0 [m]
10^{-6}
10^{-4}
10^{-2}
$\alpha_A = 1$
$P^{err} = 10^{-19}$
T = 300 K
Forbidden due to leak by tunneling
P_{leak} = 0.1 nW
τ = 0.1 ns
Forbidden due to leak by thermal activation over classical barrier
Voltage Swing ΔV_Y [V]
0
1
2
1
2
3
10^{-18}
10^{-16}
10^{-14}
10^{-12}
Forbidden due to thermal fluctuations in electron number
Node Capacitance C_Y [F]
(b)
$\alpha_A - \alpha_Y = 0.25$
Voltage Swing ΔV_Y [V]
Node Capacitance C_Y [F]
(c)
$\alpha_A - \alpha_Y = 0.1$
Voltage Swing ΔV_Y [V]
Node Capacitance C_Y [F]

Fig. 7.15. (Left page) Constraints in the voltage swing ΔV_Y of a logic 'NOT gate built from complementary working switches versus the output node capacitance C_Y: Lower limit due to thermal fluctuations in the electron number for small C_Y ($\mathcal{P}^{err} = 10^{-19}$, $T = 300$ K), lower limit due to leakage over the classical barrier for large C_Y and short delay time ($P_{leak} = 0.1$ nW, $\tau = 0.1$ ns) and a upper limit due leakage by tunneling ($P_{leak} = 0.1$ nW, $\tau = 0.1$ ns). The limits are strongly affected by the electrostatics of the switch: (a) for $\alpha_A = 1$, (b) for $\alpha_A - \alpha_Y = 0.25$, (c) for $\alpha_A - \alpha_Y = 0.1$. (adopted from [261])

might show hysteretic behaviour in the current I_{DS} with changing the voltage on the gate electrode. [27]

As pointed out, a monotonic $I_{DS}(V_{GS})$ characteristics of a conventional FET allows to compensate for variations in the characteristics of FETs by simply enlarging the voltage swing. This is not possible for transistors with non-monotonic switching behaviour – as the single-electron transistor. The lack of a monotonic $I_{DS}(V_{GS})$ characteristic is a severe disadvantage of single-electron transistors. For using an ensemble of them in electrical circuits, more severe control over the geometrical sizes and background charges is required which is hardly to achieve with present manufacturing technology. [28] Finding a solution here, however, does not annul the electrostatic design requirements.

Based on this analysis, we can even state that single-electron transistors are not smaller in spatial size than ultimate FETs:

- The channel length of electrostatically controlled transistors are determined by the same electrostatic contraints. The choice of geometry and materials' dielectric properties decides here about the performance and size. [29]
- The properties of the channel allow a more or less high 'on'-current. However, the channel width is adjustable in the conventional concept of field-effect transistors. It can be adopted to the drive-current requirements. [30] Therefore, if small 'on' current are acceptable, the channel width can be made small – if perfect control over size parameter is possible, even less than the channel length [263]. Although the size is now comparable, electron transport is conceptionally not restricted to single-electron transport.

[27] Such devices have been demonstrated as memory devices [262].

[28] Koroktov [190] gives limits for the variations in the SET parameters possible under certain conditions.

[29] A built-in energy profile along the channel might be an addition design option for determing the position of the maximum height of the barrier. This might be acheived by varying the material composition along the channel, by inducing strain etc..

[30] Due to the lower hole mobility in pMOSFETs than the electron mobility in nMOSFETs, the width w of pMOSFETs is usually three times larger than the width of nMOSFETs.

Therefore, conceptionally the single-electron transistor does not offer any advantage in digital circuits in comparison to a conventional field-effect transistor. [31]

7.10 Perspective

Using silicon technology as the base, the concept of a conventional FET will be pushed to its limits, which is definitely given when quantum mechanical tunneling causes significant leakage in the device. [32] Since the 'on' to 'off' current ratio will suffer with shrinking, the device design will finally diverge in detail driven by the trade-off between ultimate speed and low power consumption. The different designs might even be realized on the same chip to optimize the overall performance. As in the past additional materials and deposition techniques will be introduced pushing the physical concept of electrostatically controlling a *classical barrier* further. Conventional doping will be replaced by work function engineering. Devices based on molecules which mimick properties known from solid-state devices like pn-junctions or electric field effect are competing with their counterparts made in solid state semiconductors. They broaden the options, however they are not removing the fundamental design constraints derived above.

To improve in the performance of digital circuits using complementary working switches, all relations derived in the previous Sections as limitations on the switch suggest to search for a switch with $\alpha_{\mathrm{A}} > 1$. Is such a switch unphysical? An ensemble of ion channels in the membrane of neurons (nerve cells) show an exponential current dependence on the voltage drop ΔV over the cell membrane described by

$$I \propto \exp\left(\frac{\alpha\, e\, \Delta V}{k_{\mathrm{B}} T}\right) , \tag{7.45}$$

where α is in the range between six and eight. This is possible due to a conformation change of the ion channel opening or closing the pore for K^+ or Na^+ ions with ΔV. In such a channel molecule several elementary charges are linked together by the molecule backbone which feel the voltage ΔV change as a unit. Therefore such a conformation change is stable against

[31] The Coulomb blockade effect has been observed in MOSFETs of small size due to disorder potentials caused by the dopants in the channel (for example [264]). However, doping of the MOSFET channel is conceptionally not necessary, i.e., ultimate FETs do not necessarily show Coulomb blockade effects.

[32] Tunneling finally occurs through the gate insulator or directly between source and drain even in the 'off'-state of the device. The latter is dominated by band-to-band tunneling: In a nMOSFET in the 'off' state under drain-source bias, electrons can tunnel from the valence band in the channel to the conduction band of drain. In terms of the generic switch, the np-gap has to be increased suppressing this effect.

thermal fluctuations even at small membrane voltages. The current path is 'mechanically' opened and closed.

Can the concept of digital circuits based on complementary working switches be pushed further by using 'electromechanical' switches based on conformation changes of molecules? At first glance, certain conceptional options are attractive:

- Such a device concept might allow to operate the circuitry with a low voltage swing if the switch state is stabilized by electrical charges feeling *as a unit* the voltage swing in the input node.
- The electrostatic constraint described above for a pure electrostatic switch might be removed, i.e., the gate electrode need not to be that close to the device channel: The conformation change is induced by an electric field change on one site, and as a consequenece the channel is closed or opened at a different site of the molecule.
- Although the transport in 'on' state of such a device might occur by single-electron transport, a better 'on' to 'off' current ratio is achievable than in conventional SETs with fixed island and tunnel barrier parameters: The barrier for electrons between source and drain in the 'off' state can be made long by opening physically a spatial gap between source and drain, leading to a barrier in the 'off' state which is therefore less transparent for tunneling.

Whether such device concepts are feasible requires a further analysis, although I do not except here a breakthrough for digital circuits: The complexity of integrated cicruit is obtained not only by the number of transistors on a chip but by the degree of freedom in wiring these to a functional network. Actually, this wiring could not be shrinked in its spatial dimensions in the same way as the transistors. More and more wiring layers have been added. This gives further pressure on having a high 'on' to 'off' current ratio, since the node capacitance connecting the logic gates are not shrinking appropriately.

For many decades now the search has been going on for other concepts of doing computation solving certain tasks. The result can be summarized in the statement that the time evolution of any physical system can be interpreted as a system doing a sort of computation. Setting the boundary conditions and/or the initial state of the system defines the input, the final state after the time evolution the output. The problem is, how to make it useful, adoptable to purpose, robust and reliable. Such proposals abandon the idea of metal wiring logic gates, replacing the logic gates by elementary cells which physically interact in a certain way with its neighbour cells and sometimes even only for a definite period of time. Such arrangements can behave still as a classical system or even as a quantum mechanical system. Certain proposals use elements based on single-electron charging effects:

- An example for an elementary cell is an arrangement of islands which are tunnel coupled. Such cells can be charge polarized due to single-electron rearrangements between the islands. The cells are electrostatically interacting with neigbouring cells. This concept is known under the name 'quantum-dot cellular automata' (see review [265]). Several of such cells are arranged to mimick logical gates.
- Another proposal uses two tunnel-coupled quantum dots for defining a two-level system which represent a qubits – the elementary unit for a quantum computer (see [266] and references in there).
- Combining single-electron charging effects with superconductor properties allowing for a macroscopic phase coherence is another direction of realising a qubit [267, 268].

Presenting and evaluating these proposals is beyond the focus of this work which concentrates on the electrical transport through a quantum dot embedded between electrodes.

Besides this, single-electron charging effects are also discussed for the use in memory devices, combined with conventional MOSFETs [2]. These proposals are in the line of conventional floating-gate devices and devices where electrons are trapped by implanted ions in the gate dielectrics affecting the conductance of the underlying MOSFET channel.

8. Outlook

In this treatise the electrical transport through quantum dot systems is discussed. The theoretical description is supported by experimental results at each stage. Step-by-step the complexity is rised. In a retrospective glance at the treated topic, we can state: By simple energy considerations for rearranging single electrons between the quantum dot and its leads, the basic characteristics of such an arrangement are derived. The picture of sequential tunneling using rate equations covers most of the features observed in experiment. However, especially at low temperature the picture of single-electron transport breaks down. Correlated tunneling has to be taken into account leading under certain conditions even to the conductance which is equal to a spin-degenerate one-dimensional channel. Here we are at the front of the actual basic reasearch.

At present, the following aspects require further clarification and are therefore under experimental investigations in our and other laboratories:

- What kind of excitations are visible in the regions of single-electron transport? Especially small quantum dots in a lateral arrangement show energetically low-lying excitations which are below those expected from the single-particle spectrum. Quasi-selection rules – predicted by theory – have to be experimentally verified. Photoexcitation by microwave radiation might be a tool to demonstrate that excitations in the center-of-mass motion are those seen in certain transport experiments [269].
- To describe transport through molecules, additional feature have to be included, – for instance, conformation changes of the molecule. It is still an experimental challenge electrically contacting a molecule *and* offering the parameters which can be in-situ tuned to explore the system. What about model systems mimicking the respective properties?
- Correlated electron transport has to be further investigated. Testing the quantum mechanical phase coherence by dual-path interference experiments are recently presented for the Kondo state [178, 270], although not understood.
- By using a third reservoir tunnel-coupled to the quantum dot, the spectral function of the quantum dot system may directly be investigated with in-situ tuning the parameters. Up to now, only quantum dot systems with asymmetric tunnel bariers have been investigated demonstrating that a

Kondo resonance is pinned to the Fermi level of the stronger tunnel-coupled lead [271].

- Recently we found [184] a very regular pattern of enhanced and suppressed conductance in the Coulomb blockade regions of large quantum dots (enclosing about 40 electrons) with a magnetic field applied perpendicular to the plane of the 2D quantum dot system. The regions of enhanced conductance show the basic features of Kondo physics. A well-established model [125] has been used indeed explaining the behaviour. Nevertheless, the validity of the model has still to be confirmed. Theoretical investigations by C. Tejedor and coworkers hint that correlations between the electrons in the quantum dot seem to play an important role weighing the tunnel coupling.
- Recently, we predicted [272] that two electrostatically coupled quantum dots with separate leads map under certain conditions onto the Anderson impurity model. Such a system represents a spinless realization of the Anderson impurity model: Due to the electrostatic interaction the quantum dot systems become conductive. Recent experimental results [94] seems to confirm the occurrence of a Kondo state. This new realization of the Anderson impurity model would offer more tunable parameters to check theoretical predictions. Especially in a lateral arrangement, in addition the Ahonov-Bohm phase can be used as a tuning parameter. The breakdown of the Kondo state can be investigated by introducting a tunnel coupling between reservoirs.
- An open question is still how to describe the quantum dot in the transition from weakly to strongly tunnel coupled to the leads. The energy level defined for the isolated quantum dot renormalize. Experimentally, strange features have been observed in the regime where the conductance exceeds e^2/h. Their origin has still to be clarified. Some of the features remind on Coulomb blockade regions inversed in their conductance. This has been related to Fano-like resonances [273].

There is a rapid progress in understanding and in experimental use of these quantum dot systems. Especially the controlling of their properties will allow to narrow further the gap between what can be calculated and what can be realized experimentally. Quantitative comparisons will become accessible.

A. Notation and List of Used Symbols

Since the reference for applying voltages is very important for certain characteristics, the reference electrode is always explicitely indicated by the respective index. Indices in italic style are variables, indices in roman style denote named electrodes or are used to name the variable itself. Physical units are printed in roman style.

2DES	Two-**D**imensional **E**lectron **S**ystem.
A	Index (in roman style) denoting a specific electrode; input node of a logic gate.
a_B	Bohr radius.
a_B^*	Effective Bohr radius.
$\alpha_i(\boldsymbol{r})$	Dimensionless electrostatic potential profile of electrode i.
α_S, α_D, α_G, α_Y, α_A	Fraction of image charge induced on the respective electrode indicated by the index.
B	Magnetic field.
C	Index (in roman style) denoting the collector.
CB	**C**oulomb **B**lockade.
CBO	**C**oulomb-**B**lockade **O**scillations.
CIM	**C**onstant-**I**nteraction **M**odel.
const	A constant factor/additive.
C_J	Junction capacitance.
C_{ij}	Capacitance coefficient between conductor i and j.
$C_{i\Sigma}$	Total capacitance of conductor i.
$C_{i,\Sigma}^{(\infty)}$	Self-capacitance of conductor i.
C_G, C_D, C_S, C_G1, C_G2	Partial capacitances of a metal island with the respective electrode denoted by the index.
C_Σ	Total capacitance (sum of all partial capacitances).
C_Y	Capacitance of the output node Y of a logic gate.
d	Distance.
D	Index (in roman style) denoting the drain electrode.
D	Diameter.
$\boldsymbol{D}$	Dielectric field.
$\delta^3(\boldsymbol{r}-\boldsymbol{r}')$	Delta function.

e	Elementary charge, charge quantum.
$-e$	Electron charge.
$\boldsymbol{E}$	Electric field.
E	Index (in roman style) denoting the emitter.
E	Energy.
ΔE	Difference in energy.
E_{elst}	Electrostatic energy stored in a conductor arrangement.
$E_{\mathrm{pot}}(N)$	Potential Energy of N electrons.
$\Delta E_{\mathrm{pot}}^{(s)}$	Potential Energy of electron s.
E_{tot}	Total energy.
ΔE_{tot}	Difference in total energy.
E_{C}	Single-electron charging energy $e^2/2C_\Sigma$.
$\Delta E_{\mathrm{D}\to\mathrm{I}}$, $\Delta E_{\mathrm{S}\to\mathrm{I}}$, $\Delta E_{(\mathrm{D,S})\to\mathrm{I}}$, $\Delta E_{\mathrm{A}\to\mathrm{I}}$	Electrostatic energy barrier for charging a metal island by a single electron from source/drain/electrode A.
$\Delta E_{\mathrm{I}\to\mathrm{D}}$ $\Delta E_{\mathrm{I}\to\mathrm{S}}$, $\Delta E_{\mathrm{I}\to(\mathrm{D,S})}$, $\Delta E_{\mathrm{I}\to\mathrm{A}}$	Electrostatic energy barrier for discharging a metal island by a single electron to source/drain/electrode A.
$\Delta E_{\mathrm{E}\to\mathrm{QD}}$	Energy barrier for charging a single electron from emitter to the quantum dot.
$\Delta E_{\mathrm{QD}\to\mathrm{C}}$	Energy barrier for discharging a single electron from the quantum dot to the collector.
ΔE_{Q}, ΔE_{G}	Shift of electrostatic energy due to charge/gate potentials.
ΔE_{add}	Addition spectrum.
ΔE_{exc}	Excitation spectrum.
ΔE_{Y}	Electrostatic energy change on node capacitor Y.
$\Delta E_{\mathrm{Y}}^{\mathrm{min}}$	Lower limit for ΔE_{Y}.
E_{active}	Electrostatic energy dissipation with switching the output Y of a logic gate.
ϵ_0	Dielectric constant of vacuum.
ϵ	Relative dielectric constant.
$\boldsymbol{\epsilon}(\boldsymbol{r})$	Dielectric tensor depending on $\boldsymbol{r}$.
ε	Single-electron energy.
ε_{i}, ε_{f}	Initial/final single-electron energy.
ε_{F}	Fermi level.
$\varepsilon_{\mathrm{F}}^{(\mathrm{S})}$, $\varepsilon_{\mathrm{F}}^{(\mathrm{D})}$, $\varepsilon_{\mathrm{F}}^{(\mathrm{I})}$	Fermi levels of source, drain and island.
ε_{C}, ε_{E}	Single-electron energy at collector/emitter.
$\varepsilon_0^{\mathrm{C}}$	Conduction band minimum.
$\Delta\varepsilon$	Single-electron excitation energy.
η	Ideality factor of an electrostatic switch.
$\boldsymbol{F}$	Force.
f_{FD}	Fermi-Dirac function.
FIB	**F**ocused **I**on **B**eam.
FQHE	**F**ractional **Q**uantum **H**all **E**ffect.
f_{Q}, f_{G}, $f_{\mathrm{G,Q}}$	'Remaining fraction' describing the charging and

	discharging energy barriers.
$f^{(\mathrm{S})}$, $f^{(\mathrm{D})}$, $f^{(\mathrm{A})}$	'Remaining fraction' to source/drain/electrode A.
$f_{\mathrm{Q}_0^*}$, $f^{\mathrm{l}}_{\mathrm{Q}_0^*}$, $f^{\mathrm{h}}_{\mathrm{Q}_0^*}$	'Remaining fraction' accounting for 'offset charges'.
$\Phi(\boldsymbol{r})$	Electrostatic potential at $\boldsymbol{r}$.
$\Phi_{\mathrm{ion}}(\boldsymbol{r})$	Electrostatic potential at $\boldsymbol{r}$ due to $\rho_{\mathrm{ion}}(\boldsymbol{r})$.
$\Phi_{\mathrm{el}}(\boldsymbol{r})$	Electrostatic potential at $\boldsymbol{r}$ due to $\rho_{\mathrm{el}}(\boldsymbol{r})$.
$\Phi_N(\boldsymbol{r})$	Total electrostatic potential at $\boldsymbol{r}$ in presence of N electrons.
$\Phi_{\mathrm{E}}(\boldsymbol{r})$	Electrostatic potential at $\boldsymbol{r}$ due to the gate electrode with electrostatic potentials V_i.
$\Phi_{\mathrm{ext}}(\boldsymbol{r})$	External confining potential.
g	Effective Land factor.
G, G1, G2	Index (in roman style) denoting a gate electrode.
$G(\boldsymbol{r},\boldsymbol{r}')$	Green's function for a certain electrostatic arrangement.
gain	Gain factor.
Γ	Life-time broadening on an energy level.
$\Gamma^{(\mathrm{E})}$, $\Gamma^{(\mathrm{C})}$, $\Gamma^{(\mathrm{S})}$, $\Gamma^{(\mathrm{D})}$	Tunneling rates.
$\Gamma^{(\mathrm{rel})}$, $\Gamma^{(\mathrm{exc})}$	Relaxation and excitation rates.
h	Planck constant.
$\hbar$	$\hbar = h/2\pi$.
$\hbar\omega_0$	Quantization energy of a harmonic oscillator.
$\hat{\mathbf{H}}$	Hamilton operator.
i	Index.
i_x, i_y, i_z	Index.
I	Index (in roman style) denoting a (metal) island.
I_{DS}	Drain-source current.
I_{CE}	Collector-emitter current.
ΔI_{DS}	Step in drain-source current.
I_{on}, I_{off}	'On'/'off' current through switch.
$\mathrm{int}(x)$	Integer value of variable x.
IQHE	**I**nteger **Q**uantum **H**all **E**ffect.
j	Index.
k_{B}	Boltzmann constant.
k	Absolute value of wavevector, or index.
L, L_x, L_y, L_z	Length.
l^*	Oscillator length.
ℓ	Screening length.
λ	deBroglie wavelength.
λ_{F}	deBroglie wavelength at Fermi energy, Fermi wavelength.
m	Quantum number index
M	Number of electrodes in a conductor arrangement.
MBE	**M**olecular **B**eam **E**pitaxy.

m_e	Free electron mass.
m_e^*	Effective mass of a conduction band electron.
$\mathrm{mod}(x)$	$\mathrm{mod}(x) = x - \mathrm{int}(x)$.
μ_B	Bohr magneton.
μ_e	Electron mobility in a 2DES.
μ^ch	Chemical potential.
μ^elch	Electrochemical potential
μ_i^ch	Chemical potential of conductor i.
μ_i^elch	Electrochemical potential of conductor i.
$\mu_\mathrm{S}^\mathrm{elch}$, $\mu_\mathrm{D}^\mathrm{elch}$	Electrochemical potential of respective electrode denoted by the index.
$\mu_\mathrm{E}^\mathrm{elch}$	$= \max\{\mu_\mathrm{S}^\mathrm{elch}, \mu_\mathrm{D}^\mathrm{elch}\}$, electrochemical potential of emitter.
$\mu_\mathrm{C}^\mathrm{elch}$	$= \min\{\mu_\mathrm{S}^\mathrm{elch}, \mu_\mathrm{D}^\mathrm{elch}\}$, electrochemical potential of collector.
$\mu(N)$	difference in the groundstate energies between the N- and the $(N-1)$-electron system in the quantum dot.
n	Electron number $n \in \{\cdots N-1, N, N+1 \cdots\}$.
N	Total number of electrons on an island/ quantum dot.
N_0	Total number of electrons on an electrical uncharged island.
ΔN	Number of additional electrons on an island/ quantum dot.
n_0	Electron concentration in bulk.
n_s	Sheet electron concentration of a 2DES.
Δn_s	Change in sheet electron concentration of a 2DES.
ν	Landau level filling factor.
ΔN	Additional number of electrons on an previously electrically uncharged island:
ΔN_G	due to changes in the electrostatic potentials $\{V_i\}$.
ΔN_Q	due to charge in the surrounding of the island,
$\Delta N_\mathrm{G,Q}$	due to both,
ΔN_C	due to contact voltages,
$\Delta N_0^{(\mathrm{S})}$, $\Delta N_0^{(\mathrm{D})}$, $\Delta N_0^{(\mathrm{A})}$	'Offset number' of electrons on island by electron exchange with source/drain/electrode A.
N_0^l, N_0^h	Total number of electrons on node electrode Y for logic '1' and logic '0'.
N_C, N_C^h, N_C^l	Critical electron number on node Y for bit error in respective logic state.
$\Delta N_\mathrm{C}^\mathrm{h}$	$= N_0^\mathrm{h} - N_\mathrm{C}^\mathrm{h}$.
$\Delta N_\mathrm{C}^\mathrm{l}$	$= N_\mathrm{C}^\mathrm{l} - N_0^\mathrm{l}$.
P	Probability for a certain state.
P_total	Total power dissipation of a digital circuit.
P_leak	Power dissipation of logic gate due to leakage.

$\mathcal{P}^{\mathrm{err}}$	Bit error probability.
$\boldsymbol{p}_s$	Kinetic momentum of electron s.
$\hat{\mathbf{p}}$	Kinetic momentum operator.
$\hat{\mathbf{p}}_s$	Kinetic momentum operator acting on electron s.
q	Electric charge of metal island, or point charge.
q_i	Image charge induced on electrode i by q.
q_{S}, q_{D}	Image charge induced on respective electrode denoted by the index.
QD	**Q**uantum **D**ot.
Q_i	Total charge on conductor i.
Q_0^*	Total 'offset charge' of island.
ΔQ	Change of charge on a capacitor.
ΔQ_{Y}	Change of charge on output node Y of a logic gate.
$\boldsymbol{r}$, $\boldsymbol{r}'$	Position vector.
$\boldsymbol{r}_s$, $\boldsymbol{r}_{s'}$	Position vector for electron s, s'.
$\hat{\mathbf{r}}$	Position operator.
$\hat{\mathbf{r}}_s$, $\hat{\mathbf{r}}_{s'}$	Position operator acting on electron s, s'.
$\mathrm{d}^3\boldsymbol{r}$	Volume element at position $\boldsymbol{r}$.
R, R_0, R_1	Radius.
R_{J}	Junction tunnel resistance.
R_{T}, $R_{\mathrm{T}}^{(\mathrm{D})}$, $R_{\mathrm{T}}^{(\mathrm{S})}$	Tunnel resistance.
$R_{\mathrm{T}}^{\max}$	$R_{\mathrm{T}}^{\max} = \max\{R_{\mathrm{T}}^{(\mathrm{S})}, R_{\mathrm{T}}^{(\mathrm{D})}\}$.
$\rho_{\mathrm{ion}}(\boldsymbol{r})$	Fixed charge distribution due to ions or trapped electrons.
$\rho_{\mathrm{el}}(\boldsymbol{r})$	Discrete charge distribution of electrons.
s, s'	Index numbering electrons.
s	Scaling factor.
S	Index (in roman) denoting the source electrode.
S	Surface of all conductors of an arrangement.
S_i	Surface of conductor i.
$\mathrm{d}\boldsymbol{S}_i$	Directed surface element at position $\boldsymbol{r}$ at conductor i.
SET	**S**ingle-**E**lectron **T**ransistor.
σ_{on},σ_{off}	'On'/'off' conductance of a switch.
t	Time.
T	Temperature.
T_{K}	Kondo temperature.
τ	Time period. Delay time.
τ_{H}	Life time in Heisenberg uncertainty relation.
τ_e	Mean time for an electron passing the SET.
τ_N	Life time of the charge state with N electrons.
V	Volume.
$V(\boldsymbol{r})$	Confining Potential.
V_i	Electrostatic potential of electrode i.
V_{S}, V_{D}, V_{A}	Electrostatic potential of source/drain/electrode A.

V^{C}	Intrinsic contact voltage (Volta voltage).
V_{ij}^{C}	Instrinsic contact voltage between metal j and i.
$V_{i,\mathrm{I}}^{\mathrm{C}}$	Intrinsic contact voltage between metal island and electrode i.
$V_{\mathrm{DS}}^{\mathrm{C}}$, $V_{\mathrm{GS}}^{\mathrm{C}}$, $V_{\mathrm{GI}}^{\mathrm{C}}$, $V_{\mathrm{DI}}^{\mathrm{C}}$, $V_{\mathrm{SI}}^{\mathrm{C}}$	Intrinsic contact voltage between respective metals denoted by the indices.
V_{DS}	Drain-source voltage.
$V_{\mathrm{DS}}^{(\mathrm{th})}$	Threshold in drain-source voltage.
ΔV_{DS}	Step width/ difference in drain-source voltage.
V_{GS}	Gate-source voltage.
$V_{\mathrm{GS}}^{(\mathrm{th})}$	Threshold in gate-source voltage.
ΔV_{GS}	Difference in gate-source voltage V_{GS}.
ΔV	Difference in electrostatic potential.
$V_{\mathrm{2DES,S}}$	Voltage applied between 2DES and SET source.
$V_{\mathrm{Side,S}}$	Voltage applied between sidegate and SET source.
V_{BS}	Backgate-source voltage.
ΔV_{BS}	Change in backgate-source voltage.
$V_{\mathrm{BS}}^{(\mathrm{S})}(V_{\mathrm{DS}})$, $V_{\mathrm{BS}}^{(\mathrm{D})}(V_{\mathrm{DS}})$	Borderline in $(V_{\mathrm{BS}}, V_{\mathrm{DS}})$ plane for opening a single-electron transport channel on source/drain side.
ΔV_{Y}	Voltage swing on output node Y of logic gate.
$\Delta V_{\mathrm{Y}}^{\mathrm{min}}$, $\Delta V_{\mathrm{Y}}^{\mathrm{max}}$	Lower/upper limit in ΔV_{Y}.
V_{DD}	Supply voltage of a logic gate.
$V_{\mathrm{DD}}^{\mathrm{min}}$	Lower limit for V_{DD}.
x	Spatial coordinate.
x_i	Cartesian coordinate ($i \in \{1,2,3\}$).
x, y, z	Cartesian coordinates.
Y	Index (in roman style) denoting the output node of a logic gate.
$Z(\omega)$	Electric impedance.
$Z_{\mathrm{S}}(\omega)$, $Z_{\mathrm{D}}(\omega)$, $Z_{\mathrm{G}}(\omega)$	Electric impedance of terminal denoted by the index.
$\boldsymbol{\nabla}_{\boldsymbol{r}}$, $\boldsymbol{\nabla}_{\boldsymbol{r}'}$	Nabla operator acting on $\boldsymbol{r}$, $\boldsymbol{r}'$.
$\Delta_{\boldsymbol{r}}$	Laplace operator acting on $\boldsymbol{r}$.

B. Total Capacitance of the Metal Island: Increase or Decrease due to Shape Modifications of Island or Electrodes

Let us consider a metal island of a certain shape surrounded by electrodes as sketched in Fig. B.1a. The total capacitance $C_{0\Sigma}$ is due to (2.17)

$$C_{0\Sigma} = \oint_{S_0} \left\{ \epsilon_0 \boldsymbol{\epsilon}(\boldsymbol{r}) \cdot \boldsymbol{\nabla}_{\boldsymbol{r}}\, \alpha_0(\boldsymbol{r}) \right\} \mathrm{d}\boldsymbol{S}_0 \,. \tag{B.1}$$

Thus, $C_{0\Sigma}$ is determined by $\alpha_0(\boldsymbol{r})$ which describes the electrostatic potential profile of this arrangement under the boundary conditions $\alpha_0(\boldsymbol{r}) = 1$ on the island and $\alpha_0(\boldsymbol{r}) = 0$ on the metal parts. With modifying the surrounding electrodes so that they come closer to the metal island in certain regions (see Fig. B.1b), the electrostatic profile is changed to $\alpha_0^{(b)}(\boldsymbol{r})$. We assume $\boldsymbol{\epsilon}(\boldsymbol{r}) = \boldsymbol{\epsilon}^{(b)}(\boldsymbol{r})$, i.e., the local properties of the dielectric between the conductors is not affected.

From $\alpha_0(\boldsymbol{r})$ and $\alpha_0^{(b)}(\boldsymbol{r})$ fulfilling (2.7), and from a generalization of Green's theorem [274] we derive

$$\begin{aligned}
0 \overset{(2.7)}{=} & \int_{V^{(b)}} \Big\{ \alpha_0^{(b)}(\boldsymbol{r}) \cdot \boldsymbol{\nabla}_{\boldsymbol{r}} (\epsilon_0 \boldsymbol{\epsilon}(\boldsymbol{r}) \boldsymbol{\nabla}_{\boldsymbol{r}} \alpha_0(\boldsymbol{r})) \\
& \qquad - \alpha_0(\boldsymbol{r}) \cdot \boldsymbol{\nabla}_{\boldsymbol{r}} \Big(\epsilon_0 \boldsymbol{\epsilon}(\boldsymbol{r}) \boldsymbol{\nabla}_{\boldsymbol{r}} \alpha_0^{(b)}(\boldsymbol{r}) \Big) \Big\} \, \mathrm{d}^3\boldsymbol{r} \\
\overset{\text{Green}}{=} & \oint_{S^{(b)}} \epsilon_0 \boldsymbol{\epsilon}(\boldsymbol{r}) \left\{ \alpha_0(\boldsymbol{r}) \boldsymbol{\nabla}_{\boldsymbol{r}} \alpha_0^{(b)}(\boldsymbol{r}) - \alpha_0^{(b)}(\boldsymbol{r}) \boldsymbol{\nabla}_{\boldsymbol{r}} \alpha_0(\boldsymbol{r}) \right\} \mathrm{d}\boldsymbol{S} \\
= & \oint_{S_0} \epsilon_0 \boldsymbol{\epsilon}(\boldsymbol{r}) \left\{ \alpha_0(\boldsymbol{r}) \boldsymbol{\nabla}_{\boldsymbol{r}} \alpha_0^{(b)}(\boldsymbol{r}) - \alpha_0^{(b)}(\boldsymbol{r}) \boldsymbol{\nabla}_{\boldsymbol{r}} \alpha_0(\boldsymbol{r}) \right\} \mathrm{d}\boldsymbol{S} \\
& \qquad + \oint_{S^{(b)} - S_0} \epsilon_0 \boldsymbol{\epsilon}(\boldsymbol{r}) \left\{ \alpha_0(\boldsymbol{r}) \boldsymbol{\nabla}_{\boldsymbol{r}} \alpha_0^{(b)}(\boldsymbol{r}) - \alpha_0^{(b)}(\boldsymbol{r}) \boldsymbol{\nabla}_{\boldsymbol{r}} \alpha_0(\boldsymbol{r}) \right\} \mathrm{d}\boldsymbol{S}
\end{aligned}$$

The last transformation is obtained by separating the integral over the island's surface S_0 from the integral over the other electrodes' surfaces. Since $\alpha_0(\boldsymbol{r}) = \alpha_0^{(b)}(\boldsymbol{r}) = 1$ if $\boldsymbol{r} \in S_0$, $\alpha_0(\boldsymbol{r}) = 0$ if $\boldsymbol{r} \in S - S_0$, and $\alpha_0^{(b)}(\boldsymbol{r}) = 0$ if $\boldsymbol{r} \in S^{(b)} - S_0$, it leads to

$$\begin{aligned}
0 = & \oint_{S_0} \epsilon_0 \boldsymbol{\epsilon}(\boldsymbol{r}) \left\{ \boldsymbol{\nabla}_{\boldsymbol{r}} \alpha_0^{(b)}(\boldsymbol{r}) - \boldsymbol{\nabla}_{\boldsymbol{r}} \alpha_0(\boldsymbol{r}) \right\} \mathrm{d}\boldsymbol{S} \\
& + \int_{\Delta S^{(b)}} \epsilon_0 \boldsymbol{\epsilon}(\boldsymbol{r}) \cdot \alpha_0(\boldsymbol{r}) \boldsymbol{\nabla}_{\boldsymbol{r}} \alpha_0^{(b)}(\boldsymbol{r}) \, \mathrm{d}\boldsymbol{S} \,,
\end{aligned} \tag{B.2}$$

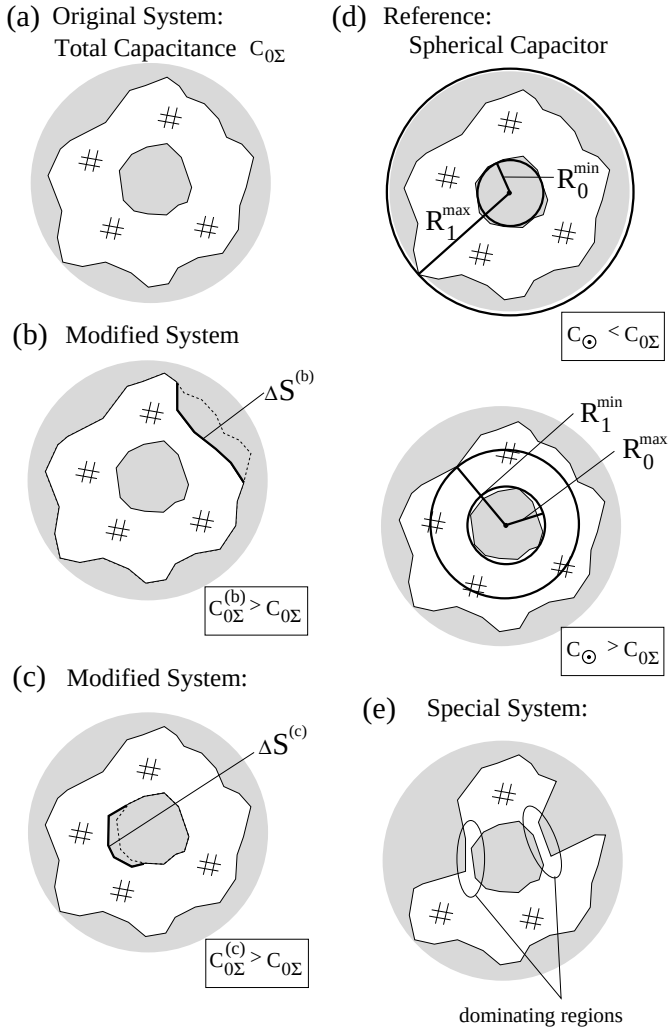

Fig. B.1. (a) The original metal island surrounded by metal electrodes. Changing the shape of the surrounding electrodes (b) or of the island (c) by reducing the dielectric space V between island and surrounding electrodes, the total island capacitance has increased. (d) The capacitance of a spherical capacitor, i.e., of a sphere with radius R_0 in the center of a hollow sphere with radius R_1 can be used to give limits for the total capacitance of the metal island in the original arrangement: A lower limit is obtained by the capacitance of a metal sphere entirely embedded in the island and the concentric hollow sphere enclosing the entire dielectric medium. An upper limit is obtained by the capacitance of a sphere enclosing the island and the concentric hollow sphere just touching the surround electrodes. (e) Regions of small distances between island and surround electrodes might dominate the total capacitance of the island.

where $\Delta S^{(b)}$ describes the surface area of the surrounding electrodes which was moved closer to the island, i.e., $\Delta S^{(b)} \notin S$ and $\Delta S^{(b)} \in V$. Since there $\alpha_0(\boldsymbol{r}) \geq 0$ and $\boldsymbol{\nabla}_{\boldsymbol{r}} \alpha_0^{(b)}(\boldsymbol{r})\, \mathrm{d}\boldsymbol{S} \leq 0$, the last integral takes a negative value. The first integral defines the difference in the total capacitance of the metal island between arrangement (a) and (b). Therefore, the total capacitance has increased from arrangement (a) to arrangement (b):

$$C_{0\Sigma}^{(b)} \geq C_{0\Sigma} \,. \tag{B.3}$$

The relation (B.3) can be stated in another way: For a given island shape, the total capacitance of this island is smallest if the surrounding metal electrodes are shifted to infinite distance from the island. This *self-capacitance* $C_{0\Sigma}^{(\infty)}$ of the metal island *gives a lower limit* to the total capacitance of the island of certain shape:

$$C_{0\Sigma} \geq C_{0\Sigma}^{(\infty)} \equiv \oint_{S_0} \left\{ \epsilon_0 \boldsymbol{\epsilon}(\boldsymbol{r}) \cdot \boldsymbol{\nabla}_{\boldsymbol{r}}\, \alpha_0^{(\infty)}(\boldsymbol{r}) \right\} \mathrm{d}\boldsymbol{S}_0 > 0 \,. \tag{B.4}$$

Instead of changing the surrounding electrodes, the metal island shape can be changed for a fixed surrounding electrode arrangement (compare Fig. B.1a and Fig. B.1c): The total capacitance increases with reducing the distance between the island electrode and the surrounding electrodes. The proof chain follows what was previously discussed between arrangement (a) and (b). But instead of integrating $\boldsymbol{\nabla}_{\boldsymbol{r}} \alpha_0(\boldsymbol{r})$ at the island surface S_0 which is modified, the capacitance is determined by integrating $\boldsymbol{\nabla}_{\boldsymbol{r}} \alpha_0(\boldsymbol{r})$ at the surface $S - S_0$ of all other electrodes which are not modified between (a) and (c):

$$\begin{aligned} C_{0\Sigma} &= \oint_{S_0} \left\{ \epsilon_0 \boldsymbol{\epsilon}(\boldsymbol{r}) \cdot \boldsymbol{\nabla}_{\boldsymbol{r}}\, \alpha_0(\boldsymbol{r}) \right\} \mathrm{d}\boldsymbol{S}_0 = \sum_{j \neq 0} C_{0,j} = \sum_{j \neq 0} C_{j,0} \\ &= \sum_{j \neq 0} - \oint_{S_j} \left\{ \epsilon_0 \boldsymbol{\epsilon}(\boldsymbol{r}) \cdot \boldsymbol{\nabla}_{\boldsymbol{r}}\, \alpha_0(\boldsymbol{r}) \right\} \mathrm{d}\boldsymbol{S}_j \\ &= - \oint_{S - S_0} \left\{ \epsilon_0 \boldsymbol{\epsilon}(\boldsymbol{r}) \cdot \boldsymbol{\nabla}_{\boldsymbol{r}}\, \alpha_0(\boldsymbol{r}) \right\} \mathrm{d}\boldsymbol{S} \,. \end{aligned} \tag{B.5}$$

Taking this, we obtain in comparing arrangement (a) with (c):

$$C_{0\Sigma}^{(c)} \geq C_{0\Sigma} \,. \tag{B.6}$$

Hence we conclude with the rule: If the volume of the dielectric filling is reduced by a moderate shape modification of the island or of the electrodes (see Fig. B.1b and c), the total capacitance increases. In contrary, if the volume is enlarged without partially decreasing the distance between island and electrodes the total capacitance decreases.

C. Estimating Upper and Lower Limits for the Total Capacitance of a Metal Island

To estimate the single-electron charging energy E_C of the metal island, it is important to know the total capacitance $C_{0\Sigma}$ of an island in its surrounding. It is shown in Appendix B that by reducing partially the distance between the surfaces of the island electrode and the surrounding electrodes – either by reshaping the island (see Fig. B.1b) or by reshaping the surrounding electrodes (see Fig. B.1c), the total capacitance of the island increases. This property allows us to give upper and lower limits for the total capacitance of a metal island in its surrounding.

For a certain island shape, the total capacitance of this island is smallest if the surrounding metal electrodes are shifted to infinite distance from the island. As derived with (B.4), this self-capacitance $C_{0\Sigma}^{(\infty)}$ of the metal island gives a *lower limit* to the total capacitance of the island of certain shape:

$$C_{0\Sigma} \geq C_{0\Sigma}^{(\infty)} \equiv \oint_{S_0} \left\{ \epsilon_0 \boldsymbol{\epsilon}(\boldsymbol{r}) \cdot \boldsymbol{\nabla}_{\boldsymbol{r}}\, \alpha_0^{(\infty)}(\boldsymbol{r}) \right\} \mathrm{d}\boldsymbol{S}_0 > 0 \,, \tag{C.1}$$

where $\alpha_0^{(\infty)}(\boldsymbol{r})$ is the electrostatic potential profile for the island with all electrodes pushed into infinite distance. To emphasize, with the self-capacitance of the island, the single-electron charging energy E_C is overestimated. To get the self-capacitance value from (C.1), still $\alpha_0^{(\infty)}(\boldsymbol{r})$ has to be known, which depends on the island shape.

A better approach to give estimates for the total or the self-capacitance is to compare the actual arrangement with simpler arrangements from which the capacitances are known.

Spherical Capacitor as a Reference. For a spheric island of radius R_0 located in the center of a hollow sphere of radius R_1 which is filled with a homogeneous isotropic dielectric medium, the electrostatic potential profile is described in spheric coordinates by

$$\alpha_\odot(r) = \left(\frac{1}{R_0} - \frac{1}{R_1} \right)^{-1} \cdot \left(\frac{1}{r} - \frac{1}{R_1} \right) \tag{C.2}$$

fulfilling (2.7) for this arrangement. This leads to the total capacitance of the sphere

$$
\begin{aligned}
C_{\odot} &= \oint_{S_0} \{\epsilon_0 \epsilon \cdot \boldsymbol{\nabla}_{\boldsymbol{r}}\, \alpha_{\odot}(\boldsymbol{r})\}\, \mathrm{d}\boldsymbol{S}_0 \\
&= \int_0^{2\pi} \int_0^{\pi} \left(\epsilon_0 \epsilon \cdot \boldsymbol{e}_r \cdot \frac{\partial}{\partial r} \alpha_{\odot}(r) \right) \cdot \left(-r^2 \sin\theta \, \mathrm{d}\theta \, \mathrm{d}\phi \cdot \boldsymbol{e}_r \right) \Bigg|_{r=R_0} \\
&= 4\pi\epsilon_0 \epsilon \cdot \frac{R_1 \cdot R_0}{R_1 - R_0} \, . \qquad \text{(C.3)}
\end{aligned}
$$

For $R_1 \to \infty$, the self-capacitance of the metal sphere with radius R_0 embedded in a homogeneous isotropic medium with the dielectric constant ϵ is obtained:

$$C_{\odot}^{(\infty)}(R_0, \epsilon) = 4\pi\epsilon_0 \epsilon \cdot R_0 \, . \qquad \text{(C.4)}$$

From that, limits for the total capacitance can be estimated (see Fig. B.1d): A lower limit is obtained by the capacitance of a metal sphere ($R_0 = R_0^{\min}$) entirely embedded in the island and the concentric hollow sphere ($R_1 = R_1^{\max}$) enclosing the entire dielectric medium:

$$C_{0\Sigma} \geq C_{\odot}\left(R_0^{\min}, R_1^{\max}, \min[\boldsymbol{\epsilon}(\boldsymbol{r}); \boldsymbol{r} \in V]\right) \, . \qquad \text{(C.5)}$$

An upper limit is obtained by the capacitance of a sphere ($R_0 = R_0^{\max}$) enclosing the island and the concentric hollow sphere ($R_1 = R_1^{\min}$) just touching the surrounding electrodes:

$$C_{0\Sigma} \leq C_{\odot}\left(R_0^{\max}, R_1^{\min}, \max[\boldsymbol{\epsilon}(\boldsymbol{r}); \boldsymbol{r} \in V]\right) \, . \qquad \text{(C.6)}$$

Cylindrical Capacitor as a Reference. For an electrode arrangement which is elongated in one direction, a better estimate might be done by using the arrangement of a tube or wire of radius R_0 and length L, surrounded coaxially by a second tube of radius R_1. It possesses the capacitance of a cylindric capacitor,

$$C_{0\Sigma}(L, R_0, R_1) = 2\pi\epsilon_0 \epsilon L \cdot \left[\ln \frac{R_1}{R_0} \right]^{-1} \, . \qquad \text{(C.7)}$$

Ellipsoidal Capacitor as a Reference. For estimating the self-capacitance, sometimes the shape of a metal island is better described by an ellipsoid than by a sphere. The lower limit for the self-capacitance of the island is obtained by completely enclosing an ellipsoid into the island, an upper limit by completely enclosing the island into an ellipsoid (see Fig. C.1). The self-capacitance of an ellipsoid with the half-axis a, b and c is given by an elliptic integral [275]

$$C_{\Theta}^{(\infty)}(a, b, c) = 8\pi\epsilon_0 \epsilon \cdot \left[\int_0^{\infty} \frac{\mathrm{d}\lambda}{\sqrt{(a^2 + \lambda)(b^2 + \lambda)(c^2 + \lambda)}} \right]^{-1} \, . \qquad \text{(C.8)}$$

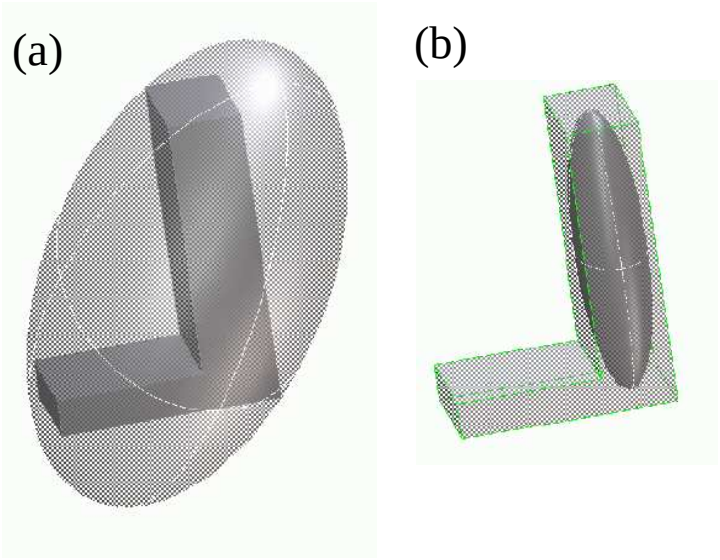

Fig. C.1. The self-capacitance of a metal island of arbirary shape (here L-shaped) is estimated by using the self-capacitance of an ellipsoid with the half axis a, b and c. (a) The metal island is fully enclosed in an ellipsoid for an upper limit, (b) the ellipsoid is fully incorporated in the metal island for a lower limit.

In case of two identical half-axes ($a = b$), the integral is analytically solved [275, 276] leading to [1]

$$C_{\Theta}^{(\infty)}(a,c) = \begin{cases} \dfrac{4\pi\epsilon_0\epsilon\sqrt{a^2-c^2}}{\arctan\sqrt{(a/c)^2-1}} & \text{, if } a=b>c\,, \\ \dfrac{4\pi\epsilon_0\epsilon\sqrt{c^2-a^2}}{\operatorname{artanh}\sqrt{1-(a/c)^2}} & \text{, if } a=b<c\,. \end{cases} \tag{C.9}$$

It includes in the limit of $a > c = 0$ the self-capacitance of a flat disk with radius $a = R_0$,

$$C_{\Theta}^{(\infty)}(R_0) = 8\epsilon_0\epsilon \cdot R_0\,, \tag{C.10}$$

and in the limit $c \gg a$ the self-capacitance of a metal wire or tube of length $2c = L$ and radius $a = R_0$,

$$C_{\Theta}^{(\infty)}(L) = 2\pi\epsilon_0\epsilon L \cdot \left[\ln\frac{L}{R_0}\right]^{-1}\,. \tag{C.11}$$

[1] Area tangens hyperbolicus: $\operatorname{artanh}(x) \equiv \frac{1}{2}\ln\left\{(1+x)/(1-x)\right\}$.

Plate Capacitor as a Reference. As already pointed out, if electrodes are very close to the island in certain surface regions, the gradient $\nabla_{\boldsymbol{r}} \alpha_0(\boldsymbol{r})$ in front of the electrodes becomes steep. These surface areas might be the dominant contributions to the total capacitance if they are large enough compared to the other surface regions. An example is given in Fig. B.1e: The total capacitance is dominated by the capacitance contributions from the marked overlap regions. Under such conditions, the total capacitance might be estimated by assuming plate capacitor arrangements with the respective distance $d^{(k)}$ and area $A^{(k)}$ for these regions:

$$C_{0\Sigma} \approx C_{0\Sigma}^{(\text{overlap})} = \sum_k \epsilon_0 \epsilon^{(k)} \cdot A^{(k)} / d^{(k)} \; . \tag{C.12}$$

Metal single-electron transistors like the one presented in Fig. 1.7 are dominated in their total capacitance by the tunnel junction areas due to the thin oxide of few nanometers. If such overlap regions do not dominate, sometimes the total capacitance of such an arrangement has been expressed by

$$C_{0\Sigma} = C_{0\Sigma}^{(\infty)} + C_{0\Sigma}^{(\text{overlap})} \; . \tag{C.13}$$

This formula is *not* strictly valid as can be seen from the previous discussion, especially if both capacitance terms are of same order.

References

1. H. Grabert and M.H. Devoret, editors. *Single Charge Tunneling*, volume B 294 of *NATO ASI Series*. Plenum Press, New York, 1992.
2. K.K Likharev. Single-electron devices and their applications. *Proceedings of the IEEE*, 87:606, 1999.
3. U. Meirav and E.B. Foxman. Single-electron phenomena in semiconductors. *Semicond. Sci. Technol.*, 10:255, 1995.
4. L.P. Kouwenhoven, Ch.M. Marcus, P.L. McEuen, S. Tarucha, R.M Westerwelt, and N.S. Wingreen. Electron transport in quantum dots. In L.L. Sohn and et al., editors, *Mesoscopic Electron Transport*. Kluwer Academic Publishers, 1997.
5. L.P. Kouwenhoven, D.G. Austing, and S. Tarucha. Few-electron quantum dots. *Rep. Prog. Phys.*, 64:701, 2001.
6. T. Chakraborty. *Quantum Dots – A survey of the properties of artifical atoms*. North-Holland, Amsterdam, 1999.
7. N.F Johnson. Quantum dots: few-body, low-dimensional systems. *J. Phys.: Condens. Matter*, 7:965, 1995.
8. D. Pfannkuche. *Aspects of Coulomb Interaction in Semiconductor Nanostructures*. Habilitationsschrift, Universität Karlsruhe, Germany, 1998.
9. D. Weinmann, W. Häusler, and B. Kramer. Transport properties of quantum dots. *Ann. Physik*, 5:652, 1996.
10. G. Schön. Single-electron tunneling. In T. Dittrich, P. Hänggi, G. Ingold, G. Kramer, B. Schön, and W. Zwerger, editors, *Quantum Transport and Dissipation*, chapter 3. VCH, 1997.
11. H. Schoeller. Transport theory of interacting quantum dots. In L.L. Sohn and et al., editors, *Mesoscopic Electron Transport*. Kluwer Academic Publishers, 1997.
12. L.L. Sohn, L.P. Kouwenhoven, and G. Schön, editors. *Mesoscopic Electron Transport*, volume E 345 of *NATO ASI Series*. Kluwer Academic Publishers, Dordrecht, 1997.
13. J.H. Davies. *The physics of low-dimensional semiconductors: an introduction*. Cambridge University Press, Cambridge, 1998.
14. C.A. Neugebauer and M.B. Webb. Electrical conduction mechanism in ultrathin, evaporated metal films. *J. Appl. Phys.*, 33:74, 1962.
15. C.J. Gorter. A possible explanation of the increase of the electrical resistance of thin metal films at low temperatures and small field strengths. *Physica*, 17:777, 1951.
16. I. Giaever and H.R. Zeller. Superconductivity of small tin particles measured by tunneling. *Phys. Rev. Lett.*, 20:1504, 1968.
17. J. Lambe and R.C. Jaklevic. Charge-quantization studies using a tunnel capacitor. *Phys. Rev. Lett.*, 22:1371, 1969.
18. R.E. Cavicchi and R.H. Silsbee. Coulomb suppression of tunneling rate from small metal particles. *Phys. Rev. Lett.*, 52:1453, 1984.

19. I.O. Kulik and R.I. Shekhter. Kinetic phenomena and charge discreteness effects in granulated media. *Sov. Phys.-JETP*, 41:308, 1975.
20. D.V. Averin and K.K. Likharev. Coulomb blockade of single-electron tunneling, and coherent oscillations in small tunnel junctions. *J. Low Temp. Phys.*, 62:345, 1986.
21. R. Wilkens, E. Ben-Jacob, and R.C. Jaklevic. Scanning-tunneling-microscope observations of Coulomb blockade and oxide polarisation in small metal droplets. *Phys. Rev. Lett.*, 63:801, 1989.
22. C. Schönenberger, H. van Houten, and H.C. Donkersloot. Single-electron tunnelling observed at room temperature by scanning-tunneling microscopy. *Europhys. Lett.*, 20:249, 1992.
23. P. Lafarge, H. Pothier, E.R. Williams, D. Esteve, C. Urbina, and M.H. Devoret. Direct observation of macroscopic charge quantization. *Z. Phys. B*, 85:327, 1991.
24. T.M. Eiles, J.M. Martinis, and M.H. Devoret. Even-odd asymmetry of a superconductor revealed by the Coulomb blockade of Andreev reflection. *Phys. Rev. Lett.*, 70:1862, 1993.
25. K.K. Likharev. Single-electron transistors: Electrostatic analogs of the DC SQUIDS. *IEEE Transactions on Magnetics*, 23:1142, 1987.
26. T.A. Fulton and G.D. Dolan. Observation of single-electron charging effects in small tunnel junctions. *Phys. Rev. Lett.*, 59:109, 1987.
27. Y.Y. Wei. *Two-Dimensional Electron System in Quantum Hall Regime Probed by Metal Single-Electron Transistor.* PhD thesis, Universität Stuttgart, Germany, 1998.
28. G.J. Dolan and J.H. Dunsmuir. Very small ($\geq$ 20 nm) lithographic wires, dots, rings and tunnel junctions. *Physica B*, 152:7, 1988.
29. D.B. Haviland, L.S. Kuzmin, P. Delsing, L.L. Likharev, and T. Claeson. Experimental evidence for the Coulomb blockade of Cooper pair tunneling and Bloch oscillations in single Josephson junctions. *Z. Phys. B*, 85:339, 1991.
30. L. Ji, P.D. Dresselhaus, S. Han, K. Lin, W. Zheng, and J.E. Lukens. Fabrication and characterization of single-electron transistors and traps. *J. Vac. Sci. Technol. B*, 12:3619, 1994.
31. J. Hüls. *Experimente zur Potentialverteilung zweidimensionaler Elektronensysteme im ganz- und gebrochenzahligen Quanten-Hall-Bereich mit Hilfe eines Einzelelektronen-Transistors als Elektrometer.* PhD thesis, Universität Hamburg, Germany, 2001.
32. D.A. Averin, A.N. Korotkov, and K.K. Likharev. Theory of single-electron charging of quantum wells and dots. *Phys. Rev. B*, 44:6199, 1991.
33. R. Wilkins, E. Ben-Jacob, and R.C. Jaklevic. Scanning-tunneling-microscope observations of Coulomb blockade and oxide polarization in small metall droplets. *Phys. Rev. Lett.*, 63:801, 1989.
34. V.A. Krupenin, D.E. Presnov, A.B. Zorin, and M.N. Niemeyer. Aluminum single electron transistors with islands isolated from the substrate. *J. Low Temp. Phys.*, 118:287, 2000.
35. R.J. Schoelkopf, P. Wahlgren, A.A. Kozhevnikov, P. Delsing, and D.E. Prober. The radio-frequency single-electron transistor (rf-SET): A fast and ultrasensitive electrometer. *Science*, 280:1238, 1998.
36. T. Fujisawa and Y. Hirayama. Transmission type rf single electron transistor operation of a semiconductor quantum dot. *Jpn. J. Appl. Phys.*, 39:2338, 2000.
37. A.N. Korotkov and M.A. Paalanen. Charge sensitivity of radio frequency single-electron transistor. *Appl. Phys. Lett.*, 74:4052, 1999.
38. A.B. Zorin, F.J. Ahlers, J. Niemeyer, T. Weimann, and H. Wolf. Background charge noise in metallic single-electron tunneling devices. *Phys. Rev. B*, 53:13682, 1996.

39. N.M. Zimmerman, J.L. Cobb, and A.F. Clark. Modulation of the charge of a single-electron transistor by distant defects. *Phys. Rev. B*, 56:7675, 1997.
40. T. Sakamoto and Nakamura K. Study of random telegraph signals in a $GaAs/Al_xGa_{1-x}As$ single-electron transistor. *Superlattices and Microstructures*, 23:413, 1998.
41. C. Bruder and H. Schoeller. Charging effects in ultrasmall quantum dots in the presence of time-varying fields. *Phys. Rev. Lett.*, 72:1076, 1994.
42. J. Weis. *Einzelelektron-Tunneltransistor: Transportspektroskopie der elektronischen Grund- und Anregungszustände in einem $GaAs/Al_xGa_{1-x}As$-Quantentopf.* PhD thesis, Universität Stuttgart, Germany, 1994.
43. J. Weis, R.J. Haug, von K. Klitzing, and K. Ploog. Single-electron tunneling transistor as a current rectifier with potential-controlled current polarity. *Semicond. Sci. Technol.*, 10:877, 1995.
44. C.W.J. Beenakker and A.A.M. Staring. Theory of the thermopower of a quantum dot. *Phys. Rev. B*, 46:9667, 1992.
45. A.S. Dzurak, C.G. Smith, M. Pepper, D.A. Ritchie, J.E.F. Frost, G.A.C. Jones, and D.G. Hasko. Observation of Coulomb blockade oscillations in the thermopower of a quantum dot. *Solid State Commun.*, 87:1145, 1993.
46. A.A.M. Staring, L.W. Molenkamp, B.W. Alphenaar, H. van Houten, O.J.A. Buyk, C.W.J. Beenakker, and C.T. Foxon. Coulomb-blockade oscillations in the thermopower of a quantum dot. *Europhys. Lett.*, 22:57, 1993.
47. L.P. Kouwenhoven, S. Jauhar, K. McCormick, D. Dixon, and McEuen P.L. Photon-assisted tunneling through a quantum dot. *Phys. Rev. B*, 50:2019, 1994.
48. H. Linke, T.E. Humphrey, A. Löfgren, A.O. Sushkov, R. Newbury, R.P. Taylor, and P. Omling. Experimental tunneling ratchets. *Science*, 286:2314, 1999.
49. M.H. Devoret, D. Esteve, H. Grabert, G.-L. Ingold, H. Pothier, and C. Urbina. Effect of the electromagnetic environment on the Coulomb blockade in ultrasamll tunnel junctions. *Phys. Rev. Lett.*, 64:1824, 1990.
50. S.M. Girvin, L.I. Glazman, M. Jonson, D.R. Penn, and M.D. Stiles. Quantum fluctuations and the single-junction Coulomb blockade. *Phys. Rev. Lett.*, 64:3183, 1990.
51. M.H. Devoret, D. Esteve, H. Grabert, G.-L. Ingold, H. Pothier, and C. Urbina. On the observability of Coulomb blockade and single-electron tunneling. *Ultramicroscopy*, 42-44:22, 1992.
52. K.K. Likharev and A.B. Zorin. Theory of the Bloch-wave oscillations in small Josephson junctions. *J. Low Temp. Phys.*, 59:347, 1985.
53. G.-L. Ingold, P. Wyrowski, and H. Grabert. On the observability of Coulomb blockade and single-electron tunneling. *Z. Phys. B*, 85:443, 1991.
54. A.A. Odintsov, G. Falci, and G. Schön. Single-electron tunneling in systems of small junctions coupled to an electromagnetic environment. *Phys. Rev. B*, 44:13089, 1991.
55. H. Higurashi, S. Iwabuchi, and Y. Nagaoka. Coulomb blockade and current-voltage characteristics of ultrasmall double tunnel junctions with external circuits. *Phys. Rev. B*, 51:2387, 1995.
56. B.J. van Wees, H. van Houton, C.W.J. Beenakker, J.G. Williamson, L.P. Kouvenhoven, D. van der Marel, and C.T. Foxon. Quantized conductance of point contacts in a two-dimensional electron gas. *Phys. Rev. Lett.*, 60:848, 1988.
57. D.A. Wharam, T.J. Thornton, R. Newbury, M. Pepper, H. Ahmed, J.E.F. Frost, D.G. Hasko, D.C. Peacock, D.A. Ritchie, and G.A.C. Jones. One-dimensional transport and the quantisation of the ballistic resistance. *J. Phys. C*, 21:L209, 1988.
58. N. Lang and W. Kohn. Theory of metal surfaces: Charge density and surface energy. *Phys. Rev. B*, 1:4555, 1970.

59. M.J. Yoo, T.A. Fulton, H.F. Hess, R.L. Willett, L.N. Dunkelberger, R.J. Chichester, L.N. Pfeiffer, and K.W. West. Scanning single-electron transistor microscopy: Imaging individual charges. *Science*, 276:579, 1997.
60. A. Yacoby, H.F. Hess, T.A. Fulton, L.N. Pfeiffer, and K.W. West. Electrical imaging of the quantum Hall state. *Solid State Comm.*, 111:1, 1999.
61. S. Ilani, A. Yacoby, D. Mahalu, and H. Shtrikman. Unexpected behaviour of the local compressibility near the $B = 0$ metal-insulator transition. *Phys. Rev. Lett.*, 84:3133, 2000.
62. T. Chakraborty and P. Pietiläinen. *The Quantum Hall Effects*. Springer, Berlin, 2nd edition, 1995.
63. K. von Klitzing, G. Dorda, and M. Pepper. New method for high-accuracy determination of the fine-structure constant based on quantized Hall resistance. *Phys. Rev. Lett.*, 45:494, 1980.
64. D.C. Tsui, H.L. Störmer, and A.C. Gossard. Two-dimensional magnetotransport in the extreme quantum limit. *Phys. Rev. Lett.*, 48:1559, 1982.
65. A. Jeffery, R.E. Elmquist, J.Q. Shields, L.H. Lee, M.E. Cage, S.H. Shields, and R.F. Dziuba. Determination of the von Klitzing constant and the fine-structure through a comparison of the quantized Hall resistance and the ohm derived from the NIST calculable capacitor. *Metrologia*, 35:83, 1998.
66. B.N. Taylor and E.R. Cohen. How accurate are the Josephson and quantum Hall effects and QED? *Physics Letters A*, 153:308, 1991.
67. B. Jeckelmann, A.D. Inglis, and B. Jeanneret. Material, device, and step independence of the quantized Hall resistance. *IEEE Trans. Instr. Meas.*, 44:269, 1995.
68. K. von Klitzing. Physics and application of the quantum Hall effect. *Physica B*, 204:111, 1995.
69. Y.Y. Wei, J. Weis, K. von Klitzing, and K. Eberl. Edge strips in the quantum Hall regime imaged by a single-electron transistor. *Phys. Rev. Lett.*, 81:1674, 1998.
70. J. Weis, Y.Y. Wei, and K. von Klitzing. Single-electron transistor probes two-dimensional electron system in high magnetic fields. *Physica E*, 3:23, 1998.
71. J. Weis, Y.Y. Wei, and K. von Klitzing. Probing the depletion region of a two-dimensional electron system in high magnetic fields. *Physica B*, 256-258:1, 1998.
72. Y.Y. Wei, J. Weis, K. von Klitzing, and K. Eberl. Single-electron transistor as an electrometer measuring chemical potential variations. *Appl. Phys. Lett.*, 71:2514, 1997.
73. H.L. Störmer, R. Dingle, Gossard A.C., W. Wiegmann, and M.D. Sturge. Two-dimensional electron gas at a semiconductor interface. *Solid State Comm.*, 29:705, 1979.
74. F. Stern and S. Das Sarma. Electron energy levels in GaAs-$Ga_xAl_{1-x}As$ heterojunctions. *Phys. Rev. B*, 30:840, 1984.
75. R. Dingle, H.L. Störmer, A.C. Gossard, and W. Wiegmann. Electron mobilities in modulation-doped semiconductor heterojunction superlattices. *Appl. Phys. Lett.*, 33:665, 1978.
76. I.A. Larkin and J.H. Davies. Edge of the two-dimensional electron gas in a gated heterostructure. *Phys. Rev. B*, 52:R5535, 1995.
77. E. Ahlswede, P. Weitz, J. Weis, K. von Klitzing, and K. Eberl. Hall potential profiles in the quantum Hall regime measured by a scanning force microscope. *Physica B*, 298:562, 2001.
78. L.D. Hallam, J. Weis, and P.A. Maksym. Screening of the electron-electron interaction by gate electrodes in semiconductor quantum dots. *Phys. Rev. B*, 53:1452, 1996.

79. H. Park, J. Park, A.K.L. Lim, E.H. Anderson, A.P. Alivisatos, and P.L. McEuen. Nanomechanical oscillations in a single-C_{60} transistor. *Nature*, 407:57, 2000.
80. M. Kastner. Artifical atoms. *Phys. Today*, 46:24, 1993.
81. R.C. Ashoori. Electrons in artifical atoms. *Nature*, 379:413, 1996.
82. Ch. Weißmantel and C. Hamann. *Grundlagen der Festkörperphysik*. Springer, Berlin, 1980.
83. E. Leobandung, L. Guo, and S.Y. Chou. Single electron and hole quantum dot transistors operating above 110 K. *J. Vac. Sci. Technol. B*, 13:2865, 1995.
84. Y. Ono, Y. Takahashi, K. Yamazaki, M. Nagase, H. Namatsu, K. Kurihara, and K. Murase. Fabrication method for IC-oriented Si single-electron transistors. *IEEE Transactions on Electron Devices*, 47:147, 2000.
85. D.C. Ralph, C.T. Black, and M. Tinkham. Gate-voltage studies of discrete electronic states in aluminum nanoparticles. *Phys. Rev. Lett.*, 78:4087, 1997.
86. A. Lorke, R.J. Luyken, A.O. Govorov, and J.P. Kotthaus. Spectroscopy of nanoscopic semiconductor rings. *Phys. Rev. Lett.*, 84:2223, 2000.
87. M. Dilger, K. Eberl, R.J. Haug, and K. von Klitzing. Self-organized growth of quantum dot-tunnel barrier systems. *Superlattices and Microstructures*, 21:533, 1997.
88. M. Dilger, R.J. Haug, K. Eberl, and K. von Klitzing. Single-electron transistors with a self-assembled quantum dot. *Semicond. Sci. Technol.*, 11:1493, 1996.
89. D.L. Klein, R. Roth, A.K.L. Lim, A.P. Alivisatos, and P.L. McEuen. A single-electron transistor made from a cadmium selenide nanocrystal. *Nature*, 389:699, 1997.
90. S.J. Tans, M.H. Devoret, Groeneveld R.J.A., and C. Dekker. Electron-electron correlations in carbon nanotubes. *Nature*, 394:761, 1998.
91. D.H. Cobden, M. Bockrath, P.L. McEuen, A.G. Rinzler, and R.E. Smalley. Spin splitting and even-odd effects in carbon nanotubes. *Phys. Rev. Lett.*, 81:681, 1998.
92. J.D. Schmid. *The Kondo Effect in Quantum Dots*. PhD thesis, Universität Stuttgart, Germany, 2000.
93. M. Keller. *Der Kondo-Effekt in Quantendots bei hohen Magnetfeldern*. PhD thesis, Universität Stuttgart, Germany, 2001.
94. U. Wilhelm. *Präparation und elektrische Charakterisierung elektrostatisch gekoppelter Quantendotsysteme – Eine Realisierung des Anderson-Störstellenmodells*. PhD thesis, Universität Stuttgart, Germany, 2000.
95. T.J. Thornton, M. Pepper, H. Ahmed, D. Andrews, and G.J. Davies. One-dimensional conduction in the 2D electron gas of a GaAs-AlGaAs heterojunction. *Phys. Rev. Lett.*, 56:1198, 1986.
96. M.A. Kastner. The single-electron transistor. *Reviews of Modern Physics*, 64:849, 1992.
97. A.D. Wieck and K. Ploog. In-plane-gated quantum wire transistor fabricated with directly written focused ion beams. *Appl. Phys. Lett.*, 56:928, 1990.
98. H. Pothier, J. Weis, R.J. Haug, and K. v. Klitzing. Realization of an in-plane-gate single-electron transistor. *Appl. Phys. Lett.*, 62:3174, 1993.
99. T. Fujisawa, Y. Hirayama, and S. Tarucha. AlGaAs/InGaAs/GaAs single-electron transistors fabricated by Ga focused ion beam implantation. *Appl. Phys. Lett.*, 64:2250, 1994.
100. T. Fujisawa and S. Tarucha. Resonant tunneling properties of single-electron transistor with a novel double-gate geometry. *Appl. Phys. Lett.*, 68:526, 1996.

101. P. Baumgartner, W. Wegscheider, M. Bichler, G. Schedelbeck, R. Neumann, and G. Abstreiter. Single-electron transistor fabricated by focused laser beam-induced doping of a GaAs/AlGaAs heterostructure. *Appl. Phys. Lett.*, 70:2135, 1997.
102. H.W. Schuhmacher, U.F. Keyser, U. Zeitler, and R.J. Haug. Nanomachining of mesoscopic electronic devices using an atomic force microscope. *Appl. Phys. Lett.*, 75:1107, 1999.
103. S. Lüscher, A. Fuhrer, R. Held, T. Heinzel, and K. Ensslin. In-plane gate single-electron transistor in Ga[Al]As fabricated by scanning probe lithography. *Appl. Phys. Lett.*, 75:2452, 1999.
104. M. Ciorga, A.S. Sachrajda, P. Hawrylak, C. Gould, P. Zawadski, S. Jullian, Y. Feng, and Z. Wasilewski. Addition spectrum of a lateral dot from Coulomb and spin-blockade spectroscopy. *Phys. Rev. B*, 61:16315, 2000.
105. M. Reed, J.N. Randall, R.J. Aggarval, R.J. Matyi, T.M. Moore, and A.E. Wetsel. Observation of discrete electronic states in a zero-dimensional semiconductor nanostructure. *Phys. Rev. Lett.*, 60:535, 1988.
106. T. Schmidt, R.J. Haug, and K. v. Klitzing. Single-electron transport in small resonant-tunneling diodes with various barrier-thickness asymmetries. *Phys. Rev. B*, 55:2230, 1997.
107. S. Tarucha, D.G. Austing, and T. Honda. Shell filling and spin effects in a few electron quantum dot. *Phys. Rev. Lett.*, 77:3613, 1996.
108. R.C. Ashoori, H.L. Stormer, J.S. Weiner, L.N. Pfeiffer, S.J. Pearton, K.W. Baldwin, and K.W. West. Single-electron capacitance spectroscopy of discrete quantum levels. *Phys. Rev. Lett.*, 68:3088, 1992.
109. D.G. Austing, S. Sasaki, S. Tarucha, S.M. Reimann, M. Koskinen, and M. Manninen. Ellipsoidal deformation of vertical quantum dots. *Phys. Rev. B*, 60:11514, 1999.
110. A. Fuhrer, S. Lüscher, T. Ihn, T. Heinzel, K. Ensslin, W. Wegscheider, and M. Bichler. Energy spectra of quantum rings. *Nature*, 413:822, 2001.
111. J.A. Folk, S.R. Patel, S.F. Godijn, Huibers A.G., S.M. Cronenwett, and C.M. Marcus. Statistics and parametric correlations of Coulomb blockade peak fluctuations in quantum dots. *Phys. Rev. Lett.*, 76:1699, 1996.
112. A.A.M. Staring, H. van Houten, C.W.J. Beenakker, and C.T. Foxon. Coulomb-blockade oscillations in disordered quantum wires. *Phys. Rev. B*, 45:9222, 1992.
113. J. Weis, R.J. Haug, K. v. Klitzing, and K. Ploog. Transport spectroscopy of a confined electron system under a gate tip. *Phys. Rev. B*, 46:12837, 1992.
114. J.T. Nicholls, J.E.F. Frost, M. Pepper, D.A. Ritchie, M.P. Grimshaw, and G.A.C. Jones. Charging effects and the excitation spectrum of a quantum dot formed by an impurity potential. *Phys. Rev. B*, 48:8866, 1993.
115. C.W.J. Beenakker. Theory of Coulomb-blockade oscillations in the conductance of a quantum dot. *Phys. Rev. B*, 44:1646, 1991.
116. L.P. Kouwenhoven, N.C. van der Vaart, A.T. Johnson, W. Kool, C.J.P.M. Harmans, J.G. Williamson, A.A.M. Staring, and C.T. Foxon. *Z. Phys. B*, 85:367, 1991.
117. L. Belkhir. Quantum and many-body effects on the capacitance of a spherical-shell quantum dot. *Phys. Rev. B*, 50:8885, 1994.
118. L.I. Glazman. Single electron tunneling. *J. Low Temp. Phys.*, 118:247, 2000.
119. A.P. Alivisatos. Semiconductor clusters, nanocrystals, and quantum dots. *Science*, 271:933, 1996.
120. A. Orlandi, M. Rontani, G. Goldoni, F. Manghi, and E. Molinari. Single-electron charging in quantum dots with large dielectric mismatch. *Phys. Rev. B*, 63:045310, 2001.

121. G. Goldoni, F. Rossi, and E. Molinari. Strong exciton binding in quantum structures through remote dielectric confinement. *Phys. Rev. Lett.*, 80:4995, 1998.
122. G. Bryant. Electronic structure of ultrasmall quantum-well boxes. *Phys. Rev. Lett.*, 59:1140, 1987.
123. U. Merkt, J. Huser, and M. Wagner. Energy spectra of two electrons in a harmonic quantum dot. *Phys. Rev. B*, 43:7320, 1991.
124. P. Maksym and T. Chakraborty. Quantum dots in a magnetic field: Role of electron-electron interaction. *Phys. Rev. Lett.*, 65:108, 1990.
125. P.L. McEuen, E.B. Foxman, J. Kinaret, U. Meirav, M.A. Kastner, N.S. Wingreen, and S.J. Wind. Self-consistent addition spectrum of a Coulomb island in the quantum Hall regime. *Phys. Rev. B*, 45:11419, 1992.
126. M. Eto. Electronic structures of few electrons in a quantum dot under magnetic fields. *Jpn. J. Appl. Phys.*, 36:3924, 1997.
127. A. Kumar, S.E. Laux, and F. Stern. Electron states in a GaAs quantum dot in a magnetic field. *Phys. Rev. B*, 42:5166, 1990.
128. M. Macucci, K. Hess, and G.J. Iafrate. Electronic energy spectrum and the concept of capacitance in quantum dots. *Phys. Rev. B*, 48:17354, 1993.
129. O. Steffens, U. Rössler, and M. Suhrke. Generalized Hund's rule in the addition spectrum of quantum dot. *Europhys. Lett.*, 42:529, 1998.
130. V. Fock. Bemerkung zur Quantelung des harmonischen Oszillators im Magnetfeld. *Z. Phys.*, 47:446, 1928.
131. C.G. Darwin. The diamagnetism of the free electron. *Proc. Cambridge Phil. Soc.*, 27:86, 1930.
132. D.B. Chklovskii, B.I. Shklovskii, and L.I. Glazman. Electrostatics of edge channels. *Phys. Rev. B*, 46:4026, 1992.
133. M. Wagner, U. Merkt, and A.V. Chaplik. Spin-singlet-spin-triplet oscillations in quantum dots. *Phys. Rev. B*, 45:1951, 1992.
134. D. Pfannkuche and S.E. Ulloa. Selection rules for spectroscopy of quantum dots. *Advances in Solid State Physics*, 35:65, 1996.
135. W. Kohn. Cyclotron resonance and de Haas-van Alphen oscillations of an interacting electron gas. *Phys. Rev.*, 123:1242, 1961.
136. D. Heitmann. Far infrared spectroscopy of quantum dots and antidot arrays. *Physica B*, 212:201, 1995.
137. D. Pfannkuche and R.R. Gerhardts. Quantum-dot helium: Effects of deviations from a parabolic confinement potential. *Phys. Rev. B*, 44:13132, 1991.
138. Z.L. Ye and E. Zaremba. Magnetoplasma excitations in anharmonic electron dots. *Phys. Rev. B*, 50:17217, 1994.
139. E. Zaremba. Magnetoplasma excitations in electron rings. *Phys. Rev. B*, 53:10512, 1996.
140. L. Brey, H.A. Fertig, R. Côté, and A.H. MacDonald. Skyrme crystal in a two-dimensional eletron gas. *Phys. Rev. Lett.*, 75:2562, 1995.
141. J.H. Oaknin, L. Martin-Moreno, J.J. Palacios, and C. Tejedor. Low-lying excitations of quantum hall droplets. *Phys. Rev. Lett.*, 74:5120, 1995.
142. D.R. Stewart, D. Sprinzak, C.M. Marcus, C.I. Duruöz, and J.S. Harris Jr. Correlations between ground and excited state spectra of a quantum dot. *Science*, 278:1784, 1997.
143. T.H. Oosterkamp, J.W. Janssen, L.P. Kouwenhoven, D.G. Austing, T. Honda, and S. Tarucha. Maximum-density droplet and charge redistributions in quantum dots at high magnetic fields. *Phys. Rev. Lett.*, 82:2931, 1999.
144. J. Weis, R.J. Haug, von K. Klitzing, and K. Ploog. Lateral transport through a single quantum dot with a magnetic field parallel to the current. *Surface Science*, 305:664, 1994.

145. B.I. Halperin, A. Stern, Y. Oreg, J.N.H.J. Cremers, J.A. Folk, and C.M. Marcus. Spin-orbit effects in a GaAs quantum dot in a parallel magnetic field. *Phys. Rev. Lett.*, 86:2106, 2001.
146. P.L. McEuen, E.B. Foxman, U. Meirav, M.A. Kastner, Y. Meir, N.S. Wingreen, and S.J. Wind. Transport spectroscopy of a Coulomb island in the quantum Hall regime. *Phys. Rev. Lett.*, 66:1926, 1991.
147. D.V. Averin and Y.V. Nazarov. Macroscopic quantum tunneling of charge and co-tunneling. In H. Grabert and M.H. Devoret, editors, *Single Charge Tunneling*, volume B 294 of *NATO ASI Series*, pages 217–247. Plenum Press, New York, 1992.
148. J. Weis, R.J. Haug, K. v. Klitzing, and K. Ploog. Competing channels in single-electron tunneling through a quantum dot. *Phys. Rev. Lett.*, 71:4019, 1993.
149. J. Weis, R.J. Haug, K. v. Klitzing, and K. Ploog. Transport spectroscopy of on a single quantum dot. *Semicond. Sci. Technol.*, 9:1890, 1994.
150. A.T. Johnson, L.P Kouwenhoven, W. de Jong, N.C. van der Vaart, C.J.P.M. Harmans, and C.T. Foxon. Zero-dimensional states and single electron charging in quantum dots. *Phys. Rev. Lett.*, 69:1592, 1992.
151. E.B. Foxman, P.L. McEuen, N.S. Wingreen, Y. Meir, P.A. Belk, N.R. Belk, and M.A. Kastner. Effects of quantum levels on transport through a Coulomb island. *Phys. Rev. B*, 47:10020, 1993.
152. J. Weis, R.J. Haug, K. v. Klitzing, and K. Ploog. Transport experiments on a quantum dot. In H.A. Cerdeira et al., editor, *Quantum Dynamics of Submicron Structures*, pages 263–274. Kluwer Academic Publishers, 1995.
153. M. Stopa. Multiple-capacitance magnetic-field-dependent Coulomb blockade energetics. *Phys. Rev. B*, 51:5494, 1995.
154. D. Weinmann, W. Häusler, and B. Kramer. Spin blockades in linear and nonlinear transport through quantum dots. *Phys. Rev. Lett.*, 74:984, 1995.
155. J.M. Kinaret, Y. Meir, Wingreen N.S., P. Lee, and X.-G. Wen. Conductance through a quantum dot in the fractional quantum Hall regime. *Phys. Rev. B*, 45:9489, 1992.
156. J.J. Palacios, L. Martin-Moreno, and C. Tejedor. Magnetotunneling through quantum boxes in a strong-correlation regime. *Europhys. Letters*, 23:495, 1993.
157. D. Pfannkuche and S.E. Ulloa. Selection rules for transport excitation spectroscopy of few-electron quantum dots. *Phys. Rev. Lett.*, 74:1194, 1995.
158. K. Jauregui, W. Häusler, D. Weinmann, and B. Kramer. Signatures of electron correlations in the transport properties of quantum dots. *Phys. Rev. B*, 53:1713, 1996.
159. T. Schmidt, R.J. Haug, V.I. Fal'ko, K. v. Klitzing, A. Förster, and H. Lüth. Observation of the local structure of Landau bands in a disordered conductor. *Phys. Rev. Lett.*, 78:4137, 1997.
160. A. Yacoby, M. Heiblum, D. Mahalu, and H. Shtrikman. Coherence and phase sensitive measurements in a quantum dot. *Phys. Rev. Lett.*, 74:4047, 1995.
161. P.W. Anderson. Localized magnetic states in metals. *Phys. Rev.*, 124:41, 1961.
162. G. Gruener and A. Zawadowski. Magnetic impurities in non-magnetic metals. *Rep. Prog. Phys.*, 37:1497, 1974.
163. J. Schmid, J. Weis, and K. Eberl. Kondo resonances in split-gate quantum dots. *Physica E*, 6:375, 2000.
164. W.J. De Haas, J. De Boer, and G.J. van der Berg. The electrical resistance of gold, copper and lead at low temperatures. *Physica*, 1:1115, 1933/34.
165. J. Kondo. Resistance minimum in dilute magnetic alloys. *Progr. Theor. Phys.*, 32:37, 1964.

166. J.R. Schrieffer and P.A. Wolff. Relation between the Anderson and the Kondo Hamiltonians. *Phys. Rev.*, 149:491, 1966.
167. K.G. Wilson. The renormalization group: Critical phenomena and the Kondo problem. *Rev. Mod. Phys.*, 47:773, 1975.
168. F.D.M. Haldane. Scaling theory of the asymmetric Anderson model. *Phys. Rev. Lett.*, 40:416, 1978.
169. L.I. Glazman and M.É. Raĭkh. Resonant Kondo transparency of a barrier with quasilocal impurity states. *JETP Lett.*, 47:453, 1988.
170. T.K. Ng and P.A. Lee. On-site Coulomb repulsion and resonant tunneling. *Phys. Rev. Lett.*, 61:1768, 1988.
171. D. Goldhaber-Gordon, H. Shtrikman, D. Mahalu, D. Abusch-Magder, U. Meirav, and M.A. Kastner. Kondo effect in a single-electron transistor. *Nature*, 391:156, 1998.
172. S.M. Cronenwett, T.H. Oosterkamp, and L.P. Kouwenhoven. A tunable Kondo effect in quantum dots. *Science*, 281:540, 1998.
173. J. Schmid, J. Weis, K. Eberl, and K. v. Klitzing. A quantum dot in the limit of strong coupling to reservoirs. *Physica B*, 256:182, 1998.
174. D.C. Ralph and R.A. Buhrman. Kondo-assisted and resonant tunneling via a single charge trap: A realization of the Anderson model out of equilibrium. *Phys. Rev. Lett.*, 72:3401, 1994.
175. Y. Meir, N.S. Wingreen, and P.A. Lee. Low-temperature transport through a quantum dot: The Anderson model out of equilibrium. *Phys. Rev. Lett.*, 70:2601, 1993.
176. J. König, J. Schmid, and H. Schoeller. Resonant tunneling through ultrasmall quantum dots: Zero-bias anomalies, magnetic-field dependence, and boson-assisted transport. *Phys. Rev. B*, 54:16820, 1996.
177. D. Goldhaber-Gordon, J. Göres, M.A. Kastner, H. Shtrikman, D. Mahalu, and U. Meirav. From the Kondo regime to the mixed-valence regime in a single-electron transistor. *Phys. Rev. Lett.*, 81:5225, 1998.
178. W.G. van der Wiel, S. De Franceschi, T. Fujisawa, J.M. Elzerman, S. Tarucha, and L.P. Kouwenhoven. The Kondo effect in the unitary limit. *Science*, 289:210, 2000.
179. N. Sivan and N.S. Wingreen. Single-impurity Anderson model out of equilibrium. *Phys. Rev. B*, 54:11622, 1996.
180. J. Schmid, J. Weis, K. Eberl, and K. v. Klitzing. Absence of odd-even parity behaviour for Kondo resonances in quantum dots. *Phys. Rev. Lett.*, 84:5824, 2000.
181. S. Sasaki, S. De Franceschi, J.M. Elzerman, W.G. van der Wiel, M. Eto, S. Tarucha, and L.P. Kouwenhoven. Kondo effect in an integer-spin quantum dot. *Nature*, 405:764, 2000.
182. J. Nygård, D.H. Cobden, and P.E. Lindelof. Kondo physics in carbon nanotubes. *Nature*, 408:342, 2000.
183. J. Schmid, J. Weis, K. Eberl, and K. v. Klitzing. Split Kondo resonances in quantum dots at finite magnetic fields. *Physica E*, 9:54, 2001.
184. M. Keller, U. Wilhelm, J. Schmid, J. Weis, K. v. Klitzing, and K. Eberl. Quantum dot in high magnetic fields: Correlated tunneling of electrons probes the spin configuration at the edge of the dot. *Phys. Rev. B*, 64:033302, 2001.
185. A.N. Korotkov, R.H. Chen, and K.K. Likharev. Possible performance of capacitively coupled single-electron transistors in digital circuits. *J. Appl. Phys.*, 78:2520, 1995.
186. T. Hiramoto and H. Ishikuro. Coulomb blockade in VLSI-compatible multiple-dot and single-dot MOSFETs. *Int. J. Electronics*, 86:591, 1999.

187. K. Matsumoto. Room temperature operated single electron transistor made by a scanning tunnelling microscopy/atomic force microscopy nano-oxidation process. *Int. J. Electronics*, 86:641, 1999.
188. Y. Ono, Y. Takahashi, K. Yamazaki, M. Nagase, H. Namatsu, K. Kurihara, and K. Murase. Si complementary single-electron inverter with voltage gain. *Appl. Phys. Lett.*, 76:3121, 2000.
189. M.I. Lutwyche and Y. Wada. Estimate of the ultimate performance of the single-electron transistor. *J. Appl. Phys.*, 75:3654, 1994.
190. A.N. Koroktov. Single-electron logic and memory devices. *Int. J. Electronics*, 86:511, 1999.
191. N. Negroponte. *Being Digital.* Alfred A. Knopf, Inc., New York, 1995.
192. J.S. Mayo. Materials for information and communication. *Scientific American*, 255:59, 1986.
193. J.S. Kilby. Miniature semiconductor integrated circuit. U.S. Patent 3,115,581, filed May 6, 1959, patented Dec. 24, 1963.
194. J.S. Kilby. Invention of the integrated circuit. *IEEE Transaction on Electron Devices*, ED-23:648, 1976.
195. R.N. Noyce. Semiconductor device-and-lead structure. U.S. Patent 2,981,877, filed July 30, 1959, patented Apr. 25, 1961.
196. G.E. Moore. Progress in digital integrated electronics. In *Proceedings of the International Electron Devices Meeting (IEDM), Technical Digest 11-13*, 1975.
197. D.J. Frank, R.H. Dennard, E. Nowak, P.M. Solomon, Y. Taur, and H.-S. Wong. Device scaling limits of Si MOSFETs and their application dependencies. *Proceedings of the IEEE*, 89:259, 2001.
198. D. Kahng. A historical perspective on the development of MOS transistors and related devices. *IEEE Transactions on Electron Devices*, ED-23:655, 1976.
199. M.M. Atalla. Semiconductor triode. U.S. Patent 3,056,888, filed Aug. 17, 1960, patented Oct. 2, 1962.
200. S.R. Hofstein and F.P. Heiman. The silicon insulated-gate field-effect transistor. *Proceedings of the IEEE*, 51:1190, 1963.
201. J.E. Lilienfeld. Method and apparatus of for controlling electric currents. U.S. Patent 1,745,175, filed Oct. 8, 1926, patented Jan. 28, 1930.
202. O. Heil. Improvements in or relating to electrical amplifiers and other control arrangements and devices. British Patent 439,457, filed Dec. 6, 1935, patented Sept., 1939.
203. W. Shockley and G.L. Pearson. Modulation of conductance of thin films of semi-conductors by surface charges. *Phys. Rev.*, 74:232, 1948.
204. W.K. Reymond. Switching circuit with a capacitor directly connected between the basis of opposite conductivity transistors. U.S. Patent 3,160,766, filed Nov. 28, 1962, patented Dec. 8, 1964.
205. R.H. Dennard, F.H. Gaensslen, Hwa-Nien Yu, E. Rideout, V.L. Bassous, and A.R. LeBlanc. Design of ion-implanted MOSFET's with very small physical dimensions. *IEEE J. of Solid-State Circuits*, 9:256, 1974.
206. D.L. Critchlow. MOSFET scaling – the driver of VLSI technology. *Proc. IEEE*, 87:659, 1999.
207. *1994 National Technology Roadmaps of the US Semiconductor Industry Association (SIA)*, 1994.
208. R.W. Keyes. Effect of randomness in the distribution of impurity ions on FET thresholds in integrated electronics. *Appl. Phys.*, 8:251, 1975.
209. R.H. Dennard. Technology challenges for ultrasmall silicon MOSFET's. *J. Vac. Sci. Technol.*, 19:537, 1981.
210. H.-S. Wong, Y. Taur, and D.J. Frank. Discrete random dopant distribution effects in nanometer-scale MOSFETs. *Microelectronics Reliability*, 38:1447, 1998.

211. M. Ono, M. Saito, T. Yoshitomi, C. Fiegna, T. Ohguro, and H. Iwai. A 40 nm gate length n-MOSFET. *IEEE Transactions on Electron Devices*, 42:1822, 1995.
212. A. Hori, H. Nakaoka, H. Umimoto, K. Yamashita, M. Takase, N. Shimizu, B. Mizuno, and S. Odanaka. A 0.05μm-CMOS with ultra shallow source /drain junctions fabricated by 5 keV ion implantation and rapid thermal annealing. In *Proceedings of the International Electron Devices Meeting (IEDM)*, 1994.
213. C. Wann, F. Assaderaghi, L. Shi, K. Chan, S. Cohen, H. Hovel, K. Jenkins, Y. Lee, D. Sadana, R. Viswanathan, S. Wind, and Y. Taur. High-performance 0.07-μm CMOS with 9.5-ps gate delay and 150 GHz f_T. *IEEE Electron Device Letters*, 18:625, 1997.
214. S. Deleonibus, C. Caillat, G. Guegan, M. Heitzmann, M.E. Nier, S. Tedesco, B. Dal'zotto, F. Martin, P. Mur, A.M. Papon, G. Lecarval, S. Biswas, and D. Souil. A 20-nm physical gate length NMOSFET featuring 1.2 nm gate oxide, shallow implanted source ad drain and BF_2 pockets. *IEEE Electron Device Letters*, 21:173, 2000.
215. Special issue: The limits of semiconductor technology. *Proceedings of the IEEE*, 89:223, 2001.
216. Y. Takahashi, M. Nagase, H. Namatsu, K. Kurihara, K. Iwdate, Y. Nakajima, S. Horiguchi, Murase K., and M. Tabe. Fabrication technique for Si single-electron transistor operating at room temperature. *Electronics Letters*, 31:136, 1995.
217. H. Ishikuro and T. Hiramoto. Quantum mechanical effects in the silicon quantum dot in a single-electron transistor. *Appl. Phys. Lett.*, 71:3691, 1997.
218. Y. Takahashi, A. Fujiwara, M. Nagase, H. Namatsu, K. Kurihara, K. Iwdate, and Murase K. Silicon single-electron devices. *Int. J. Electronics*, 86:605, 1999.
219. K. Matsumoto, M. Ishii, K. Segawa, Y. Oka, B.J. Vartanian, and J.S. Harris. Room temperature operation of a single electron transistor made by the scanning tunneling microscope nanooxidation process for the TiO_x/Ti system. *Appl. Phys. Lett.*, 68:34, 1996.
220. Y. Nakamura, Ch. Chen, and J. Tsai. 100 K operation of Al-based single-electron transistors. *Jpn. J. Appl. Phys.*, 35:1465, 1996.
221. S. Altmeyer, A. Hamidi, B. Spangenberg, and H. Kurz. 77 K single-electron transistor fabricated with 0.1 μm technology. *J. Appl. Phys.*, 81:8118, 1997.
222. J. Shirakashi and K. Matsumoto. Single-electron charging effects in Nb/Nb oxide-based single-electron transistors at room temperature. *Appl. Phys. Lett.*, 72:1893, 1998.
223. J.R. Tucker. Complementary digital logic based on the "Coulomb blockade". *J. Appl. Phys.*, 72:4399, 1992.
224. R.H. Chen, A.N. Korotkov, and K.K. Likharev. Single-electron transistor logic. *Appl. Phys. Lett.*, 68:1954, 1996.
225. K. Taniguchi and M. Kirihara. Future prospects of single-electron-tunneling (SET)-based digital circuits. *FED Journal*, 7:32, 1996.
226. A.W. Lo. Some thoughts on digital components and circuit techniques. *IRE Trans. on Electronic Computers*, 10:416, 1961.
227. A.W. Lo. Physical realization of digital logic circuits. In E. Keonjian, editor, *Micropower Electronics*. Pergamon Press, 1964.
228. R.W. Keyes. Physical limits in digital electronics. *Proceedings of the IEEE*, 5:740, 1975.
229. R.W. Keyes. Fundamental limits in digital information processing. *Proceedings of the IEEE*, 69:267, 1981.
230. R.W. Keyes. What makes a good computer device. *Science*, 230:138, 1985.

231. R.W. Keyes. Physics of digital devices. *Reviews of Modern Physics*, 61:279, 1989.
232. R.W. Keyes. Fundamental limits of silicon technology. *Proceedings of the IEEE*, 89:227, 2001.
233. R. Landauer. Can we switch by control of quantum mechanical transmission? *Physics Today*, Oct.:119, 1989.
234. R. Landauer. Advanced technology and truth in advertising. *Physica A*, 168:75, 1990.
235. R. Landauer. Is quantum mechanics useful? *Phil. Trans. R. Soc. Lond. A*, 353:367, 1995.
236. V.G. Oklobdzija. Differential and pass-transistor CMOS logic for high performance systems. *Microelectronics Journal*, 29:679, 1998.
237. A.G. Dickinson and J.S. Denker. Adiabatic dynamic logic. *IEEE J. of Solid-State Circuits*, 30:311, 1995.
238. V. Derycke, R. Martel, J. Appenzeller, and Ph. Avouris. Carbon nanotube inter- and intramolecular logic gates. *Nano Letters*, 1:453, 2001.
239. A. Bachtold, P. Hadley, T. Nakanishi, and C. Dekker. Logic circuits with carbon nanotube transistors. *Science*, 294:1317, 2001.
240. J.H. Schön, H. Meng, and Z. Bao. Self-assembled monolayer organic field-effect transistors. *Nature*, 413:713, 2001.
241. Y. Ono, K. Yamazaki, M. Nagase, S. Horiguchi, K. Shiraishi, and Y. Takahashi. Single-electron and quantum SOI devices. *Microelectronic Engineering*, 59:435, 2001.
242. K.U. Stein. Noise-induced error rate as limiting factor for energy per operation in digital IC's. *IEEE J. of Solid-State-Circuits*, 12:527, 1977.
243. I.S. Gradshteyn and I.M. Ryzhik. *Tables of Integrals, Series and Products.* Academic Press, New York and London, 1965.
244. R.M. Swanson and J.D. Meindl. Ion-implanted complementary MOS transistors in low-voltage circuits. *IEEE J. of Solid-State-Circuits*, 7:146, 1972.
245. K.N. Ratnakumar and J.D. Meindl. Short-channel MOST threshold voltage model. *IEEE J. of Solid-State Circuits*, SC-17:937, 1982.
246. G. Timp, J. Bude, F. Baumann, K.K. Bourdelle, T. Boone, J. Garno, A. Ghetti, M. Green, H. Gossmann, Y. Kim, R. Kleiman, A. Kornblit, F. Klemens, S. Moccio, D. Muller, J. Rosamilia, P. Silverman, T. Sorsch, W. Timp, D. Tennant, R. Tung, and B. Weir. The relentless march of the MOSFET gate oxide thickness to zero. *Microelectronics Reliability*, 40:557, 2000.
247. R.H. Yan, A. Ourmazd, K.F. Lee, and D.Y. Jeon. Scaling the Si metal-oxide-semiconductor field-effect transistor into the 0.1 μm regime using vertical doping engineering. *Appl. Phys. Lett.*, 59:3315, 1991.
248. R.H. Yan, A. Ourmazd, and K.F. Lee. Scaling the Si MOSFET: From bulk to SOI to bulk. *IEEE Transaction on Electron Devices*, 39:1704, 1992.
249. J.P. Colinge. Subthreshold slope of thin-film SOI MOSFET's. *IEEE Electron Device Letters*, EDL-7:244, 1986.
250. D.J Frank, S.E. Laux, and M.V. Fischetti. Monte Carlo simulation of a 30 nm dual-gate MOSFET: How short can Si go? In *Proceedings of the International Electron Devices Meeting (IEDM)*, 1992.
251. D.J. Frank and H.-S. Wong. Analysis of the design space available for high-κ gate dielectrics in nanoscale MOSFETs. *Superlattices and Microstructures*, 28:485, 2000.
252. F.G. Pikus and K.K. Likharev. Nanoscale field-effect transistors: An ultimate size analysis. *Appl. Phys. Lett.*, 71:3661, 1997.

253. Y. Taur. Analytic solutions of charge and capacitance in symmetric and asymmetric double-gate MOSFETs. *IEEE Transactions on Electron Devives*, 48:2861, 2001.
254. E. Leobandung, J. Gu, L. Guo, and S.Y. Chou. Wire-channel and wrap-around-gate metal-oxide-semiconductor field-effect transistors with a significant reduction of short channel effects. *J. Vac. Sci. Technol. B*, 15:2791, 1997.
255. G. Zimmerli, R.L. Kautz, and J.M. Martinis. Voltage gain in the single-electron transistor. *Appl. Phys. Lett.*, 61:2616, 1992.
256. E.H. Visscher, S.M. Verburgh, J. Lindeman, P. Hadley, and J.E. Mooij. Fabrication of multilayer single-electron tunneling devices. *Appl. Phys. Lett.*, 66:305, 1995.
257. Y. Ono, K. Yamazaki, and Y. Takahashi. Si single-electron transistor with high voltage gain. *IECE Trans. Electron.*, E84-C:1061, 2001.
258. M.A. Reed. Molecular-scale electronics. *Proceedings of the IEEE*, 87:652, 1999.
259. D. Goldhaber-Gordon, M.S. Montemerlo, J.Ch. Love, G.J. Opiteck, and J.C. Ellenbogen. Overview of nanoelectronic devices. *Proceedings of the IEEE*, 85:521, 1997.
260. F. Schwabl. *Quantum Mechanics*. Springer, Berlin, 1991.
261. R.H. Yan, D. Monroe, J. Weis, A. Mujtaba, and E. Westerwick. MOSFET: From bulk to SOI to bulk: Reducing operating voltage from 3, 2, to 1 Volt and below – challenges and guidelines for possible solutions. In *Proceedings of the International Electron Devices Meeting (IEDM), Technical Digest*, page 55, 1995.
262. K. Yano, T. Ishii, T. Sano, T. Mine, F. Murai, T. Hashimoto, T. Kobayashi, T. Kure, and K. Seki. Single-electron memory for giga-to-tera bit storage. *Proceedings of the IEEE*, 87:633, 1999.
263. Y. Huang, X. Duan, Y. Cui, L.J. Lauhon, K.-H. Kim, and C.M. Lieber. Logic gates and computation from assembled nanowire building blocks. *Science*, 294:1313, 2001.
264. M. Sanquer, M. Specht, L. Ghenim, S. Deleonibus, and G. Guegan. Coulomb blockade in low-mobility nanometer size Si MOSFET's. *Phys. Rev. B*, 61:7249, 2000.
265. W. Porod, C.S. Lent, G.H. Bernstein, A.O. Orlov, I. Amlani, G.L. Snider, and J.L. Merz. Quantum-dot cellular automata: computing with coupled quantum dots. *Int. J. Electronics*, 86:549, 1999.
266. E.V. Sukhorukov and D. Loss. Spintronics and spin-based qubits in quantum dots. *phys. stat. sol.*, 224:855, 2001.
267. Y. Makhlin, G. Schön, and A. Shnirman. Josephson-junction qubits with controlled couplings. *Nature*, 398:305, 1999.
268. Y. Makhlin, G. Schön, and A. Shnirman. Quantum-state engineering with josephson-junction devices. *Rev. Mod. Phys.*, 73:357, 2001.
269. H. Qin, F. Simmel, R.H. Blick, J.P. Kotthaus, W. Wegscheider, and M. Bichler. Determination of the complex microwave photoconductance of a single quantum dot. *Phys. Rev. B*, 63:035320, 2001.
270. Y. Ji, M. Heiblum, and H. Shtrikman. Transmission phase of a quantum dot with Kondo correlation near the unitary limit. *Phys. Rev. Lett.*, 88:076601, 2002.
271. F. Simmel, R.H. Blick, J.P. Kotthaus, W. Wegscheider, and M. Bichler. Anomalous Kondo effect in a quantum dot at nonzero bias. *Phys. Rev. Lett.*, 83:804, 1999.

272. U. Wilhelm, J. Schmid, J. Weis, and K. v. Klitzing. Two electrostatically coupled quantum dots as a realization of the Anderson impurity model. *Physica E*, 9:625, 2001.
273. J.. Göres, D. Goldhaber-Gordon, S. Heemeyer, and M.A. Kastner. Fano resonances in electronic transport through a single-electron transistor. *Phys. Rev. B*, 62:2188, 2000.
274. W.R. Smythe. *Static and Dynamic Electricity.* MacGraw-Hill, New York, 1968.
275. K. Simonyi. *Theoretische Elektrotechnik.* VEB Deutscher Verlag der Wissenschaften, Berlin, 4. edition, 1971.
276. I.N. Bronstein and K.A. Semendjajew. *Taschenbuch der Mathematik.* Verlag Harri Deutsch, Thun und Frankfurt (Main), 21. edition, 1981.